Ervice Vidal Pouokam Kamgne, PhD

Neue Aspekte in der gastrointestinalen Physiologie: Wirkung von Gasotransmittern und funktionalisierten Nanopartikeln sowie Erfassung physiologischer Parameter mittels Nanostrukturen

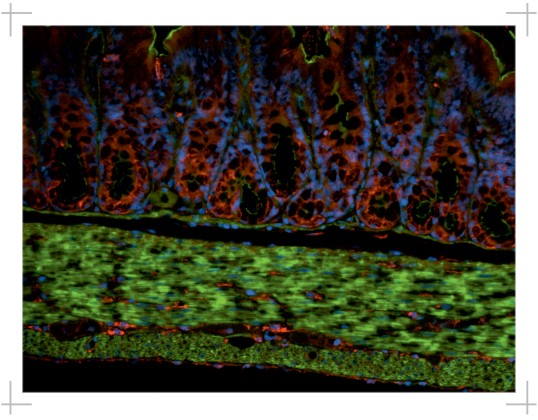

HABILITATIONSSCHRIFT
zur Erlangung der Lehrbefähigung für das Fach Veterinär-Physiologie
im Fachbereich Veterinärmedizin der Justus-Liebig-Universität Gießen

VVB LAUFERSWEILER VERLAG

Das Werk ist in allen seinen Teilen urheberrechtlich geschützt.

Die rechtliche Verantwortung für den gesamten Inhalt dieses Buches liegt ausschließlich bei dem Autoren dieses Werkes.

Jede Verwertung ist ohne schriftliche Zustimmung der Autoren oder des Verlages unzulässig. Das gilt insbesondere für Vervielfältigungen, Übersetzungen, Mikroverfilmungen und die Einspeicherung in und Verarbeitung durch elektronische Systeme.

1. Auflage 2020

All rights reserved. No part of this publication may be reproduced, stored in a retrieval system, or transmitted, in any form or by any means, electronic, mechanical, photocopying, recording, or otherwise, without the prior written permission of the Authors or the Publisher.

1st Edition 2020

© 2020 by VVB LAUFERSWEILER VERLAG, Giessen
Printed in Germany

édition scientifique
VVB LAUFERSWEILER VERLAG

STAUFENBERGRING 15, 35396 GIESSEN, GERMANY
Tel: 0641-5599888 Fax: 0641-5599890
email: redaktion@doktorverlag.de

www.doktorverlag.de

Justus-Liebig-Universität Gießen
Fachbereich Veterinärmedizin

Institut für Veterinär-Physiologie und -Biochemie

Neue Aspekte in der gastrointestinalen Physiologie: Wirkung von Gasotransmittern und funktionalisierten Nanopartikeln sowie Erfassung physiologischer Parameter mittels Nanostrukturen

HABILITATIONSSCHRIFT
zur Erlangung der Lehrbefähigung
für das Fach Veterinär-Physiologie
im Fachbereich Veterinärmedizin
der Justus-Liebig-Universität Gießen

vorgelegt von

Ervice Vidal Pouokam Kamgne, PhD

Gießen 2019

Meiner Familie

Inhaltsverzeichnis

1. Abkürzungsverzeichnis

ACh	Acetylcholin
CaCC	Calciumaktivierter Chloridkanal
cAMP	zyklisches Adenosinmonophosphat
CCh	Carbachol
CFTR	Cystic Fibrosis Transmenbrane Regulator
cGMP	zyklisches Guanosinmonophosphat
CO	Kohlenstoffmonoxid
ENS	enterische Nervensystem
ER	endoplasmatisches Reticulum
GDP	Guanosindiphosphat
GTP	Guanosintriphosphat
HNO	Nitroxyl
H_2S	Schwefelwasserstoff
IP_3	Inositoltrisphosphat
IP_3R	IP_3-Rezeptor
I_{sc}	Kurzschlussstrom
K_{ATP}	ATP-sensitiver Kaliumkanal
MLCK	Myosin-Leichte-Ketten-Kinase
MLCP	Myosin-Leichte-Ketten-Phosphatase
NHE	Natrium/Proton-Austauscher
NK1	Neurokinin1
NKCC	$Na^+/K^+/2Cl^-$-Cotransporter
NO	Stickstoffmonoxid
PG	Prostaglandin
PKA	Proteinkinase A
PKC	Proteinkinase C
PLC	Phospholipase C
RyR	Ryanodin-Rezeptor
SERCA	Calciumpumpe des sarcoplasmatischen und endoplasmatischen Reticulums
sGC	lösliche Guanylatcyklase
SKca	small conductance Ca^{2+}-abhängiger Kaliumkanal
SOCE	Speicher-gesteuerter Ca^{2+}-Einstrom
SP	Substanz P
TPeA	Tetrapentylammonium
VIP	Vasoaktives intestinales Peptid

2. Abbildungsverzeichnis

3. Auflistung der Publikationen als Teil der Habilitationsschrift

Die nachfolgend aufgelisteten Publikationen sind nicht chronologisch, sondern thematisch geordnet.

3.1 Arbeiten zur Wirkung von Gasotransmittern am Gastrointestinaltrakt

Pouokam E, Diener M. Mechanims of actions of hydrogen sulfide at rat distal colonic epithelium (2011). *Brit. J. Pharmacol*. 162: 392-404. **[Impact factor 2011: 4.409]**

Pouokam E, Diener M. Modulation of ion transport across rat distal colon by cysteine (2012). *Front. Physiol. Membr. Physiol. Biophys*. 3: Art. 43. **[Impact factor 2012: 2.97]**

Pouokam E, Bader S, Brück B, Schmidt B, Diener M. ATP-sensitive K^+ channels in rat colonic epithelium. *Pflügers Arch. Eur. J. Physiol.* (2013) 465: 865-877. **[Impact factor 2013: 3.073]**

Schindele S, **Pouokam E**, Diener M. Hypoxia/reoxygenation effects on ion transport across rat colonic epithelium. *Front. Physiol*. (2016) 7: Art. 247. **[Impact factor 2016: 4.134]**

Pouokam E, Steidle M, Diener M. Regulation of colonic ion transport by gasotransmitters. *Biol. Pharm. Bull.* (2011) 34: 789-793**. [Impact factor 2011: 1.657]**

Pouokam E, Althaus M. Epithelial electrolyte transport physiology and the gasotransmitter hydrogen sulfide. *Oxid. Med. Cell. Longevity* (2015) Vol. 2016: Art. ID 4723416. **[Impact factor 2016: 4.492]**

Pouokam E, Bell A, Diener M. Actions of Angeli's salt, a nitroxyl (HNO) donor, on ion transport across mucosa-subMukosapreprations from rat distal colon (2013). *Eur. J. Pharmacol*. 715: 133-141. **[Impact factor 2013: 2.68]**

Sowie: Bislang unveröffentlichte Daten zu HNO-Wirkungen auf die gastrointestinale Motilität (Kapitel 8.8).

3.2 Nanostrukturen und gastrointestinale Physiologie

Gasiorek F, **Pouokam E**, Diener M, Schlecht S, Wickleder M. Effects of multivalent histamine supported on gold nanoparticles: Activation of histamine receptors by derivatized histamine at subnanomolar concentrations. *Organ. Biomol. Chem.* (2015) 13: 9984-9992. **[Impactfactor 2015: 3.559]**

Mattern A, Machka F, Wickleder MS, Ilyaskina OS, Bünemann M, Diener M, **Pouokam E.** Potentiation of the activation of cholinergic receptors by multivalent presentation of ligands supported on gold nanoparticles. *Organ. Biomol. Chem*. (2018) 16: 6680-6687. **[Impact factor 2018: 3.4]**

Müntze GM, **Pouokam E**, Steidle J, Schäfer W, Sasse A, Röth K, Diener M, Eickhoff M. Acetylcholinesterase-modified AlGaN/GaN solution-gate field-effect transistors for in-situ monitoring of myenteric neuron activity. *Biosens. Bioelectr*. (2015) 77: 1048-1054 **[Impact factor 2015: 7.476]**

Hölzel S, Zyuzin MV, Wallys J, **Pouokam E**, Müßener J, Hille P, Diener M, Parak WJ, Eickhoff M. Dynamic extracellular imaging of biochemical cell activity using InGaNGaN nanowire arrays as nanophotonic probes. *Adv. Funct. Mater.* (2018) 28:1802503. **[Impact factor 2018: 13.325]**

4. Einleitung

4.1 Aufbau des Darms

Der Darm stellt den Hauptteil des Verdauungssystems dar. Er besteht generell aus dem Dünn- und dem Dickdarm, die je nach Tierart unterschiedlich ausgeprägt sind. Der Dünndarm wird vom Pylorus nach Anus in Duodenum, Jejunum und Ileum gegliedert. Das Ileum mündet in den Dickdarm, der sich aus Caecum, Colon und Rektum zusammensetzt. Die Arbeiten, die in dieser Schrift zusammengefasst sind, wurden am Jejunum, Ileum und Colon der Ratte durchgeführt.

Die Funktionen des Darms bestehen dahin, Nahrungsbestandteile zu verdauen und die entstandenen Spaltprodukte zu resorbieren, sodass sie nach der Passage durch das Epithel in die Blut- oder Lymphbahn übertreten. Unterstützt wird dies durch die Motorik der Darmwand, die neben einer mechanischen Zerkleinerung für den Weitertransport des Chymus in die unterschiedlichen gastrointestinalen Kompartimente sorgt. Außerdem weist der Darm eine Schutzfunktion auf: so stellt das Epithel eine Barriere dar, die das Körperinnere vor Fremdköpern schützt. In dem gleichen Sinne trägt das „Darmassoziierte Immunsystem“ (engl. GALT = gut-associated lymphoid tissue) dazu bei, potenziell schädliche Substanzen zu neutralisieren. Aufgrund der großen Oberfläche des Darms trägt dieser effektiv zur Aufnahme und dem Transport von Nährstoffen und Medikamenten bei. Transportvorgänge durch das Darmepithel können sowohl vom Lumen in Richtung Blutbahn (Resorption) oder umgekehrt (Sekretion) ablaufen. Letzte Aufgabe des Gastrointestinaltrakt ist die Ausscheidung unverdauter Nahrungsbestandteile oder abgeschilfterter Epithelzellen durch die Defäkation. Die **Abb.1** zeigt die schematische Struktur der Darmwand, wo grob die Schichten von innen nach außen erkennbar sind. Das sind: die Mucosa, die Submucosa, die Tunica muscularis und die Serosa, die außen das

Darmrohr überkleidet. Die Mucosa wird von Epithel ausgekleidet, welches dem Lumen zugewandt ist. Unterhalb der Mucosa liegt die Muscularis mucosae (**Abb.2a**), gefolgt von dem Nervengeflecht des Plexus submucosus.

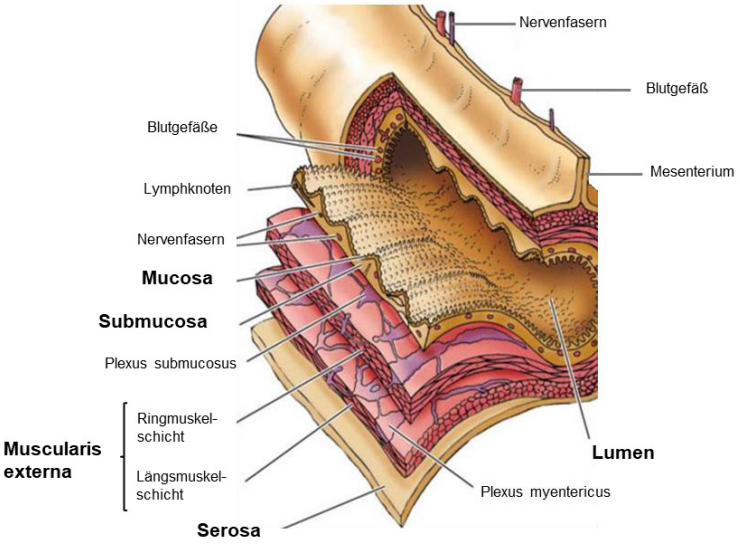

Abb.1: Struktur der Darmwand am Beispiel des Dünndarmes. Anwendung erlaubt von und modifiziert nach Purves et al. (2006).

Zwischen der Ringmuskulatur und der Längsmuskulatur ist ein weiteres Nervengeflecht eingebettet, der Plexus myentericus (**Abb.2a, b**). Eine detaillierte Struktur dieser Teile des enterischen Nervensystems (ENS) zeigt die **Abb.2b.** Einzelne Zellen dieser Nervengeflechte oder ganze Ganglien lassen sich sehr gut als neuronale Modelle zur Untersuchung neuronaler Aktivität verwenden (Browning und Lees 1996; Schäfer et al. 1997; Wada-Takahashi und Tamura 2000; Haschke et al. 2000; Vogalis und Harvey 2003; Hamodeh et al. 2004; Rehn et al. 2004; Rehn und Diener 2006; Pouokam et al. 2009). Beispielsweise wurde die Kinetik und die quantitative *„in situ“* Freisetzung des

Neurotransmitters Acetylcholin (ACh) von isolierten myenterischen Neuronen bzw. in intakten Ganglien in der **Publikation 8.11** untersucht.

Die Struktur der Darmschleimhaut weist Krypten sowohl im Dünn- als auch im Dickdarm auf. Einen Unterschied stellen aber die Zotten dar, die nur im Dünndarm vorhanden sind (**Abb.3**). Darmepithelzellen werden von intestinalen Stammzellen im Fundus, also in der Tiefe der Krypten gebildet, wandern und differenzieren sich zu hochspezialisierten Zellen entlang der Kryptenachse bis hin zur Spitze (der Zotten im Dünndarm) bzw. dem Oberflächenepithel (im Dickdarm), wo sie nach Apoptose abgestoßen werden (**Abb.4**). Die Epithelzellen sind miteinander durch Schlussleisten verbunden und bilden dadurch eine Barriereschicht. Die Schlussleisten tragen auch zur Polarität dieser Zellen bei. So wird die Seite der Zelle, die der funktionellen „Außenseite“, also dem Lumen, zugewandt ist, als luminale bzw. apikale Seite bezeichnet. Die Seite, die der Blutbahn zugewandt ist, wird als serosale bzw. basolaterale Seite bezeichnet. Im Darmepithel unterscheidet man verschiedene Zelltypen wie Paneth-Zellen (nur in den Krypten des Dünndarms und des Mastdarms, produzieren antimikrobielle Stoffe), Becherzellen (auch Goblet-Zellen genannt; produzieren Mucine), endokrine Zellen (Produktion lokaler Mediatoren und Hormone), Stammzellen sowie Enterozyten (in resorptiv aktiven Darmabschnitten des Dünn- und Dickdarms). Enterozyten tragen am apikalen Zellpol einen dichten Saum von Mikrovilli, welcher Bürstensaum genannt wird. Die Aufgaben der Enterozyten setzen sich aus der Resorption kleiner Moleküle aus der Nahrung, dem aktiven Transport von Stoffen, der Wasseraufnahme und der Sekretion von Immunglobulinen (IgA) zusammen. Die meisten Daten, die in dieser Schrift dargestellt werden, beziehen sich auf die Colonepithelzellen.

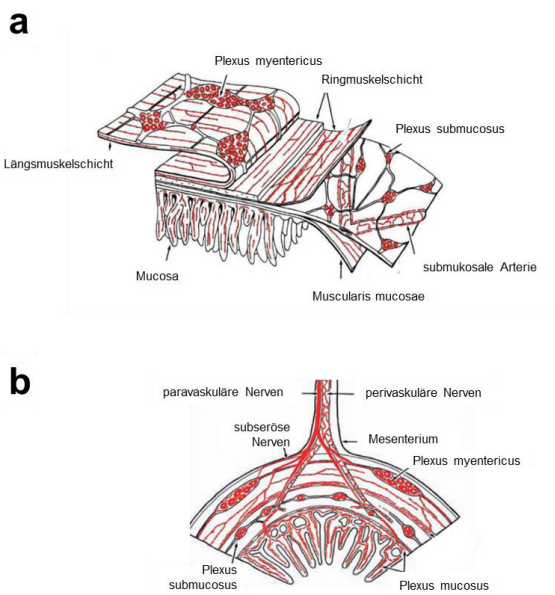

Abb.2: Topologische Anordnung (a) und Struktur (b) der Nervengeflechte des enterischen Nervensystems im Darm. Anwendung erlaubt von und modifiziert nach Furness (2006).

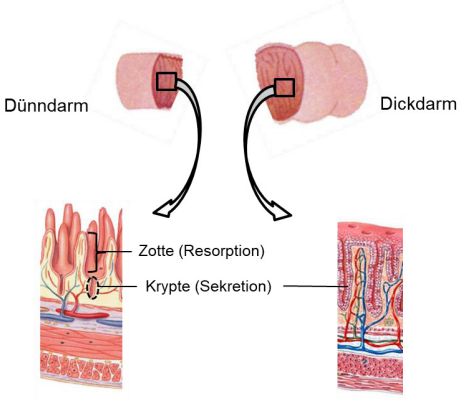

Abb.3: Darmschleimhaut des Dünn-und Dickdarms. Erlaubt von und modifiziert nach Mescher (2013).

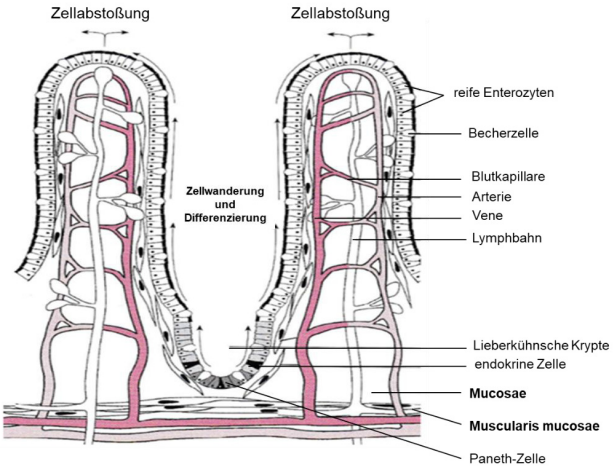

Abb.4: Aufbau des Darmepithels am Beispiel des Dünndarms. Modifiziert nach Wolffram (2009). Verwendung erlaubt vom Enke-Verlag.

4.2 Epitheliale Transportmechanismen im Colon

4.2.1.1 Transporter und Kanäle

Biomembranen sind prinzipiell selektiv durchlässig. Das bedeutet, dass sie nur bestimmte Stoffe passieren lassen. Um diese Passage kontrolliert zu gewährleisten, besitzen Zellmembranen sogenannte „Transporter“. Transportmechanismen am Darmepithel können passiv sein, das heißt „bergab“ entlang bestehender elektrochemischer Gradienten arbeiten, wodurch kein Energieaufwand für das Betreiben solcher Transporter notwendig ist. Zudem gibt es aktiven Transport, also „bergauf“ entgegen elektrochemischer Gradienten, wofür Energie, die in der Regel letztlich aus der Spaltung von ATP stammt, aufgewendet werden muss. Unter dem Begriff Transporter versteht man integrale Membranproteine, die Molekülflüsse durch eine Membran ermöglichen und so die Permeabilität der entsprechenden Membran kontrollieren. Transporter werden in zwei Superfamilien unterteilt: Die ABC (ATP binding cassette) und die SLC (solute carrier)

Transporter (Giacomini und Sugiyama 2011). Die meisten ABC Transporter sind primär aktive Transporter, die eine ATPase-Aktivität aufweisen. Die SLC Transporter hingegen sind Transporter, die entweder keine Energie benötigen (z.B. Uniporter) oder als sekundär aktive Transporter, wie z.B. Cotransporter oder Antiporter, ihre Triebkraft von primär aktiven Transportern erhalten. Kanäle sind Membranproteine, die die Passage geladener Teilchensorten oder kleiner Moleküle dem Konzentrationsgefälle und dem elektrischen Gradienten folgend verwirklichen. Kanäle weisen keine feste Stöchiometrie auf, das heißt es gibt kein festes Verhältnis in der Transportrate der zu transportierenden Substanzen. So kann eine relativ hohe Anzahl an Chloridionen durchströmen, wenn sich ein Cl^--Kanal öffnet. Auch weisen Kanäle keine Sättigungseigenschaft auf, was bedeutet, dass bei steigender Substratkonzentration die Transportrate linear ansteigt. Kanäle kommen in mindestens zwei Zuständen vor: dem „offen“ und dem „geschlossen“ Zustand, zwischen denen der Kanal stochastisch wechselt. So fungieren die Kanäle als „Poren“ im offenen Zustand. Der Stofftransport durch das Darmepithel erfolgt sowohl durch passive als auch aktive Transportmechanismen.

Die Dichtigkeit eines Epithels bestimmt zudem, ob der Stofftransport durch die Epithelschicht überwiegend parazellulär oder transzellulär stattfindet. So wird in einem lecken Epithel, wie dem Dünndarmepithel, ein relativ großer parazellulärer Transport festgestellt. Im Dickdarm dagegen ist das Epithel dicht, sodass die transepitheliale Potentialdifferenz, d.h. die elektrische Spannung zwischen der Außenseite und der der Körperflüssigkeit zugewandten Seite, relativ hoch ist. Solche Potentialdifferenzen entstehen durch Ladungsungleichgewichte, die durch strukturelle Dichtigkeiten und Ionenströme festgelegt werden. Die Dichtigkeit wird am apikalen Pol von Colonepithelzellen durch sogenannten Schlussleiten gewährleistet. Die apikale und basolaterale Membranen sind mit unterschiedlichen Transportern und Kanälen

ausgestattet. Üblicherweise ist im Dickdarm die Blutseite positiv geladen gegenüber der Lumenseite.

Das Dickdarmepithel ist in der Lage, die Transportmechanismen zwischen Resorption und Sekretion umzuschalten. Die **Abb.5** und **Abb.6** zeigen die wichtigsten Transporter und Kanäle des Dickdarmepithels, die zu Resorption und Sekretion beitragen (Böhme et al. 1991; Binder und Sandle 1994; Sandle et al. 1994; Diener und Scharrer 1994; Sandle 1998; Greger 2000; Kunzelmann und Mall 2002). Die Basolateralmembran ist überwiegend für Kaliumionen durchlässig, da sie eine hohe Anzahl von K^+-Kanälen enthält. Außerdem befindet sich hier die Na^+/K^+-ATPase, auch Na^+/K^+-Pumpe genannt, die aktiv, d.h. unter ATP-Verbrauch, Natriumionen aus der Zelle herausschleust im Austausch gegen Kaliumionen. Diese ATPase arbeitet elektrogen: für drei ausgeschleuste Natriumionen werden nur zwei Kaliumionen aufgenommen: Daraus resultiert ein Nettotransport von positiven Ladungen auf die Blutseite. Die in die Zellen gepumpten Kaliumionen verlassen die Zelle wieder über Kaliumkanäle, hier sind besonders die Ca^{2+}-abhängigen K^+-Kanäle (K_{ca}) und die ATP-sensitiven K^+-Kanäle (K_{ATP}) in der Basolateralmembran zu nennen, sodass netto gesehen nur ein Transport von Natriumionen stattfindet. Diese ATPase ist der eigentlich primär aktive Schritt, der den gesamten Ionentransport in Gang hält.

Die auf die Blutseite gelangten Na^+-Ionen werden zuvor aus dem Lumen des Magen-Darm-Traktes durch spezielle Transporteiweiße in der apikalen Membran von Dickdarmepithelzellen, den sogenannten Na^+-Kanälen (ENaC; epitheliale Natriumkanäle), aufgenommen.

Die Resorption von Na^+-Ionen erfolgt aktiv (**Abb.5**). Die Triebkraft dafür ist der Konzentrationsgradient, der von der basolateralen Na^+/K^+-ATPase aufgebaut wird. Als Folge dieses Gradienten, werden Natriumionen in die Zellen aufgenommen im Austausch

gegen Protonen durch Na^+/H^+-Austauscher (NHE). Die Tätigkeit solcher NHE löst eine Alkalinisierung der Zelle aus. Kompensatorisch wirken parallele Austauscher, die Cl^-/HCO_3^--Austauscher, dieser Alkalinisierung entgegen, um den intrazellulären pH-Wert konstant zu halten. Natriumionen können auch durch die ENaC resorbiert werden. Dies ist zum Beispiel der Fall bei einer Hyponaträmie bei Tieren wie der Ratte, bei denen unter Normalbedingung die Resorption über Austauscher erfolgt. Eine Hyponaträmie löst die Ausschüttung von Aldosteron aus der Nebennierenrinde aus und führt zum Einbau von ENaC in die apikale Membran (Canessa et al. 1993; Lingueglia et al. 1993; Canessa et al. 1994; Kunzelmann und Mall 2002).

Chloridionen werden auch im Dickdarm aktiv resorbiert. So wird auch hier der Na^+-Gradient als Triebkraft für die sekundär aktive Tätigkeit des Cl^-/HCO_3^--Austauschers verwendet (Binder und Sandle 1994; Sandle 1998; Kunzelmann und Mall 2002). Allerdings wird der Cl^-/HCO_3^--Austauscher parallel nach der Tätigkeit des Na^+/H^+-Austauschers eingeschaltet um der Alkalinisierung, wie oben erwähnt, entgegenzuwirken. So werden Chloridionen apikal aufgenommen und verlassen die Zelle hauptsächlich durch die basolaterale Membran über Cl^--Kanäle.

Kaliumionen werden im Dickdarm aktiv resorbiert und sezerniert. Die Hauptrichtung des Transports wird durch die Lage der Kaliumkonzentration im Blutplasma bestimmt. Unter Normalbedingungen herrscht eine Nettosekretion, jedoch führt ein Kaliummangel zu einer Nettoresorption von Kaliumionen. Die Kaliumresorption wird über die in der apikalen Membran eingebaute H^+/K^+-ATPase vermittelt (Übersicht bei Sandle 1998, Kunzelmann und Mall 2002).

Im Dickdarm können auch kurzkettige Fettsäuren in ihrer dissoziierten Form $SCFA^-$ aufgenommen werden (**Abb.5**). Sie sind Produkte der mikrobiellen Fermentation und als schwache Säuren liegen sie bei dem eher neutralen bis leicht sauren pH des

Dickdarminhalts zu 99 % in der dissoziierten Form vor. Acetat-, Propionat- bzw. Butyratanionen sind die eigentlichen Substrate, die von den Colonepithelzellen aufgenommen werden. Die Resorption über $SCFA^-/HCO_3^-$-Austauscher läuft nach dem sekundär aktiven Prinzip ab, wobei HCO_3^- aus der Zelle hinaus transportiert wird (Binder und Sandle 1994; Diener und Scharrer 1994; Kunzelmann und Mall 2002). In der nicht-dissoziierten Form können sie als lipophile Moleküle durch die apikale Membran diffundieren. Die Resorption der obengenannten Ionen, die auch in die Zwischenzellräume austreten, lösen eine Hyperosmolarität in diesen Räumen gegenüber dem Lumen aus, was Wassermoleküle aus dem Lumen per Osmose parazellulär anzieht.

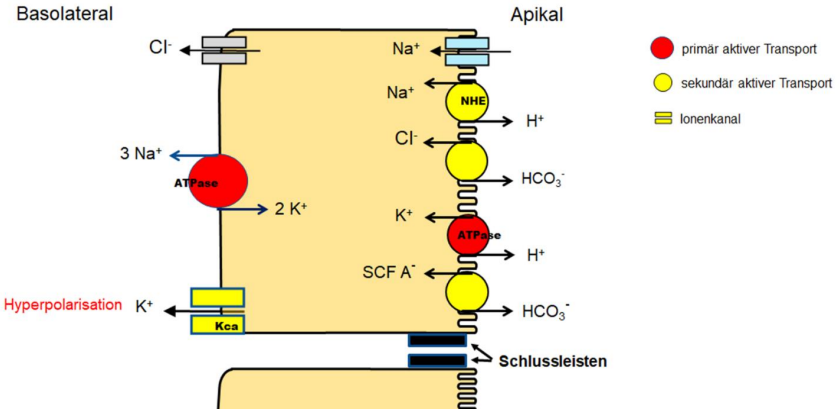

Abb.5: Wichtige Transporter und Kanäle des Colonepithels zur Resorption. In der basolateralen Mambran der Colonepithelzellen sitzen die Na^+/K^+-ATPase, die Ca^{2+}-abhängigen K^+-Kanäle und Chloridionenkanäle. In der apikalen Membran kommen K^+/H^+-ATPase, Na^+/H^+-Austauscher, Cl^-/HCO_3^--Austauscher, $SCFA^-/ HCO_3^-$ und Na^+-Kanäle vor.

Die Wasserresorption ist im Colon relativ hoch, um einen festeren Kot ausscheiden zu können. Unter Einfluss von Sekretagogen oder Toxinen können vermehrt Ionen und folglich Wasser sezerniert werden. Die wichtigsten Ionen, die so ins Lumen abgegeben werden, sind Cl^-, K^+ aber auch HCO_3^-, sowie H^+ und Na^+. Die Chloridsekretion (**Abb.6**)

erfolgt aktiv, also unter Energieverbrauch. Die Tätigkeit der basolateralen Na^+/K^+-ATPase baut den Na^+-Gradienten auf, wie oben bereits erwähnt. Parallel zur Tätigkeit der basolateralen Ca^{2+}-abhängigen K^+-Kanäle wird elektroneutral über den basolateralen Cotransporter NKKC1 die Aufnahme von Cl^--Ionen, Na^+-Ionen und K^+-Ionen gewährleistet (Übersicht bei Binder und Sandle 1994; Kunzelmann und Mall 2002).

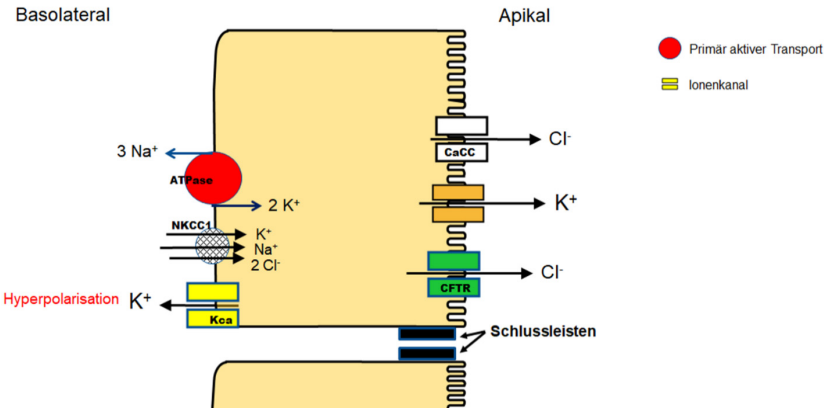

Abb.6: Wichtige Transporter und Kanäle des Colonepithels zur Sekretion. In der basolateralen Mambran der Colonepithelzellen sitzen die Na^+/K^+-ATPase, die Ca^{2+}-abhängigen K^+-Kanäle und Chloridkanäle, $Na^+/K^+/2Cl^-$-Cotransporter. In der apikalen Membran kommen Cl^- -Kanäle (Ca^{2+}-gesteuert und der cAMP-abhängige CFTR) und K^+-Kanäle vor.

Dies führt zur intrazellulären Akkumulation von Chlorionen, die die Zelle apikal verlassen, wenn sich die dort sitzenden Cl^--Kanäle, die sogenannten Cystic Fibrosis Transmembrane Conductance Regulator (CFTR) und die Ca^{2+}-gesteuerten Cl^--Kanäle (CaCC), öffnen.

Bicarbonationen können über den CFTR ins Lumen gelangen. Weitere Möglichkeiten, diese Ionen ins Lumen abzugeben, bestehen in sekundär aktiven Transportmechanismen:

So wird auch Bicarbonat über den mit dem Natrium-Protonen-Austauscher parallel geschalteten Cl^-/HCO_3^--Austauscher ins Darmlumen oder über den $SCFA^-/HCO_3^-$-Austauscher sezerniert (**Abb.5).** Bicarbonat wird dabei aus metabolisch anfallendem CO_2 gebildet, das durch eine intrazelluläre Carboanhydrase vermittelt in Kohlensäure umgewandelt wird. Die Kohlensäure zerfällt rasch zu Protonen und Bicarbonationen, die über die entsprechenden Austauscher aus der Zelle herausgebracht werden (Übersicht Binder und Sandle, 1994; Kunzelmann und Mall 2002).

Kaliumionen können auch apikal die Colonepithelzellen über K^+-Kanäle verlassen (**Abb.6**). Zur K^+-Beladung der Zellen dienen die Na^+/K^+-ATPase und der $Na^+/K^+/2Cl^-$-Cotransporter in der basolateralen Membran (**Abb.5**).

Das Colonepithel, also das Gewebe, das in den Publikationen **8.1-8.4, 8.7-10 und 8.12** im Fokus stand, ist in der Lage rasch zwischen Resorption und Sekretion umzuschalten. Es ist also notwendig, diese Eigenschaften des Epithels über extra- und intrazelluläre Signale zu regulieren.

4.2.1.2 Signaltransduktion

Signalsubstanzen, die aus Darmzellen freigesetzt werden, entfalten ihre Wirkungen lokal entweder auf benachbarte Zellen, was als parakrine Signalübertragung gilt, oder autokrin auf die Signal-produzierenden Zellen selbst. Zu den Signalsubstanzen, die auf den Gastrointestinaltrakt einwirken, gehören außerdem Hormone aus klassischen endokrinen Drüsen (etwa dem Nebennierenmark), Hormone aus diffus im Darmepithel verteilten endokrinen Zellen, Neurotransmitter und Zytokine. Die **Tabelle 1** gibt eine Übersicht der wichtigsten extrazellulären Signalsubstanzen im Colon und deren Hauptzielorte und Wirkung.

Tabelle 1: Wichtige Botenstoffe im Colon

Signalsub-stanz	Herkunft	Beschreibung	Zielort	Wirkung
Serotonin	Enterochrom-affine Zellen und enterische Nervenzellen	Biogenes Amin, Neurohormon	Colonocyten 5-HT-Rezeptoren	Steigerung der Anionensekretion, Peristaltik
VIP	Enterische Neurone	Peptid Neurohormon	VPAC Rezeptoren, Enterozyten, Intestinale Myozyten	Steigerung der Anionensekretion, Verminderung der Darmmotilität
Histamin	Mastzellen, enterische Neurone	Biogenes Amin, Immun-mediator	H-Rezeptoren, Enterozyten, enterische Neurone	Steigerung der Anionensekretion und der Motilität
Prostaglandine	Immunzellen des Dickdarms	Eikosanoide	Prostaglandin-Rezeptoren, Glatte Muskelzellen, Epithelzellen	Überwiegend Steigerung der Anionensekretion, der Sekretion von Mukus, der Motilität.
Substanz P	Enterische Neurone	Neuropeptid (Tachykinin)	Neurokinin-1 Rezeptor (NK-1R)	Steigerung der Darmmotilität, Schmerzauslösung
NO	Enterische Neurone	Gasotrans-mitter	sGC, glatte Muskelzellen, Epithelzellen	Steigerung der Anionensekretion, Peristaltik (Relaxation)
ACh	Enterische Neurone, Oberflächen-epithel	Neurotrans-mitter	ACh Rezeptoren, Epithelzellen, glatte Muskelzellen	Steigerung der Anionensekretion, Peristaltik (Kontraktion)
Noradrenalin	Endigungen der sympathischen Bahnen	Katecholamin	α und β Rezeptoren, Glatte Muskelzellen	Regulation der Darmmotilität und Durchblutung
Bradykinin	Immunzellen	Peptid, Immunmediator	B-Rezeptoren Epithelzellen, enterische Neurone	Steigerung der Anionensekretion, Regulation der Darmmotilität

Die meisten extrazellulären Botenstoffe wirken über membranständige Rezeptoren, die entweder als ionotrope oder als metabotrope Rezeptoren fungieren. Ionotrope Rezeptoren sind ligandengesteuerte Ionenkanäle, die nach Bindung des Liganden als Kanäle fungieren und Ionen durchströmen lassen. Metabotrope Rezeptoren sind G-Protein-gekoppelte Rezeptoren, die nach Bindung eines Agonisten die Aktivierung des G-Proteins veranlassen. Es folgt die Aktivierung eines Effektors, welcher zur intrazellulären Synthese eines weiteren Botenstoffs, eines sogenannten „Second Messenger“, führt (Pollard und Earnshaw 2008; Übersicht bei Aktories et al. 2009).

Second Messenger sind beispielsweise: zyklisches Adenosin-3´,5´-monophosphat (cAMP), zyklisches Guanosin-3´,5´-monophosphat (cGMP), Diacylglycerol (DAG), Inositol-1,4,5-trisphosphat (IP_3) und Ca^{2+}. G-Proteine sind Heterotrimere, die aus drei Untereinheiten bestehen: der α-Untereinheit, der β- und der γ-Untereinheit. Die α-Untereinheit bindet GTP und hydrolysiert es zu GDP. Im inaktiven Zustand hat das Trimer GDP gebunden. Die Bindung eines Agonisten führt zur Beschleunigung des Austauschs von GDP durch GTP an der α-Untereinheit. Es folgt die Dissoziation des Komplexes in die Gα-GTP-und die Gβγ-Untereinheit. Jede der beiden neu gebildeten Komponenten ist in der Lage, unabhängig voneinander getrennte Effektoren für ganz verschiedene Reaktionen zu aktivieren. Die GTPase der α-Untereinheit hydrolysiert GTP zu GDP und die Gβγ-Untereinheit reassoziiert mit dem Gα-GDP Komplex, was zur Inaktivierung der Transduktionskaskade führt. Der ganze Mechanismus dauert nur wenige Sekunden. Es gibt eine Vielzahl von G-Proteinen und deren Klassifizierung hängt von den α-Untereinheiten ab. Auf Nervenzellen, Myozyten, interstitiellen Zellen von Cajal, Immunzellen und Epithelzellen der Darmwand findet man häufig die $G\alpha_S$, Gαq, $G\alpha_{12}$, $G\alpha_{13}$. Die Aktivierung des $G\alpha_S$ stimuliert das Enzym Adenylatcyclase, welches die Umwandlung von ATP in cAMP katalysiert. Die Folge ist eine Erhöhung der zytosolischen cAMP Konzentration. Dieser Second Messenger aktiviert wiederum einen Effektor, welcher eine Kinase oder einen Kanal sein kann (Pollard und Earnshaw 2008). Bei dem Gαq aktiviert die α-Untereinheit die Isoenzyme β_1 und β_4 der Phospholipase C (PLC) (Pollard und Earnshaw 2008; Übersicht bei Aktories et al. 2009). Das Enzym katalysiert die Hydrolyse von Phosphatidylinositol-4,5-biphosphat (PIP_2) zu DAG und IP_3. Diese Produkte aktivieren unterschiedliche Effektoren, welche Kinasen für DAG oder Rezeptoren wie den IP_3R in der Membran des endoplasmatischen Retikulums für IP_3 sind.

Auch bei der Kontrolle der Darmmotilität, die im Zentrum der im **Kapitel 8.8** dargestellten Versuche liegt, spielen G-Proteine eine wichtige Rolle. Die $G\alpha_{12}$, $G\alpha_{13}$

werden in der Zellmembran von Myozyten der Darmmuskulatur (Übersicht bei Sanders 2008) exprimiert und führen zur Aktivierung des GTP-bindenden und hydrolysierenden Proteins Rho. Nach Austausch von GDP durch GTP stimuliert der Komplex Rho-GTP eine Rho-Kinase. Dieses Enzym bewirkt, dass die Myosin-Leichte-Ketten-Phosphatase (MLKP) phosphoryliert und dadurch inaktiviert wird. Parallel wird die Phosphorylierung der leichten Kette des Myosins verstärkt, was zu einer Kontraktion der glatten Muskulatur führt.

Im Allgemeinen wird über G-Protein-gekoppelte Rezeptoren nicht nur eine Weiterleitung und Übersetzung des extrazellulären Signals durch die Zellmembran gesichert, sondern auch dessen Verstärkung - entweder über die Art der Interaktion Ligand-Rezeptor oder über nachgeschaltete Effektoren - erreicht. Eine weitere Möglichkeit der Signalverstärkung im Sinne einer Potenzierung besteht in der Stimulation von G-Protein-gekoppelten Rezeptoren durch eine besondere Applikationsform, nämlich durch Nanopartikel, die dicht mit Agonisten von G-Protein-gekoppelten Rezeptoren bepackt sind. Diese multivalente Stimulation steht im Mittelpunkt der **Publikationen 8.9** und **8.10**.

Unter den intrazellulären Second Messengern spielt Ca^{2+} eine zentrale Rolle in Zellen der Darmwand. Aus diesem Grund ist die Regulation von Ca^{2+}-Strömen bzw. seiner Konzentration von großer Bedeutung. Die Regulation der Ca^{2+}-Konzentration sowohl im Extrazellularraum als auch im Intrazellularraum erfolgt durch Transportmechanismen und Pufferung. Eine Aktivierung der IP_3R veranlasst die Freisetzung von Calcium-Ionen aus intrazellulären Speichern, was zum Anstieg der zytosolischen Ca^{2+}-Konzentration führt. In vielen Zellen folgt diesem initialen Anstieg ein sogenannter kapazitativer Ca^{2+}-Einstrom durch „store-operated cation channels“ (SOCC) (Hoth und Penner 1992; Parekh und Penner 1997; Parekh 2006). Am Colonepithel der Ratte wurde solch ein La^{3+}-sensitiver Ca^{2+}-Einstrom nach Entleerung der intrazellulären Speicher gezeigt (Frings et al. 1999;

Onodera et al 2013). Dies wurde auch an myenterischen Neuronen mit Hilfe von Gd^{3+} als Inhibitor der zugrunde liegenden Kanäle nachgewiesen (Pouokam et al. 2009).

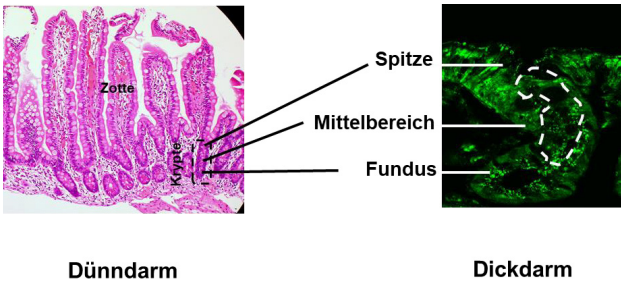

Abb.7: Die Abgabe von Anionen in das Darmlumen geschieht am apikalen Enterozytenpol. Links sind Zotten und Krypten im Dünndarm zu sehen (Uthman 2011). Eingekreist im Dickdarm ist der apikale Pol von Enterozyten, der dem Kryptenlumen zugewandt ist.

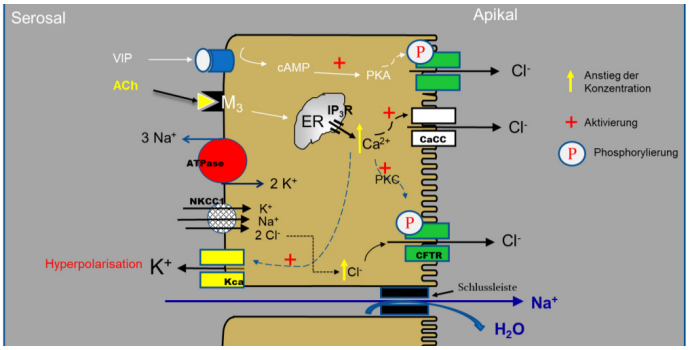

Abb.8: Mechanismen der Chloridsekretion. Na^+-Ionen folgen den Cl^--Ionen ins Lumen aus Gründen der Elektroneutralität. Die Wassersekretion folgt dem Na^+-Strom aus osmotischen Gründen.

Der Hauptmechanismus, über den ein Anstieg der zytosolischen Ca^{2+}-Konzentration eine Cl^--Sekretion auslöst, ist ein Aktivierung Ca^{2+}-abhängiger K^+-Kanäle. Die Folge ist ein Ausstrom von K^+-Ionen durch die basolaterale Membran. Dies erleichtert zum einen die

Aufnahme von Cl^- über den basolateralen NKCC1. Zum anderen ist der Ausstrom von Cl^- durch apikale Anionenkanäle verstärkt, da der basolaterale K^+-Ausstrom eine Hyperpolarisation der Membran bewirkt (**Abb.8**). Natriumionen und Wasser folgen passiv um die Elektroneutralität zu wahren bzw. zum osmotischen Ausgleich (**Abb.8**). Die Chloridionensekretion kann neuronal verstärkt werden. Acetylcholin (ACh) bindet an muskarinerge Rezeptoren vom Typ M_1 oder M_3 in der basolateralen Membran von Enterozyten (Haberberger et al. 2006) und löst dabei eine intrazelluläre Kaskade aus. Diese Rezeptoren sind Gq-Protein gekoppelte Rezeptoren, die nach Aktivierung zur Bildung des Second Messengers IP_3 führen. Der Second Messenger bindet an IP_3 Rezeptoren (IP_3R) auf dem endoplasmatischen Retikulum (ER), welche als Ca^{2+}-Kanäle fungieren. Die Kanäle werden geöffnet, vermitteln den Ausstrom von Calcium-Ionen und den Anstieg der zytosolischen Ca^{2+}-Konzentration. Mehrere Zielmoleküle werden von Calcium-Ionen aktiviert: Die Ca^{2+}-aktivierten K^+-Kanäle in der basolateralen Membran, die Ca^{2+}-aktivierten Cl^-- Kanäle (CaCC) in der apikalen Membran (Schultheis et al. 2005) oder Proteinkinasen wie etwa die PKC.

Auch der Second Messenger cAMP kann eine Sekretion auslösen, z.B. wenn das Neuropeptid VIP auf das Darmepithel einwirkt. Die von VIP ansprechbaren Rezeptoren sind Gs-gekoppelte Rezeptoren, die zur Bildung von zyklischem AMP (cAMP) führen. Solch ein Nukleotid aktiviert die Proteinkinase A, die wie die PKC in der Lage ist die Übertragung einer Phosphatgruppe auf CFTR Kanäle zu katalysieren (**Abb.8**).

4.3 Kontrolle gastrointestinaler Funktionen durch das enterische Nervensystem

Die Darmmotorik sorgt für einen gerichteten Weitertransport der Digesta innerhalb des Darmrohrs. Sie beruht auf der Aktivität der glatten Muskulatur, also der Ring- und der Längsmukulatur des Darmes. Dieser Weitertransport kann vom Zentralnervensystem über den Parasympathikus und den Sympathikus beeinflusst werden, ist aber intrinsisch von

dem enterischen Nervensystem (ENS) gesteuert. Ein Grundmuster der Darmmotorik ist die propulsive Peristaltik. Dabei ist der Auslöser des Schaltkreises, also des Reflexes, die Dehnung der Darmwand. Mechanosensorische myenterische Neurone registrieren die Dehnung, die über Interneurone Motoneuronen mitgeteilt wird. Aszendierende erregende Motoneurone projizieren oralwärts, d.h. sie innervieren die Ringmuskulatur oral der Dehnungsstelle. Deszendierende hemmende Motoneurone dagegen projizieren analwärts und innervieren die Ringmuskulatur aboral der Dehnungsstelle. Aus aszendierenden Projektionen erregender Motoneurone werden exzitatorische Transmitter freigesetzt: Acetylcholin (ACh) und das Neuropeptid Substanz P (SP), die eine Kontraktion oral des Bolus auslösen (Übersicht bei Neunlist et al. 1999; Schemann 2005).

Der hemmende Gasotransmitter Stickstoffmonoxid (NO) und die hemmenden Cotransmitter ATP oder ähnliche Purine (Christofi und Wood 1993; Wood 2004) und Vasoaktives intestinales Peptid (VIP) rufen aboral des Bolus eine Erschlaffung der Ringmuskulatur hervor. Diese kombinierten Anpassungen der Muskulatur veranlassen die Propulsion des Darminhalts in Richtung Rektum. Dieser Reflex wird in der **Abb.9** illustriert. Die Muskelzellen kontrahieren rhythmisch als Folge der Slow Waves, welche von interstitiellen Zellen nach Cajal (ICC) ausgelöst werden. In dieser Arbeit wird die Wirkung der reduzierten Form von NO, des Gasotransmitters Nitroxyl (HNO), auf die Motorik des Darms untersucht. Die bislang noch nicht publizierten Daten sind im **Kapitel 8.8** dargestellt.

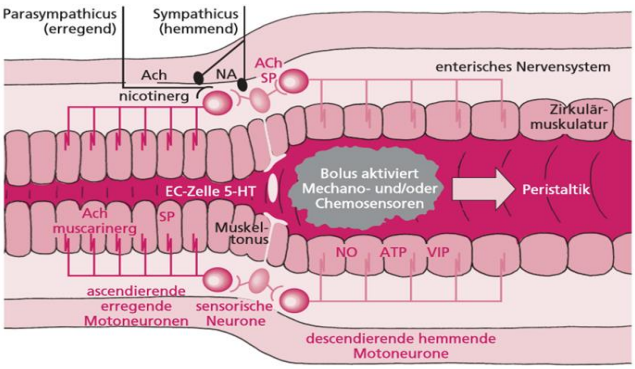

Abb.9: Ablauf und Modulation des peristaltischen Reflexes im Darm. Aus Pfannkuche und Schemann (2015), Verwendung erlaubt von Enke-Verlag. Der vom Bolus initiierte Druck an die Darmwand schaltet einen Reflexkreis: Aboral des Bolus werden inhibitorische Transmitter wie NO, ATP und VIP freigesetzt um das Darmlumen durch Erschlaffung der glatten Muskulatur weit zu stellen. Oral des Bolus werden erregende Transmitter wie ACh und SP freigesetzt, um das Darmlumen durch Kontraktion der glatten Muskulatur eng zu stellen. Beide Mechanismen führen zum Weitertransport des Bolus analwärts.

Die bislang noch nicht publizierten Daten sind im **Kapitel 8.8** dargestellt. Ähnlich wie Muskelmotoneurone existieren Neurone, die Epithelzellen innervieren, die sogenannten Sekretomotoneurone. Der Schaltkreis zur Steuerung des Epithels ähnelt dem der neuronalen Steuerung der Motorik durch den Plexus myentericus. Auch hier sind sensorische Neurone und Interneurone eingeschaltet, welche zum Teil eine Kommunikation zwischen den beiden Plexus ermöglichen. Aus den Sekretomotoneuronen des Plexus submucosus werden sowohl hemmende als auch erregende Transmitter ausgeschüttet. Erregende Transmitter lösen eine Sekretion von Anionen aus und werden daher als prosekretorisch bezeichnet. Hemmende Transmitter dagegen inhibieren die Sekretion. Eine Sekretion von Anionen, vorwiegend Chloridionen neben Bicarbonationen, ist von einer Wassersekretion begleitet. Zu den prosekretorischen Neurotransmittern

zählen ACh und VIP; hemmende Neurotransmitter dagegen sind z.B. Neuropeptid Y (NPY) und Somatostatin (Furness 2006).

Weitere Player bei der Regulation gastrointestinaler Funktionen stellen Immunzellen dar. Die Kommunikation zwischen den beiden Plexus oder zwischen den Plexus und dem Immunsystem in der Darmwand führt zu einer reflexartigen regulierten Antwort des Epithels. Einige Immunmediatoren wie z.B. Bradykinin wirken sowohl auf die Darmmotorik als auch auf das enterische Nervensystem oder den Ionentransport durch das Colonepithel (Avemary und Diener 2010, Würner et al. 2014).

4.4 Gasotransmitter und deren Wirkung im Colon

Eine neuartige Klasse von Regulatoren gastrointestinaler Funktionen sind gasförmige Moleküle, die sogenannten Gasotransmitter. Einer davon ist Kohlenstoffmonoxid (CO). Neurone, glatte Muskelzellen und Epithelzellen der Darmwand der Ratte exprimieren Hämoxygenase I und oder II zur Synthese von CO (Donat et al. 1999; Miller et al. 2001; Steidle und Diener 2011).

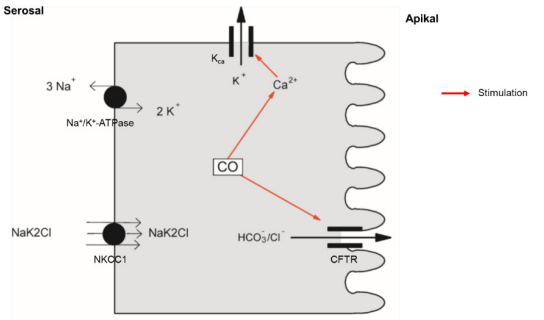

Abb.10: Kohlenstoffmonoxid-induzierte Cl^--Sekretion im Colon der Ratte. CO stimuliert über einen Anstieg der cytosolischen Ca^{2+}-Konzentration die Ca^{2+}-abhängigen K^+-Kanäle in der basolateralen Membran der Enterozyten des Colons, was zur Hyperpolarisation führt. Diese Anionen werden über apikale von CO direkt oder indirekt aktivierte Cl^--Kanäle (CFTR) sezerniert. Modifiziert nach Pouokam et al. 2011 (Publikation 8.5).

Die **Publikation 8.5** gibt eine Übersicht der Wirkung von CO auf den Ionentransport am Colonepithel der Ratte. Kohlenstoffmonoxid fördert den Einstrom von extrazellulären Calcium-Ionen in die Enterozyten und aktiviert direkt oder indirekt apikale Cl^-- Kanäle wie den CFTR. Dies führt zur Sekretion von Anionen (Cl^-/HCO^-_3), die basolateral im Falle von Cl^- durch den NKCC1-Transporter aus dem Blut aufgenommen werden. Die eingeströmten Ca^{2+}-Ionen aktivieren die Ca^{2+}-abhängigen K^+-Kanäle der basolateralen Membran, was zu einer Hyperpolarisation führt und damit die Antriebskraft für den Anionenausstrom aus der Zelle steigert (Pouokam et al. 2011).

Es gibt neben CO zwei weitere, gut etablierte Gase mit Transmitterfunktion im Darm: Stickstoffmonoxid (NO) und Schwefelwasserstoff (H_2S). Ein dritter Gasotransmitter, Nitroxyl (HNO), bekommt erst seit Kurzem viel Aufmerksamkeit. Solche Gase können von Zellen der Darmwand freigesetzt werden und autokrin oder parakrin wirken, da sie leicht innerhalb von Geweben diffundieren können. Eine vereinfachte Übersicht der Wirkungen von Gasotransmittern und der zugrunde liegenden Mechanismen an verschiedenen Geweben ist in den **Tabellen 2** bis **8** zusammengefasst. Der Fokus in den vorgelegten Publikationen wurde auf den Gastrointestinaltrakt gelegt.

Tabelle 2: Allgemeine Eigenschaften der Gasotransmitter NO, H_2S und HNO

Allgemeine Eigenschaften	Gasotransmitter		
	NO	H_2S	HNO
Thiolreaktivität	Keine direkte Reaktivität (Irvine et al. 2008)	Keine direkte Reaktivität (Zhang et al. 2015)	Hohe Reaktivität (Irvine et al. 2008)
Scavenger	Carboxy-PTIO, Hydroxocobalamin (Irvine et al. 2008)	Methämoglobin, Peroxidise, Katalase, oxidierte Form Glutathion (Wang 2012)	L-Cystein, Dithiothreitol (DTT) (Irvine et al. 2008)
Biomarker der Aktivität	Plasma cGMP (Irvine et al. 2008)	-	Plasma CGRP (Irvine et al. 2008)

Tabelle 3: NO, H_2S, HNO und das Immunsystem

Immunsystem	Gasotransmitter		
	NO	H_2S	HNO
Endzündung	Pro- und anti-inflammatorisch (Aley et al. 1998)	Pro- und anti-inflammatorisch (Wallace 2010; Ekundi-Valentim 2010)	Nicht untersucht
Nozizeption	Pro- und anti-nozizeptiv (Aley et al. 1998)	Pro- und anti-nozizeptiv (Schemann and Grundy 2009; Wallace 2010)	Pro- und anti-nozizeptiv (Eberhardt et al. 2014)

Tabelle 4: Pharmakologische Wirkung von NO, H_2S, HNO auf das Myokard

Wirkungen am Myokard	Gasotransmitter		
	NO	H_2S	HNO
Inotropie	Negativ (Irvine et al. 2008)	Negativ (Lefer 2008; Wang 2012)	Positiv (Irvine et al. 2008)
Myokard Ryanodin-Rezeptoren (Type 2)	Geringfügige Aktivierung (Irvine et al. 2008)	Unbekannt	Starke Aktivierung (Irvine et al. 2008)

Tabelle 5: Vaskuläre Wirkung von NO, H_2S und HNO

Wirkungen am Gefäßsystem	Gasotransmitter		
	NO	H_2S	HNO
Regulation Kanäle	Aktivierung K_{ca} Kanäle (Irvine et al. 2008)	Aktivierung $K_{ATP,}$ SK_{ca} Kanäle (Zhao et. al. 2001; Wallace 2010)	Aktivierung K_v, K_{ATP} Kanäle~~,~~ (Irvine et al. 2008)
Wirkung	Vasodilatator (Irvine et al. 2008)	Vasodilatator (Zhao et. al. 2001; Wallace 2010)	Vasodilatator (Irvine et al. 2008)
Vermittlung	Über sGC/cGMP (Irvine et al. 2008)	sGC/cGMP-unabhängig (Zhao et. al. 2001)	Über sGC/cGMP, Freisetzung von CGRP (Irvine et al. 2008)

Tabelle 6: Wirkung von NO, H_2S und HNO im oxidativen Stress

Oxidativer Stress	Gasotransmitter		
	NO	H_2S	HNO
Zytoprotektive / antioxidative Wirkung	Protektiv gegen Ischämie-Reperfusionsschäden Stimulation der Hämoxygenase 1 (HO-1); inkonsistente Verminderung der Lipidperoxidation (Irvine et al. 2008)	Protektiv gegen Ischämie-Reperfusions-schäden (Szabo 2007; Ji et al. 2008)	Protektiv (bei Vorbehandlung) gegen Ischämie-Reperfusion, Stimulation der Hämoxygenase 1 (HO-1); Konsistente Verminderung der Lipidperoxidation (Irvine et al. 2008)

Tabelle 7: Wirkung von NO, H_2S und HNO in der gastrointestinalen Motorik

Aktivität der Darmmuskulatur	Gasotransmitter		
	NO	H_2S	HNO
Kontraktion/ Relaxation	Relaxation (Shuttleworth und Sanders 1996)	Relaxation (Teague et al. 2002)	Relaxation (Siehe unveröffentliche Daten in „Resultate und Diskussion und **Kapitel 8.8**“)

Tabelle 8: Wirkung von NO, H_2S und HNO auf den intestinalen Ionentransport

Intestinaler epithelialer Ionentransport	Gasotransmitter		
	NO	H_2S	HNO
Anionensekretion	Cl^--Sekretion (Tamai und Gaginella 1993)	Cl^--Sekretion (Hennig und Diener 2009; Pouokam und Diener 2012).	Cl^--Sekretion (Pouokam et al. 2013)
Vermitlung: sGC/cGMP-Abhängigkeit	Donor- und konzentrationsabhängig (Sakai et al. 2002), unabhängig (Schulheiß et al. 2002)	Unabhängig (Pouokam et al. 2011)	Unabhängig (Pouokam et al. 2013)
Neuronale Beteiligung	Ja (Tamai and Gaginella 1993) Nein (Schultheiß et al. 2002)	Geringfügig (Lee et al. 2006; Hennig und Diener 2009; Krueger et al. 2010)	Nein (Pouokam et al. 2013)
Beteiligung von Prostaglandinen	Ja (Sakai et al. 2002), Nein (Schultheiß et al. 2002)	Ja (Wallace et al. 2010)	Ja (Pouokam et al. 2013)

Ein weiterer Gasotransmitter mit Wirkung im Gastrointestinaltrakt ist Hydrogensulfid (H_2S). Im Colon der Ratte wurde gezeigt, dass H_2S eine biphasische Cl^--Sekretion evoziert (Hennig und Diener 2009). Die Arbeit **Publikation 8.1** wurde durchgeführt, um die zugrundeliegenden Mechanismen aufzuklären.

H_2S wird endogen aus der Aminosäure L-Cystein synthetisiert. Diese Synthese wird von den Enzymen Cystathionin-β-Synthase und Cystathionin-γ-lyase (Wang 2002; Martin et al. 2010) katalysiert. Beide Enzyme wurden in enterischen Ganglien des Meerschweinchens und des humanen Colons (Schicho et al. 2006) sowie in der glatten

Darmmuskulatur und im Epithel des Colons der Ratte (Hennig und Diener 2009) nachgewiesen.

Stimulierung der endogenen Synthese von H_2S mit L-Cystein oder dessen Hemmung könnten paradoxerweise zu ähnlichen Wirkungen führen (Chávez-Piña et al. 2010). Als Erklärung für dieses Paradoxon werden Unterschiede sowohl in der Geschwindigkeit der Anflutung dieses Gasotransmitters als auch Unterschiede in den verwendeten Konzentrationen angenommen. So wurde die sekretorische Wirkung des H_2S-bildenden Substrats L-Cystein am Colonepithel der Ratte untersucht und mit der eines langsamen oder sehr langsamen H_2S Donors verglichen (**Publikation 8.2**). Einer der Zieleffektoren von H_2S ist der ATP-sensitive K^+-Kanal (K_{ATP}) (Zhao et. al. 2001; Übersicht bei Wallace 2010). Solche Kanäle spielen eine wichtige Rolle in den Mechanismen der H_2S-induzierten Cl^--Sekretion (Hennig und Diener 2009). Nach Permeabilisierung der apikalen Membran wurde gezeigt, dass der K_{ATP}-Hemmer Glibenclamid basolaterale K^+-Ströme am Colonepithel der Ratte hemmt (Hennig und Diener 2009). Pinacidil, ein K_{ATP}-Aktivator (Aschcroft und Gribble 2000), führte je nach Seite der Applikation (apikal oder basolateral) zu entgegengesetzten Wirkungen auf den transepithelialen Kurzschlussstrom, was Hinweise auf die Anwesenheit solcher Kanäle in der apikalen Membran lieferte (Pouokam et al. 2013). Lediglich im Dünndarm der Ratte und des Menschen wurden diese Kanäle mit dem strukturellen Kir6.1/SUR2A Komplex an den Tight-Junctions nachgewiesen (Jöns et al. 2006). Spekuliert wurde, ob solche Kanäle auch in der apikalen Membran des Colonepithels der Ratte anzutreffen wären. So wurde die Arbeit der **Publikation 8.3** durchgeführt, um diese Kanäle am Colonepithel der Ratte nachzuweisen und pharmakologisch zu charakterisieren.

Ein weiterer Gasotransmitter, Nitroxyl (HNO), bekommt erst seit Kurzem viel Aufmerksamkeit. Am Magen-Darm-Trakt ist bislang lediglich eine prosekretorische

Wirkung bekannt, die Ca^{2+}-abhängig ist und über verschiedene K^+-Kanäle (K_{ATP}, K_{Ca}), sowie teilweise durch Cyclooxygenase-Metaboliten vermittelt wird (Pouokam et al. 2013). In bisherigen Arbeiten zu diesem Gasotransmitter wurde der Fokus lediglich auf Kreislauf- (**Tabellen 2-8**) und Alkoholismus-Therapie gelegt. HNO (freigesetzt aus dem Donor-Molekül Angeli's Salz) ist aber auch in der Lage, Ionentransportvorgänge durch das Darmepithel zu verändern. Dieser Effekt und die zugrunde liegenden Mechanismen sind in **Publikation 8.7** dargestellt.

Die von mir durchgeführten Experimente zeigen außerdem, dass ein HNO-Donor (Angeli's Salz) eine intestinale Relaxation auslöst. Die Mechanismen, die dieser Relaxation zugrunde liegen, werden aktuell untersucht (**Kapitel 8.8**).

Jüngste Studien in der Literatur belegen zudem einen Crosstalk zwischen NO, H_2S und HNO-Signalwegen (Yong et al. 2011; Filipovic et al. 2013; Miljkovic et al. 2013; Eberhardt et al. 2014). Beispielsweise kann exogenes H_2S mit endogenem NO in Wechselwirkung treten und zur Bildung von HNO führen, was eventuell dazu führt, dass einige Effekte von H_2S durch HNO vermittelt werden können. In den **Tabellen 2-8** sind daher Ähnlichkeiten zwischen diesen drei Gasen aufgelistet. Laufende Versuche sollen dieses Zusammenspiel der obengenannten Gasotransmitter weiter belegen.

4.5 Hypoxie/Reoxygenation am Darm

Die obengenannten Gasotransmitter vermögen es, bei oxidativem Stress protektiv zu wirken (**Tabelle 6**). Diese Eigenschaften wurden hauptsächlich in Versuchen mit Fokus auf den Blutkreislauf festgestellt. Aber auch im Magen-Darm-Trakt stellen Hypoxie/Reoxygenation-Schäden ein wichtiges Krankheitsbild dar. Die intestinale Hypoxie als Folge einer Embolie oder einer mechanischen Kompression geht mit einer hohen Letalität einher (Haglund und Bergqvist 1999). Solch eine Verminderung der Durchblutung verschlechtert die Energieversorgung des Darmepithels, eines Gewebes mit

hohem Energieaufwand. Die Folge ist eine Beeinträchtigung und der Verlust der Barrierefunktion des Epithels. Dies geht mit einer ATP-Verarmung einher. Die Konsequenz ist die Beeinträchtigung der Tätigkeit aktiver Transportmechanismen bzw. Transporter wie der Na^+/K^+-ATPase, welche als Motor für den Ionentransport am Darmepithel gilt (Kaplan 1985). Die ATP-Verarmung führt zur Senkung des ATP/ADP-Verhältnisses, was eine relevante Folge auf die ATP- bzw. ADP-sensitiven Effektoren hat. So wird in erregbaren Organen bzw. Geweben wie im Herz, Gehirn oder in der glatten Muskulatur der Blutgefäße eine protektive Wirkung über eine Aktivierung der K_{ATP}-Kanäle gegen Schäden in Gang gesetzt (Hund und Mohler 2011). Das Öffnen dieser Kanäle hyperpolarisiert die Zellmembran und reduziert damit den Energieaufwand durch Senkung der Erregbarkeit (Übersicht bei Hibino et al. 2010). Auf der anderen Seite kann eine Reoxygenation durch Reperfusion nach Ischämie die Sauerstoffzufuhr wieder garantieren, aber auch eine Anflutung reaktiver Sauerstoffspezies auslösen. Dabei werden Radikale aus dem Superoxid Anion Radikal ($O^{\cdot-}_2$) in Mitochondrien gebildet (Dröge 2002; Gonzalez et al. 2015).

Auf der Beobachtung aufbauend, dass H_2S im Darmepithel K_{ATP}-Kanäle aktiviert (Pouokam und Diener 2011) und diese Kanäle eine protektive Funktion gegen Hypoxie-Schäden z.B. in erregbaren Geweben aufweisen, stellte sich aber die Frage, ob dies auch im Darm gilt. Die Arbeit **Publikation 8.4** wurde vorgenommen um den Einfluss der Hypoxie/Reoxygenation auf die Ionentransportmechanismen, auf die Barrierefunktion des Colonepithels der Ratte und auf die Rolle der K_{ATP}-Kanäle zu untersuchen.

4.6 Nanostrukturen als neuartige Player bei der Beeinflussung bzw. Messung physiologischer Parameter am Gastrointestinaltrakt

Wie einzelne Liganden an G-Protein gekoppelten Rezeptoren wirken ist gut erforscht. Es besteht aber die Möglichkeit bei anderen Systemen wie etwa der Selectin-Bindung von synthetischen Liganden (Dernedde et al. 2009), bei der Aktivierung von Serotonin-gesteuerten Ionenkanälen (Paolino et al. 2014) oder bei der Verstärkung der enzymatischen Aktivität der Carboanhydrase (Saada et al. 2011) durch Multivalenz, also die synchrone Stimulation benachbarter Rezeptoren mittels Nanopartikeln, die dicht mit Agonisten bepackt sind, eine extreme Steigerung der Affinität zu erreichen. Ob dies auch an G-Protein-gekoppelten Rezeptoren, die in der Kontrolle des Ionentransports durch das Darmepithel involviert sind, möglich ist, wurde in den **Publikationen 8.9** und **8.10** untersucht.

Im Colon herrscht eine starke Besiedlung durch Mikrobiota, die für den Wirtsorganismus (den Säuger) nicht verdaubare Strukturkohlenhydrate zu kurzkettigen Fettsäuren fermentieren. Durch die Resorption von solchen Fettsäuren, die als Energiesubstrat für die Colonozyten und auch den gesamten Organismus insbesondere bei herbivoren Tieren beitragen, entsteht eine Belastung für die pH-Regulation der Darmepithelzellen. Zu diesem Zweck ist das Darmepithel mit apikalen Na^+/H^+-Austauschern in der apikalen (NHE2 und NHE3) und in der basolateralen Membran (NHE1) ausgestattet (Übersicht bei Kunzelmann und Mall 2002). Die apikalen sind wahrscheinlich auch an der Resorption von kurzkettigen Fettsäuren beteiligt, indem sie Protonen für die Überführung der dissoziierten Fettsäureanionen in die ungeladene Form (freie Fettsäuren) ermöglichen, welche durch nichtionische Diffusion in die Epithelzelle aufgenommen werden können (Übersicht bei Sandle 1998; Kunzelmann und Mall 2002). Der Einfluss von aktiven Protonen-Transportmechanismen auf dieses Mikroklima kann erfasst werden. So wurde in

der **Publikation 8.12** Arrays aus pH-sensitiven InGaN/GaN Nanodrähten mit einer Raumauflösung < 0,63 µm zur dynamischen Messung der pH-Änderung in der Umgebung von Colonepithelzellen der Ratte verwendet. Die Intensität der Photolumineszenz der Nanodrähte variiert mit dem lokalen pH-Wert. Der Na^+/H^+-Austauscher (NHE) wurde in diesem Fall als Modell der pH-Regulation der Zelle in die Analyse einbezogen.

5. Methoden

Die Einzelheiten zu den Methoden können in den Publikationen im Kapitel 8 entnommen werden.

5.1 Tiere

Es wurden Wistar Ratten für die vorliegenden Untersuchungen verwendet. Organe, Gewebe, bzw. Zellen wurden nach fachgerechter und erlaubter Tötung gewonnen.

5.2 Ussing-Kammern

Elektrische Ströme, die durch Bewegung von Elektrolyten durch das Darmepithel erzeugt werden, können in sogenannten Ussing-Kammern erfasst werden. Dabei wird ein Kurzschlussstrom (I_{sc}) als Maß des Nettoionenstroms durch das Epithel gemessen. Ein Anstieg des I_{sc} bedeutet eine Sekretion von Anionen oder eine Resorption von Kationen, währenddessen ein Abfall eine Sekretion von Kationen bedeutet. Diese Methode wurde in den **Publikationen 8.1, 8.2, 8.3, 8.4, 8.7, 8.9, 8.10** verwendet.

5.3 Primäre Zellkultur und Häutchenpräparate

Zur Analyse der neuronalen Aktivität unter Einwirkung verschiedener Pharmaka wurden myenterische Nervenzellen aus dem Ileum neugeborener Ratten isoliert und kultiviert. Diese Neurone wurden direkt auf Messfläche von Biosensoren kultiviert (**Publikation 8.11**). Längsmuskelschichten oder Plexus submucosus-enthaltende Häutchenpräparate wurden vom Colon adulter Ratten für Ca^{2+}-Konzentration-Messungen zur Aufklärung der Rolle dieses Ions in verschiedensten Mechanismen isoliert (**Publikationen 8.7, 8.11**).

5.4 Isolation von Krypten und Myozyten

Krypten wurden aus dem Colon von adulten Ratten isoliert. Sie dienten als Modelle zur Untersuchung von Mechanismen der Ionentransporte auf zellulärer Ebene, da die Krypten von dem Rest der Darmwand getrennt zur Verfügung stehen. So wurden an isolierten Epithelzellen in solchen Krypten intrazelluläre Ca^{2+}-Konzentrationen bzw. Ströme (**Publikationen 8.1, 8.4, 8.7**) sowie intrazelluläre (**Publikation 8.2**) und extrazelluläre (**Publikation 8.12**) pH-Änderungs- Messungen durchgeführt. Glatte Muskelzellen wurden aus dem proximalen Colon von adulten Ratten isoliert und zur Untersuchung der Wirkung von Nitroxyl auf intrazelluläre Ca^{2+}- Konzentration verwendet (**Kapitel 8.8**).

5.5 Zelllinien

Für die Analyse der Potenzierung mit Nanopartikeln der Wirkung des ACh-Derivats CCh auf muskarinerge Rezeptoren wurden HEK293T Zellen (Human Embryonic Kidney) mit M_3 Rezeptoren, GαqYFP, Gβ1-wt, CFP-Gγ2 transfiziert und mithilfe des FRET (Förster Resonance Energy Transfer)-Verfahrens gemessen (**Publikation 8.10**). Diese Versuche wurden im Labor von Prof. Bünemann, Universität Marburg, durchgeführt.

5.6 Hypoxie/Reoxygenation

Künstliche Hypoxie in Ussing Kammern und Imaging-Messungen wurden durch N_2 Zufuhr erreicht. Die Reoxygenation erfolgte durch Zufuhr der Raumluft, welche einer Normoxie entspricht (**Publikation 8.4**).

5.7 Imaging Messungen

Ca^{2+}-Konzentrationen (**Publikationen 8.1, 8.4, 8.7, Kapitel 8.8**), Mitochondrien-Membranpotential (**Publikation 8.1**), intrazelluläres pH (**Publikation 8.2**), Superoxid Anionen (**Publikation 8.4**) und Thiolgruppen (**Publikation 8.4**) wurden mithilfe der

Farbstoffe Fura-2 bzw. Mag-Fura-2, Rhodamin123, BCECF, Mitosox und Thiol Tracker gemessen.

5.8 Analyse des biologischen Materials

Folgende Methoden wurden verwendet: Immunhistochemie/Immuncytochemie,

RT (reverse Transkription)-PCR

5.9 Nanostrukturen

Histamin- oder Carbachol-funktionalisierte Gold-Kern-Nanopartikeln wurden von der Arbeitsgruppe von Prof. Wickleder, Universität Köln, synthetisiert um per Multivalenz an entsprechenden Rezeptoren die Potenzierung der Wirkung des nativen Liganden zu erfassen (**Publikationen 8.9** und **8.10**). AChE-modifizierte InGaN/GaN Biosensoren wurden zur Messung neuronaler Aktivität in der **Publikation 8.11** gebraucht. pH-sensitive InGaN/GaN Nanodrähte mit einer Raumauflösung < 0,63 µm wurden auf leitenden Substraten von der Arbeitsgruppe von Prof. Eickhoff, jetzt Universität Bremen, erstellt. Ihre Fluoreszenz hängt von dem lokalen pH-Wert ab. Damit ist eine dynamische Imaging-Messung von pH-Änderungen im Mikroklima von Zellen machbar (**Publikation 8.12**).

5.10 Organbäder

Organbäder mit einer Volumenkapazität von jeweils 10 ml wurden für isometrische Muskelkontraktionsmessungen an isolierte Darmsegmenten verwendet (**Kapitel 8.8**).

5.11 Elektrophysiologie/Mikroelektroden

Mikroelektroden wurden verwendet, um die Wirkung des Gasotranmitters HNO auf das Membranpotential von glatten Muskelzellen zu erfassen (**Kapitel 8.8**).

6 Zusammenfassende Ergebnisse und Diskussion

6.1 Gasotransmitter und deren Wirkung im Darm

Im Gastrointestinaltrakt sind bislang die Wirkungen von vier Gasotransmittern untersucht worden. Diese Gasotransmitter sind Kohlenstoffmonoxid (CO), Stickstoffmonoxid (NO), Schwefelwasserstoff (H_2S) und Nitroxyl (HNO). Die **Publikation 8.5** gibt einen Überblick der Wirkung von CO. Wie Stickstoffmonoxid löst CO eine Vasodilatation (Kanu und Leffler 2007) aus und stimuliert das Enzym sGC (lösliche Guanylatcyclase), allerdings schwächer im Vergleich zu NO (Stone und Marletta 1994; Gibbons und Farrugia 2004). In Muskelzellen von Hirnarteriolen des Schweines wurde eine direkte Aktivierung von BK_{ca} Kanälen, welche zur Hyperpolarisation der Membran führt, nachgewiesen (Kanu und Leffler 2007). Diese Eigenschaft wurde auch für NO in Myozyten aus mesenterischen Arterien der Ratte gezeigt (Mistry und Garland 1998). In der Colon-Krebszelllinie Caco-2 wurde beobachtet, dass die Sekretion von Anionen durch den sGC-Blocker ODQ stark gehemmt wurde. In nativen Geweben dagegen spielte dieses Enzym keine Rolle, da sowohl sein Aktivator, das YC1, als auch der Enzyminhibitor ODQ die Sekretion nicht beeinflussen konnten (Steidle und Diener 2011). Ähnlich wurde eine sGC-unabhängige Anionensekretion mit dem Gasotransmitter HNO gezeigt (Pouokam et al. 2013, **Publikation 8.7**). Kohlenstoffmonoxid wirkt auf der basolateralen und apikalen Membran der Colonepithelzelle: Es fördert den Einstrom von Calcium-Ionen zur Aktivierung von apikalen Cl^--Kanälen und von basolateralen Ca^{2+}-abhängigen K^+-Kanälen. Wie genau der Ca^{2+}-Einstrom zustande kommt ist weitgehend unbekannt. Potentielle Transporterkandidaten, die diesen Strom tragen oder ermöglichen, sind nicht-selektive Kationenkanäle oder Na^+/Ca^{2+}-Austaucher, die im „reverse-mode“, also als Ca^{2+}-

Importtransporter, arbeiten, sofern der Na^+-Gradient entsprechend verändert wird (Seip et al. 2001).

Die **Publikation 8.1** befasst sich mit der Aufklärung der Mechanismen, die der durch den Gasotransmitter H_2S evozierten Cl^--Ionensekretion zugrunde liegen. Die exogene Applikation des Gasotransmitters erfolgte durch den Donor NaHS. Der Gasotransmitter bewirkte eine Cl^--Ionensekretion über die Aktivierung der basolateralen Ca^{2+}-abhängigen K^+-Kanäle, K_{ATP}-Kanäle und der Na^+/K^+-ATPase. Auch wurde die Hyperpolarisation der mitochondrialen Membran durch den Gasotransmitter anhand des Farbstoffs Rhodamin123 registriert. Ca^{2+}-Imaging Experimente zeigten eine biphasische Wirkung auf die Calcium-Ionen-Konzentration: zuerst einen kurzen Abfall, gefolgt von einem relativ lang anhaltenden Anstieg. Der Abfall resultierte aus der Ausschleusung von Ca-Ionen über den Na^+/Ca^{2+}-Austauscher. Dieser Abfall wurde durch 2′,4′-Dichlorobenzamil (DCB), einen Blocker dieses Austauschers, unterdrückt (**Abb.11**), was für eine Beteiligung des Na^+/Ca^{2+}-Austauschers spricht. Dies wurde zusätzlich durch den Einsatz eines Na^+-freien Puffers bestätigt, da das Substrat Na^+ unter diesen Bedingungen dem Transporter für seine Tätigkeit fehlte.

Da eine Aufnahme von Ca-Ionen in Organellen auch zur Senkung der zytosolischen Ca^{2+}-Konzentration führen könnte, wurden Experimente mit Mag-Fura-2 vorgenommen, einem Farbstoff, der sich spezifisch in Ca^{2+}-speichernden Organellen wie dem endoplasmatischen Retikulum einlagert. Der Gasotransmitter hatte aber keinen signifikanten Einfluss auf Fluoreszenz-Signale des Mag-Fura-2. Die Wirkung des H_2S-Donors auf die von K_{ATP}-Kanälen getragene Ionenströme zeigte zwei Komponenten: einen transienten Abfall und einen verzögerten Anstieg des Kurzschlussstroms (Pouokam und Diener 2011, **Publikation 8.1**).

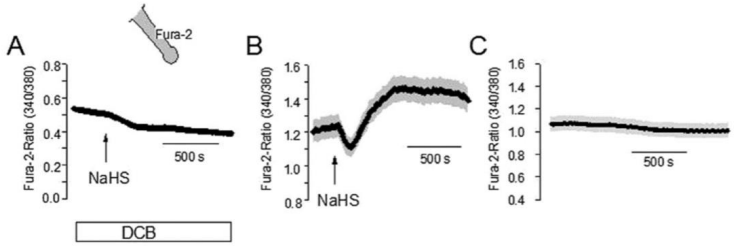

Abb.11: Änderungen der zytosolischen Ca^{2+}-Konzentration von Colonepithezellen durch den H_2S-Donor NaHS. Änderungen werden gemessen als Fura-2-Ratio in Anwesenheit des Na^+/Ca^{2+}-Austauscher-Hemmers DCB (A), in Abwesenheit des Blockers (B) im Vergleich zur zeitabhängigen Kontrolle (C). (Pouokam und Diener 2011, Publikation 8.1).

Physiologischerweise kommt es zu einem Schließen der K_{ATP}-Kanäle, wenn die zytosolische ATP-Konzentration ansteigt. Dies wäre eine mögliche Erklärung für den transienten Abfalls des Kurzschlussstroms. Eine vermehrte Synthese von ATP führt zur Depolarisation der mitochondrialen Membran durch Verminderung des H^+-Gradienten (Garlid und Paucek 2003). Diese Hypothese wurde mit Hilfe des Farbstoffs Rhodamin123 geprüft. Bei einer Depolarisation der Membran steigt dessen Fluoreszenzsignal an, während es bei einer Hyperpolarisation sinkt. Überraschenderweise induzierte H_2S einen Abfall, d.h. eine Hyperpolarisation der inneren Membran der Mitochondrien (**Abb.12**). H_2S ist dafür bekannt, die mitochondriale Atmung hemmen zu können; ein Effekt, der als Grund der protektiven Wirkung dieses Gasotransmitters gegen Ischämie/Reperfusion-Schäden am Myokard gilt (Elrod et al. 2007). Eine mögliche Erklärung für die Hyperpolarisation könnte eine lokale Erhöhung der ATP-Konzentration in der Nähe der basolateralen Membran, z.B. als Folge einer Verlangsamung des ATP-Abbauprozesses durch eine Einschränkung der Na^+/K^+-ATPase, sein. In diesem Fall würde die Akkumulation von ATP-Molekülen die Hemmung der K_{ATP}-Kanäle einleiten.

Die Geschwindigkeit der Freisetzung des Gasotransmitters H_2S und dessen lokale Konzentration könnten die Wirkung entscheidend modulieren. So wurde eine prosekretorische Wirkung dieses Gasotransmitters im Darm gezeigt, was Durchfälle in pathologischen Fällen (wie z.B. bei entzündlichen Darmerkrankungen) verschlimmern würde.

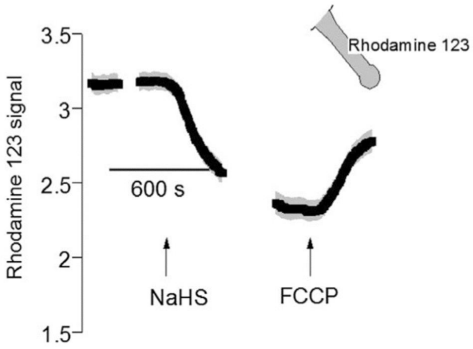

Abb.12: Änderungen des mitochondrialen Membranpotentials von Colonepithelzellen durch den H_2S-Donor NaHS. Potentialänderungen werden als Änderungen des Signals des Farbstoffs Rhodamin123 gemessen. H_2S induziert eine Hyperpolarisation. Als Kontrolle wurde der Entkoppler der Atmungskette, FCCP (Carbonylcyanid-4-(trifluormethoxy) phenylhydrazon), verwendet und wie erwartet, depolarisiert er die mitochondriale innere Membran. (Pouokam und Diener 2011, Publikation 8.1).

Ferner wurde beispielerweise an einem Akuten-Pankreatitis Modell der Maus gezeigt, dass H_2S pro-inflammatorische Eigenschaften besitzt (Tamizhselvi et al. 2007). Auch durch Hemmung der endogenen Synthese von H_2S mit Propargylglycin wurde festgestellt, dass die Ethanol-evozierte Gastritis verhindert wurde (Chávez-Piña et al. 2010). Anderseits sind positive Effekte dieses Gasotransmitters festgestellt worden: Exogenes H_2S wirkt anti-inflammatorisch und anti-nozizeptiv in Synovitis Modellen bei der Ratte (Ekundi-Valentim et al. 2010). Das Pro-Medikament ATB429, ein Derivat des H_2S-

Donors Mesalamin, ist als Therapeutikum effizienter als Mesalamin allein im Maus-Kolitis-Modell (Fiorucci et al. 2007). Diese Befunde zeigen klar, dass H_2S - je nach Freisetzungsart und Konzentration der Gasotransmitters - sowohl protektive als auch schädigende Wirkungen im Organismus ausüben kann.

Die endogene Freisetzung von H_2S über körpereigene Enzyme führt sehr wahrscheinlich zu geringen Konzentrationen des Gasotransmitters, während die exogene Applikation zu erhöhten Konzentrationen führt. Aus dem Grund wurde die endogene Synthese von H_2S aus der Aminosäure L-Cystein initiiert und dessen Wirkung mit denen der exogenen H_2S Applikation (Freisetzung aus NaHS) verglichen (Pouokam und Diener 2012, **Publikation 8.2**). Die Aminosäure L-Cystein induzierte einen konzentrationsabhängigen Abfall des I_{sc}. Dieser Effekt wurde durch Blocker der H_2S-bildenden Enzyme Aminooxyacetat (AOAA; Hemmstoff der Cystathionin-β-Synthase) und β-Cyano-L-Alanin (CLA; Hemmstoff der Cystathion-γ-Lyase) gehemmt. Dies bestätigt, dass die Änderungen der Ionenströme durch den endogen gebildeten Gasotransmitter H_2S ausgelöst werden.

Bumetanid, ein Blocker des NKCC1, blockierte ebenfalls die Wirkung von H_2S (**Abb.13**). Interessanterweise verursacht L-Cystein eine biphasische Stromänderung: einen Abfall des I_{sc} (transiente Hemmung der Cl^--Sekretion) gefolgt von einem verzögerten Anstieg (Induktion einer Cl^--Sekretion) (**Abb.13B**). Grund für den initialen Abfall des Kurzschlussstroms ist eine kurzdauernde Ansäuerung des Cytosols durch die Aminosäure. Dies wurde durch zwei Versuche nachgewiesen: Wurde statt L-Cystein Natriumcysteinat als Precursor der H_2S-Synthese verwendet, war der transiente Abfall des I_{sc} vermindert und der sekundäre Anstieg wesentlich stärker. Die Ansäuerung des Cytosols wurde außerdem in isolierten Krypten, die mit dem pH-sensitiven Farbstoffs BCECF aufgeladen waren, direkt nachgewiesen. (**Abb.14, Publikation 8.2**).

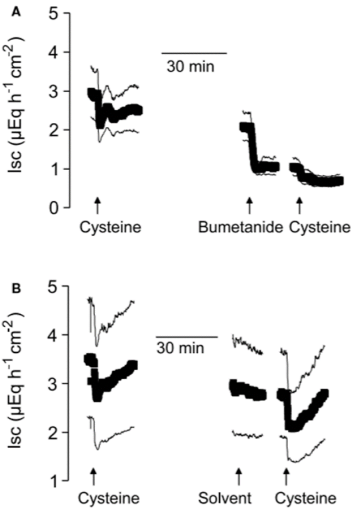

Abb.13: L-Cystein-verursachte Änderungen der transepithelialen Ionenströme am Colon der Ratte. Die Aminosäure induziert einen Abfall des I_{sc}, der zum Ausgangwert zurückkehrt (B). Der NKCC1-Blocker Bumetanid hemmt diese Wirkung (A). (Pouokam und Diener 2012, Publikation 8.2).

Viele K^+-Kanäle sind säureempfindlich, was auch die starke Hemmung der durch L-Cystein induzierten Änderungen des I_{sc} erklärte, wenn zuvor basolaterale K^+-Kanäle mit Ba^{2+} und Tetrapentylammonium (TPeA) blockiert wurden.

Exogene Anlieferung von H_2S durch den sehr langsam wirkenden Donor („slow release donor“) GYY 4137 (**Abb.15A**) oder Anflutung durch den relativ schnell wirkenden Donor Diallyltrisulfid (**Abb.15B**) bewirkten unterschiedliche Änderungen des I_{sc} (**Abb.15, Publikation 8.2**). Der anorganische Donor NaHS induzierte, wie Vorarbeiten zeigten (Hennig und Diener 2009), eine polyphasische Änderung des I_{sc} (**Abb.15, Publikation 8.2).**

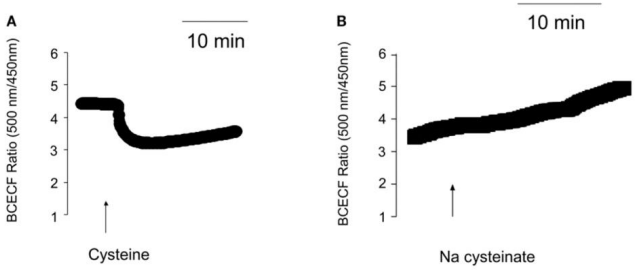

Abb.14: Änderungen durch L-Cystein (A) und das Natriumsalz des Cysteins (B) des intrazellulären pH-Wertes von Colonepithelzellen der Ratte. Der Abfall des BCECF-Ratio-Signals entspricht einer Ansäuerung des Cytosols. (Pouokam und Diener 2012, Publikation 8.2).

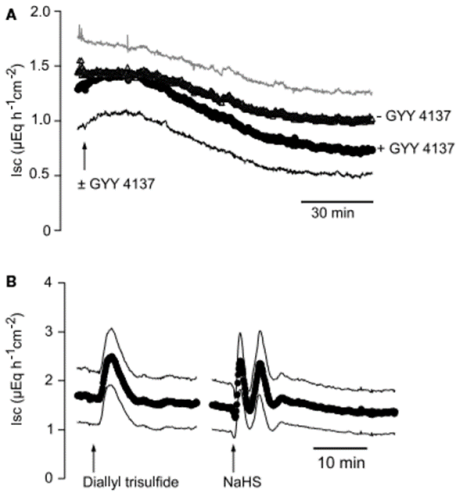

Abb.15: Vergleichende Änderungen des I_{sc} durch Gabe GYY 4137, Diallyltrisulfid und NaHS. (Pouokam und Diener 2012, Publikation 8.2).

Ähnliche divergente Effekte auf transepitheliale Ionenströme wurden mit einem anderen Gasotransmitter, dem NO, beobachtet: Serosale Natriumnitrit-Zugabe senkt den I_{sc} im Ileum der Maus (Rao et al. 1994). Hingegen induzieren andere NO-Donatoren, wie Natrium Nitroprussid (SNP), Isosorbid Dinitrat (ISDN), S-Nitroso Acetylpenicillamin

(SNAP) oder GEA 3162, einen Anstieg des I_{sc} im Ileum und Colon der Ratte (MacNaughton et al. 1993; Tamai und Gaginella 1993; Wilson et al. 1993; Li et al. 1994; Rolfe et al. 1994; Schultheis et al. 2002b).

Wie Nitroxyl (HNO) im Vergleich zu diesen relativ gut bekannten Gasotransmittern am Darmepithel wirkt, wurde in der Publikation **8.7** untersucht. Nitroxyl (HNO) löste am Colonepithel der Ratte einen konzentrationsabhängigen Anstieg des I_{sc} aus, welcher über Ionensubstitution-Versuche und basolaterale Blockade der Cl-Ionen-Aufnahme als Cl^--Sekretion identifiziert wurde. Diese Sekretion hing von Ca^{2+} ab, nicht aber von sGC, da sowohl Blockade als auch Aktivierung des Enzyms keinen Einfluss auf auf die von HNO-induzierte Sekretion hatten (**Tabelle 9,** Pouokam et al. 2013). Das Toxin Tetrodotoxin aus dem Kugelfisch, welches als Blocker spannungsabhängiger Natriumkanäle zur Unterdrückung der Ausbreitung von Aktionspotentialen eingesetzt wurde, zeigte keinen Einfluss auf die Wirkung von HNO.

Tabelle 9: Wirkung von Aktivatoren und Inhibitoren der Signalwege der pro-sekretorischen Antwort auf HNO im Colon.

	Response to Angeli's salt, ΔI_{sc} (μEq/h cm^2)	n
Without tetrodotoxin	4.71 ± 0.26	7
With tetrodotoxin	3.89 ± 0.70	7
Without indomethacin	3.14 ± 0.48	8
With indomethacin	0.63 ± 0.20[a]	8
Without indomethacin/ forskolin	3.65 ± 0.43	6
With indomethacin/forskolin	0.69 ± 0.21[a]	6
Without staurosporine	2.44 ± 0.36	8
With staurosporine	1.85 ± 0.44	8
Without H89	2.08 ± 0.47	8
With H89	2.00 ± 0.26	8
Without ODQ	2.18 ± 0.32	12
With ODQ	2.49 ± 0.36	12
Without LY 83583	1.30 ± 0.39	8
With LY 83583	1.36 ± 0.27	8
Without YC-1	2.32 ± 0.18	6
With YC-1	2.98 ± 0.36	6

Der Cyclooxygenasehemmer Indomethacin blockierte die Wirkung von HNO auf den Kurzschlussstrom. Unwirksam waren ODQ (Blockade der cGC), LY83583 (Aktivierung der cGC), Tetrodotoxin (Blockade der neuronalen Signalübertragung), Staurosporin (breit wirkender Blocker von Proteinkinasen) und H89 (Hemmstoff der Proteinkinase A) (Publikation 8.7, Pouokam et al. 2013).

Die Hemmung der Bildung von Prostaglandinen mit Indomethacin verhinderte jedoch die durch HNO induzierte Sekretion, was die Beteiligung von Eicosanoiden (produziert vor allem in der Submucosa) (Craven und DeRubertis 1983) in der Wirkung des Gastransmitters belegt. Nitroxyl entfaltete diese pro-sekretorische Wirkung durch die Aktivierung der Na^+/K^+-ATPase, der Ca^{2+}-abhängigen K^+-Kanäle und K_{ATP}-Kanäle in der basolateralen Membran. Die Letzteren weisen wichtige Schutzfunktionen im Darm auf, aber ihre Struktur ist weitgehend nicht genau bekannt. So wurde ihre Identifikation und Charakterisierung in der **Publikation 8.3** initiiert. In dieser Publikation wird gezeigt, dass die Aktivierung solche Kanäle mit Pinacidil eine Cl^--Sekretion oder dessen Hemmung auslöst, wenn Pinacidil jeweils auf die basolaterale bzw. apikale Seite zugegeben wird.

Die pharmakologischen Eigenschaften dieser Kanäle auf beiden Polen der Epithelzelle scheinen unterschiedlich zu sein. Die **Tabellen 10** und **11** belegen diese Hypothese.

Tabelle 10: Einfluss der basolateral applizierten K^+-Kanal-Inhibitoren und der neuronalen Blockade auf die serosale Pinacidil-evozierte Cl^--Sekretion.

	ΔI_{sc} evoked by serosal pinacidil ($\mu Eq h^{-1} cm^{-2}$)	
	− Inhibitor	+ Inhibitor
±Glibenclamide	0.32±0.071	0.12±0.028*
±Gliclazide	0.51±0.097	0.17±0.036*
±Tolbutamide	0.52±0.16	0.33±0.12
±TPeA	0.32±0.095	0.27±0.074
±TTX	0.28±0.13	0.49±0.10

Pinacidil als K_{ATP}-Kanal-Aktivator erhöhte die transepitheliale Cl^--Sekretion, gezeigt hier als positive ΔI_{sc} in der linken Spalte. In Anwesenheit (rechte Spalte) von K_{ATP}-Kanal-Blockern (Glibenclamid, Gliclazid, Tolbutamid) oder nach Gabe eines Blockers von K_{Ca}-Kanälen (TPeA) bzw. des Neurotoxins TTX (alle auf der basolateralen Seite appliziert), wird die Antwort zu Pinacidil nur von Gliclazid und Glibenclamid gehemmt (Publikation 8.3, Pouokam et al. 2012)

Tabelle 11: Einfluss der apikal applizierten K^+-Kanal-Inhibitoren auf die Senkung des I_{sc} durch mukosales Pinacidil

	ΔI_{sc} evoked by mucosal pinacidil ($\mu Eq h^{-1} cm^{-2}$)	
	−Inhibitor	+Inhibitor
±Ba^{2+}	−0.21±0.028	−0.46±0.061*
±Glibenclamide	−0.91±0.19	−0.73±0.079
±Gliclazide	−0.61±0.17	−0.51±0.084
±Tolbutamide	−0.32±0.13	−0.18±0.037
±TPeA	−0.52±0.24	−0.38±0.066

Pinacidil als K_{ATP}-Kanal-Aktivator verminderte die transepitheliale Cl^--Sekretion, gezeigt hier als Abfall des I_{sc} (ΔI_{sc}) in der linken Spalte. Nach Vorbehandlung (rechte Spalte) mit Blockern von K_{ATP}-Kanälen (Glibenclamid, Gliclazid, Tolbutamid), von Ca^{2+}-abhängigen K^+-Kanälen (TPeA) oder nach Gabe des unspezifischen K^+-Kanal-Blockers Ba^{2+} wird die Antwort auf apikales Pinacidil tendenziell durch Blocker von K_{ATP}-Kanälen vermindert. (Publikation 8.3, Pouokam et al. 2012).

K_{ATP}-Kanäle sind Heterooktamere, die aus 2 Typen von Untereinheiten bestehen, den sogenannten Sulfonylharnstoff-Rezeptoruntereinheiten (SUR) und den K^+-einwärts-Gleichrichtern (Kir6). Die vier identischen regulatorischen SUR-Untereinheiten bilden den äußeren Ring des Kanals. Die vier identischen Kir6-Untereinheiten bilden den inneren Ring des Kanals und umgeben die Kanalpore. Strukturell wird der Kanal aus einem Komplex der Form Kir6.x und SURy gebildet, wo „x“ für 1 oder 2 und „y“ für 1, 2A oder 2B stehen. Im Dünndarm der Ratte und des Menschen wurden diese Kanäle mit dem strukturellen Kir6.1/SUR2A-Komplex an den Tight-Junctions nachgewiesen (Jöns et al. 2006). Wie die **Abb.16** zeigt, sind die Untereinheiten der K_{ATP}-Kanäle sowohl in der basolateralen als auch in der apikalen Membran verteilt. Auch intrazellulär war eine Immunoreaktivität auf die entsprechenden Untereinheiten festzustellen. Dies ist dadurch erklärbar, da die verwendeten Antikörper auch an freien Untereinheiten, die sich in synthetisierenden Organellen oder in Vakuolen befinden könnten, binden können. Es wurden auch K_{ATP}-Kanäle in Mitochondrien nachgewiesen (Inoue et al. 1991). Anhand

der immunhistochemischen Daten ist eine strukturelle Zusammensetzung aus Kir6.1, Kir6.2, SUR1 und SUR2B denkbar, was ferner mit Hilfe der RT-PCR bestätigt wurde (Pouokam et al.2012, **Publikation 8.3**).

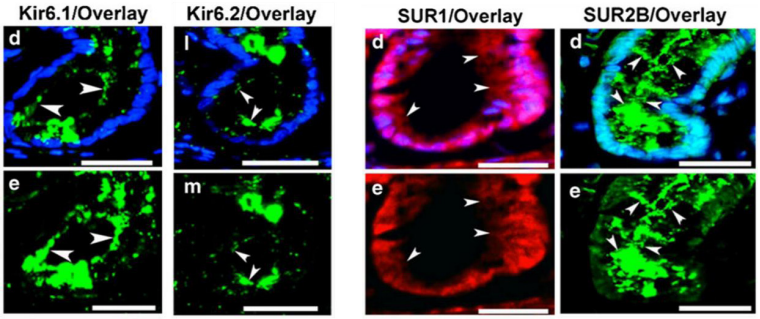

Abb.16: Untereinheiten der K_{ATP}-Kanäle in Krypten des Colons der Ratte. Pfeile zeigen die apikale Lokalisierung der Untereinheiten. Die Zellkerne (durch DAPI blau gefärbt) befinden sich am basalen Pol der Zellen. Die untere Reihe zeigt die Färbung der einzelnen Untereinheiten. Die obere Reihe zeigt die Zusammenlagerung der einzelnen Färbungen und der Kern-Gegenfärbung. (Pouokam und Diener 2012, Publikation 8.3).

Der Stoffwechselzustand einer Zelle wird mit Hilfe der K_{ATP}-Kanäle an die elektrische Aktivität der Zelle gekoppelt. Eine Aktivierung solche Kanäle führt zur Hyperpolarisation der Zellmembran und damit bei erregbaren Zellen eine Verminderung der Erregbarkeit mit der Folge der Energieeinsparung.

Auch am Kolonepithel scheinen sie an der Reaktion auf Energiemangel beteiligt zu sein. Wenn das Epithel energetisch depletiert wird (z.B. Ersatz von D-Glucose durch das nicht-metabolisierbare Molekül 2-Deoxyglucose), steigt die Gewebeleitfähigkeit deutlich an. Dieser Verlust der Integrität wird deutlich verstärkt, wenn K_{ATP}-Kanäle mit Glibenclamid blockiert werden (**Abb.17**).

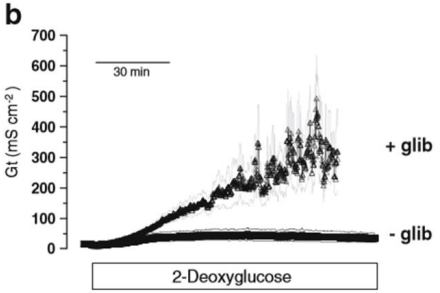

Abb.17: Die K_{ATP}-Kanäle weisen eine protektive Wirkung am Darmepithel auf. Energiedepletion durch Ersatz von D-Glucose durch die nicht-metabolisierbare 2-Deoxyglucose führt zum dramatischen Anstieg der transepithelialen Leitfähigkeit (G_t) in Anwesenheit des K_{ATP}-Kanal-Blockers Glibenclamid (Pouokam und Diener 2012, Publikation 8.3).

Übergreifend betrachtet, stellt die transepitheliale Ionensekretion ein zentrales Merkmal für die Regulation der Darmintegrität dar. Die Ionensekretion trägt zur Abwehr bei, indem die Wassersekretion, die per Osmose der Ionensekretion ins Lumen folgt, eine „Spül-Funktion" hat und Keime bzw. Toxine von den luminalen Flächen ablöst und entsorgt. Diese Grundfunktion wird physiologisch von dem Transportapparat der Enterozyten gewährleistet. Die endogene Synthese und Freisetzung von Gasotransmittern reguliert die Grundfunktionen des Epithels. Exogen zugeführte Gasotransmitter unterstützen diese Regulation (Beispiel an H_2S, **Abb.18** und **Abb.19**, Übersicht bei Pouokam und Althaus 2016). Die Kontroverse über die pro- oder antiinflammatorische Wirkung des Gasotransmitters NO (oder auch H_2S) lässt sich durch die Produktionsrate, die Dauer der Wirkung und die Art der Freisetzung des Gasotransmitters erklären (Übersicht bei Schirgi-Degen und Beubler 1995, Schultheiss et al. 2002b).

Chronisch entzündliche Darmerkrankungen, wie etwa Morbus Crohn und Colitis ulcerosa, sind mit einer erhöhten Epithelpermeabilität assoziiert (Olaison et al. 1990; Meddings 1997). Bei Morbus Crohn Patienten wurde eine Korrelation zwischen Reduktion der

epithelialen ATP-Konzentration und erhöhter parazellulärer Permeabilität am distalen Ileum nachgewiesen (Söderholm et al. 2002). Außerdem wurde eine protektive Wirkung der K_{ATP}-Kanäle in einem Colitis Modell der Ratte gezeigt, wo die Blockade der Kanäle mit Glibenclamid die Erkrankung verschlimmerte und zum Tode führte (Wallace et al. 2009). Therapeutisch sind die Angriffspunkte der Gasotransmitter im Darm also von großer Bedeutung. Entscheidend dabei sind die Konzentration, die Art der Zufuhr/Freisetzung und die Dauer der Wirkung.

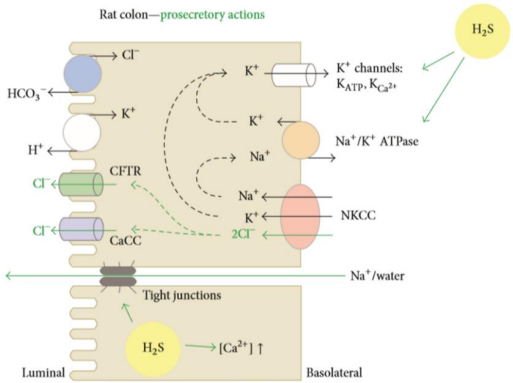

Abb.18: Direkte Wirkungen des exogen zugeführten Gasotransmitters H_2S an Epithelzellen des Colons der Ratte. Exogenes H_2S führt zur Aktivierung des Transportapparats in der basolateralen Membran, Aufnahme und Akkumulation von Anionen (vorwiegend Cl^-) und Sekretion dieser Anionen durch apikale CFTR und CaCC. Parazellulär folgen Na^+-Ionen und Wasser per Elektroneutralität und Osmose. Auch eine erhöhte Permeabilität der Tight Junctions ist die Folge. (Pouokam und Althaus 2016, Publikation 8.6).

Ein weiterer protektiver Effekt des Gasotransmitters H_2S ist die Pufferung eines Säureüberschusses im Lumen durch die Stimulation der HCO_3^--Sekretion zum Schutz der Magenwand oder der Mukosa des Duodenums gegen Geschwüre (Takeuchi et al. 2012; Blackler et al. 2014).

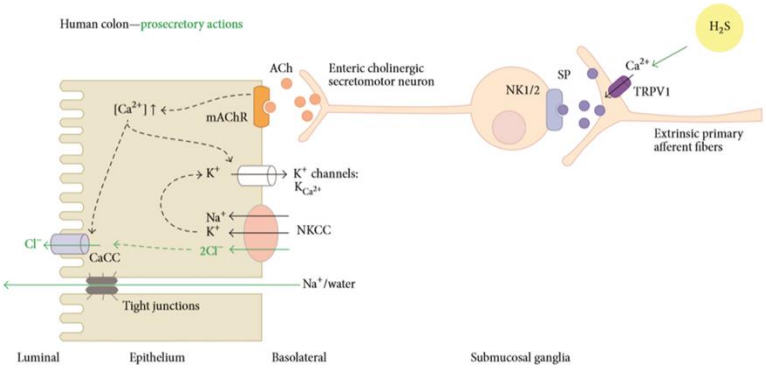

Abb.19: Indirekte Wirkungen des exogenen Gasotransmitters H_2S an Epithelzellen des humanen Colons. Exogenes H_2S aktiviert Neurone in der Submukosa. Stimuliert werden die Kationenkanäle aus der Transienten Rezeptoren-Potential-Unterfamilie V, Subtyp 1 (TRPV1) in extrinsisch primären afferenten Fasern, was zur Freisetzung von Substanz P (SP) führt. Substanz P bindet an Neurokin Rezeptoren (NK) 1 und 2 der enterischen cholinergen Sekretomotoneurone in Ganglien der Submukosa. Folglich wird ACh von den aktivierten Neuronen der Ganglien freigesetzt zur Stimulation der muskarinergen ACh Rezeptoren (mAChR). Es folgt eine Ca^{2+}-gesteuerte Anionensekretion durch CaCC. Parallel diffundieren Na^+-Ionen parazellular, gefolgt von Wassermolekülen. (Übersicht bei Krueger et al. 2010; Pouokam und Althaus 2016, Publikation 8.6).

Dazu wurde nachgewiesen, dass dieses Gas die Mukusproduktion von Becherzellen unterstützt und der Entzündungs-assoziierten Mukusdefizienz entgegenwirkt (Motta et al. 2015). Ferner wurde die protektive Wirkung der K_{ATP}-Kanäle, also ein Zieleffektor des Gasotransmitters H_2S, in Ischämie/Reperfusion- ähnlichen Geschehen am Colon der Ratte geprüft (**Publikation 8.4**). Die Hypoxie induzierte eine triphasische Änderung des I_{sc}: Einen transienten Abfall, einen Anstieg und einen langanhaltenden Abfall. Während der folgenden Reoxygenation stieg der I_{sc} langsam über den Ausgangwert. Die Gewebeleitfähigkeit zeigte einen biphasischen Anstieg unter den beiden Bedingungen. Die registrierten Änderungen werden durch Ca^{2+}-abhängige Cl^--Ströme getragen. Weder die Blockade noch die Aktivierung der K_{ATP}-Kanäle während der beiden Phasen vermochte es, die I_{sc}-Änderungen unter Hypoxie/Reoxygenation zu beeinflussen. Trolox C (ein

Radikalfänger) dagegen hemmte die I_{sc}-Änderungen nur während der Hypoxie. Überraschend zeigten Messungen mit dem Superoxid-Anion-sensitiven Farbstoff Mitosox und dem Thiol-sensitiven Farbstoff Thiol Tracker keine Änderungen der Fluoreszenz dieser Indikatoren während der beiden Phasen. Laut diesen Ergebnissen scheinen die K_{ATP}-Kanäle keine Rolle bei Ischämie/Reperfusion-Geschehen im Colon der Ratte zu spielen. Vermutet wird aber eine „Sensor-Funktion" der K_{ATP}-Kanäle für den Gasotransmitter H_2S (Pouokam und Diener 2011). Das Colon scheint resistenter gegen Ischämie/Reperfusion zu sein als zum Beispiel der Dünndarm, was auch bereits morphologische Studien gezeigt haben (Leung et al. 1992). Grund dafür könnte auch eine geringere Xanthin-Oxidase-Aktivität des Colons (Leung et al. 1992) sein, was dabei hilft, bei dem physiologisch niedrigen Sauerstoffpartialdruck in diesem Darmsegment eine zu starke Radikalbildung zu vermeiden (Zheng et al. 2015).

Der Gasotransmitter Nitroxyl hat nicht nur Wirkungen auf den transepithelialen Ionentransport, sondern beeinflusst auch die gastrointestinale Motilität. Laufende Versuche zeigen eine relaxierende Wirkung von HNO sowohl auf Längs- als auch Ringmuskelschichten des Colons (**Abb.20-21**). Die Mechanismen der Relaxation ähneln denen der anderen Gasotransmitter H_2S und NO, jedoch mit Besonderheiten. Dabei scheint HNO die MLCP und den sGC/cGMP-Weg zu aktivieren sowie die Freisetzung von Ca^{2+} aus dem sarkoplasmatischen Retikulum zu fördern um SK_{ca} Kanäle zu aktivieren. Der Ausstrom von K^+ durch solche Kanäle führt zur Hyperpolarisation der glatten Muskelzellen (**Abb.22**) und damit zur Relaxation. Die Vorinkubation mit dem Reduktionsmittel Dithiothreitol (DTT) hemmt diese Relaxation, was die starke Interaktion des Gasotransmitters mit Thiol-Gruppen ausweist. Eine potentielle Kooperation zwischen NO und H_2S zur Bildung von HNO bzw. zur HNO-ähnlichen induzierten Relaxation wäre auch vorstellbar, da DTT die von NO und H_2S induzierte Relaxation partiell hemmt.

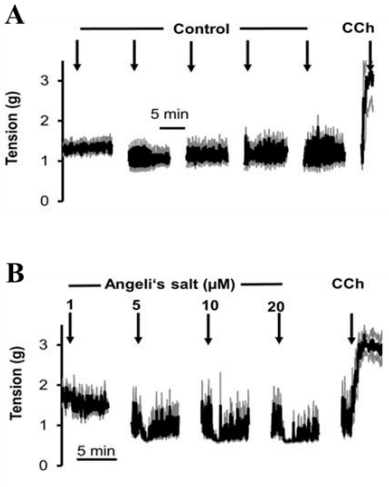

Abb.20: Der HNO-Donor Angeli's Salt induziert eine konzentrationsabhängige Relaxation von Längsmuskelschichten des proximalen Colons der Ratte. (B) zeigt den Versuch gegen die zeitgleiche Kontrolle (A). Die Vitalität der Gewebe wurde mit Carbachol (CCh; 10 µM) bestätigt (Kapitel 8.8).

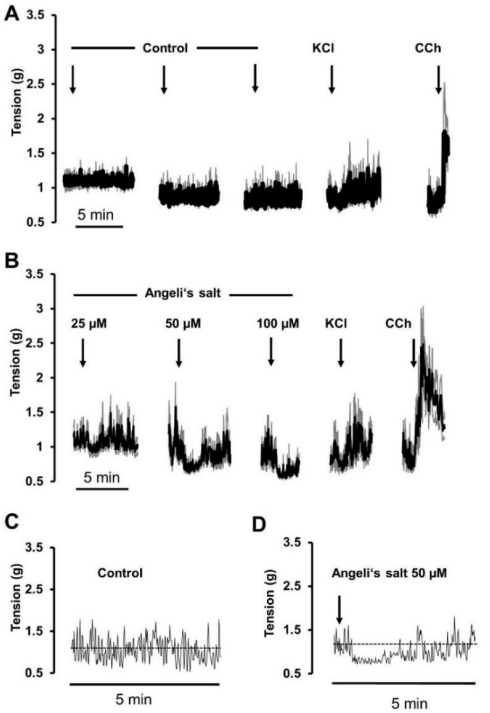

Abb.21: Der HNO-Donor Angeli's Salt induziert eine konzentrationsabhängige Relaxation von Ringsmuskelschichten des proximalen Colons der Ratte. (B) zeigt den Versuch gegen die zeitgleiche Kontrolle in (A). In (C) und (D) sind 5-min heraus gezoomte Abschnitte von einzelnen Kurven der Kontroll- und Versuchsreihe dargestellt. Die Vitalität der Gewebe wurde mit KCl (30 mM) und Carbachol (CCh, 10 µM) bestätigt (Kapitel 8.8).

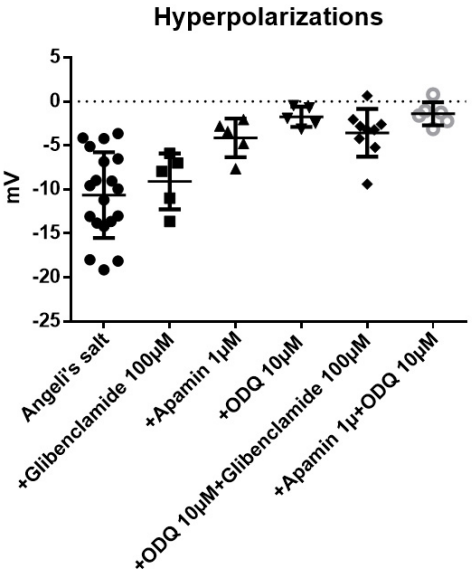

Abb.22: Der HNO-Donor Angeli's Salt induziert eine ODQ- und Apamin-sensitive, aber Glibenclamid-insensitive Hyperpolarisation von Myozyten der Ringmuskelschicht des proximalen Colons der Ratte. ODQ wurde als Hemmer der sGC und Apamin als Hemmer der SK_{ca}-Kanäle verwendet. Die Inhibitoren wurden vor Zugabe des Gasotransmitter-Donors appliziert (Kapitel 8.8).

6.2 Nanostrukturen zur Erfassung von physiologischen Parametern am Gastrointestinaltrakt

6.2.1 Signalverstärkung/Potenzierung

Second Messenger Systeme übermitteln und verstärken physiologisch Signale. Durch externe Einflüsse kann die Verstärkung dieser Signale an den Rezeptoren moduliert werden. So kann die lokale hohe Dichte von Liganden zur exponentiellen Verstärkung führen (Cairo et al. 2002). Solch ein Verfahren wird in den **Publikationen 8.9** und **8.10** ausführlicher erklärt. Es handelt sich dabei um die multivalente Präsentation an entsprechenden Rezeptoren von Liganden, die an einem Gold-Kern über Linker-Moleküle immobilisiert worden sind. Die Größe solcher Partikel variiert in Abhängigkeit von den Linker-Molekülen im Nanometer-Bereich (Turkevich et al. 1951). Die erhaltenen Nanopartikeln können bis zu 10000 native Liganden tragen (Gasiorek et al 2015). Die Geometrie bzw. Struktur der Partikeln beeinflusst erheblich die Wechselwirkung zwischen Liganden und Rezeptoren, unter anderem durch die extrem hohe lokale Konzentration der Liganden, die permanent in Wechselwirkung mit einzelnen oder benachbarten Rezeptoren treten. Im Colonepithel wurde das Ausmaß dieser Modulation auf die Cl^--Sekretion mit zwei Typen von Nanopartikeln (NP) der Größe 14 nm geprüft: Histamin-NP (Au-MUDA-HA) und Carbachol-NP (Au-MUDA-CCh). Histamin und Carbachol lösen physiologisch eine konzentrationsabhängige Cl^--Sekretion über Aktivierung von G-Protein-gekoppelte Rezeptoren aus (Strabel und Diener 1995, Schultheis et al. 2006; Bell et al. 2015, Gasiorek et al. 2015; Mattern et al. 2018).

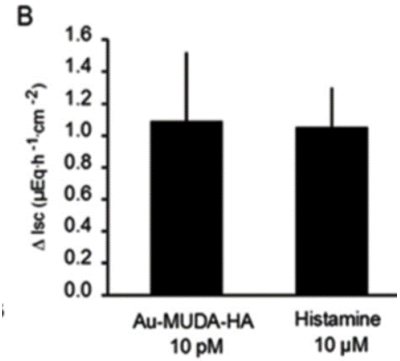

Abb.23: Potenzierung der Wirkung Au-MUDA-HA im Vergleich zu nativen Histamin Molekülen. 10 pM Histamin-Nanopartikeln und 10 µM natives Histamin weisen eine äquivalente Wirksamkeit auf. (Gasiorek et al. 2015, Publikation 8.9).

Die Spezifität der entsprechenden NP wurde nachgewiesen, indem die Standard Blocker der zu bindenden Rezeptoren eingesetzt worden waren (**Abb.24, Publikation 8.9 und 8.10**).

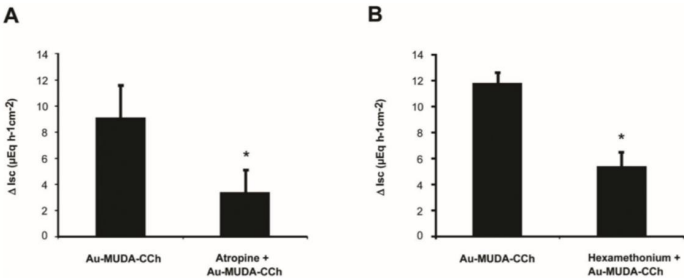

Abb.24: Spezifität der Liganden-konjugierten Nanopartikel für die Rezeptoren der entsprechenden Liganden. Atropin und Hexamethonium als Blocker von muskarinergen bzw. nikotinergen Rezeptoren hemmen die durch CCh-konjugierte NP induzierte Cl^--Sekretion am Colonepithel der Ratte. (Mattern et al. 2018, Publikation 8.10).

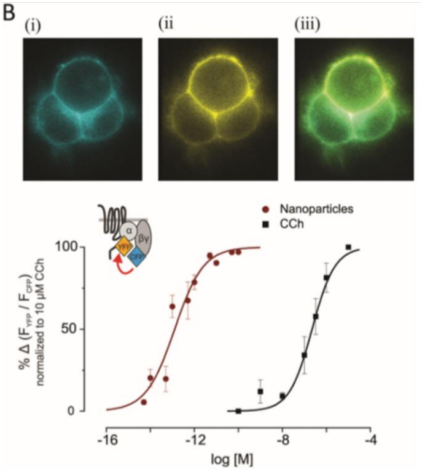

Abb.25: Gq-Protein-Aktivierung durch Stimulation von M_3R mit CCh-Nanopartikeln. FRET Messungen an HEK293T Zellen. CCh-NP bewirken eine Linksverschiebung der Konzentrationswirkungskurve mit einer EC_{50} von 127 ± 0.44 fM gegenüber 224 ± 7.12 nM für das native CCh-Molekül. Obere Bilder zeigen die CFP (i), YFP (ii) und Überlagerung CFP + YFP (iii) Fluoreszenz in der Zellmembran. (Mattern et al. 2018, Publikation 8.10).

Die multivalente Präsentation der Liganden erzielt, wie diese Arbeiten zeigen, eine Potenzierung der nativen Moleküle um einen Faktor von ca. 10^6 (**Abb.23** und **25**). Therapeutisch könnten solche funktionalisierten NP Anwendungen finden z.B. in der Therapie von Glaukom, Ileus und von Motilitätstörungen des Urogenitaltraktes.

6.2.2 *In situ* Messungen der neuronalen Aktivität und des Einflusses des epithelialen NHE auf das Mikroumgebung-pH

Mit Hilfe von Acetylcholinesterase-tragendenen AlGaN/GaN Biosensoren (Müntze et al. 2015, **Publikation 8.11)** wurde die Freisetzung ACh aus myenterischen Neuronen (isoliert oder noch in der Längsmuskulatur eingebettet) gemessen. Dieses Verfahren scheint Vorteile gegenüber den üblichen Techniken (wie die Kombination von Flüssigkeit-Chromatographie mit elektrochemischer Detektion von H_2O_2 oder mit der Elektrospray-

Ionisierung-Massenspektrometrie) zu bieten. Trotzt der hohen Empfindlichkeit der Letzteren detektieren sie in Minutenzeitspannen, währenddessen läge der Vorteil der in **Publikation 8.11** verwendeten Technik in einem kurzen Zeitfenster unter 1 Sekunde (Hai et al. 2006). Damit wäre es mit solchen schnellen Sensoren möglich „*in situ*" Signale aufzuspüren und zu messen.

Die **Publikation 8.12** befasst sich mit der Live-Messung von pH-Wert-Änderungen in der Mikroumgebung isolierter Krypten als Nachweis des Einflusses der NHE-Tätigkeit (Hölzel et al. 2018, **Abb.26**, Publikation 8.12). Die Sensoren wurden aus InGaN/GaN Nanodrähten hergestellt und erlaubten eine räumliche Auflösung unter 0,63 µm. Solch ein Verfahren könnte ein Startpunkt für weiterführende Arbeiten im Bereich des quantitativen Imagings von elektrischen bzw. biochemischen Zellprozessen sein.

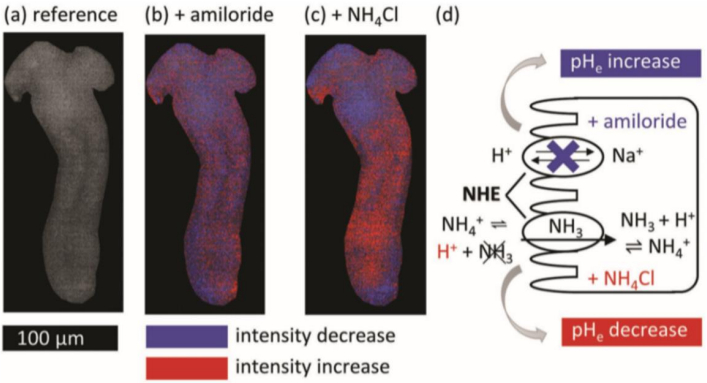

Abb.26: Detektion von lokalen pH-Änderungen einer Krypte des Colons der Ratte. Blockade des Transporters NHE mit Amilorid führt zur Alkalinisation (Blaufärbung in (b)) der Mikroumgebung der Krypte. Ansäuerung der Krypte mittels NH_4^+-Puls führt zur extrazellären Ansäuerung (Rötung in (c)). (Hölzel et al. 2018, Publikation 8.12).

7. Zusammenfassung und Perspektiven

Der Magen-Darm-Trakt ist ein komplexes System mit unterschiedlichen Funktionen. Der Darm trägt zum Beispiel zur Abwehr, Ernährung und Entgiftung bei. Störungen der grundliegenden Mechanismen dieser Funktionen führen zu erheblichen Erkrankungen. Physiologische Regulationsmechanismen dienen dazu bei Störungen der Organfunktion, etwa bei Entzündungen oder Ischämie/Reperfusion, Dysfunktionen zu vermeiden bzw. zu begrenzen. Dafür werden unter anderen Transporter, Aktivierung bzw. Deaktivierung von Enzymen oder die Verstoffwechslung hoch- oder runtergefahren um, so den Energieverbrauch anzupassen. Die Regulation der Synthese und Freisetzung von Stoffen und Sensibilisierung/Desensibilisierung des motorischen Apparats, also der kontraktilen Elemente der Zellen, kommen ebenfalls ins Spiel. So werden endogene Gasotransmitter wie H_2S und NO synthetisiert und wirken auto- oder parakrin auf Zieleffektoren wie Transporter oder Enzyme. Drei der bekannten Gasotransmitter (NO, CO und H_2S) werden endogen in der Darmwand synthetisiert; ob dies auch der Fall bei HNO ist, ist noch nicht bekannt. Die exogene Zufuhr von Gasotransmittern führt konzentrationsabhängig zu unterschiedlichen Antwortmustern, die sich den Antworten von endogen produzierten Gasotransmittern überlagern, diese maskieren oder minimieren. Die Art (endogen oder exogen und die Geschwindigkeit der Freisetzung), die Konzentration und das „Equipment“ des Gewebes an bestimmten Zielmolekülen bestimmen die Wirkung der Gasotransmitter. Dieses Prinzip wird bei der Entwicklung von Gasotransmitter-basierten Medikamenten angewendet. Da die physiologischen Prozesse im Gastrointestinaltrakt ein Resultat von Interaktionen zwischen dem enterischen Nervensystem, dem Immunsystem und dem motorischen Apparat sind, sind die Einflüsse der einzelnen Systeme zu untersuchen. Hier sind Perspektiven in der Entwicklung von adäquaten therapeutischen Molekülen zu sehen. Das vertiefte Verstehen der Schutz- bzw. Resistenzmechanismen des

Darms während der Hypoxie/Reoxygenation bzw. Ischämie/Reperfusion bietet Perspektiven zur Behandlung von Ischämie/Reperfusion-Schäden in anderen Systemen wie das kardiovaskuläre System. Die Wirkungen der Gasotransmitter werden zurzeit an Parametern der Hypoxie/Reoxygenation untersucht.

Bei Therapieansätzen werden Zellprozesse heruntergefahren, beschleunigt oder verstärkt. Die genaue Untersuchung solcher Mechanismen trägt zur Entwicklung von besseren Therapeutika bei. So wird zurzeit die Modulation von Liganden-Rezeptoren-Signalverstärkung über G-Proteine mit Hilfe von Liganden-konjugierten Nanopartikeln untersucht.

Neue Messverfahren für physiologische Parameter, die mit hoher Zeit- und/oder Raumauflösung Zellfunktionen messen, sind prinzipiell für die biomedizinische Forschung von hoher Bedeutung. Interdisziplinäre Ansätze mit anderen Fachgebieten, wie der Chemie und der Physik, ermöglichten es Biosensoren zu entwickeln, welche *„in vivo“* einsetzbar wären.

8. Vorgelegte Veröffentlichungen und unveröffentlichte Daten

Begutachtete Veröffentlichungen

8.1. "Mechanisms of actions of hydrogen sulphide at rat distal colonic epithelium"

Pouokam E, Diener M. *Brit. J. Pharmacol.* (2011) 162: 392-404

Impakt Faktor: 4.409

Eigener Anteil an der Publikation:

- Initiative: 40 %
- Projektplanung: 50 %
- Durchführung der Versuche: 50 %
- Auswertung der Experimente: 50 %
- Erstellung der Publikation: 40 %

BJP BRITISH JOURNAL OF PHARMACOLOGY
BPS BRITISH PHARMACOLOGICAL SOCIETY

BJP British Journal of Pharmacology

DOI:10.1111/j.1476-5381.2010.01026.x
www.brjpharmacol.org

RESEARCH PAPER

Mechanisms of actions of hydrogen sulphide on rat distal colonic epithelium

E Pouokam and M Diener

Institute for Veterinary Physiology, Justus-Liebig-University Giessen, Giessen, Germany

Correspondence
M. Diener, Institut für Veterinär-Physiologie, Justus-Liebig-Universität Gießen, Frankfurter Str. 100, D-35392 Gießen, Germany. E-mail: martin.diener@vetmed.uni-giessen.de

Keywords
Ca^{2+} signalling; Cl^- secretion; electrolyte transport; NaHS; rat colon

Received
18 May 2010
Revised
16 August 2010
Accepted
23 August 2010

BACKGROUND AND PURPOSE
The aim of this study was to clarify the mechanisms by which hydrogen sulphide (H_2S) affects ion secretion across rat distal colonic epithelium.

EXPERIMENTAL APPROACH
Changes in short-circuit current induced by the H_2S-donor, sodium hydrosulphide (NaHS; 10 mmol·L^{-1}), were measured in Ussing chambers after permeabilization of the apical membrane with nystatin. Cytosolic Ca^{2+} concentration ($[Ca^{2+}]_i$) and Ca^{2+} in intracellular stores were measured with fluorescent dyes. Changes in mitochondrial membrane potential were estimated with rhodamine 123.

KEY RESULTS
NaHS had a biphasic effect on overall currents across the basolateral membrane: an initial inhibition followed by a secondary stimulation. Both a scilliroside-sensitive action on the Na^+-K^+-ATPase and modulation of glibenclamide-sensitive and tetrapentylammonium-sensitive (i.e. ATP-sensitive and Ca^{2+}-dependent) basolateral K^+ channels were involved in this action. Experiments with rhodamine 123 revealed that NaHS induced a hyperpolarization of the mitochondrial membrane. NaHS evoked a biphasic change in $[Ca^{2+}]_i$, an initial decrease followed by a secondary increase, known to be mediated by the release of stored Ca^{2+}. Initial falls in $[Ca^{2+}]_i$ were not mediated by a sequestration of Ca^{2+} in intracellular Ca^{2+} storing organelles, as the Mag-Fura-2 signal was unaffected by NaHS. Falls in $[Ca^{2+}]_i$ were inhibited by 2′,4′-dichlorobenzamil, an inhibitor of the Na^+-Ca^{2+}-exchanger, and attenuated in Na^+-free buffer, suggesting a transient stimulation of Ca^{2+} outflow by this transporter, directly demonstrated by Mn^{2+} quenching experiments.

CONCLUSIONS AND IMPLICATIONS
ATP-sensitive and Ca^{2+}-dependent basolateral K^+ conductances, the basolateral Na^+-K^+-pump as well as Ca^{2+} transporters were involved in the action of H_2S in regulating colonic ion secretion.

Abbreviations
$[Ca^{2+}]_i$, cytosolic Ca^{2+} concentration; Gt, tissue conductance; Isc, short-circuit current; TPeA, tetrapentylammonium

Introduction

Intestinal ion transport, which can be switched from absorption into secretion of water and electrolytes (see Binder and Sandle, 1994), is not only controlled by classical neurotransmitters or hormones, but also by the so-called 'gaso-transmitters'. Besides nitric oxide, the prototype of this class of volatile messenger molecules, more recently hydrogen sulphide (H_2S), has been recognized and identified as a transmitter. This gas is produced from cysteine via the enzymes cystathionine-β-synthase and cystathionine-γ-lyase (Wang, 2002). In the circulation, H_2S is known as a gaso-transmitter inducing vasodilatation, decreasing cardiac inotropy, and inhibiting the proliferation of vascular smooth

© 2010 The Authors
British Journal of Pharmacology © 2010 The British Pharmacological Society

muscle (see Geng *et al.*, 2007; Lefer, 2008). Furthermore, H_2S donors have been shown to protect against burn- and smoke-induced acute lung injury in sheep (Esechie *et al.*, 2009) and to exert antiinflammatory actions in a model of rat synovitis (Ekundi-Valentim *et al.*, 2010).

In the intestine, a seminal observation in this field was the finding that enteric neurons express the key enzymes for H_2S production and that H_2S releasing drugs induce Cl^- secretion in guinea pig and human colon via excitation of submucosal secretomotor neurons. Neuronal capsaicin-sensitive cation channels, that is, transient receptor potential vanilloid receptor type 1 (TRPV1) channels are thought to be the primary target of H_2S in these two species (Schicho *et al.*, 2006; receptor and channel nomenclature follows Alexander *et al.*, 2009).

In contrast, in rat colonic epithelium, where H_2S also induces a Cl^- secretion, the neurotoxin, tetrodotoxin, only partially reduced the response in short-circuit current (Isc), a measure of net charge movement across the epithelium, which was induced by sodium hydrosulphide (NaHS), an H_2S donor (Lee *et al.*, 2006), indicating additional epithelial sites of action (Hennig and Diener, 2009). Furthermore, cystathionine-β-synthase and cystathionine-γ-lyase immunoreactivity were found within the colonic epithelium itself and isolated colonic crypts responded with changes in the cytosolic Ca^{2+} concentration ($[Ca^{2+}]_i$) in the presence of NaHS. The Isc response induced by NaHS was triphasic: an initial rise in Isc (mediated by Cl^- secretion) was followed by a transient fall (assumed to represent a transient K^+ secretion), before the Isc finally rose again to a long-lasting Cl^- secretory response. Also, the Ca^{2+} response was not monophasic; it consisted of a transient decrease of $[Ca^{2+}]_i$ followed by a long-lasting increase mediated by a release of stored Ca^{2+} via intracellular Ca^{2+} channels. The Cl^- secretory response was sensitive to serosal administration of glibenclamide, a known inhibitor of ATP-sensitive K^+ channels (see Cook and Quast, 1990), as well as tetrapentylammonium, known as an inhibitor of Ca^{2+}-dependent K^+ channels (Maguire *et al.*, 1999). This suggests that, as in smooth muscle cells from rat aorta (Zhao *et al.*, 2001) or rat insulinoma cells (Yang *et al.*, 2005), NaHS stimulates both ATP-sensitive K^+ channels and Ca^{2+}-dependent K^+ channels, which would be consistent with the observed increase in the cytosolic Ca^{2+} concentration, measured in isolated rat colonic crypts (Hennig and Diener, 2009).

In order to secrete Cl^- across the apical membrane, the basolateral membrane has to establish the driving force for anion extrusion via anion channels in the apical membrane. In the basolateral membrane, K^+ channels generate the driving force for Cl^- secretion by maintaining the negative membrane potential, which is dominated by a K^+ diffusion potential (Strabel and Diener, 1995; Warth and Barhanin, 2003), whereas the Na^+-K^+-ATPase has to maintain the K^+ concentration gradient between the intra- and the extracellular space as prerequisite for the establishment of the K^+ diffusion potential. In view of the extensive evidence for the stimulation of ATP-sensitive K^+ channels by H_2S (see above), it seemed to be of primary interest to investigate potential effects of NaHS on the basolateral membrane which dominates cellular K^+ conductance of the epithelium. The second question to be clarified was the identification of the mechanism involved in the early response of the cytosolic Ca^{2+} concentration, which is transiently decreased by NaHS, before the secondary release of stored Ca^{2+} begins. To this end, changes in Isc induced by the H_2S-donor, NaHS, were measured in Ussing chambers after permeabilization of the apical membrane with nystatin. This ionophore forms pores in the apical membrane and thereby bypasses this membrane. Consequently, all changes in Isc induced by NaHS can only result from changes in ion transport across the non-permeabilized basolateral membrane (Schultheiss and Diener, 1997). Changes of the cytosolic Ca^{2+} concentration were evaluated using Fura-2; the Ca^{2+} concentration in intracellular stores was measured with Mag-Fura-2; and changes in mitochondrial membrane potential were estimated with rhodamine 123.

Methods

Solutions

The standard solution for the Ussing chamber experiments was a buffer solution containing ($mmol \cdot L^{-1}$): NaCl 107, KCl 4.5, $NaHCO_3$ 25, Na_2HPO_4 1.8, NaH_2PO_4 0.2, $CaCl_2$ 1.25, $MgSO_4$ 1 and glucose 12. The solution was gassed with carbogen (5% CO_2 in 95% O_2, v/v); pH was 7.4. In order to apply a K^+ gradient, the KCl concentration in this buffer was increased to 13.5 $mmol \cdot L^{-1}$ at the mucosal side while reducing the NaCl concentration in order to maintain isoosmolarity. For the Na^+-free solution, NaCl was replaced by N-methyl-D-glucamine ($NMDG^+$) chloride.

For the experiments carried out with isolated crypts, the following buffers were used. The EDTA solution for the isolation contained ($mmol \cdot L^{-1}$): NaCl 107, KCl 4.5, $NaHCO_3$ 25, Na_2HPO_4 1.8, NaH_2PO_4 0.2, glucose 12.2, EDTA 10 and 1 $g \cdot L^{-1}$ bovine serum albumin (BSA). It was gassed with carbogen; pH was adjusted by Tris-base to 7.4. The

isolated crypts were stored in a high potassium Tyrode solution consisting of (mmol·L^{-1}): K gluconate 100, KCl 30, HEPES 10, NaCl 20, $MgCl_2$ 1, $CaCl_2$ 1.25, glucose 12.2, sodium pyruvate 5 and 1 g·L^{-1} BSA; pH was 7.4. For superfusion of the isolated crypts during the imaging experiments, the following buffer was used (in mmol·L^{-1}): NaCl 140, KCl 5.4, $CaCl_2$ 1.25, $MgSO_4$ 1, HEPES 10, glucose 12.2; pH was 7.4. For the Na^+-free Tyrode solution, NaCl was replaced by NMDG Cl.

Tissue preparation and crypt isolation

All animal care and experimental procedures were approved by Regierungspräsidium Gießen, Gießen, Germany. Wistar rats of both sexes were used with a weight of 180–240 g. The animals had free access to water and a standard rat diet until the day of the experiment. Animals were killed by stunning followed by exsanguination. The serosa and muscularis propria were stripped away to obtain a mucosa-submucosa preparation of the distal colon. The distal colon was distinguished from the proximal colon by the absence of palm leaf-like striae (Lindström *et al.*, 1979). Briefly, the colon was placed on a small plastic rod with a diameter of 5 mm. A circular incision was made near the anal end with a blunt scalpel, and the serosa together with the lamina propria was gently removed in a proximal direction. Two segments of the distal colon of each rat were prepared. In general, one tissue served to measure the control response evoked by NaHS and the other was treated with putative antagonists before NaHS was applied. If the antagonist had to be administered in a solvent, the control tissue was pretreated with that solvent.

For the isolation of intact crypts, the mucosa-submucosa was fixed on a plastic holder with tissue adhesive and transferred for about 7 min to the EDTA solution. The mucosa was vibrated once for 30 s in order to obtain crypts (Schultheiss *et al.*, 2002). They were collected in a high-K^+ gluconate Tyrode buffer.

Isc measurement

The mucosa–submucosa preparation was fixed in a modified Ussing chamber, bathed with a volume of 3.5 mL on each side of the mucosa. The tissue was incubated at 37°C and short-circuited by a computer-controlled voltage-clamp device (Ingenieur Büro für Mess- und Datentechnik Mussler, Aachen, Germany) with correction for solution resistance. Tissue conductance was measured every minute by the voltage deviation induced by a current pulse (±50 µA, duration 200 ms) under open-circuit conditions. Isc was continuously recorded on a chart recorder. Isc is expressed as µEq·h^{-1}·cm^{-2}, that is, the flux of a monovalent ion per time and area, with 1 µEq·h^{-1}·cm^{-2} = 26.9 µA·cm^{-2}.

Imaging experiments

Relative changes in the cytosolic Ca^{2+} concentration were measured using Fura-2 (Molecular Probes, Leiden, the Netherlands), a Ca^{2+}-sensitive fluorescent dye (Grynkiewicz *et al.*, 1985). The crypts were pipetted into the experimental chamber with a volume of about 3 mL. They were attached to the glass bottom of the chamber with the aid of poly-L-lysine (0.1 g·L^{-1}; Biochrom, Berlin, Germany). The crypts were incubated for 60 min with 2.5 µmol·L^{-1} Fura-2 acetoxymethylester (AM). Then the dye ester not taken up by the cells was washed away. The preparation was superfused hydrostatically throughout the experiment with 140 mmol·L^{-1} NaCl Tyrode. Perfusion rate was about 1 mL·min^{-1}.

Changes in the cytosolic Ca^{2+} concentration were monitored as changes in the Fura-2 ratio (R; emission at an excitation wave length of 340 nm divided by the emission at an excitation wave length of 380 nm). Experiments were carried out on an inverted microscope (Olympus IX-50; Olympus, Hamburg, Germany), equipped with an epifluorescence set-up and an image analysis system (Till Photonics, Martinsried, Germany). Several regions of interest, each with the size of about one cell, were placed over an individual crypt. The emission above 420 nm was measured from the regions of interest. Data were sampled at 0.2 Hz. The baseline in the fluorescence ratio of Fura-2 was measured for several minutes before drugs were administered. For the Mn^{2+} quench experiments, the Fura-2 fluorescence was measured at a single wavelength, 360 nm, i.e. the isoemissive wavelength of this dye. In order to quantify the Mn^{2+} quench, a sliding average over five adjacent data points (i.e. over 25 s) was calculated; the slope of the curve was obtained by calculating the first time derivative of these data.

The Ca^{2+} concentration within intracellular storing organelles (such as the endoplasmic reticulum) was estimated with the fluorescent dye, Mag-Fura-2 (Molecular Probes) as described previously (Siefjediers *et al.*, 2007). Mag-Fura-2 is a lower affinity Ca^{2+} indicator which is able to measure Ca^{2+} at a concentration of 3 µmol·L^{-1} and higher (Baylor and Hollingworth, 2000). Most of the dye accumulates in the intracellular organelles and little in the cytosol (Hofer and Machen, 1993); its fluorescence at an excitation wavelength of 340 nm increases, when the Ca^{2+} concentration increases. Crypts were incubated for 60 min with 2.5 µmol·L^{-1} Mag-Fura-2 AM.

In order to reveal changes in mitochondrial membrane potential, the fluorescent dye rhodamine 123 was used (Krippeit-Drews *et al.*, 2000). Its fluorescence at an excitation wavelength of 480 nm increases when the mitochondrial membrane potential is depolarized. For these experiments, crypts were incubated for 30 min with 26 µmol·L^{-1} rhodamine 123.

Data analysis

Values are given as means ± SEM. When means of several groups had to be compared, an analysis of variance was performed followed by *post hoc* Tukey's-test. For the comparison of two groups, either a Student's *t*-test or a Mann–Whitney *U*-test was applied. An *F*-test decided which test method had to be used. Both paired and unpaired two-tailed Student's *t*-tests were applied as appropriate. $P < 0.05$ was considered to be statistically significant.

Materials

2',4'-Dichlorobenzamil hydrochloride (DCB; from Enzo, Lörrach, Germany), glibenclamide, and nystatin were dissolved in dimethylsulphoxide (final maximal concentration 0.5%, v/v). Carbonyl cyanide 4-(trifluoromethoxy) phenylhydrazone (3) (FCCP) was dissolved in ethanol (final concentration 0.01%, v/v). Scilliroside (a generous gift from Sandoz, Basel, Switzerland) was dissolved in methanol (final concentration 0.25%, v/v). Mn^{2+} and tetrapentylammonium (TPeA) were added as chloride salts. If not indicated otherwise, drugs were from Sigma,(Taufkirchen, Germany).

Results

Effect of NaHS on currents across the basolateral membrane

Previous experiments have revealed that NaHS evokes a biphasic Cl^- secretion (interrupted by a negative Isc), which is sensitive to inhibitors of ATP-sensitive and Ca^{2+}-dependent K^+ channels (Hennig and Diener, 2009). In order to study the presumed effects of the H_2S donor on the basolateral membrane, that is, the membrane with the highest cellular K^+ conductance, more directly, the apical membrane was permeabilized by the ionophore, nystatin (100 µg·mL^{-1} at the mucosal side), and a K^+ current across basolateral K^+ channels was driven by a mucosal-to-serosal K^+ gradient (98 mmol·L^{-1} NaCl/13.5 mmol·L^{-1} KCl buffer at the mucosal and 107 mmol·L^{-1} NaCl/4.5 mmol·L^{-1} KCl at the serosal side of the tissue). Baseline Isc prior administration of nystatin amounted 0.64 ± 0.13 µEq·h^{-1}·cm^{-2} (n = 7). In average, nystatin induced a maximal increase

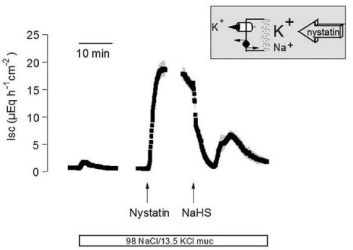

Figure 1

Biphasic change in the overall current across the basolateral membrane evoked by sodium hydrosulphide (NaHS) (10^{-2} mol·L^{-1} at the serosal side; right arrow). The apical membrane was permeabilized with nystatin (100 µg·mL^{-1} at the mucosal side; left arrow). The serosal side was exposed to a 107 mmol·L^{-1} NaCl/4.5 mmol·L^{-1} KCl buffer solution, whereas the mucosal buffer was 98 mmol·L^{-1} NaCl/13.5 mmol·L^{-1} KCl (white bar below trace), so that both basolateral K^+ channels as well as the Na^+-K^+-pump contribute to the nystatin-induced short-circuit current (Isc), as indicated by the schematic inset. Line interruptions are caused by omission of time intervals of 5–10 min in order to synchronize the tracings of individual records to the administration of drugs. Values are given as means (symbols) ± SEM (grey shaded area), n = 7. For statistics, see text.

in Isc to 19.3 ± 1.56 µEq·h^{-1}·cm^{-2} ($P < 0.05$ vs. baseline; Figure 1). Administration of NaHS (10^{-2} mol·L^{-1} at the serosal side) during the plateau phase of the nystatin-induced Isc caused a biphasic change in Isc: an initial decrease followed by a secondary increase (Figure 1). During the decreasing phase of the NaHS response, Isc fell to a value of 0.78 ± 0.14 µEq·h^{-1}·cm^{-2} and increased again to 8.34 ± 0.93 µEq·h^{-1}·cm^{-2} during the secondary phase of the response to the H_2S donor. The concentration of NaHS (10^{-2} mol·L^{-1}) was chosen as a maximal effective concentration from our previous experiments (Hennig and Diener, 2009). A ten times lower concentration of the donor (10^{-3} mol·L^{-1}), which – assuming a yield of NaHS to deliver H_2S of about 30% (Lee *et al.*, 2006) – should result in H_2S concentrations much closer to the plasma concentrations of this gasotransmitter (see Discussion), also resulted in a biphasic change in the current across the basolateral membrane (data not shown). This response, however, exhibited greater variability; so the concentration of 10^{-2} mol·L^{-1} was preferred in order to obtain consistent results.

Under these conditions, two components contribute to the nystatin-induced Isc: a stimulation of the Na^+-K^+-pump (exchanging 3 Na^+ against 2 K^+ with each transport cycle) by the apical inflow of

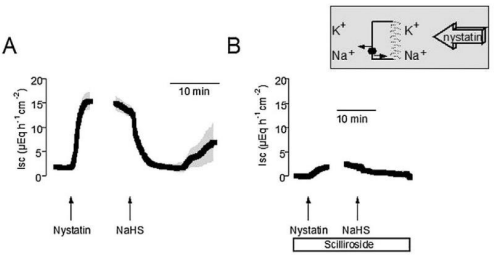

Figure 2

(A) Biphasic change in the current carried by the basolateral Na^+-K^+-pump evoked by sodium hydrosulphide (NaHS) (10^{-2} mol·L^{-1} at the serosal side; right arrow). The apical membrane was permeabilized with nystatin (100 µg·mL^{-1} at the mucosal side; left arrow). The serosal and the mucosal sides were exposed to a 107 mmol·L^{-1} NaCl/4.5 mmol·L^{-1} KCl buffer solution, so that only the Na^+-K^+-pump can contribute to the nystatin-induced short-circuit current (Isc) as indicated by the schematic inset. (B) Scilliroside (10^{-4} mol·L^{-1} at the serosal side; white bar) suppresses the secondary stimulation of pump current by NaHS. Line interruptions are caused by omission of time intervals of 5–10 min in order to synchronize the tracings of individual records to the administration of drugs. Values are given as means (symbols) ± SEM (grey shaded area), n = 8–9. For statistics, see Table 1.

Na^+ via the nystatin pores, and a current across basolateral K^+ channels driven by the applied K^+ gradient (Schultheiss and Diener, 1997). Cation substitution experiments were performed in order to distinguish between these two components. In a first attempt, the current across basolateral K^+ channels was excluded by the omission of a K^+ concentration gradient, that is, the apical membrane was permeabilized in the presence of a 107 mmol·L^{-1} NaCl/4.5 mmol·L^{-1} KCl buffer at both sides of the tissues (Figure 2). Under these conditions, NaHS (10^{-2} mol·L^{-1} at the serosal side) induced a similar, biphasic change in Isc, that is, an initial inhibition of Isc followed by a secondary increase (Figure 2A; for statistics, see Table 1). Pretreatment with scilliroside (10^{-4} mol·L^{-1} at the serosal side), a potent inhibitor of the rat Na^+-K^+-ATPase (Robinson, 1970), strongly inhibited the nystatin-induced Isc under these ionic conditions and suppressed the effect of NaHS (Figure 2B), confirming that this Isc is carried by the basolateral Na^+-K^+-ATPase.

In order to investigate the effects of NaHS on the basolateral K^+ conductance, tissues were permeabilized in the presence of a mucosal-to-serosal K^+ gradient, but in the absence of mucosal Na^+ in order to prevent a contribution of the Na^+-K^+-pump to the measured current (i.e. 98 mmol·L^{-1} NMDGCl/13.5 mmol·L^{-1} KCl buffer at the mucosal and 107 mmol·L^{-1} NaCl/4.5 mmol·L^{-1} KCl at serosal side of the tissue). Again, NaHS (10^{-2} mol·L^{-1} at the serosal side) biphasically modulated the nystatin-induced Isc under these ionic conditions; that is, an initial inhibition was followed by a secondary increase (Figure 3A). Both the nystatin-induced Isc as well as the response to NaHS were significantly

Table 1

Effect of sodium hydrosulphide (NaHS) on currents across the basolateral membrane carried by the Na^+-K^+-pump

	Pump current in the presence of scilliroside Isc (µEq·h^{-1}·cm^{-2})	Pump current without scilliroside Isc (µEq·h^{-1}·cm^{-2})
Baseline	0.00 ± 0.20*	1.74 ± 0.20
Nystatin	2.96 ± 1.03*	16.6 ± 1.82
NaHS decrease	0.11 ± 0.47	1.11 ± 0.64
NaHS peak	2.36 ± 2.41*	9.06 ± 4.57

*P < 0.05 versus Isc in the absence of scilliroside.
Effect of NaHS (10^{-2} mol·L^{-1} at the serosal side) on the current across the basolateral membrane carried by the Na^+-K^+-ATPase in the absence (right) or presence (left) of scilliroside (10^{-4} mol·L^{-1} at the serosal side). The apical membrane was permeabilized with nystatin (100 µg·mL^{-1} at the mucosal side). The serosal and the mucosal side were exposed to a 107 mmol·L^{-1} NaCl/4.5 mmol·L^{-1} KCl buffer solution. The maximal increase in Isc induced by nystatin, the maximal decrease in Isc evoked by NaHS within 20 min after administration of the drug and the maximal increase (peak) evoked by NaHS within 5–20 min after administration of the drug are given. Values are means ± SEM, n = 8–9.
ISC, short-circuit current.

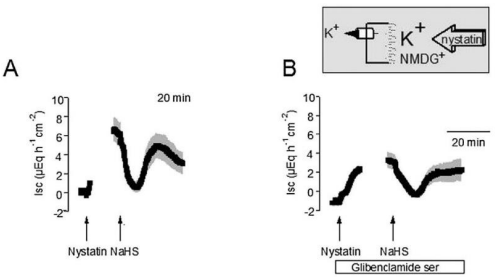

Figure 3

(A) Biphasic change in the current across the basolateral K^+ channels evoked by sodium hydrosulphide (NaHS) (10^{-2} mol·L^{-1} at the serosal side; right arrow). The apical membrane was permeabilized with nystatin (100 µg·mL^{-1} at the mucosal side; left arrow). The serosal side was exposed to a 107 mmol·L^{-1} NaCl/4.5 mmol·L^{-1} KCl buffer solution, whereas the mucosal buffer was a 98 mmol·L^{-1} NMDGCl/13.5 mmol·L^{-1} KCl, so that only basolateral K^+ channels can contribute to the nystatin-induced short-circuit current (Isc) as indicated by the schematic inset. (B) Glibenclamide (10^{-3} mol·L^{-1} at the serosal side; white bar) inhibits the secondary stimulation of Isc by NaHS. Line interruptions are caused by omission of time intervals of 5–10 min in order to synchronize the tracings of individual records to the administration of drugs. Values are given as means (symbols) ± SEM (grey shaded area), n = 6–10. For statistics, see Table 2.

($P < 0.05$) reduced, when the tissues were pretreated with glibenclamide (10^{-3} mol·L^{-1} at the serosal side, Table 2), which acts as a blocker of ATP-sensitive K^+ channels (Figure 3B; see Cook and Quast, 1990).

A further basolateral K^+ conductance, which might be a target of NaHS, is that through Ca^{2+}-dependent K^+ channels, as the H_2S donor induces a biphasic change in the cytosolic Ca^{2+} concentration, that is, an initial fall followed by an increase (Hennig and Diener, 2009). Therefore, tissues were pretreated with TPeA (10^{-4} mol·L^{-1} at the serosal side), a blocker known to inhibit preferentially Ca^{2+}-dependent K^+ channels (Maguire *et al.*, 1999). Under these conditions, nystatin induced only a small increase in K^+ current across the basolateral membrane (Table 3), emphasizing the prominent role of Ca^{2+}-dependent K^+ channels for the overall K^+ conductance of this membrane (Schultheiss and Diener, 1997). When NaHS (10^{-2} mol·L^{-1} at the serosal side) was administered, the typical initial fall in Isc induced by the drug was preserved, whereas the secondary rise in Isc was strongly reduced (Table 3), suggesting that a stimulation of TPeA-sensitive K^+ channels also contributes to this phase of the NaHS response.

Table 2

Effect of sodium hydrosulphide (NaHS) on currents carried by basolateral glibenclamide-sensitive K^+ channels

	Isc (µEq·h^{-1}·cm^{-2}) + glibenclamide	Isc (µEq·h^{-1}·cm^{-2}) – glibenclamide
Baseline	–1.16 ± 0.41*	–0.03 ± 0.26
Nystatin	3.28 ± 0.87*	6.46 ± 1.29
NaHS decrease	–0.40 ± 0.31	0.21 ± 0.54
NaHS peak	2.60 ± 1.12*	6.17 ± 1.30

*$P < 0.05$ versus Isc in the absence of glibenclamide.
Effect of NaHS (10^{-2} mol·L^{-1} at the serosal side) on the current across the basolateral K^+ conductance in the absence (– glibenclamide; right) or presence (+ glibenclamide; left) of glibenclamide (10^{-3} mol·L^{-1} at the serosal side). Tissues were permeabilized with nystatin (100 µg·mL^{-1} at the mucosal side) in the presence of 98 mmol·L^{-1} NMDGCl/13.5 mmol·L^{-1} KCl buffer at the mucosal and 107 mmol·L^{-1} NaCl/4.5 mmol·L^{-1} KCl at the serosal side of the tissue. The maximal increase in Isc induced by nystatin, the maximal decrease in Isc evoked by NaHS within 20 min after administration of the drug and the maximal increase (peak) evoked by NaHS within 5–20 min after administration of the drug are given. Values are means ± SEM, n = 6–10.
ISC, short-circuit current.

Effect of NaHS on mitochondrial membrane potential

The stimulatory effect of H_2S on ATP-sensitive K^+ channels is well known (Zhao *et al.*, 2001; Yang *et al.*, 2005), whereas the initial inhibition of this conductance, as suggested by the glibenclamide-sensitive initial fall in Isc, was unexpected. ATP-sensitive K^+ channels are inhibited by an increase in

Table 3

Effect of sodium hydrosulphide (NaHS) on currents carried by basolateral TPeA-sensitive K^+ channels

	Isc (μEq·h^{-1}·cm^{-2}) + TPeA	Isc (μEq·h^{-1}·cm^{-2}) – TPeA
Baseline	–1.89 ± 0.62*	1.43 ± 0.19
Nystatin	–1.64 ± 1.02*	6.83 ± 1.29
NaHS decrease	–4.55 ± 1.19*	–0.42 ± 1.04
NaHS peak	–3.81 ± 1.61*	3.27 ± 0.83

*P < 0.05 versus Isc in the absence of TPeA.
Effect of NaHS (10^{-2} mol·L^{-1} at the serosal side) on the current across the basolateral K^+ conductance in the absence (– TPeA; right) or presence (+ TPea; left) of tetrapentylammonium (10^{-4} mol·L^{-1} at the serosal side). Tissues were permeabilized with nystatin (100 μg·mL^{-1} at the mucosal side) in the presence of 98 mmol·L^{-1} NNMDGCl/13.5 mmol·L^{-1} KCl buffer at the mucosal and 107 mmol·L^{-1} NaCl/4.5 mmol·L^{-1} KCl at the serosal side of the tissue. The maximal increase in Isc induced by nystatin, the maximal decrease in Isc evoked by NaHS within 20 min after administration of the drug and the maximal increase (peak) evoked by NaHS within 5–20 min after administration of the drug are given. Values are means ± SEM, n = 7–8.
ISC, short-circuit current; TPeA, tetrapentylammonium.

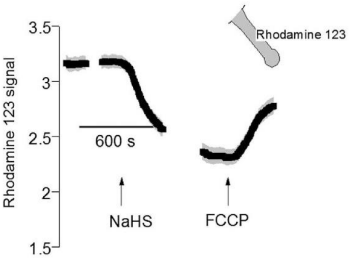

Figure 4

Hyperpolarization of the mitochondrial membrane potential by sodium hydrosulphide (NaHS) (10^{-4} mol·L^{-1}; left arrow). Isolated colonic crypts were loaded with rhodamine 123 as indicated by the inset. At the end of the experiment, Carbonyl cyanide 4-(trifluoromethoxy) phenylhydrazone (3) (FCCP; 10^{-6} mol·L^{-1}; right arrow) was administered. The rhodamine 123 fluorescence is given in arbitrary units. Line interruptions are caused by omission of time intervals of 5–10 min in order to synchronize the tracings of individual records to the administration of drugs. Values are given as means (symbols) ± SEM (grey shaded area), n = 89. For statistics, see text.

the cytosolic ATP concentration (Seino and Miki, 2003). The rate of ATP synthesis is strongly dependent on mitochondrial membrane potential (Duchen *et al.*, 1993); a high rate of ATP synthesis depolarizes the mitochondrial membrane potential due to the reduction of the H^+ gradient (Garlid and Paucek, 2003).

Therefore, in order to (indirectly) estimate whether this dual action of NaHS might be related to alterations in the cellular ATP production, changes in mitochondrial membrane potential were measured with the fluorescent dye, rhodamine 123, whose signal is quenched by this potential. For these experiments, isolated colonic crypts were used, which in our previous study (Hennig and Diener, 2009) had shown to be much more sensitive to NaHS compared with the thick mucosa–submucosa preparations used in the Ussing chamber. Therefore, the NaHS concentration was reduced to 10^{-4} mol·L^{-1}. However, in contrast to the expectation of a mitochondrial depolarization, which should result from an increase in ATP synthesis, the administration of NaHS caused a prompt decrease of the rhodamine 123 signal from 3.18 ± 0.061 to 2.34 ± 0.078 arbitrary units (P < 0.05, n = 89; Figure 4), that is, a hyperpolarization. As a control, the uncoupler of the oxidative phosphorylation, FCCP (10^{-6} mol·L^{-1}), was administered, which – as expected – caused an increase in the rhodamine 123 fluorescent signal to 2.84 ± 0.076 arbitrary units (P < 0.05 vs. the signal in the presence of NaHS). Consequently, it seems unlikely that the unconventional inhibition of ATP-sensitive basolateral K^+ conductance, which is finally superimposed by the expected stimulation due to direct interaction of H_2S with the channel molecules (Figure 3), might be caused by an increase in the cytosolic ATP level, although this conclusion remains speculative without determination of the cytosolic ATP concentration.

Effect of intracellular Ca^{2+}

In previous experiments (see also Figure 7B of the present study), we observed that NaHS induces a biphasic change in the cytosolic Ca^{2+} concentration, that is, an initial fall followed by a secondary increase mediated by a release of stored Ca^{2+}, mainly via ryanodine receptors (Hennig and Diener, 2009). As such a change in the cytosolic Ca^{2+} concentration would also affect the basolateral K^+ conductance via modulation of Ca^{2+}-dependent K^+ channels, we tried to find out, which mechanism might underlie the initial fall in $[Ca^{2+}]_i$, which is still completely unexplained.

In a first attempt, we asked the question whether an uptake of Ca^{2+} into Ca^{2+}-storing organelles such as the endoplasmic reticulum might be involved in the early NaHS response. However, NaHS did not affect, at all, the fluorescence signal of Mag-Fura-2, a

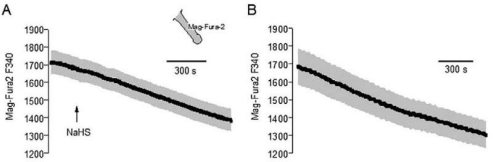

Figure 5

(A) Sodium hydrosulphide (NaHS) (10^{-4} mol·L^{-1}; arrow) does not affect the Mag-Fura-2 emission (in arbitrary units) at an excitation wavelength of 340 nm (F 340 nm, i.e. the wavelength where the dye exhibits the strongest change in fluorescence in response to changes in the Ca^{2+} concentration). (B) Time-dependent control without administration of NaHS. Isolated crypts were loaded with Mag-Fura-2 (as indicated by the inset). Values are given as means (symbols) ± SEM (grey shaded area), n = 96–97.

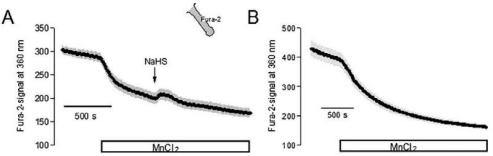

Figure 6

(A) Mn^{2+} (5 10^{-4} mol·L^{-1} $MnCl_2$; white bar) leads to a decrease in the Fura-2 signal (in arbitrary units) measured at an excitation wavelength of 360 nm (at which the Fura-2 signal is independent from the cytosolic Ca^{2+} concentration) at isolated colonic crypts (indicated by the schematic). The administration of sodium hydrosulphide (NaHS) (10^{-4} mol·L^{-1}; arrow) transiently reverses the Mn^{2+} quench, suggesting a stimulation of Ca^{2+} (Mn^{2+}) efflux by NaHS. For statistics, see text. (B) Time-dependent control without administration of NaHS. Values are given as means (symbols) ± SEM (grey shaded area) of n = 12 cells measured synchronously.

fluorescent dye, which accumulates in intracellular Ca^{2+} stores (Figure 5A; see Hofer and Machen, 1993); there was only a continuous fall in the Mag-Fura-2 signal, which was also observed in time-dependent control experiments (Figure 5B).

Consequently, the fall in the cytosolic Ca^{2+} concentration should be caused by a stimulation of Ca^{2+} efflux. To test this hypothesis, the following approach was used. The fluorescence of Fura-2 is quenched by Mn^{2+}. Mn^{2+} ions are accepted as substrate by many Ca^{2+}-transporting proteins (see Parekh and Penner, 1997; Trepakova *et al.*, 1999) and lead, once within the cell, to a quench of the Fura-2 fluorescence. When the Fura-2 fluorescence was measured at an excitation wave length of 360 nm, that is, at the isoemissive wave length, where the signal is not affected by the cytosolic Ca^{2+} concentration, the administration of Mn^{2+} (5 10^{-4} mol·L^{-1}) caused a prompt fall in the Fura-2 fluorescence signal (Figure 6). When subsequently NaHS (10^{-4} mol·L^{-1}) was administered, it caused a transient increase in the Fura-2 signal (Figure 6A), which was not observed in time-dependent control experiments (Figure 6B). The slope, by which the Fura-2 signal changed, amounted to –3.31 ± 0.27 units/5 s before and 4.27 ± 0.51 units/5 s (P < 0.05 vs. slope in the absence of NaHS, n = 84) during the steepest phase of the NaHS response. In contrast, in parallel-performed time-dependent control experiments, where no NaHS was administered, the maximal change in the Fura-2 slope only amounted to 0.79 ± 0.20 units/5 s (P < 0.05 vs. effect of NaHS, n = 72). Consequently, NaHS transiently activates a Ca^{2+} (Mn^{2+}) efflux pathway.

One prominent Ca^{2+} extruding mechanism at rat colonic crypts is a Na^+-Ca^{2+}-exchanger (Seip *et al.*, 2001). Therefore, in a final set of experiments, we tested whether a stimulation of this exchanger might be responsible for the transient fall in the cytosolic Ca^{2+} concentration induced by NaHS. When NaHS (10^{-4} mol·L^{-1}) was administered in the presence of dichlorobenzamil (2.5 10^{-6} mol·L^{-1}), a

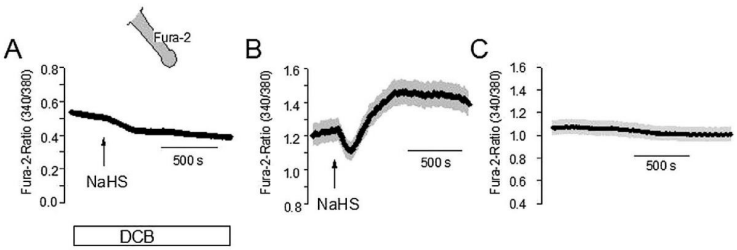

Figure 7

(A) Pretreatment with 2′,4′-dichlorobenzamil (DCB; 2.5.10^{-6} mol·L^{-1}; white bar) prevents the changes in the Fura-2 ratio evoked by sodium hydrosulphide (NaHS) (10^{-4} mol·L^{-1}; arrow) in comparison with control crypts not pretreated with DCB (B). (C) Time-dependent control without administration of NaHS. Isolated crypts were loaded with Fura-2 (as indicated by the schematic); given is the emission at an excitation wavelength of 340 nm divided by the emission at an excitation wave length of 380 nm. Values are given as means (symbols) ± SEM (grey shaded area), n = 52–84. For statistics, see Table 4.

Table 4

Effect of sodium hydrosulphide (NaHS) on the cytosolic Ca^{2+} concentration

	Δ Fura-2 ratio Initial decrease	Δ Fura-2 ratio Secondary peak
+ DCB	−0.0577 ± 0.00416*	−0.0071 ± 0.00103*
− DCB	−0.200 ± 0.0240	0.370 ± 0.0446
NMDG Cl	−0.0542 ± 0.00696*	0.0842 ± 0.00965*
NaCl	−0.131 ± 0.0203	0.247 ± 0.0471

*P < 0.05 versus response to NaHS under control conditions (i.e. without DCB or in the presence of Na^+ respectively).
Effect of NaHS (10^{-4} mol·L^{-1}) on the Fura-2 signal in the presence (+ DCB) or absence (– DCB) of DCB (2.5.10^{-4} mol·L^{-1}; upper two rows), or in the absence (NMDG Cl) or presence (NaCl) of extracellular Na^+ (lower two rows). The initial decrease (middle column) was calculated as the minimum signal reached within 4 min after administration of NaHS (10^{-4} mol·L^{-1}), whereas the secondary increase (right column) was calculated as maximum within 15 min after administration of NaHS. Data are given as change in the Fura-2 ratio (Δ Fura-2 ratio) compared with the baseline just prior to administration of NaHS and are means ± SEM, n = 52–83.
DCB, 2′,4′-dichlorobenzamil.

known inhibitor of this exchanger (see Seip *et al.*, 2001), the effect of the H_2S donor was drastically reduced (Figure 7A,B, Table 4), whereas in time-dependent control experiments a stable baseline of the Fura-2 ratio signal was measured (Figure 7C). Surprisingly, both the initial decrease as well as the secondary increase of the cytosolic Ca^{2+} concentration were inhibited, which might suggest non-specific actions of DCB on transporters other than the Na^+-Ca^{2+}-exchanger. However, when a different approach was used to inhibit the Ca^{2+} extruding action of the exchanger, that is, when the crypts were superfused with a Na^+-free solution, a similar inhibition of both phases of the NaHS response was observed (Table 4).

Discussion

In the intestine, the gaso-transmitter H_2S is known to exert several actions such as a relaxation of smooth muscle from different species (Teague *et al.*, 2002), antinociceptive (Distrutti *et al.*, 2006) or anti-inflammatory effects (Fiorucci *et al.*, 2007). A further prominent action is the induction of anion secretion (Schicho *et al.*, 2006). This anion secretion leads to an increase in Isc across the epithelium. Two phases of the Isc increase induced by the H_2S donor, NaHS, can be distinguished in rat colonic epithelium: an early one, transiently interrupted by a fall in Isc, before the current increases again to reach a long-lasting plateau (Hennig and Diener, 2009). The present data suggest that, at the basolateral membrane, three sites of action are involved in the complex Isc pattern evoked by NaHS, that is: (i) the basolateral Na^+-K^+-ATPase; (ii) glibenclamide-sensitive, ATP-sensitive K^+ channels; and (iii) TPeA-sensitive, Ca^{2+}-dependent K^+ channels.

One action of the H_2S donor, NaHS, consists in a biphasic modulation of the current across the basolateral membrane carried by the Na^+-K^+-ATPase in

apically permeabilized epithelia (Figure 2A). A transient inhibition is followed by a secondary increase in pump current. In order to confirm that this current is indeed caused by this enzyme, scilliroside was used, as the α_1-isoform of the Na^+-K^+-ATPase in rats is quite resistant to the classical Na^+-K^+-pump inhibitor, ouabain (see Edwards and Pallone, 2007). Pretreatment with this potent inhibitor of the rat Na^+-K^+-ATPase (Robinson, 1970) suppressed the action of NaHS (Figure 2B). Consequently, there seems to be a biphasic modulation by H_2S of the pump activity, which finally maintains the K^+ concentration gradient at the cell membrane and thereby sets the fundamental driving force for active ion transport. The mechanism of this modulation is not known, but it is tempting to speculate that this action may be related to a reduction of disulphide bonds within the protein by H_2S, which acts as reducing agent (Reiffenstein *et al.*, 1992), or a modification of free thiol groups. However, the Isc response evoked by NaHS at rat distal colon was not inhibited by the pretreatment of the tissue with N-ethylmaleimide (NEM; $5{\cdot}10^{-5}$ mol·L^{-1}, unpublished data), a drug assumed to block non-protein SH-groups (Chávez-Piña *et al.*, 2010), suggesting that the latter explanation is less probable.

Another site of action of H_2S in the basolateral membrane is the glibenclamide-sensitive K^+ channel (Figure 3) and such channels are considered to be classical targets of H_2S. An increase in this type of cellular K^+ conductance is known from vascular smooth muscle cells and is assumed to be mediated by a reduction of disulphide bonds within the channel protein (Zhao *et al.*, 2001). Obviously, an increase in the open probability of the channels is responsible for this response as observed in a rat insulinoma cell line (Yang *et al.*, 2005). ATP-sensitive K^+ channels serve to couple membrane potential to the metabolic state of the cell. They are octomers, composed of four channel-forming subunits ($K_{IR}6.1$ or $K_{IR}2$) and four regulatory subunits, the sulphonylurea receptors (SUR1, SUR2A or SUR2B; see Seino and Miki, 2003). Immunohistochemically, $K_{IR}6.1$ and SUR2A have been found in human and rat small intestinal epithelium (Jöns *et al.*, 2006). Basolateral administration of a K^+ channel opener such as pincacidil, which stimulates ATP-sensitive K^+ channels, evokes an increase in Isc across rat colon (Hennig and Diener, 2009), suggesting the presence of this type of cation channel in the rat colonic epithelium, although molecular or immunohistochemical evidence is still missing. Surprisingly, the effect of NaHS on the current carried by ATP-sensitive K^+ channels was also biphasic: that is, the expected activation was preceded by a transient inhibition (Figure 3).

ATP-sensitive K^+ channels are inhibited by an increase in the cytosolic concentration of ATP, which binds to the regulatory nucleotide binding site of the respective SUR subunits (Seino and Miki, 2003), so it might be hypothesized that the paradoxical, transient inhibition of the glibenclamide ATP-sensitive K^+ conductance might be caused by an increase in the ATP concentration within the cell. A high rate of ATP synthesis is known to depolarize the mitochondrial membrane potential due to the reduction of the H^+ gradient (Garlid and Paucek, 2003). However, the fluorescence signal of the fluorescent dye, rhodamine 123, which incorporates into the inner mitochondrial membrane and whose fluorescence is quenched by this potential, was reduced (and not enhanced) by NaHS, whereas a typical uncoupler of phosphorylation such as FCCP, a protonophore, which dissipates the H^+ gradient at this membrane, evoked the opposite signal (Figure 4). H_2S is known to inhibit mitochondrial respiration, probably at the level of the cytochrome C oxidase, that is, the complex IV of the mitochondrial electron transport chain; this action is thought to be the reason for the protective effect of H_2S on the myocardium after ischemia/reperfusion damage (Elrod *et al.*, 2007). This inhibition probably underlies the observed hyperpolarization of the inner mitochondrial membrane (Figure 4). Consequently, the unexpected inhibition of ATP-sensitive basolateral K^+ conductance, finally superimposed by the expected stimulation (Figure 3), is probably not related to an increase in the cytosolic ATP level, at least not on the level of the mitochondrial ATP production. Alternatively, a reduction in ATP degradation, for example, by the transient reduction in Na^+-K^+-pump activity, might cause an increase in the local concentration of ATP near the basolateral membrane and thereby transiently inhibit ATP-sensitive K^+ channels.

At first glance, an alternative explanation for the hyperpolarizing action of H_2S at the mitochondrial membrane potential might be thought. ATP-sensitive K^+ channels are also found in the inner mitochondrial membrane (Inoue *et al.*, 1991); as found with their counterparts in the cell membrane, they might also be activated by H_2S, too. However, as the K^+ concentration in the mitochondrial matrix and in the inter-membrane space are approximately equal (Garlid and Paucek, 2003), their activation would tend to depolarize the inner mitochondrial membrane.

In the basolateral membrane, apart from the ATP-sensitive K^+ conductance, the dominant Ca^{2+}-dependent K^+ conductance was also modulated in a biphasic manner by NaHS (Table 3). This response is paralleled by changes in the cytosolic Ca^{2+}

concentration (Figure 7B): a transient fall, which will lead to a decrease of basolateral K^+ conductance, and a secondary rise, which will then increase the basolateral K^+ conductance. The mechanism of the secondary increase has recently been shown to be independent from extracellular Ca^{2+}, but related to a release of Ca^{2+} from intracellular Ca^{2+} storing organelles via ryanodine receptors (Hennig and Diener, 2009), which are expressed by rat colonic epithelium (Prinz and Diener, 2008). In the present study, we focused on the pathways involved in the initial fall of the cytosolic Ca^{2+} concentration induced by the NaHS. The administration of NaHS to isolated colonic crypts transiently reversed the quench of the Fura-2 signal induced by Mn^{2+} (Figure 6A). Mn^{2+} ions are substrates for many Ca^{2+} transporters and reduce, once within the cytoplasm, the Fura-2 signal (cf. the rapid fall of the Fura-2 fluorescence in Figure 6). Consequently, these data suggest a transient stimulation of Ca^{2+} (Mn^{2+}) outflow by NaHS. The change in the cytosolic Ca^{2+} concentration could be inhibited by two different strategies to inhibit the Na^+-Ca^{2+}-exchanger in the cell membrane. Both DCB, a blocker of this exchanger (Seip *et al.*, 2001), as well as the substitution of Na^+ by the impermeant cation, $NMDG^+$, inhibited the action of NaHS on the Fura-2 signal (Figure 7A, Table 4), suggesting a transient stimulation of Na^+-Ca^{2+}-exchange by H_2S.

Another possible pathway to decrease the cytosolic Ca^{2+} concentration is the sequestration of Ca^{2+} into intracellular Ca^{2+} storing organelles such as the endoplasmic reticulum. However, the fluorescence signal of Mag-Fura-2, a low Ca^{2+} affinity fluorescent dye which accumulates in these organelles, was unaltered by NaHS (Figure 5). However, it might be possible that a part of the cytosolic Ca^{2+} is taken up into the mitochondria due to the observed hyperpolarization (Figure 4), which would in addition contribute to the decrease in the cytosolic Ca^{2+} level.

These observations about the mechanism of the prosecretory action of H_2S differ from the data obtained from guinea pig and human colon, where neuronal capsaicin-sensitive cation (TRPV1) channels are thought to be the primary target of H_2S (Schicho *et al.*, 2006). In these tissues, H_2S excites afferent nerves (shown with extracellular recordings) that are thought to release substance P, which finally leads to the activation of cholinergic secretomotor neurons as shown by experiments with specific inhibitors (Krueger *et al.*, 2010). Also in rat colon, a part of the secretory response evoked by NaHS is inhibited by the neurotoxin, tetrodotoxin (Hennig and Diener, 2009), but there is a clear epithelial component, as can be seen from the increase in the cytosolic Ca^{2+} concentration of isolated colonic crypts free of any neuronal cells. The reason for this discrepancy is unclear, but may of course represent species difference. On the other hand, we used a relatively high concentration (10^{-2} mol·L^{-1}) of NaHS, which should result in H_2S concentrations even higher than in the colonic lumen, which are estimated to be in the range of up to 10^{-3} mol·L^{-1} (Krueger *et al.*, 2010), in order to obtain a consistent induction of all phases of the Isc response (see Results). Thus, there is the possibility that a high concentration of 10^{-2} mol·L^{-1} NaHS might – in addition to the clear neuronal effects –also stimulate tetrodotoxin-resistant responses in human or guinea pig colon.

What are the functional implications of the present results? H_2S is considered as a gaseous neurotransmitter used by enteric neurons to modulate gastrointestinal functions (Schicho *et al.*, 2006; Krueger *et al.*, 2010). As shown here, this gasotransmitter affects key processes for ion transport within the epithelium such as the cytosolic Ca^{2+} concentration, the activity of the Na^+-K^+-pump, that is, the 'motor' for all active transport processes, as well as the cellular K^+ conductance, which determines the height of the membrane potential. Furthermore, organosulphur compounds from dietary compounds such as garlic are known to be converted to H_2S in a glutathione-dependent manner inside the body; this may be the reason for the cardioprotective effect of garlic (Benavides *et al.*, 2007). If this process is to start during intestinal absorption, it is possible that organosulphur compounds could also exert actions on the intestinal epithelium, such as protective action against ischaemic damage due to the observed mitochondrial hyperpolarization (Figure 4). A further potential source of H_2S *in vivo* is sulphate-reducing bacteria (such as *Desulfovibrio* or *Desulfomonas* species). They are able to reduce SO_4^{2-}, contained in food or in intestinal secretions, to sulphides including H_2S (Florin *et al.*, 1991), and thereby contribute to a permanent exposure of the epithelium, especially of the colon, to H_2S, with its pronounced effects on epithelial ion transport. Plasma levels of H_2S have been reported in the range of 50–160 10^{-6} mol·L^{-1} (Zhao *et al.*, 2003). The local concentration in the vicinity of the intestinal epithelium is unknown, but the production rate has been measured for rat ileum to be in the range of 12 10^{-9} mol·min^{-1}·g^{-1} tissue (Zhao *et al.*, 2003). It has been reported that patients with ulcerative colitis have an increased number of sulphate-reducing bacteria (Roediger *et al.*, 1993), which produce sulphides including H_2S from SO_4^{2-} in the diet or S-containing amino acids. Consequently, the ability of H_2S to modulate basolateral K^+ channels and

thereby determine the driving force for epithelial secretion may also play a role in the pathogenesis of gastrointestinal diseases.

Acknowledgements

The diligent care of Mrs B. Brück, E. Haas, B. Schmitt and A. Stockinger is a pleasure to acknowledge. This study is supported by Deutsche Forschungsgemeinschaft, grant Di 388/11-1.

Conflict of interest

The authors state no conflict of interest.

References

Alexander SPH, Mathie A, Peters JA (2009). Guide to receptors and channels (GRAC), 4th edn. Br J Pharmacol 158 (Suppl. 1): S1–S254.

Baylor SM, Hollingworth S (2000). Measurement and interpretation of cytoplasmic [Ca^{2+}] signals from calcium-indicator dyes. News Physiol Sci 15: 19–26.

Benavides GA, Squadrito GL, Mills RW, Patel HD, Isbell TS, Patel RP *et al.* (2007). Hydrogen sulfide mediates the vasoactivity of garlic. Proc Natl Acad Sci USA 104: 17977–17982.

Binder HJ, Sandle GJ (1994). Electrolyte transport in the mammalian colon. In: Johnson LR (ed.). Physiology of the Gastrointestinal Tract, 3rd edn. Raven Press: New York, pp. 2133–2171.

Chávez-Piña AE, Tapia-Alvarez GR, Navarrete A (2010). Inhibition of endogenous hydrogen sulfide synthesis by PAG protects against ethanol-induced gastric damage in the rat. Eur J Pharmacol 630: 131–136.

Cook NS, Quast U (1990). Potassium channels. Structure, classification, function and therapeutic potential. In: Cook NS (ed.). Potassium Channel Pharmacology. Ellis Horwood: New York, pp. 181–255.

Distrutti E, Sediari L, Mencarelli A, Renga B, Orlandi S, Antonelli E *et al.* (2006). Evidence that hydrogen sulfide exerts antinociceptive effects in the gastrointestinal tract by activating K_{ATP} channels. J Pharmacol Exp Ther 316: 325–335.

Duchen MR, Smith PA, Ashcroft FM (1993). Substrate-dependent changes in mitochondrial function, intracellular free calcium concentration and membrane channels in pancreatic β-cells. Biochem J 294: 35–42.

Edwards A, Pallone TL (2007). Ouabain modulation of cellular calcium stores and signaling. Am J Physiol Renal Physiol 293: F1518–F1532.

Ekundi-Valentim E, Santos KT, Camargo EA, Denadai-Souza A, Teixeira SA, Zanoni CI *et al.* (2010). Differing effects of exogenous and endogenous hydrogen sulphide in carrageenan-induced knee joint synovitis in the rat. Br J Pharmacol 159: 1463–1474.

Elrod JW, Calvert JW, Morrison J, Doeller JE, Kraus DW, Tao L *et al.* (2007). Hydrogen sulfide attenuates myocardial ischemia-reperfusion injury by preservation of mitochondrial function. Proc Natl Acad Sci USA 104: 15560–15565.

Esechie A, Enkhbaatar P, Traber DL, Jonkam C, Lange M, Hamahata A *et al.* (2009). Beneficial effect of a hydrogen sulphide donor (sodium sulphide) in an ovine model of burn- and smoke-induced acute lung injury. Br J Pharmacol 158: 1442–1453.

Fiorucci S, Orlandi S, Mencarelli A, Caliendo G, Santagada V, Distrutti E *et al.* (2007). Enhanced activity of a hydrogen sulphide-releasing derivative of mesalamine (ATB-429) in a mouse model of colitis. Br J Pharmacol 150: 996–1002.

Florin T, Neale G, Gibson GR, Christl SU, Cummings JK (1991). Metabolism of dietary sulphate: absorption and excretion in humans. Gut 32: 766–773.

Garlid KD, Paucek P (2003). Mitochondrial potassium transport: the K^+ cycle. Biochim Biophys Acta 1606: 23–41.

Geng B, Cui YY, Zhao J, Yu F, Zhu Y, Xu G *et al.* (2007). Hydrogen sulfide downregulates the aortic L-arginine/nitric oxide pathway in rats. Am J Physiol Regul Integr Comp Physiol 293: R1608–R1618.

Grynkiewicz G, Poenie M, Tsien RY (1985). A new generation of Ca^{2+} indicators with greatly improved fluorescence properties. J Biol Chem 260: 3440–3450.

Hennig B, Diener M (2009). Actions of hydrogen sulfide on ion transport across rat distal colon. Br J Pharmacol 158: 1263–1275.

Hofer AM, Machen TE (1993). Technique for in situ measurement of calcium in intracellular inositol 1,4,5-trisphophate-sensitive stores using the fluorescent indicator Mag-Fura-2. Proc Natl Acad Sci USA 90: 2598–2602.

Inoue I, Nagase H, Kishi K, Higuti T (1991). ATP-sensitive K^+ channel in the mitochondrial inner membrane. Nature 352: 244–247.

Jöns T, Wittschieber D, Beyer A, Meier C, Brune A, Thomzig A *et al.* (2006). K^+-ATP-channel-related protein complexes: potential transducers in the regulation of epithelial tight junction permeability. J Cell Sci 119: 3087–3097.

Krippeit-Drews P, Dufer M, Drews G (2000). Parallel oscillations of intracellular calcium activity and mitochondrial membrane potential in mouse pancreatic B-cells. Biochem Biophys Res Commun 267: 179–183.

Krueger D, Foerster M, Mueller K, Zeller F, Slotta-Huspenina J, Donovan J *et al.* (2010). Signaling mechanisms involved in the intestinal pro-secretory

actions of hydrogen sulfide. Neurogastroenterol Motil doi: 10.1111/j.1365-2982.2010.01571.x.

Lee SW, Hu YS, Hu LF, Lu Q, Dawe GS, Moore PK *et al.* (2006). Hydrogen sulphide regulates calcium homeostasis in microglial cells. Glia 54: 116–124.

Lefer DJ (2008). Potential importance of alterations in hydrogen sulphide (H_2S) bioavailability in diabetes. Br J Pharmacol 155: 617–619.

Lindström CG, Rosengren JE, Fork FT (1979). Colon of the rat. An anatomic, histologic and radiographic investigation. Acta Radiol Diagn 20: 523–536.

Maguire D, MacNamara B, Cuffe JE, Winter D, Doolan CM, Urbach V *et al.* (1999). Rapid responses to aldosterone in human distal colon. Steroids 64: 51–63.

Parekh AB, Penner R (1997). Store depletion and calcium influx. Physiol Rev 77: 901–930.

Prinz G, Diener M (2008). Characterization of ryanodine receptors in the rat colonic epithelium. Acta Physiol 193: 151–162.

Reiffenstein RJ, Hulbert WC, Roth SH (1992). Toxicology of hydrogen sulfide. Annu Rev Pharmacol Toxicol 1992: 109–134.

Robinson JWL (1970). The difference in sensitivity to cardiac steroids of (Na^+-K^+)-stimulated ATPase and amino acid transport in the intestinal mucosa of the rat and other species. J Physiol 206: 41–60.

Roediger WEW, Duncan A, Kapaniris O, Millard S (1993). Sulphide impairment of substrate oxidation in rat colonocytes: a biochemical basis for ulcerative colitis? Clin Sci 85: 623–627.

Schicho R, Krueger D, Zeller F, von Weyhern CWH, Frieling T, Kimura H *et al.* (2006). Hydrogen sulfide is a novel prosecretory neuromodulator in the guinea-pig and human colon. Gastroenterology 131: 1542–1552.

Schultheiss G, Diener M (1997). Regulation of apical and basolateral K^+ conductances in the rat colon. Br J Pharmacol 122: 87–94.

Schultheiss G, Kocks SL, Diener M (2002). Methods for study of ionic currents and Ca^{2+} signals in isolated colonic crypts. Biol Proced Online 3: 70–78.

Seino S, Miki T (2003). Physiological and pathophysiological roles of ATP-sensitive K^+ channels. Prog Biophys Mol Biol 81: 133–176.

Seip G, Schultheiss G, Kocks SL, Diener M (2001). Interaction between store-operated nonselective cation channels and Na^+-Ca^{2+}-exchanger during secretion in the rat colon. Exp Physiol 86: 461–468.

Siefjediers A, Hardt M, Prinz G, Diener M (2007). Characterization of inositol 1,4,5-trisphosphate (IP_3) receptor subtypes at rat colonic epithelium. Cell Calcium 41: 303–315.

Strabel D, Diener M (1995). Evidence against direct activation of chloride secretion by carbachol in the rat distal colon. Eur J Pharmacol 274: 181–191.

Teague B, Asiedu S, Moore PK (2002). The smooth muscle relaxant effect of hydrogen sulphide in vitro: evidence for a physiological role to control intestinal contractility. Br J Pharmacol 137: 139–145.

Trepakova ES, Cohen RA, Bolotina VM (1999). Nitric oxide inhibits capacitative cation influx in human platelets by promoting sarcoplasmic/endoplasmic reticulum Ca^{2+}-ATPase-dependent refilling of Ca^{2+} stores. Circulation Res 84: 201–209.

Wang R (2002). Two's company, three's a crowd: can H_2S be the third endogenous gaseous transmitter? FASEB J 16: 1792–1798.

Warth R, Barhanin J (2003). Function of K^+ channels in the intestinal epithelium. J Membr Biol 193: 67–78.

Yang W, Yang G, Jia X, Wu L, Wang R (2005). Activation of K_{ATP} channels by H_2S in rat insulin-secreting cells and the underlying mechanisms. J Physiol 569: 519–531.

Zhao W, Zhang J, Lu Y, Wang R (2001). The vasorelaxant effect of H_2S as a novel endogenous gaseous K_{ATP} channel opener. EMBO J 20: 6008–6016.

Zhao W, Ndisang JS, Wang R (2003). Modulation of endogenous production of H_2S in rat tissues. Can J Physiol Pharmacol 81: 848–853.

8.2. "Modulation of ion transport across rat distal colon by cysteine"

Pouokam E, Diener M. *Physiol. Membr. Physiol. Biophys* (2012). **3:** Art. 43.

Impakt Faktor: 2.97

Eigener Anteil an der Publikation:

- Initiative: 60 %
- Projektplanung: 50 %
- Durchführung der Versuche: 75 %
- Auswertung der Experimente: 75 %
- Erstellung der Publikation: 75 %

frontiers in PHYSIOLOGY

ORIGINAL RESEARCH ARTICLE
published: 02 March 2012
doi: 10.3389/fphys.2012.00043

Modulation of ion transport across rat distal colon by cysteine

Ervice Pouokam and Martin Diener*

Institute for Veterinary Physiology and Biochemistry, University Giessen, Giessen, Germany

Edited by:
Wolfgang G. Clauss, Justus-Liebig-University Giessen, Germany

Reviewed by:
Beate Illek, Children's Hospital and Research Center Oakland, USA
Salah Amasheh, Charité Universitätsmedizin Berlin, Germany
Yoshinori Marunaka, Kyoto Prefectural University of Medicine, Japan

***Correspondence:**
Martin Diener, Institut für Veterinär-Physiologie und –Biochemie, Justus-Liebig-Universität Gießen, Frankfurter Str. 100, D-35392 Gießen, Germany.
e-mail: martin.diener@vetmed.uni-giessen.de

The aim of this study was to identify the actions of stimulation of endogenous production of H_2S by cysteine, the substrate for the two H_2S-producing enzymes, cystathionine-β-synthase and cystathionine-γ-lyase, on ion transport across rat distal colon. Changes in short-circuit current (Isc) induced by cysteine were measured in Ussing chambers. Free cysteine caused a concentration-dependent, transient fall in Isc, which was sensitive to amino-oxyacetate and β-cyano-L-alanine, i.e., inhibitors of H_2S-producing enzymes. In contrast, Na cysteinate evoked a biphasic change in Isc, i.e., an initial fall followed by a secondary increase, which was also reduced by these enzyme inhibitors. All responses were dependent on the presence of Cl^- and inhibited by bumetanide, suggesting that free cysteine induces an inhibition of transcellular Cl^- secretion, whereas Na cysteinate – after a transient inhibitory phase – activates anion secretion. The assumed reason for this discrepancy is a fall in the cytosolic pH induced by free cysteine, but not by Na cysteinate, as observed in isolated colonic crypts loaded with the pH-sensitive dye, BCECF. Intracellular acidification is known to inhibit epithelial K^+ channels. Indeed, after preinhibition of basolateral K^+ channels with tetrapentylammonium or Ba^{2+}, the negative Isc induced by free cysteine was reduced significantly. In consequence, stimulation of endogenous H_2S production by Na cysteinate causes, after a short inhibitory response, a delayed activation of anion secretion, which is missing in the case of free cysteine, probably due to the cytosolic acidification. In contrast, diallyl trisulfide, which is intracellularly converted to H_2S, only evoked a monophasic increase in Isc without the initial fall observed with Na cysteinate. Consequently, time course and amount of produced H_2S seem to strongly influence the functional response of the colonic epithelium evoked by this gasotransmitter.

Keywords: Cl^- secretion, cysteine, cytosolic pH, electrolyte transport, H_2S, rat colon

INTRODUCTION

Colonic ion transport is not only controlled by classical neurotransmitters or hormones (for review see Binder and Sandle, 1994), but is also influenced by gasotransmitters such as nitric oxide (Toda and Herman, 2005), carbon monoxide (Steidle and Diener, 2011), or hydrogen sulfide (Schicho et al., 2006; Hennig and Diener, 2009). The latter gas is produced from the amino acid cysteine via the enzymes cystathionine-β-synthase and cystathionine-γ-lyase (Wang, 2002; Martin et al., 2010). Both enzymes are found within enteric ganglia of guinea-pig and human colon (Schicho et al., 2006) as well as in smooth muscle layers and the epithelium of rat colon (Hennig and Diener, 2009). Plasma levels of H_2S are reported in the range of 50–160 $\mu mol \cdot l^{-1}$ (Zhao et al., 2003). The local concentration within the intestinal wall is unknown, but the production rate of H_2S has been measured for rat ileum to be in the range of 12 $nmol \cdot min^{-1} \cdot g^{-1}$ tissue (Zhao et al., 2003). Furthermore, there is an upregulation of H_2S production during experimental colitis in rats (Wallace et al., 2009), so that rat colon is an interesting model to investigate the modulation of ion transport by this gasotransmitter.

Hydrogen sulfide, which can be released from a donor molecule such as NaHS (Lee et al., 2006), evokes a Cl^- secretion in guinea-pig and human colon. In these tissues, the primary action site of this H_2S donor are enteric neurons, where H_2S is thought to act at capsaicin-sensitive cation channels of the type transient receptor potential vanilloid receptor 1 (TRPV1; Schicho et al., 2006). The consequence is a release of substance P and an activation of secretomotor submucosal neurons, which finally induce epithelial anion secretion (Krueger et al., 2010). This is supported by the observation that NaHS does not evoke anion secretion in the human colonic cell line, T84 (Schicho et al., 2006). Another mechanism of action of NaHS was observed in rat colon. In this tissue, NaHS evokes a triphasic change in Isc, which is a measure of net ion movement across the epithelium. An initial increase in Isc (mediated by Cl^- secretion) was followed by a transient fall (assumed to represent a transient K^+ secretion), before the Isc finally rose again to a long-lasting Cl^- secretory response. Partial resistance against the neurotoxin, tetrodotoxin, and inhibition by glibenclamide, which acts as blocker of ATP-sensitive K^+ channels (Cook and Quast, 1990), as well as tetrapentylammonium, known as inhibitor of Ca^{2+}-dependent K^+ channels (Maguire et al., 1999), indicated an action at epithelial K^+ channels (Hennig and Diener, 2009). Direct epithelial actions of H_2S released from NaHS were observed in experiments at isolated colonic crypts loaded with

the Ca^{2+}-sensitive fluorescent dye, fura-2, where NaHS evoked a biphasic change in the cytosolic Ca^{2+} concentration ($[Ca^{2+}]_i$), i.e., an initial decrease followed by a secondary increase (Pouokam and Diener, 2011). Consequently, there seem to be pronounced species differences in the mechanism of action of NaHS.

In the literature, there is a controversy about beneficial and/or adverse effects of H_2S on intestinal functions. The above mentioned *in vitro* studies, although differing in the presumed mechanisms of action, indicate a prosecretory action of this putative gasotransmitter, which – *in vivo* – would aggravate gastrointestinal symptoms such as diarrhoe, e.g., during inflammatory bowel disease. Indeed, H_2S exerts proinflammatory actions in a mouse model of acute pancreatitis (Tamizhselvi et al., 2007). Further negative actions of H_2S on gastrointestinal integrity have been deduced from the observation that inhibition of H_2S synthesis by propargylglycine protects rats from ethanol-induced gastritis (Chávez-Piña et al., 2010). In contrast, other experimental evidence clearly demonstrates beneficial effects of this gasotransmitter. Exogenous H_2S exerts an antiinflammatory and antinociceptive action during synovitis in rats (Ekundi-Valentim et al., 2010). The H_2S-releasing derivative of mesalamine, ATB-429, is highly effective as therapeutic in a model of murine colitis (Fiorucci et al., 2007). Further protective actions of hydrogen sulfide are observed in the heart, where this gasotransmitter protects against ischemia/reperfusion damage (Ji et al., 2008). In contrast to the model of ethanol-induced gastritis (Chávez-Piña et al., 2010), where the beneficial effect of blockade of H_2S synthesis suggests proinflammatory actions of H_2S, the gastric damage caused by inhibitors of cyclooxygenases has been found to be reduced when using a cyclooxygenase inhibitor which simultaneously releases H_2S (Wallace et al., 2010). As in some studies both inhibition of H_2S synthesis as well as its stimulation by cysteine, the precursor for H_2S production, exert a similar response (Chávez-Piña et al., 2010), one reason for this discrepancy in the literature might be that the effect evoked by H_2S may differ in situations, where endogenous enzymes probably produce relative low concentrations of this gasotransmitter, and situations, in which exogenous donor molecules might release higher concentrations of H_2S.

Consequently, in the present study we investigated changes in ion transport across rat colon, in which we had previously characterized the effect of the exogenous H_2S donor, NaHS (Hennig and Diener, 2009; Pouokam and Diener, 2011), induced by cysteine as precursor of endogenous H_2S formation within the tissue. Ussing chamber experiments and experiments with the pH-sensitive dye, BCECF, were used in order to identify the mechanisms involved.

MATERIALS AND METHODS

SOLUTIONS

The standard solution for the Ussing chamber experiments was a buffer solution containing (mmol·l^{-1}): NaCl 107, KCl 4.5, $NaHCO_3$ 25, Na_2HPO_4 1.8, NaH_2PO_4 0.2, $CaCl_2$ 1.25, $MgSO_4$·1 and glucose 12. The solution was gassed with carbogen (5% CO_2 in 95% O_2, vol·vol^{-1}); pH was 7.4. For the Cl^--free buffer, NaCl and KCl were equimolarly substituted by Na gluconate and K gluconate, respectively.

For the experiments carried out with isolated crypts, the following buffers were used. The EDTA (ethylenediamino-tetraacetic acid) solution for the isolation contained (mmol·l^{-1}): NaCl 107, KCl 4.5, $NaHCO_3$ 25, Na_2HPO_4 1.8, NaH_2PO_4 0.2, glucose 12.2, EDTA 10 and 1 g·l^{-1} bovine serum albumin (BSA). It was gassed with carbogen; pH was adjusted by *tris*-base (*tris*(hydroxymethyl)-aminomethane) to 7.4. The isolated crypts were stored in a high potassium Tyrode solution consisting of (mmol·l^{-1}): K gluconate 100, KCl 30, HEPES (*N*-(2-hydroxyethyl)piperazine-*N*′-2-ethanesulfonic acid) 10, NaCl 20, $MgCl_2$ 1, $CaCl_2$ 1.25, glucose 12.2, sodium pyruvate 5, and 1 g·l^{-1} BSA; pH was 7.4. For superfusion of the isolated crypts during the imaging experiments, the following buffer was used (in mmol·l^{-1}): NaCl 140, KCl 5.4, $CaCl_2$ 1.25, $MgSO_4$ 1, HEPES 10, glucose 12.2. pH was 7.4.

TISSUE PREPARATION AND CRYPT ISOLATION

Wistar rats of both sexes were used with a weight of 180–240 g. The animals had free access to water and a standard rat diet until the day of the experiment. Animals were killed by a blow on the head followed by exsanguination (approved by Regierungspräsidium Gießen, Gießen, Germany). The serosa and muscularis propria were stripped away to obtain a mucosa–submucosa preparation of the distal colon. The distal colon was distinguished from the proximal colon by the absence of palm leaf-like striae (Lindström et al., 1979). Briefly, the colon was placed on a small plastic rod with a diameter of 5 mm. A circular incision was made near the anal end with a blunt scalpel and the serosa together with the lamina propria were gently removed in a proximal direction. Two segments of the distal colon of each rat were prepared. In general, one tissue served to measure the control response evoked by cysteine and the other to measure the response in the presence of a putative inhibitor (see below). There was no obvious segment dependence in the Isc evoked by cysteine between the early and the late distal colon (data not shown).

For the isolation of intact crypts, the mucosa–submucosa was fixed on a plastic holder with tissue adhesive and transferred for about 7 min to the EDTA solution. The mucosa was vibrated once for 30 s in order to obtain crypts. They were collected in a high-K^+ gluconate Tyrode buffer (Böhme et al., 1991).

SHORT-CIRCUIT CURRENT MEASUREMENT

The mucosa–submucosa preparation was fixed in a modified Ussing chamber, bathed with a volume of 3.5 ml on each side of the mucosa. The tissue was incubated at 37°C and short-circuited by a computer-controlled voltage-clamp device (Ingenieur Büro für Mess- und Datentechnik Mussler, Aachen, Germany) with correction for solution resistance. Tissue conductance (Gt) was measured every min by the voltage deviation induced by a current pulse (±50 μA, duration 200 ms) under open-circuit conditions. Short-circuit current (Isc) was continuously recorded on a chart-recorder. Isc is expressed as $\mu Eq \cdot h^{-1} \cdot cm^{-2}$, i.e., the flux of a monovalent ion per time and area, with $1\,\mu Eq \cdot h^{-1} \cdot cm^{-2} = 26.9\,\mu A \cdot cm^{-2}$.

In general, one tissue served to measure the control responses evoked by at least two administrations of cysteine. The other tissue was pretreated with putative inhibitors before the second cysteine administration. If the inhibitor had to be administered in

a solvent, the control tissue was pretreated with the solvent, too. After each cysteine administration, the serosal compartment was washed three times with five times the chamber volume.

IMAGING EXPERIMENTS

Relative changes in the cytosolic pH were measured using BCECF [2′,7′-*bis*(carboxyethyl)-5,6-carboxyfluorescein/acetomethoxy methyl; Life Technologies, Darmstadt, Germany], a pH-sensitive fluorescent dye (Rink et al., 1982). The crypts were pipetted into the experimental chamber with a volume of about 3 ml. They were attached to the glass bottom of the chamber with the aid of poly-L-lysine (0.1 $g \cdot l^{-1}$; Biochrom, Berlin, Germany). The crypts were incubated for 45 min with 8 $\mu mol \cdot l^{-1}$ BCECF/acetoxymethylester (AM). Then the dye ester not taken up by the cells was washed away. The preparation was superfused hydrostatically throughout the experiment with 140 $mmol \cdot l^{-1}$ NaCl Tyrode. Perfusion rate was about 1 $ml \cdot min^{-1}$.

Changes in the cytosolic pH values were monitored as changes in the BCECF ratio (R; emission at an excitation wave length of 500 nm divided by the emission at an excitation wave length of 450 nm). For each experiment, it was waited until a stable baseline had developed before cysteine or any other substance was administered. Changes in the BCECF ratio induced by free cysteine or Na cysteinate are expressed as change in relation to this baseline just prior administration of cysteine or the corresponding substance (Δ BCECF ratio). Experiments were carried out on an inverted microscope (Olympus IX-50; Olympus, Hamburg, Germany) equipped with an epifluorescence set-up and an image analysis system (Till Photonics, Martinsried, Germany). Several regions of interest, each with the size of about one cell, were placed over an individual crypt. The emission above 520 nm was measured from the regions of interest. Data were sampled at 0.2 Hz. The baseline in the fluorescence ratio of BCECF was measured for several minutes before drugs were administered.

DRUGS

BCECF/AM and diallyl trisulfide (Cayman, Ann Harbor, USA) were dissolved in dimethylsulfoxide (DMSO; final maximal concentration 0.3 $ml \cdot l^{-1}$). Bumetanide and forskolin were dissolved in ethanol (final maximal concentration 2.5 $ml \cdot l^{-1}$). Tetrodotoxin was dissolved in 2×10^{-2} $mol \cdot l^{-1}$ citrate buffer. Amino-oxyacetate (AOA), $BaCl_2$, carbachol, β-cyano-L-alanine (CLA), L-cysteine, GYY 4137 (*p*-methoxyphenyl)morpholino-phosphinodithioic acid; Cayman, Ann Harbor, USA), L-methionine, and tetrapentylammonium (TPeA) chloride were dissolved in aqueous stock solutions. Na cysteinate was prepared by dissolving free cysteine equimolarly in 1 $mol \cdot l^{-1}$ NaOH. Charybdotoxin was dissolved in an aqueous stock solution containing 1 $g \cdot l^{-1}$ BSA. If not indicated differently, drugs were from Sigma, Taufkirchen, Germany.

STATISTICS

Values are given as means ± 1 SEM. In the case that means of several groups had to be compared, an analysis of variance was performed followed by *post hoc* test of Tukey. For the comparison of two groups, either a Student's t-test or a Mann Whitney U-test was applied. An F-test decided which test method had to be used. Both paired and unpaired two-tailed Student's t-tests were applied as appropriate. $P < 0.05$ was considered to be statistically significant.

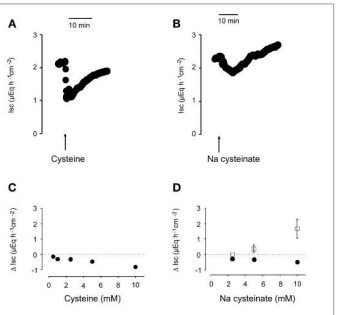

FIGURE 1 | Time course of the monophasic Isc response to free cysteine [(A), 10^{-2} mol·l^{-1} at the serosal side; indicated by the arrow] and of the biphasic response evoked by Na cysteinate [(B), 10^{-2} mol·l^{-1} at the serosal side; indicated by the arrow]. (**C,D**) Concentration-dependent initial decrease (filled circles) and secondary increase (filled squares) in Isc induced by serosal administration of free cysteine **(C)** or Na cysteinate **(D)** in mucosa–submucosa preparations of rat distal colon. The data are given as change of Isc (Δ Isc) compared to baseline (indicated by the dashed line) just prior administration of the amino acid. Each administration of the amino acid in **(C,D)** was followed by three times washing the serosal compartment with fresh, cysteine-free buffer solution. Values are given as means (symbols) ± SEM (bars), $n = 8$. The decrease in Isc was statistically significant ($P < 0.05$, paired t-test) for all concentrations of free cysteine or Na cysteinate tested, whereas the increase in Isc evoked by Na cysteinate reached statistical significance only for the highest concentration tested (10^{-2} mol·l^{-1}).

RESULTS

EFFECT OF CYSTEINE ON SHORT-CIRCUIT CURRENT

L-Cysteine, when administered to the serosal side of the tissue, induced a prompt decrease in Isc (see, e.g., **Figure 1A** for time course). The decrease in Isc was concentration-dependent (**Figure 1C**). A significant fall in baseline Isc was evoked by the lowest concentration used (5×10^{-4} $mol \cdot l^{-1}$ at the serosal side) and was maximal at a concentration of 10^{-2} $mol \cdot l^{-1}$ at the serosal side. Most of the further experiments were performed with an intermediate concentration (5×10^{-3} $mol \cdot l^{-1}$) of cysteine. The decrease in Isc was not mimicked by another S-containing amino acid, L-methionine. L-Methionine, when administered at a concentration of 5×10^{-3} $mol \cdot l^{-1}$ (at the serosal side), did not evoke a significant change in Isc ($n = 8$; data not shown). Cysteine and methionine are known to block K^+ channels of the type TREK-1 (Park et al., 2005). The failure of methionine to mimic the cysteine response indicates that such a mechanism (or non-specific osmotic effects) cannot be the reason for the change in Isc induced by cysteine.

A potential problem in the administration of free cysteine is the fact that this amino acid, despite the high buffer capacity of the buffer solution used, caused a fall in the pH of this solution, which might (and indeed does, see below) cause an acidification of the intracellular milieu (see cytosolic pH measurements below). Therefore, in a second series of experiments, cysteine was neutralized by NaOH. When administered as Na cysteinate, the time course of the Isc response evoked by the amino acid changed: an initial fall, which developed slower compared to the corresponding response evoked by free cysteine, was followed by a secondary increase above the baseline, which was not observed in the case of free cysteine (**Figure 1B**). Both phases exhibited a clear concentration dependence (**Figure 1D**). When Na cysteinate (5×10^{-3} mol·l^{-1}) was administered to the mucosal side, there was no significant change in Isc ($n = 5$, data not shown).

The effect of free cysteine (2.5×10^{-3} mol·l^{-1} at the serosal side) on Isc was significantly reduced, when the tissue was pretreated with a combination of amino-oxyacetate (5×10^{-3} mol·l^{-1} at the serosal side), an inhibitor of the enzyme cystathionine-β-synthase, and β-cyano-L-alanine (5×10^{-3} mol·l^{-1} at the serosal side), an inhibitor of the enzyme cystathionine-γ-lyase (for references to both inhibitors, see Zhao et al., 2003). In the presence of these inhibitors, cysteine only induced a fall in Isc of -0.17 ± 0.044 μEq·h^{-1}·cm^{-2} compared to -0.41 ± 0.090 μEq·h^{-1}·cm^{-2} in tissues which were – for osmotic reasons – pretreated with mannitol (10^{-2} mol·l^{-1} at the serosal side) instead of the two enzyme inhibitors ($n = 6$, $P < 0.05$; **Table 1**). When a higher concentration of cysteine (5×10^{-3} mol·l^{-1} at the serosal side) was used, the reduction in the cysteine response by these two blockers lost statistical significance. This observation would be consistent with the assumption of a competitive action of the two inhibitors on the H_2S-producing enzymes; a mechanism of inhibition, which has indeed been shown for β-cyano-L-alanine (Pfeffer and Ressler, 1967). Also both phases of the Isc response evoked by Na cysteinate were reduced by the enzyme inhibitor combination. In the presence of the inhibitors of H_2S-producing enzyme, Na cysteinate (10^{-2} mol·l^{-1} at the serosal side) evoked an initial fall in Isc of only -0.16 ± 0.029 μEq·h^{-1}·cm^{-2} ($n = 8$) compared to -0.46 ± 0.10 μEq·h^{-1}·cm^{-2} in the absence of the inhibitors ($n = 8$, $P < 0.05$). The secondary increase in Isc evoked by Na cysteinate was reduced from 1.05 ± 0.49 μEq·h^{-1}·cm^{-2} ($n = 8$) under control conditions to 0.50 ± 0.14 μEq·h^{-1}·cm^{-2} ($n = 8$) in the presence of the inhibitors, although the latter difference did not reach statistical significance due to the large variation of the control response.

Table 1 | Effect of free cysteine in the presence of inhibitors of H_2S synthesizing enzymes.

	Δ Isc (μEq·h^{-1}·cm^{-2})	
	+ AOA/CLA	− AOA/CLA
Free cysteine 2.5×10^{-3} mol·l^{-1}	-0.17 ± 0.044*	-0.41 ± 0.090
Free cysteine 5×10^{-3} mol·l^{-1}	-0.37 ± 0.088	-0.49 ± 0.094

*Effect of free cysteine (at the serosal side) in the absence (–; right column) or presence (+; middle column) of a combination of amino-oxyacetate (AOA, 5×10^{-3} mol·l^{-1} at the serosal side; cystathionine-β-synthase blocker) and β-cyano-L-alanine (CLA, 5×10^{-3} mol·l^{-1} at the serosal side, cystathionine-γ-lyase blocker). The control tissues (-AOA/CLA) were treated with mannitol (10^{-2} mol·l^{-1} at the serosal side). Data are given as change of Isc (Δ Isc) compared to baseline just prior administration of the respective cysteine concentration and are means ± SEM, n = 6. *P < 0.05 versus response to the same concentration of cysteine in the absence of the two enzyme inhibitors.*

Table 2 | Effect of free cysteine after inhibition of Cl^- secretion.

	Δ Isc (μEq·h^{-1}·cm^{-2}) evoked by free cysteine	
	Control	±Inhibitor
Cl^- free	-0.87 ± 0.14^a	-0.17 ± 0.036^b
With Cl^-	-0.78 ± 0.15^a	-0.74 ± 0.19^a
With bumetanide	-0.94 ± 0.19^a	-0.42 ± 0.10^b
Without bumetanide	-0.95 ± 0.19^a	-0.86 ± 0.21^a

The effect of free cysteine (5×10^{-2} mol·l^{-1} at the serosal side) on Isc was tested in the absence of any inhibitors (control), then in the presence or absence of the respective inhibitor (or replacement of Cl^- with the impermeable anion gluconate). The first two rows give the response to free cysteine in the absence or presence of Cl^- ion in the buffer, whereas in the subsequent rows bumetanide (10^{-4} mol·l^{-1} at the serosal side) was used as inhibitor. Data are given as change of Isc (Δ Isc) compared to baseline just prior administration of the respective cysteine administration and are means ± SEM, n = 7. Different letters (a, b) indicate statistically homogenous groups (analysis of variances followed by post hoc test of Tukey).

The negative Isc induced by cysteine did not show a desensitization. When free cysteine (5×10^{-3} mol·l^{-1} at the serosal side) was administered two times to the same tissue with a washing procedure between the individual administrations (see Materials and Methods), there was no significant decrease in the Isc response evoked by this amino acid (see, e.g., **Tables 2** and **4**, control responses). The same was observed for the biphasic change in Isc induced by Na cysteinate, which could be repetitively evoked at the same tissue without a reduction in either the initial fall nor in the final increase in Isc (see **Table 3**, control responses). In contrast, there was even a tendency (especially for Na cysteinate) that the second administration of the amino acid evoked larger changes in Isc than the first administration; a phenomenon, however, which was not studied further here.

Consequently, for all inhibitor experiments designed to clarify the mechanism of action of cysteine the following protocol was used. The response to cysteine was first measured in each tissue under control conditions, i.e., in the absence of other drugs. After a washing step, the response evoked by cysteine was measured in the presence of a putative inhibitor.

A CHANGE IN Cl^- SECRETION UNDERLIES THE CYSTEINE-INDUCED Isc

The negative Isc induced by free cysteine can, in principle, be caused by two mechanisms: an inhibition of spontaneous Cl^- secretion, which is responsible for the generation of the positive baseline Isc in rat colon (see, e.g., Strabel and Diener, 1995),

Table 3 | Effect of Na cysteinate after inhibition of Cl^- secretion.

	Δ Isc (μEq·h^{-1}·cm^{-2}) evoked by Na cysteinate			
	Control		± Inhibitor	
	Initial decrease	Peak	Initial decrease	Peak
Cl^- free	-0.59 ± 0.16^{a}	$0.24 \pm 0.16^{a,b}$	-0.17 ± 0.015^{a}	-0.03 ± 0.041^{a}
With + Cl^-	-0.81 ± 0.26^{a}	-0.11 ± 0.25^{a}	-0.59 ± 0.16^{a}	0.72 ± 0.26^{b}
With bumetanide	$-0.49 \pm 0.25^{a,b}$	0.23 ± 0.21^{b}	-0.23 ± 0.016^{a}	-0.021 ± 0.090^{a}
Without bumetanide	$-0.68 \pm 0.13^{a,b}$	0.37 ± 0.22^{a}	-1.12 ± 0.16^{b}	0.85 ± 0.61^{a}

The effect of Na cysteinate (10^{-2} mol·l^{-1} at the serosal side) on Isc was tested in the absence of any inhibitors (control), then in the presence or absence of the respective inhibitor (or replacement of Cl^- with the impermeable anion gluconate). The first two rows give the response to Na cysteinate in the absence or presence of Cl^- ion in the buffer, whereas in the subsequent rows bumetanide (10^{-4} mol·l^{-1} at the serosal side) was used as inhibitor. Data are given as change of Isc (Δ Isc) compared to baseline just prior administration of the respective Na cysteinate administration and are means ± SEM, n = 7–8. Different letters (a, b) indicate statistically homogenous groups (analysis of variances followed by post hoc test of Tukey).

or the induction of the secretion of cations, i.e., the induction of K^+ secretion (see, e.g., Hörger et al., 1998). The negative Isc evoked by free cysteine was strongly dependent on the presence of Cl^-. In the presence of Cl^-, cysteine (5×10^{-3} mol·l^{-1} at the serosal side) evoked a fall in Isc of -0.87 ± 0.14 μEq·h^{-1}·cm^{-2}. This change in Isc was reduced by about 80%, when the amino acid was administered to the same tissue after substitution of Cl^- by the impermeant anion, gluconate, on both sides of the tissue (**Table 2**). Similarly, both the initial fall as well as the secondary increase in Isc evoked by Na cysteinate (10^{-2} mol·l^{-1} at the serosal side) were significantly reduced in the absence of Cl^- (**Table 3**).

A significant inhibition of the cysteine-evoked Isc was also observed, when the Na^+–K^+–2 Cl^--cotransporter, the dominant Cl^--loading mechanism in the basolateral membrane necessary to maintain transepithelial Cl^- secretion (Kaplan et al., 1996), was blocked with bumetanide (10^{-4} mol·l^{-1} at the serosal side; **Figure 2** and **Table 2**). Bumetanide inhibited the biphasic change in Isc induced by Na cysteinate (10^{-2} mol·l^{-1} at the serosal side) to a similar extent (**Table 3**).

The further experiments, which served to elucidate the potential role of changes in K^+ transport in the negative Isc evoked by the amino acid were performed only with free cysteine in order to avoid any contamination of the measured currents with the secondary increase in Isc, i.e., the parallel induction of Cl^- secretion observed with Na cysteinate. In contrast to two maneuvers interfering with Cl^- secretion (i.e., anion substitution and inhibition of the Na^+–K^+–2 Cl^--cotransporter), inhibition of apical K^+ channels, which are a prerequisite for colonic K^+ secretion (Sørensen et al., 2010), did not change the cysteine response. None of the K^+ channel blockers tested (for references to these K^+ channel blockers, see Cook and Quast, 1990) had any significant effect on the Isc evoked by free cysteine. Neither Ba^{2+} (10^{-2} mol·l^{-1} at the mucosal side), a broad K^+ channel blocker affecting many types of K^+ channels, nor tetrapentylammonium (10^{-4} mol·l^{-1} at the mucosal side), a blocker with some preference for Ca^{2+}-dependent K^+ channels (Maguire et al., 1999), nor charybdotoxin (2×10^{-7} mol·l^{-1} at the mucosal side), a selective blocker of large-conductance (BK_{Ca}) Ca^{2+}-dependent K^+ channels (Berkefeld et al., 2010), had any significant effect on the

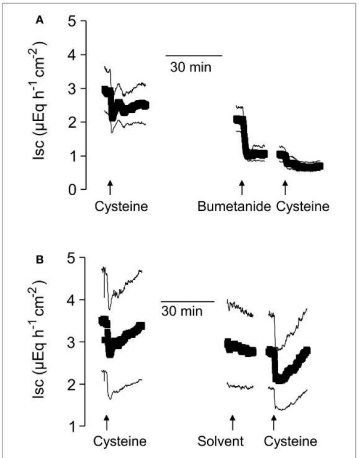

FIGURE 2 | After suppression of Cl^- secretion with bumetanide, the action of cysteine is prevented. Shown are the effects of two administrations of free cysteine (5×10^{-3} mol·l^{-1} at the serosal side; indicated by the arrows) in mucosa–submucosa preparations of rat distal colon. The line interruptions are caused by omission of current artifacts induced by washing the serosal compartment three times with five times the chamber volume, before the next administration of cysteine followed. The effect of cysteine was first tested in the absence of any inhibitors and then in the presence **(A)** or absence **(B)** of bumetanide (10^{-4} mol·l^{-1} at the serosal side). The solvent for bumetanide (ethanol) was administered to the tissues which were not treated with bumetanide. Values are means (symbols) ± SEM (lines), $n = 7$. For statistics, see **Table 2**.

negative Isc induced by free cysteine (**Table 4**). Consequently, these data allow the conclusion that the negative Isc evoked by cysteine is caused by an inhibition of spontaneous anion secretion and not due to an activation of transepithelial K^+ secretion.

This conclusion was corroborated by experiments in which K^+ channel blockers were administered to the serosal side of the tissue. A sufficient basolateral K^+ conductance is necessary to maintain basal membrane potential as driving force for Cl^- exit across apical Cl^- channels (Strabel and Diener, 1995). Blockade of basolateral K^+ channels with Ba^{2+} (10^{-2} mol·l^{-1} at the serosal side) or tetrapentylammonium (10^{-4} mol·l^{-1} at the serosal side) significantly inhibited the negative Isc evoked by free cysteine. In contrast, charybdotoxin (2×10^{-7} mol·l^{-1} at the serosal side) was ineffective (**Table 4**). In these series of experiments with K^+ channel blockers, a clear tendency for increased cysteine effects was observed in the experiments designed to measure the effect of Ba^{2+}. The reason for this discrepancy to the other experimental series may be that these experiments were performed in HCO_3^--free, HEPES buffered Tyrode solution (in order to avoid precipitation of Ba^{2+} as carbonate or sulfate salt). This phenomenon, however, was not studied further.

Table 4 | Effect of free cysteine after blockade of K^+ channels.

	Δ Isc (μEq·h^{-1}·cm^{-2}) evoked free cysteine	
	Control	**± Inhibitor**
With serosal Ba^{2+}	-1.30 ± 0.17^a	-0.78 ± 0.10^b
Without serosal Ba^{2+}	-1.57 ± 0.19^a	-2.02 ± 0.40^a
With serosal TPeA	-0.58 ± 0.12^a	-0.18 ± 0.039^b
Without serosal TPeA	-0.82 ± 0.13^a	-1.14 ± 0.28^a
With serosal CTX	-1.01 ± 0.11^a	-0.86 ± 0.13^a
Without serosal CTX	-0.81 ± 0.1^a	-0.62 ± 0.098^a
With mucosal Ba^{2+}	-0.89 ± 0.082^a	$-1.64 \pm 0.30^{a,b}$
Without mucosal Ba^{2+}	-0.80 ± 0.078^a	-1.30 ± 0.098^b
With mucosal TPeA	-0.56 ± 0.10^a	-0.63 ± 0.13^a
Without mucosal TPeA	-0.61 ± 0.067^a	-0.59 ± 0.093^a
With mucosal CTX	-0.79 ± 0.096^a	$-0.56 \pm 0.046^{a,b}$
Without mucosal CTX	-0.78 ± 0.087^a	-0.75 ± 0.15^a

The effect of free cysteine (5 × 10^{-3} mol·l^{-1} at the serosal side) on Isc was tested in the absence of any inhibitors (control) and then in the presence or absence of the respective inhibitor. The following K^+ channel blockers were applied either at the serosal or the mucosal side: Ba^{2+} (10^{-2} mol·l^{-1}), tetrapentylammonium (TPeA; 10^{-4} mol·l^{-1}), and charybdotoxin (CTX; 2.10^{-7} mol·l^{-1}). The experiments with Ba^{2+} were performed in HCO_3^--free Tyrode buffer solution in order to avoid precipitation of Ba carbonate. The reason for the apparent enhancement of the cysteine response in this buffer is unknown. Data are given as change of Isc (Δ Isc) compared to baseline just prior administration of the respective cysteine administration and are means ± SEM, n = 7–8. Different letters (a, b) indicate statistically homogenous groups (analysis of variances followed by post hoc test of Tukey).

DO ENTERIC NEURONS PARTICIPATE IN THE RESPONSE TO CYSTEINE?

Immunohistochemical experiments have demonstrated that the H_2S-producing enzymes, cystathionine-β-synthase and cystathionine-γ-lyase, are expressed within the epithelium, but also in muscle cells and neurons (Schicho et al., 2006; Hennig and Diener, 2009). Consequently, it seemed to be of interest whether enteric neurons might mediate the response evoked by cysteine. The effect of free cysteine (5×10^{-3} mol·l^{-1} at the serosal side) on Isc was unaffected when neuronal activity was blocked with tetrodotoxin (10^{-6} mol·l^{-1} at the serosal side), a blocker of voltage-dependent neuronal Na^+ channels (**Table 5**). The same resistance against tetrodotoxin was observed with Na cysteinate (5×10^{-3} mol·l^{-1} at the serosal side; **Table 5**). Consequently, cysteine obviously does not act via modulation of the activity of secretomotor submucosal neurons present in the mucosa–submucosa preparations used in this study.

EFFECTS OF CYSTEINE ON CYTOSOLIC pH

L-Cysteine is a weak acid, which causes – despite the relative high buffer capacity of the HCO_3^-/phosphate buffer used, an acidification of the extracellular solution, which might affect transepithelial transport. Administration of free cysteine in a concentration of 2.5×10^{-3} mol·l^{-1} or 5×10^{-3} mol·l^{-1} induced an acute fall in pH to 7.03 or 6.82, respectively. In order to find out whether a proton release might occur intracellularly after cellular uptake of cysteine, experiments were carried out with BCECF-loaded

Table 5 | Effect of cysteine after neuronal blockade.

	Control		± Inhibitor	
	Initial decrease	**Peak**	**Initial decrease**	**Peak**
Δ Isc (μEq·h^{-1}·cm^{-2}) EVOKED BY FREE CYSTEINE				
With tetrodotoxin	-0.56 ± 0.11^a	–	-0.56 ± 0.16^a	–
Without tetrodotoxin	-0.45 ± 0.069^a	–	-0.47 ± 0.078^a	–
Δ Isc (μEq·h^{-1}·cm^{-2}) EVOKED BY Na CYSTEINATE				
With tetrodotoxin	-0.317 ± 0.071^a	0.180 ± 0.100^a	-0.249 ± 0.055^a	0.390 ± 0.122^b
Without tetrodotoxin	-0.308 ± 0.075^a	0.064 ± 0.077^a	-0.305 ± 0.132^a	0.782 ± 0.207^b

The effect of free cysteine (5 × 10^{-3} mol·l^{-1} at the serosal side, upper two rows) and Na cysteinate (5 × 10^{-3} mol·l^{-1} at the serosal side, lower two rows) on Isc was tested in the absence of any inhibitors (control) and then in the presence or absence of tetrodotoxin (10^{-6} mol·l^{-1} at the serosal side). Data are given as change of Isc (Δ Isc) compared to baseline just prior administration of the respective cysteine administration and are means ± SEM, n = 6. Different letters (a, b) indicate statistically homogenous groups (analysis of variances followed by post hoc test of Tukey).

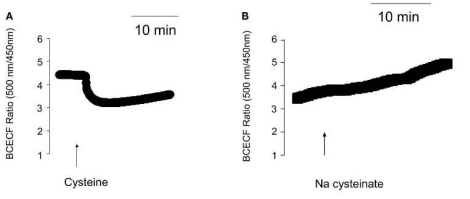

FIGURE 3 | (A) Cysteine, but not Na cysteinate induces a cytosolic acidification. Free cysteine (10^{-2} mol·l^{-1}; indicated by the arrow) induced a fall in the BCECF ratio signal. Values are given as means (symbols) ± SEM (lines), $n = 72$. **(B)** The response was not mimicked by Na cysteinate (10^{-2} mol·l^{-1}; indicated by the arrow). Values are given as means (symbols) ± SEM (lines), $n = 97$. In both cases, the ratio signal (emission at an excitation wave length of 500 nm divided by the emission at an excitation wave length of 450 nm) was measured at isolated colonic crypts.

isolated crypts. The fluorescence ratio signal of this dye decreases, when the cytosolic pH falls.

In deed, free cysteine (10^{-2} mol·l^{-1}) induced a prompt decrease in the BCECF ratio signal indicating cytosolic acidification (**Figure 3**). This fall was followed by a slow recovery, probably due to cellular pH counter-regulation. Such a phenomenon was not observed with Na cysteinate (10^{-2} mol·l^{-1}; **Figure 3B**). The sensitivity of different types of K^+ channels to cellular acidification is well known, also from isolated rat colonic crypts (Diener and Scharrer, 1994), and might be responsible for the different effects evoked by free cysteine in comparison to Na cysteinate (see Discussion). In deed, when the serosal buffer solution was acidified by administration of HCl to similar values as reached by administration of free cysteine, this caused a prompt fall in Isc of $0.95 \pm 0.22\,\mu$Eq·h^{-1}·cm^{-2} ($n = 7$, $P < 0.05$ versus baseline) in the case of an acidification to a pH of 7.0 and of $0.96 \pm 0.13\,\mu$Eq·h^{-1}·cm^{-2} ($n = 7$, $P < 0.05$ versus baseline) in the case of an acidification to a pH of 6.8. In no case, however, a secondary rise in Isc was observed as it was the case when Na cysteinate was administered.

COMPARISON WITH OTHER H_2S DONORS

The divergent response in Isc evoked by Na cysteinate, which induces a biphasic change in Isc, compared to NaHS, which stimulates a triphasic change in Isc, suggests that the speed of H_2S release might affect the biological effect at the colonic epithelium. In order to test this hypothesis in more detail, two other H_2S-releasing molecules were used (for references to these donors, see Martelli et al., 2011). GYY 4137 (5×10^{-5} mol·l^{-1} at the serosal side), a very slow H_2S-releasing molecule, did not evoke any increase in Isc. Instead, a slow fall in Isc was observed which appeared to be faster than the usual time-dependent decrease in Isc observed over prolonged time-periods in mucosa–submucosa preparations of rat distal colon (**Figure 4A**). In contrast, diallyl trisulfide, a compound found in garlic, which is converted intracellularly to H_2S by reaction with glutathione, evoked a monophasic increase in Isc in all concentrations tested (up to 1.5×10^{-4} mol·l^{-1} at the serosal side). When administered in a concentration of 1.5×10^{-5} mol·l^{-1} at the serosal side, diallyl trisulfide evoked an increase of $0.89 \pm 0.22\,\mu$Eq·h^{-1}·cm^{-2} above baseline ($P < 0.05$, $n = 7$; **Figure 4B**). In contrast, a roughly equieffective concentration of the fast H_2S donor, NaHS (2.5×10^{-3} mol·l^{-1} at the serosal side), evoked the typical multiphasic change in Isc as reported earlier (Hennig and Diener, 2009), i.e., a quick increase in Isc by $1.06 \pm 0.14\,\mu$Eq·h^{-1}·cm^{-2} above baseline ($P < 0.05$, $n = 7$), followed by a transient fall and finally a secondary increase of $1.60 \pm 0.22\,\mu$Eq·h^{-1}·cm^{-2} above baseline ($P < 0.05$, $n = 7$; **Figure 4B**). Consequently, three different H_2S-releasing drugs evoked different patterns of Isc responses across the colonic mucosa.

INTERACTIONS WITH SECRETAGOGUES

As cysteine modulates basal anion secretion (**Figure 1**), it seemed to be of interest to study whether this activator of endogenous H_2S synthesis might be able to interfere with the response of the epithelium to secretagogues. Ca^{2+}-dependent secretagogues such as the stable acetylcholine derivate, carbachol, typically induce a strong, but only transient increase in Isc (see, e.g., Strabel and Diener, 1995). Therefore, the effect of Na cysteinate on the carbachol response was measured by pretreatment with this amino acid. In the absence of Na cysteinate, carbachol evoked an increase in Isc of $9.11 \pm 1.62\,\mu$Eq·h^{-1}·cm^{-2} ($n = 6$), which only amounted to $6.84 \pm 1.83\,\mu$Eq·h^{-1}·cm^{-2} in the presence of Na cysteinate (5×10^{-5} mol·l^{-1} at the serosal side, $n = 6$, **Figures 5A,B**), although this difference did not reach statistical significance. Similar experiments were performed with free cysteine. In the absence of free cysteine, carbachol (5×10^{-5} mol·l^{-1} at the serosal side) evoked an increase in Isc above baseline which amounted to $7.66 \pm 0.63\,\mu$Eq·h^{-1}·cm^{-2} ($n = 6$). In contrast, after pretreating the tissue with free cysteine (5×10^{-3} mol·l^{-1} at the serosal side), Isc increased by only $4.20 \pm 1.02\,\mu$Eq·h^{-1}·cm^{-2} ($n = 7$, $P < 0.05$ versus response to carbachol in the absence of free cysteine).

In contrast to Ca^{2+}-dependent secretagogues, stimulation of the cAMP-pathway with forskolin, an activator of adenylate cyclase(s) (Seamon and Daly, 1981), leads to a stable increase in Isc (see **Figure 5D**), so that cysteine could be administered

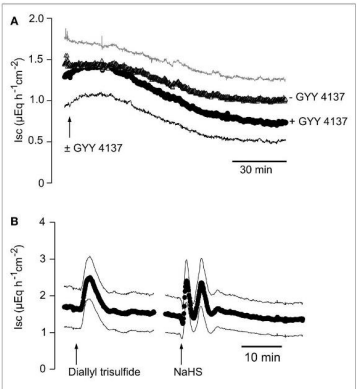

FIGURE 4 | (A) Comparison of the Isc evoked by different H_2S donors. The very slow H_2S-releasing molecule, GYY 4137 (5×10^{-4} mol·l^{-1} at the serosal side; arrow; black symbols and curve marked with + GYY 4137), did not evoke an increase in Isc in mucosa–submucosa preparations of rat distal colon. In contrast, a slow decrease in Isc, which had the tendency (not statistically significant) to be more pronounced compared to time-dependent control experiments (– GYY 4137) not pretreated with GYY 4137 (gray symbols) was observed. **(B)** The slow H_2S donor, diallyl trisulfide (1.5×10^{-3} mol·l^{-1} at the serosal side; left arrow), causes a transient, monophasic increase in Isc, whereas the fast H_2S donor, NaHS, administered in an equieffective concentration (2.5×10^{-3} mol·l^{-1} at the serosal side; right arrow), induced a triphasic change in Isc. Values are means (symbols) ± SEM (lines), $n = 5$–7. In the case of the experiments with GYY 4137, for graphical reasons for the time-dependent control experiments (– GYY 4137) only +SEM (gray line) and for the group treated with GYY 4137 (+ GY 4137) only −SEM (black line) are shown. For statistics, see text.

during the plateau phase of the current induced by forskolin (5×10^{-6} mol·l^{-1} at the mucosal and the serosal side). Under these conditions, Na cysteinate only evoked a transient and small decrease in Isc (**Figure 5C**). A similar response was observed with free cysteine. For example, administration of free cysteine in a concentration of 5×10^{-3} mol·l^{-1} (at the serosal side) induced a transient decrease of the forskolin-induced Isc by -0.55 ± 0.028 µEq·h^{-1}·cm^{-2} ($n = 7$), which is not larger than the effect of cysteine on baseline Isc in the absence of forskolin (see e.g. control series in **Table 2** and **Table 4**). So similar as it was observed with another gasotransmitter, carbon monoxide (Steidle and Diener, 2011), which when given alone evokes anion secretion but reduces the carbachol-induced Isc, also hydrogen sulfide impairs Ca^{2+}-dependent secretion, probably because both gasotransmitters interfere with intracellular Ca^{2+} signaling (Hennig and Diener, 2009; Pouokam and Diener, 2011; Steidle and Diener, 2011).

DISCUSSION

Hydrogen sulfide is recognized as a neurotransmitter in the enteric nervous system, i.e., the central regulator responsible for the control of most gastrointestinal functions (Jimenez, 2010). Expression of cystathionine-β-synthase and cystathionine-γ-lyase, the key enzymes for H_2S production (Wang, 2002), in smooth muscle and in epithelial cells from rat colon suggests additional paracrine actions of this gaseous molecule (Hennig and Diener, 2009). As stated in the Introduction, the biological role of H_2S during inflammatory processes is discussed controversially because this gasotransmitter has been reported to aggravate (see, e.g., Chávez-Piña et al., 2010) as well as to ameliorate (see, e.g., Fiorucci et al., 2007; Wallace et al., 2009) inflammatory processes. The observation that the exogenous H_2S donor NaHS evokes a strong Cl^- secretion across the colon of different species *in vitro* (Schicho et al., 2006; Hennig and Diener, 2009), i.e., would finally induce secretory diarrhoe *in vivo*, is – at first glance – in contradiction to the observed therapeutic effect of a H_2S-releasing mesalamine-derivative (ATB-429) in a model of mouse colitis (Fiorucci et al., 2007). Interestingly, a similar controversy about pro/antiinflammatory or proabsorptive/prosecretory actions exists for a second gasotransmitter, NO (see, e.g., Schirgi-Degen and Beubler, 1995; Schultheiss et al., 2002), suggesting that depending on differences in time, location, or amplitude of the production of these gasotransmitters the physiological response may differ in a fundamental way.

The present results demonstrate that cysteine (especially when administered as Na cysteinate), the precursor for endogenous H_2S synthesis, has a biphasic effect on anion secretion: an initial decrease followed by prolonged increase in Isc above the former baseline (**Figure 1B**). This second phase, i.e., a rise above the former baseline, is missing in the case of free cysteine (**Figure 1A**). Most probably the intracellular acidification, which is evoked by free cysteine, but not by Na cysteinate (**Figure 3**), is responsible for the missing ability of the presumed stimulation of H_2S synthesis to induce anion secretion (see below). Plasma cysteine concentrations in human blood are in the range of 0.3 mmol·l^{-1} (Van den Brandhof et al., 2001). So the concentrations used in the present study are clearly above physiological level. However, our aim was not mimic the physiological situation, but to stimulate maximally endogenous H_2S production, which is shown here by the amino-oxyacetate- and β-cyano-L-alanine-sensitive changes in Isc.

Both phases of the response to Na cysteinate, i.e., the initial fall as well as the secondary rise in Isc, were inhibited in the presence of bumetanide or after substitution of Cl^- by an impermeant anion confirming the modulation of Cl^- secretion by Na cysteinate (**Table 3**). This response differs from the change in Isc evoked by the exogenous H_2S donor, NaHS, which evokes a polyphasic Cl^- secretion in the same tissue (Hennig and Diener, 2009). Theoretically, the negative Isc induced by cysteine might also be caused by the activation of K^+ secretion, as both an inhibition of anion secretion as well as a stimulation of cation secretion exert the same effect on the transepithelial potential difference, i.e., the serosal side gets less positive. However, none of the K^+ channel blockers tested (Ba^{2+}, tetrapentylammonium, or charybdotoxin),

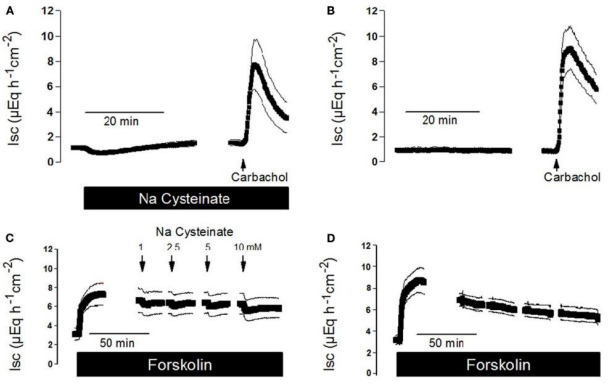

FIGURE 5 | (A) Interaction of Na cysteinate with the Isc evoked by secretagogues. Pretreatment with Na cysteinate (5×10^{-3} mol·l^{-1} at the serosal side; black bar) slightly reduced the increase in Isc evoked by carbachol (5×10^{-5} mol·l^{-1} at the serosal side; arrow) in mucosa–submucosa preparations of rat distal colon compared to a time-dependent control not treated with Na cysteinate **(B)**. **(C)** Na cysteinate (10^{-3} to 10^{-2} mol·l^{-1} at the serosal side; arrows) caused transient reductions in the Isc evoked by forskolin (5×10^{-4} mol·l^{-1} at the mucosal and the serosal side; black bar) compared to a time-dependent control not treated with Na cysteinate **(D)**. Line interruptions are caused by omission of time intervals of 5–10 min in order to synchronize the tracings of individual records to the administration of drugs. Values are means (symbols) ± SEM (lines), $n = 6$. For statistics, see text.

when administered at the mucosal side in order to block apical K^+ channels mediating apical efflux of K^+ during potassium secretion, had any effect on the decrease in Isc induced by free cysteine suggesting that an induction of K^+ secretion is not involved in the effect of cysteine (**Table 4**).

In contrast, two of these K^+ channel blockers, i.e., Ba^{2+} and tetrapentylammonium, when administered at the serosal side in order to block basolateral K^+ channels, reversibly inhibited the Isc response evoked by free cysteine (**Table 4**). This observation would fit to a mechanism, in which free cysteine reduces basolateral K^+ conductance. This K^+ conductance, which is dependent on the number of K^+ channels, their single channel conductance and their open probability, keeps the membrane potential at hyperpolarized values. If the K^+ channels involved are already inhibited by one of the K^+ channel blockers, this action of cysteine is no more possible. In the case of free cysteine, the observed cytosolic acidification (**Figure 3A**) might – at first glance – offer a reasonable explanation for the inhibition of basal Cl^- secretion by free cysteine, as epithelial K^+ conductance is known to be sensitive to a fall in cytosolic pH (Diener and Scharrer, 1994). Any inhibition of K^+ conductance, will reduce the driving force for Cl^- exit across the apical membrane via apical anion channels and thereby lead to an inhibition of transepithelial anion secretion.

This acidification and the presumed inhibition of cellular K^+ conductance is probably the reason why the second, prosecretory response evoked by the pH-neutral form of the amino acid, Na cysteinate, is missing in the case of free cysteine. Nevertheless, a fall in pH cannot be the reason for the initial inhibition in basal anion secretion evoked by Na cysteinate (see fall in Isc, e.g., in **Figure 1B**), as Na cysteinate does not affect cytosolic pH in the epithelial cells (**Figure 3B**). As this fall in Isc as well as the increase in Isc evoked by Na cysteinate was sensitive to inhibition of H_2S-synthesizing enzymes (see Results), these results suggest that the functional response induced by this gasotransmitter depends on the velocity of the H_2S release and/or the local concentration reached. This is supported by the comparison with compounds known to release H_2S at different velocity. Whereas the very slowly releasing compound GYY 4137 never induced an increase in Isc, but only evoked a prolonged fall in baseline Isc (**Figure 4A**), diallyl trisulfide only increased Isc, and the rapidly releasing molecule NaHS polyphasically changed the current across the colonic epithelium (**Figure 4B**). Consequently, the local concentration of H_2S seems to critically determine whether this gasotransmitter exerts a prosecretory or an antisecretory action in the gastrointestinal mucosa.

ACKNOWLEDGMENTS

The diligent care of Mrs. B. Brück, E. Haas, B. Schmitt, and A. Stockinger is a pleasure to acknowledge. Supported by Deutsche Forschungsgemeinschaft, grant Di 388/11-1.

REFERENCES

Berkefeld, H., Fakler, B., and Schulte, U. (2010). Ca^{2+}-activated K^+ channels: From protein complexes to function. *Physiol. Rev.* 90, 1437–1459.

Binder, H. J., and Sandle, G. J. (1994). "Electrolyte transport in the mammalian colon," in *Physiology of the Gastrointestinal Tract*, 3rd Edn, ed. L. R. Johnson (New York: Raven Press), 2133–2171.

Böhme, M., Diener, M., and Rummel, W. (1991). Calcium- and cyclic-AMP-mediated secretory responses in isolated colonic crypts. *Pflügers Arch.* 419, 144–151.

Chávez-Piña, A. E., Tapia-Alvarez, G. R., and Navarrete, A. (2010). Inhibition of endogenous hydrogen sulfide synthesis by PAG protects against ethanol-induced gastric damage in the rat. *Eur. J. Pharmacol.* 630, 131–136.

Cook, N. S., and Quast, U. (1990). "Potassium channels. Structure, classification, function and therapeutic potential," in *Potassium Channel Pharmacology*, ed. N. S. Cook (New York: Ellis Horwood), 181–255.

Diener, M., and Scharrer, E. (1994). The effect of short-chain fatty acids on Cl- and K^+ conductance in rat colonic crypts. *Pflügers Arch.* 426, 472–480.

Ekundi-Valentim, E., Santos, K. T., Camargo, E. A., Denadai-Souza, A., Teixeira, S. A., Zanoni, C. I., Grant, A. D., Wallace, J. L., Muscará, M. N., and Costa, S. K. (2010). Differing effects of exogenous and endogenous hydrogen sulphide in carrageenan-induced knee joint synovitis in the rat. *Br. J. Pharmacol.* 159, 1463–1474.

Fiorucci, S., Orlandi, S., Mencarelli, A., Caliendo, G., Santagada, V., Distrutti, E., Santucci, L., Cirino, G., and Wallace, J. L. (2007). Enhanced activity of a hydrogen sulphide-releasing derivative of mesalamine (ATB-429) in a mouse model of colitis. *Br. J. Pharmacol.* 150, 996–1002.

Hennig, B., and Diener, M. (2009). Actions of hydrogen sulfide on ion transport across rat distal colon. *Br. J. Pharmacol.* 158, 1263–1275.

Hörger, S., Schultheiss, G., and Diener, M. (1998). Segment-specific effects of epinephrine on ion transport in the colon of the rat. *Am. J. Physiol. Gastrointest. Liver Physiol.* 275, G1367–G1376.

Ji, Y., Pang, Q. F., Xu, G., Wang, L., Wang, J. K., and Zeng, Y. M. (2008). Exogenous hydrogen sulfide postconditioning protects isolated rat hearts against ischemia-reperfusion injury. *Eur. J. Pharmacol.* 587, 1–7.

Jimenez, M. (2010). Hydrogen sulfide as a signaling molecule in the enteric nervous system. *Neurogastroenterol. Motil.* 22, 1149–1153.

Kaplan, M. R., Mount, D. B., Delpire, E., Gamba, G., and Hebert, S. C. (1996). Molecular mechanisms of NaCl cotransport. *Annu. Rev. Physiol.* 58, 649–668.

Krueger, D., Foerster, M., Mueller, K., Zeller, F., Slotta-Huspenina, J., Donovan, J., Grundy, D., and Schemann, M. (2010). Signaling mechanisms involved in the intestinal prosecretory actions of hydrogen sulfide. *Neurogastroenterol. Motil.* 22, 1224–1231.

Lee, S. W., Hu, Y. S., Hu, L. F., Lu, Q., Dawe, G. S., Moore, P. K., Wong, P. T., and Bian, J. S. (2006). Hydrogen sulphide regulates calcium homeostasis in microglial cells. *Glia* 54, 116–124.

Lindström, C. G., Rosengren, J. E., and Fork, F. T. (1979). Colon of the rat. An anatomic, histologic and radiographic investigation. *Acta Radiol. Diagn. (Stockh.)* 20, 523–536.

Maguire, D., MacNamara, B., Cuffe, J. E., Winter, D., Doolan, C. M., Urbach, V., O'Sullivan, G. C., and Harvey, B. J. (1999). Rapid responses to aldosterone in human distal colon. *Steroids* 64, 51–63.

Martelli, A., Testai, L., Breschi, M. C., Blandizzi, C., Virdis, A., Taddei, S., and Calderone, V. (2011). Hydrogen sulphide: novel opportunity for drug discovery. *Med. Res. Rev.* 31, doi:10.1002/med20234

Martin, G. R., McKnight, G. W., Dicay, M. S., Coffin, C. S., Ferraz, J. G. P., and Wallace, J. L. (2010). Hydrogen sulphide synthesis in the rat and mouse gastrointestinal tract. *Dig. Liver Dis.* 42, 103–109.

Park, K. J., Baker, S. A., Cho, S. Y., Sanders, K. M., and Koh, S. D. (2005). Sulfur-containing amino acids block stretch-dependent K^+ channels and nitrergic responses in the murine colon. *Br. J. Pharmacol.* 144, 1126–11387.

Pfeffer, M., and Ressler, C. (1967). β-Cyanoalanine, an inhibitor of rat liver cystathionase. *Biochem. Pharmacol.* 16, 2299–2308.

Pouokam, E., and Diener, M. (2011). Mechanims of actions of hydrogen sulfide at rat distal colonic epithelium. *Br. J. Pharmacol.* 162, 392–404.

Rink, T. J., Tsien, R., and Pozzan, T. (1982). Cytoplasmic pH and free $Mg2^+$ in lymphocytes. *J. Cell Biol.* 95, 189–196.

Schicho, R., Krueger, D., Zeller, F., von Weyhern, C. W. H., Frieling, T., Kimura, H., Ishii, I., De Giorgio, R., Campi, B., and Schemann, M. (2006). Hydrogen sulfide is a novel prosecretory neuromodulator in the guinea-pig and human colon. *Gastroenterology* 131, 1542–1552.

Schirgi-Degen, A., and Beubler, E. (1995). Significance of nitric oxide in the stimulation of intestinal fluid absorption in the rat jejunum in vivo. *Br. J. Pharmacol.* 114, 13–18.

Schultheiss, G., Seip, G., Kocks, S. L., and Diener, M. (2002). $Ca2^+$-dependent and $Ca2^+$-independent Cl- secretion stimulated by the nitric oxide donor, GEA 3162, in rat colonic epithelium. *Eur. J. Pharmacol.* 444, 21–30.

Seamon, K. B., and Daly, J. W. (1981). Forskolin: a unique diterpene activator of cyclic AMP-generating systems. *J. Cyclic Nucleotide Res.* 7, 201–224.

SØrensen, M. V., Matos, J. E., Praetorius, H. A., and Leipziger, J. (2010). Colonic potassium handling. *Pflügers Arch.* 459, 645–656.

Steidle, J., and Diener, M. (2011). Effects of carbon monoxide on ion transport across rat distal colon. *Am. J. Physiol. Gastrointest. Liver Physiol.* 300, G207–G216.

Strabel, D., and Diener, M. (1995). Evidence against direct activation of chloride secretion by carbachol in the rat distal colon. *Eur. J. Pharmacol.* 274, 181–191.

Tamizhselvi, R., Moore, P. K., and Bhatia, M. (2007). Hydrogen sulfide acts as a mediator of inflammation in acute pancreatitis: in vitro studies using isolated mouse pancreatic acinar cells. *J. Cell. Mol. Med.* 11, 315–326.

Toda, N., and Herman, A. G. (2005). Gastrointestinal function regulation by nitrergic efferent nerves. *Pharmacol. Rev.* 57, 315–338.

Van den Brandhof, W. E., Haks, K., Schouten, E. G., and Verhoef, P. (2001). The relation between plasma cysteine, plasma homocysteine and coronary atherosclerosis. *Atherosclerosis* 157, 403–409.

Wallace, J. L., Caliendo, G., Santagada, V., and Cirino, G. (2010). Markedly reduced toxicity of a hydrogen sulphide-releasing derivative of naproxen (ATB-346). *Br. J. Pharmacol.* 159, 1236–1246.

Wallace, J. L., Vong, L., McKnight, W., Dicay, M., and Martin, G. R. (2009). Endogenous and exogenous hydrogen sulfide promotes resolution of colitis in rats. *Gastroenterology* 137, 569–578.

Wang, R. (2002). Two's company, three's a crowd: can H2S be the third endogenous gaseous transmitter? *FASEB J.* 16, 1792–1798.

Zhao, W., Ndisang, J. S., and Wang, R. (2003). Modulation of endogenous production of H2S in rat tissues. *Can. J. Physiol. Pharmacol.* 81, 848–853.

Conflict of Interest Statement: The authors declare that the research was conducted in the absence of any commercial or financial relationships that could be construed as a potential conflict of interest.

Received: 25 January 2012; paper pending published: 07 February 2012; accepted: 17 February 2012; published online: 02 March 2012.

Citation: Pouokam E and Diener M (2012) Modulation of ion transport across rat distal colon by cysteine. Front. Physio. ***3****:43. doi: 10.3389/fphys.2012.00043*

This article was submitted to Frontiers in Membrane Physiology and Biophysics, a specialty of Frontiers in Physiology.

Copyright © 2012 Pouokam and Diener. This is an open-access article distributed under the terms of the Creative Commons Attribution Non Commercial License, which permits non-commercial use, distribution, and reproduction in other forums, provided the original authors and source are credited.

8.3 "ATP-sensitive K^+ channels in rat colonic epithelium"

Pouokam E, Bader S, Brück B, Schmidt B, Diener M. *Pflügers Arch. Eur. J. Physiol* (2013) **465:** 865-877

Impakt Faktor: 3.073

Eigener Anteil an der Publikation:

- Initiative: 70 %
- Projektplanung: 75 %
- Durchführung der Versuche: 70 %
- Auswertung der Experimente: 80 %
- Erstellung der Publikation: 80 %

Pflugers Arch - Eur J Physiol
DOI 10.1007/s00424-012-1207-7

ION CHANNELS, RECEPTORS AND TRANSPORTERS

ATP-sensitive K^+ channels in rat colonic epithelium

Ervice Pouokam · Sandra Bader · Brigitta Brück · Bärbel Schmidt · Martin Diener

Received: 7 December 2012 / Revised: 10 December 2012 / Accepted: 10 December 2012
© Springer-Verlag Berlin Heidelberg 2012

Abstract ATP-sensitive K^+ (K_{ATP}) channels couple the metabolic state of a cell to its electrical activity. They consist of a hetero-octameric complex with pore-forming Kir6.x (Kir6.1, Kir6.2) and regulatory sulfonylurea receptor (SUR) subunits. Functional data indicate that K_{ATP} channels contribute to epithelial K^+ currents at colonic epithelia. However, their molecular identity and their properties are largely unknown. Therefore, changes in short-circuit current (I_{sc}) induced by the K_{ATP} channel opener pinacidil (5 10^{-4} $mol\,l^{-1}$) were measured in Ussing chambers under control conditions and in the presence of different blockers of K_{ATP} channels. The channel subunits expressed by the colonic epithelium were identified by immunohistochemistry and by RT-PCR. The K^+ channel opener, when administered at the serosal side, induced an increase in I_{sc} consistent with the induction of transepithelial Cl^- secretion after activation of basolateral K^+ channels, whereas mucosal administration of pinacidil resulted in a negative I_{sc}. The increase in I_{sc} evoked by serosal pinacidil was inhibited by serosal administration of glibenclamide (5 10^{-4} $mol\,l^{-1}$) and gliclazide (10^{-6} $mol\,l^{-1}$), but was resistant even against a high concentration (10^{-2} $mol\,l^{-1}$) of tolbutamide. In contrast, none of these inhibitors (administered at the mucosal side) reduced significantly the negative I_{sc} induced by mucosal pinacidil. Instead, pinacidil inhibited Cl^- currents across apical Cl^- channels in basolaterally depolarized epithelia indicating that the negative I_{sc} induced by mucosal pinacidil is due to a transient inhibition of Cl^- secretion. In mRNA prepared from isolated colonic crypts, messenger RNA for both pore-forming subunits, Kir6.1 and Kir6.2, and two regulatory subunits (SUR1and SUR2B) was found. Expression within the colonic epithelium was confirmed for these subunits by immunohistochemistry. In consequence, K_{ATP} channels are present in the basolateral membrane of the colonic epithelium; their exact subunit composition, however, has still to be revealed.

Keywords ATP-sensitive K^+ channels · Cl^- secretion · Distal colon

Introduction

Potassium channels which are inhibited by cytosolic ATP have been found in several tissues including the heart, where they were originally discovered [24], skeletal muscles [32], the brain [1], smooth muscle [33], and other cell types like the pancreatic β-cells [2, 9]. The activity of ATP-sensitive K^+ (K_{ATP}) channels is essentially voltage-independent, but depends on intracellular nucleotides, especially ATP and MgADP, which inhibit and stimulate the channels, respectively. Thus, they couple the metabolic state of a given cell to its electrical activity, contributing thereby to crucial functions such as insulin secretion both in response to sulfonylureas and to glucose [2], regulation of the vascular smooth muscle tone and therefore the regulation of blood pressure [11], and cytoprotection [6].

An individual K_{ATP} channel consists of a hetero-octameric complex of two distinct types of protein subunits: a pore-forming subunit Kir6.x (Kir6.1 or Kir6.2) and a regulatory subunit that belongs to the sulfonylurea receptor (SUR) subfamily, a member of the ATP-binding cassette (ABC) protein superfamily [5]. Four Kir6.x subunits, which belong to the Kir6 family of inwardly rectifying K^+ channels, form the ion conducting pore (for review, see [29]). Kir6.1 and Kir6.2 share about 71 % amino acid identity

E. Pouokam · S. Bader · B. Brück · B. Schmidt · M. Diener (✉)
Institute for Veterinary Physiology and Biochemistry,
Justus-Liebig-University, Frankfurter Str. 100,
Giessen, Germany
e-mail: martin.diener@vetmed.uni-giessen.de

Published online: 22 December 2012

[16]. They are supplemented by four SUR subunits (for review, see [29]). Two isoforms of SUR are known: SUR1 and SUR2, which are derived from two different genes. Alternative splicing of SUR2 mRNA creates two further variants, i.e. SUR2A and SUR2B [8, 16, 19], with SUR2B as the subtype showing the wider expression pattern. SUR2A and SUR2B contain a nucleotide binding site and are the action site for inhibitors such as sulfonylurea derivatives (e.g., glibenclamide or tolbutamide) or activators such as pinacidil (for review, see [29]). SUR2A and SUR2B differ only in their carboxyl-terminal 42 amino acids [19], whereas SUR1 and SUR2B possess a similar C-terminus (for review, see [29]).

Expression of Kir6.x and SUR subunits in different combinations yields the tissue-specific K_{ATP} channel subtypes with different electrophysiological and pharmacological properties [17, 19, 38]. Thus, the combination Kir6.2/SUR1 forms the pancreatic β-cell type K_{ATP} channels [16], and Kir6.2/SUR2A makes up the dominant K_{ATP} channel type in the cardiac muscle [17]. Kir6.2/SUR2B probably constitutes the K_{ATP} channels in non-vascular smooth muscles [19], while Kir6.1/SUR2B forms the vascular smooth muscle type K_{ATP} channels [38].

ATP-sensitive K^+ channels also play a role in vectorial ion transport across the colonic epithelium. In order to secrete Cl^- across the apical membrane, the basolateral membrane has to establish the driving force for anion extrusion. Chloride efflux via anion channels in the apical membrane is driven by the negative membrane potential, which is dominated by a K^+ diffusion potential [33, 35], whereas the Na^+-K^+-ATPase has to maintain the K^+ concentration gradient between the intra- and the extracellular compartment as a prerequisite for the establishment of a K^+ diffusion potential. Previous studies showed the importance of these channels for colonic secretion: the Cl^- secretory response evoked by the gasotransmitter H_2S was sensitive to serosal administration of glibenclamide, a known inhibitor of the K_{ATP} channels [14]. Apical permeabilization of the epithelium evoked the stimulation of a glibenclamide-sensitive basolateral K^+ conductance by H_2S [27].

During these experiments, we observed opposing actions of pinacidil, a known K_{ATP} channel opener [4], on the short-circuit current (I_{sc}). These actions depended on the side (basolateral or apical) where the channel opener was administered [14]. Thus, we speculated that K_{ATP} channels might be present as well on the apical side. With the exception of human and rat small intestine, where K_{ATP} channels made up of the Kir6.1/SUR2A complex have been found in the region of the tight junctions [20], no information is available about the expression pattern of this type of ion channels in the intestinal epithelium. Therefore, a pharmacological characterization of the current evoked by the K_{ATP} channel opener pinacidil as well as an immunohistochemical and molecular biological characterization via reverse transcriptase polymerase chain reaction (RT-PCR) of the putative K_{ATP} channels in rat colonic epithelium was performed in the present study.

Material and methods

Animals

Female and male Wistar rats with a body mass of 200–250 g were used. The animals were bred and housed at the institute for Veterinary Physiology and Biochemistry of the Justus-Liebig-University Giessen at an ambient temperature of 22.5 °C and air humidity of 50–55 % on a 12 h:12 h light–dark cycle with free access to water and food until the time of the experiment. Animals were killed by a blow on the head followed by exsanguination (approved by Regierungspräsidium Giessen, Giessen, Germany).

Solutions

Most Ussing chamber experiments were carried out in a bathing solution containing (in millimoles per liter): 107 NaCl, 4.5 KCl, 25 $NaHCO_3$, 1.8 Na_2HPO_4, 0.2 NaH_2PO_4, 1.25 $CaCl_2$, 1 $MgSO_4$, 12.2 glucose. Glucose was equimolarly replaced by 2-deoxyglucose when an energetic depletion of the epithelium was intended. The buffer for the depolarization of the basolateral membrane contained (in millimoles per liter): KCl 111.5, $NaHCO_3$ 25, Na_2HPO_4 0.2, $CaCl_2$ 1.25, $MgSO_4$ 1 and glucose 12.2. In order to obtain a serosal-to-mucosal Cl^- gradient, 107 mmol l^{-1} of Cl^- (in the form of KCl) of this buffer solution was replaced equimolarly by the impermeable anion gluconate in the apical bathing solution thus containing (in millimoles per liter): K gluconate 107, KCl 4.5, $NaHCO_3$ 25, Na_2HPO_4 0.2, $CaCl_2$ 1.25, $MgSO_4$ 1, glucose 12.2. All these solutions were gassed with carbogen (5 % (vol/vol) CO_2 and 95 % (vol/vol) O_2) at 37 °C and at a pH of 7.4 (adjusted by $NaHCO_3$/HCl). The Ussing chamber experiments with Ba^{2+} were carried out in a Tyrode solution containing (in millimoles per liter): 140 NaCl, 5.4 KCl, 1.25 $CaCl_2$, 1 $MgCl_2$, 10 HEPES (*N*-(2-hydroxyethyl)piperazine-*N*′-2-ethansulfonic acid), 12.2 glucose; pH of 7.4, which was gassed with O_2.

For crypt isolation, a Ca^{2+}- and Mg^{2+}-free Hank's balanced solution was used containing 10 mmol l^{-1} ethylenediamine tetraacetic acid (EDTA), penicillin (10000 units ml^{-1}), and streptomycin (10 mg ml^{-1}); pH was 7.4 (adjusted by Tris/HCl). For the immunohistochemical experiments, a 100 mmol^{-1} phosphate buffer was used containing (mmol l^{-1}): 80 Na_2HPO_4 and 20 NaH_2PO_4; pH was 7.4 (adjusted by NaOH/HCl).

Ussing chamber experiments

The serosa and muscularis propria were stripped away by hand to obtain a mucosa–submucosa preparation from the distal colon. Briefly, the colon was placed on a small plastic rod with a diameter of 5 mm. A circular incision was made near the anal end with a blunt scalpel and the serosa, together with the muscularis propria, were gently removed in a proximal direction.

The mucosa–submucosa preparation was fixed in a modified Ussing chamber bathed with a volume of 3.5 ml on each side of the mucosa. The tissue was incubated at 37 °C and short-circuited by a computer-controlled voltage-clamp device (Ingenieur Büro für Mess- und Datentechnik Mussler, Aachen, Germany) with correction for solution resistance. Tissue conductance (Gt) was measured every minute by the voltage deviation induced by a current pulse (±50 μA, duration 200 ms) under open-circuit conditions. Short-circuit current (I_{sc}) is expressed as microequivalents per hour per square centimeter, i.e., the flux of a monovalent ion per time and area, with 1 $\mu Eq h^{-1} cm^{-2} = 26.9\ \mu A cm^{-2}$. A positive I_{sc} reflects the secretion of anions (or the electrogenic absorption of cations). In some tables, the maximal increase in I_{sc} evoked by serosal administration of pinacidil (Table 2) or the maximal decrease in I_{sc} evoked by mucosal administration of pinacidil (Table 3) reached within 10–15 min is given as difference to the baseline just prior administration of the drug.

Immunohistochemical experiments

The tissue was fixed overnight in phosphate buffer (100 mmol l^{-1}) containing 40 $g l^{-1}$ paraformaldehyde and embedded in gelatin (gelatin type A from porcine skin; 100 g l^{-1}). The tissue was frozen in N_2-cooled isopentane; sections (about 2 μm thick) were cut and mounted on glass slides coated with gelatin containing chrome alaun (chromium(III) potassium sulfate; 0.5 g l^{-1}). For immunofluorescence staining, after rehydration in phosphate buffer, the sections were incubated for 2 h in phosphate buffer containing 2 ml l^{-1} Triton-X-100, 30 g l^{-1} BSA, and 100 ml l^{-1} donkey serum (Millipore, Schwalbach, Germany) to block unspecific binding sites. The blocking solution was then removed and the sections were incubated with the primary antibody for 24 h at 4 °C. Each primary antibody (for sources and dilutions, see Table 1) was dissolved in phosphate buffer containing 1 ml l^{-1} Triton-X-100, 5 g l^{-1} milk powder, 10 g l^{-1} BSA and 10 $ml l^{-1}$ donkey serum. After rinsing with phosphate buffer, the sections were incubated with the secondary antibody (see Table 1). After a further rinse with phosphate buffer, the sections were incubated for 5 min with $3 \cdot 10^{-7}$ mol l^{-1} 4′,6-diamidino-2-phenylindoldilactate (DAPI; Molecular Probes, Leiden, The Netherlands) for nuclear staining. As a negative control, some sections were incubated with a solution that did not contain the primary antibodies (see Figs. 4, 5, and 6).

Isolation of intact colonic crypts

The colon was initially rinsed with Hank's balanced salt solution containing Ca^{2+} and Mg^{2+}. The mucosa–submucosa preparation was fixed on a plastic holder with tissue adhesive and transferred for about 7 min to the Hank's-EDTA solution. The mucosa was vibrated once for 30 s in order to obtain crypts [28]. They were collected in RPMI 1640 medium (PAA, Cölbe, Germany) supplemented with penicillin (10,000 units ml^{-1})/streptomycin (10 mg ml^{-1}) and centrifuged 3 min at 1000×g. After discarding the supernatant, the pellet was resuspended in about 10 ml Hank's balanced salt solution containing Ca^{2+} and Mg^{2+} and centrifuged for 5 min at 1000×g. After this step, the pellet was used for mRNA isolation.

Reverse transcriptase polymerase chain reaction experiments

For RT-PCR studies, isolated colonic crypts were transferred into lysis buffer (Qiagen, Heiden, Germany) and homogenized using a mixer mill (NM301; Retsch, Haan, Germany) with a frequency of 300 Hz. Total RNA was extracted using the Nucleo Spin® RNA XS kit (Macherey-Nagel, Düren, Germany) RNA was reverse transcribed with Tetro cDNA synthesis Kit (Bioline, Germany).

For the PCR reaction Eppendorf MasterMix (Eppendorf, Hamburg, Germany) was used with 1.5 $mmol l^{-1}$ $MgCl_2$. Published primers [37, 39] were used against rat Kir6.1 (http://www.ncbi.nlm.nih.gov; accession code D42145; expected product length 339 bp), Kir 6.2 (accession code D86039; expected product length 297 bp), SUR1 (accession code L40624; expected product length 388 bp), SUR2A (accession code D83598; expected product length 501 bp), and SUR2B (accession code AF019628; expected product length 436 bp). Primers were obtained from Eurofins MWG Synthesis, Ebersberg, Germany. Each PCR started with a denaturation period of 1 min at 94 °C, followed by an annealing phase of 1.5 min at 60 °C and an elongation phase of 1 min at 72 °C; the whole cycle was repeated 40 times. For control of the PCR reaction glyceraldehyde-3-phosphate dehydrogenase (GAPDH; accession code BC059110; forward 744–763, backward 1027–1046; expected product length 303 bp) was used. The reaction product was visualized after electrophoresis in a 3 % (weight/vol) agarose gel (Peqlab, Erlangen, Germany) and staining with Roti®-Gel Stain (Carl Roth, Karlsruhe, Germany).

Table 1 Antibodies used

Target	Host species	Supplier	Final dilution	Specificity control of primary antibodies in Western blot
Kir6.1	Goat (polyclonal)	Santa Cruz (sc-11224)	1:50	[26]
Kir6.2	Goat (polyclonal)	Santa Cruz (sc-11228)	1:50	[41]
SUR1	Rabbit (polyclonal)	Santa Cruz (sc-25683)	1:50	[26]
SUR2A	Goat (polyclonal)	Santa Cruz (sc-32462)	1:50	Not available
SUR2A	Goat (polyclonal)	Santa Cruz (sc32461)	1:50	Not available
SUR2B	Goat (polyclonal)	Santa Cruz (sc-5793)	1:50	[26]
Goat IgG	Donkey	Invitrogen (A11055), Alexa Fluor 488 conjugated	1:200	–
Rabbit IgG	Donkey	Jackson ImmunoResearch (711-165-152), AffiniPure Cy3 conjugated	1:400	–

Drugs

Amiloride, diazoxide, glibenclamide (Boehringer Mannheim, Mannheim, Germany), gliclazide, pinacidil, and tolbutamide were dissolved in dimethylsulphoxide (DMSO; final maximal DMSO concentration 5 $ml l^{-1}$). Forskolin and indomethacin were dissolved in ethanol (final maximal concentration 1.4 $ml l^{-1}$). Tetrodotoxin was dissolved in $2{\cdot}10^{-2}$ $mol l^{-1}$ citrate buffer. Barium chloride and tetrapentylammonium chloride were dissolved in an aqueous stock solution. If not indicated differently drugs were from Sigma, Taufkirchen, Germany.

Statistics

Results are given as mean±standard error of the mean (SEM) with the number (n) of investigated tissues. For the comparison of two groups either a Student's t test or a Mann–Whitney U test was applied. An F-test decided which test method had to be used. Both paired and unpaired two-tailed Student's t tests were applied as appropriate. To compare more than two samples, an analysis of variance was performed followed by post-hoc test of Tukey. $P<0.05$ was considered to be statistically significant.

Results

Basic effects of pinacidil and diazoxide on I_{sc}

As reported recently [14], the K_{ATP} channel opener pinacidil - depending on the site of administration - evoked opposing effects on I_{sc} across rat distal colon, i.e. an increase in I_{sc} after serosal administration and a decrease in I_{sc} after mucosal administration (see control responses in Table 2 and 3). In some tissues, the initial decrease in I_{sc} evoked by mucosal pinacidil was followed by a secondary rise in I_{sc} above the former baseline (see, e.g. black curve in Fig. 3a).

The response to pinacidil did not show a desensitization. When the drug was administered repeatedly to the same tissue in a concentration of $5{\cdot}10^{-4}$ $mol l^{-1}$, which had been shown to be maximally effective in concentration-response experiments [14], there was no significant difference between the change in I_{sc} induced by three administrations of the drug, neither in the increase in I_{sc} induced by serosal (Fig. 1a) nor in the decrease in I_{sc} induced by mucosal administration of pinacidil (Fig. 1b). Similar opposing effects on I_{sc} were observed with another K^+ channel opener, diazoxide ($5{\cdot}10^{-4}$ $mol\ l^{-1}$). When administered at the serosal side, this drug induced an increase in I_{sc} of 0.40± 0.093 $\mu Eq h^{-1} cm^{-2}$ (n=8), whereas after mucosal administration a decrease in I_{sc} of −1.28±0.43 $\mu Eq h^{-1} cm^{-2}$ (n=8) was measured. As observed for pinacidil, there was no desensitization upon repetitive administration of diazoxide

Table 2 Sensitivity of the I_{sc} response evoked by serosal pinacidil to basolateral K^+ channel blockers and neuronal blockade

	ΔI_{sc} evoked by serosal pinacidil ($\mu Eq h^{-1} cm^{-2}$)	
	− Inhibitor	+ Inhibitor
±Glibenclamide	0.32±0.071	0.12±0.028*
±Gliclazide	0.51±0.097	0.17±0.036*
±Tolbutamide	0.52±0.16	0.33±0.12
±TPeA	0.32±0.095	0.27±0.074
±TTX	0.28±0.13	0.49±0.10

The effect of pinacidil ($5{\cdot}10^{-4}$ $mol l^{-1}$ at the serosal side) on I_{sc} was first tested in the absence of any other drugs (− *Inhibitor*; *second column*) and then in the presence of a putative blocker (+ *Inhibitor*; third column). Inhibitors used were: glibenclamide ($5{\cdot}10^{-4}$ $mol l^{-1}$ at the serosal side), gliclazide (10^{-6} $mol l^{-1}$ at the serosal side), tolbutamide (10^{-2} $mol l^{-1}$ at the serosal side), tetrapentylammonium (TPeA; $5{\cdot}10^{-4}$ $mol l^{-1}$ at the serosal side), and tetrodotoxin (TTX; 10^{-6} $mol l^{-1}$ at the serosal side). Data are given as increase in I_{sc} compared to baseline just prior administration of pinacidil and are means±SEM, n= 6–8. * $P<0.05$ versus response to pinacidil under control conditions

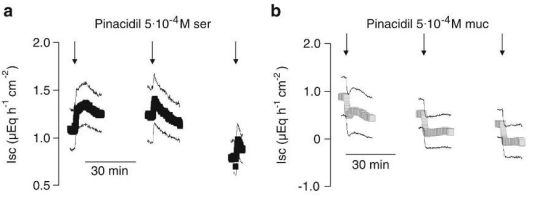

Fig. 1 Effect of repeated administration of pinacidil ($5{\cdot}10^{-4}$ mol l^{-1}) administered either at the serosal **a** or the mucosal side **b** of the tissue. The individual administrations were separated from each other by washing the compartment in which the K^+ channel opener had been administered three times by five times the chamber volume as indicated by the interruptions of the current tracings. Data are means (*symbols*)±SEM (*lines*); n = 7. No significant differences were observed between the individual administrations (analysis of variances followed by Tukey's test)

(n=8, data not shown). Therefore, in all subsequent experiments, the response induced by pinacidil was first tested under control conditions, i.e. in the absence of any inhibitors, and then in the presence of drugs presumed to interfere with the response evoked by the K^+ channel opener.

The action of serosal pinacidil is consistent with the activation of basolateral K_{ATP} channels

The increase in I_{sc} induced by serosal administration of pinacidil ($5{\cdot}10^{-4}$ mol l^{-1}) was significantly reduced by about two thirds in the presence of glibenclamide ($5{\cdot}10^{-4}$ mol l^{-1} at the serosal side; Table 2), a typical blocker of ATP-sensitive K^+ channels (for references, see [10]). Surprisingly, inhibition was not mimicked by tolbutamide, although a quite high concentration of this blocker (10^{-2} mol·l^{-1} at the serosal side) was used. Because of the unexpected tolbutamide resistance, these experiments were repeated using diazoxide ($5{\cdot}10^{-4}$ mol l^{-1} at the serosal side) as agonist. However, also the response to this K^+ channel opener proved to be resistant against tolbutamide (data not shown). In contrast to tolbutamide, gliclazide (10^{-6} mol l^{-1} at the serosal side) inhibited the pinacidil response. After pretreatment with this inhibitor, the long-lasting increase in I_{sc} evoked by serosal pinacidil was even reverted in a decrease, i.e. the response which was usually observed after mucosal administration of pinacidil (Fig. 2a). As expected, the effect of serosal pinacidil was resistant against tetrapentylammonium (Table 2), which preferentially inhibits Ca^{2+}-dependent K^+ channels [22]. As serosal pinacidil might also affect secretomotor neurons within the submucosal plexus, which could contribute to the secretory response evoked by this K^+ channel opener, the effect of pinacidil ($5{\cdot}10^{-4}$ mol l^{-1} at the serosal side) was tested in the presence of the neurotoxin, tetrodotoxin. However, neuronal blockade by tetrodotoxin (10^{-6} mol l^{-1} at the serosal side) did not prevent the pinacidil-induced increase in I_{sc} (Table 2).

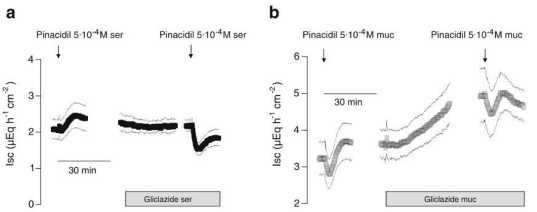

Fig. 2 Effect of repeated administration of pinacidil ($5{\cdot}10^{-4}$ mol l^{-1}) administered either at the serosal **a** or the mucosal side **b** of the tissue. The individual administrations were separated from each other by washing the compartment in which the K^+ channel opener had been administered three times by five times the chamber volume as indicated by the interruptions of the current tracings. The second administration of pinacidil was performed in the presence of gliclazide (10^{-6} mol l^{-1}; gray bar) administered either at the serosal (**a**) or the mucosal (**b**) side of the tissue. Data are means (*symbols*)±SEM (*lines*); n=6–8. For statistics, see Tables 2 and 3

Table 3 Sensitivity of the I_{sc} response evoked by mucosal pinacidil to apical K^+ channel blockers

	ΔI_{sc} evoked by mucosal pinacidil ($\mu Eq h^{-1} cm^{-2}$)	
	−Inhibitor	+Inhibitor
±Ba^{2+}	−0.21±0.028	−0.46±0.061*
±Glibenclamide	−0.91±0.19	−0.73±0.079
±Gliclazide	−0.61±0.17	−0.51±0.084
±Tolbutamide	−0.32±0.13	−0.18±0.037
±TPeA	−0.52±0.24	−0.38±0.066

The effect of pinacidil ($5 \cdot 10^{-4}$ mol l^{-1} at the mucosal side) on I_{sc} was first tested in the absence of any other drugs (−Inhibitor; second column) and then in the presence of a putative blocker (+Inhibitor; third column). Inhibitors used were: Ba^{2+} (10^{-2} mol l^{-1} at the mucosal side), glibenclamide ($5 \cdot 10^{-4}$ mol l^{-1} at the mucosal side), gliclazide (10^{-6} mol l^{-1} at the mucosal side), tolbutamide (10^{-2} mol l^{-1} at the mucosal side), and tetrapentylammonium (TPeA; $5 \cdot 10^{-4}$ mol l^{-1} at the mucosal side). The experimental series with Ba^{2+} was carried out in a HCO_3^- -free, HEPES-buffered solution (see Methods) in order to avoid precipitation of Ba^{2+} as carbonate salt. Data are given as decrease in I_{sc} compared to baseline just prior administration of pinacidil and are means±SEM, n=6–7

*P<0.05 versus response to pinacidil under control conditions

The action of mucosal pinacidil represents an unspecific inhibition of apical Cl^- channels

In contrast, when the same K^+ channel blockers were tested for their ability to interfere with the decrease in I_{sc} evoked by mucosal administration of pinacidil, which we had previously assumed to represent K^+ secretion induced by opening of apical K^+ channels [27], none of these blockers was effective (Table 3 and Fig. 2b for gliclazide, i.e. the potent inhibitor of the I_{sc} response evoked by serosal pinacidil). Mucosal gliclazide itself evoked a paradox increase in I_{sc}, but did not inhibit the decrease in I_{sc} induced by the K^+ channel opener. Even in the presence of Ba^{2+}, a broad channel blocker affecting most types of K^+ channels [10], no inhibition (and even a paradox enhancement of the response to mucosal pinacidil) was observed (Table 3), suggesting that the negative I_{sc} induced by mucosal administration of this K^+ channel activator might be related to effects of the drug on the movements of ions other than K^+.

Therefore, experimental series were designed to find out whether mucosal pinacidil might interfere with electrogenic Na^+ or Cl^- transport. Preincubation with amiloride (10^{-6} mol l^{-1} at the mucosal side) did not inhibit the negative I_{sc} induced by pinacidil ($5 \cdot 10^{-4}$ mol l^{-1} at the mucosal side; n = 14; data not shown) suggesting that pinacidil did not alter currents across epithelial Na^+ channels. Therefore, as a final hypothesis it was tested whether the negative I_{sc} evoked by mucosal pinacidil might reflect inhibition of basal anion secretion. Two approaches were used for this purpose. The first was based on the fact that spontaneous anion secretion across rat colon depends on the continuous stimulation of the epithelium by prosecretory neurotransmitters and prostaglandins [34]. Therefore, the effect of pinacidil ($5 \cdot 10^{-4}$ mol l^{-1} at the mucosal side) was tested in the absence or presence of combination of tetrodotoxin and indomethacin (each 10^{-6} mol l^{-1} at the serosal side). Under these conditions, in tissues where mucosal pinacidil only evoked a transient decrease in I_{sc} (red curve in Fig. 3a), the blocker combination suppressed the negative I_{sc} induced by pinacidil. In other tissues where pinacidil evoked a strong increase in I_{sc} after a transient decrease (black curve in Fig. 3a), both phases were suppressed by the blocker combination. This suggests that in some tissues mucosal pinacidil might diffuse in a sufficient concentration towards the basolateral membrane and activate there ATP-sensitive K^+ channels (see above); a response, however, which can only induce a transepithelial Cl^- secretion via hyperpolarization of the membrane when apical Cl^- channels are kept open by prosecretory neurotransmitters and prostaglandins.

In order to study this unexpected inhibitory effect of mucosal pinacidil on Cl^- secretion more directly, Cl^- currents across the apical membrane were measured in depolarized epithelia (via K^+ depolarization) using a chemical Cl^- gradient as driving force for Cl^- currents across the apical membrane [15]. When a Cl^- secretion was prestimulated by forskolin ($5 \cdot 10^{-6}$ mol l^{-1} at the mucosal and the serosal side), pinacidil ($5 \cdot 10^{-4}$ mol l^{-1} at the mucosal side) caused a transient inhibition of forskolin-induced I_{sc} (Fig. 3b). As under these conditions only Cl^- movement across apical Cl^- channels [12], can contribute to I_{sc}, these experiments clearly indicate that pinacidil, when administered at the mucosal side, transiently inhibits Cl^- secretion.

Immunodetection of the ATP-sensitive K^+ channel subunits in rat colonic epithelium

To determine which of the ATP-sensitive K^+ channel subunits are expressed by the rat colonic epithelium, immunostaining for the pore-forming subunits Kir6.1 and Kir6.2 as well as for the three regulatory subunits SUR1, SUR2A and SUR2B was performed. Nuclear staining with DAPI (blue fluorescence, Figs. 4, 5, and 6) was used to mark the shape of the crypts invaginating into the lamina propria.

A strong signal for the two pore-forming subunits, Kir6.1 and Kir6.2, was observed in the epithelial layer with no obvious gradient between the surface region and the cells in the depth of the crypt (Fig. 4). Only a weak staining was found in the smooth muscle layer of the muscularis propria as a weak punctuated band. The negative controls, in which the primary antibodies had been omitted, did not reveal a

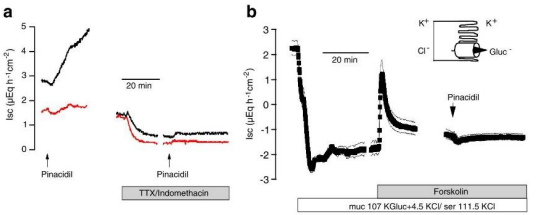

Fig. 3 **a** Individual tracing depicting the inhibition of the I_{sc} response evoked by pinacidil ($5{\cdot}10^{-4}$ mol·l^{-1} at the mucosal side) by a combination of tetrodotoxin and indomethacin (both 10^{-6} mol·l^{-1} at the serosal side, *gray rectangle*) in order to suppress basal anion secretion. Two examples from a total of 6 experiments were selected, a tissue (*red curve*), where mucosal pinacidil only evoked a transient decrease in I_{sc}, which was suppressed by the blocker combination, and another tissue (*black curve*), where pinacidil evoked a strong increase in I_{sc} after a transient decrease, which both were suppressed by the blocker combination. Due to this large variability of the I_{sc} pattern evoked by pinacidil, averaging of the individual I_{sc} response as it was performed in Figs. 1–2 was not meaningful. **b** Effect of pinacidil ($5{\cdot}10^{-4}$ mol·l^{-1} at the mucosal side) on Cl^- currents across the apical membrane. Tissues were basolaterally depolarized (111.5 mmol l^{-1} KCl at the serosal side in the presence of a Cl^- gradient (107 mmol l^{-1} K gluconate/4.5 mmol l^{-1} KCl at the mucosal side) as indicated by the schematic inset. A positive I_{sc} indicates the transport of anions from the serosal to the mucosal side (or the transport of cations in the reverse direction). Forskolin ($5{\cdot}10^{-6}$ mol·l^{-1} at the mucosal and the serosal side) was used to prestimulate Cl^- secretion. Data are means (*symbols*)±SEM (*lines*); n=8. On average, pinacidil evoked a decrease in I_{sc} by 0.36± 0.067 µEq·h^{-1}·cm^{-2} (n=8, P<0.05) under these conditions

signal excluding unspecific binding of the secondary antibodies used. The staining for the regulatory subunits SUR1 and SUR2B, however, was quite similar in the epithelial layer and the smooth muscle cells of the muscularis propria (Figs. 5 and 6). Again, for both regulatory subunits, there was no obvious gradient in the expression patterns of immature crypt and mature surface epithelium.

In contrast to the primary antibodies used for Kir6.1, Kir 6.2, SUR1, or SUR2B detection, in which the specific detection of the respective subunits in rat tissues has been verified by Western blot analysis (see Table 1 for references), primary antibodies against SUR2A with Western blots controls were missing. Therefore, we tried two different commercial antibodies (see Table 2) against this subunit. The first antibody (sc-32462) did not reveal a staining, neither in the colonic epithelium nor rat heart, which was used as control (data not shown). A second antibody used (sc-32461) revealed an immunoreactivity within the rat colonic wall. However, this reactivity was not inhibited by preincubation with the respective antigenic peptide indicating nonspecific binding of the antibody.

RT-PCR

Due to the lack of specific tools for the detection of SUR2A expression by immunohistochemical analysis, RT-PCR experiments were performed to investigate the expression of all subunits of ATP-sensitive K^+ channels at the mRNA level. The transcripts of the pore-forming and the regulatory subunits of ATP-sensitive K^+ channels were identified starting with mRNA prepared from isolated crypt, i.e. colonic epithelial cells devoid of connective tissue or smooth muscle, using published primers [37, 39]. Heart tissue was used as positive control due to its known ability to express the pore forming subunits Kir6.1 and Kir6.2 as well as the SUR subunits SUR1, SUR2A and SUR2B (for references, see [40]). For Kir6.1, a 340-bp band was observed in colonic epithelium, i.e. isolated crypts (Fig. 7a). Initially, several control tissues such as intact colon (i.e. mRNA isolated from the complete colonic wall), heart, and pancreas from rats were used as positive control tissues in order to check the quality of the PCR reaction. For Kir6.1, a 340 bp band was not only observed in homogenates from isolated colonic crypts, but also in intact colon or pancreas (data not shown).

With a similar approach, Kir6.2 was detected in rat colonic crypts with a 297 bp product (Fig. 7b). In accordance with the immunohistochemical experiments, SUR subunits were found in the colonic epithelium, i.e. the isolated crypts, with a 388 bp product specific for SUR1 and a 436 bp product specific for SUR2B (Fig. 8). Water controls without template DNA did not show any amplificates (Figs. 7 and 8).

Function of the ATP-sensitive potassium channels in the rat distal colon

Taking into account that the activity of K_{ATP} channels is linked to the metabolic status of a cell, it seemed to be of interest to investigate changes in I_{sc} induced by energy depletion in the absence and presence of blockers of these ion channels. Therefore, D-glucose was replaced by 2-

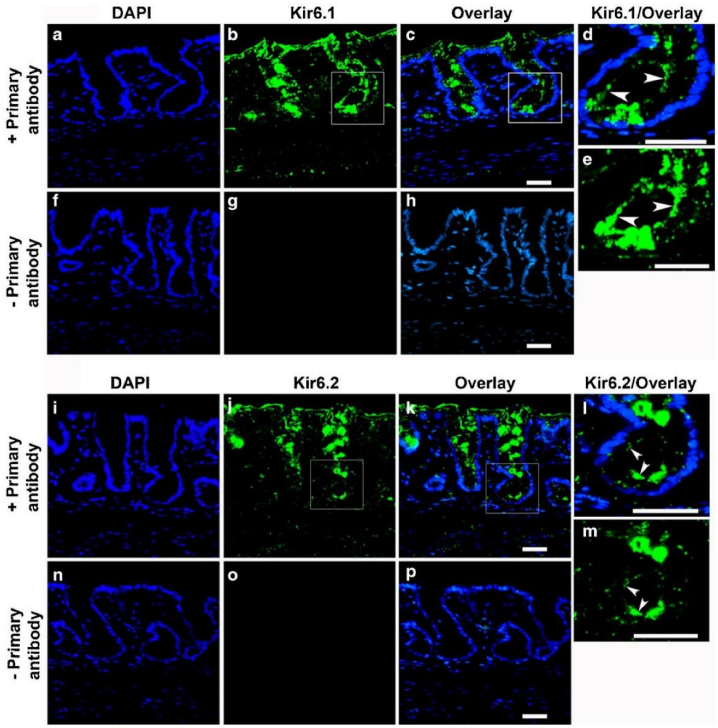

Fig. 4 Distribution of the Kir6.1 and Kir6.2 subunits of the ATP-sensitive K^+ channels in the rat colonic wall. For each picture, the orientation is as follows: *lower part* muscularis propria; *upper part* surface area of the colonic epithelium. From *left to right*, *first column* nuclear staining with 4′,6-diamidino-2-phenylindoldilactate (*DAPI*) (*blue*); *second column* Kir6.1 (**b**) or Kir6.2 (**j**); *third column*: overlay of both; *far right column*: **d**, **e**, **l** and **m** are higher magnifications of the selected areas (see *white frames*) in **c**, **b**, **k**, and **j**, respectively. *Arrows* show the apical localization of the corresponding subunits. *Second* (**f**–**h**) and *fourth* (**n**–**p**) *rows* negative controls obtained in the absence of primary antibody against the respective subunit. Typical results from three independent experiments. *Bar* 50 μm

deoxyglucose, an inhibitor of glycolysis, in the buffer. Under these conditions, remarkable changes in the I_{sc} and the conductance were observed: a triphasic change in the I_{sc}, consisting of a transient increase followed by a secondary peak and a late long-lasting decrease (Fig. 9a) as well as an increase in tissue conductance (Gt). The changes in I_{sc} induced by energy depletion were only weakly affected by glibenclamide ($5{\cdot}10^{-4}$ mol l^{-1} at the serosal side). In the presence of this inhibitor, the first peak of I_{sc} was slightly reduced from 2.30± 0.38 μEq$h^{-1}cm^{-2}$ in the absence of this blocker compared to 1.51±0.40 μEq$h^{-1}cm^{-2}$ (n=7, difference not

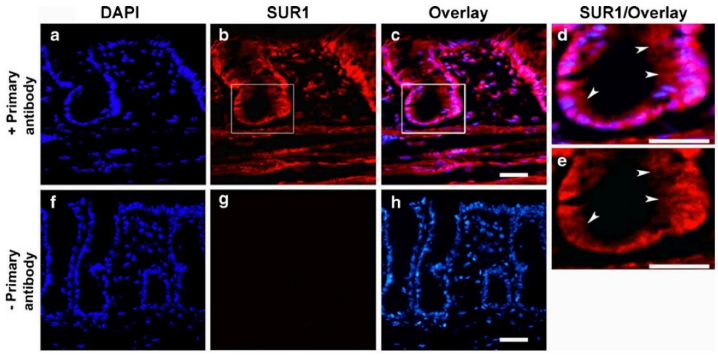

Fig. 5 Distribution of the SUR1 subunits of the ATP-sensitive K^+ channels in the rat colonic wall. For each picture, the orientation is as follows: lower part: muscularis propria; *upper part* surface area of the colonic epithelium. From *left to right*, *first column* nuclear staining with 4′,6-diamidino-2-phenylindoldilactate (*DAPI*) (*blue*); *second column*: SUR1 (**b**); *third column* overlay of both; *far right column*: **d** and **e** are higher magnifications of the selected areas (see *white frames*) in **c** and **b**, respectively. *Arrows* show the apical localization of the corresponding subunits. *Second row* (**f**–**h**): negative controls obtained in the absence of primary antibody against the respective subunit. Typical results from three independent experiments. *Bar* 50 μm

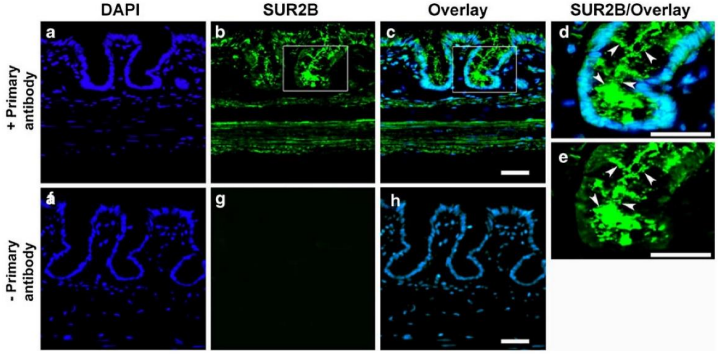

Fig. 6 Distribution of the SUR2B subunits of the ATP-sensitive K^+ channels in the rat colonic wall. For each picture, the orientation is as follows: *lower part* muscularis propria; *upper part* surface area of the colonic epithelium. From *left to right*: *first column* nuclear staining with 4′,6-diamidino-2-phenylindoldilactate (*DAPI*) (*blue*); *second column* SUR2B (**b**); *third column* overlay of both; *far right column* **d** and **e** are higher magnifications of the selected areas (see *white frames*) in **c** and **b**, respectively. *Arrows* show the apical localization of the corresponding subunits. *Second row* (**f**–**h**) negative controls obtained in the absence of primary antibody against the respective subunit. Typical results from three independent experiments. *Bar* 50 μm

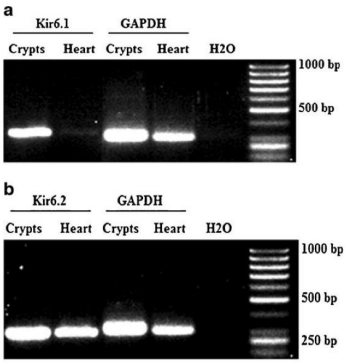

Fig. 7 RT-PCR detection of mRNA expression of ATP-sensitive K^+ channels Kir6.x subunits. The agarose gel shows bands of cDNA fragments amplified using primer pairs specific for Kir6.1 (fragment size of 340 bp; A) or primer pairs specific for Kir6.2 (fragment size of 297 bp; B). The mRNA was isolated from colonic crypts (i.e., pure epithelial cells). Transcripts from heart tissue were used as control to check the efficiency of the selected primers. GAPDH in isolated crypts (fragment size of 303 bp) served as further control to check the quality of the PCR reaction. Representative results from three independent experiments for each pore-forming subunit. Water control without template DNA did not show any amplificates

significant) in its presence. More dramatically, the changes in Gt were altered by this inhibitor. In the absence of glibenclamide, Gt rose from 17.1±2.5 to 56.1±20.5 mScm^{-2} (n=6, Fig. 9b, lower curve). In contrast, in the presence of glibenclamide, Gt rose from 15.1 ±1.6 mScm^{-2} (n=7) to values far above 100 mScm^{-2} (Fig. 9b, upper curve) suggesting an impairment of epithelial integrity. These data indicate that inhibition of ATP-sensitive K^+ channels dramatically increases the susceptibility of the colonic epithelium to energetic depletion.

Discussion

As reported earlier [14] and extended in the present study, the I_{sc} response evoked by the K^+ channel opener pinacidil depends on the side of administration of the drug (Fig. 1). After serosal administration, an increase in I_{sc} is observed, which is consistent with the assumption of an activation of basolateral K^+ channels. The increase in the basolateral K^+ conductance will cause a hyperpolarization of this membrane leading to apical chloride efflux via an increase in the electrical driving force for anion secretion. The consequence is that the transepithelial potential difference is increased, as the serosal side reaches more positive values and the I_{sc} necessary to compensate this potential difference under voltage-clamp conditions rises. The opposite change in I_{sc} was observed after mucosal administration of pinacidil or diazoxide, which proved, however, to represent an unexpected, transient inhibition of apical Cl^- channels (see below).

The action sites of pinacidil at K_{ATP} channels are the SUR subunits, with some preference for SUR2-subunits (for review, see [29]). The increase in I_{sc} evoked by serosally administered pinacidil was inhibited by blockers of K_{ATP} channels such as glibenclamide or gliclazide (Table 2). These are sulfonylurea derivatives with glibenclamide possessing an additional benzamido moiety [3]. They act via binding to different sites at the SUR-subunit of the K_{ATP} channels. SUR1 possesses both a sulfonylurea- and a benzamido-binding site, whereas SUR2A only exhibits a benzamido-binding site. Furthermore, there is a complex interaction of K_{ATP} channel blockers with intracellular MgADP. For example, in the absence of tolbutamide, MgADP inhibits K_{ATP} channels from pancreatic β-cells by binding at the Kir6.2 subunit, but activates the channels by

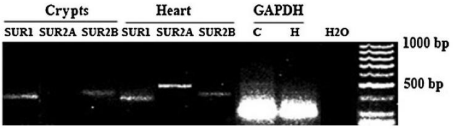

Fig. 8 RT-PCR detection of mRNA expression of the SUR subunits of ATP-sensitive K^+ channels. The agarose gel shows bands of DNA fragments amplified using primer pairs specific for SUR1 (fragment size of 388 bp), SUR2A (fragment size of 501 bp), and SUR2B (fragment size of 436 bp). The mRNA was isolated from colonic crypts, i.e. colonic epithelium. Transcripts from heart tissue were used as a positive control to check the efficiency of the selected primers. GAPDH from isolated crypts (*C*, fragment size of 303 bp) and heart (*H*) served as further controls to check the quality of the PCR reaction. Representative result from three independent experiments. Water control without template DNA did not show any amplificates

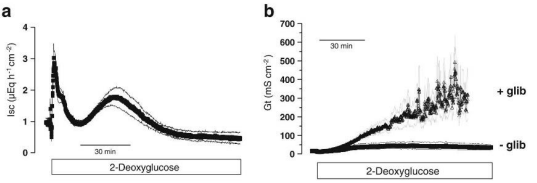

Fig. 9 **a** Changes in short-circuit current (I_{sc}) across rat colonic epithelium evoked by substitution of glucose by the glycolysis inhibitor 2-deoxyglucose (12.2 mmoll^{-1} at the mucosal and the serosal side). 2-Deoxyglucose induced a triphasic change in the I_{sc} over 2 h. An initial increase and a delayed secondary increase followed by a long-lasting decrease. **b** Changes in tissue conductance (Gt) evoked by 2-deoxyglucose in the absence (*lower curve*, *filled squares*, *−glib*) or the presence (*upper curve*, *open triangles*, *+glib*) of glibenclamide ($5{\cdot}10^{-4}$ moll^{-1} at the serosal side). In the presence of this blocker, the conductance dramatically increased with large scattering of the data. Data are means (*symbols*)±SEM (*lines*); n=6–7. For statistics, see text

binding at its SUR1 subunit; this latter action vanishes in the presence of tolbutamide so that the stimulatory action of ADP at the pore-forming Kir subunit is suppressed. The consequence is a tissue-specific sensitivity against K_{ATP} channel blockers depending on the molecular composition of the K_{ATP} channels expressed [13] which renders e.g. the Kir6.2/SUR2A combination (found, e.g. in heart) resistant against tolbutamide (reviewed by [3]).

The most potent inhibition of the basolateral K_{ATP} channel activation by pinacidil was reached with gliclazide (10^{-6}moll^{-1} at the serosal side; Table 2), a sulfonylurea derivative which structurally differs from tolbutamide by a single 3-amino-aza octane ring. Moreover, gliclazide alone did not change the basal I_{sc}, but reversed the electrical response evoked by serosal pinacidil from the usual increase into a decrease in I_{sc} (Fig. 2a). An explanation for this phenomenon might be that a part of the lipophilic drug, pinacidil, reaches also the apical membrane after serosal administration, so the increase in I_{sc} evoked by serosal pinacidil due to stimulation of Cl^- secretion is reduced under control conditions by the simultaneous inhibitory action of apical Cl^- channels. If the activation of basolateral K_{ATP} channels is prevented by serosal gliclazide, this latter action is unmasked. Also, Ca^{2+}-dependent K^+ channels contribute to the K^+ conductance of the basolateral membrane and to the maintenance of transepithelial anion secretion. However, inhibition of these K^+ channels with TPeA failed to inhibit the effect of pinacidil (Tables 2–3) excluding a role of these channels in the response to the K^+ channel opener. Glucoresponsive enteric neurons expressing Kir6.2 and SUR1 and sensitive to both tolbutamide and diazoxide have been found in guinea pig [21]. Since also colonic secretomotor neurons might be equipped with ATP-sensitive K^+ channels, it was of interest to study the possible involvement of secretomotor neurons in the I_{sc} increase evoked by pinacidil. However, neuronal blockade with tetrodotoxin did not change the effect of the K^+ channel activator (Table 2).

In contrast to the response evoked by serosally administered pinacidil, none of the inhibitors tested significantly reduced the negative I_{sc} evoked by mucosally administered pinacidil (Table 3), suggesting that the action of mucosal pinacidil does not represent activation of apical K^+ channels as previously assumed by us [27]. In contrast, the negative I_{sc} induced by mucosal pinacidil represents the inhibition of apical Cl^- channels as shown in basolaterally depolarized epithelia with a serosal-to-mucosal Cl^- concentration as driving force for Cl^- flux (Fig. 3b). Interestingly, for two other K_{ATP} channel activators, i.e. minoxidil and diazoxide, inhibition of Cl^- currents at CFTR-expressing 3 T3 fibroblasts has been shown [30]; a similar effect might underlie the antisecretory effect of mucosal pinacidil.

In order to obtain hints about the possible subunit composition(s) which might form the K_{ATP} channels in the colonic epithelium, we performed an immunohistochemical analysis of the rat colonic wall using antibodies against the three SUR- and two Kir6.x subunits. The presence of Kir6.2 (Fig. 4j–k) and SUR2B (Fig. 6b–c) in the muscularis propria is consistent with the identification of the complex Kir6.2/SUR2B as the typical non-vascular smooth muscle K_{ATP} channel [19]. Furthermore, an immunohistochemical signal was observed for SUR1 and SUR2B and both Kir6.x subunits within the colonic epithelium (Figs. 4, 5, and 6). Their expression in the epithelium was confirmed by an independent method, i.e. RT-PCR starting with mRNA obtained from isolated colonic crypts (Fig. 7 and 8). Consequently, similarly as, e.g. in the heart [40] or in vascular smooth muscle [7], more than one type of the pore-forming Kir6.x and of the regulatory SUR subunit is expressed by the colonic epithelium.

The present data only allow a description of the regional distribution of the different K_{ATP} channel subunits along the crypt-surface axis. The pore-forming Kir6.x subunits (Fig. 4) and the two SUR subunits studied (Figs. 5 and 6) exhibited a uniform expression along the crypt-surface axis. The distribution of the different subunits within an individual epithelial cell, however, can only be considered very cautiously from the present data. Both for the pore-forming Kir6.x subunits (Fig. 4) as well as for the two regulatory SUR subunits studied (Figs. 5 and 6) larger parts of the cytoplasm of the cells exhibited an immunohistochemical signal. This is, however, not unexpected, as the antibodies will also bind to channel subunits present in cell organelles involved in the synthesis of these proteins such as endoplasmic reticulum or involved in the regulation of channel density in the plasma membrane such as endocytotic vesicles. Furthermore, K_{ATP} channels are also found in mitochondria [18]. So these organelles will contribute to a more uniform distribution of the immunohistochemical signal of the corresponding subunits within a cell.

To our knowledge, the present results are the first evidence for the expression of the K_{ATP} channels subunits Kir6.1, Kir6.2, SUR1, and SUR2B on the mRNA and the protein level in colonic epithelium. The question, which of the theoretically possible combination(s) of the respective pore-forming Kir6.x and the regulatory SUR subunits finally form the octameric K_{ATP} channels in the basolateral membrane, however, is still open and requires further studies.

Nevertheless, we have shown previously that K_{ATP} channels as well as Ca^{2+}-dependent K^+ channels contribute to ion transport regulation and induction of anion secretion at rat distal colonic epithelium by the gasotransmitter, H_2S [14, 27]. Their pharmacological properties, i.e. the sensitivity against glibenclamide and gliclazide, but resistance against tolbutamide, contrasts with the tolbutamide sensitivity shown in human distal colon [22] where those channels additionally promote Na^+ absorption. These K_{ATP} channels obviously exert a protective action against energy depletion as their inhibition leads to a dramatic increase in tissue conductance (Fig. 9b) compared to tissues which were only exposed to energy depletion via exposure to 2-deoxyglucose in the absence of glibenclamide. This observation is in line with previous observations in rat small intestine, showing regulation of the paracellular permeability by the complex Kir6.1-SUR2A [20]. The exact mechanism, how these channels protect epithelial integrity, remains to be determined. However, activation of K_{ATP} channels will hyperpolarize the membrane and thereby reduce K^+ efflux, as the membrane potential is closer to the K^+ equilibrium potential. This should reduce the energy demand of the cell for recycling of K^+ into the cytosol via the Na^+-K^+-pump, which is one of the main energy consuming enzymes within a cell. In a pathophysiological perspective, inflammatory bowel diseases including colitis and Crohn's disease are associated with increased intestinal permeability [23, 25]. A decrease in epithelial ATP levels and increase in paracellular permeability have been shown in the distal ileum in patients with Crohn's disease [31]. Moreover, a protective function of K_{ATP} channels has been shown in rats with colitis, as a blockade of these channels with glibenclamide worsened the disease and increased mortality [36]. Consequently, K_{ATP} channels seem to affect both transepithelial ion transport as well as the permeability of the colonic epithelium.

Acknowledgments Supported by Deutsche Forschungsgemeinschaft, grant Di 388/11-1.

References

1. Amoroso S, Schmid-Antomarchi H, Fosset M, Lazdunski M (1990) Glucose, sulphonylureas, and neurotransmitter release: role of ATP-sensitive K^+ channels. Science 247:852–854
2. Ashcroft FM, Harrison DE, Ashcroft SJ (1984) Glucose induces closure of single potassium channels in isolated rat pancreatic beta-cells. Nature 312:446–448
3. Ashcroft FM, Gribble FM (1999) ATP-sensitive K^+ channels and insulin secretion: their role in health and disease. Diabetologia 42:903–919
4. Ashcroft FM, Gribble FM (2000) New windows on the mechanism of action of K_{ATP} channel openers. Trends Pharmacol Sci 21:439–445
5. Babenko AP, Aguilar-Bryan L, Bryan J (1998) A view of SUR/KIR6.x, KATP channels. Annu Rev Physiol 60:667–687
6. Blondeau N, Plamondon H, Richelme C, Heurteaux C, Lazdunski M (2000) K_{ATP} channel openers, adenosine agonists and epileptic preconditioning are stress signals inducing hippocampal neuroprotection. Neuroscience 100:465–474
7. Cao K, Tang G, Hu D, Wang R (2002) Molecular basis of ATP-sensitive K^+ channels in rat vascular smooth muscles. Biochem Biophys Res Commun 296:463–469
8. Chutkow WA, Makielski JC, Nelson DJ, Burant CF, Fan Z (1999) Alternative splicing of SUR2 exon 17 regulates nucleotide sensitivity of the ATP-sensitive potassium channels. J Biol Chem 274:13656–13665
9. Cook DL, Hales CN (1984) Intracellular ATP directly blocks K^+ channels in pancreatic B-cells. Nature 311:271–273
10. Cook NS, Quast U (1990) Potassium channels. Structure, classification, function and therapeutic potential. In: Cook NS (ed) Potassium channel pharmacology. Ellis Horwood, New York, pp 181–255
11. Edwards G, Weston AH (1993) The pharmacology of ATP-sensitive K^+ channels. Annu Rev Pharmacol Toxicol 33:597–637
12. Greger R (2000) Role of CFTR in the colon. Annu Rev Physiol 62:467–491
13. Gribble FM, Tucker SJ, Seino S, Ashcroft FM (1998) Tissue specificity of sulfonylureas: studies on cloned cardiac and beta-cell K_{ATP} channels. Diabetes 47:1412–1418
14. Hennig B, Diener M (2009) Actions of hydrogen sulfide on ion transport across rat distal colon. Brit J Pharmacol 158:1263–1275
15. Hennig B, Schultheiss G, Kunzelmann K, Diener M (2008) Ca^{2+}-induced Cl^- efflux at rat distal colonic epithelium. J Membrane Biol 221:61–72

16. Inagaki N, Gonoi T, Clement JP, Namba N, Inazawa J, Gonzalez G, Aguilar-Bryan L, Seino S, Bryan J (1995) Reconstitution of I_{KATP}: an inward rectifier subunit plus the sulphonylurea receptor. Science 270:1166–1170
17. Inagaki N, Gonoi T, Clement JP, Wang CZ, Aguilar-Bryan L, Bryan J, Seino S (1996) A family of sulfonylurea receptors determines the pharmacological properties of ATP-sensitive K^+ channels. Neuron 16:1011–1017
18. Inoue I, Nagase H, Kishi K, Higuti T (1991) ATP-sensitive K^+ channel in the mitochondrial inner membrane. Nature 352:244–247
19. Isomoto S, Kondo C, Yamada M, Matsumoto S, Higashiguchi O, Horio Y, Matsuzawa Y, Kurachi Y (1996) A novel sulfonylurea receptor forms with BIR (Kir6.2) a smooth muscle type ATP-sensitive K^+ channel. J Biol Chem 271:24321–24324
20. Jöns T, Wittschieber D, Beyer A, Meier C, Brune A, Thomzig A, Ahnert-Hilger G, Veh RW (2006) K^+-ATP-channel-related protein complexes: potential transducers in the regulation of epithelial tight junction permeability. J Cell Sci 119:3087–3097
21. Liu M, Seino S, Kirchgessner A (1999) Identification and characterization of glucoresponsive neurons in the enteric nervous system. J Neurosci 19:10305–10317
22. Maguire D, MacNamara B, Cuffe JE, Winter D, Doolan CM, Urbach V, O' Sullivan GC, Harvey BJ (1999) Rapid responses to aldosterone in human distal colon. Steroids 64:51–63
23. Meddings JB (1997) Review article: intestinal permeability in Crohn's disease. Aliment Pharmacol Ther 11(Suppl 3):47–53
24. Noma A (1983) ATP-regulated K^+ channels in cardiac muscle. Nature 305:147–148
25. Olaison G, Sjödahl R, Tagesson C (1990) Abnormal intestinal permeability in Crohn's disease. A possible pathogenic factor. Scand J Gastroenterol 25:321–8
26. Ploug KB, Edvinsson L, Olesen J, Jansen-Olesen I (2006) Pharmacological and molecular comparison of K_{ATP} channels in rat basilar and middle cerebral arteries. Eur J Pharmacol 553:254–262
27. Pouokam E, Diener M (2011) Mechanims of actions of hydrogen sulfide at rat distal colonic epithelium. Brit J Pharmacol 162:392–404
28. Schultheiss G, Kocks SL, Diener M (2002) Methods for the study of ionic currents and Ca^{2+}-signals in isolated colonic crypts. Biol Proced Online 3:70–78 (http://www.biologicalprocedures.com/)
29. Seino S, Miki T (2003) Physiological and pathophysiological roles of ATP-sensitive K^+ channels. Progr Biophys Mol Biol 81:133–176
30. Sheppard DN, Welsh MJ (1992) Effect of ATP-sensitive K^+ channel regulators on cystic fibrosis transmembrane conductance regulator chloride channels. J Gen Physiol 100:573–591
31. Söderholm JD, Olaison G, Peterson KH, Franzén LE, Lindmark T, Wirén M, Tagesson C, Sjödahl R (2002) Augmented increase in tight junction permeability by luminal stimuli in the non-inflamed ileum of Crohn's disease. Gut 50:307–313
32. Spruce AE, Standen NB, Standfield PR (1985) Voltage-dependent ATP-sensitive potassium channels of skeletal muscle membrane. Nature 316:736–738
33. Standen NB, Quayle JM, Davies NW, Brayden JE, Huang Y, Nelson MT (1989) Hyperpolarizing vasodilatators activate ATP-sensitive K^+ channels in arterial smooth muscle. Science 245:177–180
34. Strabel D, Diener M (1995) Evidence against direct activation of chloride secretion by carbachol in the rat distal colon. Eur J Pharmacol 274:181–191
35. Tilmann M, Kunzelmann K, Fröbe U, Cabantchik I, Lang HJ, Englert HC, Greger R (1991) Different types of blockers of the intermediate-conductance outwardly rectifying chloride channel in epithelia. Pflügers Arch Eur J Physiol 418:556–563
36. Wallace JL, Vong L, McKnight W, Dicay M, Gary RM (2009) Endogenous and exogenous hydrogen sulfide promotes resolution of colitis in rats. Gastroenterology 137:569–578
37. Wulfsen I, Hauber HP, Schiemann D, Bauer CK, Schwarz JR (2000) Expression of mRNA for voltage-dependent and inward-rectifying K channels in GH3/B6 cells and rat pituitary. J Neuroendocrinol 12:263–272
38. Yamada M, Isomoto S, Matsumoto S, Kondo C, Shindo T, Horio Y, Kurachi Y (1997) Sulphonylurea receptor 2B and Kir6.1 form a sulphonylurea-sensitive but ATP-insensitive K^+ channel. J Physiol 499:715–720
39. Zhou M, He HJ, Hirano M, Sekiguchi M, Tanaka O, Kawahara K, Abe H (2010) Localization of ATP-sensitive K^+ channel subunits in rat submandibular gland. J Histochem Cytochem 58:499–507
40. Zhou M, He HJ, Suzuki R, Liu KX, Tanaka O, Sekiguchi M, Itoh H, Kawahara K, Abe H (2007) Localization of sulfonylurea receptor subunits, SUR2A and SUR2B, in rat heart. J Histochem Cytochem 55:795–804
41. Zhou M, Tanaka O, Sekiguchi M, He HJ, Yasuoka Y, Itoh H, Kawahara K, Abe H (2005) ATP-sensitive K^+-channel subunits on the mitochondria and endoplasmic reticulum of rat cardiomyocytes. J Histochem Cytochem 53:1491–1500

8.4 “Hypoxia/reoxygenation effects on ion transport across rat colonic epithelium”

Schindele S, **Pouokam E**, Diener M. *Front. Physiol. Membr. Physiol. Biophys* (2016). 7: 247

Impakt Faktor: 4.134

Eigener Anteil an der Publikation:

- Initiative: 40 %
- Projektplanung: 60 %
- Durchführung der Versuche: 20 %
- Auswertung der Experimente: 60 %
- Erstellung der Publikation: 60 %

frontiers in Physiology

ORIGINAL RESEARCH
published: 21 June 2016
doi: 10.3389/fphys.2016.00247

Hypoxia/Reoxygenation Effects on Ion Transport across Rat Colonic Epithelium

*Sabine Schindele, Ervice Pouokam and Martin Diener**

Institute of Veterinary Physiology and Biochemistry, University Giessen, Giessen, Germany

Ischemia causes severe damage in the gastrointestinal tract. Therefore, it is interesting to study how the barrier and transport functions of intestinal epithelium change under hypoxia and subsequent reoxygenation. For this purpose we simulated hypoxia and reoxygenation on mucosa-submucosa preparations from rat distal colon in Ussing chambers and on isolated crypts. Hypoxia (N_2 gassing for 15 min) induced a triphasic change in short-circuit current (I_{sc}): a transient decrease, an increase and finally a long-lasting fall below the initial baseline. During the subsequent reoxygenation phase, I_{sc} slightly rose to values above the initial baseline. Tissue conductance (G_t) showed a biphasic increase during both the hypoxia and the reoxygenation phases. Omission of Cl^- or preincubation of the tissue with transport inhibitors revealed that the observed changes in I_{sc} represented changes in Cl^- secretion. The radical scavenger trolox C reduced the I_{sc} response during hypoxia, but failed to prevent the rise of I_{sc} during reoxygenation. All changes in I_{sc} were Ca^{2+}-dependent. Fura-2 experiments at loaded isolated colonic crypts revealed a slow increase of the cytosolic Ca^{2+} concentration during hypoxia and the reoxygenation phase, mainly caused by an influx of extracellular Ca^{2+}. Surprisingly, no changes could be detected in the fluorescence of the superoxide anion-sensitive dye mitosox or the thiol-sensitive dye thiol tracker, suggesting a relative high capacity of the colonic epithelium (with its low O_2 partial pressure even under physiological conditions) to deal with enhanced radical production during hypoxia/reoxygenation.

Keywords: Cl^- secretion, electrolyte transport, intracellular Ca^{2+}, rat colon

OPEN ACCESS

Edited by:
Catia Sternini,
University of California, Los Angeles, USA

Reviewed by:
Elisabetta Barocelli,
University of Parma, Italy
Muriel Larauche,
University of California, Los Angeles, USA

****Correspondence:***
Martin Diener
martin.diener@vetmed.uni-giessen.de

Specialty section:
This article was submitted to Gastrointestinal Sciences, a section of the journal Frontiers in Physiology

Received: *22 March 2016*
Accepted: *03 June 2016*
Published: *21 June 2016*

Citation:
Schindele S, Pouokam E and Diener M (2016) Hypoxia/Reoxygenation Effects on Ion Transport across Rat Colonic Epithelium. Front. Physiol. 7:247. doi: 10.3389/fphys.2016.00247

INTRODUCTION

Intestinal hypoxia, e.g., caused by arterial or venous thromboembolism or mechanical compression, is a severe gastroenterologic disease associated with a high lethality (Haglund and Bergqvist, 1999). A reduction in mucosal blood flow impairs energy supply to the high energy demanding intestinal epithelium leading to severe mucosal damage and a loss of the barrier function of the epithelium. This damage may be even exaggerated after reperfusion/reoxygenation due to the production of reactive oxygen species. The generation of these oxidants begins already during the hypoxic phase due to the accumulation of hypoxanthine and the proteolytic conversion of xanthine dehydrogenase into xanthine oxidase. Hypoxanthine is oxidized to xanthine, which is then further oxidized to uric acid; both reactions lead to the production of superoxide ($O_2^-\bullet$). When oxygen supply is restored during reperfusion/reoxygenation, radical production is exaggerated by $O_2^-\bullet$ generation in mitochondria (Dröge, 2002; Gonzalez et al., 2015).

Beside radical production, a further challenge for the epithelium during the ischemic/hypoxic phase is the fall in ATP production, with severe consequences for the activity of ATP-dependent enzymes such as the Na^+-K^+-ATPase, which is the motor for transcellular absorption or secretion of many solutes across epithelia (Kaplan, 1985). In excitable tissues such as heart, brain or vascular smooth muscle cells, however, the fall of the ATP/ADP ratio triggers a protective mechanism, i.e., the activation of ATP-sensitive K^+ (K_{ATP}) channels. The opening of these channels hyperpolarizes the membrane and thereby decreases energy demand via reduced excitability (for review of these channels, see Hibino et al., 2010). Ionic currents sensitive to sulphonylurea derivatives (which are prototypical blockers of K_{ATP} channels), however, have also been measured across the basolateral membrane of colonic epithelium of man (Maguire et al., 1999) and rat (Hennig and Diener, 2009). These channels function as heterooctamers (Babenko et al., 1998) consisting of four pore-forming subunits (K_{ir}) building an inwardly-rectifying K^+ channel and four regulatory, sulphonylurea-binding (SUR) subunits. On the molecular level, two pore-forming isoforms (K_{ir} 6.1 and K_{ir} 6.2) and two regulatory subunits (SUR1, SUR2B) have been identified on the mRNA as well as the protein level in colonic epithelium (Pouokam et al., 2013). As these channels play a central role in the protection of excitable tissues against hypoxia (e.g., Hund and Mohler, 2011), we investigated the impact of hypoxia/reoxygenation on the barrier and ion transport functions of the intestinal epithelium and the contribution of these channels to the changes induced. Ussing chamber experiments with mucosa-submucosa preparations and imaging experiments with isolated crypts from rat colon were conducted for this investigation.

MATERIALS AND METHODS

Tissue Preparation

Wistar rats of both sexes were used with a body mass of 170–220 g for imaging experiments or of 180–280 g for Ussing chamber experiments. The animals were bred and housed at the institute of veterinary physiology and biochemistry of the Justus-Liebig-University Giessen at an ambient temperature of 22.5°C and air humidity of 50–55% on a 12 h: 12 h light-dark cycle with free access to water and food until the time of the experiment. The rats were numbed by a stroke on the head and killed by cervical dislocation (approved by the named animal welfare officer of the Justus Liebig University, administrative number 487_M) and performed according to the German and European animal welfare law.

The colon was flushed with an ice-cold Tyrode solution and then put into ice-cold bathing solution. The serosa and muscularis propria were stripped away by hand to obtain the mucosa-submucosa preparation of the distal colon. Briefly, the colon was placed on a small plastic rod with a diameter of 5 mm. A circular incision was made near the anal end with a blunt scalpel and the serosa together with the tunica muscularis were gently removed in the proximal direction. Two segments of the distal colon of each rat were used for the experiments.

Solutions

The Ussing chamber experiments were carried out in a Tyrode solution containing (in $mmol \cdot l^{-1}$): NaCl 140, KCl 5.4, HEPES (N-(2-hydroxyethyl)piperazine-N′-2-ethanesulfonic acid) 10, glucose 12.2, $CaCl_2$ 1.25, $MgCl_2$ 1. The pH was adjusted with NaOH to 7.4. For the Cl^--free buffer, NaCl and KCl were replaced equimolarly by Na gluconate and K gluconate. For the Ca^{2+}-free buffer, $CaCl_2$ was omitted. For crypt isolation, a Ca^{2+}- and Mg^{2+}-free Hanks's balanced solution was used containing 10 $mmol \cdot l^{-1}$ EDTA (ethylenediamine tetraacetic acid), pH was adjusted with tris-base (tris(hydroxymethyl)-aminomethane) to 7.4. The isolated crypts were stored in a high potassium Tyrode solution consisting of ($mmol \cdot l^{-1}$): K gluconate 100, KCl 30, HEPES 10, NaCl 20, $MgCl_2$ 1, $CaCl_2$ 1.25, glucose 12.2, sodium pyruvate 5 and 1 $g \cdot l^{-1}$ BSA; pH was 7.4. All solutions were either gassed with room air to mimic normoxic conditions or with N_2 to induce hypoxia.

Crypt Isolation for Imaging Experiments

For the isolation of intact colonic crypts, the mucosa-submucosa preparation was fixed on a plastic holder with tissue adhesive and transferred for about 5–7 min to the EDTA solution. The tissue sample was vibrated once for about 30 s in order to isolate intact crypts. They were collected in high K^+ Tyrode buffer, similar to the intracellular medium (Böhme et al., 1991). The isolation procedure was performed at 38°C.

The crypts were attached to the surface of a cover slip (diameter 22 mm) with the aid of poly-L-lysine (0.1 $mg \cdot ml^{-1}$; Biochrom, Berlin, Germany). For Ca^{2+}-imaging, they were incubated for 60 min with 2.5 $\mu mol \cdot l^{-1}$ fura-2 acetoxymethylester (AM) in the presence of 0.05 $g \cdot l^{-1}$ pluronic acid (Life Technologies, Darmstadt, Germany). Afterwards, the dye which was not taken up by the cells was washed away. Then the preparation was transferred to a gas-tight hypoxia chamber (own design; see inset of **Figure 6**). The chamber had a volume of 2 ml. It was perfused with 140 $mmol \cdot l^{-1}$ NaCl Tyrode at about 5 $ml \cdot min^{-1}$. In order to mimic normoxic or hypoxic conditions, the superfusing solutions were continuously gassed with air or with N_2.

Changes in the cytosolic Ca^{2+} concentration were monitored as changes in the fura-2-ratio (emission at an excitation wave length of 340 nm divided by the emission at an excitation wave length of 380 nm; emission was measured at a wave length above 410 nm). In order to measure mitochondrial production of hydrogen peroxide (H_2O_2), the crypts were incubated for 60 min with $5 \cdot 10^{-6}$ $mol \cdot l^{-1}$ mitosox at room temperature. Potential production of superoxide anion ($O_2^- \bullet$) was monitored as changes in the mitosox signal (emission above 580 nm at an excitation wave length of 390 nm). For the registration of changes in the cytosolic concentration of reduced glutathione (GSH), the crypts were incubated with for 60 min with $2 \cdot 10^{-5}$ $mol \cdot l^{-1}$ thiol tracker violet stain at room temperature. The GSH concentration was monitored as changes in the thiol tracker violet signal (emission above 410 nm at an excitation wave length of 380 nm).

The imaging experiments were carried out on an inverted microscope (Olympus IX-50; Olympus, Hamburg, Germany), equipped with an epifluorescence set-up and an image analysis

system (Till Photonics, Martinsried, Germany). Several regions of interest (ROI's) were selected, each one with the size of one cell. Data were sampled at 0.2 Hz. The baseline in the fluorescence signal was measured for several minutes before any drug was added.

Short-Circuit Current Measurement

The tissue was fixed in a modified Ussing chamber, bathed with a volume of 3.5 ml on each side of the mucosa-submucosa preparation and short-circuited by a computer-controlled voltage-clamp device (Ingenieur Büro Mußler, Aachen, Germany) with correction for solution resistance. The tissue was incubated at 37°C and the electric activities were measured on an area of 1 cm^2. Tissue conductance (G_t) was measured every min by the voltage deviation induced by a current pulse (±50 μA, duration 200 ms) under open-circuit conditions. Short-circuit current (I_{sc}) was continuously recorded on a chart recorder. I_{sc} is expressed as $\mu Eq \cdot h^{-1} \cdot cm^{-2}$, i.e., the flux of monovalent ion per time and area with $1\ \mu Eq \cdot h^{-1} \cdot cm^{-2} = 26.9\ \mu A \cdot cm^{-2}$.

Drugs

$BaCl_2$ and $GdCl_3$ were dissolved in an aqueous stock solution. Bumetanide was dissolved in ethanol (final maximal concentration 0.25% v/v). 2-APB (2-aminoethoxydiphenyl borate), glibenclamide (Boehringer Mannheim, Mannheim, Germany), NPPB, pinacidil and trolox C were dissolved in dimethylsulphoxide (final maximal concentration 0.25% v/v). All fluorescent dyes were obtained from Life Technologies, (Darmstadt, Germany). If not indicated differently, drugs were from Sigma (Taufkirchen, Germany).

Statistics

Results are given as means ± one standard error of the mean (SEM) with the number n of analyzed tissues or cells received from at least three animals. For the comparison of two groups, either a student's *t*-test or a Mann-Whitney *U*-test was used. An *F*-test decided, which test method had to be used. To compare more than two groups, an analysis of variance was performed followed by *post-hoc* Tukey's -test. $P < 0.05$ was considered to be statistically significant.

RESULTS

Hypoxia and Subsequent Reoxygenation Modulate Ion Transport across Rat Colonic Epithelium

Hypoxia reached by means of N_2 gassing for 15 min in Ussing chambers was preceded and followed by room air gassing in order to mimic normoxia and reoxygenation, respectively. Baseline in short-circuit current (I_{sc}), which is a measure of net ion movement across the epithelium, at the end of the normoxic period amounted to 1.55 ± 0.98 $\mu Eq \cdot h^{-1} \cdot cm^{-2}$ ($n = 8$). As a response to hypoxia, a triphasic change (**Figure 1A**) in I_{sc} was induced. It consisted of an initial, transient decrease (Dec1 in **Figure 1A**) of −0.91 ± 0.20 $\mu Eq \cdot h^{-1} \cdot cm^{-2}$ under the initial baseline. This was followed by a transient rise (peak) of 0.57 ± 0.17 $\mu Eq \cdot h^{-1} \cdot cm^{-2}$ and finally a long-lasting decrease (Dec2 in **Figure 1A**) of −1.26 ± 0.19 $\mu Eq \cdot h^{-1} \cdot cm^{-2}$ (**Table 1**) under the initial baseline. Approximately 10 min after the start of the hypoxic phase, the I_{sc} reached a stable plateau (**Figure 1A**). Reoxygenation caused the I_{sc} to rise again after a delay of about 7 min. After 15 min in air gassing, the I_{sc} had risen by 0.37 ± 0.20 $\mu Eq \cdot h^{-1} \cdot cm^{-2}$ (**Table 1**) compared to the baseline at the end of the N_2 period and further rose to value of 1.69 ± 1.38 $\mu Eq \cdot h^{-1} \cdot cm^{-2}$ ($n = 8$) above the current during the hypoxic period, when the reoxygenation period was extended to a duration of 30 min (**Figure 1A**). In time-dependent control experiments with continuous air gassing, only a slight increase in I_{sc} was observed (**Figure 1B**), which rose by 0.35 ± 0.2 $\mu Eq \cdot h^{-1} \cdot cm^{-2}$ ($n = 15$) in the same time interval as described above for the hypoxia/reoxygenation experiments.

Hypoxia caused a strong increase in tissue conductance (G_t). It rose from 28.6 ± 3.4 $mS \cdot cm^{-2}$ at the end of the normoxic period to 42.5 ± 7.2 $mS \cdot cm^{-2}$ ($n = 8$, $P < 0.05$) during

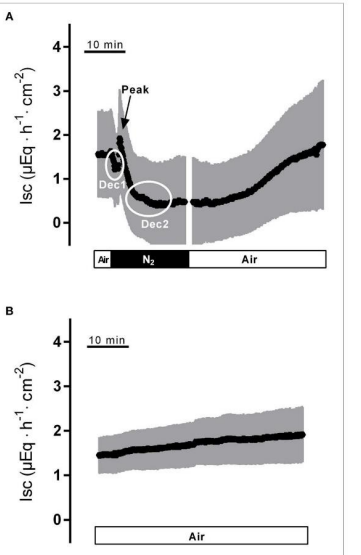

FIGURE 1 | Effect of hypoxia (N_2, black bar) and reoxygenation on I_{sc} (A) in comparison to a time-dependent control (B) continuously gassed with air (white bar). Dec1, Peak and Dec2 mark the minimal respective maximal changes in I_{sc} quantified in **Tables 1**– **3**. Values are means (symbols) ± SEM (gray area), $n = 8$ **(A)** or 15 **(B)**. For statistics, see **Table 1**.

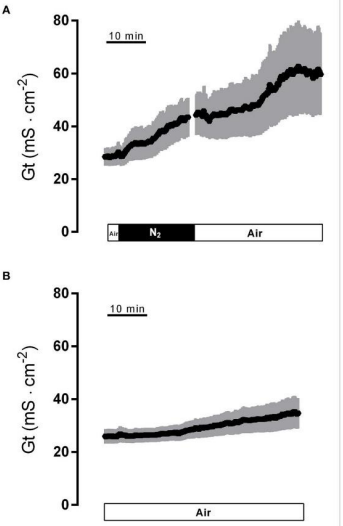

FIGURE 2 | Effect of hypoxia (N_2; black bar) and reoxygenation on tissue conductance (A) in comparison to a time-dependent control (B) continuously gassed with air (white bar). Values are means (symbols) ± SEM (gray area), $n = 8$ **(A)** or 15 **(B)**.

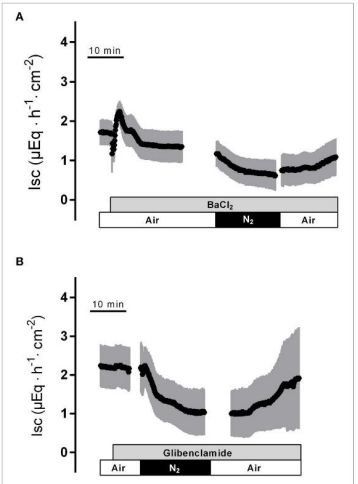

FIGURE 3 | The nonselective K^+ channel blocker Ba^{2+} (10^{-2} mol·l^{-1} at the serosal side; gray bar) suppresses the peak in I_{sc} induced by hypoxia (A), whereas the K_{ATP} channel blocker glibenclamide ($5{\cdot}10^{-4}$ mol·l^{-1} at the serosal side) was ineffective (B). Values are means (symbols) ± SEM (gray area), $n = 6$–10. For statistics, see **Table 1**.

the hypoxic phase. Switching back to air gassing during the reoxygenation phase did not lead to a recovery of the G_t, which remained stable at an elevated level for about 15 min, before a secondary rise in G_t was observed (**Figure 2A**). In time-dependent control experiments with continuous air gassing, only a slight increase in G_t was observed (**Figure 2B**) from 26.5 ± 2.8 mS·cm^{-2} to 34.0 ± 5.6 mS·cm^{-2} in the same time interval as described above for the hypoxia/reoxygenation experiments. Due to the strong secondary increase in G_t during the late reoxygenation phase, which suggests a damage of the colonic epithelium, in all subsequent experiments the reoxygenation period was limited to 15 min.

Involvement of K^+ Channels

To find out whether K^+ channels play a role in the response to hypoxia and subsequent reoxygenation, blockers of K^+ conductances known to be involved in rat colonic epithelial ion transport (Strabel and Diener, 1995; Schultheiss and Diener, 1997; Warth and Barhanin, 2003) were used. Preincubation of the tissue with Ba^{2+} (10^{-2} mol·l^{-1} at the serosal side), a nonselective K^+ channel blocker (Cook and Quast, 1990), caused a significant reduction in the peak of I_{sc} observed during hypoxia (**Figure 3A**, **Table 1**). Administration of serosal $BaCl_2$ caused a paradox transient increase in I_{sc}, which is known to represent the transient activation of Ca^{2+}-calmodulin dependent Cl^- secretion (Hardcastle et al., 1985).

In order to investigate the involvement of K_{ATP} channels, the tissue was pretreated with glibenclamide ($5{\cdot}10^{-4}$ mol·l^{-1}, at the serosal side), an inhibitor of this type of K^+channels (for review of the drugs acting on K_{ATP} channels, see Seino and Miki, 2003). However, neither the triphasic change in I_{sc} during hypoxia nor the secondary rise in I_{sc} during the reoxygenation were altered in the presence of glibenclamide (**Figure 3A**, **Table 1**). Also preincubation with pinacidil ($5{\cdot}10^{-4}$ mol·l^{-1}, at the serosal side), an opener of K_{ATP} channels, did not alter the currents induced by hypoxia/reoxygenation (**Table 1**) suggesting that K_{ATP} channels are not involved in the induction of the currents by hypoxia/reoxygenation in this tissue.

The Currents Induced by Hypoxia/Reoxygenation Represent Changes in Cl^- Secretion

Changes in I_{sc} across colonic epithelium often represent changes in anion secretion. In order to be secreted, Cl^- is taken up across the basolateral membrane via the Na^+-K^+-$2Cl^-$ cotransporter (NKCC1) and leaves the cell via apical anion channels mainly of the CFTR (cystic fibrosis transmembrane conductance regulator) type (for review see Greger, 2000). The driving for Cl^- exit across these channels is the negative membrane potential, which is dominated by a K^+ diffusion potential generated by K^+ efflux via basolateral K^+ channels (Strabel and Diener, 1995; Warth and Barhanin, 2003). In order to find out, whether the changes in I_{sc} observed during hypoxia/reoxygenation represent changes in Cl^- transport, blockers of key ion transporters involved in Cl^- secretion were used.

In the presence of bumetanide (10^{-3} mol·l^{-1} at the serosal side), an inhibitor of the NKCC1 (for review see Greger, 2000), all three phases of the current response observed during hypoxia were significantly reduced (**Table 2**). Also the subsequent rise in I_{sc} during the reoxygenation phase was diminished (**Figure 4A**), although this inhibition did not reach statistical significance (**Table 2**). In order to block apical Cl^- channels, NPPB (10^{-4} mol·l^{-1} at the mucosal side), a Cl^- channel blocker (Diener and Rummel, 1989), was used. NPPB suppressed the currents induced by hypoxia and reduced (without reaching statistical significance) the secondary rise in I_{sc} during the reoxygenation period (**Figure 4B**, **Table 2**). Both bumetanide as well as NPPB induced a fall in I_{sc}, which has to be expected after blockade of basolateral Na^+-K^+-$2Cl^-$ cotransporter and of apical anion channels, respectively, because basal I_{sc} in rat colon is dominated by a spontaneous anion secretion, mainly of Cl^- (Strabel and Diener, 1995).

Substitution of Cl^- with the impermeable anion gluconate showed similar effects (**Table 2**) indicating that hypoxia and subsequent reoxygenation modulate Cl^- transport across the colonic epithelium.

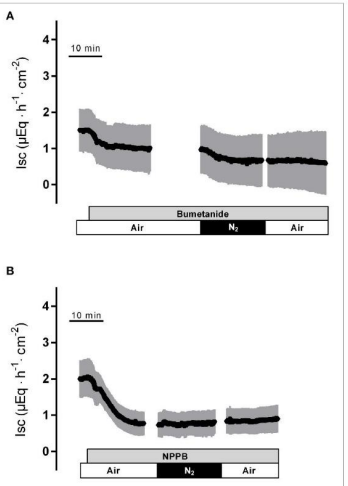

FIGURE 4 | The response to hypoxia/reoxygenation is suppressed by bumetanide (10^{-3} mol·l^{-1} at the serosal side; gray bar in A) or NPPB (10^{-4} mol·l^{-1} at the mucosal side; gray bar in B). Values are means (symbols) ± SEM (gray area), n = 8–9. For statistics, see **Table 2**.

Intracellular Messenger Substances Involved in the Changes in I_{sc}

The reoxygenation phase following hypoxia mimics the reperfusion situation following ischaemia *in vivo*, which is known to be concomitant with an increased production of oxidants and radicals (Kowaltowski et al., 2009). In order to find out, whether radicals, which are known to act as intracellular signaling molecules (Dröge, 2002), play a role in the currents induced by hypoxia/reoxygenation, tissues were pretreated with trolox C, a derivate of α-tocopherol (Lee et al., 2014; Vergauwen et al., 2015). In the presence of this radical scavenger, the initial decrease and the peak in I_{sc} during the hypoxic phase tended to be reduced and the secondary decrease in I_{sc} was significantly inhibited by 55%. Surprisingly, the increase in I_{sc} during the reoxygenation period remained unaltered in the presence of trolox C (**Table 2**).

A second messenger known to be involved, e.g., in the response of endothelial cells to hypoxia/reoxygenation is Ca^{2+} (Schäfer et al., 2003). As this second messenger is also able to induce intestinal Cl^- secretion predominantly via stimulation of basolateral Ca^{2+}-dependent K^+ channels (Böhme et al., 1991) supported by the transient opening of Ca^{2+}-dependent apical Cl^- channels (Hennig et al., 2008), the involvement of Ca^{2+} in the I_{sc} response evoked by hypoxia/reoxygenation was investigated.

In the absence of serosal Ca^{2+}, the peak in I_{sc} during the early hypoxic period was significantly reduced suggesting that this phase is caused by the transient stimulation of Ca^{2+}-dependent Cl^- secretion. When in addition the release of Ca^{2+} from intracellular stores was inhibited with 2-APB (10^{-4} mol·l^{-1}), a blocker of inositol-1,4,5-trisphosphate (IP_3) receptors (Maruyama et al., 1997), all three phases of the I_{sc} response during hypoxia were significantly diminished (**Table 3**).

Changes in the Cytosolic Ca^{2+} Concentration

Ca^{2+} measurements at fura-2-loaded isolated crypts in imaging experiments revealed a slow increase of the cytosolic Ca^{2+}

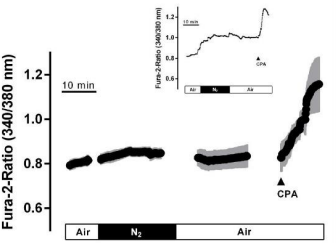

FIGURE 5 | In fura-2 imaging experiments with isolated crypts a moderate increase in the cytosolic Ca^{2+} concentration during hypoxia was observed followed by a secondary increase during the reoxygenation phase. At the end of the experiment, cyclopiazonic acid (CPA; 10^{-5} mol·l^{-1}; filled arrow) was administered as viability control. Values are means (symbols) ± SEM (gray area), $n = 40$. The inset shows an original tracing which exemplifies the increase in the fura-2 ratio signal more clearly, as the time ensemble presented in the averaged figure tends to dampen signal amplitudes if not all cells respond synchronously. For statistics, see **Table 4**.

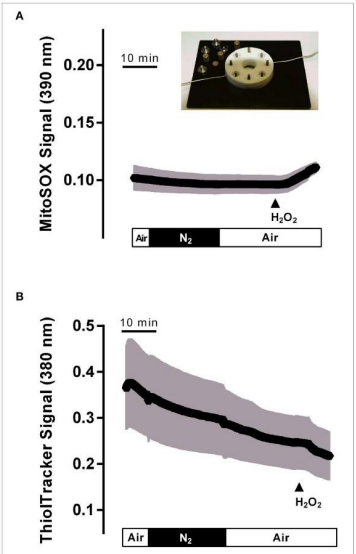

FIGURE 6 | Hypoxia (N_2 gassing; black bar)/reoxygenation did not affect mitochondrial radical production (A) or cytosolic glutathione concentration (B) in isolated colonic crypts. Values are means (symbols) ± SEM (gray area), $n = 75$–90. At the end of the experiments, H_2O_2 (10^{-2} mol·l^{-1}; filled arrow) was administered as control. The inset shows the hypoxia chamber, in which the crypts (mounted between two glass slides fixed between teflon rings) were superfused with N_2- or air-gassed solutions.

concentration during hypoxia (**Figure 5**). When switching back to the perfusion of the chamber with air-gassed buffer solutions, the fura-2 ratio signal further increased (**Table 4**). At the end of the experiment, intracellular Ca^{2+} stores were depleted by cyclopiazonic acid (10^{-5} mol·l^{-1}), an inhibitor of sarcoplasmic-endoplasmic Ca^{2+}-ATPases (SERCA; Plenge-Tellechea et al., 1997), which served as viability control. Cyclopiazonic acid induced a consistent and prompt increase in the fura-2 ratio signal thus excluding irreversible changes of the colonic epithelium during the hypoxic period. The increase in the cytosolic Ca^{2+} concentration was abolished when the crypts were superfused with a Ca^{2+}-free solution either alone or in combination with the IP_3 receptor blocker 2-APB (10^{-4} mol·l^{-1}). The same was observed, when the crypts were pretreated with Gd^{3+} ($5{\cdot}10^{-6}$ mol·l^{-1}), a blocker of nonselective cation channels (Frings et al., 1999) responsible for store-operated Ca^{2+} entry in these cells (**Table 4**).

When the crypts were pretreated with the radical scavenger trolox C (10^{-4} mol·l^{-1}), no increase in the fura-2 ratio was induced by hypoxia and also the secondary increase during the reoxygenation period was abolished (**Table 4**).

Involvement of Reactive Oxygen Species

As the production of oxidants in mitochondria starts with the conversion of the superoxide anion ($O_2^-\bullet$) to hydrogen peroxide (H_2O_2), a reaction catalyzed by the enzyme superoxide dismutase (Yu, 1994), it was of interest to check the production of potential oxidants in the isolated crypts during hypoxia/reoxygenation. For this purpose, the fluorescent dye mitosox was used. However, the mitosox signal was unaltered during the hypoxia and the subsequent reoxygenation period (**Figure 6A**). The mitosox fluorescence (arbitrary units) fell by −0.005 ± 0.002 during the hypoxia and by −0.004 ± 0.002 ($n = 50$) during reoxygenation. In time-dependent control experiments (without hypoxia/reoxygenation), a similar change of the mitosox signal by −0.005 ± 0.002 and by −0.004 ± 0.003 ($n = 44$) in the same time intervals was observed. At the end of the experiment H_2O_2 (10^{-2} mol·l^{-1}) was administered in order to prove the validity of the method. As expected, hydrogen peroxide induced a strong increase in the mitosox fluorescence signal by 0.12 ± 0.004 ($n = 50$) in the hypoxia group and by 0.16 ± 0.01 ($n = 44$) in the time-dependent control experiments.

Physiological protection against oxidants is insured by glutathione (GSH), the main reducing agent in the cytosol (Mandavilli and Janes, 2010), which keeps thiols in the reduced state in intact cells. In order to find out, whether cytosolic glutathione might "trap" the expected production of

TABLE 1 | Effect of drugs modulating K^+ channel activity on the I_{SC} induced by hypoxia/reoxygenation.

Condition	Changes in I_{SC} (ΔI_{SC}) induced by hypoxia and reoxygenation ($\mu Eq \cdot h^{-1} \cdot cm^{-2}$)				
	Hypoxia			Reoxygenation	
	Initial decrease (Dec1) 0–5 min	Peak hypoxia 0–5 min	Secondary decrease (Dec2) 5–15 min	Peak reoxygenation 3–15 min	*n*
Control	−0.91 ± 0.20	0.57 ± 0.17	−1.26 ± 0.19	0.37 ± 0.20	8
$BaCl_2$	−0.54 ± 0.12	−0.15 ± 0.11*	−0.81 ± 0.16	0.47 ± 0.15	10
Glibenclamide	−0.80 ± 0.18	0.24 ± 0.09	−1.24 ± 0.33	0.78 ± 0.55	6
Pinacidil	−0.60 ± 0.18	0.49 ± 0.13	−1.14 ± 0.28	0.54 ± 0.14	5

*The effects of hypoxia and reoxygenation on I_{SC} were tested in presence of different K^+ channel blockers or activators (all administered to the serosal side). Values were taken as follows (see also **Figure 1**): Dec1: minimal I_{SC} during min 0–5 of the hypoxic period; peak hypoxia: maximal I_{SC} during min 0–5 of the hypoxic period; Dec2: minimal I_{SC} during min 5–15 of the hypoxic period; peak reoxygenation: maximal I_{SC} during min 3–15 of the reoxygenation period. The first row shows the response to hypoxia followed by reoxygenation in the absence of inhibitors. Drugs used were: Ba^{2+} (a nonselective K^+ channel blocker; 10^{-2} mol·l^{-1}), glibenclamide (an inhibitor of K_{ATP} channels; $5 \cdot 10^{-4}$ mol·l^{-1}) and pinacidil (an opener of K_{ATP} channels; $5 \cdot 10^{-4}$ mol·l^{-1}). Data are given as change of I_{SC} (ΔI_{SC}) compared to the baseline just prior the start of the respective gassing period and are means ± SEM. n = number of tissues. *P < 0.05 vs. control (analysis of variances followed by post-hoc test of Tukey).*

TABLE 2 | The transepithelial currents induced by hypoxia/reoxygenation represent changes in Cl^- secretion and are blunted by a radical scavenger.

Condition	Changes in I_{SC} (ΔI_{SC}) induced by hypoxia and reoxygenation ($\mu Eq \cdot h^{-1} \cdot cm^{-2}$)				
	Hypoxia			Reoxygenation	
	Initial decrease (Dec1) 0–5 min	Peak hypoxia 0–5 min	Secondary decrease (Dec2) 5–15 min	Peak reoxygenation 3–15 min	*n*
With Cl^-	−0.91 ± 0.20	0.57 ± 0.17	−1.26 ± 0.19	0.37 ± 0.91	8
Cl^--free	−0.39 ± 0.07*	−0.08 ± 0.06*	−0.47 ± 0.01*	0.17 ± 0.07	8
NPPB	−0.14 ± 0.06*	0.09 ± 0.05*	−0.14 ± 0.09*	0.17 ± 0.07	9
Bumetanide	−0.31 ± 0.05*	0.04 ± 0.02*	−0.49 ± 0.06*	0.12 ± 0.12	8
Trolox C	−0.40 ± 0.12	0.15 ± 0.10	−0.55 ± 0.14*	0.36 ± 0.06	6

*The effects of hypoxia and reoxygenation on I_{SC} were tested in the absence (Cl^- being replaced by the impermeable anion gluconate) of chloride ions, after blockade of Cl^- channels with NPPB, after blockade of the Na^+-K^+-$2Cl^-$ cotransporter with bumetanide, or scavenging of oxidants with trolox C. For definitions of the parameters measured, see legend of **Table 1**. For better orientation, in the 1st row (with Cl^-) the control response to hypoxia/reoxygenation from **Table 1** is shown again. Concentrations of the inhibitors were: NPPB (10^{-4} mol·l^{-1} at the mucosal side), bumetanide (10^{-3} mol·l^{-1} at the serosal side), trolox C ($2 \cdot 10^{-4}$ mol·l^{-1} at the serosal side). Data are given as change of I_{SC} (ΔI_{SC}) compared to the baseline just prior the start of the respective gassing period and are means ± SEM. n = number of tissues. *P < 0.05 vs. control (analysis of variances followed by post-hoc test of Tukey).*

TABLE 3 | Role of Ca^{2+} in the hypoxia/reoxygenation-evoked changes in I_{SC}.

Condition	Changes in I_{SC} (ΔI_{SC}) induced by hypoxia and reoxygenation ($\mu Eq \cdot h^{-1} \cdot cm^{-2}$)				
	Hypoxia			Reoxygenation	
	Initial decrease (Dec1) 0–5 min	Peak hypoxia 0–5 min	Secondary decrease (Dec2) 5–15 min	Peak reoxygenation 3–15 min	*n*
With Ca^{2+}	−0.91 ± 0.20	0.57 ± 0.17	−1.26 ± 0.19	0.37 ± 0.91	8
0 Ca^{2+}	−0.86 ± 0.14	0.20 ± 0.05*	−0.94 ± 0.15	0.50 ± 0.07	13
0 Ca^{2+} + 2-APB	−0.20 ± 0.06*	0.05 ± 0.02*	−0.28 ± 0.10*	0.21 ± 0.05	8

*The effects of hypoxia and reoxygenation on I_{SC} were tested in the presence (1st row) or absence of Ca^{2+} althar alone (2nd row) or combined with 2-APB (3rd row; 10^{-4} mol·l^{-1} at the serosal side). For definitions of the parameters measured, see legend of **Table 1**. For better orientation, in the 1st row (with Ca^{2+}) the control response to hypoxia/reoxygenation (**Table 1**) is shown again. Ca^{2+} was omitted from the serosal side of the tissue. Data are given as change of I_{SC} (ΔI_{SC}) compared to the baseline just prior the start of the respective gassing period and are means ± SEM. n = number of tissues. *P < 0.05 vs. control (analysis of variances followed by post-hoc test of Tukey).*

oxidants during hypoxia/reoxygenation, changes in the cytosolic glutathione concentration were monitored by loading the colonic crypts with thiol tracker. However, no change in the signal of this fluorescent indicator was observed during the hypoxic period, i.e., during superfusion with N_2-gassed solutions, or the subsequent reoxygenation period. Instead, a continuous, time-dependent decrease of the signal, which probably reflects bleaching of the dye, was observed (**Figure 6B**). The thiol tracker signal (arbitrary units) fell from the beginning to the end of the hypoxia period by −0.06 ± 0.009 and by −0.11 ± 0.01 (n = 90) during the subsequent reoxygenation phase. These values were not different from the changes in time-dependent control

TABLE 4 | Changes in the cytosolic Ca^{2+} concentration of isolated crypts during hypoxia/reoxygenation.

	Δ fura-2 ratio (340/380 nm)			
Condition	**Hypoxia (means measured over the final 3 min)**	**Reoxygenation (means measured over the final 3 min)**	**Cyclopiazonic acid (peak response)**	***n***
Control	0.0008 ± 0.01	0.03 ± 0.02*	0.22 ± 0.03	40
Trolox C	−0.07 ± 0.32*	0.00 ± 0.42	0.42 ± 0.57	46
Gd^{3+}	−0.01 ± 0.01	−0.01 ± 0.02	0.3 ± 0.02*	57
0 Ca^{2+}	−0.10 ± 0.01*	−0.11 ± 0.03*	0.17 ± 0.01	60
0 Ca^{2+} + 2-APB	0.02 ± 0.01	−0.001 ± 0.01	0.08 ± 0.005	36

*Changes in the fura-2 ratio signal induced by hypoxia and subsequent reoxygenation under control conditions (with Ca^{2+}), in the presence of the radical scavenger trolox C (10^{-4} mol·l^{-1}), after blockade of store-operated Ca^{2+} channels with Gd^{3+} ($5{\cdot}10^{-6}$ mol·l^{-1}), in the absence of Ca^{2+} ions or after additional blockade of IP_3 receptors with 2-APB (10^{-4} mol·l^{-1}). Data are given as change of fura-2 ratio [Δfura-2 ratio (340/380 nm)] compared to the baseline just prior the start of the respective gassing period or prior administration of cyclopiazonic acid 10^{-5} mol·l^{-1}) and are means ± SEM. n = number of tissues *P < 0.05 vs. control (analysis of variances followed by post-hoc test of Tukey).*

experiments, where the thiol tracker fluorescence fell by −0.07 ± 0.005 and −0.09 ± 0.006 ($n = 75$) in the respective time periods. At the end of each experiment, H_2O_2 (10^{-2} mol·l^{-1}) was administered. Hydrogen peroxide induced a prompt decrease of the thiol tracker signal by −0.04 ± 0.005 ($n = 90$) in the hypoxia experiments and by −0.04 ± 0.005 ($n = 75$) in the time-dependent control experiments, as has to be expected after challenging the cell with oxidants.

DISCUSSION

The intestinal epithelium is strongly affected by changes in oxygen supply, which has an influence on the expression, cellular localization or activity of several transporters for ions and nutrients in the gut (Ward et al., 2014). In the present study, we observed a triphasic change in electrogenic ion transport measured as I_{sc} across rat distal colon during hypoxia: a transient decrease followed by a short rise in I_{sc}, before the current finally fell below the initial baseline (**Figure 1A**). Anion substitution experiments (**Table 2**) and experiments in which Cl^- secretion was blocked either by inhibition of the Na^+-K^+-$2Cl^-$-cotransporter (**Figure 4A**), which represents the dominant Cl^- uptake mechanism across the basolateral membrane (Russell, 2000), or inhibition of Cl^- channels (**Figure 4B**) responsible for Cl^- exit across the apical membrane (Greger, 2000), revealed that these changes in I_{sc} represent changes in Cl^- secretion.

The transient increase in I_{sc} ("peak" in **Figure 1A**) thus represents a short-lasting stimulation of anion secretion. Chloride secretion is under the control of intracellular second messengers such as Ca^{2+}, cAMP and cGMP (Binder and Sandle, 1994). The secretory response was inhibited in the absence of serosal Ca^{2+}, especially when this maneuver was combined by the additional presence of 2-ABP blocking the release of intracellularly stored Ca^{2+} via IP_3 receptors (**Table 4**). Furthermore, hypoxia leads to modest, but consistent increase in the cytosolic Ca^{2+} concentration of isolated colonic crypts loaded with the Ca^{2+}-sensitive dye fura-2 (**Figure 5**). Therefore, this current probably reflects a stimulation of Ca^{2+}-dependent Cl^- secretion during hypoxia. The dominant mechanism, by which an increase in the cytosolic Ca^{2+} concentration stimulates Cl^- secretion is the activation of Ca^{2+}-dependent basolateral K^+ channels, which hyperpolarizes the membrane and thereby increases the driving force for Cl^- exit across apical anion channels (Böhme et al., 1991; Strabel and Diener, 1995). This process is supported by the transient opening of Ca^{2+}-dependent Cl^- channels in the apical membrane (Hennig et al., 2008). Indeed, in human colonic epithelium chemically induced hypoxia has been shown to activate intermediate conductance Ca^{2+}-dependent K^+ channels (Loganathan et al., 2011). An increase in the cytosolic Ca^{2+} concentration will also stimulate apical Ca^{2+}-dependent K^+ channels, which are found in the brushborder membrane, too (Schultheiss and Diener, 1997). This may underlie the Ca^{2+}-dependent (**Table 3**) initial fall in I_{sc} ("Dec1" in **Figure 1A**) during hypoxia preceding the transient Cl^- secretion leading to a rise in I_{sc}. How these changes in ion transport are initiated is finally unclear. However, during hypoxia epithelial cells release adenosine as shown on T84 cells (Matthews et al., 1995), a human colonic tumor cell line. Thus, paracrine mediators may be involved in the control of epithelial ion channel activity during hypoxia/reoxygenation.

The central role of K^+ channels in the initial response to hypoxia is underlined by the action of Ba^{2+}, which suppressed the peak in I_{sc} during hypoxia (**Figure 3A**) and tended to reduce the initial fall in I_{sc} at the onset of hypoxia (**Table 2**). Surprisingly, despite functional, morphological and molecular biological evidence demonstrating the expression of ATP-sensitive K^+ channels in the basolateral membrane of rat colonic epithelium (Pouokam et al., 2013), neither blockade of these channels with glibenclamide (**Figure 3B**) nor activation with pinacidil prior the onset of hypoxia had any effect on the electrogenic response evoked by hypoxia or reoxygenation. So despite the expected fall in the cytosolic ATP concentration after impairment of mitochondrial oxidative phosphorylation during hypoxia, K_{ATP} channels do not contribute to the changes in colonic ion transport during hypoxia. This clearly contrasts the response of the epithelium from that of excitable tissues, where these channels represent an important protective mechanism via hyperpolarization of the membrane, which finally reduces excitability and thereby the energy demand of these cells (Hibino

et al., 2010). Consequently, in colonic epithelia K_{ATP} channels must exert other functions, such as to sense the gasotransmitter H_2S (Pouokam and Diener, 2011).

The final response, however, of the epithelium to hypoxia consists in a long-lasting fall in I_{sc} (**Figure 1A**) consistent with an inhibition of anion secretion. Several mechanisms may underlie this reduction in transepithelial current. For example, in T84 cells a decrease in the intracellular level of cGMP and cAMP, i.e., 2 s messengers responsible for activation of transepithelial Cl^- secretion, has been observed during hypoxia (Taylor et al., 1998b). Also the activation of an AMP kinase during hypoxia is known to downregulate especially cAMP-induced anion secretion (Collins et al., 2011). Furthermore, already a reduction in the cytosolic ATP concentration alone might directly impair the opening of the CFTR channel, the dominant Cl^- channel in the apical membrane (Greger, 2000), as this member of the ABC (ATP-binding cassette) protein family needs phosphorylation for activation and in addition ATP hydrolysis for its gating (Gadsby et al., 2006). On the long-term, there seems even to be a downregulation of this channel on the transcriptional level during hypoxia via the HIF-1 (hypoxia-inducible factor-1) pathway as shown in the colonic cells lines T84 and Caco-2 (Zheng et al., 2009).

Concomitant with the change in I_{sc}, there is a strong increase in tissue conductance, i.e., in the ionic permeability, of the epithelium during hypoxia, which even further rises after a short delay during the reoxygenation period (**Figure 2A**). A small increase in G_t was also observed in the time-dependent control experiments (**Figure 2B**). This is probably due to the experimental design, in which we decided to switch between "normoxic" conditions (i.e., gassing with room air containing 20.9% (v/v) O_2 instead of pure oxygen), and N_2 gassing, to mimic better the *in vivo* situation of ischemia/reperfusion. Obviously, this seems to limit the normally observed "longevity" of colonic specimens in Ussing chamber setups, which are usually gassed with 95–100% (v/v) O_2. In T84 cells, a release of epithelial cytokines such as tumor necrosis factor-α has been shown to play a role in the increase in G_t during hypoxia, which probably reflects an increased permeability of the tight junctions (Taylor et al., 1998a). However, this does not necessarily represent only an unspecific damage of the epithelium due to hypoxia, but may in addition involve a regulated process as inhibition of Ca^{2+}-dependent K^+ channels has been shown to reduce the increase in the paracellular permeability during energy depletion in human colon (Loganathan et al., 2011).

Experiments with the radical scavenger trolox C suggest that both the long-lasting inhibition of I_{sc} during the late hypoxia period (**Table 2**) as well as the rise of the cytosolic Ca^{2+} concentration during this period (**Table 4**) involved reactive oxygen species. However, no changes could be detected in the fluorescence of the superoxide anion-sensitive dye mitosox (**Figure 6A**) or the thiol-sensitive dye thiol tracker (**Figure 6B**) indicating that the expected increase in $O_2^-\bullet$ or a compensatory fall in the cytosolic glutathione level were below the level of detection and at least much smaller compared to the changes induced by a strong oxidant such as H_2O_2. *In vivo*, the situation is most likely different due to the infiltration of the intestinal wall with neutrophil granulocytes, which are a strong source of oxidants (Gonzalez et al., 2015). On the other hand, morphological studies performed at rat intestine suggest that ischemia causes only a modest histological damage in the colon in comparison to small intestine (Leung et al., 1992). Especially, in contrast to the small intestine, colonic mucosal damage was not enhanced by reperfusion, which might correlate with the low level of xanthine oxidase activity (about only 10% of that observed in small intestine) and thus a smaller production rate of reactive oxygen species in this segment of the gut (Leung et al., 1992). This suggests a relative high capacity of the colonic epithelium with its low O_2 partial pressure even under physiological conditions (Zheng et al., 2015) to deal with enhanced radical production during hypoxia/reoxygenation.

The colonic epithelium is exposed to daily fluctuations of nutrient contents, microflora and mesenteric blood circulation. Adaptive mechanisms have been developed for facing such threats. Chloride secretion may be a "priming" consequence of epithelial cells which are regularly exposed to stimuli like inflammation correlated with hypoxia, which often is associated clinically with diarrhea (Zheng et al., 2009; Ward et al., 2014). The goal of this secretion could be "flushing" pathogens from the epithelium as if a microbial assault was running.

AUTHOR CONTRIBUTIONS

Conception and design of the work (SS, EP, MD); acquisition (SS, EP), analysis and interpretation of data (SS, EP, MD); drafting, revising and final approval the manuscript (SS, EP, MD).

ACKNOWLEDGMENTS

The diligent care of Mrs. B. Brück, E. Haas, B. Schmitt, and A. Stockinger is a pleasure to acknowledge. We thank Prof. Dr. K. D. Schlüter for his help in adapting the hypoxia chamber.

REFERENCES

Babenko, A. P., Aguilar-Bryan, L., and Bryan, J. (1998). A view of SUR/KIR6.x, KATP channels. *Annu. Rev. Physiol.* 60, 667–687. doi: 10.1146/annurev.physiol.60.1.667

Binder, H. J., and Sandle, G. I. (1994). "Electrolyte transport in the mammalian colon," in *Physiology of the Gastrointestinal Tract*, ed L. R. Johnson (New York, NY: Raven Press), 2133–2171.

Böhme, M., Diener, M., and Rummel, W. (1991). Calcium- and cyclic-AMP-mediated secretory responses in isolated colonic crypts. *Pflügers Arch. Eur. J. Physiol.* 419, 144–151. doi: 10.1007/BF00373000

Collins, D., Kopic, S., Bachlechner, J., Ritter, M., Winter, D. C., and Geibel, J. P. (2011). Hypoxia inhibits colonic ion transport via activation of AMP kinase. *Ann. Surg.* 254, 957–963. doi: 10.1097/SLA.0b013e31821d477f

Cook, N. S., and Quast, U. (1990). "Potassium channels. Structure, classification, function and therapeutic potential," in *Potassium Channel Pharmacology*, ed N. S. Cook (New York, NY: Ellis Horwood), 181–255.

Diener, M., and Rummel, W. (1989). Actions of the Cl^- channel blocker NPPB on absorptive and secretory transport processes of Na^+ and Cl^- in rat descending colon. *Acta Physiol. Scand.* 137, 215–222. doi: 10.1111/j.1748-1716.1989.tb08741.x

Dröge, W. (2002). Free radicals in the physiological control of cell function. *Physiol. Rev.* 82, 47–95. doi: 10.1152/physrev.00018.2001

Frings, M., Schultheiss, G., and Diener, M. (1999). Electrogenic Ca^{2+} entry in the rat colonic epithelium. *Pflügers Arch. Eur. J. Physiol.* 439, 39–48. doi: 10.1007/s004249900159

Gadsby, D. C., Vergani, P., and Csanidy, L. (2006). The ABC protein turned chloride channel whose failure causes cystic fibrosis. *Nature* 440, 477–483. doi: 10.1038/nature04712

Gonzalez, L. M., Moeser, A. J., and Blikslager, A. T. (2015). Animal models of ischemia-reperfusion-induced intestinal injury: progress and promise for translational research. *Am. J. Physiol. Gastrointest. Liver Physiol.* 308, G63–G75. doi: 10.1152/ajpgi.00112.2013

Greger, R. (2000). Role of CFTR in the colon. *Annu. Rev. Physiol.* 62, 467–491. doi: 10.1146/annurev.physiol.62.1.467

Haglund, U., and Bergqvist, D. (1999). Intestinal ischemia - the basics. *Langenbeck's Arch. Sur.* 384, 233–238. doi: 10.1007/s004230050197

Hardcastle, J., Hardcastle, P. T., and Noble, J. M. (1985). The secretory action of barium chloride in rat colon. *J. Physiol.* 361, 19–33. doi: 10.1113/jphysiol.1985.sp015630

Hennig, B., and Diener, M. (2009). Actions of hydrogen sulfide on ion transport across rat distal colon. *Brit. J. Pharmacol.* 158, 1263–1275. doi: 10.1111/j.1476-5381.2009.00385.x

Hennig, B., Schultheiss, G., Kunzelmann, K., and Diener, M. (2008). Ca^{2+}-induced Cl^- efflux at rat distal colonic epithelium. *J. Membrane Biol.* 221, 61–72. doi: 10.1007/s00232-007-9078-0

Hibino, H., Inanobe, A., Furutani, K., Murakami, S., Findlay, I., and Kurachi, Y. (2010). Inwardly rectifying potassium channels: their structure, function, and physiological roles. *Physiol. Rev.* 90, 291–366. doi: 10.1152/physrev.00021.2009

Hund, T. J., and Mohler, P. J. (2011). Differential roles for SUR subunits in K_{ATP} channel membrane targeting and regulation. *Am. J. Physiol. Heart Circul. Physiol.* 300, H33–H35. doi: 10.1152/ajpheart.01088.2010

Kaplan, J. H. (1985). Ion movements throught the sodium pump. *Annu. Rev. Physiol.* 47, 535–544. doi: 10.1146/annurev.ph.47.030185.002535

Kowaltowski, A. J., De Souza-Pinto, N. C., Castilho, R. F., and Vercesi, A. E. (2009). Mitochondria and reactive oxygen species. *Free Radic. Biol. Med.* 47, 333–343. doi: 10.1016/j.freeradbiomed.2009.05.004

Lee, J. H., Kim, B., Jin, W. J., Kim, J. W., Kim, H. H., Ha, H., et al. (2014). Trolox inhibits osteolytic bone metastasis of breast cancer through both PGE_2-dependent and independent mechanisms. *Biochem. Pharmacol.* 91, 51–60. doi: 10.1016/j.bcp.2014.06.005

Leung, F. W., Su, K. C., Passaro, E. Jr., and Guth, P. H. (1992). Regional differences in gut blood flow and mucosal damage in response to ischemia and reperfusion. *Am. J. Physiol. Gastrointest. Liver Physiol.* 263, G301–G305.

Loganathan, A., Linley, J. E., Rajput, I., Hunter, M., Lodge, J. P. A., and Sandle, G. I. (2011). Basolateral potassium (IK_{Ca}) channel inhibition prevents increased colonic permeability induced by chemical hypoxia. *Am. J. Physiol. Gastrointest. Liver Physiol.* 300, G146–G153. doi: 10.1152/ajpgi.00472.2009

Maguire, D., MacNamara, B., Cuffe, J. E., Winter, D., Doolan, C. M., Urbach, V., et al. (1999). Rapid responses to aldosterone in human distal colon. *Steroids* 64, 51–63. doi: 10.1016/S0039-128X(98)00096-8

Mandavilli, B. S., and Janes, M. S. (2010). Detection of intracellular glutathione using thiol tracker violet stain and fluorescence microscopy. *Curr. Protoc. Cytometry* Chapter 9, Unit 9.35. doi: 10.1002/0471142956.cy0935s53

Maruyama, T., Kanaji, T., Nakade, S., Kanno, T., and Mikoshiba, K. (1997). 2APB, 2-aminoethoxydiphenyl borate, a membrane-penetrable modulator of $Ins(1,4,5)P_3$-induced Ca^{2+} release. *J. Biochem.* 122, 498–505. doi: 10.1093/oxfordjournals.jbchem.a021780

Matthews, J. B., Tally, K. J., Smith, J. A., Zeind, A. J., and Hmjez, B. J. (1995). Activation of Cl secretion during chemical hypoxia by endogenous release of adenosine in intestinal epithelial monolayers. *J. Clin. Invest.* 96, 117–125. doi: 10.1172/JCI118010

Plenge-Tellechea, F., Soler, F., and Fernadez-Belda, F. (1997). On the inhibition mechanism of sarcoplasmic or endoplasmic reticulum Ca^{2+}-ATPases by cyclopiazonic acid. *J. Biol. Chem.* 272, 2794–2800. doi: 10.1074/jbc.272.5.2794

Pouokam, E., Bader, S., Brück, B., Schmidt, B., and Diener, M. (2013). ATP-sensitive K^+ channels in rat colonic epithelium. *Pflügers Arch. Eur. J. Physiol.* 465, 865–877. doi: 10.1007/s00424-012-1207-7

Pouokam, E., and Diener, M. (2011). Mechanims of actions of hydrogen sulfide at rat distal colonic epithelium. *Brit. J. Pharmacol.* 162, 392–404. doi: 10.1111/j.1476-5381.2010.01026.x

Russell, J. M. (2000). Sodium-potassium-chloride cotransport. *Physiol. Rev.* 80, 211–276. doi: 10.1016/B978-0-12-374373-2.00027-3

Schäfer, C., Walther, S., Schäfer, M., Dieterich, L., Kasseckert, S., Abdallah, Y., et al. (2003). Inhibition of contractile activation reduces reoxygenation-induced endothelial gap formation. *Cardiovasc. Res.* 58, 149–155. doi: 10.1016/S0008-6363(02)00842-8

Schultheiss, G., and Diener, M. (1997). Regulation of apical and basolateral K^+ conductances in the rat colon. *Brit. J. Pharmacol.* 122, 87–94. doi: 10.1038/sj.bjp.0701353

Seino, S., and Miki, T. (2003). Physiological and pathophysiological roles of ATP-sensitive K^+ channels. *Progr. Biophys. Mol. Biol.* 81, 133–176. doi: 10.1016/S0079-6107(02)00053-6

Strabel, D., and Diener, M. (1995). Evidence against direct activation of chloride secretion by carbachol in the rat distal colon. *Eur. J. Pharmacol.* 274, 181–191. doi: 10.1016/0014-2999(94)00728-P

Taylor, C. T., Dzus, A. L., and Colgan, S. P. (1998a). Autocrine regulation of epithelial permeability by hypoxia: role for polarized release of tumor necrosis factor alpha. *Gastroenterology* 114, 657–668. doi: 10.1016/S0016-5085(98)70579-7

Taylor, C. T., Lisco, S. J., Awtrey, C. S., and Colgan, S. P. (1998b). Hypoxia inhibits cyclic nucleotide-stimulated epithelial ion transport: role for nucleotide cyclases as oxygen sensors. *J. Pharmacol. Exp. Ther.* 284, 568–575.

Vergauwen, H., Tambuyzer, B., Jennes, K., Degroote, J., Wang, W., De Smet, S., et al. (2015). Trolox and ascorbic acid reduce direct and indirect oxidative Stress in the IPEC-J2 Cells, an *in vitro* model for the porcine gastrointestinal tract. *PLoS ONE* 10:e0120485. doi: 10.1371/journal.pone.0120485

Ward, J. B. J., Keely, S. J., and Keely, S. J. (2014). Oxygen in the regulation of intestinal epithelial transport. *J. Physiol.* 592, 2473–2489. doi: 10.1113/jphysiol.2013.270249

Warth, R., and Barhanin, J. (2003). Function of K^+ channels in the intestinal epithelium. *J. Membr. Biol.* 193, 67–78. doi: 10.1007/s00232-002-2001-9

Yu, B. P. (1994). Cellular defenses against damage from reactive oxygen species. *Physiol. Rev.* 74, 139–162.

Zheng, L., Kelly, C. J., and Colgan, S. P. (2015). Physiologic hypoxia and oxygen homeostasis in the healthy intestine. A review in the theme: cellular responses to hypoxia. *Am. J. Physiol. Cell Physiol.* 309, C350–C360. doi: 10.1152/ajpcell.00191.2015

Zheng, W., Kuhlicke, J., Jäckel, K., Eltzschig, H. K., Singh, A., Sjöblom, M., et al. (2009). Hypoxia inducible factor-1 (HIF-1)-mediated repression of cystic fibrosis transmembrane conductance regulator (CFTR) in the intestinal epithelium. *FASEB J.* 23, 204–213. doi: 10.1096/fj.08-110221

Conflict of Interest Statement: The authors declare that the research was conducted in the absence of any commercial or financial relationships that could be construed as a potential conflict of interest.

Copyright © 2016 Schindele, Pouokam and Diener. This is an open-access article distributed under the terms of the Creative Commons Attribution License (CC BY). The use, distribution or reproduction in other forums is permitted, provided the original author(s) or licensor are credited and that the original publication in this journal is cited, in accordance with accepted academic practice. No use, distribution or reproduction is permitted which does not comply with these terms.

8.5. "Regulation of colonic ion transport by gasotransmitters [Review]"

Pouokam E, Steidle M, Diener M. *Biol. Pharm. Bull (2012)* **34:** 789-793.

Impakt Faktor: 1,657

Eigener Anteil an der Publikation:

- Initiative: 20 %
- Projektplanung: 30 %
- Durchführung der Versuche: 30 %
- Auswertung der Experimente: 40 %
- Erstellung der Publikation: 40 %

June 2011 *Biol. Pharm. Bull.* **34**(6) 789—793 (2011) 789

Current Topics

Cellular Physiology of Channels and Transporters in Gastrointestinal Tracts

Regulation of Colonic Ion Transport by Gasotransmitters

Ervice Pouokam, Julia Steidle, and Martin Diener*

Institute for Veterinary Physiology, University of Giessen; Frankfurter Str. 100, D-35392 Giessen, Germany.

Received November 15, 2010

Gaseous molecules such as nitric oxide (NO), hydrogen sulfide (H_2S), or carbon monoxide (CO) are involved in the regulation of colonic water and salt transport, which can be switched between absorption and secretion. Nitric oxide is produced from the amino acid L-arginine by different isoforms of the enzyme NO synthase, which are expressed both by enteric neurones and by the colonic epithelium. NO donors evoke a transepithelial Cl^- secretion *in vitro*. Most actions of NO are mediated by a stimulation of guanosine 5′ cyclic monophosphate (cGMP) synthesis *via* activation of the soluble guanylate cyclase. In rat colon, NO possesses several main action sites: a stimulation of apical Cl^- channels most probably not related to cGMP-dependent phosphorylation, and an increase in the cytosolic Ca^{2+} concentration, which stimulates a Ca^{2+}-dependent K^+ conductance in the basolateral membrane. Hydrogen sulfide, produced during the metabolism of the amino acid L-cysteine, also evokes a Cl^- secretion, either by stimulation of secretomotor submucosal neurones as in guinea-pig colon or by activating Ca^{2+}-dependent and ATP-sensitive K^+ channels as in rat colon. The third gasotransmitter, CO, produced during the degradation of heme, evokes anion secretion carried by Cl^- and HCO_3^-. This response is mainly caused by the activation of apical anion channels and a stimulation of Ca^{2+}-dependent K^+ channels *via* an increase of the cytosolic Ca^{2+} concentration. Consequently, gaseous molecules produced by enteric neurones, epithelial cells, as well—in the case of H_2S—the microbial flora affect key transport enzymes involved in colonic ion transport.

Key words gasotransmitter; ion channel; ion transport; carbon monoxide; hydrogen sulfide; nitric oxide

1. INTRODUCTION

Colonic ion transport can be switched from absorption into secretion of water and electrolytes.[1)] Under healthy conditions there is a net colonic absorption of Na^+ and Cl^-, the two quantitatively most important anorganic ions transported in the large intestine. This absorption is physiologically replaced by net secretion, predominantly of Cl^-, *e.g.* after mechanical distension of the gut wall in order to produce a fluid film for the protrusion of intestinal content.[2)] Under pathophysiologic conditions, this active secretion of Cl^- plays a prominent role for the development of secretory diarrhea, *e.g.* after exposure of the gut wall to certain bacterial products such as cholera toxin or different toxins produced from *Escherichia coli*, vibrio cholerae or other toxigenic bacteria.[3)]

In order to be secreted Cl^- ions are accumulated above electrochemical equilibrium by a Na^+–K^+–$2Cl^-$-cotransporter in the basolateral membrane, the prominent Cl^- loading transporter in this membrane beside a Cl^-–HCO_3^--exchanger at the same location.[4,5)] When apical Cl^- channels open, which are predominantly of the cystic fibrosis transmembrane regulator (CFTR) channel type,[6)] there is an efflux of Cl^- into the colonic lumen, followed by a paracellular flux of Na^+ for reasons of electroneutrality, and a flux of water for osmotic reasons.

The switching between absorption and secretion is controlled by classical neurotransmitters, predominantly released from the submucosal plexus, hormones and paracrine substances, which in general act on membrane-bound receptors in order to modify intracellular second messenger systems regulating ionic transport across the epithelium. However, since several years it has become evident that small gaseous molecules, the so-called gasotransmitters, can act as signalling molecules to affect intestinal transport, too. The first of these gasotransmitters which has been discovered was nitric oxide (NO).[7)] More recently, hydrogen sulfide (H_2S) and carbon monoxide (CO) have been described to act as gasotransmitters in the gastrointestinal tract. The aim of this review is to give an overview about actions of these gasotransmitters on colonic ion transport and the mechanisms involved.

2. NITRIC MONOXIDE

Nitric oxide is produced from the amino acid L-arginine by the enzyme nitric oxide synthase (NOS), from which three isoforms are known.[8)] NOS-1 (neuronal NOS, n-NOS) is the main form expressed in neurones, including enteric neurones of rat colon.[9)] NOS-1 plays a role in cell communication, *e.g.* between inhibitory motorneurones of the enteric nervous system and smooth muscle cells.[10)] The isoform NOS-2 (inducible NOS, i-NOS) is located in parts of the immune and the cardiovascular system and is upregulated during inflammation. The third enzyme of the NOS-family, NOS-3 (endothelial NOS, e-NOS), produces NO in blood vessels; it is involved in the regulation of vascular functions.

The gas NO is a free radical which is able to pass the plasma membrane *via* diffusion. Most of its actions are mediated through activation of its main intracellular receptor, the soluble guanylate cyclase. This cytosolic enzyme produces the second messenger guanosine 5′ cyclic monophosphate (cGMP) from guanosine 5′-triphosphate (GTP). Cyclic GMP exerts most of its actions *via* stimulation of protein kinase G catalyzing the phosphorylation of target proteins, by direct effects on ion channels, or *via* modulation of cGMP-regulated phosphodiesterases which control the degradation of

* To whom correspondence should be addressed. e-mail: Martin.Diener@vetmed.uni-giessen.de

© 2011 Pharmaceutical Society of Japan

cAMP, *i.e.* of another second messenger.[7,11] Other effects of NO can be mediated by *S*-nitrosylation of proteins.[12]

Nitric oxide liberating drugs evoke Cl^- secretion across the colon of different species such as rat,[13] guinea-pig,[14] man,[15] or pig.[16] For example, the NO liberating drug 1,2,3,4-oxatriazolium,5-amino-3-(3,4-dichlorophenyl)-chloride (GEA 3162) induces a Cl^- secretion across rat colon, which can be measured in voltage-clamp experiments in Ussing chambers as increase in short-circuit current.[17] Several action sites in the secretory mechanism of the epithelial cells have been found. An action site at the apical membrane could be identified in epithelia which had been basolaterally depolarized by use of a buffer with a high K^+ concentration. This shifts the K^+ diffusion potential, which dominates the membrane potential of the basolateral membrane with its high K^+ permeability to values near zero and reduces its resistance due to the high concentration of permeant ions (Fig. 1A). Consequently, the transepithelial potential (and also the measured short-circuit current) are dominated by the apical membrane.[18,19] Under these conditions, the NO donor stimulated a Cl^- current across the apical membrane (driven by a Cl^- concentration gradient), which was inhibited by glibenclamide, a typical inhibitor of the CFTR channel.[6] This inhibition was resistant against inhibitors of protein kinases suggesting a possible direct action of NO on the channel (or a regulator of it) not involving phosphorylation of CFTR, which is the classical pathway to regulate the activity of this anion channel.

Experiments at isolated colonic crypts loaded with the Ca^{2+}-sensitive fluorescent dye fura-2 revealed that GEA 3162 evoked an increase of the cytosolic Ca^{2+} concentration due to an influx of extracellular Ca^{2+}. This influx was mediated by an activation of a nonselective cation conductance as shown by whole-cell patch-clamp studies. The increase of the cytosolic Ca^{2+} concentration is most probably the reason for the activation of a basolateral K^+ conductance. Ca^{2+}-dependent K^+ channels constitute a large fraction of the conductance of this membrane. Their activation leads to a hyperpolarization of the cell membrane thereby increasing the driving force for the efflux of negatively charged Cl^- anions across apical anion channels.[20] This activation can be measured in the Ussing chamber when the apical membrane is permeabilized with the ionophore nystatin in the absence of mucosal Na^+. This can *e.g.* be reached after replacement of Na^+ with the impermeant cation *N*-methyl-D-glucamine in order to avoid a contribution of the current generated by the $3Na^+$–$2K^+$–ATPase, driving a K^+ current across basolateral K^+ channels by a K^+ concentration gradient between the mucosal and the serosal buffer solution (Fig. 1B). This current across basolateral K^+ channels was stimulated by the NO donor. Furthermore, also the pump current was enhanced by GEA 3162. This was measured when the permeabilization of the apical membrane was performed in the absence of a K^+ concentration gradient (thus no current is driven across basolateral K^+ channels), but in the presence of mucosal Na^+, which enters the cell *via* the nystatin pores and thereby stimulates the $3Na^+$–$2K^+$–ATPase (Fig. 1C). Consequently, the gasotransmitter NO affects several key transport enzymes involved in colonic Cl^- secretion (Fig. 2). Interestingly, in rat small intestine *in vivo* also a proabsorptive role of NO has been observed.[21,22] The reasons for this discrepancy between the *in vivo* and the *in vitro* measurements are completely unknown.

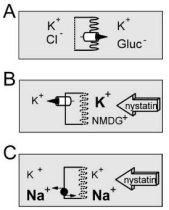

Fig. 1. Manoeuvres for the Selective Study of Different Conductances across Colonic Epithelium

(A) The apical Cl^- conductance can be measured when the basolateral membrane is depolarized by a high K^+ concentration in the buffer at the serosal side of the tissue; a Cl^- current across the apical membrane can be driven by a serosal to mucosal Cl^- concentration gradient (*e.g.*, 111.5 mmol·l^{-1} KCl solution at the serosal side; 107 mmol·l^{-1} K gluconate/4.5 mmol·l^{-1} KCl solution at the mucosal side).[17] (B) Actions of a drug on the basolateral K^+ conductance can be studied when the apical membrane is permeabilized with the ionophore nystatin in the absence of mucosal Na^+ (*e.g.*, after replacement of Na^+ with the impermeant cation *N*-methyl-D-glucamine) in order to avoid a contribution of the current generated by the $3Na^+$–$2K^+$–ATPase when Na^+ would enter the cell from the mucosal compartment *via* the nystatin pores. A K^+ current can then be driven by applying a mucosal to serosal K^+ concentration gradient (*e.g.*, 107 mmol·l^{-1} NaCl/4.5 mmol·l^{-1} KCl at the serosal side; 98 mmol·l^{-1} NMDGCl/13.5 mmol·l^{-1} KCl at the mucosal side). (C) Actions of a drug on the pump current carried by the basolateral $3Na^+$–$2K^+$–ATPase can be studied when the apical membrane is permeabilized by nystatin in the presence of Na^+ but in the absence of a K^+ concentration gradient (*e.g.*, 107 mmol·l^{-1} NaCl/4.5 mmol·l^{-1} KCl at the serosal and the mucosal side). Abbreviations: $Gluc^-$: gluconate, $NMDG^+$: *N*-methyl-D-glucamine.

3. HYDROGEN SULFIDE

A further molecule working as gasotransmitter is H_2S. Hydrogen sulfide is produced from the amino acid L-cysteine by the action of the enzymes cystathionin-β-synthase (CBS) and cystathionin-γ-lyase (CSE).[23] The best characterised actions of this gasotransmitter concern circulation as H_2S induces vasodilatation, decreases cardiac inotropy, and inhibits the proliferation of vascular smooth muscle cells.[24] Two main intracellular action sites of H_2S are known from different cell systems. This includes the ability of H_2S to stimulate ATP-sensitive K^+ channels, an effect that is well characterized *e.g.* at smooth muscle cells from rat aorta resulting in a lowering of blood pressure,[25] or at rat insulinoma cells, where H_2S modulates insulin secretion.[26] A further effect of H_2S consists of an increase in the cytosolic Ca^{2+} concentration, demonstrated *e.g.* at microglial cells from the rat.[27] In these cells H_2S stimulates both the release of stored Ca^{2+} from thapsigargin-sensitive stores, as well as an influx of extracellular Ca^{2+}.

In the gastrointestinal tract H_2S is known to relax smooth muscle from different species[28] and to induce anion secretion across the colonic epithelium.[29] There is evidence for the spontaneous production of H_2S within the gut wall[30] and for the expression of the key enzymes for H_2S formation in enteric neurones[29] or the intestinal epithelium.[31] However, the action sites of H_2S involved in the induction of colonic secretion seem to differ strongly in a species-dependent manner. In guinea-pig colon an exogenous H_2S donor such as

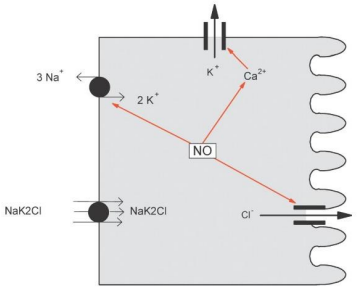

Fig. 2. Action Sites of NO at Rat Colonic Epithelium

Nitric oxide most probably directly stimulates apical Cl^- channels. Further actions are an increase in the cytosolic Ca^{2+} concentration, which determines the K^+ conductance of the basolateral membrane and an increase in the current carried by the Na^+–K^+–ATPase.

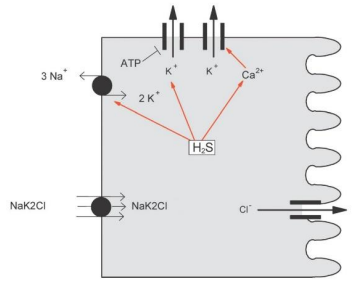

Fig. 3. Action Sites of H_2S at Rat Colonic Epithelium

Hydrogen sulfide most probably directly affects basolateral ATP-dependent K^+ channels and modifies the activity of Ca^{2+}-dependent K^+ channels *via* modulation of the cytosolic Ca^{2+} concentration. A further site of action in the basolateral membrane is the Na^+–K^+–ATPase.

NaHS induces a Cl^- secretion *via* stimulation of secretomotor neurones of the submucosal plexus; an action which is probably mediated by capsazepine-sensitive transient receptor potential vanilloid 1 (TRPV 1) ion channels.[29] In contrast, in rat colon the same H_2S donor induces a polyphasic Cl^- secretion, which leads to an increase in short-circuit current transiently interrupted by a negative current (assumed to represent a transient K^+ secretion).[31]

Hydrogen sulfide exerts several actions at the basolateral membrane (Fig. 3). Experiments with blockers of different types of K^+ channels demonstrate that the H_2S donor NaHS has a biphasic effect (an initial inhibition followed by a stimulation) on two types of basolateral K^+ conductances, *i.e.* ATP-sensitive K^+ channels, which are inhibited by glibenclamide, and Ca^{2+}-dependent K^+ channels, which are sensitive to quarternary amines such as tetrapentylammonium.[32] This forces anion secretion by enhancing the driving force for Cl^- efflux across the apical membrane. The action of H_2S on basolateral K^+ channels is supported by a biphasic change in the $3Na^+$–$2K^+$-pump current.

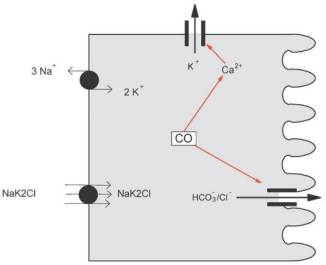

Fig. 4. Action Sites of CO at Rat Colonic Epithelium

Carbon monoxide most probably directly affects apical anion channels and stimulates the activity of Ca^{2+}-dependent K^+ channels *via* an increase of the cytosolic Ca^{2+} concentration.

Experiments at fura 2-loaded colonic crypts demonstrate that the modulation of the basolateral K^+ conductance is paralleled by a change in the cytosolic Ca^{2+} concentration, which consists in a transient fall followed by a long-lasting increase. Different mechanisms underlye these two phases: the initial fall is probably mediated by an efflux of Ca^{2+} from the cytosol into the extracellular space. This response is dependent on the presence of extracellular Na^+ and is blocked by 2′,4′-dichlorobenzamil, an inhibitor of the Na^+–Ca^{2+}-exchanger, suggesting a transient stimulation of Ca^{2+} outflow by this transporter, which was directly demonstrated by Mn^{2+} quenching experiments.[32] In contrast, the secondary rise of the cytosolic Ca^{2+} concentration was independent from the presence of extracellular Ca^{2+}.[31] The pathway, by which this influx occurs, is not known. Possible effects of H_2S on apical ion conductances are still to be examined.

4. CARBON MONOXIDE

A third gaseous molecule has been recognized to act as gasotransmitter in mammals, *i.e.* CO. Carbon monoxide is a product generated from the metabolism of heme, contained *e.g.* in hemoglobin or many other cellular enzymes such as *e.g.* catalase, by the action of heme oxygenases. This process is catalysed by two enzymes, the inducible isoform heme oxygenase I (HO-I) and the constitutive isoform heme oxygenase II (HO-II).[33] A third isoform, HO-III, has been cloned but is probably of minor functional significance because it catalyzes heme degradation to a much smaller degree than the other two enzymes.[34] Like NO, carbon monoxide has pronounced actions on blood circulation, for example it induces vasodilatation.[35] Carbon monoxide—like NO—can stimulate the soluble guanylate cyclase in cells by binding to the heme iron in the enzyme and thereby enhance the intracellular production of cGMP.[36] Although the stimulation

of cellular cGMP production by CO has clearly been shown, at the level of the isolated enzyme CO is a quite weak activator of the soluble guanylate cyclase when compared with the action of NO.[37] A further action site of CO, which has been characterized *e.g.* in porcine arteriolar smooth muscle cells, is a direct, *i.e.* cGMP-independent activation of K^+ channels leading to a hyperpolarisation of the membrane.[35] Another interaction known with ion channels is the cGMP-independent inhibition of Na^+ channels in alveolar epithelium, which may be caused by a modification of histidine residues in the ion channels (or regulators of them) as concluded from experiments with diethyl pyrocarbonate, a histidine-modifying agent.[38]

In the gut wall, enteric neurones, the key players in the regulation of intestinal functions, express the enzymes for CO production such as heme oxygenase II.[39,40] Both heme oxygenase I and heme oxygenase II are expressed in the rat colon as observed immunohistochemically and by reverse transcription-polymerase chain reaction (RT-PCR). Immunoreactivity of heme oxygenase I was found mainly in the muscularis propria whereas heme oxygenase II was localized in addition within the colonic epithelium.[41] A CO-releasing molecule, tricarbonyldichlororuthenium(II) dimer (CORM-2), evokes a concentration-dependent anion secretion carried by changes in the transepithelial transport of Cl^- and HCO_3^-.[42] A similar induction of Cl^- secretion by a CO donor or pretreatment with heme to stimulate endogenous CO production is already known from the colonic tumor cell line, Caco-2.[43] In these cells, the CO-induced secretion was reduced by an inhibitor of the soluble guanylate cyclase (ODQ; 1*H*-[1,2,4]oxadiazolo[4,3-*a*]quinoxalin-1-one), which is consistent with the 'classical' CO signalling pathway. However, CORM-2 induced anion secretion in rat distal colon was neither affected by ODQ nor reduced after pretreatment with an activator of this pathway (YC1; 3-[5′-hydroxymethyl-2′-furyl]-1-benzylindazole) suggesting an action of CO independent from the stimulation of this enzyme.

Carbon monoxide possesses action sites both at the apical and the basolateral membrane. In basolaterally depolarized epithelia, CORM-2 stimulated a Cl^- conductance which was sensitive against a typical Cl^- channel blocker such as 5-nitro-2-(3-phenylpropylamino)-benzoate (NPPB). The most simple explanation for this observation would be the assumption of a direct interaction of CO with apical anion channels. In the basolateral membrane, CORM-2 activated a Ba^{2+}-sensitive K^+ conductance. Again, this was paralleled by an increase in the cytosolic Ca^{2+} concentration suggesting an activation of Ca^{2+}-dependent K^+ channels by the CO donor (Fig. 4). The increase in the cytosolic Ca^{2+} concentration depended on the influx of extracellular Ca^{2+} but not on a release of Ca^{2+} from intracellular stores. The pathway, by which this Ca^{2+} influx occurs, is unknown; putative candidates for colonic epithelial cells are the capacitive Ca^{2+} influx, which is mediated by nonselective cation channels in these cells,[44] or the Na^+–Ca^{2+} exchanger, which can act as a Ca^{2+}-loading mechanism when working in the reverse mode.[45]

5. OUTLOOK

Gasotransmitters represent a relatively new pathway to modulate physiological functions including regulation of colonic ion transport. They are not only produced in the enteric nervous system to be released during excitation of these neurones, but the enzymes involved in their synthesis are also found within the intestinal epithelium suggesting a role in paracrine regulation of epithelial functions. A further site of production, at least in the case of H_2S, is the microbial flora which can use (as alternative to methane) this gas as a kind of hydrogen sink to bind H_2 produced during fermentation of carbohydrates. Consequently, there seems to be an exciting interaction between the key players in the regulation of intestinal functions *via* gasotransmitters, which has still to be elucidated in future experiments.

Acknowledgement The cited work of the authors was supported by Deutsche Forschungsgemeinschaft, Grants Di 388/3, Di 388/6, Di 388/9 and Di 388/11.

REFERENCES

1) Binder H. J., Sandle G. J., "Physiology of the Gastrointestinal Tract," ed. by Johnson L. R., Raven Press, New York, 1994.
2) Diener M., Rummel W., *Eur. J. Pharmacol.*, **178**, 47—57 (1990).
3) Kunzelmann K., Mall M., *Physiol. Rev.*, **82**, 245—289 (2002).
4) Schultheiss G., Hörger S., Diener M., *Acta Physiol. Scand.*, **164**, 219—228 (1998).
5) Rajendran V. M., Black J., Ardito T. A., Sangan P., Alper S. L., Schweinfest C., Kashgarian M., Binder H. J., *Am. J. Physiol. Gastrointest. Liver Physiol.*, **279**, G931—G942 (2000).
6) Greger R., *Annu. Rev. Physiol.*, **62**, 467—491 (2000).
7) Waldman S. A., Murad F., *Pharmacol. Rev.*, **39**, 163—196 (1987).
8) Knowles R. G., Moncada S., *Biochem. J.*, **298**, 249—258 (1994).
9) Sitmo M., Rehn M., Diener M., *Am. J. Physiol. Gastrointest. Liver Physiol.*, **293**, G886—G893 (2007).
10) Toda N., Herman A. G., *Pharmacol. Rev.*, **57**, 315—338 (2005).
11) Bender A. T., Beavo J. A., *Pharmacol. Rev.*, **58**, 488—520 (2006).
12) Broillet M. C., *Cell. Mol. Life Sci.*, **55**, 1036—1042 (1999).
13) Wilson K. T., Xie Y., Musch M. W., Chang E. B., *J. Pharmacol. Exp. Ther.*, **266**, 224—230 (1993).
14) MacNaughton W. K., *Life Sci.*, **53**, 585—593 (1993).
15) Stack W. A., Filipowicz B., Hawkey C. J., *Gut*, **39**, 93—99 (1996).
16) Gäbel G., Garz B., Ahrens F., Aschenbach J. R., *J. Comp. Physiol. B*, **173**, 177—186 (2003).
17) Schultheiss G., Seip G., Kocks S. L., Diener M., *Eur. J. Pharmacol.*, **444**, 21—30 (2002).
18) Fuchs W., Larsen E. H., Lindemann B., *J. Physiol.*, **267**, 137—166 (1977).
19) Schultheiss G., Diener M., *Br. J. Pharmacol.*, **122**, 87—94 (1997).
20) Böhme M., Diener M., Rummel W., *Pflügers Arch. Eur. J. Phys.*, **419**, 144—151 (1991).
21) Schirgi-Degen A., Beubler E., *Br. J. Pharmacol.*, **114**, 13—18 (1995).
22) Schirgi-Degen A., Beubler E., *Eur. J. Pharmacol.*, **316**, 257—262 (1996).
23) Wang R., *FASEB J.*, **16**, 1792—1798 (2002).
24) Geng B., Cui Y. Y., Zhao J., Yu F., Zhu Y., Xu G., Zhang Z., Tang C., Du J., *Am. J. Physiol. Regul. Integr. Comp. Physiol.*, **293**, R1608—R1618 (2007).
25) Zhao W., Zhang J., Lu Y., Wang R., *EMBO J.*, **20**, 6008—6016 (2001).
26) Yang W., Yang G., Jia X., Wu L., Wang R., *J. Physiol.*, **569**, 519—531 (2005).
27) Lee S. W., Hu Y. S., Hu L. F., Lu Q., Dawe G. S., Moore P. K., Wong P. T., Bian J. S., *Glia*, **54**, 116—124 (2006).
28) Teague B., Asiedu S., Moore P. K., *Br. J. Pharmacol.*, **137**, 139—145 (2002).
29) Schicho R., Krueger D., Zeller F., Von Weyhern C. W. H., Frieling T., Kimura H., Ishii I., De Giorgio R., Campi B., Schemann M., *Gastroenterology*, **131**, 1542—1552 (2006).
30) Zhao W., Ndisang J. F., Wang R., *Can. J. Physiol. Pharmacol.*, **81**, 848—853 (2003).
31) Hennig B., Diener M., *Br. J. Pharmacol.*, **158**, 1263—1275 (2009).

32) Pouokam E., Diener M., *Br. J. Pharmacol.*, **162**, 392—404 (2011).
33) Maines M. D., *Annu. Rev. Pharmacol. Toxicol.*, **37**, 517—554 (1997).
34) Hayashi S., Omata Y., Sakamoto H., Higashimoto Y., Hara T., Sagara Y., Noguchi M., *Gene*, **336**, 241—250 (2004).
35) Kanu A., Leffler C. W., *Am. J. Physiol. Heart Circ. Physiol.*, **293**, H3193—H3200 (2007).
36) Gibbons S. J., Farrugia G., *J. Physiol.*, **556**, 325—336 (2004).
37) Stone J. R., Marletta M. A., *Biochemistry*, **33**, 5636—5640 (1994).
38) Althaus M., Fronius M., Buchäckert Y., Vadász I., Clauss W. G., Seeger W., Motterlini R., Morty R. E., *Am. J. Respir. Cell Mol. Biol.*, **41**, 639—650 (2009).
39) Donat M. E., Wong K., Staines W. A., Krantis A., *J. Auton. Nerv. Syst.*, **77**, 4—12 (1999).
40) Miller S. M., Reed D., Sarr M. G., Farrugia G., Szurszewski J. H., *Neurogastroenterol. Motil.*, **13**, 121—131 (2001).
41) Steidle J., Diener M., *Am. J. Physiol. Gastrointest. Liver Physiol.*, **300**, G207—G216 (2011).
42) Steidle J., Diener M., *Acta Physiol.* (Oxford), **195** (Suppl. 669), 52 (2009).
43) Uc A., Husted R. F., Giriyappa R. L., Britigan B. E., Stokes J. B., *Am. J. Physiol. Gastrointest. Liver Physiol.*, **289**, G202—G208 (2005).
44) Frings M., Schultheiss G., Diener M., *Pflügers Arch. Eur. J. Phys.*, **439**, 39—48 (1999).
45) Seip G., Schultheiss G., Kocks S. L., Diener M., *Exp. Physiol.*, **86**, 461—468 (2001).

8.6 "Epithelial electrolyte transport physiology and the gasotransmitter hydrogen sulphide" [Review]

Pouokam E. and Althaus M. *Oxid.Med. Cell. Longevity.* (2015) Art. ID 4723416.

Impakt Faktor: 4.492

Eigener Anteil an der Publikation:

- Initiative: 50 %
- Projektplanung: 50 %
- Durchführung der Versuche: 50 %
- Auswertung der Experimente: 50 %
- Erstellung der Publikation: 50 %

Hindawi Publishing Corporation
Oxidative Medicine and Cellular Longevity
Volume 2016, Article ID 4723416, 13 pages
http://dx.doi.org/10.1155/2016/4723416

Review Article

Epithelial Electrolyte Transport Physiology and the Gasotransmitter Hydrogen Sulfide

Ervice Pouokam[1] and Mike Althaus[2]

[1]*Institute for Veterinary Physiology and Biochemistry, Justus-Liebig University, Frankfurter Strasse 100, 35392 Giessen, Germany*
[2]*Institute for Animal Physiology, Justus-Liebig University, Heinrich-Buff-Ring 26, 35392 Giessen, Germany*

Correspondence should be addressed to Ervice Pouokam; ervice.pouokam-kamgne@vetmed.uni-giessen.de
and Mike Althaus; mike.althaus@bio.uni-giessen.de

Received 29 October 2015; Accepted 17 December 2015

Academic Editor: Yi C. Zhu

Copyright © 2016 E. Pouokam and M. Althaus. This is an open access article distributed under the Creative Commons Attribution License, which permits unrestricted use, distribution, and reproduction in any medium, provided the original work is properly cited.

Hydrogen sulfide (H_2S) is a well-known environmental chemical threat with an unpleasant smell of rotten eggs. Aside from the established toxic effects of high-dose H_2S, research over the past decade revealed that cells endogenously produce small amounts of H_2S with physiological functions. H_2S has therefore been classified as a "gasotransmitter." A major challenge for cells and tissues is the maintenance of low physiological concentrations of H_2S in order to prevent potential toxicity. Epithelia of the respiratory and gastrointestinal tract are especially faced with this problem, since these barriers are predominantly exposed to exogenous H_2S from environmental sources or sulfur-metabolising microbiota. In this paper, we review the cellular mechanisms by which epithelial cells maintain physiological, endogenous H_2S concentrations. Furthermore, we suggest a concept by which epithelia use their electrolyte and liquid transport machinery as defence mechanisms in order to eliminate exogenous sources for potentially harmful H_2S concentrations.

1. Introduction

"All things are poisons, for there is nothing without poisonous qualities. It is only the dose which makes a thing poison." This famous quote from Paracelsus (1493–1541) is still important for research in physiology and especially for recent investigations on a toxic gas, hydrogen sulfide, and its potential role as a physiologically relevant signalling molecule.

Hydrogen sulfide (H_2S) is well known as an environmental chemical threat and even more for its unpleasant smell of rotten eggs. The odour threshold for H_2S is about 0.003–0.02 ppm and concentrations above 50 ppm have toxic effects such as irritations of the eye and respiratory tract [1]. At 150–200 ppm H_2S, the olfactory sense for this gas is lost and higher concentrations lead to the formation of pulmonary oedema, unconsciousness, and eventually death [1]. The toxic effects of H_2S are mainly based on the inhibition of the mitochondrial respiratory chain, especially cytochrome c oxidase [2, 3]. However, consistent with the principle of Paracelsus, research of the past decade has revealed that cells endogenously produce small amounts of H_2S which are not simply a metabolic by-product and play an important role in cellular signalling processes [4]. Similar to nitric oxide (NO) or carbon monoxide (CO), H_2S has therefore been classified as a "gasotransmitter," a gaseous cellular signalling molecule [4, 5]. Furthermore, a therapeutic potential for low-dose H_2S has been discovered [4] and H_2S-releasing pharmacological compounds have been designed [6] and are currently evaluated as potential therapeutics in various models of disease [7].

A major challenge for cells and tissues is the maintenance of physiological (low) concentrations of H_2S in order to prevent potential toxicity. In this review article, we describe epithelial reactions to H_2S. We focus on epithelia of the respiratory and intestinal tract since these tissues are predominantly exposed to a variety of exogenous and potentially dangerous sources for H_2S, that is, inhaled H_2S in the lung and microbiota-generated H_2S in the gut. Furthermore, epithelial cells endogenously produce low concentrations of H_2S with potential implications for cellular signalling

processes. In line with the principle of Paracelsus, epithelia therefore have to find a balance between potentially toxic exogenous and physiological, endogenous H_2S concentrations. In the following sections we will describe the chemistry as well as sources of H_2S to which epithelia are exposed, their reactions to exogenous and endogenous H_2S, and potential physiological/pathophysiological implications with respect to epithelial function.

2. Hydrogen Sulfide: Properties, Exogenous Sources, and Enzymatic Production

2.1. Chemical Properties of Hydrogen Sulfide. H_2S is a colourless and flammable gas characterized by its rotten eggs or blocked sewer smell. At 20°C, one gram of H_2S will dissolve in 242 mL water. Temperature and time influence the concentration of H_2S; temperature elevation increases the solubility of this gas. Oxidation occurring over time in solution leads to precipitation of elemental sulfur, giving a cloudy aspect to the solution (for review see [4]). Experimental work with this molecule is complicated since H_2S evaporates easily from aqueous solutions with a half-life on the minute time-scale [4, 8, 9]. In solution, H_2S is a weak acid, dissociating into the hydrosulfide anion or thiolate form HS^- and the sulfide anion S^{2-} building the following equilibrium:

$$H_2S \longleftrightarrow HS^- \longleftrightarrow S^{2-} \quad (1)$$

with p*K*a1 and p*K*a2 values of 6.9 and >12, respectively.

Consequently, at 37°C and physiological pH, there are almost equal amounts of H_2S and HS^- (but no S^{2-}) in cells and tissues and nearly a 20% H_2S/80% HS^- ratio in extracellular fluid or plasma [4]. H_2S is highly lipophilic with a dipole moment of 0.97 [10], allowing for a rapid cell membrane permeation [11] and hence potential interference with cell respiration. Diffusion of H_2S into the cells is hence a primary problem of respiratory and intestinal epithelia which are predominantly exposed to exogenous and potentially dangerous levels of H_2S.

2.2. Exogenous and Endogenous H_2S Sources

2.2.1. Exogenous H_2S Sources. There are organic and inorganic sources of H_2S (Figure 1). The pulmonary epithelium can be exposed to H_2S by inhalation of environmental H_2S gas (Figure 1(a)). H_2S may be released by volcanoes as natural gas or contained in sulfur deposits or (healing) sulfur springs. Additional significant H_2S sources are industrial processes such as petroleum refinery, rayon manufacturing, and paper, swine, and pulp mill industry [4]. 125,000 employees in 73 industries of the United States are potentially exposed to H_2S [4].

In the intestinal tract, methionine- or cysteine-rich diet may end up as H_2S production/release. The intestinal flora may produce H_2S via sulfate-reducing bacteria (SRB) (Figure 1(b), Table 1). SRBs use several substrates like short-chain fatty acids, other organic acids, or alcohol as electron donors for reduction of sulfate or other oxidized sulfur molecules to produce H_2S. Furthermore, endogenous substrates in the large intestine, such as sulfated polysaccharides (sulfomucins), can be used by the microflora for H_2S generation [12, 13]. Sulfates may also be directly delivered by food such as dried fruits, nuts, bread, wine, or brassica vegetables. The key bacterial enzyme used during these processes is dissimilatory sulfite reductase [14]. Furthermore, Shatalin and colleagues demonstrated that clinically relevant and pathogenic nonsulfur bacteria such as *Bacillus anthracis*, *Pseudomonas aeruginosa*, *Staphylococcus aureus,* and *Escherichia coli* produce H_2S endogenously [15]. These species contain orthologues of the mammalian H_2S-generating enzymes cystathionine-β-synthase (CBS), cystathionine-γ-lyase (CSE), and 3-mercaptopyruvate sulfurtransferase (3MST) and metabolize cysteine [15]. Overall, up to millimolar H_2S concentrations can occur in the content of human colon [13, 16] due to food compounds and activity of the intestinal flora.

In experimental studies, exogenous H_2S is mainly administered by "H_2S donors." Sulfur salts such as NaHS, Na_2S, and Lawesson's reagent are routinely used for H_2S delivery. However, these molecules are fast donors (in fact, these salts readily dissociate), contrasting with a continuous and more physiologically relevant production and release of H_2S which may occur in the body. Synthetic slow-releasing H_2S donors are, for example, GYY4137 or ATB-429 (for review, see [6, 17]). Natural H_2S donors are, for example, compounds in garlic extracts such as diallyl poly(di,tri)sulfides which slowly release H_2S. Also the sulfur-compounds S-allylcysteine (SAC) and allicin are found in garlic. These organic polysulfides may react with intracellular thiols like glutathione (GSH) to produce H_2S [4].

2.2.2. Endogenous, Intracellular H_2S. H_2S is endogenously produced by various cell types, including epithelial cells, as a result of L-cysteine metabolism. For the detailed biochemistry of cellular H_2S production pathways, the reader is referred to excellent recent review articles [18, 19]. In the past years, a growing body of evidence suggests a concept by which intracellular H_2S concentrations are determined by (1) its enzymatic production; (2) its intracellular storage as bound sulfane sulfur; and (3) its oxidative degradation by mitochondria.

(1) Enzymatic H_2S Production. H_2S is generated by three enzymes: CBS, CSE and 3MST. L-cysteine is the substrate for pyridoxal-5′-phosphate (vitamin B6) dependent CBS and CSE. However, it can be synthesized from L-methionine through the transsulfuration pathway catalysed by methionine adenosyltransferase (MAT) and glycine N-methyltransferase (GNMT). Serine is then transferred to homocysteine leading to cystathionine, a reaction catalysed by CBS. CSE converts cystathionine to cysteine. Cysteine may be converted to L-cystine which in turn will be converted to thiocysteine and further to H_2S. CSE and CBS together catalyse the production of H_2S from cysteine. The abovementioned processes occur within the cytosol. Cysteine aminotransferase (CAT) and 3-mercaptopyruvate sulfur transferase (MPST), both found in cytosol and mitochondria, catalyse

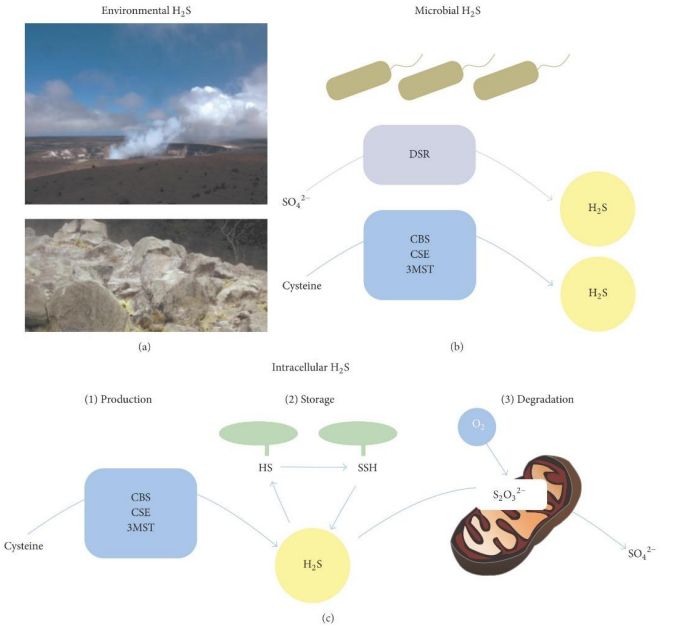

FIGURE 1: Sources of hydrogen sulfide. (a) Environmental hydrogen sulfide (H_2S) occurs due to geothermal activities such as volcanoes, sulfur deposits, or sulfur springs. The pictures show the Halema'uma'u crater (top) and sulfur deposit (bottom) on Hawaii Big Island. (b) Microbial production of H_2S. Sulfate-reducing bacteria dissimilate sulfate into H_2S via dissimilatory sulfite reductase (DSR). Mesophilic bacteria use orthologues of the mammalian H_2S-generating enzymes cystathionine-β-synthase (CBS), cystathionine-γ-lyase (CSE), and 3-mercaptopyruvate sulfurtransferase (3MST) in order to generate H_2S from cysteine. (c) Mammalian cells produce H_2S from cysteine via CBS, CSE, and 3MST (1). H_2S can be stored in a reductant-labile intracellular pool as bound sulfane sulfur (2). The degradation of H_2S occurs via oxidative metabolic pathways in mitochondria (3).

the conversion of cysteine to 3-mercaptopyruvate and H_2S, respectively [4, 9, 20].

In addition, there is enzyme-free generation of H_2S; however, this represents only a minor source of this gasotransmitter. Here, oxidation of sulfide produces thiosulfate, which in turn interacts with intracellular thiols such as GSH to release H_2S.

(2) Intracellular H_2S-Storage. Enzymatically produced H_2S can be intracellularly stored as bound sulfane sulfur [18]. This occurs by the oxidative formation of hydrodisulfides or persulfides, for example, by modification of the sulfur of cysteine residues in proteins, which establish a reductant-labile pool of sulfane sulfur [18, 21]. A study by Shibuya and colleagues demonstrated that HEK293-F cells expressing 3MST contained larger amounts of sulfane sulfur than nontransfected cells or cells expressing enzymatically inactive 3MST [22]. This indicates that enzymatically produced H_2S is transformed into bound sulfane sulfur, thereby reducing the concentration of free intracellular H_2S.

(3) Mitochondrial H_2S-Degradation. H_2S affects mitochondrial respiration by inhibiting cytochrome c oxidase [2] with an IC_{50} value of 0.32 μM in colonic epithelial cell

Table 1: H_2S-producing bacteria of the digestive tract.

Bacteria genus	Location	Process	References
Veillonella	Oral cavity and stomach	Metabolism of carbohydrates/lactate	[23] [24]
Actinomyces	Oral cavity and small intestine	Metabolism of lactate	[23] [24]
Prevotella	Oral cavity	Metabolism of short-chain fatty acids	[23] [24]
Desulfosarcina, Desulfotomaculum, Desulfonema, Desulfovibrio (Desulfomonas), Desulfococcus, Desulfobacter	Human and animal colon	Reduction of sulfate or other oxidized sulfur compounds using H_2 or lactate	[25] [26] [14]

homogenates [27]. Despite this finding, colonic epithelial cells are surprisingly resistant to even millimolar H_2S concentrations [13, 27] due to a detoxifying sulfide metabolism [13]. Remarkably, low (micromolar) concentrations of H_2S are even able to stimulate cellular respiration and represent an energy substrate for epithelial cells (for excellent review see [13]). H_2S is metabolized in mitochondria by the sulfide oxidation pathway [18, 28]. In the presence of oxygen, sulfide:quinone oxidoreductases (SQR) oxidize H_2S to persulfide which is subsequently oxidized into sulfite via dioxygenase. Sulfite is further transferred into thiosulfate by rhodanese. Thiosulfate reductase and sulfite oxidase eventually metabolize thiosulfate into sulfate which is excreted. Interestingly, epithelial tissues which are predominantly exposed to H_2S, such as colon epithelia, have a particular high metabolic, H_2S-detoxifying capacity [29, 30].

The oxidative metabolism of H_2S in mitochondria implies that concentrations of free H_2S in normoxic tissues are low. The group of Olson demonstrated with H_2S-specific amperometric sensors that endogenous H_2S production inversely correlates with oxygen concentrations [28, 31–33]. Hence, significant amounts of H_2S are only produced in anoxic environments and rapidly disappear in the presence of oxygen. This dynamic relationship between oxygen and H_2S indicates the necessity to maintain free H_2S concentrations low and, furthermore, led to the hypothesis that H_2S might be a cellular oxygen sensor [28, 34, 35].

In sum, recent evidence suggests that there is a dynamic intracellular life-cycle of H_2S. Its enzymatic production is antagonized by storage as bound sulfane sulfur and oxidative metabolism, thereby limiting the concentration of free H_2S to the submicromolar range [36, 37]. Aside from the intracellular biochemical mechanisms to maintain low H_2S concentrations, there are epithelial mechanisms which prevent the exposure to potentially dangerous, high H_2S concentrations. This will be described in the next sections.

3. Epithelial Reactions to H_2S

Similar to nervous, connective and muscle tissues, epithelia are a basic type of animal tissue. They are continuous sheets of tightly packed cells lining the surfaces and cavities of the body [38]. Epithelial cells are attached to each other by protein complexes such as tight junctions. The structure of an epithelium depends on the morphology of its cells and on the amount of cell layers it is made of. In monolayer epithelia (also called simple epithelia) the cells rest on the basal membrane. Flat and scale-like cells are characteristic of simple squamous epithelia. Cube-shaped cells constitute the simple cuboidal epithelium while simple columnar epithelia (gastrointestinal tract) are built of column-shaped cells. The cell nuclei may be disposed at different levels allowing for a pseudocellular stratification, a characteristic of the pseudostratified columnar epithelium which can be ciliated (trachea, upper respiratory tract) or not (penile urethra). When made of many layers, the epithelium is qualified as "stratified." Here, the shape of the upper most cells determines the type of epithelium. Hence, stratified squamous keratinized (skin) or not (oesophagus), stratified cuboidal (ducts of sweat glands), or stratified columnar (conjunctiva) epithelia can be distinguished. The lower most cell layers may comprise different types of cells. A further characteristic of stratified epithelia, besides keratinization, is their ability to contract and stretch. For the latter, they are called transitional epithelia (urothelium).

Epithelia are multifunctional structures which protect from mechanical forces or physical trauma, from desiccation or toxins. They act as barriers against pathogens, regulating exchanges of, for example, water and electrolytes between the *milieu intérieur* and the *milieu extérieur*. The epithelia of the lung or the digestive tract are especially faced with building a protective barrier towards the outer environment on the one hand and at the same time allowing for efficient exchange, such as the respiratory gases or food components, on the other. Vectorial transport of electrolytes and water is a fundamental feature of these epithelia, regulating the diffusion barrier for respiratory gases in the lung, or exchanging nutrients and water from intestinal content. Furthermore, these epithelia use secretory mechanisms as a defence reaction against potentially harmful substances by flushing their outer surfaces. Hence, the epithelial electrolyte and water transport machinery represents both a key feature for normal physiology of these organs and primary defence mechanism. In the following section we discuss the impact of H_2S,

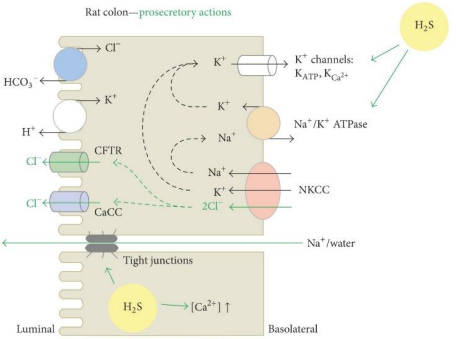

FIGURE 2: Epithelial ion transport responses to exogenous hydrogen sulfide in rat colon. Channels and transport mechanisms activated by H_2S in the rat colonic epithelium. Anion (Cl^-) secretion through the cystic fibrosis transmembrane conductance regulator (CFTR) or calcium-dependent chloride channels (CaCC) is enabled after building up a cytosolic anion potential, which results from the activation of basolateral transporters notably: the Na^+/K^+-ATPase maintaining the K^+ concentration gradient between the intracellular and the extracellular spaces; the Ca^{2+}-dependent ($K_{Ca^{2+}}$) and ATP-sensitive (K_{ATP}) K^+ channels, responsible for the driving force allowing for uptake of Cl^- via the basolateral Na^+-K^+-Cl^- cotransporter type 1 (NKCC1). H_2S donors induce activation of the Na^+/K^+-ATPase and basolateral K^+ conductance, enabling intracellular accumulation of Cl^-, which will be secreted via the CFTR or CaCC. Also, the apical Na^+/Ca^{2+} exchanger was activated in parallel with increase in paracellular permeability.

in both potentially harmful and physiological concentrations, on electrolyte and water transport mechanisms in intestinal and pulmonary epithelia.

3.1. H_2S and Intestinal Epithelia

3.1.1. Intestinal Epithelial Responses to Exogenous H_2S. The intestinal epithelium fulfils the above mentioned epithelial functions, with a more or less secretory or absorptive profile depending on the segment. The determination of intestinal epithelial functions finds its origins in its cellular organization. Intestinal epithelia are organized into finger-like protrusions called villi, absent in the colon, and invaginations called crypts of Lieberkühn (short: crypts). Four types of cells constitute the intestinal epithelium: enterocytes, goblet cells, Paneth cells, and enteroendocrine cells. The Paneth cells, absent in the colon, are located in the crypts and promote defence by their antimicrobial secretions. Also, pluripotent stem cells are located in the crypts; their mitosis generates the other cells, which migrate up the crypt-villus axis and differentiate. The goblet cells produce and secrete mucus, protecting against shear stress and chemical damage [38]. Enteroendocrine cells produce hormones or peptides for digestion or chemical sensors for digestive reflexes. Enterocytes are polarized cells representing the absorptive cell lineage. They carry an apical brush border which is responsible for enzymatic digestion, as well as ion, water, and nutrient uptake. These transport pathways may be transcellular passive (facilitated or not), active, or paracellular through cell junctions such as tight junctions.

Intestinal ion transport, which can be switched from absorption into secretion of water and electrolytes, is controlled by neurotransmitters and hormones, but also gasotransmitters such as CO, NO, H_2S, and nitroxyl (HNO) [39, 40].

The colonic epithelium absorbs water and electrolytes under basal conditions; however, distention of the gut wall by intestinal content induces electrolyte secretion in order to generate a fluid film which facilitates the protrusion of the content. The switch to secretion is also observed after exposure of the epithelium to bacterial products and observed in the development of secretory diarrhoea under pathophysiological conditions. Secretion by the colonic epithelium is predominantly driven by a transepithelial secretion of chloride ions into the lumen, which osmotically facilitates liquid secretion. In order to secrete chloride across the apical membrane of the epithelial cells, the basolateral membrane has to establish a driving force for anion efflux via anion channels (e.g., cystic fibrosis transmembrane conductance regulator, CFTR, or Ca^{2+}-sensitive chloride channels) located in the apical membrane (Figure 2). In the basolateral membrane, potassium channels generate the driving force for chloride secretion by maintaining the negative membrane potential which is dominated by a potassium diffusion potential [41,

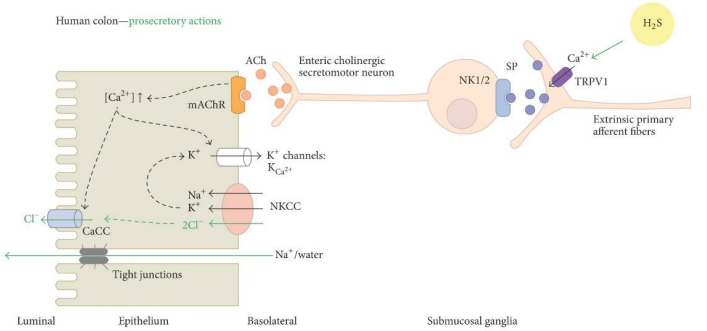

FIGURE 3: Exogenous hydrogen sulfide stimulates electrolyte secretion in human colon via activation of submucosal neurons. H_2S stimulates TRPV1 channels in extrinsic primary afferent fibres, which leads to the release of substance P (SP). SP binds to neurokinin receptors (NK) 1 and 2 of enteric cholinergic secretomotor neurons in submucosal ganglia. The subsequently released acetyl choline (ACh) binds to muscarinergic acetyl choline receptors (mAChR) in the epithelial cells. This stimulates a rise in intracellular calcium concentrations which triggers electrolyte secretion by activating calcium-dependent chloride (CaCC) and potassium ($K_{Ca^{2+}}$) channels.

42]. The Na^+/K^+-ATPase maintains the potassium concentration gradient between the intra- and the extracellular space as a prerequisite for the establishment of the potassium diffusion potential (Figure 2).

H_2S affects key ion transport processes within the colonic epithelium. In rat, guinea pig, and human colon preparations H_2S (applied by sulfur salts) elicits a secretory response [43–45]. In rat colon, H_2S activates the apical membrane Na^+/Ca^{2+} exchanger extruding Ca^{2+} (Figure 2). It also induces an increase in cytosolic Ca^{2+} concentration as a result of the release of stored Ca^{2+} from intracellular organelles via IP_3-receptors or ryanodine receptors (RyR). Cytosolic accumulation of Ca^{2+} triggers the opening of basolateral Ca^{2+}-dependent potassium channels (K_{Ca}). Furthermore, an ATP-sensitive basolateral potassium (K_{ATP}) conductance is activated in the presence of H_2S. The K_{ATP} channels carrying this conductance may consist of the following combinations: Kir6.1/SUR1, Kir6.1/SUR2B, Kir6.2/SUR1, or Kir6.2/SUR2B [46]. They also exert a protective function against energy depletion as their inhibition by glibenclamide under this condition causes a huge increase in the colonic epithelium conductance [46]. The protective characteristic of K_{ATP} channels was also demonstrated in rats with colitis as their blockade with glibenclamide worsened the disease and increased mortality [47].

Both basolateral potassium conductance (K_{ATP} and K_{Ca}) build the driving force for apical chloride efflux (Figure 2). Furthermore, the Na^+/K^+-ATPase is also activated by H_2S [45]. In addition to the secretion of chloride, potassium is also secreted and the epithelial permeability increases [43, 48]. As a consequence of these secretion processes, sodium ions move paracellularly to the lumen (for electroneutrality) and water follows osmotically.

Aside from the direct effect of H_2S on ion channels and transporters within the epithelium, exogenous H_2S indirectly stimulates chloride secretion by activating secretomotor neurons in human and guinea pig colon mucosa/submucosa preparations [44] (Figure 3). This is supported by the facts that (1) the H_2S-induced secretory response in these preparations is inhibited by tetrodotoxin and (2) it is absent in the human colon epithelial cell line T84 [44]. The reason for the different actions of H_2S in rat and human/guinea pig colon preparations is unknown but might be explained by differences in the species. In human/guinea pig colon, H_2S activates the transient receptor potential vanilloid receptor 1 (TRPV1) in extrinsic primary afferent fibres, which results in a release of substance P [49]. Substance P binds to neurokinin receptors (NK) in enteric cholinergic secretomotor neurons [49]. The subsequent release of acetylcholine by these neurons stimulates epithelial chloride secretion via a muscarinergic receptor- and calcium-mediated signalling axis (Figure 3).

In addition to the described effects of H_2S on the secretion of chloride ions, H_2S activates bicarbonate secretion which in turn neutralizes excess acid produced in the gastrointestinal lumen thereby protecting from gastric or duodenal mucosa ulcers [50, 51]. Furthermore, H_2S increases mucus production from goblet cells, reversing inflammation-associated mucus deficiency [52].

The secretory response to exogenous H_2S could be interpreted as a defence mechanism of the intestinal epithelium which prevents potentially harmful H_2S concentrations

which might exceed the oxidative capacities of the epithelial cells. Since the oxidative capacity is particularly high in intestinal epithelia [30] the secretory response would be triggered by rather high exogenous H_2S concentrations. In sum, exogenous H_2S triggers a secretory epithelial response in the intestine which prevents toxic effects of H_2S as well as onset of inflammatory processes by flushing the exogenous sources for H_2S from the epithelial wall.

3.1.2. Endogenous H_2S Production in Intestinal Epithelia. Gut tissue produces and releases H_2S [53] and the H_2S-generating enzymes CBS and CSE have been found within rat colonic epithelium [43]. The local H_2S concentration within the intestinal wall is unknown but the production rate of H_2S in rat ileum is in the range of 12 nmol/min/g tissue [54]. Consistent with the described prosecretory actions of H_2S, inhibitors of CBS and CSE dose-dependently decreased basal anion secretion across rat distal colon preparations, indicating that endogenous H_2S production might contribute to basal (secretory) ion transport mechanisms in the epithelium [43]. These observations seem to contrast the principle of oxidative degradation of H_2S under normal physiological conditions (see Section 2.2.2); however, the environment of the gut might generate local, even subcellular anoxic milieus which would allow for enzymatic H_2S production. Whether or not endogenous H_2S influences basal secretory processes via the same mechanisms and ion channels/transporters as exogenous H_2S is unknown. Furthermore, the administration of the H_2S "precursor" L-cysteine stimulated a secretory response in guinea pig colon preparations, which was sensitive to CBS and CSE inhibitors as well as the TRP channel inhibitor capsaicin [44]. This indicates that the indirect secretory epithelial response in this preparation (see Section 3.1.1) does occur not only due to exogenous H_2S, but also as a result of enhanced intracellular H_2S production in submucosal neurons. Whether such endogenous H_2S production in submucosal neurons occurs under physiological (normoxic) conditions and contributes to ion transport regulation is unknown.

3.1.3. H_2S in Intestinal Epithelia: Pharmacological Aspects. The local concentration of H_2S as well as the velocity of the H_2S-generating pathway determines whether H_2S acts as a prosecretory (as described above) or as an antisecretory agent. This was demonstrated by assessing chloride secretion by rat enterocytes using different H_2S-generating compounds: GYY4137 as a very slow releaser, L-cysteine and diallyl trisulfide as relatively slow releasers, and NaHS as a fast releaser. The last two compounds activated chloride secretion whereas L-cysteine and GYY4137 induced the opposite (antisecretory) effect [48]. Such concentration-dependent proabsorptive/prosecretory epithelial actions have already been described for NO and indicate that the kinetics of production, degradation, and even formation of reactive intermediates determines the physiological effects of gasotransmitters. These facts should be considered when evaluating (1) the contribution of (endogenous and exogenous) H_2S to the pathogenesis of diseases as well as (2) H_2S-releasing molecules for therapeutic purposes.

For example, pro- and anti-inflammatory effects are ascribed to H_2S (for review, see [4]). In rat models of colitis, inflammation was resolved by NaHS, Lawesson's reagent, and diallyl trisulfide. These H_2S donors achieved such a positive action by downregulating the expression of proinflammatory cytokines (IL-1β, TNF, INFγ, IL-12, and IL-13) and of chemokines (for review, see [7]). This is consistent with the observed therapeutic effects of, for example, the slow-release ATB-429 in a mouse model of colitis [55]. By contrast, other studies describe detrimental effects such as proinflammatory actions or impairment of gastrointestinal integrity [56–58].

In a rat model of colitis, the secretory response to H_2S was reduced in colon epithelial preparations. This reduction was prevented when the animals were fed on a S-reduced diet (which reduces microflora-mediated H_2S formation), but not by inhibitors of H_2S-generating enzymes [59]. This is consistent with an enhanced number of SRBs and faecal H_2S production in patients with ulcerative colitis [60, 61]. These findings indicate that alteration in exogenous, that is, colonic, microflora-derived H_2S, determines the efficacy of H_2S-liberating molecules in diseased tissues. This appears to be reasoned in a desensitisation of the intestinal epithelium to repeated exposure to H_2S [43]. Again, this example demonstrates that the kinetics of H_2S production and local concentration are important determinants of epithelial reactions to this molecule.

3.2. H_2S and Pulmonary Epithelia

3.2.1. Pulmonary Epithelial Responses to Exogenous H_2S. In contrast to secretory actions of H_2S in the intestine, a growing body of evidence suggests that H_2S inhibits epithelial electrolyte absorption in a variety of tissues and species [33, 62–68], including epithelia of the lung. Electrolyte absorption by pulmonary epithelial cells is facilitated by the activity of basolaterally localised Na^+/K^+-ATPases which establish an electrochemical driving force for the entry of sodium ions through cation channels and/or transporters in the apical epithelial membrane [69]. The concerted action of these apical entry pathways and basolateral Na^+/K^+-ATPases generates a vectorial absorption of sodium ions across the epithelium. Consequently, sodium absorption facilitates the paracellular absorption of chloride ions and water (Figure 4).

The rate-limiting step for sodium absorption in many vertebrate epithelia including those of the lungs is the epithelial sodium channel (ENaC) [70–73]. Experimental evidence from lung epithelial preparations suggests that exogenous H_2S reduces ENaC-mediated epithelial electrolyte absorption (Figure 4). H_2S-releasing compounds such as the sulfur salts NaHS and Na_2S decreased basal ENaC-mediated sodium absorption in airway epithelial preparations from pigs and mice [62], as well as distal lung tissues from rats [33] and amphibians [63]. Consistent with the concept that lung liquid clearance largely depends on ENaC-mediated sodium transport [74–76], the sulfur salts decreased the basal rate of transepithelial liquid absorption in rat lungs [33, 68]. A decreased capacity to absorb excess lung liquid would facilitate the formation of liquid accumulation in lungs. Mice

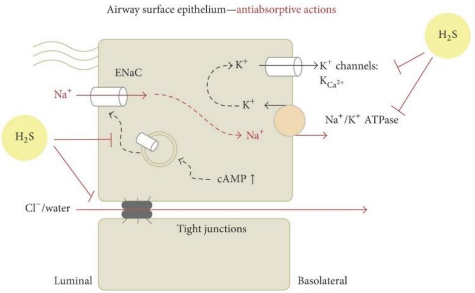

FIGURE 4: Airway epithelial ion transport responses to exogenous hydrogen sulfide. In airway surface epithelia, H_2S decreases basal absorption of Na^+ and eventually water by decreasing the electrochemical driving forces for apical entry of Na^+ through epithelial sodium channels (ENaC). This occurs by inhibition of the basolateral Na^+/K^+-ATPase as well as $K_{Ca^{2+}}$ channels. Furthermore, exogenous H_2S prevents the translocation of subapical vesicles containing ENaCs to the membrane thereby abrogating the action of proabsorptive, cAMP-dependent stimuli.

and rats develop such pulmonary oedema after exposure to exogenous H_2S [68, 77, 78]. Furthermore, pulmonary oedema formation is characteristic for patients who suffer from acute H_2S poisoning [79], thus providing further evidence that exogenous H_2S reduces epithelial sodium and liquid absorption in lungs.

The precise mechanism how ENaC-mediated epithelial sodium absorption is impaired by H_2S has not been completely clarified. Patch-Clamp and heterologous expression experiments revealed that there is no direct effect of acute H_2S exposure on ENaC activity [62, 66, 67]. By contrast, long-term exposure to H_2S (NaHS) reduces the expression of the ENaC α-subunit by ERK1/2 mediated signalling [68]. However, the observed inhibition of ENaC-mediated epithelial sodium absorption by H_2S occurs too fast (within minutes) [33, 62, 63] to be explained by changes in gene expression of sodium transporting molecules. As mentioned above, the electrochemical driving force for apical sodium entry through ENaC is generated by the basolateral Na^+/K^+-ATPase. Apical membrane permeabilisation studies revealed that the activity of the Na^+/K^+-ATPase is reduced by H_2S [62, 63] (Figure 4). As described, the Na^+/K^+-ATPase is also influenced by H_2S in rat distal colon epithelia [45]. Furthermore, it is speculated that H_2S-induced inhibition of sodium-uptake in larval zebrafish might be due to impaired Na^+/K^+-ATPase activity [65], further indicating that this enzyme is a molecular target for H_2S.

Aside from the Na^+/K^+-ATPase, basolateral potassium channels contribute to the electrochemical driving force for sodium absorption by maintaining a negative membrane potential which facilitates cation influx at the apical epithelial plasma membrane. It was demonstrated that H_2S inhibits basolateral potassium channels in lung epithelia [62, 63] (Figure 4). Inhibitor studies suggest that K_{Ca} channels are likely targeted by H_2S; however, the precise type of basolateral potassium channel has yet to be identified. Inhibition of potassium channels as well as the Na^+/K^+-ATPase impairs the electrochemical gradient which is necessary for ENaC-mediated sodium influx and thereby reduces overall transepithelial sodium and, consequently, liquid absorption.

How H_2S leads to a decreased activity of these basolateral transporting molecules remains unknown. As mentioned above, the rapid effects of H_2S suggest changes in the activity of the transporting molecules rather than changes in their expression levels. This might be achieved by either changing their transport activity rates or, alternatively, their abundance in the basolateral plasma membrane.

In rat renal tubular epithelial cells, NaHS induces endocytosis of the Na^+/K^+-ATPase thereby inhibiting renal sodium absorption [64]. This occurs via a signalling cascade which is initiated by activation of the epidermal growth factor receptor by H_2S. In H441 lung epithelial cells, there is no change in membrane abundance of the Na^+/K^+-ATPase within the time course of sodium transport inhibition by H_2S [62], indicating that in lung epithelia H_2S rather interferes with the transport activity of this enzyme.

Activity changes of transport proteins might be achieved by a posttranslational modification due to H_2S. Initially it was suggested that H_2S is able to directly modify thiol groups in proteins (including K_{ATP} channels), a mechanism which was referred to as S-sulfhydration [80, 81], although persulfidation is the more correct term [82]. Recently it became clear that H_2S alone is not able to modify thiol groups, but derivatives of H_2S such as polysulfides [83] or reaction products of H_2S and NO such as nitroxyl (HNO) are able to do so [82]. Elegant work by Eberhardt and colleagues recently dissected

a mechanism underlying the activation of a member of the TRP channel family (TRPA1) by H_2S. These authors observed that HNO, which is formed by a redox reaction between H_2S and NO, induced calcium influx into neurons from dorsal root ganglia of wild type, but not TRPA1-*knock-out* mice [84]. The primary targets for HNO are thiols [85] and the N-terminal region of TRPA1 contains cysteine residues which are necessary for activation of the channel by sulfhydryl-reactive agents [86, 87]. Mutation of these residues to lysine prevented the activation of human TRPA1 by HNO [84]. Furthermore, the authors demonstrated that HNO induces a formation of disulfide bonds and suggest a model by which disulfide bond formation between two cysteine pairs induces a conformational change which leads to channel opening [84].

Whether a similar mechanism would also account for the observed inhibition of the Na^+/K^+-ATPase and basolateral potassium channels in lung epithelia remains to be investigated. Interestingly, NO also inhibits basolateral transporting molecules in H441 lung epithelial cells, with similar kinetics to H_2S [88], and posttranslational thiol-modification modulates the activity of the Na^+/K^+-ATPase [89]. Furthermore, HNO was recently shown to influence the Na^+/K^+-ATPase and basolateral potassium channels in distal rat colon epithelia [40], suggesting that these molecules represent molecular targets for reactive derivatives of H_2S. However, it has to be noted that H_2S stimulates the Na^+/K^+-ATPase in the rat colon, whereas an inhibition of the Na^+/K^+-ATPase was observed in airway surface epithelia. This discrepancy might be explained by variations in the Na^+/K^+-ATPase subunit composition. The Na^+/K^+-ATPase consists of core α- and β-subunit, of which there are four and three isoforms, respectively [90]. In addition, these core α/β-complexes assemble with an additional subunit of the FXYD protein family [91]. Tissue-dependent differences in the molecular Na^+/K^+-ATPase compositions might account for the different reactions to H_2S. Furthermore, basolateral potassium channels indirectly influence Na^+/K^+-ATPase activity by either enhancing or diminishing basolateral potassium-recycling and hence activity of the Na^+/K^+-ATPase. It is possible that the potassium channel repertoire of the basolateral membrane indirectly contributes to the observed variety in responses to H_2S.

Aside from the influence of H_2S on basal epithelial sodium transport processes, H_2S reduces the efficacy of proabsorptive stimuli. In lung epithelia, H_2S abrogated the stimulation of ENaC-mediated sodium transport and lung liquid clearance by β-adrenergic receptor agonists [33]. This is the result of an impairment of the cAMP/protein kinase A signalling axis, although the molecular target for H_2S remains unknown. In amphibian A6 (renal) cells, H_2S prevented the activation of ENaC by reactive oxygen species [66] and advanced glycation end-products [67], likely due to antioxidative mechanisms.

In sum, the currently available data indicate antiabsorptive actions of exogenous H_2S on electrolyte absorbing pulmonary epithelia.

3.2.2. Endogenous H_2S Production in Pulmonary Epithelia. In the human respiratory system, CBS/CSE have been detected in nasal mucosa [92, 93], submucosal glands [92, 93], and human H441 airway epithelial cells [33]. 3MST has only been detected at the mRNA level in human H441 cells [33]. In rodents, CBS/CSE are present in mouse airway epithelium [94], whereas CSE/3MST but not CBS were detected in rat lung homogenates [95]. All three proteins are present in airways and alveoli of cow and sea lion lungs [31]. These data indicate that pulmonary epithelia contain H_2S-generating pathways. Consistently, using H_2S-specific amperometric sensors it was shown that rat lung homogenates [95] as well as H441 epithelial cell lysates [33] produce detectable amounts of H_2S.

However, H_2S production is only detectable in the absence of oxygen (see Section 2.2.2). Consistently, inhibition of H_2S-generating enzymes under normoxic conditions does not alter baseline sodium absorption by these cells [62]. This indicates that H_2S is not a basal regulator of pulmonary epithelial sodium transport processes and the observed inhibition of sodium and water absorption rather represents an epithelial reaction to either exogenous H_2S or deregulated endogenous H_2S generation under pathophysiological conditions.

3.2.3. H_2S in Lung Epithelia: Physiological and Pathophysiological Aspects. How can these findings be integrated into a physiological context? The antiabsorptive and prosecretory epithelial responses can be interpreted as an epithelial defence mechanism against potentially harmful H_2S concentrations which exceed the oxidative H_2S-degrading capacities of the epithelial cells. Liquid accumulation at the luminal side of the epithelia would eliminate the potential sources of H_2S (such as microbiota) by "flushing" of epithelia-covered compartments.

The main epithelial defence mechanism in the lung is airway mucociliary clearance [96, 97], whereas in the distal, alveolar regions of the lungs, primary defence against potential pathogens is maintained by alveolar macrophages. The entire epithelial surface of the airways is covered by a thin film of liquid, the airway surface liquid (ASL). This ASL is composed of a liquid phase surrounding the cilia of the airway epithelial cells, the periciliary liquid (PCL), and a gel-like mucus layer on top of the PCL [98]. The mucus layer is a trap for inhaled particles and potential pathogens. Due to ciliary movement, the PCL as well as the mucus layer moves towards the larynx, thereby clearing the trapped particles/pathogens from the lungs. Mucus clearance depends on the degree of hydration of the mucus gel: an increase in ASL volume enhances mucociliary clearance [96, 97, 99]. Hence, mechanisms which result in hydration of the ASL will eventually strengthen mucociliary clearance and clear the pulmonary epithelial surface from potential pathogens. The ASL volume and, consequently, the degree of mucus hydration are regulated by liquid secretion and absorption across the pulmonary epithelium.

The liquid feeding the PCL/ASL is produced by submucosal glands [96], a process which depends on vectorial

anion secretion by serous cells of the glands [97]. A recent study demonstrated that submucosal glands of pig tracheal epithelia secrete liquid upon exposure to bacteria such as *Pseudomonas aeruginosa* [100], thereby showing that liquid secretion and augmented mucociliary clearance are a primary defence mechanism in the airways. Whether or not H_2S elicits anion secretion in submucosal glands is currently unknown. In experiments addressing liquid secretion/absorption rates in fluid-filled rat lungs, there was no effect of H_2S over that of the ENaC-inhibitor amiloride, indicating that H_2S does not induce a detectable liquid secretion [33]. However, in this preparation the major liquid movements occur across the large surface of the alveolar regions. A potential contribution of gland secretion of the upper airways might be difficult to detect with this approach.

Aside from liquid secretion by submucosal glands, the surface epithelium of the airways is considered to absorb excess liquid [96]. This concept is supported by an anatomical view of the epithelia-covered lung structures. The alveolar surface of the human lung is by a magnitude of 10^5 larger than that of the trachea [101]. Given that the epithelial surface liquid (alveolar liquid and ASL) is continuously transported towards the larynx, the volume of liquid lining the airway epithelia should also increase by the same magnitude. However, the height of the liquid layer lining the epithelia is relatively constant, indicating that excess volume is absorbed by the surface epithelial cells of the airways [101]. A reduction in epithelial sodium and liquid absorption would therefore result in a volume increase of the ASL. An *in vitro* approach using cultured human airway epithelia demonstrated that volume increase of the ASL results in a higher rate of mucus transport [102]. Furthermore, patients with the hereditary disease Pseudohypoaldosteronism Type 1 have a reduced ENaC activity in the airways and thus an increased ASL volume [99]. Consistently, these patients display a mucus transport rate which is profoundly above that of normal subjects [99]. This example demonstrates that a reduction in ENaC-mediated sodium absorption eventually results in an increased mucociliary clearance and would therefore be consistent with the idea of an H_2S-induced "defence-flushing" of epithelial surfaces. The occurrence of rhinorrhoea during exposure to H_2S [103] is consistent with an increased amount of surface liquid in the respiratory system. Furthermore, the formation of rhinorrhoea or, in the distal lung, pulmonary oedema due to H_2S poisoning might be interpreted as a hyperresponsive epithelial defence reaction to exogenous H_2S.

4. Conclusion and Perspective

The herein reviewed findings teach a concept by which physiological effects elicited by H_2S critically depend on its concentration as well as kinetics of its production and metabolism. In accordance with Paracelsus' principle, the local concentration is the critical factor which allows the separation of physiology and toxicology of H_2S. The precise determination of local H_2S concentrations is still a major technical challenge (for review see [36, 37]) and hampers the classification of toxic, physiological, and beneficial roles for this molecule.

The currently available data on (1) the biochemistry of endogenous H_2S production; (2) its correlation with oxygen availability; and (3) epithelial reactions to exogenous H_2S suggest that normal physiology aims to maintain a low endogenous H_2S concentration which is likely in the submicromolar range. The future challenges will be to understand pathophysiological conditions, in which these systems are impaired, and the precise determination of concentration windows which allow for pharmacological interference. Furthermore, the contribution of exogenous (i.e., microbiota-derived) H_2S in experimental studies should be taken into consideration. At this stage it appears most suitable to close with the introductory quote: "*All things are poisons, for there is nothing without poisonous qualities. It is only the dose which makes a thing poison.*"

Conflict of Interests

The authors declare that there is no conflict of interests regarding the publication of this paper.

Acknowledgments

The authors would like to thank Pawel Piotr Szczesniak and Fabrizio Santangelo for helpful comments and discussions. Professor Martin Diener is acknowledged for outstanding support. Mike Althaus is supported by a grant from the German Research Foundation (DFG, AL1453/1-2).

References

[1] R. J. Reiffenstein, W. C. Hulbert, and S. H. Roth, "Toxicology of hydrogen sulfide," *Annual Review of Pharmacology and Toxicology*, vol. 32, pp. 109–134, 1992.

[2] L. C. Petersen, "The effect of inhibitors on the oxygen kinetics of cytochrome c oxidase," *Biochimica et Biophysica Acta (BBA)—Bioenergetics*, vol. 460, no. 2, pp. 299–307, 1977.

[3] J. P. Collman, S. Ghosh, A. Dey, and R. A. Decréau, "Using a functional enzyme model to understand the chemistry behind hydrogen sulfide induced hibernation," *Proceedings of the National Academy of Sciences of the United States of America*, vol. 106, no. 52, pp. 22090–22095, 2009.

[4] R. Wang, "Physiological implications of hydrogen sulfide: a whiff exploration that blossomed," *Physiological Reviews*, vol. 92, no. 2, pp. 791–896, 2012.

[5] R. Wang, "Two's company, three's a crowd: can H_2S be the third endogenous gaseous transmitter?" *The FASEB Journal*, vol. 16, no. 13, pp. 1792–1798, 2002.

[6] K. Kashfi and K. R. Olson, "Biology and therapeutic potential of hydrogen sulfide and hydrogen sulfide-releasing chimeras," *Biochemical Pharmacology*, vol. 85, no. 5, pp. 689–703, 2013.

[7] J. L. Wallace and R. Wang, "Hydrogen sulfide-based therapeutics: exploiting a unique but ubiquitous gasotransmitter," *Nature Reviews Drug Discovery*, vol. 14, no. 5, pp. 329–345, 2015.

[8] E. R. Deleon, G. F. Stoy, and K. R. Olson, "Passive loss of hydrogen sulfide in biological experiments," *Analytical Biochemistry*, vol. 421, no. 1, pp. 203–207, 2012.

[9] C. Szabō, "Hydrogen sulphide and its therapeutic potential," *Nature Reviews Drug Discovery*, vol. 6, no. 11, pp. 917–935, 2007.

[10] J. R. D. Nelson, J. D. R. Lide, and A. A. Maryott, *Selected Values of Electric Dipole Moments for Molecules in the Gas Phase*, vol. 10 of *NSRDS-NBS*, U.S. Government Printing Office, Washington, DC, USA, 1967.

[11] J. C. Mathai, A. Missner, P. Kügler et al., "No facilitator required for membrane transport of hydrogen sulfide," *Proceedings of the National Academy of Sciences of the United States of America*, vol. 106, no. 39, pp. 16633–16638, 2009.

[12] C. Willis, J. Cummings, G. Neale, and G. Gibson, "In vitro effects of mucin fermentation on the growth of human colonic sulphate-reducing bacteria," *Anaerobe*, vol. 2, pp. 117–122, 1996.

[13] F. Blachier, A.-M. Davila, S. Mimoun et al., "Luminal sulfide and large intestine mucosa: friend or foe?" *Amino Acids*, vol. 39, no. 2, pp. 335–347, 2010.

[14] P. D. Scanlan, F. Shanahan, and J. R. Marchesi, "Culture-independent analysis of desulfovibrios in the human distal colon of healthy, colorectal cancer and polypectomized individuals," *FEMS Microbiology Ecology*, vol. 69, no. 2, pp. 213–221, 2009.

[15] K. Shatalin, E. Shatalina, A. Mironov, and E. Nudler, "H_2S: a universal defense against antibiotics in bacteria," *Science*, vol. 334, no. 6058, pp. 986–990, 2011.

[16] G. T. Macfarlane, G. R. Gibson, and J. H. Cummings, "Comparison of fermentation reactions in different regions of the human colon," *Journal of Applied Bacteriology*, vol. 72, no. 1, pp. 57–64, 1992.

[17] Z. J. Song, M. Y. Ng, Z.-W. Lee et al., "Hydrogen sulfide donors in research and drug development," *MedChemComm*, vol. 5, no. 5, pp. 557–570, 2014.

[18] H. Kimura, "Metabolic turnover of hydrogen sulfide," *Frontiers in Physiology*, vol. 3, article 101, 2012.

[19] H. Kimura, "Physiological role of hydrogen sulfide and polysulfide in the central nervous system," *Neurochemistry International*, vol. 63, no. 5, pp. 492–497, 2013.

[20] C. E. Paulsen and K. S. Carroll, "Cysteine-mediated redox signaling: chemistry, biology, and tools for discovery," *Chemical Reviews*, vol. 113, no. 7, pp. 4633–4679, 2013.

[21] T. S. Bailey, L. N. Zakharov, and M. D. Pluth, "Understanding hydrogen sulfide storage: probing conditions for sulfide release from hydrodisulfides," *Journal of the American Chemical Society*, vol. 136, no. 30, pp. 10573–10576, 2014.

[22] N. Shibuya, M. Tanaka, M. Yoshida et al., "3-Mercaptopyruvate sulfurtransferase produces hydrogen sulfide and bound sulfane sulfur in the brain," *Antioxidants & Redox Signaling*, vol. 11, no. 4, pp. 703–714, 2009.

[23] J. Washio, T. Sato, T. Koseki, and N. Takahashi, "Hydrogen sulfide-producing bacteria in tongue biofilm and their relationship with oral malodour," *Journal of Medical Microbiology*, vol. 54, no. 9, pp. 889–895, 2005.

[24] I. Sekirov, S. L. Russell, L. Caetano M Antunes, and B. B. Finlay, "Gut microbiota in health and disease," *Physiological Reviews*, vol. 90, no. 3, pp. 859–904, 2010.

[25] T. Florin, G. Neale, G. R. Gibson, S. U. Christl, and J. H. Cummings, "Metabolism of dietary sulphate: absorption and excretion in humans," *Gut*, vol. 32, no. 7, pp. 766–773, 1991.

[26] D. H. Bergey and J. G. Holt, *Bergey's Manual of Determinative Bacteriology*, Williams & Wilkins, Baltimore, Md, USA, 9th edition, 1993.

[27] X. Leschelle, M. Goubern, M. Andriamihaja et al., "Adaptative metabolic response of human colonic epithelial cells to the adverse effects of the luminal compound sulfide," *Biochimica et Biophysica Acta—General Subjects*, vol. 1725, no. 2, pp. 201–212, 2005.

[28] K. R. Olson, "Hydrogen sulfide as an oxygen sensor," *Clinical Chemistry and Laboratory Medicine*, vol. 51, no. 3, pp. 623–632, 2013.

[29] J. Furne, J. Springfield, T. Koenig, E. DeMaster, and M. D. Levitt, "Oxidation of hydrogen sulfide and methanethiol to thiosulfate by rat tissues: a specialized function of the colonic mucosa," *Biochemical Pharmacology*, vol. 62, no. 2, pp. 255–259, 2001.

[30] S. Mimoun, M. Andriamihaja, C. Chaumontet et al., "Detoxification of H_2S by differentiated colonic epithelial cells: implication of the sulfide oxidizing unit and of the cell respiratory capacity," *Antioxidants and Redox Signaling*, vol. 17, no. 1, pp. 1–10, 2012.

[31] K. R. Olson, N. L. Whitfield, S. E. Bearden et al., "Hypoxic pulmonary vasodilation: a paradigm shift with a hydrogen sulfide mechanism," *The American Journal of Physiology—Regulatory Integrative and Comparative Physiology*, vol. 298, no. 1, pp. R51–R60, 2010.

[32] R. A. Dombkowski, M. G. Naylor, E. Shoemaker et al., "Hydrogen sulfide (H_2S) and hypoxia inhibit salmonid gastrointestinal motility: evidence for H_2S as an oxygen sensor," *Journal of Experimental Biology*, vol. 214, no. 23, pp. 4030–4040, 2011.

[33] A. M. Agné, J. Baldin, A. R. Benjamin et al., "Hydrogen sulfide decreases β-adrenergic agonist-stimulated lung liquid clearance by inhibiting ENaC-mediated transepithelial sodium absorption," *American Journal of Physiology—Regulatory, Integrative and Comparative Physiology*, vol. 308, no. 7, pp. R636–R649, 2015.

[34] P. J. Kemp and V. Telezhkin, "Oxygen sensing by the carotid body: is it all just rotten eggs?" *Antioxidants and Redox Signaling*, vol. 20, no. 5, pp. 794–804, 2014.

[35] K. R. Olson, "Hydrogen sulfide as an oxygen sensor," *Antioxidants & Redox Signaling*, vol. 22, no. 5, pp. 377–397, 2015.

[36] K. R. Olson, "Hydrogen sulfide: both feet on the gas and none on the brake?" *Frontiers in Physiology*, vol. 4, article 2, 2013.

[37] K. R. Olson, E. R. DeLeon, and F. Liu, "Controversies and conundrums in hydrogen sulfide biology," *Nitric Oxide*, vol. 41, pp. 11–26, 2014.

[38] L. G. van der Flier and H. Clevers, "Stem cells, self-renewal, and differentiation in the intestinal epithelium," *Annual Review of Physiology*, vol. 71, pp. 241–260, 2009.

[39] E. Pouokam, J. Steidle, and M. Diener, "Regulation of colonic ion transport by gasotransmitters," *Biological and Pharmaceutical Bulletin*, vol. 34, no. 6, pp. 789–793, 2011.

[40] E. Pouokam, A. Bell, and M. Diener, "Actions of Angeli's salt, a nitroxyl (HNO) donor, on ion transport across mucosa—submucosa preparations from rat distal colon," *European Journal of Pharmacology*, vol. 715, no. 1–3, pp. 133–141, 2013.

[41] D. Strabel and M. Diener, "Evidence against direct activation of chloride secretion by carbachol in the rat distal colon," *European Journal of Pharmacology*, vol. 274, no. 1–3, pp. 181–191, 1995.

[42] R. Warth and J. Barhanin, "Function of K+ channels in the intestinal epithelium," *Journal of Membrane Biology*, vol. 193, no. 2, pp. 67–78, 2003.

[43] B. Hennig and M. Diener, "Actions of hydrogen sulphide on ion transport across rat distal colon," *British Journal of Pharmacology*, vol. 158, no. 5, pp. 1263–1275, 2009.

[44] R. Schicho, D. Krueger, F. Zeller et al., "Hydrogen sulfide is a novel prosecretory neuromodulator in the Guinea-pig and human colon," *Gastroenterology*, vol. 131, no. 5, pp. 1542–1552, 2006.

[45] E. Pouokam and M. Diener, "Mechanisms of actions of hydrogen sulphide on rat distal colonic epithelium," *British Journal of Pharmacology*, vol. 162, no. 2, pp. 392–404, 2011.

[46] E. Pouokam, S. Bader, B. Brück, B. Schmidt, and M. Diener, "ATP-sensitive K^+ channels in rat colonic epithelium," *Pflugers Archiv—European Journal of Physiology*, vol. 465, no. 6, pp. 865–877, 2013.

[47] J. L. Wallace, L. Vong, W. McKnight, M. Dicay, and G. R. Martin, "Endogenous and exogenous hydrogen sulfide promotes resolution of colitis in rats," *Gastroenterology*, vol. 137, no. 2, pp. 569.e1–578.e1, 2009.

[48] E. Pouokam and M. Diener, "Modulation of ion transport across rat distal colon by cysteine," *Frontiers in Physiology*, vol. 3, article 43, 2012.

[49] D. Krueger, M. Foerster, K. Mueller et al., "Signaling mechanisms involved in the intestinal pro-secretory actions of hydrogen sulfide," *Neurogastroenterology & Motility*, vol. 22, no. 11, p. 1224-e320, 2010.

[50] K. Takeuchi, E. Aihara, M. Kimura, K. Dogishi, T. Hara, and S. Hayashi, "Gas mediators involved in modulating duodenal HCO3-secretion," *Current Medicinal Chemistry*, vol. 19, no. 1, pp. 43–54, 2012.

[51] R. W. Blackler, B. Gemici, A. Manko, and J. L. Wallace, "NSAID-gastroenteropathy: new aspects of pathogenesis and prevention," *Current Opinion in Pharmacology*, vol. 19, pp. 11–16, 2014.

[52] J. Motta, K. L. Flannigan, T. A. Agbor et al., "Hydrogen sulfide protects from colitis and restores intestinal microbiota biofilm and mucus production," *Inflammatory Bowel Diseases*, vol. 21, no. 5, pp. 1006–1017, 2015.

[53] D. R. Linden, L. Sha, A. Mazzone et al., "Production of the gaseous signal molecule hydrogen sulfide in mouse tissues," *Journal of Neurochemistry*, vol. 106, no. 4, pp. 1577–1585, 2008.

[54] W. Zhao, J. F. Ndisang, and R. Wang, "Modulation of endogenous production of H_2S in rat tissues," *Canadian Journal of Physiology and Pharmacology*, vol. 81, no. 9, pp. 848–853, 2003.

[55] S. Fiorucci, S. Orlandi, A. Mencarelli et al., "Enhanced activity of a hydrogen sulphide-releasing derivative of mesalamine (ATB-429) in a mouse model of colitis," *British Journal of Pharmacology*, vol. 150, no. 8, pp. 996–1002, 2007.

[56] R. Tamizhselvi, P. K. Moore, and M. Bhatia, "Inhibition of hydrogen sulfide synthesis attenuates chemokine production and protects mice against acute pancreatitis and associated lung injury," *Pancreas*, vol. 36, no. 4, pp. e24–e31, 2008.

[57] R. Tamizhselvi, P. K. Moore, and M. Bhatia, "Hydrogen sulfide acts as a mediator of inflammation inacute pancreatitis: in vitro studies using isolated mouse pancreatic acinar cells," *Journal of Cellular and Molecular Medicine*, vol. 11, no. 2, pp. 315–326, 2007.

[58] A. E. Chávez-Piña, G. R. Tapia-Álvarez, and A. Navarrete, "Inhibition of endogenous hydrogen sulfide synthesis by PAG protects against ethanol-induced gastric damage in the rat," *European Journal of Pharmacology*, vol. 630, no. 1–3, pp. 131–136, 2010.

[59] J. Steidle, L. Würner, and M. Diener, "Altered response to hydrogen sulphide during experimental colitis in rats," *Journal of Animal Physiology and Animal Nutrition*, vol. 97, no. 5, pp. 942–950, 2013.

[60] W. E. W. Roediger, J. Moore, and W. Babidge, "Colonic sulfide in pathogenesis and treatment of ulcerative colitis," *Digestive Diseases and Sciences*, vol. 42, no. 8, pp. 1571–1579, 1997.

[61] J. Levine, C. J. Ellis, J. K. Furne, J. Springfield, and M. D. Levitt, "Fecal hydrogen sulfide production in ulcerative colitis," *The American Journal of Gastroenterology*, vol. 93, no. 1, pp. 83–87, 1998.

[62] M. Althaus, K. D. Urness, W. G. Clauss, D. L. Baines, and M. Fronius, "The gasotransmitter hydrogen sulphide decreases Na^+ transport across pulmonary epithelial cells," *British Journal of Pharmacology*, vol. 166, no. 6, pp. 1946–1963, 2012.

[63] A. Erb and M. Althaus, "Actions of hydrogen sulfide on sodium transport processes across native distal lung epithelia (*Xenopus laevis*)," *PLoS ONE*, vol. 9, no. 6, Article ID e100971, 2014.

[64] S. Ge, M. Zhao, D. Wu et al., "Hydrogen sulfide targets EGFR Cys797/Cys798 residues to induce Na^+/K^+-ATPase endocytosis and inhibition in renal tubular epithelial cells and increase sodium excretion in chronic salt-loaded rats," *Antioxidants & Redox Signaling*, vol. 21, no. 15, pp. 2061–2082, 2014.

[65] Y. Kumai, C. S. Porteus, R. W. M. Kwong, and S. F. Perry, "Hydrogen sulfide inhibits Na^+ uptake in larval zebrafish, *Danio rerio*," *Pflügers Archiv—European Journal of Physiology*, vol. 467, no. 4, pp. 651–664, 2015.

[66] J. Zhang, S. Chen, H. Liu et al., "Hydrogen sulfide prevents hydrogen peroxide-induced activation of epithelial sodium channel through a PTEN/$PI(3,4,5)P_3$ dependent pathway," *PLoS ONE*, vol. 8, no. 5, Article ID e64304, 2013.

[67] Q. Wang, B. Song, S. Jiang et al., "Hydrogen sulfide prevents advanced glycation end-products induced activation of the epithelial sodium channel," *Oxidative Medicine and Cellular Longevity*, vol. 2015, Article ID 976848, 10 pages, 2015.

[68] L. Jiang, J. Wang, C. Su et al., "α-ENaC, a therapeutic target of dexamethasone on hydrogen sulfide induced acute pulmonary edema," *Environmental Toxicology and Pharmacology*, vol. 38, no. 2, pp. 616–624, 2014.

[69] M. Althaus, "Gasotransmitters: novel regulators of epithelial Na^+ transport?" *Frontiers in Physiology*, vol. 3, article 83, 2012.

[70] S. Kellenberger and L. Schild, "Epithelial sodium channel/degenerin family of ion channels: a variety of functions for a shared structure," *Physiological Reviews*, vol. 82, no. 3, pp. 735–767, 2002.

[71] V. Bhalla and K. R. Hallows, "Mechanisms of ENaC regulation and clinical implications," *Journal of the American Society of Nephrology*, vol. 19, no. 10, pp. 1845–1854, 2008.

[72] B. C. Rossier, M. E. Baker, and R. A. Studer, "Epithelial sodium transport and its control by aldosterone: the story of our internal environment revisited," *Physiological Reviews*, vol. 95, no. 1, pp. 297–340, 2015.

[73] L. G. Palmer, A. Patel, and G. Frindt, "Regulation and dysregulation of epithelial Na^+ channels," *Clinical and Experimental Nephrology*, vol. 16, no. 1, pp. 35–43, 2012.

[74] R. E. Olver, C. A. Ramsden, L. B. Strang, and D. V. Walters, "The role of amiloride-blockable sodium transport in adrenaline-induced lung liquid reabsorption in the fetal lamb," *Journal of Physiology*, vol. 376, pp. 321–340, 1986.

[75] R. E. Olver, D. V. Walters, and S. M. Wilson, "Developmental regulation of lung liquid transport," *Annual Review of Physiology*, vol. 66, pp. 77–101, 2004.

[76] M. Althaus, W. G. Clauss, and M. Fronius, "Amiloride-sensitive sodium channels and pulmonary edema," *Pulmonary Medicine*, vol. 2011, Article ID 830320, 8 pages, 2011.

[77] R. C. Francis, K. Vaporidi, K. D. Bloch, F. Ichinose, and W. M. Zapol, "Protective and detrimental effects of sodium sulfide and hydrogen sulfide in murine ventilator-induced lung injury," *Anesthesiology*, vol. 115, no. 5, pp. 1012–1021, 2011.

[78] J. Wang, H. Zhang, C. Su et al., "Dexamethasone ameliorates H_2S-induced acute lung injury by alleviating matrix metalloproteinase-2 and -9 expression," *PLoS ONE*, vol. 9, no. 4, Article ID e94701, 2014.

[79] T. L. Guidotti, "Hydrogen sulfide: advances in understanding human toxicity," *International Journal of Toxicology*, vol. 29, no. 6, pp. 569–581, 2010.

[80] A. K. Mustafa, M. M. Gadalla, N. Sen et al., "H_2S signals through protein S-Sulfhydration," *Science Signaling*, vol. 2, no. 96, p. ra72, 2009.

[81] A. K. Mustafa, G. Sikka, S. K. Gazi et al., "Hydrogen sulfide as endothelium-derived hyperpolarizing factor sulfhydrates potassium channels," *Circulation Research*, vol. 109, no. 11, pp. 1259–1268, 2011.

[82] M. R. Filipovic, "Persulfidation (S-sulfhydration) and H_2S," in *Chemistry, Biochemistry and Pharmacology of Hydrogen Sulfide*, vol. 230 of *Handbook of Experimental Pharmacology*, pp. 29–59, Springer, New York, NY, USA, 2015.

[83] H. Kimura, "Hydrogen sulfide and polysulfides as biological mediators," *Molecules*, vol. 19, no. 10, pp. 16146–16157, 2014.

[84] M. Eberhardt, M. Dux, B. Namer et al., "H_2S and NO cooperatively regulate vascular tone by activating a neuroendocrine HNO-TRPA1-CGRP signalling pathway," *Nature Communications*, vol. 5, article 4381, 2014.

[85] J. M. Fukuto and S. J. Carrington, "HNO signaling mechanisms," *Antioxidants and Redox Signaling*, vol. 14, no. 9, pp. 1649–1657, 2011.

[86] A. Hinman, H.-H. Chuang, D. M. Bautista, and D. Julius, "TRP channel activation by reversible covalent modification," *Proceedings of the National Academy of Sciences of the United States of America*, vol. 103, no. 51, pp. 19564–19568, 2006.

[87] L. J. Macpherson, A. E. Dubin, M. J. Evans et al., "Noxious compounds activate TRPA1 ion channels through covalent modification of cysteines," *Nature*, vol. 445, no. 7127, pp. 541–545, 2007.

[88] M. Althaus, A. Pichl, W. G. Clauss, W. Seeger, M. Fronius, and R. E. Morty, "Nitric oxide inhibits highly selective sodium channels and the Na^+/K^+-ATPase in H441 cells," *American Journal of Respiratory Cell and Molecular Biology*, vol. 44, no. 1, pp. 53–65, 2010.

[89] Y. Yang, X. Jin, and C. Jiang, "S-glutathionylation of ion channels: insights into the regulation of channel functions, thiol modification crosstalk, and mechanosensing," *Antioxidants & Redox Signaling*, vol. 20, no. 6, pp. 937–951, 2014.

[90] E. Tokhtaeva, R. J. Clifford, J. H. Kaplan, G. Sachs, and O. Vagin, "Subunit isoform selectivity in assembly of Na,K-ATPase α-β heterodimers," *The Journal of Biological Chemistry*, vol. 287, no. 31, pp. 26115–26125, 2012.

[91] K. Geering, "FXYD proteins: new regulators of Na-K-ATPase," *American Journal of Physiology—Renal Physiology*, vol. 290, no. 2, pp. F241–F250, 2006.

[92] S. J. Park, T. H. Kim, S. H. Lee et al., "Expression levels of endogenous hydrogen sulfide are altered in patients with allergic rhinitis," *The Laryngoscope*, vol. 123, no. 3, pp. 557–563, 2013.

[93] J. W. Hwang, Y. J. Jun, S. J. Park et al., "Endogenous production of hydrogen sulfide in human sinus mucosa and its expression levels are altered in patients with chronic rhinosinusitis with and without nasal polyps," *American Journal of Rhinology and Allergy*, vol. 28, no. 1, pp. 12–19, 2014.

[94] A. Madurga, A. Golec, A. Pozarska et al., "The H_2S-generating enzymes cystathionine β-synthase and cystathionine γ-lyase play a role in vascular development during normal lung alveolarization," *American Journal of Physiology—Lung Cellular and Molecular Physiology*, vol. 309, no. 7, pp. L710–L724, 2015.

[95] J. A. Madden, S. B. Ahlf, M. W. Dantuma, K. R. Olson, and D. L. Roerig, "Precursors and inhibitors of hydrogen sulfide synthesis affect acute hypoxic pulmonary vasoconstriction in the intact lung," *Journal of Applied Physiology*, vol. 112, no. 3, pp. 411–418, 2012.

[96] M. R. Knowles and R. C. Boucher, "Mucus clearance as a primary innate defense mechanism for mammalian airways," *The Journal of Clinical Investigation*, vol. 109, no. 5, pp. 571–577, 2002.

[97] J. H. Widdicombe and J. J. Wine, "Airway gland structure and function," *Physiological Reviews*, vol. 95, no. 4, pp. 1241–1319, 2015.

[98] M. Althaus, "ENaC inhibitors and airway re-hydration in cystic fibrosis: state of the art," *Current Molecular Pharmacology*, vol. 6, no. 1, pp. 3–12, 2013.

[99] E. Kerem, T. Bistritzer, A. Hanukoglu et al., "Pulmonary epithelial sodium-channel dysfunction and excess airway liquid in pseudohypoaldosteronism," *The New England Journal of Medicine*, vol. 341, no. 3, pp. 156–162, 1999.

[100] X. Luan, V. A. Campanucci, M. Nair et al., "Pseudomonas aeruginosa triggers CFTR-mediated airway surface liquid secretion in swine trachea," *Proceedings of the National Academy of Sciences of the United States of America*, vol. 111, no. 35, pp. 12930–12935, 2014.

[101] J. H. Widdicombe, "Regulation of the depth and composition of airway surface liquid," *Journal of Anatomy*, vol. 201, no. 4, pp. 313–318, 2002.

[102] R. Tarran, B. R. Grubb, J. T. Gatzy, C. W. Davis, and R. C. Boucher, "The relative roles of passive surface forces and active ion transport in the modulation of airway surface liquid volume and composition," *Journal of General Physiology*, vol. 118, no. 2, pp. 223–236, 2001.

[103] B. Doujaiji and J. A. Al-Tawfiq, "Hydrogen sulfide exposure in an adult male," *Annals of Saudi Medicine*, vol. 30, no. 1, pp. 76–80, 2010.


The Scientific World Journal
Gastroenterology Research and Practice
MEDIATORS INFLAMMATION
Journal of Diabetes Research
Disease Markers
Journal of Immunology Research
Hindawi
Submit your manuscripts at
http://www.hindawi.com
International Journal of Endocrinology
PPAR Research
BioMed Research International
Journal of Ophthalmology
Stem Cells International
eCAM
Evidence-Based Complementary and Alternative Medicine
Journal of Obesity
Journal of Oncology
Computational and Mathematical Methods in Medicine
Behavioural Neurology
Parkinson's Disease
AIDS Research and Treatment
Oxidative Medicine and Cellular Longevity

8.7 "Actions of Angeli´s salt, a nitroxyl (HNO) donor, on ion transport across mucosa-subMukosapreparations from rat distal colon"

Pouokam E, Bell A, Diener M. .*Eur. J. Pharmacol* (2013) **715:** 133-141.

Impakt Faktor: 2.68

Eigener Anteil an der Publikation:

- Initiative: 75 %
- Projektplanung: 75 %
- Durchführung der Versuche: 85 %
- Auswertung der Experimente: 90 %
- Erstellung der Publikation: 90 %

European Journal of Pharmacology 715 (2013) 133–141

Contents lists available at ScienceDirect

European Journal of Pharmacology

journal homepage: www.elsevier.com/locate/ejphar

Pulmonary, gastrointestinal and urogenital pharmacology

Actions of Angeli's salt, a nitroxyl (HNO) donor, on ion transport across mucosa—submucosa preparations from rat distal colon

Ervice Pouokam, Anna Bell, Martin Diener*

Institute for Veterinary Physiology and Biochemistry, Justus-Liebig-University Giessen, Germany

ARTICLE INFO

Article history:
Received 12 March 2013
Received in revised form
3 May 2013
Accepted 20 May 2013
Available online 4 June 2013

Keywords:
Angeli's salt
Ca^{2+}
Electrolyte transport
Nitroxyl
Rat colon

ABSTRACT

The aim of this study was to investigate whether nitroxyl (HNO), a redox variant of the radical gasotransmitter nitric oxide (NO) with therapeutically promising properties, affects colonic ion transport. Changes in short-circuit current (I_{sc}) induced by the HNO donor Angeli's salt were recorded in Ussing chambers. Cytosolic Ca^{2+} concentration was measured with fura-2. The nitroxyl donor induced a concentration-dependent increase in I_{sc} across rat distal colon which was due to a stimulation of chloride secretion. The secretion induced by Angeli's salt (5×10^{-4} mol/l) was not altered by the NO scavenger 2-(4-carboxyphenyl)-4,5-dihydro-4,4,5,5-tetramethyl-1H-imidazolyl-1-oxy-3-oxide (carboxy-PTIO), but was abolished by the HNO scavenger L-cysteine. The response was not dependent on the activity of soluble guanylate cyclase or enteric neurons, but was inhibited by indomethacin. Experiments with apically permeabilized epithelia revealed the activation of basolateral K^+ channels and a stimulation of the current carried by the basolateral Na^+—K^+-pump by Angeli's salt. The secretion induced by Angeli's salt was reduced in the absence of extracellular Ca^{2+}. A prominent increase in the cytosolic Ca^{2+} concentration was evoked by Angeli's salt predominantly in subepithelial cells within the submucosa, which had the same dependence on extracellular Ca^{2+} as the Angeli's salt-induced Cl^- secretion. Consequently, Angeli's salt induces a soluble guanylate cyclase-independent, Ca^{2+}-dependent Cl^- secretion via activation of the Na^+—K^+-ATPase and of basolateral K^+ channels. Cyclooxygenase metabolites produced within the submucosa seem to be involved in this response.

© 2013 Elsevier B.V. All rights reserved.

1. Introduction

Intestinal ion transport, which can be switched between absorption and secretion of water and electrolytes (for review see Binder and Sandle (1994)), is not only controlled by classical neurotransmitters or hormones, but also by the so-called "gasotransmitters" such as hydrogen sulfide (Schicho et al., 2006; Hennig and Diener, 2009; Pouokam and Diener, 2011), carbon monoxide (Steidle and Diener, 2011), and nitric oxide (Tamai and Gaginella, 1993; Toda and Herman, 2005). The latter gas is a signaling molecule whose physiological and pharmacological properties have been intensively studied during the last decades. Among other properties, nitric oxide (NO) plays a modulatory role on vascular tone and is involved in inflammation, angiogenesis and fibrolysis (Moncada and Higgs, 2006). Most of the research based on NO focused on the uncharged free radical ·NO and its oxidized variants such as nitrite (NO_2^-), nitrate (NO_3^-), peroxynitrite ($ONOO^-$), nitrogen dioxide (NO_2), or dinitrogen trioxide (N_2O_3). However, reduced variants of NO such as hydroxylamine (NH_2OH) or nitroxyl (HNO), the one-electron reduced and protonated sibling of NO, have been somewhat neglected. Recent evidence suggests that HNO might be endogenously produced and may show different pharmacological properties compared to NO (for review see Paolocci et al. (2007)). Thus, HNO can be generated by NO synthase(s) in the absence of the cofactor tetrahydrobiopterine (Rusche et al., 1998) or from oxidation of hydroxylamine (Donzelli et al., 2008). Nitroxyl can also be generated when NO is catabolyzed by cytochrome C (for review see Reisz et al. (2010)) or by xanthine oxidase (Saleem and Ohshima, 2004).

The growing evidence of a potential endogenous production of HNO and its ability to cross cell membranes (Fukuto et al., 2008) suggests that this molecule might exert physiologic paracrine effects in the organism. Indeed, it has been shown that HNO causes a vasodilatation of arteries (Fukuto et al., 1992; Ellis et al., 2000; Irvine et al., 2003; Favaloro and Kemp-Harper, 2007). Pharmacologically, HNO exerts an inotropic action (Paolocci et al., 2007). Furthermore, HNO is established as an antialcoholic agent as it inhibits the enzyme aldehyde dehydrogenase by modification of the active site cysteine thiolate (for review, see Paolocci et al. (2007)).

* Correspondence to: Institut für Veterinär-Physiologie und -Biochemie, Justus-Liebig-Universität Gießen, Frankfurter Straße, 35392 Gießen, Germany.
Tel.: +49 641 9938161; fax: +49 641 9938159.
E-mail address: Martin.Diener@vetmed.uni-giessen.de (M. Diener).

0014-2999/$ - see front matter © 2013 Elsevier B.V. All rights reserved.
http://dx.doi.org/10.1016/j.ejphar.2013.05.031

The last finding also reveals the thiophilicity of HNO, a property that has been confirmed by further studies showing the inhibition of other thiol enzymes (for review, see Paolocci et al. (2007)), the activation of cardiac sarcoplasmic reticulum ATPase (SERCA) at a cysteine residue (Lancel et al., 2009), or interactions with thiol residues on receptors or ion channels (Cheong et al., 2005). The thiophilicity of nitroxyl may result in a reversible modification of thiol proteins via formation of disulfide bonds or in an irreversible thiol protein modification via sulfinamide formation (Fukuto et al., 2009). In addition, nitroxyl has been reported to interact with metals, reducing iron (preferentially in the ferric state in heme or non-heme proteins), copper, and manganese (for review, see Irvine et al. (2008)). Finally, an activation of soluble guanylate cyclase/cGMP pathway has been identified as part of the mechanism of action of HNO (Irvine et al., 2003; Favaloro and Kemp-Harper, 2007; Paolocci et al. 2007). This is responsible e.g. for the activation of voltage-dependent K^+ (K_v) channels in rat mesenteric arteries (Irvine et al., 2003; Favaloro and Kemp-Harper, 2009) or ATP-sensitive K^+ (K_{ATP}) channels in the rat coronary vasculature (Favaloro and Kemp-Harper, 2007).

In contrast to NO (see e.g. Schultheiss et al. (2002a,b)), potential effects of HNO on gastrointestinal tract such as epithelial ion transport and the mechanisms involved are unknown. Therefore, changes in short-circuit current (I_{sc}), a measure of net ion transport across the epithelium, induced by a HNO donor, Angeli's salt, were measured in Ussing chambers under different conditions in a model epithelium, i.e. rat distal colon.

2. Material and methods

2.1. Animals

Female and male Wistar rats with a body mass of 200—250 g were used. The animals were bred and housed at the institute for Veterinary Physiology and Biochemistry of the Justus-Liebig-University Giessen at an ambient temperature of 22.5 °C and air humidity of 50—55% on a 12 h: 12 h light—dark cycle with free access to water and food until the time of the experiment. Experiments were approved by Regierungspräsidium Giessen, Giessen, Germany.

2.2. Solutions

If not indicated differently (as e.g. in ion substitution experiments), all Ussing chamber experiments were performed using a buffer solution on both sides of the tissue containing (mmol/l): NaCl 107, KCl 4.5, $NaHCO_3$ 25, Na_2HPO_4 1.8, NaH_2PO_4 0.2, $CaCl_2$ 1.25, $MgSO_4$ 1 and glucose 12. The solution was gassed with carbogen (5% CO_2 in 95% O_2, v/v); pH was 7.4. In order to apply a K^+ gradient, the KCl concentration in the buffer was increased to 13.5 mmol/l at the mucosal side while reducing the NaCl concentration in order to maintain isoosmolarity. For the Na^+-free solution, NaCl was replaced by N-methyl-D-glucamine ($NMDG^+$) chloride. For the depolarization of the basolateral membrane, a 111.5 mmol/l KCl solution was used, in which NaCl was replaced by equimolar KCl on the serosal side. In order to apply a serosal to mucosal Cl^- gradient, 107 mmol/l Cl^- was replaced by the impermeable anion gluconate in the apical bathing solution. In the Cl^--free buffer, NaCl and KCl were substituted by Na gluconate and K gluconate (KGluc), respectively. The Ca^{2+} concentration in the Cl^--free buffer was increased to 5.75 mmol/l to compensate for the Ca^{2+}-buffering properties of gluconate (Kenyon and Gibbons, 1977). For the experiments carried out with isolated crypts, the following buffers were used: the EDTA solution for the isolation contained (mmol/l): NaCl 107, KCl 4.5, $NaHCO_3$ 25, Na_2HPO_4 1.8, NaH_2PO_4 0.2, glucose 12.2, EDTA 10 and 1 g/l bovine serum albumin (BSA). It was gassed with carbogen; pH was adjusted by tris-base (tris(hydroxymethyl)-aminomethane) to 7.4. The isolated crypts were stored in a high potassium Tyrode solution consisting of (mmol/l): K gluconate 100, KCl 30, HEPES (N-(2-hydroxyethyl)piperazine-N'-2-ethanesulfonic acid) 10, NaCl 20, $MgCl_2$ 1, $CaCl_2$ 1.25, glucose 12.2, sodium pyruvate 5 and 1 g/l BSA; pH was 7.4. For superfusion of the isolated crypts and the submucosal sheets during the imaging experiments, the following buffer was used (in mmol/l): NaCl 140, KCl 5.4, $CaCl_2$ 1.25, $MgSO_4$ 1, HEPES 10, glucose 12.2; pH was 7.4. For the Ca^{2+}-free solution, Ca^{2+} was omitted.

2.3. Tissue preparation and isolation of intact colonic crypts

Animals were killed by stunning followed by exsanguination. The serosa and muscularis propria were stripped away by hand to obtain a mucosa—submucosa preparation of the distal colon. Briefly, the colon was placed on a small plastic rod with a diameter of 5 mm. A circular incision was made near the anal end with a blunt scalpel, and the serosa together with the lamina propria was gently removed in a proximal direction. Two segments of the distal colon of each rat were prepared.

For the isolation of colonic crypts, the mucosa—submucosa preparation was glued on a plastic holder with tissue adhesive. The specimen was incubated for 7 min in the EDTA solution. Then the tissue was vibrated once for 30 s, which results in a separation of the cell contacts within the surface epithelium and a detachment of the basal cell contacts of the crypt cells from the basement membrane, so that isolated crypts are released from the mucosa. The crypts were collected in a high K^+ gluconate Tyrode buffer; the storage in this intracellular-like high K^+ low Cl^- buffer strongly prolongs the survival of the enterocytes (Schultheiss et al., 2002a).

In order to obtain intact submucosal sheets for Ca^{2+} imaging experiments, the submucosa-mucosa preparation, still fixed on the rod, was opened along the mesenteric border and placed on a glass plate. With the mucosal surface upwards, the proximal end of the tissue was clamped with a clip between a microscope slide and the upper end of the glass plate. The distal end of the colon was fixed with a blunt object slide. With a fresh and sharp slide the mucosa was cut transversely without damaging the underlying submucosal layer. Then the mucosa was carefully removed with the edge of a second microscope slide. The resulting submucosal layer was dissected into small pieces of about 8 mm x 8 mm and attached to cover slips (diameter 22 mm) coated with poly-L-lysine (molecular weight > 300,000; Biochrom, Berlin, Germany). The submucosal preparations were used in fura-2 experiments immediately after the tissue was fixed.

2.4. Short-circuit current measurement

The mucosa—submucosa preparation was fixed in a modified Ussing chamber bathed with a volume of 3.5 ml on each side of the mucosa. The tissue was incubated at 37 °C and short-circuited by a computer-controlled voltage-clamp device (Ingenieur Büro für Mess- und Datentechnik Mussler, Aachen, Germany) with correction for solution resistance. Tissue conductance (G_t) was measured every minute by the voltage deviation induced by a current pulse ($\pm$ 50 μA, duration 200 ms) under open-circuit conditions. Short-circuit current (I_{sc}) was continuously recorded. I_{sc} is expressed as μEq/h cm^2, i.e. the flux of a monovalent ion per time and area, with 1 μEq/h cm^2 = 26.9 μA/cm^2.

For the measurement of basolateral ion currents, the apical membrane was permeabilized by mucosal administration of nystatin (100 μg/ml). Nystatin was ultrasonicated immediately before use. The I_{sc} response to the ionophore was tested in the presence

or absence of a K^+ gradient (13.5 mmol/l at the mucosal and 4.5 mmol/l at the serosal side). When Angeli's salt was administered after apical permeabilization, the increase in I_{sc} evoked by the HNO donor was calculated as difference to the current extrapolated by linear regression from current data during the last 3 min before administration of the drug (ΔI_{sc}; see left inset in Fig. 5A).

To depolarize the basolateral membrane, the tissue was exposed to a high K^+ buffer (111.5 mmol/l KCl) at the serosal side. Under these conditions, the basolateral membrane is electrically eliminated and changes in I_{sc} reflect changes in current across the apical membrane (Schultheiss and Diener, 1997).

2.5. Imaging experiments

Relative changes in the cytosolic Ca^{2+} concentration were measured using fura-2 (Life Technologies, Darmstadt, Germany), a Ca^{2+}-sensitive fluorescent dye. The crypts were pipetted into the experimental chamber with a volume of about 3 ml. Like the submucosal preparations, the crypts were attached to the glass bottom of the chamber with the aid of poly-L-lysine (0.1 g/l). The crypts or submucosal preparations were incubated for 60 min with 2.5 μmol/l fura-2 acetoxymethylester (AM) and 0.05 g/l pluronic acid (Life Technologies, Darmstadt, Germany). Then the dye ester not taken up by the cells was washed away. The preparation was superfused hydrostatically throughout the experiment with 140 mmol/l NaCl Tyrode or Ca^{2+}-free Tyrode where appropriate. The perfusion rate was about 2 ml/min. Changes in the cytosolic Ca^{2+} concentration were monitored as changes in the fura-2 ratio (R; emission at an excitation wave length of 340 nm divided by the emission at an excitation wave length of 380 nm).

Experiments were carried out on an inverted microscope (Olympus IX-50; Olympus, Hamburg, Germany), equipped with an epifluorescence set-up and an image analysis system (Till Photonics, Martinsried, Germany). Several regions of interest, each with the size of about one cell, were selected. The emission above 420 nm was measured from the regions of interest. Data were sampled at 0.2 Hz. The baseline in the fluorescence ratio of fura-2 was measured for several minutes before drugs were administered.

2.6. Drugs

Angeli's salt ($Na_2(ONNO_2)$; disodium diazen-1-ium-1,2,2-triolate; Cayman Chemical, Ann Arbor, MI, USA), cyclopiazonic acid (CPA; Alexis, Grünberg, Germany), N-5-isoquinolinesulphonamide (H89), nystatin, 1H-[1,2,4]oxadiazolo [4,3-a]quinoxalin-1-one (ODQ; Tocris, Bristol, UK), staurosporine, and 3-(5′-hydroxymethyl-2′-furyl)-1-benzylindazole (YC-1; Alexis, Grünberg, Germany) were dissolved in dimethylsulfoxide (final maximal concentration 0.5%, v/v). 6-Anilino-5,8-quinolinequinone (LY 83583, Calbiochem, Bad Soden, Germany), bumetanide, forskolin (Calbiochem, Bad Soden, Germany), and indomethacin were dissolved in ethanol (final maximal concentration 0.25%, v/v). Scilliroside (generous gift from Sandoz, Basel, Switzerland) was dissolved in methanol (final concentration 0.25%, v/v). Tetrodotoxin was dissolved in 2×10^{-2} mol/l citrate buffer. $BaCl_2$, 2-(4-carboxyphenyl)-4,5-dihydro-4,4,5,5-tetramethyl-1H-imidazolyl-1-oxy-3-oxide (carboxy-PTIO), L-cysteine, GEA 3162 (1,2,3,4-oxatriazolium-5-amino-3-(3,4-dichlorophenyl chloride), and tetrapentylammonium chloride (TPeA) were dissolved in aqueous stock solutions. If not indicated otherwise, drugs were from Sigma (Taufkirchen, Germany).

Inactivated Angeli's salt was prepared as described in the literature (Fukuto et al., 2008) by incubation in the standard HCO_3^--buffered solution at 37 °C overnight under continuous supply of carbogen (95% O_2, 5% CO_2, v/v). Drug concentrations were selected according to the references cited at the first use of each drug and supported in most cases by own preliminary experiments.

2.7. Statistics

Results are given as means ± S.E.M., with the number (n) of investigated tissues or cells. When means of several groups had to be compared, an analysis of variance was performed followed by post-hoc Tukey's-test. For the comparison of two groups, either a Student's t-test or a Mann—Whitney U-test was applied. An F-test decided which test method had to be used. Both paired and unpaired two-tailed Student's t-tests were applied as appropriate. $P < 0.05$ was considered to be statistically significant.

3. Results

3.1. Effect of Angeli's salt on short-circuit current

The HNO donor Angeli's salt, administered at the serosal side, induced a concentration-dependent increase in I_{sc} (Fig. 1). This was paralleled by a small increase in tissue conductance (G_t), which amounted to 0.24 ± 0.20 mS/cm² for 10^{-4} mol/l and 1.60 ± 0.15 mS/cm² for 5×10^{-4} mol/l ($P < 0.05$, $n = 6$—8). For subsequent experiments, the highest concentration of Angeli's salt (5×10^{-4} mol/l at the serosal side) was used. The increase in I_{sc} was transient as the I_{sc} returned to baseline values within 25—30 min (Fig. 2).

A repetitive administration of Angeli's salt (5×10^{-4} mol/l at the serosal side) to the same tissue did not induce a desensitization (Fig. 2). It was therefore possible to investigate the actions of this drug upon repetitive administration to the same tissue in the presence or absence of pharmacological drugs (inhibitors/activators) without altering tissue properties.

To exclude contaminations either from any impurity or from Angeli's salt-derived nitrite, control experiments with decomposed Angeli's salt were performed. When used in the same concentrations (up to 5×10^{-4} mol/l at the serosal side), decomposed Angeli's salt did not evoke any change in I_{sc} ($n = 4$, data not shown).

3.2. Identification of the NO congener responsible for the response to Angeli's salt

Angeli's salt is a classical HNO donor, whose degradation at concentrations over 10^{-5} mol/l may, however, result in the

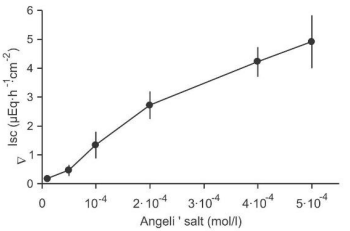

Fig. 1. Concentration-dependent increase in I_{sc} across rat distal colon induced by serosal administration of Angeli's salt. After each administration, the respective compartment was washed three times with 5 times the chamber volume, before the next concentration of the drug was administered. Values are means (filled circles) ± S.E.M. (vertical lines), $n = 6$—8.

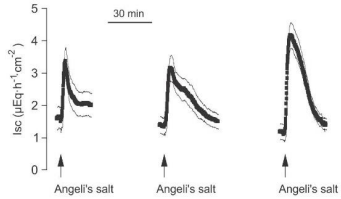

Fig. 2. Repetitive administration of Angeli's salt (5×10^{-4} mol/l at the serosal side, arrows) did not induce a desensitization of the tissue. Line interruptions between subsequent administrations of the HNO donor are caused by omission of current artefacts induced by washing the serosal compartment three times with 5 times the chamber volume. Values are means (symbols) ± S.E.M. (parallel continuous lines), $n=8$.

formation of ·NO. Also a conversion of HNO to ·NO might occur by oxidation catalyzed by superoxide dismutase (for review, see Irvine et al. (2008)). In order to discriminate which molecule effectively mediates the responses to Angeli's salt in the colonic preparations, scavengers were used. In the presence of L-cysteine (10^{-3} mol/l at the serosal side), which acts as a HNO scavenger (Favaloro and Kemp-Harper, 2009), the response to Angeli's salt (5×10^{-4} mol/l at the serosal side) was reduced from 1.32 ± 0.22 μEq/h cm^2 to 0.43 ± 0.02 μEq/h cm^2, i.e. inhibited by 67% ($P<0.05$). On the other hand, carboxy-PTIO (2×10^{-4} mol/l at the serosal side), a NO scavenger (Akaike et al., 1993), did not affect the increase in I_{sc} evoked by Angeli's salt (increase in I_{sc} 2.67 ± 0.53 μEq/h cm^2 in the presence compared to 2.77 ± 0.69 μEq/h cm^2 in the absence of carboxy-PTIO, $n=8$ each), although carboxy-PTIO reduced the response to a NO donor, GEA 3162 (10^{-4} mol/l at the serosal side), by 50% ($n=7$—8; data not shown). Consequently, the increase in I_{sc} evoked by Angeli's salt is mediated by HNO, but not by the radical, NO.

3.3. Ionic nature of the I_{sc} response

Anion substitution experiments were performed in order to find out the ionic nature of the I_{sc} induced by Angeli's salt. When administered first under control conditions, i.e. with Cl^- ions on both sides of the tissue, Angeli's salt (5×10^{-4} mol/l at the serosal side) evoked an increase in I_{sc} of 2.41 ± 0.42 μEq/h cm^2 ($n=8$). After replacement of Cl^- by the impermeant anion, gluconate, however, the increase in I_{sc} only amounted to 0.054 ± 0.027 μEq/h cm^2 ($P<0.05$ versus control response in the presence of Cl^-, $n=8$). Finally, a third administration of Angeli's salt after replacing the Cl^--free buffer by a Cl^- containing buffer yielded again an increase in I_{sc} of 1.02 ± 0.18 μEq/h cm^2 ($n=8$, Fig. 3). Similarly, blockade of the Na^+—K^+—2Cl^--cotransporter, the dominant Cl^--loading transporter at the basolateral membrane involved in Cl^- secretion (Binder and Sandle, 1994), with bumetanide (10^{-3} mol/l at the serosal side), significantly inhibited the increase in I_{sc} induced by Angeli's salt (5×10^{-4} mol/l at the serosal side; Table 1).

A prerequisite for epithelial Cl^- secretion is a negative membrane potential as driving force for apical Cl^- efflux via anion channels, which is generated predominantly by the activity of basolateral K^+ channels. In accordance with this general mode, the nonselective K^+ channel blocker Ba^{2+} (10^{-2} mol/l at the serosal side) suppressed the I_{sc} induced by Angeli's salt (5×10^{-4} mol/l at the serosal side; Table 1). In consequence, these series of experiments clearly indicate that the current response evoked by the HNO donor represents transepithelial Cl^- secretion.

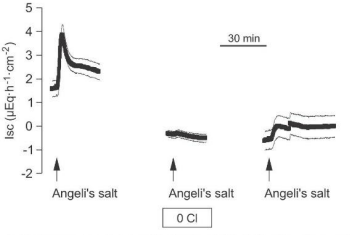

Fig. 3. The increase in the I_{sc} induced by Angeli's salt (5×10^{-4} mol/l at the serosal side, arrows) is abolished in the absence (0 Cl, white bar) of chloride at the mucosal and the serosal side. Line interruptions between two administrations of Angeli's salt are caused by omission of current artefacts induced by washing the serosal compartment three times with 5 times the chamber volume. Values are means (symbols) ± S.E.M. (parallel continuous lines), $n=8$. For statistics, see text.

Table 1
Effects of transport inhibitors on I_{sc} induced by Angeli's salt.

	Response to Angeli's salt, ΔI_{sc} (μEq/h cm^2)	n
Without serosal bumetanide	2.09 ± 0.24	8
With serosal bumetanide	0.65 ± 0.07[a]	8
Without serosal Ba^{2+}	1.96 ± 0.29	6
With serosal Ba^{2+}	0.04 ± 0.01[a]	6

The effect of the HNO donor Angeli's salt (5×10^{-4} mol/l at the serosal side) was tested first under control conditions, i.e. in the absence of any inhibitor, and then in the presence of the putative inhibitor. Inhibitor concentrations were: Ba^{2+} (K^+ channel blocker; 10^{-2} mol/l at the serosal side), bumetanide (blocker of the Na^+—K^+—2Cl^--cotransporter; 10^{-3} mol/l at the serosal side). The experiments with Ba^{2+} were performed in HEPES-buffered Tyrode solution in order to avoid precipitation of barium carbonate. Values are given as difference to the baseline in I_{sc} just before administration of Angeli's salt (ΔI_{sc}) and are means ± S.E.M.

[a] $P<0.05$ versus I_{sc} in the absence of the corresponding inhibitor.

3.4. Missing effects of Angeli's salt on apical Cl^- currents

In order to find out whether activation of transepithelial Cl^- secretion by Angeli's salt is caused by a direct activation of apical Cl^- channels, experiments with basolaterally depolarized epithelia 111.5 mmol/l KCl solution at the serosal side) were performed in which a serosal-to-mucosal Cl^- concentration gradient (107 mmol/l K gluconate/4.5 mmol/l KCl at the mucosal side) was used to drive currents across apical Cl^- channels. However, under these conditions Angeli's salt (5×10^{-4} mol/l at the serosal side) was completely ineffective (Fig. 4), indicating that Angeli's salt does not stimulate apical Cl^- conductance.

3.5. Effects of Angeli's salt on currents across the basolateral membrane

As Angeli's salt had no effect on apical Cl^- channels, putative effects of the mediator at the basolateral membrane were studied, which delivers the driving force for anion secretion, i.e. the negative membrane potential. This is dominated by a K^+ diffusion potential generated by the efflux of K^+ via basolateral K^+ channels (Strabel and Diener, 1995; Warth and Barhanin, 2003), whereas the Na^+—K^+-ATPase has to maintain the K^+ concentration gradient between the intra- and the extracellular space as prerequisite for the establishment of the K^+ diffusion potential. For this purpose, the apical membrane was permeabilized with the ionophore, nystatin (100 μg/ml at the mucosal side), and adequate ionic

compositions of the buffer solutions were selected in order to study overall current, currents across basolateral K^+ channels, or currents generated by the Na^+—K^+-pump.

First it was tested, whether Angeli's salt does exert actions at electrogenic transport processes at the basolateral membrane. For this purpose, ionic conditions were selected, in which both the electrogenic Na^+—K^+-pump as well as basolateral K channels contribute to the current across this membrane. Therefore, the mucosal solution (98 mmol/l NaCl/13.5 mmol/l KCl) contained Na^+ (to stimulate the $3Na^+$—$2K^+$-pump after apical permeabilization) and established a K^+ concentration gradient towards the serosal side (K^+ concentration three times higher than in the 107 mmol/l NaCl/4.5 mmol/l KCl at the serosal side) to drive a current across basolateral K^+ channels. Under these conditions, nystatin stimulated the I_{sc} from a basal value of 1.08 ± 0.22 μEq/h cm^2 ($n=6$) to a maximum of 19.5 ± 2.97 μEq/h cm^2 ($P<0.05$ versus baseline; $n=6$, Fig. 5). As reported earlier (Schultheiss and Diener, 1997), this current then declines slowly. When Angeli's salt (5×10^{-4} mol/l at the serosal side) was administered during this decaying phase, it caused a transient stimulation of I_{sc} across the apical membrane (Fig. 5), which increased in average by 1.50 ± 0.48 μEq/h cm^2 ($n=6$) above the extrapolated spontaneous fall in I_{sc} (as indicated by the left inset in Fig. 5).

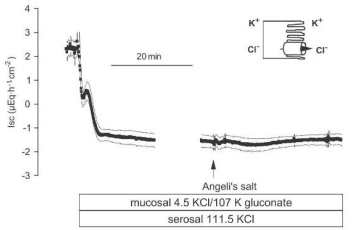

Fig. 4. Angeli's salt (5×10^{-4} mol/l at the serosal side, arrow) does not activate a Cl^- conductance in the apical membrane. When applied after depolarization of the basolateral membrane (111.5 mmol/l KCl at the serosal side, white bar) in the presence of a serosal to mucosal Cl^- gradient (107 mmol/l K gluconate/4.5 mmol/l KCl in the mucosal bathing solution, white bar; ionic gradient indicated by the schematic drawing), Angeli's salt was ineffective. Line interruptions are caused by omission of time intervals in order to synchronize the tracings of individual records to the administration of drugs. The large drop in I_{sc} induced by the solution change probably reflects the compensation of an offset potential due to applied asymmetric ion conditions. Values are means (symbols) ± S.E.M. (parallel continuous lines), $n=8$.

The nystatin-induced increase in I_{sc} was unaffected by bumetanide (10^{-3} mol/l at the serosal side). The peak current evoked by nystatin (100 μg/ml at the mucosal side) amounted to 12.9 ± 2.43 μEq/h cm^2 ($n=6$) in the presence of bumetanide (compared to 13.8 ± 1.20 μEq/h cm^2 in its absence ($n=7$)) and was further enhanced by Angeli's salt (5×10^{-4} mol/l at the serosal side; data not shown) suggesting that the current measured under these conditions represents ion flow across successfully permeabilized epithelial cells.

In order to distinguish between effects of Angeli's salt on pump currents and currents across basolateral K^+ channels, cation substitution experiments were performed. The pump current can be selectively studied, when the apical permeabilization is carried out in the absence of a K^+ gradient, i.e. with symmetrical 107 mmol/l NaCl/4.5 mmol/l KCl at both sides of the tissue. Also under these conditions, Angeli's salt (5×10^{-4} mol/l at the serosal side) induced an increase in I_{sc} of 2.05 ± 0.58 μEq/h cm^2 ($n=8$). Pretreatment with scilliroside (10^{-4} mol/l at the serosal side), a potent inhibitor of the rat Na^+—K^+-ATPase (Robinson, 1970), strongly inhibited the nystatin-induced I_{sc} under these ionic conditions and almost suppressed the response to Angeli's salt, which was reduced to only 0.099 ± 0.041 μEq/h cm^2 ($P<0.05$ versus response in the absence of scilliroside; $n=8$), confirming that this Angeli's salt-stimulated I_{sc} is carried by the basolateral Na^+—K^+-ATPase.

In a second step, the contribution of basolateral K^+ conductances to the Angeli's salt response was investigated. Tissues were

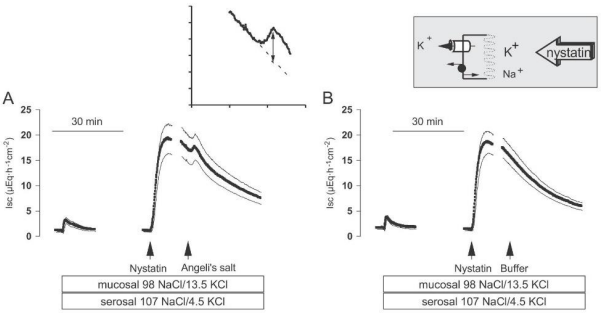

Fig. 5. (A) Change in the overall current across the basolateral membrane evoked by Angeli's salt (5×10^{-4} mol/l at the serosal side, right arrow). The apical membrane was permeabilized with nystatin (100 μg/ml at the mucosal side, left arrow) in the presence of 98 mmol/l NaCl/13.5 mmol/l KCl at the mucosal side (white bar below trace) whereas the basolateral side was exposed to a 107 mmol/l NaCl/4.5 mmol/l KCl buffer solution, so that both the basolateral K^+ channels as well as the Na^+—K^+-pump contribute to the nystatin-induced I_{sc} as indicated by the schematic inset at the right side. The inset at the left shows the difference (arrow) between the maximal increase in the I_{sc} induced by the HNO donor in regard to the extrapolated decreasing phase of the nystatin-induced I_{sc} (dashed line). (B) Time-dependent control under the same conditions in the absence of Angeli's salt. Line interruptions are caused by omission of time intervals in order to synchronize the tracings of individual records to the administration of drugs. Values are given as means (symbols) ± S.E.M. (parallel continuous lines), $n=6$. For statistics, see text.

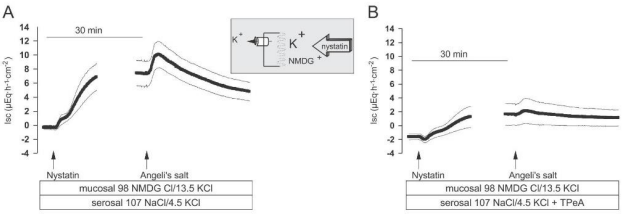

Fig. 6. (A) Angeli's salt (5×10^{-4} mol/l at the serosal side, right arrow) stimulates the current across basolateral K^+ channels. The apical membrane was permeabilized with nystatin (100 µg/ml at the mucosal side, left arrow) in the absence of Na^+ (to suppress pump currents) and in the presence of a mucosal-to-serosal K^+ gradient (98 mmol/l NMDGCl/13.5 mmol/l KCl at the mucosal and 107 mmol/l NaCl/4.5 mmol/l KCl at the serosal side as indicated by the schematic inset). (B) This current is inhibited by tetrapentylammonium (TPeA; 10^{-4} mol/l at the serosal side), a K^+ channel blocker. Line interruptions are caused by omission of time intervals in order to synchronize the tracings of individual records to the administration of drugs. Values are given as means (symbols) ± S.E.M. (parallel continuous lines), $n=8$. For statistics, see text.

permeabilized in the presence of a mucosal-to-serosal K^+ gradient, but mucosal Na^+ was replaced by the cation $NMDG^+$ (see Section 2) in order to prevent a contribution of the Na^+—K^+-pump to the measured current (see inset in Fig. 6). Also under these ionic conditions, Angeli's salt (5×10^{-4} mol/l at the serosal side) stimulated a current across the basolateral membrane. Under control conditions, this current amounted to 3.47 ± 0.54 µEq/h cm^2 ($n=8$, Fig. 6A). Pretreatment of the tissues with tetrapentylammonium, a blocker known to inhibit preferentially Ca^{2+}-dependent K^+ channels (Maguire et al., 1999), significantly inhibited the response to Angeli's salt as the Angeli's salt-induced I_{sc} only amounted to 0.81 ± 0.36 µEq/h cm^2 ($P<0.05$ versus response in the absence of tetrapentylammonium; $n=8$, Fig. 6B). Consequently, Angeli's salt stimulates several key processes in the basolateral membrane involved in transepithelial anion secretion.

3.6. *Involvement of subepithelial structures in the response to Angeli's salt*

Subepithelial components such as neurotransmitters released from enteric neurons or eicosanoids produced within the submucosa can contribute to induction of epithelial anion secretion. Submucosal secretomotor neurons, however, are obviously not involved in the mediation of the response to Angeli's salt, as pretreatment of the tissue with tetrodotoxin (10^{-6} mol/l at the serosal side), a neuronal blocker which blocks voltage-dependent neuronal Na^+ channels, did not significantly affect the current induced by Angeli's salt (Table 2). In contrast, a significant inhibition of the response to Angeli's salt (5×10^{-4} mol/l at the serosal side) was observed in the presence of the cyclooxygenase (s) inhibitor, indomethacin (10^{-6} mol/l at the serosal side, Table 2) suggesting that prostaglandins may play a role in the induction of the Angeli's salt-induced secretory response. As prostaglandins are necessary to keep the apical CFTR channel in an open state via cAMP-dependent phosphorylation and therefore blockade of prostaglandin synthesis also inhibits the response to Ca^{2+}-dependent secretagogues (Strabel and Diener, 1995), it was tested whether a low concentration of forskolin (5×10^{-7} mol/l at the mucosal and the serosal side), an activator of adenylate cyclase (s), might overcome inhibition by indomethacin. However, this was not the case as in the combined presence of indomethacin and forskolin, Angeli's salt (5×10^{-4} mol/l at the serosal side) evoked only an increase in I_{sc} of 0.69 ± 0.21 µEq/h cm^2 compared to 3.65 ± 0.43 µEq/h cm^2 in the respective control group (Table 2).

Table 2
Effects of inhibitors or activators of signaling pathways on I_{sc} induced by Angeli's salt.

	Response to Angeli's salt, ΔI_{sc} (µEq/h cm^2)	n
Without tetrodotoxin	4.71 ± 0.26	7
With tetrodotoxin	3.89 ± 0.70	7
Without indomethacin	3.14 ± 0.48	8
With indomethacin	0.63 ± 0.20[a]	8
Without indomethacin/ forskolin	3.65 ± 0.43	6
With indomethacin/forskolin	0.69 ± 0.21[a]	6
Without staurosporine	2.44 ± 0.36	8
With staurosporine	1.85 ± 0.44	8
Without H89	2.08 ± 0.47	8
With H89	2.00 ± 0.26	8
Without ODQ	2.18 ± 0.32	12
With ODQ	2.49 ± 0.36	12
Without LY 83583	1.30 ± 0.39	8
With LY 83583	1.36 ± 0.27	8
Without YC-1	2.32 ± 0.18	6
With YC-1	2.98 ± 0.36	6

The effect of Angeli's salt (5×10^{-4} mol/l at the serosal side) was tested first under control conditions, i.e. in the absence of any inhibitor or activator, and then in the presence of the putative inhibitor or activator. Drug concentrations were as follows: indomethacin (cyclooxygenase(s) inhibitor; 10^{-6} mol/l at the mucosal and serosal side) either alone or in combination with forskolin (activator of adenylate cyclase (s); 5×10^{-7} mol/l at the serosal side), H89 (protein kinase A inhibitor; 2×10^{-5} mol/l at the mucosal and the serosal side), LY 83583 (inhibitor of soluble guanylate cyclase; 10^{-5} mol/l at the mucosal and the serosal side), ODQ (inhibitor of soluble guanylate cyclase; 10^{-5} mol/l at the mucosal and the serosal side), staurosporine (broad protein kinase inhibitor; 10^{-6} mol/l at the serosal side), tetrodotoxin (blocker of neuronal Na^+ channels; 10^{-6} mol/l at the serosal side), YC-1 (activator of soluble guanylate cyclase; 10^{-5} mol/l at the serosal side). Values are given as difference to the baseline in I_{sc} just before administration of Angeli's salt (ΔI_{sc}) and are means ± S.E.M.

[a] $P<0.05$ versus I_{sc} in the absence of the respective drug.

3.7. *Intracellular mediation*

Activation of the CFTR channels for Cl^- secretion is operated by an increase in their phosphorylation state (Greger, 2000). For this reason, the interference of protein kinases with the Angeli's salt-induced Cl^- secretion was investigated. In the presence of staurosporine (10^{-6} mol/l at the serosal side), which inhibits a broad range of serine/threonine protein kinases (Tamaoki et al., 1986), the response to the HNO donor was not affected (Table 2). Also H89 (2×10^{-5} mol/l at the mucosal and the serosal side), a specific protein kinase A inhibitor, was ineffective (Table 2).

Table 3
Effects of inhibitors of Ca^{2+} signaling on I_{sc} induced by Angeli's salt.

Conditions	Response to Angeli's salt ΔI_{sc} (μEq/h cm^2)	n
Control	2.60 ± 0.69^a	8
Serosal Ca^{2+}-free	0.83 ± 0.23^b	8
Serosal Ca^{2+}-free+cyclopiazonic acid	0.64 ± 0.16^b	8

The effect of Angeli's salt (5×10^{-4} mol/l at the serosal side) was tested first under control conditions, i.e. in the absence of any inhibitor (control), and then in the presence of the putative inhibitor. For the Ca^{2+}-free solution, Ca^{2+} was removed from the serosal side. The concentration of cyclopiazonic acid (SERCA inhibitor) amounted to 10^{-5} mol/l (at the mucosal and the serosal side).Values are calculated as the difference from the baseline in short-circuit current (I_{sc}) just before administration of Angeli's salt (ΔI_{sc}) and are means $\pm$ S.E.M.. Different letters (a, b) indicate statistically homogenous groups (analysis of variances followed by post-hoc test of Tukey).

In vascular tissues, it has been shown that HNO acts via activation of the soluble guanylate cyclase and accumulation of cGMP (Favaloro and Kemp-Harper, 2007; Irvine et al., 2003; Paolocci et al., 2007). To check whether a similar process occurs in the rat colon, tissues were pre-incubated with inhibitors of the soluble guanylate cyclase prior administration of the HNO donor. Two inhibitors were used: LY 83583 (Mülsch et al., 1989; 10^{-5} mol/l at the mucosal and the serosal side) and ODQ (Hussain et al., 1997; 10^{-5} mol/l at the mucosal and the serosal side). None of them, however, inhibited the effect of Angeli's salt (5×10^{-4} mol/l at the serosal side; Table 2). Also when soluble guanylate cyclase was preactivated with YC-1 (10^{-5} mol/l at the serosal side), a known stimulator of this enzyme (Evgenov et al., 2006), the response to Angeli's salt was unaltered (Table 2), pointing out that its effect strongly differs from that of typical NO donors, as nitric oxide activates soluble guanylate cyclase (for review, see Paolocci et al. (2007) and Irvine et al. (2008)). As a control, we tested the ability of the inhibitor of the soluble guanylate cyclase, LY 83583, to interfere with the secretory response evoked by the lipophilic NO donor GEA 3162 (10^{-4} mol/l at the serosal side). LY 83583 significantly reduced the response to GEA 3162 from 2.45 ± 0.17 μEq/h cm^2 in the absence of the inhibitor to 0.95 ± 0.15 μEq/h cm^2 in the presence of the inhibitor ($P < 0.05$; $n = 6$), indicating that NO, but not HNO, mediates its action on rat colon via activation of soluble guanylate cyclase.

Calcium ions are known to be involved in the intracellular regulation of colonic anion secretion (Binder and Sandle, 1994). Therefore and as the sensitivity of the Angeli's salt-induced K^+ current across the basolateral membrane against tetrapentylammonium, a blocker of Ca^{2+}-dependent K^+ channels (Fig. 6), suggested an action site of HNO at Ca^{2+}-dependent transporters, we tested whether the I_{sc} response evoked by the HNO donor was dependent on Ca^{2+}. Omission of Ca^{2+} from the serosal compartment led to a significant reduction of the I_{sc} induced by Angeli's salt (5×10^{-4} mol/l at the serosal side) by about 68% ($P < 0.05$, Table 3), indicating that extracellular Ca^{2+} plays a crucial role in the mechanism of Angeli's salt-induced anion secretion. Under the same conditions, depletion of intracellular Ca^{2+} stores with cyclopiazonic acid (10^{-5} mol/l at the mucosal and the serosal side), a blocker of sarcoplasmic-endoplasmic reticulum ATPase (see e.g. Prinz and Diener (2008)), reduced the Angeli's salt-induced I_{sc} by further 20% (Table 3), hinting at the additional involvement of intracellular Ca^{2+} stores.

3.8. Fura-2 experiments

In order to study this Ca^{2+}-dependence in more detail, isolated colonic crypts were loaded with the Ca^{2+}-sensitive dye, fura-2. Surprisingly, Angeli's salt in concentrations, which induced a strong increase in I_{sc} in the Ussing chamber, i.e. 10^{-5} mol/l and 10^{-4} mol/l, did not change the fura-2 ratio signal in this isolated epithelial preparation devoid of submucosal structures ($n = 48$, data not shown). Only at the highest concentration used, i.e. 5×10^{-4} mol/l, a marginal increase in the fura-2 signal was observed, which was more pronounced in the cells at the depth of the crypts than in the middle (and not observed at the surface cells; data not shown), where Angeli's salt caused a slow increase of the fura-2 ratio signal by 0.093 ± 0.012 against 0.086 ± 0.013 in the middle ($n = 38$—54, Fig. 7A and B). However, these increases were quite low. All the cells tested responded with significant increases in the fura-2 signal to cyclopiazonic acid confirming the viability of the cells used (Fig. 7A and B).

As these changes were surprisingly low, we asked the question whether the strong Ca^{2+}-dependence of Angeli's salt-induced anion secretion (Table 3) might take place at subepithelial cells within the submucosa. Therefore, isolated sheets of submucosa were loaded with fura-2 and used for imaging experiments. In these sheets, three cellular structures can clearly be recognized: vascular cells, identified by their linear arrangement, submucosal ganglia, recognized as oval cell agglomerates, and single cells, to which fibroblasts, mast cells and others might contribute (Fig. 7C). Nearly all submucosal cells responded to Angeli's salt (10^{-4} mol/l) with a strong increase in the fura-2 ratio signal (Fig. 7D). This was also observed in submucosal ganglia (data not shown), which were, however, not further considered as the epithelial anion secretion evoked by the HNO donor had been proven resistant against the neurotoxin, tetrodotoxin (Table 2). In average, in non-neuronal subepithelial cells, the fura-2 ratio increased by 0.808 ± 0.130 ($n = 23$, Table 4). In the absence of Ca^{2+}, the fura-2 ratio signal was significantly reduced by about 67% (Table 4).

4. Discussion

At our knowledge, the present study is the first investigation on the action of nitroxyl (HNO) on electrolyte transport in the colonic epithelium. The results demonstrate that Angeli's salt induces a concentration-dependent increase in the I_{sc} across rat distal colon (Fig. 1) without any signs of desensitization upon repetitive administration (Fig. 2). The response started immediately after administration of the donor, likely related to the fast diffusion of HNO across cell membranes (Fukuto et al., 2008).

Angeli's salt is a classical HNO donor, but HNO may be oxidized to NO intracellularly e.g. in mitochondria by cytochrome C (for review, see Reisz et al. (2010)) or extracellularly by copper ions (Nelli et al., 2000). Thus the question arises as if the observed results are related to HNO or its NO congener. Specific scavengers utilized, carboxy-PTIO for the radical $\cdot$NO and L-cysteine for HNO, revealed that the mediator of the effects of Angeli's salts was indeed HNO.

Ion substitution approaches revealed that Angeli's salt induced a Cl^- secretion (Fig. 3 and Table 1). Since HNO is a NO congener, this fits to previous studies showing that NO stimulates Cl^- secretion (Tamai and Gaginella, 1993). In contrast to NO-evoked Cl^- secretion, which is inhibited by tetrodotoxin (Tamai and Gaginella, 1993), Angeli's salt-induced anion secretion was resistant against this neurotoxin (Table 2). This does, however, not totally exclude a participation of enteric neurons as tetrodotoxin only blocks the generation and propagation of neuronal action potentials, but will not affect a release of neurotransmitters from nerve endings induced e.g. by direct depolarization of the presynaptic membrane.

The activity of different ion transporters involved in transepithelial Cl^- secretion is changed in the presence of Angeli's salt.

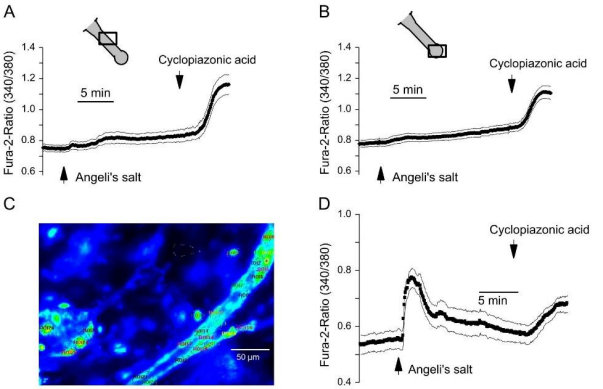

Fig. 7. Changes in the fura-2 ratio evoked by Angeli's salt (5×10^{-4} mol/l, left arrow) in the middle region (A) or the fundus region (B) of isolated colonic crypts as indicated by the schematic insets. (C) Photograph of an isolated, fura-2 loaded submucosal sheet. Beside a submucosal ganglion (left lower corner) and a blood vessel (right side) numerous isolated single cells loaded with fura-2 can be recognized. (D) Change in the fura-2 ratio of submucosal cells induced by Angeli's salt (10^{-4} mol/l, left arrow). Cyclopiazonic acid (10^{-5} mol/l, right arrows) was used for cell viability control. Values are given as means (symbols) ± S.E.M. (parallel continuous lines), $n = 13$—27. For statistics, see text.

Table 4
Effects of the HNO donor on the fura-2 ratio signal in submucosal cells.

Inhibitor	Response to Angeli's salt (Δfura-2 ratio)	*n*
With Ca^{2+}	0.808 ± 0.130	23
Ca^{2+}-free	0.264 ± 0.023[a]	21

Effect of Angeli's salt (10^{-4} mol/l) on the fura-2 ratio of submucosal cells under control conditions and in the nominal absence of Ca^{2+}. For the nominal Ca^{2+}-free solution, Ca^{2+} was omitted in the buffer. Values are given as change in the fura-2 ratio (Δfura-2 ratio) compared with the baseline just prior to administration of Angeli's salt and are means ± S.E.M.

[a] $P < 0.05$ versus increase in the fura-2 ratio in the presence of Ca^{2+}.

The basolateral membrane exerts a key role in anion secretion across the intestinal epithelium as it generates the driving force for anion efflux by generation of a negative membrane potential. Several transporters are involved in this process such as the Na^+—K^+-pump establishing the K^+ concentration gradient and basolateral K^+ channels.

The HNO donor induced a monophasic stimulation of the current across the basolateral membrane carried by the Na^+—K^+-ATPase in apically permeabilized epithelia in the absence of a K^+ concentration gradient, i.e. under conditions, where currents across basolateral K^+ channels are suppressed. To make sure that this current was caused by the enzyme, scilliroside (Robinson, 1970) was used as pump inhibitor, as the α_1-isoform of the Na^+—K^+-ATPase in rats is quite resistant to the classical Na^+—K^+-pump inhibitor, ouabain (see Edwards and Pallone (2007)). Pretreatment with this inhibitor of the rat Na^+—K^+-ATPase suppressed the action of Angeli's salt. Consequently, there seems to be a monophasic modulation by Angeli's salt of the pump activity, which finally maintains the K^+ concentration gradient at the cell membrane and thereby sets the fundamental driving force for active ion transport. A similar activation has been observed previously at the same tissue with the NO donor, GEA 3162 (Schultheiss et al., 2002b). The mechanism underlying this action has yet to be identified. One may speculate — based on the high thiophilicity of HNO — that it might directly interact with the pump at thiol groups within the enzyme. Another possible explanation could be a direct reduction of disulfide bonds within the enzyme by HNO, which also serves as a reductant (Lopez et al., 2007).

Furthermore, Angeli's salt increased the K^+ conductance in the basolateral membrane. The HNO donor increased the dominant tetrapentylammonium-sensitive Ca^{2+}-dependent K^+ conductance in this membrane under Na^+-free conditions, i.e. conditions, where the stimulatory effect of Angeli's salt on the Na^+—K^+-pump current is absent (Fig. 6). Knowing the dependency of the HNO-induced I_{sc} on Ca^{2+} (Table 3) and the capability of Angeli's salt to induce (an albeit weak) increase in cytosolic Ca^{2+} concentration in isolated crypts (Fig. 7A and B) and subepithelial cells (Table 4 and Fig. 7D), Angeli's salt should activate the basolateral K^+ channels. The primary action site of Angeli's salt is the hyperpolarization of the basolateral membrane via these mechanisms as after depolarization of this membrane its action was abolished (Fig. 4).

Nitroxyl has been reported to be able to activate the soluble guanylate cyclase similar as does NO (Irvine et al., 2003; Favaloro and Kemp-Harper, 2007; Paolocci et al., 2007). However, in rat distal colon the I_{sc} induced by Angeli's salt was independent from the activity of the soluble guanylate cyclase as neither prior inhibition of this enzyme with ODQ nor prior activation with YC-1 had any effect on the response evoked by a subsequent administration of Angeli's salt (Table 2). However, also from other tissues guanylate cyclase-independent actions are known, for example the activation of voltage-dependent K^+ channels in rat mesenteric arteries (Irvine et al., 2003; Favaloro and Kemp-Harper, 2009).

The secretory property of the HNO donor was not influenced by tetrodotoxin, but was sensitive to the cyclooxygenase(s) inhibitor

indomethacin (Table 2). Inhibition was not overcome by forskolin (Table 2), indicating that this inhibition does not represent an indirect dependence of the secretory response by the effect of prostaglandins on the apical Cl^- conductance as it is observed e.g. for carbachol (Strabel and Diener, 1995).

Calcium ions play a crucial role in the response to Angeli's salt as removal of extracellular Ca^{2+} or inhibition of intracellular Ca^{2+} release inhibited the Cl^- secretion induced by Angeli's salt (Table 3). The strongest inhibition was observed, when the normal Ca^{2+}-containing serosal buffer was exchanged against a nominal Ca^{2+} free buffer solution indicating that Angeli's salt acts mainly via an influx of extracellular Ca^{2+} across the plasma membrane.

Surprisingly, Angeli's salt induced only a marginal increase in the cytosolic Ca^{2+} concentration of the epithelial cells as shown by fura-2 experiments at isolated colonic crypts (Fig. 7A and B). However, when the cells within the submucosa were tested for their sensitivity against the HNO donor, they turned out to be much more sensitive compared to the epithelium (Fig. 7D). This response exhibited the same dependence on the presence of extracellular Ca^{2+} as was the case for Angeli's salt-induced Cl^- secretion (Table 3). Together with the observed indomethacin-sensitivity of the I_{sc} stimulated Angeli's salt (see above) and the fact that subepithelial cells are the main source for prostaglandin formation in rat colon (Craven and DeRubertis, 1983), these results suggest that one action site of Angeli's salt are subepithelial cells which modulate epithelial ion transport via the release of paracrine acting mediators.

Taken together, HNO induces Cl^- secretion via activation of the Na^+—K^+-ATPase and basolateral K^+ channels. The mechanism does not depend on soluble guanylate cyclase, but seems to be mediated by cyclooxygenase products. Thus actions of the HNO donor Angeli's salt on intestinal ion transport differ fundamentally from those of its redox variant, the radical gasotransmitter NO.

Acknowledgment

The diligent care of Mrs. B. Brück, E. Haas, B. Schmitt, and A. Stockinger is a pleasure to acknowledge. Supported by Deutsche Forschungsgemeinschaft, Grant Di 388/11-1.

References

Akaike, T., Yoshida, M., Miyamoto, Y., Sato, K., Kohno, M., Sasamoto, K., Miyazaki, K., Ueda, S., Maeda, H., 1993. Antagonistic action of imidazolineoxyl N-oxides against endothelium-derived relaxing factor/NO through a radical reaction. Biochemistry 32, 827–832.

Binder, H.J., Sandle, G.J., 1994. Electrolyte transport in the mammalian colon. In: Johnson, L.R. (Ed.), Physiology of the Gastrointestinal Tract, third ed. Raven Press, New York, NY, pp. 2133–2171.

Cheong, E., Tumbev, V., Abramson, J., Salama, G., Stoyanovsky, D.A., 2005. Nitroxyl triggers Ca^{2+} release from skeletal and cardiac sarcoplasmic reticulum by oxidizing ryanodine receptors. Cell Calcium 37, 87–96.

Craven, P.A., DeRubertis, F.R., 1983. Pattern of prostaglandin synthesis and degradation in isolated superficial and proliferative colonic epithelial cells compared to residual colon. Prostaglandins 26, 583–604.

Donzelli, S., Espey, M.G., Flores-Santana, W., Switzer, C.H., Yeh, G.C., Huang, J., Stuehr, D.J., King, S.B., Miranda, K.M., Wink, D.A., 2008. Generation of nitroxyl by heme protein-mediated peroxidation of hydroxylamine but not N-hydroxy-L-arginine. Free Radical Biol. Med. 45, 578–584.

Edwards, A., Pallone, T.L., 2007. Ouabain modulation of cellular calcium stores and signaling. Am. J. Physiol. Renal Physiol. 293, F1518–F1532.

Ellis, A., Li, C.G., Rand, M.J., 2000. Differential actions of L-cysteine on responses to nitric oxide, nitroxyl anions and EDRF in the rat aorta. Br. J. Pharmacol. 129, 315–322.

Evgenov, O.V., Pacher, P., Schmidt, P.M., Haskó, G., Schmidt, H.H.H.W., Stasch, J.P., 2006. NO-independent stimulators and activator of soluble guanylate cyclase: discovery and therapeutic potential. Nat. Rev. Drug Discov. 5, 755–768.

Favaloro, J.L., Kemp-Harper, B.K., 2007. The nitroxyl anion (HNO) is a potent dilator of rat coronary vasculature. Cardiovasc. Res. 73, 587–596.

Favaloro, J.L., Kemp-Harper, B.K., 2009. Redox variants of NO (NO• and HNO) elicit vasorelaxation of resistance arteries via distinct mechanisms. Am. J. Physiol. Heart Circ. Physiol. 296, H1274–280.

Fukuto, J.M., Bianco, C.L., Tyler, A.C., 2009. Nitroxyl (HNO) signaling. Free Radical Biol. Med. 47, 1318–1324.

Fukuto, J.M., Chiang, K., Hszieh, R., Wong, P.S.Y., Chaudhurri, G., 1992. The pharmacological activity of nitroxyl: a potent vasodilator with activity similar to nitric oxide and/or endothelium-derived relaxing factor. J. Pharmacol. Exp. Ther. 263, 546–551.

Fukuto, J.M., Jackson, M.I., Kaludercic, N., Paolocci, N., 2008. Examining nitroxyl (HNO) in biological systems. Methods Enzymol. 440, 411–431.

Greger, R., 2000. Role of CFTR in the colon. Annu. Rev. Physiol. 62, 467–491.

Hennig, B., Diener, M., 2009. Actions of hydrogen sulfide on ion transport across rat distal colon. Br. J. Pharmacol. 158, 1263–1275.

Hussain, A.S., Marks, G.S., Brien, J.F., Nakatso, K., 1997. The soluble guanylyl cyclase inhibitor 1H-[1,2,4]oxadiazolo[4,3-a]quinoxalin-1-one (ODQ) inhibits relaxation of rabbit aortic rings induced by carbon monoxide, nitric oxide, and glyceryltrinitrat. Can. J. Physiol. Pharmacol. 75, 1034–1037.

Irvine, J.C., Favaloro, J.L., Kemp-Harper, B.K., 2003. NO- activates soluble guanylate cyclase and K+ channels to vasodilate resistance arteries. Hypertension 41, 1301–1307.

Irvine, J.C., Ritchie, R.H., Favaloro, J.L., Andrews, K.L., Widdop, R.E., Kemp-Harper, B.K., 2008. Nitroxyl (HNO): the Cinderella of the nitric oxide story. Trends Pharmacol. Sci. 29, 601–608.

Kenyon, J.L., Gibbons, W.R., 1977. Effects of low-chloride solutions on action potentials of sheep cardiac purkinje fibers. J. Gen. Physiol. 70, 635–660.

Lancel, S., Zhang, J., Evangelista, A., Trucillo, M.P., Tong, X.Y., Siwik, D.A., Cohen, R.A., Colucci, S., 2009. Nitroxyl activates SERCA in cardiac myocytes via glutathiolation of cysteine 674. Circ. Res. 104, 720–723.

Lopez, B.E., Shinyashiki, M., Han, T.H., Fukuto, J.M., 2007. Antioxidant actions of nitroxyl (HNO). Free Radical Biol. Med. 42, 482–491.

Maguire, D., MacNamara, B., Cuffe, J.E., Winter, D., Doolan, C.M., Urbach, V., O'Sullivan, G.C., Harvey, B.J., 1999. Rapid responses to aldosterone in human distal colon. Steroids 64, 51–63.

Moncada, S., Higgs, E.A., 2006. The discovery of nitric oxide and its role in vascular biology. Br. J. Pharmacol. 147 (Suppl. 1), S193–S201.

Mülsch, A., Bechtold, A., Pohl, U., Busse, R., Bassenge, E., 1989. LY 83583 (6-anilino-5,8-quinolinedione) blocks nitrovasodilator-induced cyclic GMP increases and inhibition of platelet activation. Naunyn-Schmiedeberg's Arch. Pharmacol. 340, 119–125.

Nelli, S., Hillen, M., Buyukafsar, K., Martin, W., 2000. Oxidation of nitroxyl anion to nitric oxide by copper ions. Br. J. Pharmacol. 131, 356–362.

Paolocci, N., Jackson, M.I., Lopez, B.E., Miranda, K., Tocchetti, C.G., Wink, D.A., Hobbs, A.J., Fukuto, J.M., 2007. The pharmacology of nitroxyl (HNO) and its therapeutic potential: not just the Janus face of NO. Pharmacol. Ther. 113, 442–458.

Pouokam, E., Diener, M., 2011. Mechanisms of actions of hydrogen sulfide at rat distal colonic epithelium. Br. J. Pharmacol. 162, 392–404.

Prinz, G., Diener, M., 2008. Characterization of ryanodine receptors in the rat colonic epithelium. Acta Physiol. 193, 151–162.

Reisz, J.A., Bechtold, E., King, B., 2010. Oxidative heme protein-mediated nitroxyl (HNO) generation. Dalton Trans. 39, 5203–5212.

Robinson, J.W.L., 1970. The difference in sensitivity to cardiac steroids of (Na^+—K^+)-stimulated ATPase and amino acid transport in the intestinal mucosa of the rat and other species. J. Physiol. 206, 41–60.

Rusche, K.M., Spiering, M.M., Marletta, M.A., 1998. Reactions catalyzed by tetrahydrobiopterin-free nitric oxide synthase. Biochemistry 37, 15503–15512.

Saleem, M., Ohshima, H., 2004. Xanthine oxidase converts nitric oxide to nitroxyl that inactivates the enzyme. Biochem. Biophys. Res. Commun. 315, 455–462.

Schicho, R., Krueger, D., Zeller, F., von Weyhern, C.W.H., Frieling, T., Kimura, H., Ishii, I., De Giorgio, R., Campi, B., Schemann, M., 2006. Hydrogen sulfide is a novel prosecretory neuromodulator in the guinea-pig and human colon. Gastroenterology 131, 1542–1552.

Schultheiss, G., Diener, M., 1997. Regulation of apical and basolateral K^+ conductances in the rat colon. Br. J. Pharmacol. 122, 87–94.

Schultheiss, G., Kocks, S.L., Diener, M., 2002a. Methods for the study of ionic currents and Ca^{2+}-signals in isolated colonic crypts. Biol. Proced. Online 3, 70–78 ⟨http://www.biologicalprocedures.com/⟩.

Schultheiss, G., Seip, G., Kocks, S.L., Diener, M., 2002b. Ca^{2+}-dependent and Ca^{2+}-independent Cl^- secretion stimulated by the nitric oxide donor, GEA 3162, in rat colonic epithelium. Eur. J. Pharmacol. 444, 21–30.

Steidle, J., Diener, M., 2011. Effects of carbon monoxide on ion transport across rat distal colon. Am. J. Physiol. Gastrointest. Liver Physiol. 300, G207–G216.

Strabel, D., Diener, M., 1995. Evidence against direct activation of chloride secretion by carbachol in the rat distal colon. Eur. J. Pharmacol. 274, 181–191.

Tamai, H., Gaginella, T., 1993. Direct evidence for nitric oxide stimulation of electrolyte secretion in the rat colon. Free Radical Res. Commun. 19, 229–239.

Tamaoki, T., Nomoto, H., Takahashi, I., Kato, Y., Morimoto, M., Tomita, P., 1986. Staurosporine, a potent inhibitor of phospholipid/Ca^{++} dependent protein kinase. Biochem. Biophys. Res. Commun. 135, 397–402.

Toda, N., Herman, A.G., 2005. Gastrointestinal function regulation by nitrergic efferent nerves. Pharmacol. Rev. 57, 315–338.

Warth, R., Barhanin, J., 2003. Function of K^+ channels in the intestinal epithelium. J. Membr. Biol. 193, 67–78.

8.8 "Wirkungen des HNO-Donors Angeli´s salt auf die gastrointestinale Motilität" [Unveröffentlichte Befunde]

Mechanisms associated to nitroxyl (HNO)-induced relaxation in the intestinal smooth muscle.

Mirko Gastreich-Seelig[1], Marcel Jimenez[2], Ervice Pouokam[1]*

[1]Institute for Veterinary Physiology and Biochemistry, Justus-Liebig-University Giessen, Germany

[2]Department of Cell Biology, Physiology and Immunology and Neurosciences Institute, Universitat Autònoma de Barcelona, Barcelona, Spain.

Running title: HNO and intestinal motility

*Send correspondence to: Ervice Pouokam, Institut für Veterinär-Physiologie und -Biochemie, Justus-Liebig-Universität Gießen, Frankfurter Str. 100, Fax: Int-49-641-9938159, Tel: Int-49-641-9938160, 35392 Gießen, Germany. Email: Ervice.Pouokam-Kamgne@vetmed.uni-giessen.de

Abstract

Aim: The role of nitroxyl (HNO) as signaling molecule in the gastrointestinal tract is not known. We investigated the properties of this gasotransmitter in the regulation of gastrointestinal contractility focussing on its possible interaction with other gasotransmitters such as NO and H_2S.

Methods: Organ bath, Ca^{2+} imaging and microelectrode recordings were performed on rat intestinal samples, using Angeli's salt as HNO donor.

Results: Angeli's salt caused a concentration-dependent relaxation of longitudinal or circular muscle strips of the ileum and the proximal colon. This relaxation was strongly inhibited by the Rho-kinase inhibitor Y-27632 (10 μM), by the reducing agent DTT or by the inhibitor of soluble guanylate cyclase (sGC) ODQ (10 μM) alone or in combination with the inhibitors of the endogenous synthesis of H_2S β-cyano-L-alanine (5 mM) and amino-oxyacetate (5 mM). Preventing endogenous synthesis of NO by the NO synthase inhibitor L-NAME (200 μM) did not affect the relaxation induced by HNO. HNO induced an increase of cytosolic Ca^{2+} concentration in colonic myocytes. It also elicited myocyte membrane hyperpolarization that amounted to -10.6 ± 1.1 mV. ODQ (10 μM) and Apamin (1 μM), a selective inhibitor of small conductance Ca^{2+}-activated K^+ channels (SK), strongly antagonized this effect.

Conclusion:

HNO relaxes the gastrointestinal tract musculature by hyperpolarizing myocytes via activation of the sGC/cGMP/PKG pathway similarly to NO, inhibiting the RhoK and activating MLCP as do both NO and H_2S, but also increasing cytosolic Ca^{2+} for activation of SK_{Ca} contributing to hyperpolarization.

Abbreviations

AOAA, amino-oxyacetate; CLA, β-cyano-L-alanine; DTT, 1,4-dithiothreitol; GI, gastrointestinal; L-NAME, N_{ω}-nitro-L-arginine methylester hydrochloride; MLCP, myosin light chain phosphatase; ODQ, 1H-[1,2,4]oxadiazolo [4,3-a]quinoxalin-1-one; RhoK, Rhokinase; RMP, resting membrane potential, sGC, soluble guanylate cyclase;

Key words: Ca^{2+}, gasotransmitters, membrane potential, motility, Nitroxyl (HNO), small conductance Ca^{2+}-activated K^{+} channels (SK), soluble guanylate cyclase.

1. Introduction

Gastrointestinal motility is regulated by enteric neurotransmitters inducing contraction and relaxation of the smooth muscle cells. Excitatory neurotransmitters such as acetylcholine (ACh) elicit smooth muscle cell depolarization and contraction, whereas inhibitory neurotransmitters cause smooth muscle hyperpolarization and relaxation. Inhibitory junction potentials are mainly due to ATP (or a related purine) and NO causing a transient fast inhibitory junction potential (IJPf) followed by a sustained IJP (IJPs), respectively. Hydrogen sulphide (H_2S) and nitric oxide (NO) are two endogenous signalling gasotransmitters in the enteric nervous system with inhibitory effects on gastrointestinal smooth muscle.[1,2,3,4]

These two gasotransmitters exert their actions on smooth muscles via different mechanisms. In canine colonic smooth muscle cells, exogenous NO caused accumulation of cytosolic cGMP.[5] Endogenous NO either depresses the release of ACh from interneurons in descending enteric pathways or facilitates ACh release in the ascending pathways; both mechanisms involve soluble guanylate cyclase (sGC).[6] The relative contribution of these pathways in the action of NO may differ depending on either the species or the segment of the gastrointestinal tract concerned. In contrast, H_2S does activate the opening of ATP-sensitive K^+ (K_{ATP}) channels and the closure of voltage-dependent K^+ channels (K_v) in guinea-pig gastric antrum myocytes.[7] In human, rat and mouse colon and jejunum, relaxant effects of H_2S are dependent on apamin-sensitive small conductance Ca^{2+} activated K (SK) and on K_{ATP} channels.[8] In addition, activation of the myosin light chain phosphatase (MLCP) may account for the relaxing properties of H_2S as shown in murine gastric fundus.[9]

A third gasotransmitter, nitroxyl (HNO), is getting more attention.[10,11,12,13]. Its positive inotropic and lusitropic effects are important therapeutic actions in the heart. So far, HNO properties have been investigated mainly in the cardiovascular system.[10,12] In the gastrointestinal tract, upon repetitive application in Ussing chambers, the HNO-donor Angeli's salt induced a Ca^{2+}-dependent Cl^- secretion without desensitization.[11] The mechanism of action clearly differed from that of the secretion induced by its sibling NO, because it did not depend on the activity of the sGC, which is the prototypical site of action of NO. In contrast, HNO-evoked secretion was blocked by indomethacin suggesting that cyclooxygenase metabolites such as prostaglandins mediate the response, to which an activation of the basolateral Na^+-K^+-ATPase, Ca^{2+}-dependent K^+ and ATP-sensitive K^+ channels contributed.[11]

Recent studies showed a cross-talk of H_2S and NO signalling pathways.[12,14,15,16] Both gasotransmitters (NO delivered by sodium nitroprusside (SNP) and H_2S delivered by sodium sulphide (Na_2S)) underwent a fast chemical reaction (at pH 7.4 and under aerobic conditions), forming the intermediate $[(CN)_5FeN(O)SH]^{3-}$, which is converted to thiocyanate products; the latter being catalyzed by rhodaneses allowing therefore for elimination of toxic cyanide.[15,16] During this interplay between both gases, H_2S can also interact with the S-nitrosothiol HSNO to generate HNO and disulphides ($RSSR^{'}$).[15,16] Thus, the combination NO/H_2S and therefore HNO appears therapeutically very interesting as it is less toxic than the combination SNP/thiosulfate used for example in acute hypertensive crises to regulate blood pressure.[15] It has been recently confirmed that NO and H_2S cooperatively generate HNO in cells, as for example, a strong increase in the HNO-sensor CuBOT1 was observed in dorsal root ganglia (DRG) neurons only when both gases were simultaneously applied.[12] As endogenous NO may be transformed to HNO by H_2S,[12] some effects of H_2S may be ascribed to HNO.

Since HNO presents interesting clinical properties, we aimed to investigate the properties of this agent in the regulation of intestinal contractility, revealing its specific characters in regard to the well-known gasotransmitters NO and H_2S. To our knowledge, this is the first report studying neuromuscular actions of HNO in the GI tract.

2. Results

2.1. Nitroxyl relaxes gastrointestinal muscle

The HNO donor Angeli's salt induced a reduction in the basal tone, a decrease in spontaneous contractions leading to a reduction in the AUC of all three intestinal muscle preparations tested. In ileal longitudinal muscle, concentrations above 25 μM induced a transient fall in muscle tone, which lasted for 3 - 5 min (Fig. 1B). Concentrations lower than 25 μM were ineffective (data not shown). Muscle tone remained stable in time-dependent controls treated with the solvent only (Fig. 1A). Also, contractions induced by KCl (30 mM) or carbachol (10 μM) were unaffected after washout of the HNO donor (Fig. 1A, B). Concentration-response curves based either on the amplitude of the maximal relaxation induced by the HNO donor (Fig. 3A) or on the integrated change in muscle tone over a 3 min period (Fig. 3B) revealed a flat concentration-dependence of the effect of Angeli's salt.

Also, longitudinal muscle from the proximal colon responded with a concentration-dependent relaxation (Fig. 1D, E; 3C, D), which was not observed in parallely performed time-dependent control experiments (Fig. 1C). In contrast to the ileum, the longitudinal muscle strips from the colon responded to the HNO donor at much lower concentrations. However, with higher concentrations of Angeli's salt, the duration of the induce relaxation was prolonged. Contraction induced by carbachol (10 μM) was unaffected (Fig. 1D, E).

A relaxing effect induced by Angeli's salt was also observed in circular muscle preparations from proximal colon (Fig. 2B) in comparison to a control series (Fig. 2A). The effect of the HNO donor was concentration-dependent and showed a maximum at a concentration of 50 µM with respect to the amplitude of relaxation (Fig. 3E) and the decrease in the area under the curve over a 3 min period (Fig. 3F). Angeli's salt not only reduced basal muscle tone but also suppressed the phasic contractions as shown when considering records from individual muscle preparations with an extended time scale (Fig. 2C, D).

The frequency of phasic spontaneous contractions of longitudinal muscle strips from the colon was significantly ($p < 0.05$, Mann-Whitney U-test) reduced by Angeli's salt. At 50 µM, the HNO donor reduced the frequency from 3.0 ± 0.6 (n = 7) cpm to 0.6 ± 0.0 cpm (n = 7). Similarly, they were reduced from 1.8 ± 0.6 cpm (n = 8) to 0.0 ± 0.0 cpm (n = 8) with 100 µM of the donor.

All further experiments were performed with longitudinal muscle strips from the proximal colon and two concentrations of the HNO donor, 50 µM and 100 µM were selected for further isometric measurements.

2.2. HNO interferes with the cholinergic pathway for relaxation

In order to investigate a possible interaction of HNO with MLCP, longitudinal muscle strips of the proximal colon were pre-contracted with 10 µM carbachol and the amplitude of relaxation caused by HNO was compared in the presence or absence of one of the following smooth muscle contractile apparatus desensitizers calyculin A (inhibitor of the MLCP) or Y-27632 (inhibitor of Rho-kinase). A preliminary test for the validity of Y-27632 (10 µM) as inhibitor of the cholinergic pathway was conducted. Indeed, this inhibitor significantly reduced the contraction induced by CCh (Fig. 4A). In the presence

of Y-27632, the relaxation induced by 50 µM Angeli's salt was slightly reduced from -0.59 ± 0.14 g (n = 7) to -0.28 ± 0.05 g (n = 11), whereas the relaxation induced by 100 µM of HNO donor was reversed into a contraction of +0.24 ± 0.03 g (n = 11; measured 1 min after administration of the donor) in comparison to the untreated control, where HNO evoked a relaxation of 0.35 ± 0.03 g (n = 7 (Fig. 4B).

A potentiation of the cholinergic-evoked contraction is expected by inhibiting MLCP, for example with calyculin A. Indeed, the contractile response induced by CCh was slightly increased from 0.71 ± 0.28 g (n = 10) to 0.97 ± 0.15 g (n = 11) in the presence of 100 nM calyculin A (Fig. 4C). MLCP blockade slightly potentiated the relaxing effect of 50 µM Angeli's salt and attenuated numerically the relaxing response to 100 µM Angeli's salt; none of these effects, however, reached statistical significance (Fig. 4D).

2.3. Interplay between NO, H_2S and HNO

The relaxing properties of NO depend on activation of sGC. The potential interplay between NO, H_2S and HNO may also involve this enzyme. To test this hypothesis, the relaxing action of these three gasotransmitters was measured in the presence of the sGC inhibitor ODQ (10 µM). As expected, the inhibitor significantly blocked (Fig. 5A) the relaxation induced by the NO donor sodium nitroprusside (SNP, 1 mM) from -1.02 ± 0.23 g (n = 6) to -0.32 ±0.05 g (n = 9). Among the other donors, only 50 µM Angeli's salt was significantly sensitive to the blocker as the relaxation was reduced from -0.37 ± 0.11 g (n = 7) to -0.03 ± 0.06 g (Fig. 5C, n = 8). The relaxation induced by the H_2S donor sodium hydrogen sulphide (NaHS 100 µM) was not affected by ODQ; it amounted to -0.88 ± 0.24 g (n = 5) in the absence and -0.61 ± 0.11 g (Fig. 5B) in the presence of the sGC blocker (Fig. 5B). Increasing the concentration of AS to 100 µM partially overcome the ODQ-

induced inhibition, suggesting the presence of GC dependent and GC independent inhibitory pathways (Fig. 5D).

To assess the potential importance of endogenously produced NO in HNO induced relaxation, the relaxing activity of Angeli's salt was measured after a 30 min preincubation period of the tissue with the NOS inhibitor L-NAME (200 µM). L-NAME did not affect HNO-induced relaxation (Fig. 5E and F) as the maximal relaxation was statistically unchanged from -1.29 ± 0.18 g (control, n = 8) to -1.32 ± 0.27 g (test, n = 7) for 50 µM Angeli's salt and from -0.68 ± 0.05 g (control, n = 8) to -0.75 ± 0.12 g (test, n = 7) for 100 µM Angeli's salt. Calculating AUC led to the same conclusion. Similar values of AUC were calculated for control and test (in the presence of L-NAME): -163.3 ± 20.2 g·180s (control, n = 8) versus -148.1 ± 19.4 g·180s (test, n =7) for 50 µM Angeli's salt and -91.6 ± 6.2 g·180s (control, n = 8) versus -77.8 ± 17.3 g·180s (test, n =7) for 100 µM Angeli's salt.

The impact of endogenously produced H_2S on HNO action was investigated using inhibitors of the H_2S-producing enzymes. Thus, amino-oxyacetate (AAOA, 5 mM, cystathionine-β-synthase inhibitor) and β-cyano-L-alanine (CLA, 5 mM, cystathionine-γ-lyase blocker) were used in the presence or absence of the sGC blocker ODQ (10 µM). Inhibition of endogenous synthesis of H_2S alone led to the reduction of the basal tonus by -0.56 ± 0.08 g (AUC: -81.54 ± 13.22 g.180s, n = 6) versus -0.10 ± 0.01 g for control (AUC: -3.85 ± 0.84 g.180s, n = 6). This reduction lasted approximately 5 min. Preventing H_2S synthesis, however, only slightly reduced the relaxation induced by 50 µM Angeli's salt as shown in Table 1. A simultaneous blockade of endogenous synthesis of H_2S and sGC almost abolished the Angeli's salt-evoked relaxation (Table 1).

Nitroxyl is highly thiophilic and may interact with thiol groups. In the presence of DTT (500 µM), known to maintain SH groups in reduced state or reduce protein disulphide bonds, the relaxing property of HNO donor was significantly impaired (Table 2). Simultaneous administration of the H_2S donor (NaHS, 100 µM) and NO donor (SNP, 1 mM) evoked a relaxation that was partially but not significantly sensitive to DTT (Table 2).

2.4. Mechanism of action and particularity of HNO

2.4.1 Calcium ions mobilization for relaxation

H_2S induces the opening of K_{ATP} channels and the closure of voltage-dependent K^+ channels in guinea-pig gastric antrum myocytes[17] or activates small conductance calcium-activated potassium channels (SK_{Ca}) in mouse colon.[7] HNO has been shown to stimulate sarco-endoplasmic reticulum Ca^{2+}-ATPase (SERCA) in cardiomyocytes.[10] To assess the role of Ca^{2+} in the HNO induced relaxation, calcium imaging was performed on isolated myocytes of the proximal colon.

In myocytes from the longitudinal layer, Angeli's salt (50 µM) caused a significant increase in the fura-2 ratio signal from 0.21 ± 0.08 (n = 22) to 0.44 ± 0.09 (n = 48) ($P < 0.001$, paired t-test). In myocytes isolated from the circular layer the response was weaker, as the HNO donor increased the fura-2 ratio from 0.008 ± 0.001 (control; n = 13) to 0.057 ± 0.011 (test; n = 15) ($P < 0.001$; unpaired t-test). A representative result of 6 controls and 13 tests is shown in Figure 6. All the cells tested responded with significant increase in the fura-2 signal to 30 mM KCl confirming the viability of the cells used (Fig. 6 B and C).

2.4.2. HNO elicits membrane hyperpolarization of colonic myocytes

Accumulation of cytosolic Ca^{2+} as observed in fura-2 experiments (Fig. 6) might be responsible for alternative mechanisms of relaxation different from activation of GC

pathways (Figs. 1-3). Consequently, HNO inducing relaxation indicates a more complex mechanism. Electrophysiological experiments on myocytes unveiled that the HNO donor Angeli's salt (50 µM) induced cell membrane hyperpolarization by - 10.64 ± 1.11 mV (n = 19) from a resting membrane potential of -40 mV (-38 to -45 mV, 95 % confidence interval) (Fig. 8).

The enteric inhibitory neurotransmitters NO, ATP or related purines and H_2S, may induce GI myocyte relaxation via activation of sGC/cGMP, or $P2Y_1$ purine receptors or K_{ATP}, respectively.[6,8,18,19] To identify the target candidates for HNO-induced relaxation, the hyperpolarization induced by Angeli's salt was challenged by ODQ (10 µM, inhibitor of the sGC), the bee venom apamin (1 µM, inhibitor of the SKca), and glibenclamide (100 µM, inhibitor of K_{ATP}. As expected, the amplitude of the IJP was strongly reduced by apamin (1 µM) from – 22.89 ± 2.08 mV (n = 12) to – 6.39 ± 0.76 mV (n = 5) or any drug combination based on it (apamin + ODQ, from -22.89 ± 2.08 mV, n = 12 to -3.83 ± 1.59 mV, n = 5) (Fig. 7A and C). In the presence of apamin, only the second component associated to the IJPs was recorded (Fig. 7 A). This second component was sensitive to ODQ (Fig. 7 A). Accordingly, both MRS2500 and apamin reduced the fast component of the IJP (Fig. 7A, B and C) whereas ODQ (and L-NAME, not shown) reduced the second component of the IJP (Figure 7A and C). Apamin additionally elicits a slight depolarization as the resting membrane potential (RMP) is shifted upwards (Fig. 7A). All these results confirm the co-transmission process already described in several species including the rat colon[19] and the human small intestine[20].

2.4.3 HNO targets sGC and SK_{Ca}

As shown in Fig. 8, only glibenclamide did not modify the HNO donor-induced hyperpolarization as the amplitude of hyperpolarization did not significantly change in the

presence of this blocker (-9.08 ± 1.42 mV, n = 5) compared to control (Angeli's salt 50 µM, -10.64 ± 1.11 mV, n = 19). Apamin and ODQ significantly reduced the Angeli's salt-evoked hyperpolarization from -10.64 ± 1.11 mV (n = 19) to -4.13 ± 0.98 mV (n = 5) for the first inhibitor and from -10.64 ± 1.11 mV (n = 19) to -1.73 ± 0.51 mV (n = 5) for the second one. Also combining ODQ with either glibenclamide or apamin resulted in a very strong inhibition of Angeli's salt effect (Fig. 8F). For the first combination, the hyperpolarization was significantly reduced from -10.64 ± 1.11 mV (n = 19) to -3.55 ± 0.90 mV (n = 9) and from -10.64 ± 1.11 mV (n = 19) to -1.39 ± 0.53mV (n = 6) for the second one. These data lead to the conclusion that the hyperpolarization evoked by HNO is mediated by activation of SKca channels and sGC, the latter being the predominant pathway.

2.4.4 HNO is a tone regulator

Based on the electrophysiological measurements, the question arising as if the relaxation elicited by HNO in organ bath was only relying on the activation of sGC or whether SKca had to be addressed. However, the relaxing action of HNO was not reduced, either in the presence of apamin or MRS2500 (Table 3). This might be due to a major contribution of GC pathway in inhibitory mechanisms. Accordingly, we tested the effect of apamin in the presence of ODQ. However, as shown in 5C Angeli's salt (50 µM) barely relaxes longitudinal muscle strips by -7.36 ± 4.00 g·180s (n =7) and -5.97 ± 2.37 g·180s (n =7), in the absence or presence of apamin; respectively.

3. Discussion

3.1. HNO presents similar relaxation properties as H_2S and NO

Nitric oxide and hydrogen sulphide are both known to relax intestinal smooth muscle cells.[20,21] In the present study we show that also HNO, released by the donor Angeli's salt, elicits a relaxation of both circular and longitudinal muscle strips from the rat ileum or colon (Fig. 1, 2 and 3) as do NO and H_2S in different species including rat.[21,22,23,24] This relaxation reaches a maximum within 3 minutes after application of the donor, which also matches with the profile of NO or H_2S in their relaxing property.[8,25] Both the basal tone and the frequency of phasic contractions are reduced by the gasotransmitter. The recovery used to occur after 5 min from the onset of the HNO donor (Fig. 2D as example). This recovery profile might be due to the short half-life of the donor which is approximately 2 - 3 minutes at physiological pH and temperature[27] or the pathways used to achieve the relaxation. Also NO and H_2S present similar periods of action depending on their concentration or the mode of administration or even the donor used.

3.2. HNO acts on the contractile apparatus of intestinal myocytes

Neuromuscular transmission regulates smooth muscle contraction by either excitatory transmitters like ACh or inhibitory transmitters like NO. The excitatory neurotransmitter ACh binds to muscarinic G-protein coupled-receptors, initiating a physiological cascade through $G\alpha_{q/11}$ leading step by step to activation of phospholipase Cβ (PLCβ), synthesis of IP_3 which binds to IP_3R on sarcoplasmatic reticulum for intracellular release of Ca^{2+}. In addition to this pathway, receptor-operated (ROC) and stretch-activated (SAC) non-selective cation channels are activated and positively regulate voltage dependent calcium channels (VDCC), allowing for Ca^{2+} entry. Another parallel pathway is the G protein regulation of GDP-GTP exchange factor (Rho-GEF), RhoA and activation of Rho-kinases (RhoK). Activation of RhoK and PKC by diacylglycerol (DAG) or by Ca^{2+} lead to phosphorylation and therefore inactivation of myosin light chain phosphatase (MLCP), the

enzyme causing relaxation by dephosphorylating light chain of myosin. Accumulating Ca^{2+} activates the protein calmodulin initiating the activation of kinases such as PKC or myosin light chain kinase (MLCK). The latter phosphorylates light chain of myosin launching cross-bridge cycling.[27] Relaxation is operated by repolarization or hyperpolarization counter-acting depolarization that resulted from excitation. This can be achieved by activation of Ca^{2+}-dependent potassium channels like SKca in smooth muscle cells or alternatively in PDGFRα+ cells that might transduce purinergic inputs to smooth muscle cells. Relaxation can also be achieved by activating MLCP or by extrusion or restoring of cytosolic Ca^{2+}.

In the present study, blocking the RhoK by the specific inhibitor Y-27632[28,29] blocked the response to CCh (Fig. 4A). This confirms that the agonist activates RhoK during muscarinic contraction. In the presence of this inhibitor, the HNO donor induced relaxation was strongly reduced (Fig. 4B), revealing an inactivating property of HNO on the RhoK in the absence of the blocker. Such an inactivation of RhoK by HNO should shift the balance towards a potentiation of MLCP activity, resulting in a relaxation. However, the contraction observed with 100 µM (Fig. 4B) indicates a switch in the appropriate pathway depending on the concentration of HNO, which when it is higher may correct a persistent blockade of RhoK or activity of MLCP. A possible reason for this unexpected contraction might be the rise in the cytosolic Ca^{2+} concentration induced by HNO (Fig. 6), which might be able to elicit a contraction, when the RhoK is inhibited. A contrasting result was obtained in resistance arteries where NO relaxing activity was potentiated with Y-27632.[30]

On the other hand, inhibition of MLCP activity for example by its specific blocker calyculin A[30,31] should strengthen the contractile mechanism initiated for example by CCh. A partial effect was observed indeed (Fig. 4C). A previous work on arteries also showed

increasing contractions upon administration of calyculin A.[31] Thus, preincubation with this inhibitor leads to an enhanced pre-contraction status of the tissues. Under this condition, the HNO donor's relaxing effect was potentiated (Fig. 4D) at 50 µM what is not expected considering a potential inhibitory property of this gasotransmitter on RhoK as mentioned above. Such a property would have slightly weakened the MLCP inhibition by calyculin A as MLCP is physiologically inactivated by RhoK, but the potentiation observed would have not occurred. Apparently, a pre-contraction may change the priority of HNO for target selection. This can be observed with a higher concentration of the gasotransmitter (100 µM, Fig. 4D) where the expected reduction in relaxing action of HNO occurs, indicating indeed a direct activation of MLCP or an indirect activation through inhibition of RhoK by HNO. This property activating MLCP is also known for NO[30,32] and H_2S.[9] Figure 9 summarizes the mechanisms of HNO actions on the contractile apparatus.

3.3. NO and H_2S influence the HNO-evoked relaxation

The strong inhibition of the NO-evoked relaxation by ODQ (Fig. 5A) was expected since animals that lack GC have no response to NO[33]. Although several interactions between NO and H_2S have been reported[34], we did not observe a significant reduction of NAHS response when tissue was incubated with ODQ (Fig 5B). Based on the data obtained with L-NAME, it seems that endogenously synthesized NO does not directly contribute to the relaxation induced by exogenous HNO.

It is known that AAOA may increase spontaneous motility.[35] However, in the present experiments we observed a transient reduction of the basal tone when endogenous synthesis of H_2S was hindered by both AOAA and CLA, indicating a contribution of endogenous H_2S to the maintenance of basal muscle tone of rat colonic musculature. The relaxation induced by exogenous HNO may be partly potentiated by endogenous H_2S as

the HNO-evoked maximal relaxation was slightly reduced by the combination AOAA/CLA (Table 1). This indicates a potential switch in the predominant pathway(s) for relaxation depending on the concentration and the nature of the gasotransmitter(s) present *in situ*. Only additional administration of ODQ in the presence of AOAA/CLA abolished AS-evoked relaxation. If a cooperative interplay between NO and H_2S could lead to endogenous synthesis of HNO, release of HNO could be indirectly sensed by its interaction with thiol groups knowing its high thiophillicity. This thiophilic property was revealed with DTT (Table 2). The relaxation obtained by the simultaneously administration of the NO donor SNP and the H_2S donor NaHS was partly sensitive to DTT, indicating indeed a partial thiophilic characteristic under both gasotransmitters. Thus, exogenous NO and H_2S may partially lead to an HNO-like effect. Whether endogenously produced NO cooperates with endogenous H_2S for HNO-like effects, still has to be investigated in more detail, as we used in the present study only one NOS inhibitor (L-NAME) at a single concentration.

3.4. Mechanism of action of HNO.

In contrast to previous findings showing an activation of the SERCAs in cardiomyocytes,[10] cytosolic accumulation of Ca^{2+} upon administration of the HNO donor also makes sense as this could activate SKca in colonic myocytes, leading to hyperpolarization and therefore to relaxation. The corresponding hyperpolarization was observed under non-cholinergic non-adrenergic conditions to isolate inhibitory responses (Fig. 8). Under these pharmacological conditions, the K_{ATP} channels known as H_2S target[7,8] did not play a role in the response to HNO as shown by the missing sensitivity against glibenclamide, the prototypical blocker of this class of ion channels (Fig. 8). In the contrary, the HNO-evoked hyperpolarization was dependent both on sGC and SKca as the

hyperpolarization was strongly reduced by the corresponding inhibitors ODQ and apamin, respectively (Fig. 8). One possibility is that HNO might be acting on enteric inhibitory neurons causing the release of purines acting on P2Y1 receptors that activate SK_{Ca} channels. However, MRS2500 did not modify the mechanical relaxation induced by HNO (Table 3) and therefore it is possible that the effect of HNO is not on enteric inhibitory neurons but a direct effect on post-junctional cells. These results are consistent with calcium measurements in colonic myocytes. Whether these mechanisms are located only in smooth muscle cells or other post-junctional cells such as ICC or PDGFRα cells is currently unknown.

All these results indicate a clear activation of SKca and sGC/cGMP/PKG pathway by HNO in colonic myocytes. NO activates the sGC/cGMP/PKG pathway, but other types of K^+ channels namely the KNO1, KNO2 and the BK channels.[36]

4. Conclusion

We can conclude that HNO presents similarities with NO and H_2S when it comes to mechanisms of action or pathways regulated. All three gasotransmitters cause GI tract relaxation. HNO causes relaxation via activation of the sGC/cGMP/PKG pathway leading to hyperpolarization (like NO), activation of SK_{Ca} channels (like H_2S), activation of MLCP (like both NO and H_2S), and inhibition of RhoK. It also corrects impaired pathways and induces a fine-tuning between motility regulating properties of NO and H_2S. HNO may also present a motility “sensor” property. It interferes with disulphide bonds and the amplitude of its response may be dependent on the balance -S-S-/SH at its targets. HNO alone may act as a hybrid gasotransmitter between NO and H_2S with more regulatory properties and some particularites. Consequently, HNO appears to be an excellent candidate for substituting NO and or H_2S in the therapy of diverse GI tract

disorders. Nitroxyl-prodrugs (temposil, dipsan) have being used so far as alcohol deterrent agents or undergo clinical trials (CXL 1427).[13] Investigating on the appropriate *in situ* concentration and the ideal therapeutic window as it is known for each drug[37] could be a great benefit for the GI-tract.

5. Methods

5.1. Animals

Female and male Wistar (160 - 220 g) or Sprague-Dawley rats (12 - 18 weeks old) were used. The animals were bred and housed at the institute for Veterinary Physiology and Biochemistry of the Justus-Liebig-University Giessen (Wistar rats) or at the institute of Veterinary Physiology of the Universitat Autònoma de Barcelona (Sprague-Dawley rats) at an ambient temperature of 22.5 °C and air humidity of 50 - 55 % on a 12 h: 12 h light-dark cycle with free access to water and food until the time of the experiment. The animals were anaesthetized with CO_2 and killed by exsanguination. Experiments were approved by the named animal welfare officer of the Justus Liebig University (administrative number 577_M) or by the Ethics Committee of the Universitat Autònoma de Barcelona and performed according to the German and European animal welfare law.

5.2. Isometric force measurements

For isometric force measurements, the muscle strips were obtained as follows: the abdomen of euthanized animals was opened, the ileum and colon were collected and the lumen carefully cleaned. After a short period in ice-cold buffer gassed with 5 % (v/v) CO_2/95 % (v/v) O_2, the tissues were cut into 1.5 cm long pieces which were then fixed in the organ bath. The chamber was filled with warm (37°C) and gassed (5 % CO_2/95 % O_2, v/v) buffer solution. For longitudinal muscle strips, the pretension was set at 1.5 g and

after an equilibrium period of at least 15 min, the tension was lowered to 1 g. For circular muscle strips (1 cm x 0.5 cm) the tension was continuously set at 1 g. The baseline was measured for five minutes before administration of any drug. As viability control, 10 µM carbachol and/or 30 mM KCl were administered at the end of each experiment.

Isometric force was measured via a BioAmp-04/8 amplifier system and sampled via an A/D-converter with a sampling rate of 1 Hz (Föhr Medical Instruments, Seeheim, Germany). For data analysis, the baseline just prior administration of a drug was measured as mean over 1 min. To calculate the maximal relaxation induced by Angeli's salt, the maximal reduction in muscle tone within 5 min after administration of the agonist was calculated and expressed as difference to the baseline just prior administration of Angeli's salt (ΔForce; see e.g. Fig. 4). As the action of Angeli's salt on muscle tone was only transient, in addition the changes in the area under the curve (AUC) over a 3 min interval (g·180 s) before and after administration of the HNO donor was calculated (see inset in Fig. 3). To determine the frequency of phasic spontaneous contractions, first time derivatives (dg/dt) were calculated. Only waves passing a threshold set at 0.1 $g \cdot s^{-1}$ were counted as contraction during a 1 min period before (control) and 3 min after administration of HNO. The calculated frequency was expressed as contractions/min (cpm).

5.3. Isolation of myocytes

Ca^{2+} imaging experiments were performed at isolated myocytes from the proximal colon. The longitudinal muscle layer (devoid of mesenterium) from the colon was removed and cut in small pieces of about 0.1 x 0.1 cm. These pieces were collected and transferred into the digestion solution consisting of collagenase type II (0.5 $mg \cdot ml^{-1}$) and trypsin inhibitor (0.25 $mg \cdot ml^{-1}$) in Hank's balanced salt solution (Ca^{2+}- and Mg^{2+}-free). If cells from the

circular muscle layer had to be prepared, after stripping away the longitudinal muscle layer, the mucosa layer was scrapped off using the edge of a glass slide; the remaining tissue was minced then proceeded as with the longitudinal layer. The tissues were then enzymatically digested for 30 min at 37°C then vortexed for 10 s and centrifuged 2000 rpm for 3 min. The supernatant was discarded and the digestion solution added to the pellet. After shortly mixing, a second incubation period at 37 °C for 30 min followed. The preparation was then vortexed for 5 s and centrifuged at 1500 rpm for 3 min. The supernatant was discarded and the myocytes resuspended in DMEM F12 medium supplemented with fetal calf serum until the beginning of measurements.

5.4. Microelectrode recordings

For microelectrode recordings, the colon of Sprague-Dawley rats was removed and placed in carbogenated (95 % O_2 and 5 % CO_2, v/v) Krebs solution, then opened along the mesenteric border. The mucosal and submucosal layers were gently removed and 3 x 5 mm muscle strips were cut in a circular direction.

Electrophysiological experiments were performed with colonic strips pinned in a Sylgard®-coated chamber with the circular muscle layer facing upwards. The tissue was continuously perfused with carbogenated Krebs solution at 37 ± 1°C and allowed to equilibrate for 1 h. Phentolamine, propranolol and atropine (all at 1 μM) were added to block α- and β-adrenoceptors and muscarinic receptors, respectively, so that the action of Angeli's salt could be measured under non-adrenergic non-cholinergic (NANC) conditions. To obtain stable microelectrode impalements, nifedipine 1 μM was added to abolish mechanical activity. Circular smooth muscle cells were impaled using glass microelectrodes filled with 3 M KCl (30 - 60 MΩ of tip resistance). Membrane potential was measured by using a standard Duo 773 electrometer (WPI Inc., Sarasota, FL, USA).

Tracings were displayed on an oscilloscope (Racal-Dana Ltd, Windsor, UK) and simultaneously digitalized (100 Hz) with a PowerLab 4/30 system and Chart 5 software for Windows (both from ADInstrument, Castle Hill, NSW, Australia). Inhibitory junction potentials (IJP) were elicited by electrical field stimulation (EFS) using two silver chloride plates placed 1.5 cm apart perpendicular to the longitudinal axis of the preparation. The protocol consisted of single pulse trains of EFS (0.4 ms pulse duration) at supramaximal voltage (30 - 40 V). The resting membrane potential (RMP) and both the amplitude as well as the duration of the IJP were measured and compared before and after drug incubation.

5.5. Ca^{2+} Imaging

The myocytes suspension was spun down at 1500 rpm for 1 min. After discarding the supernatant, the cells were resuspended in warm (37 °C) Tyrode solution containing the Ca^{2+}-sensitive fluorescent dye fura-2 (6 µM; Life Technologies, Darmstadt, Germany) and pluronic acid (1.2 $mg \cdot l^{-1}$; Life Technologies, Darmstadt, Germany) and incubated for 1 hour at 37 °C. After incubation, 30 µl of the myocyte suspension were spread onto a poly-L-lysine-coated coverslip and incubated at room temperature for 15 min, before it was washed carefully. The coverslip was then mounted in the experimental chamber with a volume of about 3 ml. The preparation was superfused hydrostatically with warm Tyrode solution (37 °C). Perfusion was stopped only if the drug applied had to be applied via a pipette. The perfusion rate was about 2 $ml \cdot min^{-1}$. Changes in the cytosolic Ca^{2+} concentration were monitored as changes in the fura-2 ratio (R; emission at an excitation wave length of 340 nm divided by the emission at an excitation wave length of 380 nm). Experiments were carried out on an inverted microscope (Olympus IX-50; Olympus, Hamburg, Germany), equipped with an epifluorescence set-up and an image analysis

system (Till Photonics, Martinsried, Germany). Several regions of interest, each with the size of about one cell, were selected. The emission above 420 nm was measured from the regions of interest. Data were sampled at 0.2 Hz. The baseline in the fluorescence ratio of fura-2 was measured for several minutes before drugs were administered.

5.6. Solutions and drugs

The organ bath Parsons solution consisted of (in mM): NaCl 107, KCl 4.5, $NaHCO_3$ 25, Na_2HPO_4 1.8, NaH_2PO_4 0.2, $CaCl_2$ 1.25, $MgSO_4$ 1 and glucose 12. The solution was gassed with carbogen (5 % CO_2 in 95 % O_2, v/v); pH was 7.4. The composition of the Krebs solution was (in mM): glucose 10.1, NaCl 115.5, $NaHCO_3$ 21.9, KCl 4.6, NaH_2PO_4 1.1, $CaCl_2$ 2.5, and $MgSO_4$ 1.2 bubbled with a carbogen (pH 7.4). The myocytes were dissociated in Ca^{2+}- and Mg^{2+}-free Hank's balanced salt solution (HBSS, Life Technologies, Paisley, UK). For superfusion of the isolated myocytes during the imaging experiments, a Tyrode solution was used (in mM): NaCl 140, KCl 5.4, $CaCl_2$ 1.25, $MgSO_4$ 1, HEPES 10, glucose 12.2; pH was 7.4.

Angeli's salt (Cayman Chemical, Ann Arbor, MI, USA) was dissolved in 0.01 N NaOH. Nifedipine was dissolved in 96 % (v/v) ethanol. Calyculin A (New England, Ipswitch, USA), glibenclamide and ODQ (Tocris, Bristol, England) were dissolved in DMSO. Amino-oxyacetate (AOAA), apamine (Alomone Labs, Jerusalem, Israel), atropine sulfate, carbachol, β-cyano-l-alanine (CLA), MRS2500 (Tocris, Bristol, England), 1,4-dithiothreitol (DTT), N_ω-nitro-L-arginine methylester hydrochloride (L-NAME), phentolamine, propranolol, sodium hydrogen sulfide (NaHS), sodium nitroprusside (SNP; Enzo Life, Lausen, Switzerland), and Y-27632 (Tocris, Bristol, UK) were dissolved in aqueous solutions. If not stated explicitly, drugs were purchased from Sigma Aldrich, St Louis, USA.

5.7. Data analysis and statistics

In general results are given as means ± standard error of the mean (SEM. The number of investigated tissues or cells is indicated n. When means of several groups had to be compared, an analysis of variance was performed followed by Bonferroni or Tuckey *post hoc* test. For the comparison of two groups, either a paired or an unpaired Student's t-test or a Mann-Whitney U-test was applied. Statistical analysis was performed with GraphPad Prism 6. Data were considered significant when $P < 0.05$.

Acknowledgement

The diligent care of Mrs. B. Buß, E. Haas, B. Schmitt, A. Stockinger and Emma Martínez is a pleasure to acknowledge. We thank Prof. Martin Diener for helpful discussion. Supported by Deutsche Forschungsgemeinschaft, grant PO 2143/1-1 and the ERASMUS + Program.

Conflict of interest

The authors state no conflict of interest.

References

1. Schemann M. Control of gastrointestinal motility by the "gut brain"-The enteric nervous system. *J. Pediatr. Gastroenterol. Nutr.,*. 2005;45:S4-S6.
2. Wood JD. Enteric nervous system: reflexes, pattern generators and motility. *Curr. opin. Gastroenterol.,* 2008;24:149-158.
3. Gallego D, Malagelada C, Accarino A, De Giorgio R, Malagelada JR, Azpiroz F, Jimenez M. Nitrergic and purinergic mechanisms evoke inhibitory neuromuscular

transmission in the human small intestine. *Neurogastroenterol Motil.,* 2014;26:419-429.

4. Jimenez M, Clave P, Accarino A, Gallego D. Purinergic neuromuscular transmission in the gastrointestinal tract: functional basis for future clinical and pharmacological studies. *Br. J. Pharmacol.,* 2014;171:4360-4375.
5. Shuttleworth CW, Xue C, Ward SM, de Vente J, Sanders KM. Immunohistochemical localization of 3',5'-cyclic guanosine monophosphate in the canine proximal colon: responses to nitric oxide and electrical stimulation of enteric inhibitory neurons. *Neuroscience*, 1993;56:513-522.
6. Smith TK, McCarron SL. Nitric oxide modulates cholinergic reflex pathways to the longitudinal and circular muscle in the isolated guinea-pig distal colon. *J Physiol*., 1998;512:893-906.
7. Zhao P, Huang X, Wang ZY, Qiu ZX, Han YF, Lu HL, Kim YC, Xu WX. Dual effect of exogenous hydrogen sulfide on the spontaneous contraction of the gastric smooth muscle in guinea-pig. *Eur. J. Pharmacol.,* 2009;616:223-228.
8. Gallego D, Clavé P, Donovan J, Rahmati R, Grundy D, Jiménez M, Beyak MJ. The gaseous mediator hydrogen sulphide inhibits in vitro motor patterns in the human, rat and mouse colon and jejunum. *Neurogastroenterol Motil.,* 2008;20:1306-1316.
9. Dhaese I., Lefebvre AR. Myosin light chain phosphatase activation is involved in the hydrogen sulfide-induced relaxation in mouse gastric fundus. *Eur. J. Pharmacol.,* 2009;606:180-186.
10. Irvine JC, Ritchie RH, Favaloro JL, Andrews KL, Widdop RE, Kemp-Harper BK. Nitroxyl (HNO): the Cinderella of the nitric oxide story. *Trends Pharmacol. Sci.*, 2008; 29:601-608.
11. Pouokam E, Bell A, Diener M. Actions of Angeli's salt, a nitroxyl (HNO) donor, on ion transport across mucosa-submucosa preparations from rat distal colon. *Eur. J. Pharmacol.,* 2013;715:133-141.
12. Eberhardt M, Dox M, Namer B, Miljkovic J, Cordasic N, Will C, Kichko TI, De La Roche J, Fischer M, Suarez SS, Bikiel D, Dorsch K, Leffler A, Babes A, Lampert A, Kennerz JK, Jacobi J, Marti MA, Doctorovich F, Högestätt ED, Zygmunt PM, Ivanovic-Burmazovic I, Messlinger K, Reeh P, Filipovic MR. H_2S and NO

cooperatively regulate vascular tone by activating a neuroendocrine HNO-TRPA1-CGRP signalling pathway. *Nat Commun*. 2014;5:4381

13. Cowart D, Venuti R, Guptill J, Noveck R, Foo S. A phase 1 study of the safety and pharmacokinetics of the intravenous nitroxyl prodrug, CXL-1427. *JACC* .2015;65(10S).

14. Yong QC, Cheong JL, Hua F, Deng LW, Khoo YM, Lee HS, Perry A, Wood M, Whiteman M, Bian JS. Regulation of heart function by endogenous gaseous mediators-crosstalk between nitric oxide and hydrogen sulfide. *Antioxid. Redox Signal.,* 2011;14:2081-2091.

15. Filipovic MR, Eberhardt M, Prokopovic V, Mikuskovic, Orescanin-Dusic Z, Reeh P, Ivanovic-Burmazovic I. Beyond H_2S and NO interplay: Hydrogen sulfide and nitroprusside react directly to give nitroxyl (HNO). A new pharmacological source of HNO. *J. Med. Chem*., 2013;56:1499-1508.

16. Miljkovic JL, Kenkel I, Ivanovic-Burmazovic I, Filipovic MR. Generation of HNO and HSNO from nitrite by heme-iron-catalysed metabolism with H2S. *Angew. Chem. Int. Ed.,* 2013;52:12061-12064.

17. Wang R. Physiological implications of hydrogen sulfide: a whiff exploration that blossomed. *Physiol. Rev*., 2012;92:791-896.

18. He XD, Goyal RK. Nitric oxide involvement in the peptide VIP-associated inhibitory junction potential in the guinea pig ileum. *J. Physiol.,* 1993;461:485-499.

19. Grasa L, Gil V, Gallego D, Jimenez M. P2Y1 receptors mediate inhibitory neurotransmission in the rat colon. *Br. J. Pharmacol*., 2009;158:1641-1652.

20. Shuttleworth CW, Sanders KM. Involvement of nitric oxide in neuromuscular transmission in canine proximal colon. *Proc Soc Exp Biol Med*., 1996;211:16-23.

21. Teague B, Asiedu S, Moore PK. The smooth muscle relaxant effect of hydrogen sulphide in vitro:evidence for a physiological role to control intestinal contractility. *Br. J. Pharmacol*., 2002;137:139-145.

22. Tam FS, Hillier K. The role of nitric oxide in mediating non-adrenergic non-cholinergic relaxation in longitudinal muscle of human taenia coli. *Life Sci.,* 1992;51:1277-1284.

23. Stark ME, Bauer AJ, Sarr MG, Szurszewski JH. Nitric oxide mediates inhibitory nerve input in human and canine jejunum. *Gastroenterology,*1993;104:398-409.

24. Boeckxstaens GE, Pelckmans PA, Herman AG, Van Maercke YM. Involvement of nitric oxide in the inhibitory isolation of the human isolated colon. *Gastroenterology,* 1993;104:690-697.

25. Gallego D, Malagelada C, Accarino A Gori A, Malagelada JR, Azpiroz F, De Giorgio R, Jimenez M. Functional neuromuscular impairment in severe intestinal dysmotility. *Neurogastroenterol Motil.,* 2018;30:e13458.

26. Switzer CH, Flores-Santana W, Mancardi D, Donzelli S, Basudhar D, Ridnour LA, Miranda KM, Fukuto JM, Paolocci N, Wink DA. The emergence of nitroxyl (HNO) as a pharmacological agent. *Biochim. Biophys Acta*., 2009;1787:835-840.

27. Sanders KM. Regulation of smooth muscle excitation and contraction. *Neurogastroenterol Motil*., 2008;20:39-53.

28. Uehata M, Ishizaki T, Satoh H, Ono T, Kawahara T, Morishita T, Tamawaka H, Yamagami K, Inui J, Maekawa M, Narumiya S. Calcium sensitization of smooth muscle mediated by a Rho-associated protein kinase in hypertension. *Nature,* 1997;389:990-994.

29. Narumiya S, Ishizaki T, Ufhata M. Use and properties of ROCK-specific inhibitor Y-37632. *Meth. Enzymol*., 2000;325:273-284.

30. Bolz SS, Vogel L, Sollinger D, Derwand R, de Wit C, Loirand G, Pohl U. Nitric oxide-induced decrease in Calcium sensitivity of resistance arteries is attributable to activation of the myosin light chain phosphatase and antagonized by the RhoA/Rho Kinase pathway. *Circulation,* 2003;107:3081-3087.

31. Ishihara H, Ozaki H, Sato K, Hori M, Karaki H, Watabe S, Kato Y, Fusetani N, Hashimoto K, Uemura D. Calcium-independent activation of contractile apparatus in smooth muscle by calyculin -A. *J Pharmacol Exp Ther.* 1989;250:388-396.

32. Gallego D, Mane N, Gil V, Martinez-cutillas M, Jimenez M. Mechanisms responsible for neuromuscular relaxation in the gastrointestinal tract. *Rev. Esp Enferm Dig*., 2016; 108 :721-731.

33. Groneberg D, König P, Wirth A, Offermans S, Koesling D, Friebe A. Smooth Muscle–Specific Deletion of Nitric Oxide–Sensitive Guanylyl Cyclase Is Sufficient to Induce Hypertension in Mice. *Circulation*, 2010; 121:401-409.

34. Szabo Csaba. Hydrogen sulphide, an enhancer of vascular nitric oxide signalling: mecahnisms and implications. *Am. J. Physiol. Cell Physiol*., 2017;312: C3-C15.

35. Gil V, Gallego D, Jimenez M. Effects of inhibitors of hydrogen sulphide synthesis on rat colonic motility. *Br. J Pharmacol*. 2011;164:485-498.

36. Koh SD, Campbell JD, Carl A, Sanders KM. Nitric oxide activates multiple potassium channels in canine colonic smooth muscle. *J. Physiol*. 1995; 489:735-43.

37. Paolocci N, Jackson MI, Lopez BE, Miranda K, Tocchetti CG, Wink DA, Hobbs AJ, Fukuto JM. The pharmacology of nitroxyl (HNO) and its therapeutic potential: not just the janus face of NO. *Pharmacol Ther*., 2007;113:442–458.

Tables

Table 1 Impact of AOAA/CLA in the presence or not of ODQ on Angeli's salt-evoked relaxation.

	ΔForce (g)	**AUC (g·180s)**	**n**
Angeli's salt alone	-0.70 ± 0.05	-96. 4 ± 6.8	6
AOAA/CLA + Angeli's salt	-0.54 ± 0.07	-71.7 ± 10.0	6
Angeli's salt alone	-0.97 ± 0.13	-133.0 ± 24.0	5
AOAA/CLA/ODQ + Angeli's salt	-0.31 ± 0.04**	-1.8 ± 1.5**	5

Blockade of endogenous synthesis of H_2S with both AOAA and CLA (both 5 mM) slightly reduced the relaxation induced by Angeli's salt (50 μM) in longitudinal muscle from rat colon. Additional blockade of the sGC with ODQ (10 μM) significantly inhibited the response to Angeli's salt. ** $P < 0.01$ versus control in the absence of the corresponding blockers (Mann-Whitney U-test).

Table 2 Impact of protection of thiol groups on Angeli's salt- or SNP- and NaHS-evoked relaxation.

	ΔForce (g)	**AUC (g·180s)**	**n**
Angeli's salt alone	-1.49 ± 0.25	-186.8 ± 25.9	5
DTT + Angeli's salt	-0.83 ± 0.07*	-90.4 ± 10.9*	8
NaHS + SNP	-0.73 ± 0.09	-103.3 ± 18.9	5
DTT + NaHS + SNP	-0.59 ± 0.07	-76.4 ± 10.6	8

The reducing agent DTT (500 μM) significantly inhibited the relaxation induced by Angeli's salt (50 μM), but only slightly reduced the relaxation induced by NaHS (H_2S donor; 100 μM) and SNP (NO donor; 1 mM). Longitudinal muscle from rat colon. * $P < 0.05$ versus control in the absence of the corresponding blocker (Mann-Whitney U-test).

Table 3 Amplitude of Angeli's salt-evoked relaxation in the presence of apamin and MRS2500

	ΔForce (g)	**n**
Angeli's salt alone	-0.62 ± 0.11	8
Angeli's salt in the presence of apamin	-0.71 ± 0.12	11
Angeli's salt alone	-0.62 ± 0.14	5
Angeli's salt in the presence of MRS 2500	-0.69 ± 0.05	5

Blockade of SKca with apamin (1 μM) or of purine receptors P2Y1 with MRS2500 (1 μM) does not inhibit the relaxation evoked by Angeli's salt (50 μM) in longitudinal muscle from rat colon.

Figures

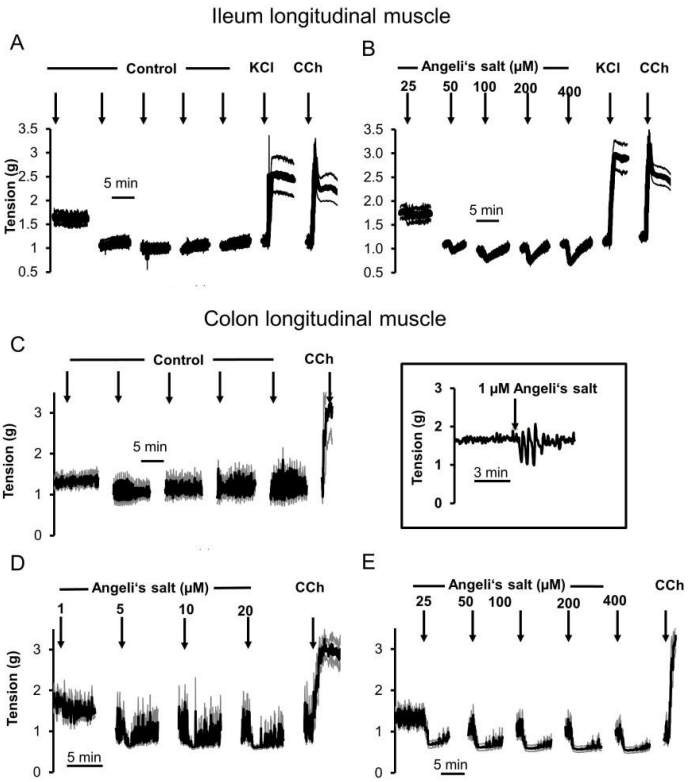

Fig. 1: Relaxation induced by different concentrations of Angeli's salt (1 - 400 µM, arrows) on longitudinal segments of rat ileum (B) or proximal colon (D, E) and time-dependent control experiments (A) or (C), where only the solvent of Angeli's salt was administered. The inset (middle) shows an original tracing of an individual colonic longitudinal muscle strip with a transient relaxation induced by 1 µM Angeli's salt, which is hard to recognize in the ensemble average depicted in Fig. 1D resulting from the averaging of 8 muscle strips responding asynchronously with a short relaxation induced by the HNO donor. Line interruptions are caused by omitting washing periods of about 10 min, where the content of the organ bath was exchanged 3 times before the next concentration of Angeli's salt was administered. KCl (30 mM) and or carbachol (CCh; 10 µM) were used to check tissue viability. Values are means (black lines) ± SEM (grey lines), n = 5 -11.

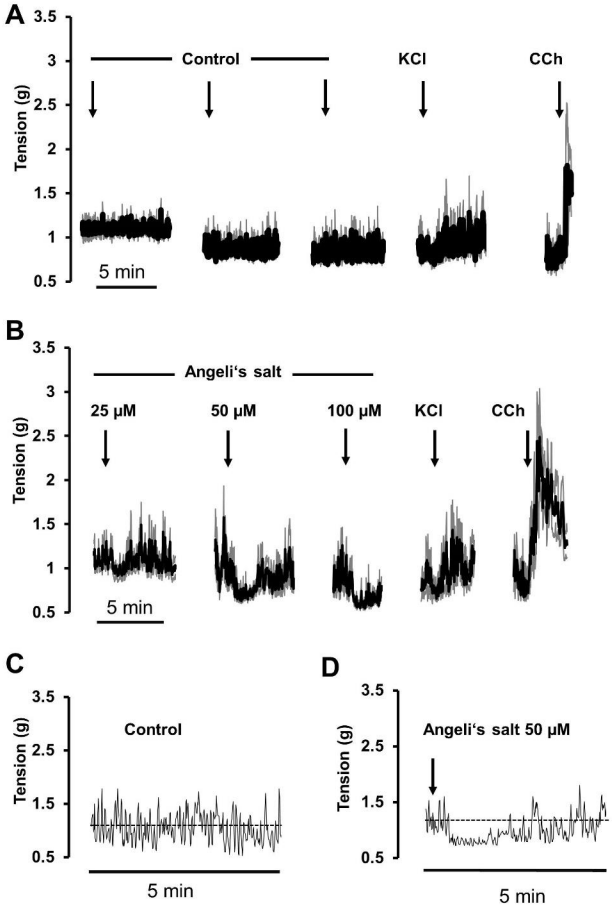

Fig. 2: The HNO donor Angeli's salt (25 - 100 µM, arrows) induces a relaxation of circular segments of rat proximal colon (B) compared to a time-dependent control (A), where only the solvent of Angeli's salt was administered. Line interruptions are caused by omitting washing periods of about 10 min, where the content of the organ bath was exchanged 3 times before the next concentration of Angeli's salt was administered. KCl (30 mM) and carbachol (CCh; 10 µM) were used to check tissue viability. Data in A, B are means (black lines) ± SEM (grey lines), n =5 - 6. (C) and (D) are higher magnifications of 5 min intervals of an individual muscle preparation contained in the respective ensemble averages in (A) and (B). For statistics, see Fig. 3.

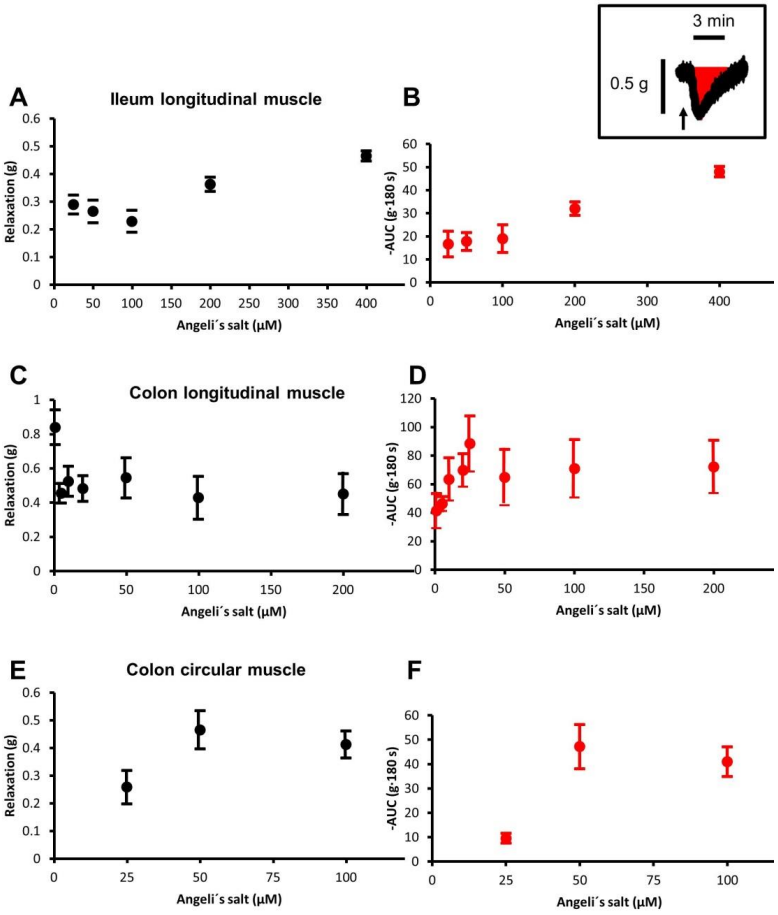

Fig. 3: Concentration-dependent relaxation induced by Angeli's salt in ileal longitudinal muscle (A, B), colonic longitudinal (C, D) and colonic circular muscle (E, F). The relaxing effect is either expressed as maximal reduction in muscle tone (Δg; difference to baseline just prior administration of the drug (A, C, E) or reduction of the area under the curve (AUC) over a 3 min period compared to the 3 min period just prior administration of Angeli's salt as illustrated by the schematic inset where the arrow marks the administration of Angeli's salt. Concentration-response curves in the colonic longitudinal muscle was constructed from two independent series of experiments (see Fig. 1), in which the effect of 1 – 20 µM and 25 – 400 µM Angeli's salt was tested, respectively. Values are means ± SEM, n = 6 - 11.

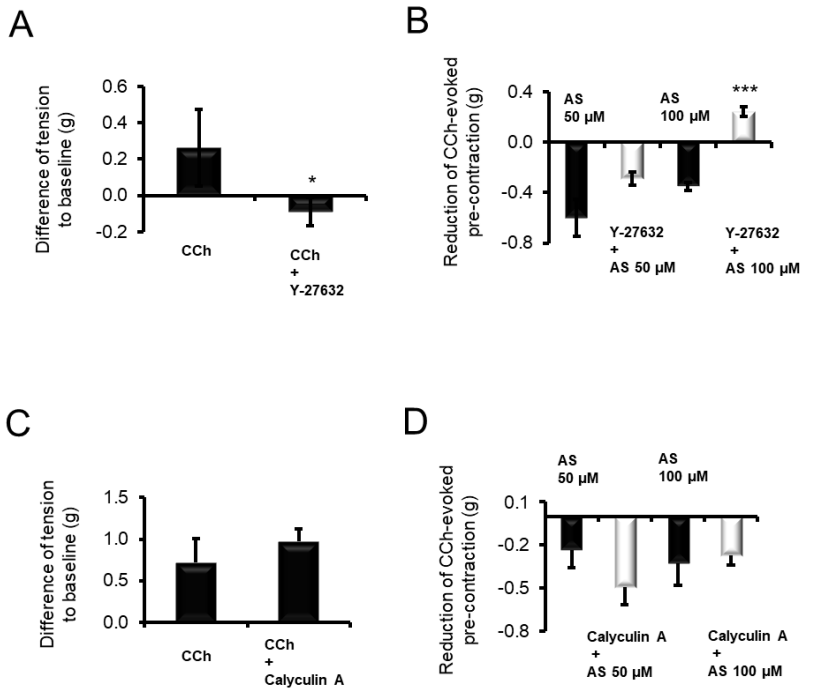

Fig. 4: Inhibition of Rho kinases by Y-27632 (10 µM) prevents the contraction induced by CCh (10 µM) of longitudinal muscle strips from proximal colon (A) and reduces the relaxation induced by HNO donor Angeli's salt (AS). Data in (B) are expressed as difference between the muscle tone just prior administration of Angeli's salt and the muscle tone averaged over a 1 min period starting 1 min after administration of the HNO. Potentiating (C) the contractile action of the cholinergic system with calyculin A (100 nM) strengthens or weakens the relaxing action of HNO (D). Values are means ± SEM, n = 7-12. * $P < 0.05$, *** $P < 0.001$ versus control in the absence of the corresponding blocker (Mann-Whitney U-test). For statistics, see text.

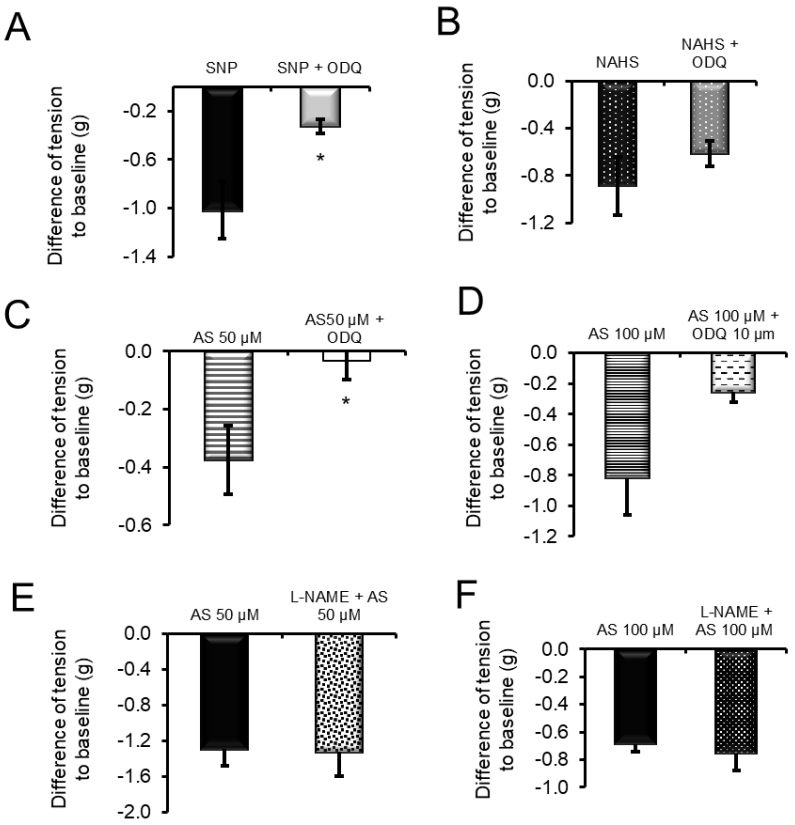

Fig. 5: The relaxing effect of the nitric oxide donor sodium nitroprusside (SNP; 1 mM) and 50 µM Angeli's salt (AS) was significantly inhibited in the presence of the sGC inhibitor ODQ (10 µM) (A, C). When the concentration of Angeli's salt was increased to 100 µM, this inhibition failed to reach significance (D). Relaxation induced by the H_2S donor sodium hydrogen sulfide (NaHS; 100 µM) was unaffected by ODQ (B). Inhibition of NOS with L-NAME (200 µM) did not affect HNO-induced relaxation (E, F). n = 5-9. * $P < 0.05$, versus control in the absence ODQ (Mann-Whitney U-test). For statistics, see text.

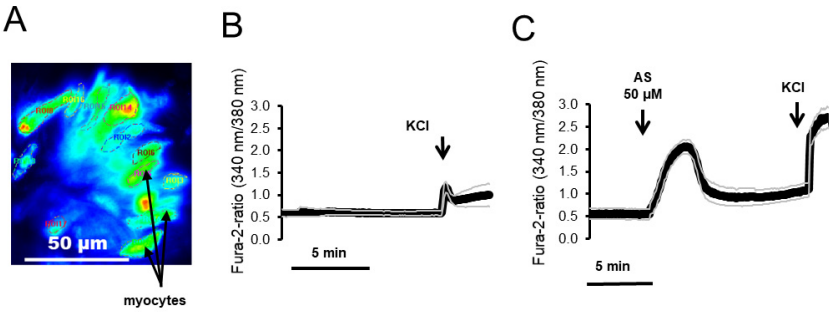

Fig. 6: Changes in the fura-2 ratio evoked by Angeli's salt (50 µM) in isolated rat colonic myocytes. A: Photograph of isolated myocytes loaded with fura-2. Angeli's salt induces an increase in the fura-2 ratio (C) compared to a time-dependent control (B). KCl (30 mM) was used for cell viability control. Values are given as means (symbols) ± SEM (parallel continuous lines), n = 6 for the time-dependent control and n = 13 for the test group with the HNO donor. For statistics, see text.

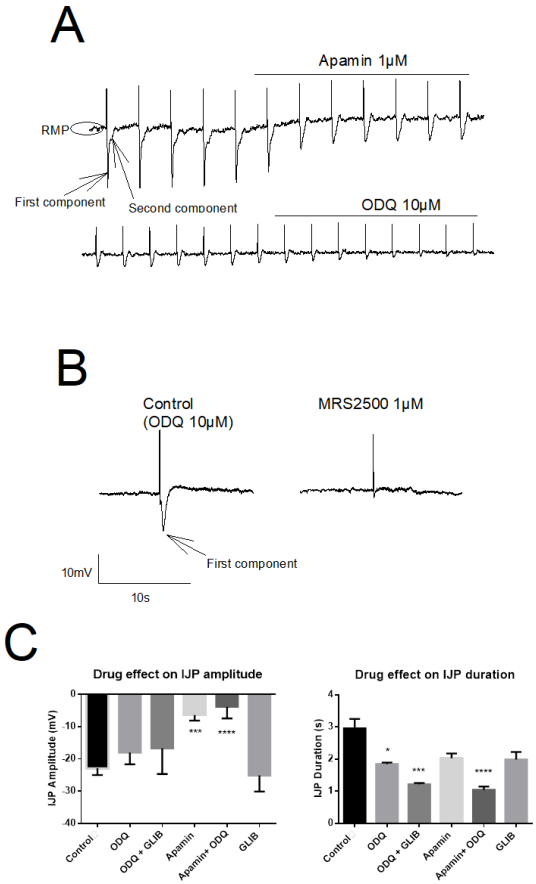

Fig. 7: Identification of the IJPf and IJPs evoked by EFS under NANC conditions. (A) Apamin blocks the IJPf (1st component in A), while ODQ blocks the IJPs (2nd component in A). Apamin induces a shift of the resting membrane potential (RMP) to more positive values. (A~~B~~) The IJPf isolated after suppression of the IJPs by ODQ was also sensitive against MRS2500 (C) The amplitude of the IJP was strongly inhibited by apamin; this inhibition was not enhanced, when in addition ODQ was administered. In contrast, the duration of the IJP was significantly reduced by ODQ; this effect was significantly enhanced when in addition glibenclamide or apamin were present. Concentrations of drugs were: apamin 1 µM, glibenclamide 100 µM, ODQ 10 µM. Values in (C) are means ± SEM, n = 3-12. * $P < 0.05$, *** $P < 0.001$, **** $P < 0.0001$, versus control in the absence of any drug (analysis of variance followed by Bonferroni test). For statistics, see text.

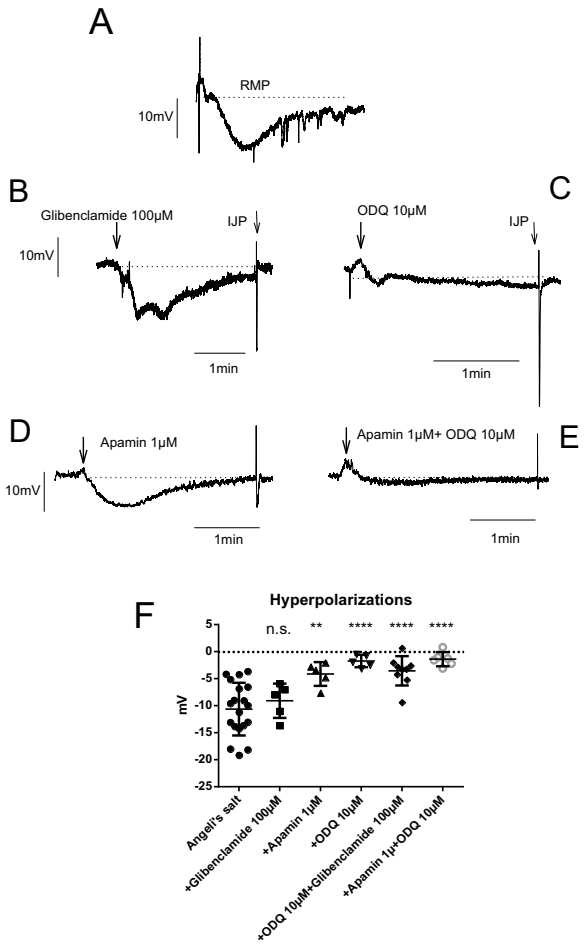

Fig. 8: The hyperpolarization caused by the HNO donor Angeli's salt (25 µM; A) is insensitive to glibenclamide (B, F, n = 5), but sensitive to apamin (D, F, n = 5) or highly sensitive to ODQ alone (C, F, n = 5) or in combination with apamin (E, F, n = 6) or glibenclamide (F, n = 9). The discontinuous horizontal lines represent the resting membrane potential (RMP). Values are means SD, n values refer to (F), while (A), (B), (C), (D) and (E) are representative original tracings. ** $P < 0.01$, **** $P < 0.0001$, versus control in the absence of any drug (analysis of variance followed by Bonferroni test). For statistics, see text.

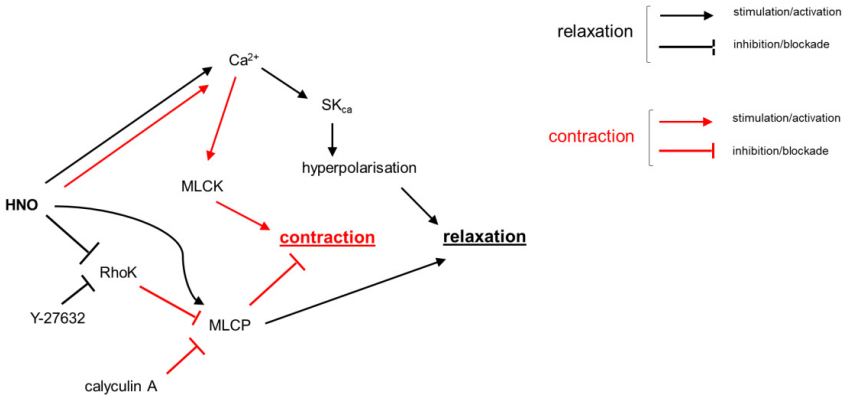

Fig. 9: HNO may induce relaxation either directly by activating MLCP or indirectly inhibiting the RhoK. Additional increase in cytosolic Ca^{2+} concentration activates SKca for hyperpolarization and relaxation. Blocking RhoK with Y-27632 shunts HNO-effects, inducing a shift towards Ca^{2+}-mediated responses which also activates MLCK for contraction.

8.9 "Effects of multivalent histamine supported on gold nanoparticles: Activation of histamine receptors by derivatized histamine at subnanomolar concentrations"

Gasiorek F, **Pouokam E**, Diener M, Schlecht S, Wickleder M. *Organ. Biomol. Chem.* (2015) 13: 9984 - 9992.

Impakt Faktor: 3.559

Eigener Anteil an der Publikation:

- Initiative: 20 %
- Projektplanung: 40 %
- Durchführung der Versuche: 50 %
- Auswertung der Experimente: 50 %
- Erstellung der Publikation: 50 %

Organic & Biomolecular Chemistry

PAPER

View Article Online
View Journal | View Issue

Open Access Article. Published on 20 August 2015. Downloaded on 8/22/2018 9:27:06 AM.
This article is licensed under a Creative Commons Attribution 3.0 Unported Licence.

Cite this: *Org. Biomol. Chem.*, 2015, **13**, 9984

Effects of multivalent histamine supported on gold nanoparticles: activation of histamine receptors by derivatized histamine at subnanomolar concentrations†

Friederike Gasiorek,[a] Ervice Pouokam,[b] Martin Diener,*[b] Sabine Schlecht[a] and Mathias S. Wickleder*[a]

Colloidal gold nanoparticles with a functionalized ligand shell were synthesized and used as new histamine receptor agonists. Mercaptoundecanoic acid moieties were attached to the surface of the nanoparticles and derivatized with native histamine. The multivalent presentation of the immobilized ligands carried by the gold nanoparticles resulted in extremely low activation concentrations for histamine receptors on rat colonic epithelium. As a functional read-out system, chloride secretion resulting from stimulation of neuronal and epithelial histamine H_1 and H_2 receptors was measured in Ussing chamber experiments. These responses were strictly attributed to the histamine entities as histamine-free particles Au–MUDOLS or the monovalent ligand AcS–MUDA–HA proved to be ineffective. The vitality of the tissues used was not impaired by the nanoparticles.

Received 3rd July 2015,
Accepted 5th August 2015
DOI: 10.1039/c5ob01354b
www.rsc.org/obc

Introduction

During the past 20 years, the number of applications of nano- and microdevices in the fields of biotechnology and biomedicine has been increased drastically.[1,2] Most promising tools are nanoparticles.[3] They represent nanoscale materials with unique chemical and physical properties due to their size. These are for example optical absorption (metal nanoparticles), photoluminescence (semiconductor quantum dots) or magnetic behaviour (iron oxides). Their applicability derives not only from the fact that their dimension range is in the size of some biomolecules like proteins or receptors, but also that through simple surface modification a huge variety of interactions can be achieved. The basic requirement for every application is the proper surface functionalization of the particles, which determines their interaction with the environment. In this study we chose gold nanoparticles as a template because of their well-known synthesis and functionalization with small molecules.[4,5] Moreover they are biocompatible. We took these particles and applied the concept of multivalency for the interaction with biological tissue. Multivalent presentation of immobilized ligands is a common concept in ligand–receptor interactions and can result in high affinities of ligands that possess only moderate binding constants in a similar concentration range when they are presented in their monovalent form.[6–8] Simplifying binding structures reduces the synthetic complexity of the molecules immobilized on the nanoparticles and has the advantage of being synthetically well accessible. Multivalent carriers can either inhibit or activate biological processes in a different way than the monovalent analogue. Usually the effective concentration is much lower.[9] There are only few examples where this concept is applied on receptor–ligand interactions with neurotransmitters. Paolino *et al.* synthesized dendrimeric tetravalent ligands for the activation of ligand-gated ion channels.[10] Indeed they found activation concentrations in the low picomolar range. Saada *et al.* synthesized gold nanoparticles coated with histamine and applied the conjugates for enzyme activation.[11] They also found an enhancement of the activation properties for these conjugates. Mediators such as histamine are key regulators of physiological processes such as ion transport across epithelial barriers. Chloride secretion is one of these processes occurring for example at the colonic epithelium.[12,13] Such a secretion can be activated *via* stimulation of histamine H_1 and/or H_2 receptors as previously shown.[14–16] The receptor activity can also be blocked by inhibitors, which are well-known for the histaminic receptors. Mediators or neurotransmitters represent an inter-

[a]*Institute of Inorganic and Analytical Chemistry, Justus-Liebig-University, Heinrich-Buff-Ring 58, 35392 Giessen, Germany. E-mail: friederike.gasiorek@anorg.chemie.uni-giessen.de*
[b]*Institute for Veterinary Physiology and Biochemistry, Justus-Liebig-University, Frankfurter Straße 100, 35392 Giessen, Germany. E-mail: martin.diener@vetmed.uni-giessen.de*
†Electronic supplementary information (ESI) available. See DOI: 10.1039/c5ob01354b

This journal is © The Royal Society of Chemistry 2015

Open Access Article. Published on 20 August 2015. Downloaded on 8/22/2018 9:27:06 AM.
This article is licensed under a Creative Commons Attribution 3.0 Unported Licence.

esting class of bioactive molecules and yet there is no study on multivalent ligand presentation on biological systems. In this paper we report the immobilization and multivalence of the biogenic amine histamine on gold nanoparticles as well as its biological function in receptor activation.

Results and discussion

Synthesis of the gold nanoparticles

By attaching histamine derivatives on gold nanoparticles we developed a new conjugate for the interaction with compatible receptors. Water soluble gold nanoparticles with a terminally functionalized thiol shell were prepared and used as a scaffold for the multivalent presentation of histamine. Gold nanoparticles with an average diameter of 14 nm were synthesized by a modification of a well-known method developed by Turkevich *et al.* (Fig. 1).[17,18]

In an aqueous solution Au(III) was reduced by sodium citrate which serves not only as reducing agent but also as a ligand to prevent aggregation of the formed particles. Even if the solvent is limited to water or polar equivalents like DMSO, the resulting size of the particles can be defined by the molar ratios of the starting materials, the reaction temperature and time. By this method, gold nanoparticles with a diameter of 14 nm (NP 1, Fig. 1) could be obtained. Depending on the size of the particles, the surface is coated with several thousand ligands with respect to the steric demand of a single ligand. The resulting nanoparticles are stabilized by electrostatic repulsion of the negatively charged citrate ions adsorbed on their surface. This layer can be easily replaced by ligands with a stronger binding affinity, such as for example thiols.[19,20] Thus, in a second step the ligand shell was substituted by a bivalent ligand. Bivalent ligands give access to further functionalization steps at the ligand periphery. One end binds to the surface and gives stability to the particle whereas the other end is exposed to the solution. Depending on the thiol moiety, the particles possess different stabilities at different pH values. There is a wide variety of ligands suitable for exchange still providing stability in aqueous media. Often poly (ethylene glycol) (PEG) is used as a ligand as it provides enough colloidal stability and reduces nonspecific adsorption. Besides "PEGylation", ω-functionalized thiol surfactants with free carboxylic acid groups are a versatile type of ligand and are often used in aqueous solution. They offer an additional anchor point for further attachments of biological molecules. Herein we chose 11-mercaptoundecanoic acid (MUDA). On the one hand, a new bond between Au and S with high affinity is built upon transfer, ensuring a complete replacement of citrate due to strong binding affinities. On the other hand, the free carboxylic acid can serve as an anchor for further coupling reactions with amines. In addition, the long alkyl chain provides enough flexibility for the active moiety to interact multivalently with the receptor. The ligand exchange with MUDA giving NP 2 proceeded completely as it is indicated in the infra-red (IR) spectra (Fig. 2).

The final step towards the fully functionalized nanoparticle was accomplished by peptide coupling with EDC (1-ethyl-3-(3-dimethylaminopropyl)carbodiimide) and NHS (*N*-hydroxy-succinimide). The free carboxylic acid is activated by EDC and forms with NHS *in situ* a so called 'active ester'. This reacts easier with amine moieties of *e.g.* amino acids or peptides. Although the prepared NHS ester is sufficiently stable for the reaction, it hydrolyses within hours depending on the pH of the reaction solution. To ensure the coupling, another equivalent of histamine, EDC and NHS were added after two hours. The excess of coupling agents and byproducts of the reaction were removed by purification with dialysis against water (MWCO 3500, three times). The characterization of the synthesized and functionalized nanoparticles NP 1–3 was per-

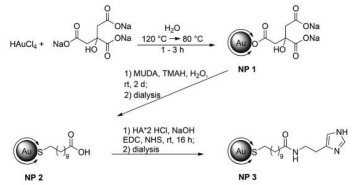

Fig. 1 Synthetic procedure for gold nanoparticles with a mean diameter of 14 nm (NP 1) followed by ligand exchange with 11-mercaptoundecanoic acid (NP 2) and functionalization with histamine (NP 3, Au–MUDA–HA). Double arrows at the Au core represent the ligand.

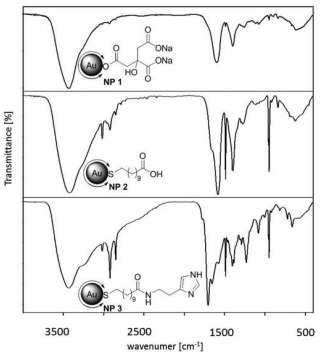

Fig. 2 IR spectra of (a) Au–Citrate NP 1, (b) Au–MUDA NP 2 and (c) Au–MUDA–HA NP 3; vibration for the amide bond is found at 1641 cm^{-1}.

Open Access Article. Published on 20 August 2015. Downloaded on 8/22/2018 9:27:06 AM.
This article is licensed under a Creative Commons Attribution 3.0 Unported Licence.

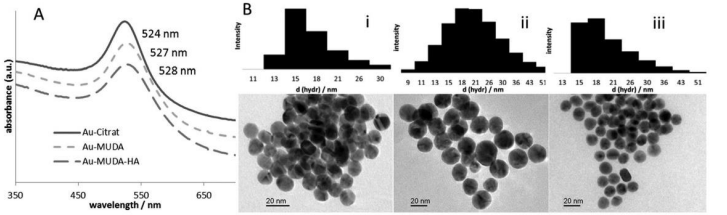

Fig. 3 (A) UV/Vis spectra of the stepwise functionalization of Au–Citrate NP 1, Au–MUDA NP 2 and Au–MUDA–HA NP 3 nanoparticles. (B) TEM images and DLS measurements with values for the distribution of the hydrodynamic diameters of (i) Au–Citrate NP 1 d = 14.0 ± 0.9 nm, d_{hydr} = 16.7 ± 3.0 nm, (ii) Au–MUDA NP 2 d = 14.5 ± 1.2 nm, d_{hydr} = 24.1 ± 6.7 nm and (iii) Au–MUDA–HA NP 3 d = 14.3 ± 0.7 nm, d_{hydr} = 19.3 ± 2.9 nm; d = diameter.

formed with different methods. For the characterization of the core transmission electron microscope (TEM) images, dynamic light scattering (DLS) measurements and UV/Vis spectroscopy were used. The images shown in Fig. 3 indicate that the synthesized nanoparticles have mostly a spherical shape; the average diameter determined by TEM is 14.0 ± 0.9 nm. The hydrodynamic diameter of the nanoparticles in solution obtained by DLS measurements was determined by 16.7 ± 3.0 nm. The absorption maximum was found at 524 nm. The position and form of the maximum is also a hint for the size of the nanoparticles, as it derives from a distinctive plasmon resonance at the gold surface depending on the shape of the material. The obtained data confirmed that the average diameter of the particles cores and the maxima of absorption remained unchanged after ligand exchange reaction and functionalization. The slight shift can be explained due to the new ligand. The affinity to a gold surface is higher for thiolated ligands than for citrate and therefore effects on the plasmon resonance of the particle. Nonetheless, neither the exchange of the ligands nor the purification *via* dialysis had an effect on the agglomeration state. Also the functionalization at the ligand periphery did not alter the particles significantly. In addition to these methods, the success of the ligand exchange was verified by IR spectroscopy (Fig. 2). Identification of the newly formed amide bond at 1641 cm^{-1} gives evidence for the successful coupling. Again the colloidal solution was purified by dialysis. Unlike the particles with MUDA as ligand shell, the final functionalization with histamine provides a good stability at physiological pH value and in a standard buffer solution for the Ussing chamber experiments (see below). The number of the ligands at the surface determined by TGA is about 10 000 for 14 nm gold nanoparticles, however determination is difficult due to small amounts of product. In order to find out whether the size of the nanoparticles could be a limiting factor for their properties, two other sizes were investigated. Following the same synthetic procedure as described above but with different reaction conditions, 25 nm nanoparticles were obtained. Also, 7 nm nanoparticles were prepared using dodecanethiol-protected particles from the Stucky method as basic material.[21]

As a negative control for the biochemical application, gold nanoparticles NP 4 (Fig. 4) with a sulfated ligand shell were

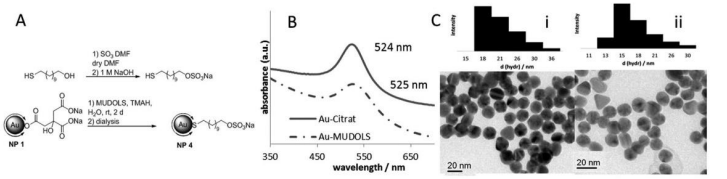

Fig. 4 (A) Synthetic procedure for the preparation of Au–MUDOLS NP 4, (B) UV/Vis spectra of Au–Citrate NP 1 and Au–MUDOLS NP 4, (C) TEM images and DLS measurements with values for the distribution of the hydrodynamic diameters of (i) Au–Citrate NP 1 d = 14.0 ± 0.9 nm, d_{hydr} = 16.7 ± 3.0 nm, (ii) Au–MUDOLS NP 4 d = 14.3 ± 1.3 nm, d_{hydr} = 18.6 ± 2.5 nm; d = diameter.

Open Access Article. Published on 20 August 2015. Downloaded on 8/22/2018 9:27:06 AM.
This article is licensed under a Creative Commons Attribution 3.0 Unported Licence.

synthesized. We already reported from sulfated ligands for the inhibition of selectin binding.[22] A structurally similar and simple ligand is sulfated 11-mercaptoundecanol (MUDOLS), which can be immobilized on gold nanoparticles in the same way as mentioned before. Again citrate-stabilized gold nanoparticles NP 1 served as basic material.

The sulfated ligand was synthesized separately and then attached to the surface *via* ligand exchange reaction. TEM images, DLS measurements and UV/Vis spectra (Fig. 4) indicated that the colloidal solution was intact and the nanoparticles were stable. Sulfated nanoparticles showed excellent stability over a wide range of pH value due to interparticle repulsion through a negatively charged ligand shell. Unlike the unsulfated Au–MUDA particles they are perfectly stable at physiological pH.

When looking at multivalent effects, the monovalent ligand 3 (Fig. 5) also has to be investigated. Thus the complete ligand was synthesized separately. To prevent the formation of a disulfide bond between two molecules, the thiol moiety was protected with an acetyl group.

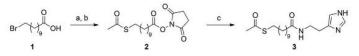

Fig. 5 Synthesis of the monovalent analogue AcS–MUDA–HA (3) starting from 11-bromoundecanoic acid 1. Reaction conditions: (a) KSOAc, DMF, 2 h, rt, (b) NHS, DCM, 18 h, rt, (c) EDC, HA·2HCl, NEt_3, DCM, 6 h, rt.

Functionality of the histamine-nanoparticles

From all the synthesized nanoparticles of different sizes, only the 14 nm nanoparticles yielded consistent effects on short-circuit current (I_{sc}) when they were administered to rat colonic mucosa mounted in Ussing chambers. Therefore, this type of particles was used for all subsequent experiments. To investigate the functionality of the Au–MUDA–HA nanoparticles, their ability to induce chloride secretion was compared with that of native histamine, which induces a strong chloride secretion across rat colonic epithelium.[15,16] Indeed, the histamine-conjugated nanoparticles induced a concentration-dependent increase in I_{sc}, which is a measure for net ion transport across the epithelium (Fig. 6).

These changes in I_{sc} reflect a secretion of chloride ions as they were abolished in Cl^--free buffer solution (Fig. 6). However, repetitive administration of these particles led to a desensitization of the tissue (Table 1). Thus in all subsequent experiments, each tissue was only exposed once to a single concentration of the Au–MUDA–HA nanoparticles (10^{-11} mol l^{-1} at the serosal side). The tissue conductance (G_t) was not significantly changed by the nanoparticles (10^{-11} mol l^{-1} at the serosal side); G_t amounted to 14.4 ± 1.87 mS cm^{-2} before and 14.7 ± 1.96 mS cm^{-2} after administration of the particles (n = 6; difference not significant). Viability of the tissue was also not impaired by the Au–MUDA–HA nanoparticles as both the Ca^{2+}-dependent secretagogue carbachol (5×10^{-5} mol l^{-1} at the serosal side), *i.e.* a stable derivative of acetylcholine,[23] as well as the cAMP-dependent secretagogue forskolin (5×10^{-6} mol l^{-1} at the mucosal and the serosal side), which stimulates the intracellular production of cAMP,[24] induced a prompt rise in I_{sc} in all tissues (Fig. 6). As the response to histamine evokes

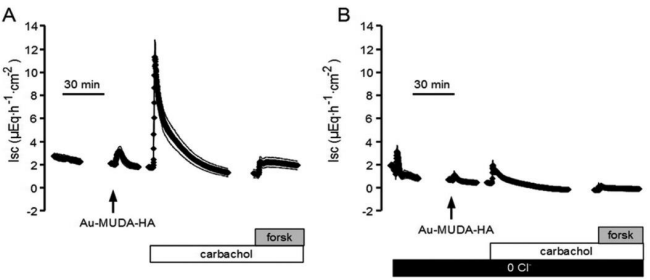

Fig. 6 Au–MUDA–HA (10^{-11} mol l^{-1} at the serosal side, arrow) induced an increase in I_{sc} (A), which was almost abolished in the absence of chloride (0 Cl^-; black bar, (B). At the end of the experiments, the secretagogues carbachol (5×10^{-5} mol l^{-1} at the serosal side, white bars) and forskolin (forsk; 5×10^{-6} mol l^{-1} at the mucosal and the serosal side, grey bars, (A and B), known to induce chloride secretion, were administered. Line interruptions are caused by omission of time intervals in order to synchronize the tracings of individual records to the administration of drugs. Values are means (symbols) ± SEM (parallel continuous lines), n = 6–8.

Open Access Article. Published on 20 August 2015. Downloaded on 8/22/2018 9:27:06 AM.
This article is licensed under a Creative Commons Attribution 3.0 Unported Licence.

Table 1 Effects of additive concentrations of Au–MUDA–HA 14 nm on I_{sc} and H_1 and H_2 receptors

	Increase in short-circuit current ΔI_{sc} (μEq h^{-1} cm^{-2})		
	Au–MUDA–HA 14 nm		
No inhibitor	1.09 ± 0.43^{b}	$0.61 \pm 0.11^{a,b}$	$0.42 \pm 0.11^{a,b}$
Mepyramine + cimetidine	0.083 ± 0.041^{a}	0.13 ± 0.033^{a}	0.13 ± 0.02^{a}

Cumulative administration of gradually increased concentrations (10^{-11}, 5×10^{-11}, 10^{-10} mol l^{-1}, at the serosal side) of Au–MUDA–HA induced an increase in I_{sc} concomitant with an obvious desensitization of the tissue as indicated by the reduced I_{sc} response after repeated administration. Given is the control response in the absence of any inhibitors and the response to Au–MUDA–HA in the combined presence of mepyramine (10^{-4} mol l^{-1} at the serosal side) and cimetidine (10^{-4} mol l^{-1} at the serosal side). Values are given as difference to the baseline in I_{sc} just before administration of the corresponding agonist (ΔI_{sc}) and are means ± SEM, $n = 6$. Different letters (a, b, c) indicate statistically homogenous groups (analysis of variances followed by *post hoc* test of Tukey).

chloride secretion in part *via* stimulation of histamine receptors located on submucosal neurons, the effect of the inhibitory neurotoxin tetrodotoxin, which inhibits the propagation of action potentials *via* blockade of voltage-dependent Na^+ channels, on the I_{sc} evoked by the Au–MUDA–HA nanoparticles was investigated.[16,25] Ideed, in the presence of tetrodotoxin (10^{-6} mol l^{-1} at the serosal side), the I_{sc} evoked by Au–MUDA–HA (10^{-11} mol l^{-1} at the serosal side) only amounted to 0.69 ± 0.20 μEq h^{-1} cm^{-2} ($n = 6$) in comparison to 2.92 ± 0.64 μEq h^{-1} cm^{-2} in untreated control tissues ($P < 0.05$, $n = 6$).

The response to native histamine is mediated by stimulation of histamine H_1 and histamine H_2 receptors.[16] In accordance with that observation, the increase in I_{sc} evoked by Au–MUDA–HA (10^{-11} mol l^{-1} at the serosal side) was strongly inhibited by a combination of the histamine H_1 receptor blocker, mepyramine (10^{-4} mol l^{-1} at the serosal side), and the histamine H_2 receptor blocker, cimetidine (10^{-4} mol l^{-1} at the serosal side, Table 1). Mepyramine is a substituted ethylamine derivative, whereas cimetidine has an imidazole ring system similar to native histamine.[26] Both drugs act as competitive inhibitors of the G-protein coupled histamine receptors type 1[26] and type 2,[27] respectively.

Viability of the tissue was not altered, as forskolin, the activator of adenylate cyclase(s),[24] evoked an increase in I_{sc} of 11.90 ± 1.10 μEq h^{-1} cm^{-2} ($n = 6$) in the absence and of 10.72 ± 1.18 μEq h^{-1} cm^{-2} ($n = 6$, difference not significant) in the presence of the histamine receptors antagonists.

Controls with histamine-free nanoparticles

In order to make sure that the effects of the nanoparticles are not unspecific artefacts resulting from the assembly components of the particles, controls were performed either with the conjugator AcS–MUDA–HA or with the sulfated moiety Au–MUDOLS. As shown in Fig. 7, these components failed to induce a rise in I_{sc}. Furthermore, Au–MUDOLS impaired the viability of the epithelium as it prevented the secretion induced by a subsequent administration of forskolin (5×10^{-6} mol l^{-1} at the mucosal and the serosal side).

Potency of the Au–MUDA–HA nanoparticles

The highest changes in the I_{sc} or the G_t induced by the nanoparticles were obtained at the concentration 10^{-11} mol l^{-1}. For the I_{sc}, the change amounted to 1.09 ± 0.42 μEq h^{-1} cm^{-2}. When comparing this response with a concentration-response curve of native histamine (Fig. 8) it turned out that a comparable increase in I_{sc} (1.05 ± 0.24 μEq h^{-1} cm^{-2}) was obtained with histamine in a concentration of 10^{-5} mol l^{-1} (Fig. 8B). Assuming a maximum of 10 000 histaminic units at the surface determined by TGA, the relative potency is still some magnitudes higher. In other words, the conjugation to the 14 nm nanoparticles strongly enhanced the potency of histamine to evoke anion secretion.

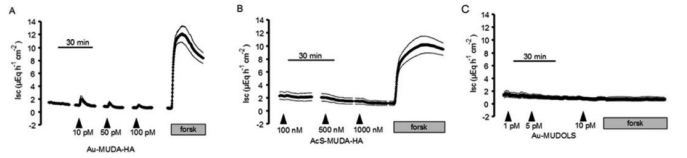

Fig. 7 Au–MUDA–HA (10^{-11}, 5×10^{-11}, 10^{-10} mol l^{-1}, administered cumulatively at the serosal side, arrows) induced an increase in I_{sc}. (B) AcS–MUDA–HA (10^{-7}, 5×10^{-7}, 10^{-6} mol l^{-1}, at the serosal side, arrows) was ineffective. (C) Au–MUDOLS (10^{-12}, 5×10^{-12}, 10^{-11} mol l^{-1}, at the serosal side, arrows) failed to change the I_{sc}. All particles except Au–MUDOLS preserved the secretory function of the tissues as they did not impair the effect of the secretagogue forskolin (forsk; 5×10^{-6} mol l^{-1} at the mucosal and the serosal side, grey bars). Values are means (symbols) ± SEM (parallel continuous lines), $n = 4–8$.

This journal is © The Royal Society of Chemistry 2015

Open Access Article. Published on 20 August 2015. Downloaded on 8/22/2018 9:27:06 AM.
This article is licensed under a Creative Commons Attribution 3.0 Unported Licence.

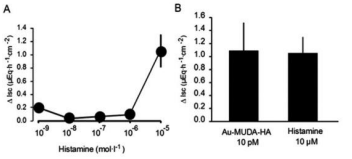

Fig. 8 (A) Histamine induced a concentration-dependent increase in I_{sc}. (B) Shows the potency of Au–MUDA–HA *versus* histamine; an equivalent potency between Au–MUDA–HA and histamine was obtained with 10^{-11} mol l^{-1} and 10^{-5} mol l^{-1}, respectively. Values are given as increase in I_{sc} above baseline in short-circuit current (ΔI_{sc}) just before administration of the corresponding drug and are means ± SEM, n = 6–8.

Conclusion

The gold nanoparticles with an average diameter of 14 nm were loaded with the histamine derivative and showed excellent activation properties in the Ussing chamber experiments. Compared to native histamine, the nanoparticles were more effective at extremely low concentrations. It was found that the newly developed conjugate was able to induce a concentration-dependent chloride secretion across rat colonic epithelium *via* stimulation of histamine H_1 and H_2 receptors. These receptors, which are composed of 487 or 359 amino acids, respectively, belong to the class of G-protein coupled receptors with seven transmembrane spanning regions. Upon binding of the agonist, these receptors induce the exchange of guanosine diphosphate (GDP) against guanosine triphosphate (GTP) at the a-subunit of trimeric GTP-binding proteins. The consequence is the dissociation of the G-protein in the GTP-binding a-subunit and a b/g-complex and the activation of intracellular enzymes such as phospholipase C or adenylate cyclase, which then activate intracellular second messenger pathways.[28] An explanation for this stimulation might be the high local density of the immobilized ligand. The molecular recognition between the receptors on the surface and ligands bound to the nanoparticles is strengthened through the geometric arrangement given by the spherical shape. The density of the binding moieties allows simultaneous binding resulting in a lower activation concentration.[29] The interaction can be blocked with same inhibitors used for native histamine. To ensure the response originated only from multivalent histamine supported on gold nanoparticles and not from any unspecific interactions with the biological tissue, the monovalent ligand AcS–MUDA–HA or the gold nanoparticles with a simple sulfated moiety from 11-mercaptoundecanol were synthesized and tested in parallel. Indeed, no chloride secretion could be observed. All particles tested in this study preserved the basic functions of the tissues except for Au–MUDOLS. Only the particles with the sulfated moiety harmed the tissues irreversibly. Among the three sizes of particles tested (7 nm, 14 nm and 25 nm), only the intermediate size 14 nm showed consistent effects on transepithelial Cl^- secretion, indicating a size-dependence. The smaller nanoparticles exhibited unspecific interactions whereas the bigger particles evoked no signal in the Ussing chamber experiments. The observed size dependence might correlate with the number of histamine molecules at the surface. The density of immobilized histamine moieties at 14 nm core size and the spatial arrangement are both essential for the activation of histaminic receptors bound on an epithelium. For a detailed insight into the mechanisms of receptor activation further experiments will be conducted on the ligand–receptor-complex which is formed during the activation process. But also the length of the spacer between the particle core and the active moiety influences the interplay, as it was shown in one of our previous studies on multivalent interactions of gold nanoparticles in selectin binding.[22] Further investigations shall be conducted on this influence. In summary the present work is another example for the influence of multivalent interactions in biological systems. This concept can also be transferred to other receptor antagonists and to different neurotransmitters.

Experimental section

All reactions of nanoparticles in aqueous solution were carried out in purified Millipore water. Organic solvents were distilled before use. All chemicals were purchased from commercial sources and used as received. The ligand exchange reactions and coupling reactions were done under inert conditions. All glass vessels were washed with aqua regia and distilled water prior to use. NMR spectra were recorded on Bruker BioSpin Avance III AV600 (600 MHz), AV400 (400 MHz) or AV200 (200 MHz) spectrometers using tetramethylsilane (TMS) as an internal standard with chemical shifts given in ppm relative to TMS (δ = 0.00 ppm) or the respective solvent peaks. ^{1}H NMR data are reported as follows: chemical shifts (multiplicity [ppm], coupling constants [Hz], integration, classification). Multiplicity is recorded as s = singlet, br s = broadened singlet, d = doublet, t = triplet, q = quartet, m = multiplet. For ^{13}C NMR, chemical shifts and structural assignments are reported where applicable. Because of the rigidity of the alkyl chains in the thiol shells and the resulting large differences in the relaxation times of different protons, no integrals are given for the proton NMR data of the gold colloids. IR spectra were obtained on a Bruker IFS48 spectrometer in ATR mode. Electrospray ionization mass spectra (ESI-MS) were recorded on a Finnigan LCQDuo spectrometer using methanol solutions of the respective. TEM measurements were performed on a Philips CM30 STEM (300 kV, LaB6-cathode) equipped with a GATAN digital camera. TEM images were recorded using a digital micrograph. The average particle core sizes were determined by measuring at least 100 individual particles from recorded TEM images. The UV/Vis spectra were plotted with an Agilent 8453 spectrophotometer (Agilent Technologies Inc., Santa

Open Access Article. Published on 20 August 2015. Downloaded on 8/22/2018 9:27:06 AM.
This article is licensed under a Creative Commons Attribution 3.0 Unported Licence.

Clara, CA, USA). Dynamic light scattering measurements were performed with a StabiSizer PMX 200C from Particlemetrix (Meerbusch, Germany).

Chemical syntheses

Citrate-coordinated gold nanoparticles NP 1 (Au–Citrate Ø 14 nm). Citrate-coordinated gold nanoparticles were synthesized by a variation of a procedure first published by Turkevich. A solution of 50 mg (0.127 mmol) $HAuCl_4 \cdot 3H_2O$ in 195 mL of Millipore water was heated to reflux for 20 min. Under vigorous stirring a solution of 224 mg (0.52 mmol) of sodium citrate in 5 mL of Millipore water was added quickly. The reaction mixture was held at 80 °C for 2 h. Then the solution was cooled to 0 °C in an ice bath and filtered (0.2 μm pore size). A clear red solution with a particle concentration of 2.7 nM was obtained and stored at 4 °C.

^{1}H NMR (400 MHz, D_2O): δ/ppm = 2.61 (bs, CH_2); IR (KBr disc, ν/cm^{-1}): 3426.8 (νO–H), 1598.2 (νC=O), 1397.6, 1258.4, 618.0; TEM: d = 14.0 ± 0.9 nm; UV/Vis: λ_{max} = 522 nm; DLS: d_{hydr} = 16.7 ± 3.0 nm.

11-Mercaptoundecanoic acid coordinated gold nanoparticles NP 2 (Au–MUDA Ø 14 nm). An amount of 21 mg 11-mercaptoundecanoic acid (0.1 mmol, 10^5 equiv.) was dissolved in 8.5 mL Millipore water under the addition of 50 μL tetramethylammonium hydroxide (TMAH). 5 mL of a 2.7 nM solution of citrate-protected gold nanoparticles in water was added dropwise and the solution was stirred for 24 h. The nanoparticles solution was dialysed against 300 mL water three times (3500 MWCO). A clear red solution with a particle concentration of 1 nM was obtained and stored at 4 °C.

^{1}H NMR (400 MHz, D_2O): 3.17 (s, 16H, TMAH), 2.76 (t, CH_2), 2.16 (t, CH_2), 1.73 (quin, CH_2), 1.54 (m, CH_2), 1.40 (m, CH_2), 1.30 (bs, CH_2); IR (KBr disc, ν/cm^{-1}): 3422.8, 3018.5, 2920.1 & 2849.8 (νC–H), 1583.5 (νC=O), 1487.9, 1396.2, 1274.9, 956.8, 948.2, 625.0; TEM: d = 14.5 ± 1.2 nm, UV/Vis: λ_{max} = 527 nm, DLS: d_{hydr} = 24.1 ± 6.7 nm.

Sodium 11-mercaptoundecyl sulfate coordinated gold nanoparticles NP 4 (Au–MUDOLS Ø 14 nm). An amount of 30 mg 11-mercaptoundecanyl sulfate was dissolved in 8.5 mL Millipore water and 50 μL tetramethylammonium hydroxide (TMAH) was added. 5 mL of a 2.7 nM solution of citrate-protected gold nanoparticles in water was added dropwise and the solution was stirred for 24 h. The nanoparticles solution was dialysed against 300 mL water three times (3500 MWCO) and stored at 4 °C.

^{1}H NMR (400 MHz, D_2O): δ/ppm = 4.00–3.89 (m, CH_2), 2.70–2.60 (m, CH_2), 1.68–1.51 (m, CH_2), 1.37–1.23 (m, CH_2); IR (KBr disc, ν/cm^{-1}): 2918.7 & 2849.9 (νC–H), 1614.8, 1470.0, 1261.7 & 1205.1 & 1128.1 (ν(R–OSO_2–OR), 1068.8, 966.4, 831.8, 718.9, 628.7, 586.3; TEM: d = 14.3 ± 1.3 nm; UV/Vis: λ_{max} = 525 nm; DLS: d_{hydr} = 18.6 ± 2.5 nm.

Synthesis of histamine functionalized gold nanoparticles NP 3 (Au–MUDA–HA Ø 14 nm). 10 mL of a 1 nM solution Au–MUDA were set in a glass vessel washed with aqua regia and distilled water. 18 mg histamine dihydrochloride (0.1 mmol), 17 mg EDC (0.11 mmol) and 15 mg HOBt (0.11 mmol) and 50 μL NEt_3 were added to the nanoparticle solution. The reaction mixture was stirred overnight and subsequently dialysed against water three times (3500 MWCO) and stored at 4 °C.

^{1}H NMR (400 MHz, D_2O): 7.55 (s, 1H, CH), 6.81 (s, 1H, CH), 2.73–2.86 (m, 2H, CH_2(HA)), 2.57–2.71 (m, 3H, CH_2(HA) + NH)), 2.41–2.53 (m, 2H), 2.21–2.34 (m, 4H), 2.10–2.21 (m, 3H), 2.03 (t, J = 7.7, 1H), 1.52–1.68 (m, 1H), 1.36–1.48 (m, 1H), 1.18 (bs, 8H, CH_2), IR (KBr disc, ν/cm^{-1}): 3018.8, 2921.4 & 2850.0 (νC–H), 1641.1 (νC=O, amide), 1596.3 (νCO–NH), 1488.2, 1404.2, 957.1, 948.6, TEM: d = 14.3 ± 0.7 nm, UV/Vis: λ_{max} = 528 nm, DLS: d_{hydr} = 19.3 ± 2.9 nm.

Sodium 11-mercaptoundecyl sulfate (MUDOLS). In a flame-dried vessel under argon atmosphere, 353 mg of 11-mercaptoundecanol (1.72 mmol, 1 equiv.) was dissolved in 3 ml dry DMF. Separately, 395 mg of SO_3·DMF complex (2.5 mmol, 1.5 equiv.) were dissolved in 1 mL dry DMF and added to the solution. After stirring for 1 h at room temperature the solvent was removed under reduced pressure (OPV) and the residue was dissolved in 4 mL of 1 M NaOH. A white precipitate appeared. 15 mL of ethanol were added and washed three times. The product was dried in vacuum. 280 mg of a colorless solid (0.91 mmol, 53%) could be obtained. The dimer was formed.

^{1}H NMR (200 MHz, DMSO-d_6): δ/ppm = 3.68 (t, J = 6.6 Hz, 2 H, CH_2), 3.35 (t, J = 6.3 Hz, 2H, CH_2), 2.27–2.61 (m, 4H, CH_2), 2.56–2.49 (m, 2H, CH_2), 1.67–1.52 (m, 4H, CH_2), 1.36–1.24 (m, 10H, CH_2); ^{13}C NMR (200 MHz, DMSO-d_6): δ/ppm = 65.6, 60.7, 32.5, 29.1, 29.0, 28.9, 28.8, 28.6, 28.5, 27.7, 25.5; ESI-MS: m/z = 633.1593 ([M + Na]$^+$, calcd 633.1612).

11-(Acetylthio)undecanoic acid (AcS–MUDA). 500 mg 11-bromoundecanoic acid (1.89 mmol, 1 equiv.) were dissolved in 70 mL absolute DMF under argon atmosphere. Separately 520 mg potassium thioacetate (4.56 mmol, 2.4 equiv.) were suspended in 8 mL absolute DMF under argon atmosphere and added dropwise to the first solution. The reaction mixture was stirred for 2 hours at room temperature. The precipitate was filtered off, washed several times with water and dried in vacuum. 414 mg of a colorless solid (1.59 mmol, 84%) could be obtained.

^{1}H NMR (200 MHz, $CDCl_3$): δ/ppm = 2.79 (t, J = 7.17, 2H, CH_2), 2.27 (t, J = 7.17, 2H, CH_2), 2.25 (s, 3H, CH_3), 1.61–1.52 (m, 2H, CH_2), 1.52–1.44 (m, 2H, CH_2), 1.32–1.16 (m, 12H, CH_2); ^{13}C NMR (100 MHz, $CDCl_3$): δ/ppm = 196.2 (C_{qt}, C=O, acetyl), 179.4, 33.9, 30.7, 29.5, 29.4, 29.3, 29.2, 29.1, 29.1, 29.0, 28.8, 24.7; ESI-MS: m/z = 283.1335 ([M + Na]$^+$, calcd 283.1344).

2,5-Dioxopyrrolidin-1-yl-11-(acetylthio)undecanoate (AcS–MUDA–NHS). 195 mg NHS (1.7 mmol, 1.1 equiv.) and 700 mg AcS–MUDA (1.55 mmol, 1 equiv.) were dissolved in DCM under stirring at room temperature. 350 mg DCC (1.7 mmol, 1.1 equiv.) were separately dissolved in 5 mL DCM and added slowly. After 30 min a white precipitate appeared. The reaction mixture was stirred overnight. The solvent was removed under reduced pressure. 506 mg (1.42 mmol, 92%) of a colorless powder were obtained.

^{1}H NMR (400 MHz, $CDCl_3$): δ/ppm = 2.81–2.77 (m, CH_2), 2.53 (t, J = 7.34, 2H, CH_2), 2.25 (s, 3H, CH_3), 1.71–1.63 (m, 2H, CH_2), 1.52–1.47 (m, 2H, CH_2), 1.38–1.17 (m, 12H, CH_2); ^{13}C

Open Access Article. Published on 20 August 2015. Downloaded on 8/22/2018 9:27:06 AM.
This article is licensed under a Creative Commons Attribution 3.0 Unported Licence.

NMR (100 MHz, $CDCl_3$): δ/ppm = 196.1 (C_q, C=O, acetyl), 169.3 (2 × C_q, C=O), 168.7 (C_q, C=O), 30.9 (CH_3), 30.7, 29.5, 29.3, 29.2, 29.2, 29.1, 29.0, 28.8, 28.7, 25.6 (2 × CH_2), 24.6; ESI-MS: m/z = 380.1502 ($[M + Na]^+$, calcd 380.1508).

***S*-(11-((2-(1*H*-Imidazol-4-yl)ethyl)amino)-11-oxoundecyl) ethanethioate 4 (AcS–MUDA–HA).** 97 mg AcS–MUDA (0.27 mmol, 1 equiv.) were dissolved in DMF to form a clear solution. 34 mg HA·2HCl (0.30 mmol, 1.1 equiv.) and a few drops NEt_3 were added and the solution was stirred overnight. Subsequently 50 mL water were added and a white solid appeared. The precipitate was filtered off and washed three times with water. The crude product was dissolved in $CHCl_3$, filtered again and purified *via* column chromatography ($CHCl_3$/MeOH 9/1 R_f = 0.7). After evaporation 70 mg (0.19 mmol, 70%) of a colorless powder were obtained.

^{1}H NMR (400 MHz, $CDCl_3$): δ/ppm = 7.50 (s, 1H, CH), 6.75 (s, 1H, CH), 6.33 (br s, 1H, NH), 3.52–3.42 (m, 2H, CH_2(HA)), 2.79–2.69 (m, 2H, CH_2(HA)), 2.53–2.39 (m, 2H, CH_2), 2.56 (s, 3H, CH_3), 2.10 (t, J = 7.24 Hz, 2H, CH_2), 1.59–1.43 (m, 4H, CH_2), 1.26–1.14 (m, 12H, CH_2); ^{13}C NMR (100 MHz, $CDCl_3$): δ/ppm = 196.4 (C_q, C=O, acetyl), 173.7 (C_q, C=O, amide), 134.8 (CH, C_{ar}), 127.6 (C_q, C_{ar}), 118.6 (CH, C_{ar}), 39.2 (CH_2(HA)), 36.9 (CH_2 (HA)), 30.7 (CH_3), 29.5, 29.3, 29.3, 29.2, 29.1, 28.7, 28.4, 26.9, 25.7; ESI-MS: m/z = 354.2221 ($[M + H]^+$, calcd 354.2210).

Animals

Female and male Wistar rats with a body mass of 200–250 g were used. The animals were bred and housed at the institute for Veterinary Physiology and Biochemistry of the Justus-Liebig-University Giessen at an ambient temperature of 22.5 °C and air humidity of 50–55% on a 12 h : 12 h light–dark cycle with free access to water and food until the time of the experiment. Experiments were approved by the named animal welfare officer of the Justus Liebig University (administrative number 487_M) and performed according to the German and European animal welfare law.

Solutions

The standard solution for the Ussing chamber experiments was a buffer solution containing (mmol l^{-1}): NaCl 107, KCl 4.5, $NaHCO_3$ 25, Na_2HPO_4 1.8, NaH_2PO_4 0.2, $CaCl_2$ 1.25, $MgSO_4$ 1 and glucose 12. The solution was gassed with carbogen (5% CO_2 in 95% O_2, v/v); pH was 7.4. For the Cl^--free buffer, NaCl and KCl were substituted by Na gluconate and K gluconate (KGluc), respectively. The Ca^{2+} concentration in the Cl^--free buffer was increased to 5.75 mmol l^{-1} to compensate for the Ca^{2+}-buffering properties of gluconate.[30]

Tissue preparation

Animals were killed by stunning followed by exsanguination. The serosa and tunica muscularis were stripped away by hand to obtain a mucosa–submucosa preparation of the distal colon. Briefly, the colon was placed on a small plastic rod with a diameter of 5 mm. A circular incision was made near the anal end with a blunt scalpel, and the serosa together with the tunica muscularis was gently removed in a proximal direction. Two segments of the distal colon of each rat were prepared.

Short-circuit current measurements

The mucosa–submucosa preparation was fixed in a modified Ussing chamber bathed with a volume of 3.5 ml on each side of the mucosa. The tissue was incubated at 37 °C and short-circuited by a computer-controlled voltage-clamp device (Ingenieur Büro für Mess- und Datentechnik Mussler, Aachen, Germany) with correction for solution resistance. Tissue conductance (G_t) was measured every minute by the voltage deviation induced by a current pulse (±50 μA, duration 200 ms) under open-circuit conditions. Short-circuit current (I_{sc}) was continuously recorded on a chart-recorder. I_{sc} is expressed as μEq h^{-1} cm^{-2}, *i.e.* the flux of a monovalent ion per time and area, with 1 μEq h^{-1} cm^{-2} = 26.9 μA cm^{-2}. At the end of each experiment, tissue viability was tested by administration of the cholinergic agonist, carbachol (5 × 10^{-5} mol l^{-1} at the serosal side) and/or the administration of forskolin (5 × 10^{-6} mol l^{-1} at the mucosal and the serosal side), an activator of adenylate cyclase(s), which induce a strong Ca^{2+}-respective cAMP-dependent Cl^- secretion.[23,24]

Drugs

Au–MUDOLS, Au–MUDA–HA, carbachol, cimetidine, histamine dihydrochloride, and mepyramine were dissolved in aqueous stock solutions. Forskolin (Calbiochem, Bad Soden, Germany) was dissolved in ethanol (final maximal concentration 0.25%, v/v). Tetrodotoxin was dissolved in 2 × 10^{-2} mol l^{-1} citrate buffer. If not indicated otherwise, drugs were from Sigma, (Taufkirchen, Germany).

Statistics

Results are given as means ± SEM, with the number (n) of investigated tissues. When means of several groups had to be compared, an analysis of variance was performed followed by *post hoc* Tukey's-test. For the comparison of two groups, a Mann-Whitney *U*-test was applied. $P < 0.05$ was considered to be statistically significant.

Acknowledgements

We wish to acknowledge Anne Schulze (Institute of Inorganic and Analytical Chemistry, Justus-Liebig-University at Giessen) for the TEM images.

References

1 H. Goesmann and C. Feldmann, *Angew. Chem., Int. Ed.*, 2010, **49**, 1362.
2 K. Park, *ACS Nano*, 2013, **7**, 7442.
3 R. Shenhar and V. M. Rotello, *Acc. Chem. Res.*, 2003, **36**, 549.
4 M.-C. Daniel and D. Astruc, *Chem. Rev.*, 2004, **104**, 293.

Open Access Article. Published on 20 August 2015. Downloaded on 8/22/2018 9:27:06 AM.
This article is licensed under a Creative Commons Attribution 3.0 Unported Licence.

5 S. Panigrahi, S. Basu, S. Praharaj, S. Pande, S. Jana, A. Pal, S. Ghosh and T. Pal, *J. Phys. Chem. C*, 2007, **111**, 4596.
6 M. Mammen, S.-K. Choi and G. M. Whitesides, *Angew. Chem., Int. Ed.*, 1998, **110**, 2908.
7 C. Fasting, C. A. Schalley, M. Weber, O. Seitz, S. Hecht, B. Koksch, J. Dernedde, C. Graf, E.-W. Knapp and R. Haag, *Angew. Chem., Int. Ed.*, 2012, **51**, 10472.
8 J. E. Gestwicki, C. W. Cairo, L. E. Strong, K. A. Oetjen and L. L. Kiessling, *J. Am. Chem. Soc.*, 2002, **124**, 14922.
9 J. Dernedde, S. Enders, H.-U. Reissig, M. Roskamp, S. Schlecht and S. Yekta, *Chem. Commun.*, 2009, 932.
10 M. Paolino, L. Mennuni, G. Giuliani, M. Anzini, M. Lanza, G. Caselli, C. Galimberti, M. C. Menziani, A. Donati and A. Cappelli, *Chem. Commun.*, 2014, **50**, 8582.
11 M.-C. Saada, J.-L. Montero, D. Vullo, A. Scozzafava, J.-Y. Winum and C. T. Supuran, *J. Med. Chem.*, 2011, **54**(5), 1170.
12 M. Böhme, M. Diener and W. Rummel, *Pflügers Arch. Eur. J. Physiol.*, 1991, **419**, 144.
13 R. Greger, *Annu. Rev. Physiol.*, 2000, 467.
14 Y. Z. Wang and H. J. Cooke, *Gasterointest. Liver Physiol.*, 1990, **258**, 887.
15 G. Schultheiss, B. Hennig, W. Schunack, G. Prinz and M. Diener, *Eur. J. Pharmacol.*, 2006, **546**, 161.
16 A. Bell, M. Althaus and M. Diener, *Pflügers. Arch. Eur. J. Physiol.*, 2015, **467**, 1809.
17 J. Turkevich, P. C. Stevenson and J. Hillier, *Discuss. Faraday Soc.*, 1951, **11**, 55.
18 J. Wilcoxon, *J. Phys. Chem. B*, 2009, **113**(9), 2647.
19 S.-Y. Lin, Y.-T. Tsai, C.-C. Chen, C.-M. Lin and C.-h. Chen, *J. Phys. Chem. B*, 2004, **108**(7), 2134.
20 R. P. Briñas, M. Maetani and J. J. Barchi, *J. Colloid Interface Sci.*, 2013, **392**, 415.
21 N. Zheng, J. Fan and G. D. Stucky, *J. Am. Chem. Soc.*, 2006, **128**, 6550.
22 M. Roskamp, S. Enders, F. Pfrengle, S. Yekta, V. Dekaris, J. Dernedde, H.-U. Reissig and S. Schlecht, *Org. Biomol. Chem.*, 2011, **9**, 7448.
23 D. Strabel and M. Diener, *Eur. J. Pharmacol.*, 1995, **274**, 181.
24 R. J. Bridges, W. Rummel and B. Simon, *N. S. Arch, Pharmacol.*, 1983, **323**, 355.
25 F. Hug, M. Diener and E. Scharrer, *Z. Ernahrungswiss.*, 1996, **35**, 323.
26 J. C. Garrison and T. W. Rall, in *Goodmann and Gilman's The Pharmacological Basis of Therapeutics*, ed. A. G. Gilman, T. W. Rall, A. S. Nies and P. Taylor, Pergamon Press, New York, 8th edn, 1990, p. 574.
27 L. L. Brunton, in *Goodmann and Gilman's The Pharmacological Basis of Therapeutics*, ed. A. G. Gilman, T. W. Rall, A. S. Nies and P. Taylor, Pergamon Press, New York, 8th edn, 1990, p. 897.
28 P. Panula, P. L. Chazot, M. Cowart, R. Gutzmer, R. Leurs, W. L. S. Liu, H. Stark, R. L. Thurmond and H. L. Haas, *Pharmacol. Rev.*, 2015, **67**(3), 601.
29 C. W. Cairo, J. E. Gestwicki, M. Kanai and L. L. Kiessling, *J. Am. Chem. Soc.*, 2002, **124**, 1615.
30 J. Kenyon and W. R. Gobbins, *J. Gen. Physiol.*, 1977, **70**, 635.

8.10 "Potentiation of the activation of cholinergic receptors by multivalent presentation of ligands supported on gold nanoparticles"

Mattern A, F Machka MS, Wickleder OS, Ilyaskina M, Bünemann M, Diener M, **Pouokam E** *Organ. Biomol. Chem.* **16** (6684): 6680-6687.

Impakt Faktor: 3.423

Eigener Anteil an der Publikation:

- Initiative: 80 %
- Projektplanung: 70 %
- Durchführung der Versuche: 35 %
- Auswertung der Experimente: 40 %
- Erstellung der Publikation: 75 %

Published on 29 August 2018. Downloaded by UNIVERSITAT GIESSEN on 1/23/2019 9:52:34 AM.

Organic & Biomolecular Chemistry

PAPER

View Article Online
View Journal | View Issue

Check for updates

Cite this: Org. Biomol. Chem., 2018, 16, 6680

Potentiation of the activation of cholinergic receptors by multivalent presentation of ligands supported on gold nanoparticles

A. Mattern,[a] F. Machka,[b] M. S. Wickleder,[a] O. S. Ilyaskina,[c] M. Bünemann,[c] M. Diener[d] and E. Pouokam ★[d]

Gold nanoparticles (NP) with a functionalized ligand shell offer the possibility to potentiate the action of agonists at the receptor site by multivalency. In order to find out whether this can be realized for the pharmacologically important class of cholinergic receptors known to be involved in the regulation of most organ functions, carbachol-functionalized gold NPs (Au-MUDA-CCh) with an average diameter of 14 nm were synthesized. As functional read-out, cholinergic agonist-induced anion secretion was measured as increase in short-circuit current (I_{sc}) across rat proximal colon in Ussing chambers. Similarly to the corresponding native agonist acetylcholine, Au-MUDA-CCh induced a concentration-dependent increase in I_{sc}, which represents chloride secretion across the epithelium. This response was inhibited by atropine and hexamethonium indicating the activation of muscarinic and nicotinic receptors by the functionalized NPs. A strong potentiation of ligand–receptor interaction was a key benefit of functionalized NPs over native agonists. This was observed with physiological approaches as measurements of changes in I_{sc} revealed a nearly equivalent response evoked by 1 pM Au-MUDA-CCh and 500 nM native CCh. To better determine this potentiation at the receptor level, pharmacological approaches based on the signaling cascade of ACh-induced activation of muscarinic receptors were used. FRET (Förster Resonance Energy Transfer) measurements performed on HEK293T cells transiently transfected with M_3-R, $G\alpha_q$-YFP, $G\beta_1$-wt and CFP-$G\gamma_2$, revealed that both Au-MUDA-CCh and native CCh activated G-proteins with EC_{50} amounting to 127 ± 0.44 fM and 224 ± 7.12 nM, respectively. Thus, the functionalization of the NPs with CCh yields a potentiation by over 10^6, a property that could find usage in specific targeting, activation and compensation of pathologically reduced expression of receptors of interest.

Received 15th July 2018,
Accepted 28th August 2018
DOI: 10.1039/c8ob01686k
rsc.li/obc

Introduction

The field of NPs is a highly interdisciplinary field which is rapidly evolving, as they represent an interesting and applicable tool for many applications. In the year 2000 the number of publications pertaining to "nanoparticles" was less than 2100. Ten years later almost 25 000 publications focused on this area.[1] Nanoparticles are a good strategy to overcome biological barriers such as the brain blood barrier or the intestinal epithelium. They also offer the possibility to enhance ligand–receptor interaction by multivalency, *i.e.* the simultaneous operation of multiple molecular recognition events between two structures. The potential applications of NPs are enormous, not only for biological purpose. They can be used for cellular and molecular dynamics, for *in vivo* or live imaging, for improving contrast agents or as quantum dots for example in combination with magnetic resonance imaging.[2,3]

In this work, we chose to use gold NPs because of their robust synthesis and easily functionalizable surface. In addition to these properties, gold NPs possess high biocompatibility.[4] Therefore, it is essential to accurately characterize the synthesized and functionalized nanoparticles. Their properties in biological systems are easily influenced by their shape, size and functionalization.

The surface structure of gold NPs plays an important role in the appearance of particles within the body. Citrate-stabilized gold NPs are mainly localized at the endosomes of the cells.[5] However, amine-functionalized gold NPs possess a positive surface charge and interact with negatively charged nucleic acids, conferring on them a higher potential of gene transfection.[6] With diverse functionalized gold NPs, targeted localiz-

[a]Institute of Inorganic Chemistry, University of Cologne, Cologne, Germany
[b]Institute of Inorganic and Analytical Chemistry, Justus Liebig University, Giessen, Germany
[c]Institute for Pharmacology and Pharmacy, Philipps University, Marburg, Germany
[d]Institute for Veterinary Physiology and Biochemistry, Justus Liebig University, Giessen, Germany. E-mail: Ervice.Pouokam-Kamgne@vetmed.uni-giessen.de

This journal is © The Royal Society of Chemistry 2018

Published on 29 August 2018. Downloaded by UNIVERSITAT GIESSEN on 1/23/2019 9:52:34 AM.

ation of the particles in different cell organelles can be achieved. In this way, bio-imaging[7] and targeted drug delivery could be realised[8] improving therapeutics. With gold NPs, a multitude of diseases can be diagnosed and treated. Furthermore, NPs possess a large surface-to-volume ratio and therefore they can be loaded with an abundant amount of the active compound. Stable gold NPs are good candidates for biological or medical applications. Carbachol (CCh) unlike acetylcholine is resistant against acetylcholinesterase and more stable in aqueous solutions. As carbachol is used therapeutically to treat glaucoma or to stimulate motility of the gastrointestinal or the urogenital tract, CCh-coated nanoparticles which retain their pharmacological properties might be of potential interest.

The architectural concept of the NPs used in this work is based on our previous work,[9] that is the multivalent presentation of immobilized ligands, in this case the acetylcholine derivative carbachol. Such a presentation may result in drastic changes in the affinity of the ligand for the corresponding receptors. Here we report the influence of such a concept on the cholinergic receptors.

Results and discussion

Based on previous work by Gasiorek *et al.*,[9] 14 nm NPs showed consistent effects on short circuit current (I_{sc}). In this paper we report the three-step synthesis of carbachol-functionalized gold NPs, presenting an average size of 14 nm. Since they were synthesized for potential biological applications, it was necessary to obtain monodisperse nanoparticles. The established method by Turkevich *et al.*[10] promised good results in aqueous media. With a solvent system which closely mimicked *in vivo* conditions, a good biocompatibility might be expected.

Reaction temperature and duration affect particle size and shape as Gasiorek *et al.*[9] described previously. In this work, predominantly spherical NPs with a diameter of 14 nm were synthesized. NPs in aqueous media were stored at 4 °C to curb a future growth and aggregation of the NPs, which could be favored at higher temperatures due to a larger kinetic energy.[11]

Citrate itself acts as reducing agent as well as a stabilising ligand during this reaction. Because of its relatively weak reducing and stabilising character, the NPs synthesized by this method have comparatively large diameters. Due to weak electrostatic interactions between citrate ligands and particle surface, the NPs represent good starting particles for ligand exchange reactions.

Thiols are often used as suitable ligands for this type of reaction. This is due to the strong covalent Au–S-bond between ligands and core formed which results in a large affinity on the particle surface[12] allowing for a better stabilization. Thiol ligands with longer chain lengths also stabilize NPs due to steric interactions. In the present study, 11-mercaptoundecanoic acid (MUDA) was used as a bifunctional thiol linker. Its free carboxylic acid moiety can act as an anchor for coupling reactions in order to immobilize another molecule (such as a biogenic amine) at the ligand periphery. MUDA also possesses a flexible chain, which favors sterical stability. A ligand exchange was performed according to a procedure described by Gasiorek *et al.*;[9] an Au-citrate solution was stirred at room temperature and the new ligand was added in excess. The pH value was maintained at a basic environment (pH > 8) after the addition of TMAH. Subsequently, the reaction mixture was purified *via* dialysis against water (3 × 2 h with 300 ml, MWCO 3500).

Thereafter the functionalization of the NPs took place. *N*-(3-Dimethylaminopropyl)-*N*′-ethylcarbodiimide hydrochloride (EDC) and *N*-hydroxysuccinimide (NHS) were used as peptide coupling reagents to form an *in situ* active ester, which reacted with the amino units to form the corresponding amides. Here we used carbachol (CCh) as amine in place of acetylcholine the native ligand of cholinergic receptors, due to its stability as cholinergic agonist. To perform the reaction, coupling agents as well as the amine were added in excess to the Au-MUDA solution in order to guarantee functionalization (Fig. 1). To achieve a basic pH value, triethyl amine (NEt_3) was added. Subsequently, the solution was purified *via* dialysis against water (3 × 2 h with 300 ml, MWCO 3500). This yielded Au-MUDA-CCh as a clear pink solution.

CCh with a positive charge at the quaternary amine was considered to be rather difficult to immobilize. To prevent the solution from agglomeration, the pH value had to be controlled. A basic pH value during synthesis and throughout the purification process (*via* dialysis) guaranteed a stable nanoparticle solution and was necessary to obtain the desired results. The purified functionalized NP solution was stable above pH 5. At lower pH values like 4, NPs precipitated. Thus, the stability of the NP solution is guaranteed in the neutral pH range meaning under physiological conditions. As a consequence, such particles are suitable for biological applications.

All NP solutions were characterized with different methods. Several analyses were required in order to characterize the entire core–ligand-structure of the NP. With TEM and UV-Vis spectroscopy the size and the shape of the particle core was elucidated. With NMR and IR spectroscopy, the structure of the organic framework was analyzed. DLS measurements however provided information regarding the whole NP by measuring the hydrodynamic diameter. TEM images (Fig. 2B) of the carbachol-functionalized gold NPs showed monodisperse spherical particles with a diameter of 14.1 ± 0.8 nm. Moreover, TEM images indicate that no significant change in size and dispersity occurred during functionalization of the nanoparticles, when comparing to the other determined average diameters of Au-citrate (d_{TEM} = 13.9 ± 0.5 nm) and Au-MUDA (d_{TEM} = 14.1 ± 1.1 nm). Furthermore, the hydrodynamic diameter was not significantly influenced by functionalization of the nanoparticles. The hydrodynamic diameter of Au-MUDA-CCh was slightly larger than d_{TEM} with d_{hydr} = 15 ± 4 nm. The Polydispersity Index (PDI) indicates an estimation for the polydispersity of a sample.[13] PDI is defined as the square of the quotient of the standard deviation (σ) of the par-

View Article Online

Published on 29 August 2018. Downloaded by UNIVERSITAT GIESSEN on 1/23/2019 9:52:34 AM.

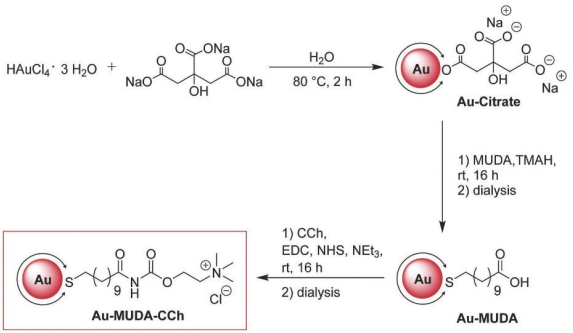

Fig. 1 Synthetic route of carbachol-functionalized gold NPs including the synthesis of Au-citrate NP(ø14 nm), followed by a ligand exchange reaction with 11-mercaptoundecanoic acid as a bifunctional thiol linker to Au-MUDA and functionalization with carbachol to Au-MUDA-CCh. Double-ended arrows surrounding the Au core represent the ligand.

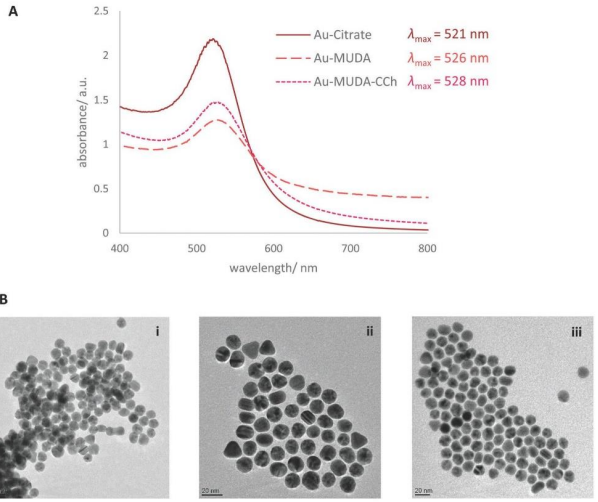

Fig. 2 (A) UV-Vis spectra of Au-citrate, Au-MUDA and Au-MUDA-CCh; (B) TEM images of (i) Au-citrate d = 13.9 ± 0.5 nm, (ii) Au-MUDA d = 14.1 ± 1.1 nm and (iii) Au-MUDA-CCh d = 14.1 ± 0.8 nm.

 This journal is © The Royal Society of Chemistry 2018

Published on 29 August 2018. Downloaded by UNIVERSITAT GIESSEN on 1/23/2019 9:52:34 AM.

ticle diameter distribution and the mean hydrodynamic diameter (d_{hydr}) [eqn (1)].[14] Au-MUDA-CCh has a PDI of 0.08.

$$PDI = \left(\frac{\sigma}{d_{hydr}}\right)^2 \quad (1)$$

Fig. 2A shows the UV-Vis spectra of different nanoparticle solutions. The absorption maximum of Au-citrate was at 521 nm. However, a slight shift was observed for Au-MUDA with λ_{max} = 526 nm after the ligand exchange reaction. As we described previously,[9] the plasmon resonance of the nanoparticles was affected by the new introduced thiol ligand. After functionalization with CCh, a minimal shift to λ_{max} = 528 nm was observed for Au-MUDA-CCh.

To prove the functionalization and analyse the ligands on the gold nanoparticle surface, NMR and IR were used. The ^{1}H NMR spectrum taken after the ligand exchange reaction to Au-MUDA has shown the different proton signals related to the new bifunctional thiol linker MUDA. Whereas the spectrum of Au-MUDA-CCh showed new signals above δ = 3 ppm which can be correlated to CCh. Especially the intensive singlet proton signal at δ = 3.15 ppm can be assigned to 9 H of the trimethyl ammonia unit of CCh. IR spectroscopy assisted in identifying the linking amide bond between the mercaptoacid MUDA and CCh as an amine. The characteristic amide bond band was found at 1640.8 cm^{-1}. Thus, the successful coupling could be proved.

Functionality of the CCh-nanoparticles

Based on our previous work[9] showing that 14 nm conjugated NPs yielded consistent effects on short-circuit current (I_{sc}) when they were administered to rat colonic mucosa mounted in Ussing chambers, we selected this size of particles for the

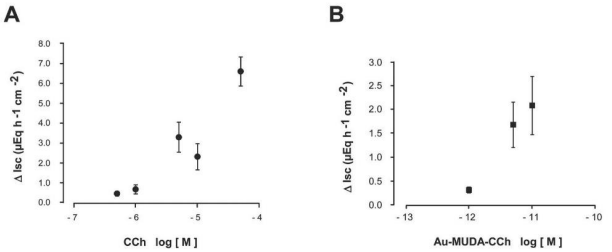

Fig. 3 Native CCh (A) and the Au-MUDA-CCh NP(B) induced a concentration-dependent increase in I_{sc}. Values are given as increase in I_{sc} above baseline in short-circuit current (ΔI_{sc}) just before administration of the corresponding drug and are means ± SEM, n = 6.

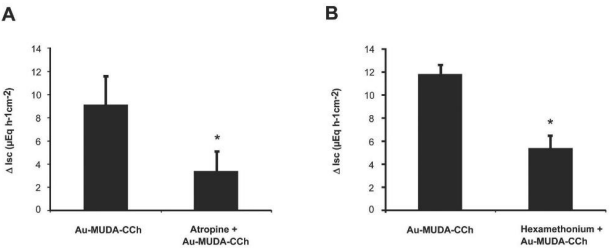

Fig. 4 The response induced by the Au-MUDA-CCh (10 pM, administered at the serosal side) was significantly inhibited in the presence of the muscarinic acetylcholine receptor blocker atropine (1 µM, at the serosal side, A) or in the presence of the nicotinic acetylcholine receptor blocker hexamethonium (100 µM, at the serosal side, B). Values are given as increase in I_{sc} above baseline in short-circuit current (ΔI_{sc}) just before administration of the corresponding drug and are means ± SEM, n = 6–7, *P < 0.05 (Mann–Whitney U-test).

Published on 29 August 2018. Downloaded by UNIVERSITAT GIESSEN on 1/23/2019 9:52:34 AM.

present studies. Therefore, the functionality of 14 nm Au-MUDA-CCh NPs was investigated. Carbachol, as stable derivative of ACh is known as a potent secretagogue, which activates chloride secretion across rat colonic epithelium.[15] In the present study, both native carbachol and the Au-MUDA-CCh NPs induce a concentration-dependent increase in I_{sc}, which is a measure for net ion (in this case chloride ions) transport across the epithelium (Fig. 3A and B).

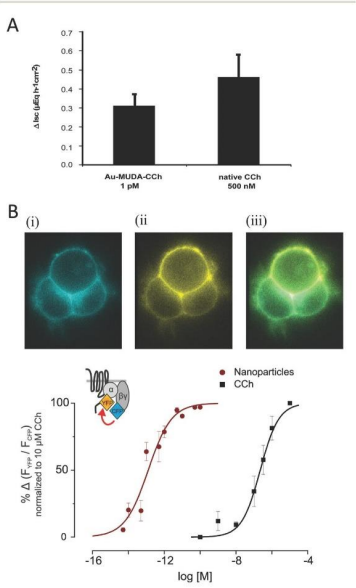

Fig. 5 (A) 0.5 μM native CCh and 1 pM Au-MUDA-CCh NP yielded approximately the same response in Ussing chambers experiments. (B) G_q activation *via* stimulating M_3-R with carbachol nanoparticles. The change of FRET ratio increment was normalized to 10 μM saturating carbachol concentration. The concentration response curves of $G\alpha_q$ activation by NP (EC_{50} 127 ± 0.44 fM, red) were found to be significantly left shifted in comparison to $G\alpha_q$ activation by carbachol (CCh) (EC_{50} 224 ± 7.12 nM, black). All concentration-response data are represented by the mean of at least 10 independent experiments ± SEM for each condition. Statistical analysis was performed by ANOVA with Bonferroni *post-hoc* test (*$P < 0.05$). The insets (i), (ii) and (iii) show YFP and CFP membrane staining. Images of transiently transfected (see Methods) HEK293T cells with CFP (i), YFP (ii) and overlay (iii) staining were taken using an inverted fluorescence microscope with a 100× oil immersion objective 100 ms exposure time, 2% YFP (500 nm) and/or CFP (425 nm) LEDs intensity.

As ACh or carbachol exert their physiological effects *via* activation of muscarinic (mAChR) or nicotinic (nAChR) acetylcholine receptors, it was of interest to prove whether the Au-MUDA-CCh NPs present the same specificity for those receptors. Pretreatment of the tissue with blockers of mAChR or nAChR, *i.e.* atropine (1 μM at the serosal side) or hexamethonium (100 μM at the serosal side), respectively, led to a strong reduction of the I_{sc} evoked by the Au-MUDA-CCh NPs (10 pM at the serosal side, Fig. 4A and B).

Very low concentrations of Au-MUDA-CCh NPs yielded consistent increase in the I_{sc}, indicating an increase in the potency of the native agonist. For example, 0.5 μM native CCh and 1 pM Au-MUDA-CCh NPs were found to be nearly equieffective (Fig. 5A). To better determine this potentiation, molecular approaches based on the signalling cascade of acetylcholine-induced activation of muscarinic receptors were used.

Potentiation of the native CCh-effects by CCh-conjugated nanoparticles

Muscarinic receptors are G protein-coupled receptors, amplifying extracellular signals *via* association/dissociation of the trimeric G proteins, consisting of α, β, and γ subunits. There are basically many variants of those subunits.[16] In the present work, the subunits $G\beta_1$-wt (wild type) and $G\gamma_2$ were used. The Gα subunit was conjugated to the yellow fluorescence protein (YFP) and the $G\gamma_2$ subunit to the cyan fluorescence protein (CFP). FRET (Förster Resonance Energy Transfer) measurements were then performed on HEK293T cells, transiently transfected with M_3-R, $G\alpha_q$YFP, $G\beta_1$-wt and CFP-$G\gamma_2$. Native CCh and Au-MUDA-CCh NP activated G_q proteins with EC_{50} amounting to 224 ± 7.12 nM and 127 ± 0.44 fM, respectively (Fig. 5B). Thus, the functionalization of the NPs with carbachol yields a potentiation by over 10^6 at the level of the addressed receptors. Considering a single gold core carries approximately 10 000 ligands[9] and only an area of the bead faces the receptor (s) at time, this potentiation may in fact be even stronger.

Conclusion

In summary, we were able to synthesize carbachol-coated gold NPs (Au-MUDA-CCh). Carbachol is a synthetic choline ester and positively charged quaternary ammonium compound that mimics the effects of the native ligand acetylcholine on nicotinic and muscarinic acetylcholine receptors. This acetylcholine derivative was chosen because of its stability and resistance to endogenous esterases such as acetylcholine esterase (AChE). This enzyme is the main limiting factor in acetylcholine's actions. The synthesized Au-MUDA-CCh NPs with a 14 nm size were specific for both acetylcholine receptors as their effects were inhibited by the well-known nicotinic and muscarinic receptor blockers hexamethonium and atropine, respectively. The multivalent presentation of the ligands as it was done in this work yields at least a 10^6-fold increase in the potency of the native monovalent ligand. As NPs may be engin-

 This journal is © The Royal Society of Chemistry 2018

Published on 29 August 2018. Downloaded by UNIVERSITAT GIESSEN on 1/23/2019 9:52:34 AM.

eered to target specific cells, tissues or organs, the present conjugated NPs may present an advantage for overcoming biological barriers and improve treatments for example an alternative in the therapy of myasthenia gravis, a neuromuscular disease characterized by muscle weakness due to reduced ligand release at the synapses and contra-productive cleavage of the native ligand ACh under physiological conditions by AChE. In our previous paper,[9] histamine NPs were used as proof of principle for multivalent stimulation of G-protein coupled receptors by functionalized nanoparticles. However, stimulation of histamine receptors is pharmacologically of no importance as these receptors mediate allergic reactions. This is different with cholinergic receptors, for which carbachol is a potent agonist. Carbachol is used medically in the therapy of glaucoma or to stimulate motility of the gastrointestinal or the urogenital tract, so carbachol-functionalized NPs might have therapeutic application.

Experimental section

All aqueous-based syntheses were performed in demineralized water. Organic solvents were distilled before use. All other chemicals were purchased from commercial sources and used as received. All glass vessels were washed with aqua regia and demineralized water prior to use. For dialysis of the NP solutions, membranes of regenerated cellulose "ZelluTrans" with different pore sizes by Carl Roth GmbH were used. The dialysis membrane was immersed in the solvent (demineralized water) for 30 min prior to use. All dialyses were performed at room temperature.

^{1}H NMR spectra were recorded on Bruker Avance II 400 MHz (AV II 400) und Bruker Avance III HD 400 MHz (AV III 400) spectrometers. Chemical shifts are given in ppm relative to respective solvent peaks. ^{1}H NMR data are reported as follows: chemical shifts (multiplicity [ppm], classification). Multiplicity is recorded as s = singlet, br s = broadened singlet, d = doublet, t = triplet, q = quartet, m = multiplet. IR measurements were performed on a Bruker ALPHA IR spectrometer utilizing KBr cells/Bruker IFS48 spectrometer in ATR mode. TEM images were taken on a Philips CM30/STEM (300 kV, LaB_6-cathode) equipped with a GATAN digital camera. For sample preparation, a 10 µl NP solution was placed on a carbon-coated copper grid. Determination of the average particle size and standard deviation was achieved by measuring 100 individual particles. Dynamic light scattering (DLS) measurements were performed with a STABISIZER® PMX-200 from Particlemetrix. UV/Vis spectra were recorded with an Agilent 8453 spectrophotometer (Agilent Technologies Inc.). Zeta-potentials were measured on a NanoZS by Malvern.

Chemical synthesis

Synthesis of citrate coordinated gold NPs (Au-citrate ∅ 14 nm). Citrate coordinated gold NPs were synthesized according to the procedure described by Turkevich *et al.*[10] $HAuCl_4 \cdot 3H_2O$ (50 mg, 0.13 mmol) was dissolved in water (195 ml) and heated under reflux for 20 min. A solution of sodium citrate dihydrate (224 mg, 0.76 mmol) in water (5 ml) was added quickly under vigorous stirring. The reaction mixture was stirred at 80 °C for 2 h before being cooled to 0 C and filtered (0.2 µm pore size). A clear red solution with a particle concentration of 7.5 nM was obtained and stored at 4 °C.

^{1}H NMR (400 MHz, D_2O): δ/ppm = 2.61 (bs, 4 H, CH_2); **IR** (KBr disc): ν/cm^{-1} = 3425.4 (ν_{O-H}), 1595.4 ($\nu_{C=O}$), 1249.3, 620.0; **TEM:** d = 13.9 ± 0.5 nm; **UV/Vis:** λ_{max} = 521 nm; **DLS:** d_{hydr} = 13 ± 3 nm; **ζ potential:** ζ = −35.9 ± 5.15 mV.

Ligand exchange synthesis of 11-mercaptoundecanoic acid coordinated gold NPs (Au-MUDA ∅ 14 nm). The ligand exchange reaction was performed according to the procedure described by Gasiorek *et al.*[9] 11-Mercaptoundecanoic acid (MUDA, 22 mg, 0.10 mmol) and tetramethylammonium hydroxide (TMAH, 50 µl, 0.55 mmol) were added to Au-citrate solution (10 ml) and stirred at room temperature for 16 h. The solution was purified *via* dialysis against water (3 × 2 h with 300 ml, MWCO 3500) to obtain a clear pink solution with a particle concentration of 7.5 nM which was stored at 4 °C.

^{1}H NMR (400 MHz, D_2O): δ/ppm = 2.60–2.52 (m, 2 H, CH_2), 2.35–2.23 (m, 2 H, CH_2), 1.95–1.91 (m, 4 H, CH_2), 1.36–1.05 (m, 12 H, CH_2); **IR** (KBr disc): ν/cm^{-1} = 3422.8, 3018.5, 2916.2 (ν_{C-H}), 2847.7 (ν_{C-H}), 1565.1 ($\nu_{C=O}$),1411.3; **TEM:** d = 14.1 ± 1.1 nm; **UV/Vis:** λ_{max} = 526 nm; **DLS:** d_{hydr} = 15 ± 3 nm; **ζ potential:** ζ = −36.5 ± 7.75 mV.

Synthesis of carbachol functionalised gold NPs (Au-MUDA-CCh ∅ 14 nm). Carbachol (CCh, 3 mg, 0.016 mmol), *N*-(3-dimethylaminopropyl)-*N'*-ethylcarbodiimide hydrochloride (EDC, 3 mg, 0.016 mmol), *N*-hydroxysuccinimide (NHS, 2 mg, 0.017 mmol) and triethyl amine (NEt_3, 50 µl, 0.36 mmol) were added to Au-MUDA solution (10 ml) and stirred at room temperature for 16 h. The clear pink solution was purified *via* dialysis against water (3 × 2 h with 300 ml, MWCO 3500) and stored at 4 °C.

^{1}H NMR (400 MHz, D_2O): δ/ppm = 4.48–4.42 (m, 2 H, CH_2), 3.67–3.62 (m, 2 H, CH_2), 3.15 (s, 9 H, CH_3), 2.75–2.64 (m, 2 H, CH_2), 1.69–1.55 (m, 2 H, CH_2), 1.53–1.43 (m, 4 H, CH_2), 1.40–1.18 (m, 12 H, CH_2); **IR** (KBr disc): ν/cm^{-1} = 3426.7 (ν_{O-H}), 2921.0 (ν_{C-H}), 2848.8 (ν_{C-H}), 1640.8 ($\nu_{C=O,\ amide}$), 1576.0, 1487.8, 1465.0, 1408.3, 1342.9, 1238.0, 1099.6, 948.7, 721.5, 663.4; **TEM:** d = 14.1 ± 0.8 nm; **UV/Vis:** λ_{max} = 528 nm; **DLS:** d_{hydr} = 15 ± 4 nm; **ζ potential:** ζ = 56.6 ± 7.50 mV.

Animals

Female and male Wistar rats with a body mass of 200–250 g were used. The animals were bred and housed at the institute for Veterinary Physiology and Biochemistry of the Justus-Liebig-University Giessen at an ambient temperature of 22.5 °C and air humidity of 50–55% on a 12 h : 12 h light–dark cycle with free access to water and food until the time of the experiment. Experiments were approved by the named animal welfare officer of the Justus Liebig University (administrative number 577_M) and performed according to the German and European animal welfare law.

Published on 29 August 2018. Downloaded by UNIVERSITAT GIESSEN on 1/23/2019 9:52:34 AM.

Solutions

The standard solution for the Ussing chamber experiments was a buffer solution containing (mM): NaCl 107, KCl 4.5, $NaHCO_3$ 25, Na_2HPO_4 1.8, NaH_2PO_4 0.2, $CaCl_2$ 1.25, $MgSO_4$ 1 and glucose 12. The solution was gassed with carbogen (5% CO_2 in 95% O_2, v/v); pH was 7.4. For cell culture, Dulbecco's modified Eagle's High glucose medium was used.

Cell culture and transfection

HEK293T cells (a kind gift from M. Lohse, Würzburg, Germany) were cultured in DMEM Dulbecco's modified Eagle's High glucose medium supplemented with 10% (v/v) fetal bovine serum, 2 mM L-glutamine, 100 units per ml penicillin, and 0.1 mg ml^{-1} streptomycin at 37 °C (all substances purchased from Biochrom, Berlin, Germany), 5% (v/v) CO_2. Cells were transiently transfected with (µg DNA, 6 cm dish) 0.5 M_3-R (Missouri S&T cDNA Resource Center, Rolla, MO), 0.8 $G\alpha_q$YFP,[17] 0.5 $G\beta_1$-wt[18] and 0.2 CFP-$G\gamma_2$[19] by Effectene Transfection Reagent according to the manufacturer's instructions (Qiagen, Hilden, Germany). FRET experiments were performed 48 hours after transfection at room temperature in external buffer (mM) (NaCl 137, KCl 5.4, HEPES 10, $CaCl_2$ 2, $MgCl_2$ 1) at pH 7.3 on cells, which were plated on 6-well plates 25 mm coverslips (cover glasses were pre-incubated 30 min with poly-L-lysine) one day after transfection.

Single-cell FRET imaging

FRET (Förster Resonance Energy Transfer) measurements were performed on single transiently transfected HEK293T cells plated on poly-L-lysine-coated coverslips. Activation of Gq protein by stimulating muscarinic M_3 receptors (M_3-R) with NP was determined as the $G\alpha_q$ YFP-labelled subunit and N-terminus CFP labelled $G\gamma_2$ subunit rearrangement as described by Wolters *et al.* (2015).[20] The recording of YFP (yellow fluorescence protein) and CFP (cyan fluorescence protein) emission were recorded by dual-emission imagining using an inverted fluorescence microscope (Eclipse Ti; Nikon, Düsseldorf, Germany) as described in Milde *et al.* (2013)[21] supplemented with a light-emitting diode (LED) excitation system (pE-2; CoolLED, Andover, UK) containing LEDs emitting light at 425 for CFP and 500 nm for YFP excitation when intensity set to 2%. Recording interval was set to 500 ms in correlation to the time of exposure. Obtained fluorescence data were corrected for background fluorescence, false YFP excitation CFP spillover, and bleaching effects. FRET ratio was defined as selective YFP intensity divided to selective CFP intensity. Calculated absolute changes in FRET ratio represented as the average values of last 20 seconds application of respective concentration of agonist.

Tissue preparation

Animals were killed by stunning followed by exsanguination. The serosa and tunica muscularis were stripped away by hand to obtain a mucosa–submucosa preparation of the proximal colon. Briefly, the colon was placed on a small plastic rod with a diameter of 5 mm. A circular incision was made near the anal end with a blunt scalpel, and the serosa together with the tunica muscularis was gently removed in a proximal direction. Two segments of the proximal colon of each rat were prepared.

Short-circuit current measurements

The mucosa–submucosa preparation was fixed in a modified Ussing chamber bathed with a volume of 3.5 ml on each side of the mucosa. The tissue was incubated at 37 °C and short-circuited by a computer-controlled voltage-clamp device (Ingenieur Büro für Mess-und Datentechnik Mussler, Aachen, Germany) with correction for solution resistance. Short-circuit current (I_{sc}) was continuously recorded on a chart-recorder. I_{sc} is expressed as µEq h^{-1} cm^{-2}, *i.e.* the flux of a monovalent ion per time and area, with 1 µEq h^{-1} cm^{-2} = 26.9 µA cm^{-2}.

Drugs

Au-MUDA-CCh, carbachol, atropine, hexamethonium were dissolved in aqueous stock solutions. If not indicated otherwise, drugs were from Sigma (Steinheim, Germany).

Statistics

Results are given as means ± SEM, with the number (n) of investigated tissues. Statistical analysis was performed by ANOVA followed by a Bonferroni *post-hoc* test. For small groups, a Mann–Whitney U-test was applied. $P < 0.05$ was considered statistically significant.

Conflicts of interest

There are no conflicts to declare.

Acknowledgements

All chemical syntheses were performed at the Institute of Inorganic and Analytical Chemistry, Justus-Liebig-University at Giessen. We wish to acknowledge Anne Schulze (Institute of Inorganic and Analytical Chemistry, Justus-Liebig-University at Giessen) for the TEM images.

References

1 The American Chemical Society, *Program package Scifinder*, Washington, 2017.
2 J. Estelrich, M. J. Sánchez-Martín and M. A. Busquets, Nanoparticles in magnetic resonance imaging. From simple to dual contrast agents, *Int. J. Nanomed.*, 2015, **10**, 1727–1741.
3 M. Oostendorp, *et al.*, Gadolinium-labeled quantum dots for molecular magnetic resonance imaging. R1 versus R2 mapping, *Magn. Reson. Med.*, 2010, **64**, 291–298.
4 Y. Chen, Y. Xianyu and X. Jiang, Surface Modification of Gold Nanoparticles with Small Molecules for Biochemical Analysis, *Acc. Chem. Res.*, 2017, **50**, 310–319.

 This journal is © The Royal Society of Chemistry 2018

Published on 29 August 2018. Downloaded by UNIVERSITAT GIESSEN on 1/23/2019 9:52:34 AM.

5 B. D. Chithrani, A. A. Ghazani and W. C. W. Chan, Determining the size and shape dependence of gold nanoparticle uptake into mammalian cells, *Nano Lett.*, 2006, **6**, 662–668.
6 D. A. Giljohann, *et al.*, Gold nanoparticles for biology and medicine, *Angew. Chem., Int. Ed.*, 2010, **49**, 3280–3294.
7 P. M. Tiwari, K. Vig, V. A. Dennis and S. R. Singh, Functionalized Gold Nanoparticles and Their Biomedical Applications, *Nanomaterials*, 2011, **1**, 31–63.
8 J. D. Gibson, B. P. Khanal and E. R. Zubarev, Paclitaxel-functionalized gold nanoparticles, *J. Am. Chem. Soc.*, 2007, **129**, 11653–11661.
9 F. Gasiorek, E. Pouokam, M. Diener, S. Schlecht and M. S. Wickleder, Effects of multivalent histamine supported on gold nanoparticles: activation of histamine receptors by derivatized histamine at subnanomolar concentrations, *Org. Biomol. Chem.*, 2015, **13**, 9984–9992.
10 J. Turkevich, P. C. Stevenson and J. Hillier, A Study of the Nucleation and Growth Processes in the Synthesis of Colloidal Gold, Discuss, *Faraday Soc.*, 1951, 55–75.
11 S. K. Balasubramanian, *et al.*, Characterization, purification, and stability of gold nanoparticles, *Biomaterials*, 2010, **31**, 9023–9030.
12 J. Zong, S. L. Cobb and N. R. Cameron, Peptide-functionalized gold nanoparticles: versatile biomaterials for diagnostic and therapeutic applications, *Biomater. Sci.*, 2017, **5**, 872–886.
13 P. Hirschle, *et al.*, Exploration of MOF nanoparticle sizes using various physical characterization methods – is what you measure what you get?, *CrystEngComm*, 2016, **18**, 4359–4368.
14 K. N. Clayton, J. W. Salameh, S. T. Wereley and T. L. Kinzer-Ursem, Physical characterization of nanoparticle size and surface modification using particle scattering diffusometry, *Biomicrofluidics*, 2016, **10**, 54107.
15 D. Strabel and M. Diener, Evidence against direct activation of chloride secretion by carbachol in the rat distal colon, *Eur. J. Pharmacol.*, 1995, **274**, 181–191.
16 M. Hillenbrand, C. Schori, J. Schöppe and A. Plückthun, Comprehensive analysis of heterotrimeric G-protein complex diversity and their interactions with GPCRs in solution, *Proc. Natl. Acad. Sci. U. S. A.*, 2015, **112**, E1181–E1190.
17 T. E. Hughes, H. Zhang, D. E. Logothetis and C. H. Berlot, Visualization of a functional Galpha q-green fluorescent protein fusion in living cells. Association with the plasma membrane is disrupted by mutational activation and by elimination of palmitoylation sites, but not be activation mediated by receptors or AlF4-, *J. Biol. Chem.*, 2001, **276**, 4227–4235.
18 M. Bünemann, M. Frank and M. J. Lohse, Gi protein activation in intact cells involves subunit rearrangement rather than dissociation, *Proc. Natl. Acad. Sci. U. S. A.*, 2003, **100**, 16077–16082.
19 P. Hein and M. Bünemann, Coupling mode of receptors and G proteins, *Naunyn-Schmiedeberg's Arch. Pharmacol.*, 2009, **379**, 435–443.
20 V. Wolters, C. Krasel, J. Brockmann and M. Bünemann, Influence of gαq on the dynamics of m3-acetylcholine receptor-g-protein-coupled receptor kinase 2 interaction, *Mol. Pharmacol.*, 2015, **87**, 9–17.
21 M. Milde, A. Rinne, F. Wunder, S. Engelhardt and M. Bünemann, Dynamics of Gαi1 interaction with type 5 adenylate cyclase reveal the molecular basis for high sensitivity of Gi-mediated inhibition of cAMP production, *Biochem. J.*, 2013, **454**, 515–523.

This journal is © The Royal Society of Chemistry 2018

8.11 "Acetylcholinesterase-modified AlGaN/GaN solution-gate field-transistors for in-situ monitoring of myenteric neuron activity"

Müntze GM, **Pouokam E**, Steidle J, Schäfer W, Sasse A, Röth K, Diener M, Eickhoff M. *Biosens. Bioelectr* (2015) 77: 1048-1054

Impakt Faktor: 7.476

Eigener Anteil an der Publikation:

- Initiative: 10 %
- Projektplanung: 25 %
- Durchführung der Versuche: 40 %
- Auswertung der Experimente: 30 %
- Erstellung der Publikation: 30 %

Biosensors and Bioelectronics 77 (2016) 1048–1054

Contents lists available at ScienceDirect

Biosensors and Bioelectronics

journal homepage: www.elsevier.com/locate/bios

In situ monitoring of myenteric neuron activity using acetylcholinesterase-modified AlGaN/GaN solution-gate field-effect transistors

Gesche Mareike Müntze [a,*], Ervice Pouokam [b], Julia Steidle [b], Wladimir Schäfer [a], Alexander Sasse [a], Kai Röth [a], Martin Diener [b], Martin Eickhoff [a]

[a] I. Physikalisches Institut, Justus-Liebig-Universität Gießen, Heinrich-Buff-Ring 16, 35392 Gießen, Germany
[b] Institut für Veterinär-Physiologie und -Biochemie, Justus-Liebig-Universität Gießen, Frankfurter Straße 100, 35392 Gießen, Germany

ARTICLE INFO

Article history:
Received 13 October 2015
Received in revised form
23 October 2015
Accepted 26 October 2015
Available online 30 October 2015

Keywords:
EnFET
Acetylcholineseterase
AlGaN/GaN HEMT
Neuron activity
Bioelectronics
Cell-transistor hybrid

ABSTRACT

The response characteristics of acetylcholinesterase-modified AlGaN/GaN solution-gate field-effect transistors (AcFETs) are quantitatively analyzed by means of a kinetic model. The characterization shows that the covalent enzyme immobilization process yields reproducible AcFET characteristics with a Michaelis constant K_M of (122 ± 4) μM for the immobilized enzyme layer. The increase of K_M by a factor of 2.4 during the first four measurement cycles is attributed to partial denaturation of the enzyme. The AcFETs were used to record the release of acetylcholine (ACh) by neuronal tissue cultivated on the gate area upon stimulation by rising the extracellular K^+ concentration. The neuronal tissue constituted of isolated myenteric neurons from four to 12 days old Wistar rats, or sections from the *muscularis propria* containing the myenteric plexus from adult rats. For both cases the AcFET response was demonstrated to be related to the activity of the immobilized acetylcholinesterase using the reversible acetylcholinesterase blocker donepezil. A concentration response curve of this blocking agent revealed a half maximal inhibitory concentration of 40 nM which is comparable to values measured by complementary *in vitro* methods.

© 2015 Elsevier B.V. All rights reserved.

1. Introduction

The development of acetylcholinesterase (AChE)-based biosensors is of interest for various branches of research. As inhibition of AChE leads to accumulation of the neurotransmitter ACh and thus dysfunction in the cholinergic neurotransmission or even death (Spradling and Dillman, 2011; Storm et al., 2000), one application field of AChE-based biosensors is the study of AChE inhibitors such as organophosphorus pesticides (Arduini et al., 2013; Dzyadevych et al., 2004; Meng et al., 2013) and neurotoxins (Arduini et al., 2010). Furthermore, AChE-based biosensors can be used for the detection and quantification of the neurotransmitter ACh itself. This application is particularly important for geriatric medicine as a decreased level of brain ACh can be associated with memory disturbance (Ikarashi et al., 2004). In this context, the determination of ACh and the related choline acetyltransferase activity give insight into the pathogenesis of diseases such as Parkinson's disease (Dubois et al., 1983) and Alzheimer's disease (Bartus et al., 1982; Chauhan and Pundir, 2014; White and Cummings, 1996).

Since ACh is not only produced by cholinergic neurons but also by non-neuronal cells such as the urothelium (Lips et al., 2007), the colonic epithelium (Bader et al., 2014) and the airway epithelium (Kummer et al., 2008), the detection of ACh also plays a significant role in the study of the non-neuronal cholinergic system (Wessler and Kirkpatrick, 2008).

At present, mainly methods sensitive in the (sub-)fmol-range are used to prove the cellular production and/or the release of ACh. Examples are liquid chromatography combined with the electrochemical detection of hydrogen peroxide (Huang et al., 1995), matrix-assisted laser desorption ionization time-of-flight mass spectrometry (Persike et al., 2010) and liquid chromatography in combination with electrospray ionization mass spectrometry (Uutela et al., 2005). Although being highly sensitive, these methods only offer a time resolution on the minute scale and hence *in situ* application is not possible. In contrast, AChE-based biosensors offer the advantage of possible *in situ* analysis with a time resolution on the (sub-)second scale (Hai et al., 2006). The operating principles of AChE-based biosensors developed so far are diverse. Among those are fluorometric (Meng et al., 2013; Wei

* Corresponding author. Fax: +49 641 99 33139.
E-mail address: gesche.m.muentze@exp1.physik.uni-giessen.de (G.M. Müntze).

http://dx.doi.org/10.1016/j.bios.2015.10.076
0956-5663/© 2015 Elsevier B.V. All rights reserved.

et al., 2014), amperometric (Arduini et al., 2010; Chauhan and Pundir, 2014) and potentiometric (Dzyadevych et al., 2004; Härtl et al., 2008; Hai et al., 2006; Kharitonov et al., 2000; Sohn et al., 2013) biosensors with the lowest ACh concentration detectable being 1 μM using a potentiometric sensor (Härtl et al., 2008; Hai et al., 2006). Despite this relatively high detection limit of 1 μM when compared to the methods described above, the applicability of a potentiometric AcFET in an "artificial synapse" (Hai et al., 2006) has been discussed. Here, the authors argued that the detection limit of an AcFET (1 μM) could be reached when neurons cultured on the gate area are releasing ACh as the volume between the neurons and the gate area is limited (Fromherz, 2003) and ACh concentrations up to several 100 μM have been reported in the synaptic cleft (Kuffler and Yoshikami, 1975).

In the present work, we realize such an "artificial synapse" with myenteric neurons from the myenteric plexus embedded in the *muscularis propria*, and isolated myenteric neurons cultured on the gate area of an AlGaN/GaN AcFET, combined with *in situ* detection of ACh release by means of an AcFET. As part of this work, the AlGaN/GaN AcFETs are quantitatively analyzed with respect to reproducibilty and stability of the covalent immobilization process for AChE by means of a kinetic model (Glab et al., 1991) to ensure their functionality for monitoring neuron activity.

2. Materials and methods

2.1. Preparation of solution-gate FET

AlGaN/GaN AcFETs were prepared using pH-sensitive AlGaN/GaN high electron mobility transistors (HEMTs) consisting of a GaN/$Al_{0.27}Ga_{0.73}$N/GaN (800 nm/18 nm/1 nm) heterostructure grown by metal organic chemical vapor deposition on silicon (111) substrates (DOWA, Japan). The sheet carrier density and the carrier mobility at room temperature were determined from Hall-effect measurements to $(2.0 \pm 0.2) \cdot 10^{13}$ cm^{-2} and (744 ± 62) $cm^2 V^{-1} s^{-1}$, respectively.

Patterning of transistor mesastructures with gate dimensions of (1.2×0.5) mm^2 was achieved by ion beam etching using a ME 601 system (Veeco Instruments, Plainview, USA) with an argon ion source. Ti/Au (30 nm/150 nm) ohmic contacts for source and drain were deposited by thermal evaporation and annealed for 30 s at 820 °C in vacuum.

For measurements in electrolyte solution passivation of electrical contacts was accomplished with silicone rubber (Scrintec 901; Carl Roth, Karlsruhe, Germany), the active gate area remained uncovered.

2.2. Immobilization of acetylcholinesterase

Covalent immobilization of AChE (*electrophorus electricus*, EC 3.1.1.7, C3389, Sigma-Aldrich, Taufkirchen, Germany) on the gate area of the pH-sensitive HEMTs was carried out adapting a procedure from refs. (Baur et al., 2005; Gabrovska et al., 2008; Müntze et al., 2015): First, the samples were wet chemically oxidized in a mixture of sulfuric acid (98%; Carl Roth, Karlsruhe, Germany) and hydrogen peroxide (≥30%; Fluka, Taufkirchen, Germany) (H_2SO_4:H_2O_2, 3:1) followed by silanization with (3-aminopropyl) triethoxysilane (≥98%; Sigma-Aldrich, Taufkirchen, Germany). Second, they were incubated in 20 mM aqueous glutaraldehyde solution (diluted from: 50% in water; Sigma-Aldrich, Taufkirchen, Germany) before covalent attachment of AChE was performed in a solution with an enzyme concentration of 400 nM in the presence of cyanoborohydride (coupling buffer; Sigma, Taufkirchen, Germany) in a humid controlled environment at 5 °C for 20 h. The resulting AcFETs (schematically shown in Fig. S1) were stored in 10 mM phosphate buffered saline (PBS) solution (pH 7.5) with a sodium chloride concentration of 137 mM and a potassium chloride concentration of 2.7 mM at a temperature of 5 °C (all salts according to Ph. Eur. from Carl Roth, Karlsruhe, Germany).

2.3. AcFET characterization and monitoring of neuron activity

The AcFETs were operated with a drain-source voltage (U_{DS}) of 200 mV while the gate-source potential (U_{GS}) was applied via an Ag/AgCl reference electrode in a three-electrode measurement set-up resulting in a transconductance of about 60 μS during operation (Müntze et al., 2015).

Calibration measurements and stability tests were performed in current-clamping mode where U_{GS} was adjusted with a computer-controlled potentiostat in order to compensate the changes in I_{DS} caused by a change in pH due the formation of acetic acid in the enzymatic reaction of AChE (cf. Fig. S2). Hence, here the AcFET's signal is the required ΔU_{GS} and the relation of pH and ΔU_{GS} is given by the AcFETs' pH-sensitivity. The obtained response curves were then evaluated according to the kinetic model of Glab et al. (1991) utilizing the procedure described in Müntze et al. (2015), thus facilitating the determination of model parameters directly related to the covalently immobilized enzyme layer. For measurements of neuron activity U_{GS} was clamped and the I_{DS} transients were recorded. The measurements were started after the AcFETs had equilibrated with the surrounding electrolyte and only a linear drift in I_{DS} was obtained. The latter was determined over a period of 300 s before any chemical was added and then subtracted from the recorded transients in I_{DS}.

The calibration measurements and the stability analysis were conducted in a stirred PBS solution with a buffer concentration [BF] of 0.5 mM, a sodium chloride concentration of 25 mM and a potassium chloride concentration of 0.1 mM at 35 °C. All calibration measurements were regularly performed at pH 7.7 while the stability measurements have been performed at pH 7.5, mimicking physiological conditions for measuring vital tissue and cells. For quantitative analysis of the AcFET response the concentration of the substrate acetylthiocholine (ATCh; ≥99.0%; Sigma, Taufkirchen, Germany) which is equivalently processed by AChE as the neurotransmitter ACh (Ellman et al., 1961) was varied by pipetting from a 100 mM stock solution into the measurement volume of 100 ml.

The measurements for monitoring neuron activity of isolated myenteric neurons, and myenteric neurons from the myenteric plexus embedded in the *muscularis propria*, as well as the corresponding reference measurements have been carried out in a modified Tyrode solution containing phosphate buffer (1 mM), potassium chloride (KCl, 5.4 mM), sodium chloride (140 mM), calcium chloride (1.25 mM), magnesium chloride (1 mM) and glucose (12.2 mM) at a pH of 7.5 adjusted with sodium hydroxide/hydrogen chloride. To stimulate the neurons, the membrane was depolarized by rising the extracellular K^+ concentration by 30 mM, using a 3 M KCl stock solution (Carl Roth, Karlsruhe, Germany). The reversible AChE blocker donepezil (≥98%; Sigma, Taufkirchen, Germany) as well as ATCh were pipetted from stock solutions with a concentration of 100 mM, respectively.

Between successive experiments monitoring neuron activity and for transport, the samples were stored in a standard Tyrode solution containing HEPES (10 mM; ≥98%; Carl Roth, Karlsruhe, Germany), potassium chloride (5.4 mM), sodium chloride (140 mM), calcium chloride (1.25 mM), magnesium chloride (1 mM) and glucose (12.2 mM; ≥95.5%; Carl Roth, Karlsruhe, Germany) at a pH of 7.4 adjusted with sodium hydroxide/hydrogen chloride.

2.4. Tissue preparation

Isolated myenteric neurons were obtained from four to 12 days old Wistar rats while the myenteric plexus was obtained by preparing the *muscularis propria* from female and male Wistar rats with a body mass of (140–160) g. Experiments were approved by Regierungspräsidium Gießen, Gießen, Germany. Myenteric neurons were isolated and cultured as described previously (Pouokam et al., 2009). Then, 20 µl of the cell suspension were transferred to the gate of the AcFET which was incubated overnight at 37 °C in an atmosphere of 5% (v/v) CO_2 in 95% (v/v) air.

The *muscularis propria* was obtained by removing the colon of adult rats and placing it on a small plastic rod with a diameter of 5 mm. A circular incision was made near the anal end with a blunt scalpel. Then, the *serosa* and the *muscularis propria* embedding the myenteric plexus, were gently removed and transferred to a glass plate. One piece of (1×2) mm^2 was then placed on the gate of an AcFET using fine forceps, covered by polyester gauze (pore size 70 µm) and fixed with a plastic clip.

3. Results and discussion

3.1. Characterization of AcFETs

It has recently been shown that the kinetic model introduced by Glab et al. (1991) is an adequate tool to quantitatively analyze the enzyme-modified FET (EnFET) response curves of pH-affecting enzymes on the example of an AlGaN/GaN EnFET with a covalently immobilized layer of penicillinase (Müntze et al., 2015). This approach is also used here in order to assess the reproducibility and stability of the utilized immobilization procedure by quantitatively analyzing the AcFET characteristics as a prerequisite for the monitoring of myenteric neuron activity.

In Fig. 1 four response curves of freshly prepared AcFETs from differing production dates directly after preparation are compared. The good agreement between the different measurements, particularly in the sensitive region at substrate concentrations smaller than 100 µM (inset Fig. 1), indicates the good reproducibility of the AcFET preparation. Furthermore, Fig. 1 shows that the standard deviation of the measurement points and thus the error of each measurement point is small. As this finding is representative for all response curves presented here, the standard deviation is not shown for ATCh concentrations below 500 µM in the following to ensure the legibility of the presented data.

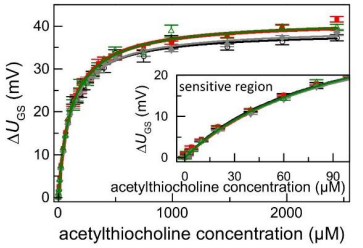

Fig. 1. Comparison of the response curves of four different AcFETs at pH 7.7 with the relative standard deviation of the measurement points given. The inset shows the sensitive region at substrate concentrations smaller than 100 µM in detail. Solid lines represent fits according to the kinetic model discussed in the text.

Table 1
Extracted model parameters for the AcFETs shown in Fig. 1.

AcFET	K_M (µM)	k_V (µM)	$\bar{k}_H$	$\bar{k}_{BF}$ (10^{-2})
○	113	3.5	0.001	2.0
■	128	1.0	0.003	0.5
△	123	0.4	0.021	0.2
◆	123	2.2	0.003	1.1

The lowest detectable ATCh concentration ([ATCh]) was 1 µM with a corresponding value of $\Delta U_{GS}=(0.81 \pm 0.27)$ mV. Hence, taking into account the transistor's geometry as well as the thickness of the AChE layer, which is approximately 15 nm when considering the size of the molecules as stated in refs. (Bierbaum et al., 1995; Bourne et al., 1999), this corresponds to a total number of approximately 10^7 substrate molecules (≈ 10 amol) in the sensing layer.

Fitting with the kinetic model (Glab et al., 1992) according to the procedure outlined in Müntze et al. (2015) yields an average Michealis constant K_M of (122 ± 4) µM which lies within the range of 84 µM (Barteri et al., 2005) to 900 µM (Gabrovska et al., 2008) published for AChE from *electrophorus electricus*. The normalized rate constants, which have been introduced in Glab et al. (1991) and are briefly discussed in Supporting Information, have been determined by averaging the values given in Table 1 to $k_V = (1.8 \pm 1.1)$ µM, $\bar{k}_H=(0.007 \pm 0.007)$ and $\bar{k}_{BF}=(1.0 \pm 0.6) \cdot 10^{-2}$. It should be noted that all these parameters are considerably smaller than 1 with the normalized rate constants being defined by the ratio of the maximum reaction velocity v_{max} (k_V), the transport rate constant of protons k_H ($\bar{k}_H$) and the transport rate constant of the buffer k_{BF} ($\bar{k}_{BF}$) to the transport rate constant of the substrate molecule k_S, respectively. Hence, all three quantities (v_{max}, k_H, k_{BF}) are much smaller than k_S contrary to the findings for penicillinase in Müntze et al. (2015), where k_H as well as k_{BF} were larger than k_S and k_V was about three orders of magnitude larger than in the case of AChE presented here.

The reason for this comparatively high value of k_S is that AChE is one of the most efficient enzymes known (Nolte et al., 1980) and consequently each substrate molecule reaching the covalently immobilized AChE at the gate surface is immediately converted. As a result, a large concentration gradient between the gate surface ([ATCh] ≈ 0) and the surrounding electrolyte (constant [ATCh]) for the substrate ATCh is established and causes a high value for the transport rate constant k_S.

To assess the AcFETs' stability, an AcFET was measured repeatedly over the course of 77 days while storage was only interrupted for measurements. In this time span eight measurements were taken on day 0, 2, 4, 14, 21, 35, 49, and 77 after preparation, as displayed in Fig. 2A. The results show that both, the sensitive region and the saturation region, are altered during the first four measurements within two weeks after AcFET preparation: The saturation signal decreases continuously by about 50% while the sensitivity s of the device for ATCh (estimated by a linear fit of the response curve in the sensitive region up to [ATCh]= 100 µM) is lowered from (186 ± 21) µV µM^{-1} (1st measurement) to (69 ± 9) µV µM^{-1} (4th to 8th measurement) as shown in Fig. 2B. Starting from the 4th measurement on day 14 stable response curves were obtained that allow the quantitative determination of the administered ATCh concentration up to 100 µM.

The values extracted for K_M increase steadily from 134 µM until they reach a constant value of (316 ± 20) µM from day 14 (4th measurement) on. As K_M equals $(k_{-1}+k_2)/k_1$, the ratio of the reaction constants of the dissociation ($k_{-1}+k_2$) and formation (k_1) of the enzyme–substrate complex, this increase over time could be

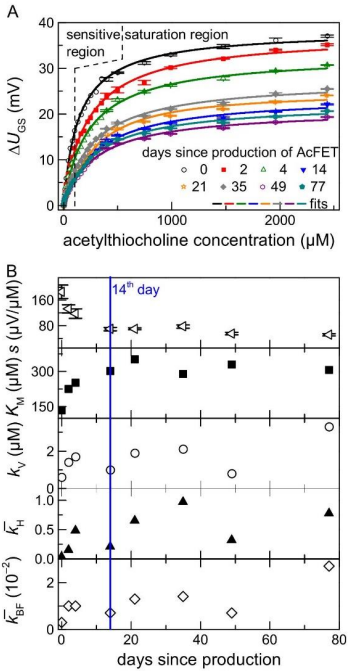

Fig. 2. Chronological development of an AcFET over the course of 77 days. Evolution of (A) response curves with the relative standard deviation of the measurement points given for [ATCH] ≥ 500 μM as well as fit and (B) sensitivity s with its standard deviation derived by the linear fit as well as extracted model parameters.

due to an increased dissociation rate or a decreased formation rate of the enzyme–substrate complex. As AChE is already one of the most efficient enzymes (Nolte et al., 1980) it is unlikely that it will convert the substrate faster into the products of the enzymatic reaction when stored. In contrast, a decrease in k_1 due to a partial denaturation of AChE during the first two weeks of storage causing a slower formation of the enzyme–substrate complex and/or its faster dissociation into substrate and enzyme is more plausible.

As the sensitivity of the device is directly related to the velocity of the enzymatic reaction $v \sim k_2/K_M$ (for $[S] \to 0$) (Johnson and Goody, 2011; Michaelis and Menten, 1913) the related increase in K_M by about a factor of 2.4 could explain the decrease of the sensitivity by a factor of about 2.7 during the first four measurements.

The other three extracted model parameters show an increase during this period until they saturate at values of $k_V = (1.8 \pm 0.7)$ μM, $\bar{k}_H = (0.584 \pm 0.257)$ and $\bar{k}_{BF} = (1.4 \pm 0.6) \cdot 10^{-2}$ (Fig. 2B). This increase can be explained by a decrease in k_S which equally affects all three parameters. As k_S depends on the concentration gradient of the substrate at the enzymatic layer, a decrease in k_S is related to a smaller concentration gradient which can be either explained by partial denaturation of AChE as discussed above and/or a lower amount of AChE on the gate surface, *exempli gratia* a detachment of AChE.

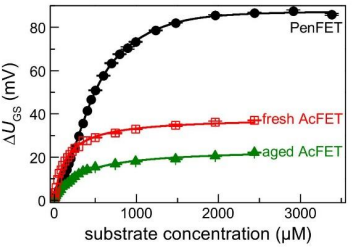

Fig. 3. Comparison of PenFET with a freshly prepared AcFET and an aged AcFET (14 days old). Solid lines represent fits. The relative standard deviation of the measurement points is given for substrate concentrations greater and equal to 500 μM.

To gain further insight into the AcFET characteristics the response curve of a freshly prepared AcFET and an aged AcFET (response curves after day 0 and 14 in Fig. 2A) are compared to the response curve of a penicillinase-modified FET (PenFET) analyzed in Müntze et al. (2015) in Fig. 3, demonstrating that the three different response curves are clearly distinguishable.

The freshly prepared AcFET exhibits the highest sensitivity of (186 ± 21) μV μM^{-1} in the low concentration regime. The sensitivity of the PenFET with (104 ± 1) μV μM^{-1}, determined up to a substrate concentration of 500 μM, is higher than the sensitivity of (69 ± 5) μV μM^{-1} obtained for the aged AcFET. As the ratio of k_2 to K_M for AChE $(2 \cdot 10^8$ M^{-1} s^{-1} (Nolte et al., 1980)) is an order of magnitude larger than for penicillinase $(0.28 \cdot 10^8$ M^{-1} s^{-1} (Guo et al., 1999)) it is expected that the sensitivity of an AcFET should be higher than that of a PenFET. As for the aged AcFET this statement does not hold we assign the decrease in sensitivity to partial denaturation of AChE.

In the saturation region the difference between the AcFET and the PenFET response curves are even more pronounced. The saturation signal of the PenFET with about 85 mV is 2.5 times and 4 times higher than the saturation signal of the freshly prepared AcFET and the aged AcFET, respectively. This result can be explained with regard to the molecular weight of the respective enzymes. AChE has a molecular weigth of 280 kDa (Rosenberry et al., 1974) and thus is more than 10 times heavier than penicillinase (M=22 kDa (Davies and Abraham, 1974)). *Ergo*, on a transistor with a constant gate area, as is the case here, it is expected that a (sub-)monolayer of enzyme contains less enzymes in case of AChE. Hence, the density of enzymes on the gate area for an AcFET is smaller than for a PenFET if the same transistor geometry is used and a lower saturation signal is expected. This reasoning also leads to the conclusion that the lower saturation signal of the aged AcFET compared to the freshly prepared AcFET could be due to a detachment of AChE from the gate surface. Thus, we have shown that that AlGaN/GaN FETs in combination with the applied covalent functionalization process provide a platform for quantitative comparison of different immobilized enzymes, here

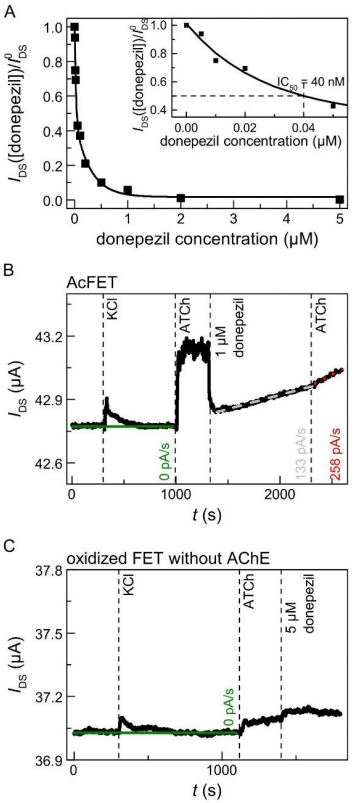

Fig. 4. Reference measurements. (A) Concentration response curve of donepezil; (B) response of an AcFET to the addition of KCl, ATCh and donepezil; (C) response of an oxidized FET covered with isolated myenteric neurons to the addition of KCl, ATCh and donepezil. B and C are plotted on the same I_{DS} scale for better comparison.

penicillinase and acetylcholinesterase.

3.2. Monitoring the ACh release of myenteric neurons

In this paragraph measurements of myenteric neuron activity utilizing AcFETs are described. Prior to those experiments it was assessed that the AcFETs do not show any interfering response to the chemicals used throughout those measurements: KCl (stimulant), donepezil (reversible AChE blocker) and ATCh (neurotransmitter analog).

Furthermore, a concentration response curve of an AcFET to the reversible AChE blocker donepezil (Fig. 4A) was measured to ensure that the AChE on the gate area can be blocked by donepezil in an equal fashion as *in vitro*. To obtain this concentration response curve the ratio of the change in I_{DS} for a given donepezil concentration (I_{DS}([donepezil]) to the initial increase in I_{DS} due to the addition of 200 μM ATCh (I^0_{DS}) was plotted against the administered donepezil concentration. The resulting data points were fitted by a double exponential decay fit from which a half maximal inhibitory concentration (IC_{50}) of 40 nM could be deduced which is comparable to literature values (Contreras et al., 1999).

Subsequently, the response of an AcFET to the addition of KCl, ATCh and donepezil (cf. Fig. 4B) was evaluated. The addition of KCl causes an immediate spike in I_{DS} due to a transient inhomogeneity in the ionic concentrations. However, as indicated by the solid line, it does not have a persistent effect on I_{DS}. Then, the substrate ATCh was added in a concentration of 200 μM. As the substrate is enzymatically converted into acetic acid and thiocholine the pH is lowered until a steady state is reached which leads to a steplike increase in I_{DS} by about 400 nA. The following addition of donepezil in a concentration of 1 μM results in a decrease of I_{DS} as the acid production is blocked. The ensuing slope of the I_{DS} transient of 133 pA/s (dashed line in Fig. 4B) is attributed to the fact that donepezil is a reversible AChE blocker. *Id est*, some acetic acid is still produced which leads to a continuous decrease in pH and thus an increase in I_{DS}.

The subsequent second addition of ATCh causes an increase in the slope of the I_{DS} transient proving that the AcFET is still functioning properly as it re-enhances the production of acetic acid. This behavior is indicated by the dotted line in Fig. 4B, reflecting a slope of 258 pA/s that is about two times higher than before the second addition of ATCh.

A third reference measurement was performed with an AlGaN/GaN solution-gate FET without AChE attached, covered with isolated myenteric neurons from four to 12 days old Wistar rats testing the device selectivity. As can be seen from the solid line in Fig. 4C the stimulation of the neurons with KCl does not affect the I_{DS} transient after relaxation of the initial spike in I_{DS}, demonstrating that the covalently immobilized AChE is essential for successful monitoring of myenteric neuron activity. The subsequent addition of ATCh in a concentration of 200 μM results in a steplike increase in I_{DS} by 40 nA attributed to AChE produced by the neurons on the AcFET's gate area. This latter effect can be neglected when compared to the step height of 400 nA in Fig. 4B. A final addition of donepezil in a concentration of 5 μM does not affect the I_{DS} transient. While it is desirable that the addition of donepezil does not alter the slope of the I_{DS} transient it is not yet understood why it does not block the increase in I_{DS} due to the ATCh addition as it is the case in Fig. 4B. A possible explanation might be the expression of butyrylcholinesterase activity by the myenteric neurons, which would further cleave acetylcholine, but would be resistant against donepezil.

Next, measurements for monitoring neuron activity of myenteric neurons from adult Wistar rats' myenteric plexus still embedded in the *muscularis propria* (Fig. 5A) and of isolated myenteric neurons from four to 12 days old rats (Fig. 5B) were carried out. In contrast to the reference measurements in Fig. 4B and C the stimulation of neurons by addition of KCl leads to an increase in I_{DS} over time (cf. dashed/dotted line in Fig. 5A and B). The slope of the I_{DS} transient represents a continuous reduction of pH that is attributed to the release of ACh by the stimulated neurons which is enzymatically converted into acetic acid and choline.

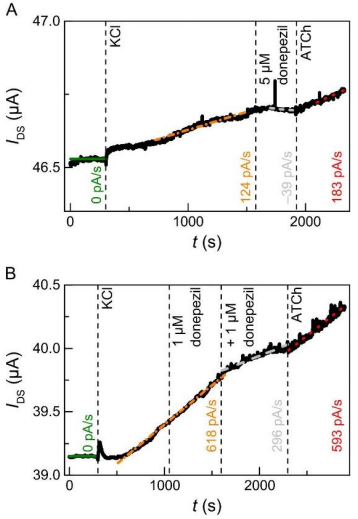

Fig. 5. Monitoring of neuron activity: (A) myenteric neurons from the myenteric plexus still embedded in the *muscularis propria* from adult rats covering the gate area of an AcFET; (B) isolated myenteric neurons from four to 12 days old Wistar rats, cultured on the gate area of an AcFET.

In case of myenteric neurons embedded in the *muscularis propria*, it is noticeable that the initial spike in I_{DS} after the addition of KCl is missing. This observation is attributed to the fact that the tissue sample of the *muscularis propria* covers the entire gate area and hence forms a diffusion barrier.

The addition of donepezil in a concentration of 5 µM results in a decrease of the slope in the I_{DS} transient to − 39 pA/s (cf. dashed line in Fig. 5A), comparable to the behavior before stimulation. This observation reflects the effect of donepezil blocking the enzymatic degradation of ACh by AChE. In combination with the reference measurements this demonstrates that the response of the neuron-covered AcFET observed after KCl addition directly reflects the AcFET sensing ACh released by the stimulated neurons. The ensuing increase in the slope (cf. dotted line in Fig. 5A, 183 pA/s) in response to the addition of the neurotransmitter analog ATCh illustrates that the AcFET is still operational.

After the experiment the tissue sample was removed from the AcFET and its vitality confirmed by fluorometric calcium imaging utilizing fura-2 acetoxymethylester (Life Technologies, Darmstadt, Germany) as exemplarily shown in Fig. S3.

The second experiment displayed in Fig. 5B with isolated myenteric neurons cultured on the gate area qualitatively shows the same results as in case of the neurons embedded in the *muscularis propria*. However, the I_{DS} transient spikes directly after the addition of KCl and the slope of the I_{DS} transient (618 pA/s compared to 124 pA/s) is five times larger. As the isolated neurons do not cover the gate area completely, *id est* part of the gate is in direct contact with the electrolyte, the AcFET can register the transient inhomogeneity in the ionic concentrations explaining the spike in I_{DS} after the addition of KCl. Additionally, the isolated neurons are no longer embedded in the *muscularis propria*, which all analytes have to permeate before they can reach the gate surface in case of the neurons still embedded in the *muscularis propria*. Hence, ACh released from isolated neurons can reach the EnFET surface more easily as reflected by the higher slope of the I_{DS} transient.

It should also be noticed that the onsets of the increase in I_{DS} differ by about 100 s: In case of the isolated myenteric neurons (Fig. 5B) the increase starts about 200 s after the addition of KCl, and after about 300 s in case of myenteric neurons still embedded in the *muscularis propria* (Fig. 5A). This behavior can be explained assuming that I_{DS} has to increase by 20 nA over its base line value before being detectable (equivalent to a detection limit of about 5 µM for an aged AcFET with a sensitivity of (0.069 ± 0.005) mV µM^{-1} and a transconductance of 60 µS). Taking the different slopes into account, the onset is expected after 32 s for isolated myenteric neurons and after 161 s for neurons embedded in the *muscularis propria*, respectively. Hence, assuming that ACh being released by isolated neurons or neurons embedded in the *muscularis propria* needs the same time to reach the AcFET's gate the expected time difference is in good agreement with the experimental result.

Subsequent addition of donepezil in a concentration of 1 µM does not show any measurable effect on the slope of the I_{DS} transient. Only a second addition of donepezil, resulting in a total concentration of 2 µM, leads to a decrease of the slope from 618 pA/s (cf. dashed/dotted line in Fig. 5B) to 296 pA/s (cf. dashed line in Fig. 5B) and thus a decrease in the enzymatic acid production. *Id est*, the block is not complete. This finding illustrates that the donepezil concentration needed to block an AcFET covered with myenteric neurons is significantly higher than the concentration needed to block a bare AcFET (cf. Fig. 4A). The reason for this is that in case of the neuron-covered AcFET not only the AChEs covalently immobilized on the gate area but as well the AChEs produced by the neurons have to be blocked.

The final addition of ATCh results in a re-increase in the slope of the I_{DS} transient from 296 pA/s (cf. dashed line in Fig. 5B) to 593 pA/s (cf. dotted line in Fig. 5B), proving that the utilized AcFET has been functioning properly throughout the experiment.

In case of the isolated myenteric neurons a vitality test analogous to the one performed on the myenteric neurons embedded in tissue was not possible because the current AcFET's geometry does not allow focusing of the fluorescent microscope. Neither is the non-invasive removal of the isolated neurons from the gate area possible. As the measurement results in Fig. 5A and B are equivalent and the vitality of the neurons after the experiment in case of the myenteric neurons embedded in tissue was shown, the vitality of the isolated neurons throughout the experiment was assumed.

4. Conclusions

AlGaN/GaN-based AcFETs were quantitatively analyzed with respect to sensitivity, stability and reproducibility by application of a kinetic model as introduced by Glab et al. in 1991. We could show that the device preparation is reproducible and that alterations during the first four measurement cycles can be primarily attributed to a partial denaturation of immobilized AChE. In further measurements the AcFET showed stable response characteristics and allowed quantitative and comparative investigation of enzyme kinetics demonstrating that the kinetic model is highly suitable for the study of enzyme characteristics, as long as the enzymatic reaction does affect the pH.

The successful detection of ACh released by isolated myenteric neurons from four to 12 days old Wistar rats, and by neurons of the myenteric plexus embedded in the *muscularis propria* from adult rats demonstrates that AlGaN/GaN AcFETs are a suitable tool for the *in situ* detection of released ACh in general. This application could also be expanded to the analysis of non-neuronal tissue. However, in such cases the amount of released ACh might be smaller than in case of neuronal tissue and thus a modification of the AcFET design in order to increase the transconductance and hence the sensitivity might be required.

Acknowledgments

The authors gratefully acknowledge financial support from the Deutsche Forschungsgemeinschaft (DFG, EI 518/5-1) and by the Förderfonds from the Justus-Liebig-Universität Gießen (BioChip).

Appendix A. Supplementary material

Supplementary data associated with this article can be found in the online version at http://dx.doi.org/10.1016/j.bios.2015.10.076.

References

Arduini, F., Amine, A., Moscone, D., Palleschi, G., 2010. Microchim. Acta 170, 193–214.
Arduini, F., Guidone, S., Amine, A., Palleschi, G., Moscone, D., 2013. Sens. Actuat. B: Chem. 179, 201–208.
Bader, S., Klein, J., Diener, M., 2014. Eur. J. Pharmacol. 733, 23–33.
Barteri, M., Pala, A., Rotella, S., 2005. Biophys. Chem. 113, 245–253.
Bartus, R.T., Dean, R.L., Beer, B., Lippa, A.S., 1982. Science 217, 408–417.
Baur, B., Steinhoff, G., Hernando, H., Purrucker, O., Tanaka, M., Nickel, B., Stutzmann, M., Eickhoff, M., 2005. Appl. Phys. Lett. 87, 263901–1–263901–3.
Bierbaum, K., Kinzler, M., Woll, C., Grunze, M., 1995. Langmuir 11, 512–518.
Bourne, Y., Grassi, J., Bougis, P.E., Marchot, P., 1999. J. Biol. Chem. 274, 30370–30376.
Chauhan, N., Pundir, C.S., 2014. Biosens. Bioelectron. 61, 1–8.
Contreras, J.-M., Rival, Y.M., Chayer, S., Bourguignon, J.-J., Wermuth, C.G., 1999. J. Med. Chem. 42, 730–741.
Davies, R.B., Abraham, E.P., 1974. Biochem. J. 143, 115–127.
Dubois, B., Ruberg, M., Javoy-Agid, F., Ploska, A., Agid, Y., 1983. Brain Res. 288, 213–218.
Dzyadevych, S.V., Arkhypova, V.N., Martelet, C., Jaffrezic-Renault, N., Chovelon, J.-M., El'skaya, A.V., Soldatkin, A.P., 2004. Electroanal. 16, 1873–1882.
Ellman, G.L., Courtney, K.D., Andres, V., Featherstone, R.M., 1961. Biochem. Pharmacol. 7, 88–95.
Fromherz, P., 2003. Phys. E: Low-dimens. Sys. Nanostruct. 16, 24–34.
Gabrovska, K., Marinov, I., Godjevargova, T., Portaccio, M., Lepore, M., Grano, V., Diano, N., Mita, D.G., 2008. Int. J. Biol. Macromol. 43, 339–345.
Glab, S., Koncki, R., Hulanicki, A., 1991. Analyst 116, 453–458.
Glab, S., Koncki, R., Holona, I., 1992. Analyst 117, 1671–1674.
Guo, F., Huynh, J., Dmitrienko, G.I., Viswanatha, T., Clarke, A.J., 1999. Biochim. Biophys. Acta (BBA) – Protein Struct. Mol. Enzym. 1431, 132–147.
Härtl, A., Baur, B., Stutzmann, M., Garrido, J.A., 2008. Langmuir 24, 9898–9906.
Hai, A., Ben-Haim, D., Korbakov, N., Cohen, A., Shappir, J., Oren, R., Spira, M.E., Yitzchaik, S., 2006. Biosens. Bioelectron. 22, 605–612.
Huang, T., Yang, L., Gitzen, J., Kissinger, P.T., Vreeke, M., Heller, A., 1995. J. Chromatogr. B 670, 323–327.
Ikarashi, Y., Harigaya, Y., Tomidokoro, Y., Kanai, M., Ikeda, M., Matsubara, E., Kawarabayashi, T., Kuribara, H., Younkin, S.G., Maruyamae, Y., Shoji, M., 2004. Neurobiol. Aging 25, 483–490.
Johnson, K.A., Goody, R.S., 2011. Biochemistry 50, 8264–8269.
Kharitonov, A.B., Zayats, M., Lichtenstein, A., Katz, E., Willner, I., 2000. Sens. Actuat. B: Chem. 70, 222–231.
Kuffler, S.W., Yoshikami, D., 1975. J. Physiol. 251, 465–482.
Kummer, W., Lips, K.S., Pfeil, U., 2008. Histochem. Cell Biol. 130, 219–234.
Lips, K.S., Bschleipfer, T., Schukowski, K., Weidner, W., Wessler, I., Schwantes, U., Koepsell, H., Kummer, W., 2007. Eur. Urol. 51, 1042–1053.
Meng, X., Wei, J., Ren, X., Ren, J., Tang, F., 2013. Biosens. Bioelectron. 47, 402–407.
Michaelis, L., Menten, M.L., 1913. Biochem. Z. 49, 333–369.
Müntze, G.M., Baur, B., Schäfer, W., Sasse, A., Howgate, J., Röth, K., Eickhoff, M., 2015. Biosens. Bioelectron. 64, 605–610.
Nolte, H.-J., Rosenberry, T.L., Neumann, E., 1980. Biochemistry 19, 3705–3711.
Persike, M., Zimmermann, M., Klein, J., Karas, M., 2010. Anal. Chem. 82, 922–929.
Pouokam, E., Rehn, M., Diener, M., 2009. Eur. J. Pharmacol. 615, 40–49.
Rosenberry, T.L., Chen, Y.T., Bock, E., 1974. Biochemistry 13, 3068–3078.
Sohn, I.-Y., Kim, D.-J., Jung, J.-H., Yoon, O.J., Thanh, T.N., Quang, T.T., Lee, N.-E., 2013. Biosens. Bioelectron. 45, 70–76.
Spradling, K.D., Dillman, J.F., 2011. Adv. Mol. Toxicol. 5, 111–144.
Storm, J.E., Rozman, K.K., Doull, J., 2000. Toxicology 150, 1–29.
Uutela, P., Reinilä, R., Piepponen, P., Ketola, R.A., Kostiainen, R., 2005. Rapid Commun. Mass Spectrom. 19, 2950–2956.
Wei, J., Ren, J., Liu, J., Meng, X., Ren, X., Chen, Z., Tang, F., 2014. Biosens. Bioelectron. 52, 304–309.
Wessler, I., Kirkpatrick, C.J., 2008. Br. J. Pharmacol. 154, 1558–1571.
White, K.E., Cummings, J.L., 1996. Compr. Psychiatry 37, 188–195.

8.12 "Dynamic extracellular imaging of biochemical cell Activity using InGaNGaN nanowire arrays as nanophotonic orobes"

Hölzel S, Zyuzin MV, Wallys J, **Pouokam E**, Müßener J, Hille P, Diener M, Parak WJ, Eickhoff M. *Adv. Funct. Mater.* (2018) 28:1802503.

Impakt Faktor: 13.325

Eigener Anteil an der Publikation:

- Initiative: 15 %
- Projektplanung: 30 %
- Durchführung der Versuche: 20 %
- Auswertung der Experimente: 25 %
- Erstellung der Publikation: 25 %

FULL PAPER
Nanophotonics
ADVANCED FUNCTIONAL MATERIALS
www.afm-journal.de

Dynamic Extracellular Imaging of Biochemical Cell Activity Using InGaN/GaN Nanowire Arrays as Nanophotonic Probes

Sara Hölzel, Mikhail V. Zyuzin, Jens Wallys, Ervice Pouokam, Jan Müßener, Pascal Hille, Martin Diener, Wolfgang J. Parak, and Martin Eickhoff*

The application of InGaN/GaN nanowire heterostructure arrays as photonic probes for dynamic imaging of biochemical and cellular processes in an incident light fluorescence microscope is demonstrated. The photoluminescence intensity of InGaN/GaN nanowires sensitively depends on the pH value of the surrounding solution, making them suitable probes for the optical detection of biochemical processes accompanied by local pH variations. Grown on a conductive substrate, the nanowire arrays can be operated in a well-defined electrochemical working point with high sensitivity and stability. The achievable pH and bias resolution as well as signal-to-noise ratio are assessed as a function of the working point and for different integration times. A bias resolution of 1 mV and a pH resolution of 0.03 are achieved at a time resolution below 25 ms. The application for dynamic imaging of the activity of isolated intestinal crypts from Wistar rats is demonstrated. Here, the pH change in the vicinity of the crypt is quantified and attributed to the activity of the sodium-proton exchanger (NHE). Imaging of the effect of amiloride and NH_4Cl on its activity is demonstrated with a spatial resolution of <0.63 µm and reveals that NH_4Cl-induced NHE activation preferentially occurs in the upper part of the crypt.

1. Introduction

Semiconductor biosensors that offer the possibility for spatially resolved dynamic imaging of biochemical processes are of high interest for applications in medical screening, pathology, or medical research.[1–3] In such an approach not only optical excitation, but also optical readout of the transducer response within the boundary conditions provided by a standard optical microscope setup is an important requirement for application. This is in contrast to the complex electronic infrastructure that is required in the case of sensor arrays based on solution gate field-effect transistors.[4–7] In this concept, the temporal evolution of the measurand is transformed into an optical response that is detectable at room temperature and under physiological conditions. The resulting dynamic (bio-)chemical contrast superimposed to the optical microscope image enables a substantial enhancement of functionality. To satisfy the resulting simultaneous demands for a high luminescence efficiency and a high spatial resolution, the minority carrier lifetime can be artificially reduced, as it is the case in semiconductor nanostructures that currently represent the only material platform that fulfills these requirements.

Fluorescent semiconductor nanoparticles (NPs), so-called quantum dots (QDs; e.g., CdSe, ZnSe, and ZnS), have received a lot of interest.[8] The NP core size, typically below 10 nm, can be adjusted during the cheap fabrication process and determines the emission wavelength. In addition, nonradiative surface recombination can be reduced in core–shell heterostructures, resulting in efficient luminescence also at room temperature.[9] Therefore, QDs are good labels for bioimaging and detection.[10–12] Bioimaging in the form of immunostaining can be achieved by specific binding of functionalized luminescent

S. Hölzel, Dr. J. Müßener, Dr. P. Hille, Prof. M. Eickhoff
Institute of Solid State Physics
University of Bremen
28359 Bremen, Germany
E-mail: shoelzel@ifp.uni-bremen.de
S. Hölzel, Dr. J. Wallys, Dr. J. Müßener, Dr. P. Hille, Prof. M. Eickhoff
Institute of Experimental Physics I
Justus Liebig University Giessen
35392 Giessen, Germany
Dr. M. V. Zyuzin, Prof. W. J. Parak
Philipps-Universität Marburg
Renthof 7, 35037 Marburg, Germany
The ORCID identification number(s) for the author(s) of this article can be found under https://doi.org/10.1002/adfm.201802503.
Dr. M. V. Zyuzin
Department of Nanophotonics and Metamaterials
ITMO University
St. Petersburg 197101, Russia
Dr. E. Pouokam, Prof. M. Diener
Institute for Veterinary Physiology and Biochemistry
Justus Liebig University Giessen
35392 Giessen, Germany
Prof. W. J. Parak
Universität Hamburg
Center for Hybrid Nanostructures
Luruper Chaussee 149, 22607 Hamburg, Germany

DOI: 10.1002/adfm.201802503

 © 2018 WILEY-VCH Verlag GmbH & Co. KGaA, Weinheim

NPs to antibodies, followed by fluorescence imaging.[13] Semiconductor NPs have also been applied to record the motion of the cytoplasm by tracing the NP fluorescence over time[11] and are frequently used for microscope-assisted applications in diagnostics and life science. Concerning the detection of (bio-)molecules, fluorescence resonant energy transfer to molecules that specifically bind to the functionalized NP shell results in a quenched fluorescence intensity or a redshift of the fluorescence light that can both be observed and located in an optical microscope image.[14]

While the detection of neural action potentials by changes in QD fluorescence has been discussed since a decade,[15] experimental realization suffers from low signal-to-noise ratios (SNRs).[16,17] Instead of recording electrical activity, changes in cellular metabolism can also be detected by pH measurements.[18] However, the electrochemical potential of NPs with respect to the surrounding electrolyte cannot be defined, disabling the relation of quantitative detection of changes in surface potential to changes in the local pH value. Moreover, cytotoxic effects of CdSe/ZnS NPs,[19] one of the most frequently used NP types for optical labeling and detection, are still a topic of discussion with respect to potential in vivo applications.

Recently, we have shown that the photoluminescence (PL) properties of GaN and InGaN nanowires (NWs) in aqueous solutions sensitively respond to variation in the ion concentration of the surrounding electrolyte.[20] The material system of the group III-nitrides (III-N) in general has been demonstrated to be excellently suited for biochemical applications, as it exhibits a high electrochemical stability, is nontoxic to living cells, and exhibits a high pH sensitivity of about 55 mV pH^{-1}.[21–23] The reproducible covalent immobilization of organic molecules on the GaN surface with maintaining their functionality has also been demonstrated.[24,25]

Self-assembled GaN-based NWs and nanowire heterostructures (NWHs), first reported in 1997,[26] combine a low density of structural defects with the excellent optical and electrochemical properties of the III-N material system. On the one hand, they open the possibility for the study of fundamental material properties such as doping[27,28] or quantum confinement effects in embedded AlGaN/GaN or InGaN/GaN heterostructures, where the incorporation of indium allows shifting the range of absorption and photoluminescence emission to the visible part of the spectrum.[29,30] On the other hand, employing the interaction of photoexcited carriers and chemical surface processes, such InGaN/GaN NWs have recently been applied as fluorescence probes for the analysis of water adsorption[31] or for optical gas detection.[32] In ref. [33] InGaN/GaN NW arrays have been used as a photoelectrode for the realization of photoelectrochemical biosensors, benefiting from growth on a conductive substrate. This latter fact was also employed in ref. [20] where the possibility of adjusting a well-defined electrochemical working point has been used to realize pH-sensitive photonic probes based on InGaN/GaN NWs.

Here, we state that the combination of the unique chemical surface properties of the group III-nitride materials with the excellent optoelectronic properties and the high surface-to-volume ratio of InGaN/GaN NWs as nanophotonic probes allows the realization of optochemical electrodes (OCEs) for extracellular dynamic imaging of biochemical and cellular processes. We assess the applicability and performance within the boundary conditions defined by a standard fluorescence microscope, benefiting from the possibility of operating the OCE at an electrochemically well-defined working point. The latter allows the optimization of sensitivity and stability and enables spatially resolved, quantitative analysis of local pH variations caused by cellular processes. We demonstrate the potential of this approach by monitoring transcellular activity of isolated intestinal crypts from Wistar rats as a model system while inhibiting the activity of the Na^+/H^+ exchanger (NHE) (by amiloride or energy depletion with 2,4-dinitrophenol (DNP)) and during uptake of NH_3 from the extracellular space.

2. Results and Discussion

2.1. Basic Characterization of InGaN/GaN NW Nanophotonic Probes

The InGaN/GaN NWs in the heterostructure arrays used in the present experiments consist of a GaN base and an InGaN top region, as schematically shown in **Figure 1**a. Scanning electron microscope (SEM) images of the investigated arrays are presented in Figure 1 in side view (a) and top view (b).

The NW heterostructure ensembles feature an intense, broad photoluminescence emission band ranging from 450 to 700 nm (≈2.7–1.8 eV, respectively) (cf. **Figure 2**) at room

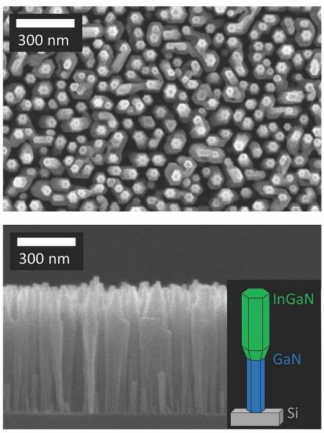

Figure 1. a) Side-view and b) top-view scanning electron microscopy image of an InGaN/GaN NW ensemble. The inset in (a) shows the schematic of the heterostructure.

 © 2018 WILEY-VCH Verlag GmbH & Co. KGaA, Weinheim

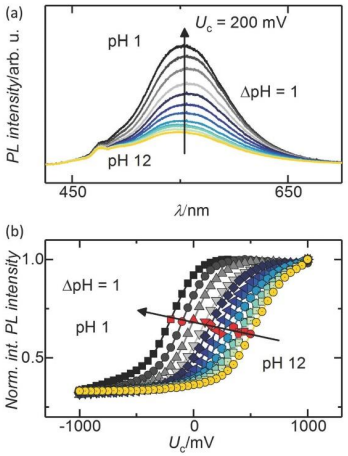

Figure 2. a) Room temperature PL spectra of the InGaN/GaN NW heterostructure arrays at a cathodic bias of 200 mV for different pH. b) Integrated PL intensities (400–700 nm) of InGaN peak in dependence of the cathodic bias voltage for different pH. The position of the working points is indicated in red.

temperature. The width of this emission band is due to an inhomogeneous indium distribution within each NW and wire-to-wire fluctuations.[30,34]

When operated as working electrode in an electrochemical cell, the photoluminescence characteristics depend on the solution pH and on the applied bias with respect to the reference electrode. In Figure 2a, the PL spectra of an InGaN/GaN NW heterostructure array at a cathodic bias voltage (U_c) of 200 mV are shown for different electrolyte pH. In Figure 2b, the integrated PL intensities normalized to the maximum as a function of U_c are compared for different pH.

The PL intensity of the InGaN/GaN NW heterostructure arrays sensitively responds to changes of the solution pH and the applied bias. At constant bias, a decreasing pH of the electrolyte solution results in an enhancement of the PL intensity as it is also the case for an increasing U_c at constant pH. In ref. [20] this behavior was attributed to a bias-dependent variation in the effective surface band bending that leads to an enhanced confinement of photoexcited holes as minority carriers inside the NW for increasing cathodic bias or decreasing pH (positive surface charge), while the transfer of holes and thus a decrease in radiative recombination rate is found for anodic bias or increasing pH (negative surface charge) (see Figure S1 in the Supporting Information). The adjustment of the carrier confinement is reversible so that the PL changes can be instantaneously changed back; i.e., in the case of a change in pH the response time is only limited by the fluid exchange in the measurement chamber.[20]

Based on the calibration diagrams for the dependence of the PL intensity on U_c in Figure 2b, the photoelectrochemical working point, i.e., the point of highest sensitivity, is defined as the inflection point of the S-shaped curves for a fixed pH (cf. Figure 2b, red data points). In this point, the highest PL response to variations in the surface potential at a given pH is expected.

The pH-induced shift of the calibration curves in the acidic pH range (pH = 1–4) is about 120 mV pH^{-1}, and 80 mV pH^{-1} for the neutral to alkaline pH range, which equals a resolution of pH differences of 0.008–0.0125 for a variation in the surface potential by 1 mV.

In the following, the pronounced sensitivity of the PL characteristics with respect to variations in the pH will be employed for the application of InGaN/GaN NW heterostructure arrays as nano-optical probes that provide information on local pH changes or local changes in the surface potential caused by biochemical processes. Spatially resolved detection of the pH changes, i.e., imaging of the biochemical activity, will be performed by recording time-dependent fluorescence images of the sample in a standard optical microscope setup using a modified electrochemical cell, which allows the immersion of the objective lenses into the electrolyte.

As the most critical issue for this application, the stability of the InGaN/GaN NW heterostructure arrays was assessed in comparison to pH-sensitive probes that are currently in use for biochemical imaging applications.[35] In addition to absorption or fluorescence-based optical probes that do either change the color or show a difference in their fluorescence properties,[35] nanoparticles such as semiconductor quantum dots[36,37] are frequently used as optical transducers and have recently been improved with respect to their stability against photobleaching.[38]

It should be noted that in comparison to these approaches InGaN/GaN nanowires do also hold a high surface-to-volume ratio but can be operated independently from the surrounding pH and without the need for additional functional groups linked to the surface. Here, we exemplarily compare the stability of the InGaN/GaN NWs heterostructures to that of poly(fluorescein isothiocyanate allylamine hydrochloride) (PAH-FITC) and CdSe quantum dots by time-dependent fluorescence measurements in 10×10^{-3} M phosphate-buffered salt (PBS) at pH 7 under continuous excitation.

The intensities of the different fluorescent probes, displayed in **Figure 3**a, are normalized to the initial value. The CdSe QDs and the dye PAH-FITC were immobilized on a silicon substrate and coated with two bilayers of poly(sodium 4-styrenesulfonate)/poly(allylamine hydrochloride) (PSS/PAH) for stabilization.[39] They are denoted as CdSe QDs/$(PSS/PAH)_2$ and PAH-FITC/$(PSS/PAH)_2$ in the following. The NWs samples and the silicon substrates functionalized with QDs and fluorescent dye (FITC) were continuously irradiated for 45 min and fluorescence images were recorded every 2 min. Afterward, the images were analyzed as described below and the fluorescence intensities were derived and plotted versus irradiation time.

 © 2018 WILEY-VCH Verlag GmbH & Co. KGaA, Weinheim

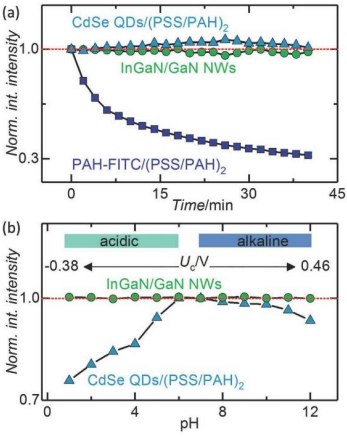

Figure 3. a) Transient fluorescence measurements of an InGaN/GaN NW heterostructure ensemble biased at 1 V, unbiased CdSe QDs on Si with $(PSS/PAH)_2$, and unbiased PAH-FITC on Si with $(PSS/PAH)_2$ at pH 7. The intensities are normalized to the initial value. Both the NW heterostructure and the CdSe QD electrode exhibit a stable fluorescence intensity over the investigated time interval. Excitation wavelengths were 470 ± 40 nm, the detection wavelengths were 525 ± 50 nm for PAH-FITC and CdSe QDs, and 615 nm for the NW heterostructure, respectively. The integration times were 500 ms for CdSe-QDs and for PAH-FITC, and 200 ms for InGaN/GaN NWs. A tenfold objective lens was used. b) Comparison of the fluorescence intensities of CdSe QDs and InGaN/GaN NWs as a function of the pH. The integrated intensities are normalized to the starting value of the series for the QDs and the InGaN/GaN NWs (starting value at $U_c = 0.2$ V). For the QDs, an irreversible decrease of the fluorescence is detected for the acidic series from pH 6 to pH 1. In the alkaline series, the pH values were increased from pH 7 to pH 12. At alkaline pH, the fluorescence intensity decreases. The photoluminescence intensity of the InGaN/GaN NWs can be kept constant by application of an appropriate bias potential U_c from −0.38 to 0.46 V, respectively. By doing so, the PL intensity was adjusted to the PL intensity at $U_c = 0.2$ V at pH = 7. No permanent degradation was observed. A tenfold objective lens was used.

In the transient fluorescence measurements, both InGaN/GaN NW heterostructures and CdSe QDs sample exhibit an almost constant PL intensity. The PL intensity of the QDs exhibits a slight increase in the beginning, known as "photobrightening."[40] Note that, however, for longer illumination times CdSe QDs suffer from photobleaching. The PL intensity of the InGaN/GaN NWs sample merely decreases less than 2% in the investigated time interval. In contrast, PAH-FITC samples show strong photobleaching with a fast decrease of 50% in less than 20 min, as it was also reported earlier.[41,42]

Whereas both the InGaN/GaN NWs and the QDs exhibit acceptable long-term stability of the photoluminescence, the application of the unbiased CdSe QDs is restricted to a small range in the neutral pH regime of 6 < pH < 8[43] and 6 < pH < 9,[44] respectively, as an irreversible decrease of the PL intensity is observed outside this pH range, as shown in Figure 3b.

The instability of CdSe QDs for acidic and alkaline pH has also been reported in refs. [43] and [44]. Beyond neutral pH, CdSe QDs may start to corrode.[44] In contrast, the possibility of operating InGaN/GaN NW arrays at a well-defined electrochemical potential allows the definition of a working point. While the pH was varied between pH = 1 and pH = 12 the respective bias potential U_c was simultaneously adjusted between −0.38 and 0.46 V to compensate for the pH-induced changes in PL intensity, thus keeping it at the same value as initially recorded for $U_c = 0.2$ V at pH = 7. As a result, the surface band bending remained constant and degradation due to oxidation processes was suppressed in the entire pH range (Figure 3b).

Recently, carbon-based nanomaterials (carbon dots) were investigated as optical probes for bioimaging and fluorescence-based sensing[45,46] and were shown to be applicable only in comparatively small pH ranges between pH = 9 and pH = 14[45] or between pH = 6 and pH = 12.[46] Also in that case photoelectrochemical control, i.e. operation in a well-defined working point of optimized sensitivity and stability around pH = 7.4 as demonstrated for the InGaN/GaN nanowire OCEs in the present study, is not possible.

2.2. Analysis in Fluorescence Microscope Environment

To further assess the pH and bias response of InGaN/GaN NW heterostructure ensembles that can be recorded when operated as an OCE in an optical microscope environment, i.e., for the experimental conditions described above, the evolution of the fluorescence images was studied as a function of both U_c and pH value of the electrolyte solution.

In a first step, the integrated luminescence intensity of an area of ≈15 000 µm² (for an NW density of ≈180 NWs µm^{-2} this corresponds to 2.7×10^6 excited NWs) was recorded as a function of U_c for different pH values between pH = 2 and pH = 10 in steps of ΔpH = 1, as depicted in **Figure 4**a. For each pH, the intensity increases with increasing U_c, following the S-shape behavior shown in Figure 2b[20] and saturates at an intensity of 40% above the starting value for low pH and of 65% of the starting value at higher pH. For more acidic conditions the deflection point shifts to smaller values of U_c by 200 mV pH^{-1} for acidic pH and 40 mV pH^{-1} for the neutral and alkaline pH range, which equal a resolution of pH differences of 0.005–0.025 for 1 mV bias resolution. The micrographs in Figure 4b show the fluorescence images of a patterned OCE (width of the NW ring patterns: 20 µm) for pH values of 6, 3, and 1 at $U_c = 100$ mV demonstrate that a chemical contrast due to spatially varying pH can already be detected by the naked eye.

The achievable resolution with respect to variations in the surface potential or pH was investigated in more detail, exemplarily summarized in **Figure 5**. Figure 5a depicts the mean intensity between $U_c = 670$ and $U_c = 680$ mV with a step width

 © 2018 WILEY-VCH Verlag GmbH & Co. KGaA, Weinheim

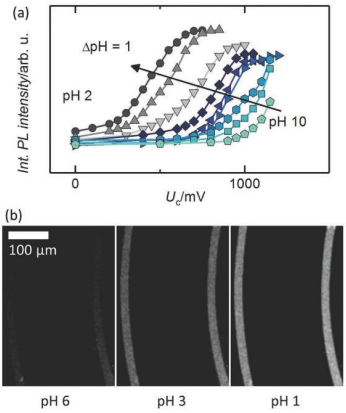

Figure 4. a) Integrated luminescence intensity of microscope images of an InGaN/GaN NW array as a function of U_c for different pH. The electrochemical working point with maximum linear sensitivity is indicated in the figure by a black arrow. The exposure time was 100 ms and a 63-fold objective lens was used. b) Fluorescence images of a patterned InGaN/GaN NW array (ring width: 20 µm) recorded with a fluorescence microscope and a tenfold objective at U_c = 100 mV for pH 6, 3, and 1. The exposure time was 300 ms.

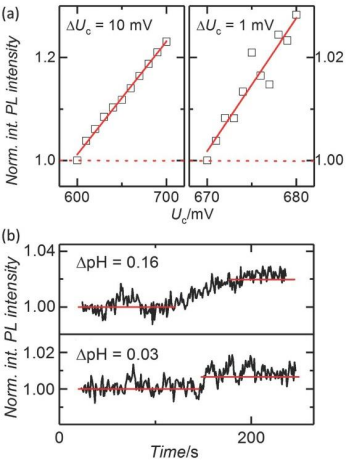

Figure 5. a) Integrated PL intensity for a PBS solution pH 7.2 in dependence of the applied bias voltage from U_c = 670 to U_c = 680 mV with a step size of 1 mV, which can be clearly resolved. The exposure time was 100 ms and a 63-fold objective lens was used. b) Transient measurements of the PL intensity in variation of the solution pH at U_c = 400 mV with an exchange of the electrolyte solution with 19.26 mL min^{-1}. The pH resolution limit is below ΔpH = 0.03 for a ten times magnification and an integration time of 300 ms. The integration times are $t_{int.}$ = 500 ms (ΔpH = 0.16) and $t_{int.}$ = 300 ms (ΔpH = 0.03).

of 1 mV. The integrated intensities can clearly be distinguished for bias changes of 1 mV. Figure 5b exemplary shows two transients of a pH drop of ΔpH = 0.16 and ΔpH = 0.03 starting from pH = 7.0 recorded at U_c = 400 mV with integration times ($t_{int.}$) of 500 and 300 ms, respectively.

These results show that the bias resolution of an InGaN/GaN NW OCE in combination with a fluorescence microscope is better than ΔU_c = 1 mV. The pH change from pH = 7 to pH = 6.97 in the transient measurement in Figure 5b demonstrates that the pH resolution for an integration time of 300 ms is better than ΔpH = 0.03 in that regime.

In general, the achievable resolution depends on the sample structure, but also on the measurement settings, in particular on the integration time $t_{int.}$, which determines the achievable SNR in the luminescence measurement. Here, we have analyzed the SNR of fluorescence images of InGaN/GaN NWHs as a function of U_c and $t_{int.}$ by transient recordings of the fluorescence intensity while U_c was varied from 0 V to U_c and then back to 0 V with increasing bias steps of ΔU_c = 100 mV up to 1 V. The integrated intensities are compared for the integration times 25, 50, and 100 ms, respectively. The results are depicted in **Figure 6**a.

From these results, the respective signal-to-noise ratios are calculated as ratios of signal amplitude by noise-standard deviation according to

$$\mathrm{SNR} = \frac{\bar{I}(U_c)}{\sigma\left(\bar{I}(U_c)\right)} \quad (1)$$

with $\bar{I}$ being the mean value of the integrated intensity at U_c and with the standard deviation σ. The resulting SNRs as a function of U_c are shown for the different integration times in Figure 6b.

The noise amplitude in the integrated fluorescence intensities in Figure 6a decreases with increasing $t_{int.}$, i.e., the detection limit increases when the integration time is increased. The calculated SNRs, shown in Figure 6b, are independent from U_c. The SNR shows a distinct dependence on the integration time and increases from $t_{int.}$ = 25 ms to $t_{int.}$ = 100 ms by a factor of 1.32.

2.3. Biochemical Application

The high sensitivity of InGaN/GaN NW OCEs toward local pH changes and variations in the surface potential in combination with the operation at a well-defined electrochemical

 © 2018 WILEY-VCH Verlag GmbH & Co. KGaA, Weinheim

ADVANCED SCIENCE NEWS
www.advancedsciencenews.com

ADVANCED FUNCTIONAL MATERIALS
www.afm-journal.de

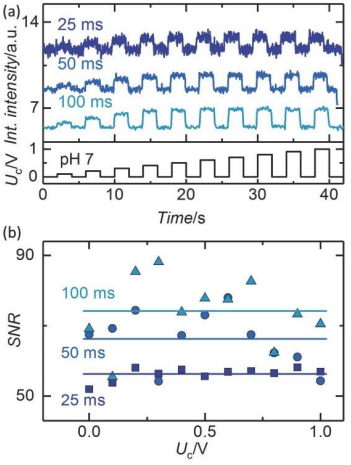

Figure 6. a) Integrated intensities in dependence of U_c for three different integration times. Increasing the integration time results in an increase of the signal-to-noise ratio. b) The SNR increases with increasing the integration time from 25 to 100 ms by 1.32. Here, a tenfold objective is used.

working point with high sensitivity and electrochemical stability represents excellent prerequisites for the application in extracellular space and time resolved imaging of biochemical processes accompanied by local pH changes or potential fluctuations caused by cell activity and metabolism.

As a model system for cellular biochemical transport mechanisms, we have analyzed the electroneutral sodium/proton antiport in the cell membrane via sodium-proton exchanger (NHE). Due to the limited means for extracellular pH detection, this process is usually studied as a function of the intracellular pH.[47–49] In this line, the cells are loaded with a pH-sensitive dye that might undergo photobleaching.[50,51] Ion-sensitive field-effect transistors in close proximity to the cell were demonstrated to allow for measurements of the extracellular pH changes of the NHE,[52,53] but lack the opportunity of imagining or spatially resolved analysis. Here, we demonstrate that InGaN/GaN NW probes can be used to dynamically image the cell activity by monitoring blocking of the NHE and the NH_3 uptake by the cell.

Isolated intestinal crypts from Wistar rats as a model system were extracted and deposited on the surface of the InGaN/GaN NW OCE with each nanowire acting as an extracellular pH probe according to the preparation process described below.

As a first assessment for the functionality of the OCE, the influence of the addition of 1.3×10^{-3} M DNP solution to the buffer solution was studied.

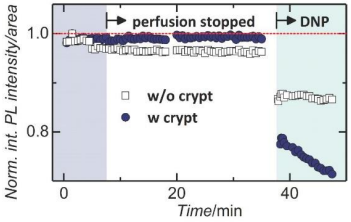

Figure 7. Analysis of the crypt activity using InGaN/GaN NW OCE is shown by constantly perfusing the electrolyte solution without additives and an addition of a solution with 1.3×10^{-3} M 2,4-dinitrophenol (DNP) after 38 min. The intensities for the nanowires with and without crypt do not show a change until the addition of DNP. After adding DNP to the electrolyte solution, the intensity of the area with crypt decreases whereas the intensity of the area without crypt shows a constant signal. The images were recorded at U_c = 200 mV with an integration time of $t_{int.}$ = 250 ms and a tenfold objective lens.

DNP is an uncoupler of oxidative phosphorylation, the mechanism leading to ATP (adenosine triphosphate) synthesis in mitochondria. As a consequence of DNP application, activity of pumps such as the Na^+/K^+ pump depending on ATP slows down. The Na^+/K^+ pump is located in the basolateral membrane of enterocytes (crypt cells) and builds an extracellularly oriented Na^+ concentration gradient by extruding 3 Na^+ while taking 2 K^+ up into the cell. The reduced intracellular concentration of Na^+ energizes the Na^+/H^+ exchanger for Na^+ uptake and H^+ extrusion. After such an indirect inhibition, the rate of transport via the NHE is depressed,[54] which results in a reduced affinity of the Na^+-H^+-exchange for H^+.[55] As this is a measure for extracellular alkalization, it is expected to result in an intensity decrease of the OCE luminescence.

The results displayed in **Figure 7** show that the intensity of the OCE areas with and without crypts do not show any changes in intensity when the system is perfused with modified Tyrode's solution. Since the DNP solution was directly added into the measurement chamber, the peristaltic pump was stopped before the addition, which does not lead to a change in fluorescence intensity. The addition of DNP to the buffer solution results in an initial decrease of the intensity in both regions due to enhanced light absorption in the fluid. In the following, the OCE fluorescence intensity in the region without crypt remains constant, whereas it continuously decreases in the areas with crypt due to a running down of the NHE activity after energy depletion and therefore de-energization of the antiporter. This result highlights the mechanistic of cell regulation of pH and energy. The estimated pH change in the investigated time interval based on the results of Figure 4a is $\Delta pH = 1.85$. Studies on the ATP dependence of NHE reported in ref. [54] showed a pH change of about $\Delta pH = 1$ upon ATP activation of depleted cells, in reasonable agreement with the present findings.

Spatially resolved analysis of the extracellular pH change induced by the activity of the Na^+/H^+ antiporter of the crypt

© 2018 WILEY-VCH Verlag GmbH & Co. KGaA, Weinheim

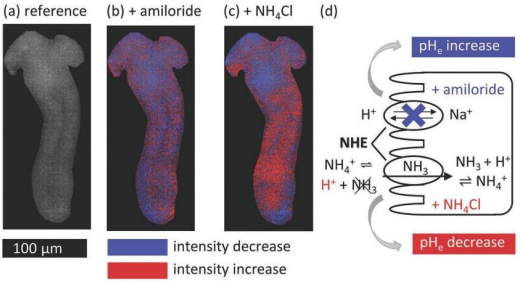

Figure 8. a) Spatially resolved image of the crypt on top of the NW array in the presence of modified Tyrode's solution as reference. b,c) Intensity decrease (blue) and increase (red) after changing the buffer solution to modified Tyrode's solution with b) 0.1×10^{-3} M amiloride and c) 20×10^{-3} M NH_4Cl. The spatially resolved intensity change provides a chemical contrast that is generated by the OCE. The addition of amiloride results in a net intensity decrease, i.e., a local alkalization in the vicinity of the cell that is attributed to the blocking of the NHE with amiloride (②, cf. Figure 9). In contrast, the intensity increases in the presence of ammonium chloride as NH_3 is taken up by the cells via nonionic diffusion across the cell membrane resulting in an enhanced dissociation of NH_4^+ in the extracellular medium to keep the chemical equilibrium constant (③, cf. Figure 9). d) Schematic of an epithelial cell with resulting change of the extracellular pH. The blocking of the amiloride-sensitive NHE in the apical surface is shown in blue and the extracellular acidification due to cellular uptake of NH_3 in red. The integration time was $t_{int.} = 250$ ms and a tenfold objective lens was used. (a)–(c) represent only the section with crypt of the images.

was analyzed by direct evaluation of the transient fluorescence image of the OCE area covered with crypt during changes of the buffer solution using the charge-coupled device (CCD) camera (211 megapixel, monochrome, 1200 pixel × 1600 pixel resolution) of the microscope.

In **Figure 8**b the evolution of the fluorescence intensity image upon addition of the NHE inhibitor amiloride (0.1×10^{-3} M amiloride) is shown, while Figure 8c displays the effect of the addition of ammonium chloride (20×10^{-3} M NH_4Cl). The measurement was performed at $U_c = 200$ mV.

In Figure 8a, a fluorescence image of the OCE covered with crypt in modified Tyrode's solution at pH 7.4 is shown. In this image, which serves as reference for the determination of the changes in fluorescence intensity, the contour and the surface of the cell are apparent.

Comparison to the image obtained after changing to the buffer solution with 0.1×10^{-3} M amiloride (Figure 8b) shows that the fluorescence intensity decreases almost homogenously along the crypt's surface. This decrease corresponds to an increase of the pH in close vicinity of the cell due to inhibition of the NHE activity with amiloride (Figure 8d). In contrast, Figure 8c depicts an image of the intensity increase upon addition of 20×10^{-3} M NH_4Cl to the buffer solution caused by a decreasing pH. The image clearly shows that this preferably occurs in the lower part of the crypt.

The reason for this regional difference probably reflects known differences in the expression of pH-regulatory ion transporters along the crypt axis. The undifferentiated cells near the crypt fundus show only a low activity of Na^+/H^+ exchange.[47] In contrast, the more differentiated cells near the surface region absorb Na^+ and Cl^- via Na^+/H^+ exchanger(s) and Cl^-/HCO_3^- (OH^-) exchanger(s). In the presence of NH_4Cl (which causes an intracellular alkalization; Figure 8d), this will reduce the activity of cellular proton export via NHE, which will therefore reduce the extracellular acidification measured here near those regions of the crypt with high NHE activity, i.e., in the upper part of the crypts. The intensity decrease in the lower part of the cell is due to a slight difference in cell position.

Chemical imaging using the NW array bears the advantage of locating the areas of biochemical activity and thus allows identifying the possible origin of the observed effects. Intestinal crypts are found in the tunica mucosa and they form glands with lamina epithelialis mucosae on the inside, which is constituted of epithelial cells.[56] Crypts absorb water and ions like Na^+ from the chyme via channels or carriers such as the NHE. The NHE is an amiloride-sensitive transport protein whose activity is inhibited in the presence of amiloride and its derivatives by occupation of extracellular Na^+-binding sites[57] (realized by purging with a reference buffer solution with 0.1×10^{-3} M amiloride in the experiments). As a result, the proton transport is suppressed and the pH of the extracellular environment increases, thus leading to a decrease in PL intensity during this interval ((b) in Figure 8 and ② in **Figure 9**).

Loading of the cell with ammonia (realized by the addition of 20×10^{-3} M NH_4Cl to the buffer solution) results in a decreased intracellular proton concentration and consequently in an reduced proton extrusion, which can be recognized in the reduction of slope of the PL signal change induced by amiloride after the intracellular alkalization (**Table 1**; amiloride II)

 © 2018 WILEY-VCH Verlag GmbH & Co. KGaA, Weinheim

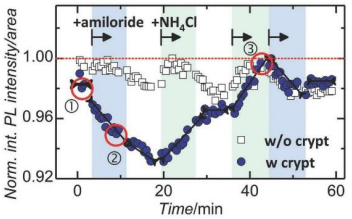

Figure 9. Transient behavior of the mean fluorescence intensity of the OCE during exchange of buffer solutions. The delay due to the electrolyte exchange is considered. After the addition of 0.1×10^{-3} M amiloride, the PL intensity of the area with crypt decreases significantly compared to the reference region. The addition of 20×10^{-3} M NH_4Cl results in a re-increase of the PL intensity. The changes in PL intensity of reference region can be assigned to small differences in pH and temperature of the buffer solutions. The measurements were recorded at $U_c = 200$ mV with an integration time of $t_{int.} = 250$ ms and a tenfold objective lens.

in comparison to the control situation with physiological intracellular pH (Table 1; amiloride I).

For the measurement conditions applied here (10x objective lens, image recording with 1200 pixel × 1600 pixel resolution) the achievable spatial resolution is better than 0.63 µm.

The images shown in Figure 8 were quantitatively analyzed to associate the intensity changes with the cell activity or specifically the NHEs of the crypts. For that purpose, the integrated intensities of transient fluorescence mappings with the presence of the NHE-inhibitor amiloride or NH_4Cl were recorded where the intensities were analyzed as a function of the buffer solutions, which involved the presence of the NHE-inhibitor amiloride or NH_4Cl used for alkalization of the cell. The properties of the arrays allow establishing a relation between the intensity changes and changes of the extracellular pH.

All images were quantitatively evaluated by an integration of the intensity of the OCE covered with crypts and of reference region of the OCE itself. For this purpose, an image mask was created for each image that defines the cell outline and allows for correction of the cell motion on the OCE. The mask generation is described in more detail below. Figure 9 shows the evolution of the resulting mean PL intensity for those parts of the InGaN/GaN NW electrode covered with crypt (blue) compared to those without crypt (white) for alternating exposure to amiloride and NH_4Cl-containing buffer solutions. The intensities are normalized to the area and to their maximum value for better comparison.

Table 1. Summary of calculated slopes (change of normalized intensity per area per time) in the presence of 0.1×10^{-3} M amiloride and 20×10^{-3} M NH_4Cl for the first (I) and the second (II) sequence.

Slope/10^{-3}/(area * min)	+ amiloride I	+ amiloride II	+ NH_4Cl I	+ NH_4Cl II
NWs covered with crypt	−3.04	−2.44	3.17	3.96
NWs	−0.37	−1.62	−0.88	0.85

In the areas of the OCE covered with crypt a pronounced decrease of the PL intensity was recorded in both sequences with the amiloride-containing buffer solution. In turn, the presence of NH_4Cl results in a strong luminescence increase. In contrast, the reference regions without crypt show only a small decrease in PL intensity in the periods containing amiloride and nonsystematic small variations for the presence of ammonium chloride. These small intensity fluctuations are assigned to variations in buffer pH and temperature induced by the buffer exchange. The slopes of the intervals with NHE blocker and activator in the electrolyte solution were calculated and are summarized in Table 1.

The slopes of the PL signal in the OCE areas covered with crypt during the two different intervals with the amiloride-containing buffer reveal that the dynamics of the intensity changes are significantly dominated by the cell activity, resulting in comparable evolution of the recorded signal during the respective sequences (I, II) of intervals with addition of amiloride and NH_4Cl.

The decrease in the PL intensity of the results with crypt in both amiloride sequences can be correlated to the blocking of the NHE because alkalization of the electrolyte results in a decrease of the PL intensity for InGaN/GaN NWs.

The differences in the respective luminescence transients recorded for the regions with and without crypts demonstrate that the observed changes can be unambiguously assigned to blocking the NHE by amiloride and to the extracellular acidification due to cellular uptake of NH_3. The estimated pH change extracted from the calibration curves based on a sensitivity of 35.8 mV pH^{-1} for this sample in that pH regime is $\Delta pH = +0.68$ for amiloride and $\Delta pH = -0.84$ for NH_4Cl, which are comparable to the intracellular pH changes determined by pH-sensitive fluorescent dyes with $\Delta pH \approx 0.5$ for the inhibition with amiloride[58] and $\Delta pH = 0.68–1.1$ for the NH_4Cl pulse.[47,58,59]

The technique presented here allows for reproducible measurements with small variations found for the absolute pH changes caused by fluctuations in the biochemical activity of the isolated intestinal crypts, as demonstrated in Figure S4 of the Supporting Information. Thus, the pH change upon blocking of the NHE (NH_3 uptake) with amiloride (NH_4Cl) was determined to be in the range of $\Delta pH(\text{amiloride}) = (+0.78 \pm 0.23)$ ($\Delta pH(NH_4Cl) = (-0.59 \pm 0.25)$) considering the results of three different measurements.

Recently, ratiometric fluorescence sensors were demonstrated to monitor the extracellular pH with a simultaneous high spatiotemporal resolution.[60] However, due to stability issues such probes are applicable only in weak alkaline or acidic environments[60] and the achievable pH resolution of $\Delta pH = 0.1$ is significantly lower than the pH resolution demonstrated for InGaN/GaN NWHs here ($\Delta pH = 0.03$). Optical cell imaging based on surface-enhanced Raman scattering showed a subendosomal spatial resolution, but very limited temporal resolution still and a pH resolution of only $\Delta pH = 0.2$.[61]

pH-measurement experimental techniques based on the pH-sensitive fluorescent dye 2′,7′-bis(2-carboxyethyl)-5,6-carboxyfluorescein (BCECF) (used in the ester form BCECF acetoxymethyl ester (BCECF-AM)) allowed for the determination of the intracellular pH.[47,49] However, such techniques encounter a couple of problems regarding signal gain due to the leakage of the dye, the very small fluorescence emission profile evoked

 © 2018 WILEY-VCH Verlag GmbH & Co. KGaA, Weinheim

by pH-dependent changes, the poor signal-to-noise characteristics in ratio imaging and the bleaching of the dye.[62] The latter can only be improved by the advanced method of the ratio of fluorescence intensities measured at two different excitation wavelengths (recommended: $\lambda_{exc} = 490$ nm and $\lambda_{exc} = 440$ nm), while the emission is supposed to be measured at $\lambda_{em} = 535$ nm. Nevertheless, a fast bleaching renders any measurement impossible as even the ratio could not be calculated.

3. Conclusion

We have shown that InGaN/GaN nanowire arrays as optochemical electrodes provide an excellent technology platform for optical detection and extracellular imaging of cellular processes that are accompanied by local pH changes in a standard fluorescence microscope. In contrast to existing optical imaging technologies, the substrate supported nanowires arrays presented here can be operated in a working point of optimized sensitivity, i.e., an optimized signal-to-noise ratio, and enhanced stability, thus allowing long-term monitoring of cellular processes with spatially resolved quantitative evaluation of the related pH changes. We have demonstrated that a pH resolution lower than 0.03 and a time resolution below 25 ms can be achieved. Visualization of the correlation energy/pH upon DNP application was possible. Furthermore, the visualization of the effect of amiloride and NH_4Cl on the activity of the NHE of isolated intestinal crypts by chemical imaging has been demonstrated with a spatial resolution of <0.63 µm and reveals that NH_4Cl-induced activation of the NHE preferentially occurs in the upper part of the crypt. The resulting pH changes upon blocking of the NHE (NH_3 uptake) with amiloride (NH_4Cl) have been determined to be $\Delta pH = +0.69$ ($\Delta pH = -0.84$).

In addition to the visualization of local pH changes demonstrated here, the OCEs should also be capable of visualizing electrical modulations generated by electrogenic cells. Further improvement of the imaging performance in terms of spatial and time resolution by optimization of the photoluminescence efficiency of the NW heterostructures could also allow imaging of neuronal action potentials, as it has been done in similar sensors, but with electric readout.[63] For such experiments the substrate supported NWs could also be used for the electrical excitation. On that account, the interaction between the cell and the OCE can be further optimized by adjusting the surface morphology in terms of NW density and aspect ratio. We anticipate that the integration of InGaN/GaN nanowire-based optochemical electrodes in fluorescence microscopy can be a starting point for more advanced studies of quantitative imaging of chemical and electrical coupling in biochemical and cellular processes.

4. Experimental Section

Reagents: A 10×10^{-3} M PBS solution with a NaCl concentration of 137×10^{-3} M and a KCl concentration of 2.7×10^{-3} M was used. NaCl (purity > 99.8%), Na_2HPO_4 (≥99.5%), KH_2PO_4 (≥98%), and KCl (≥99%) for PBS solution were purchased from Carl Roth (Karlsruhe, Germany).

For modified Tyrode's solution 140×10^{-3} M NaCl, 1×10^{-3} M phosphate buffer, 5.4×10^{-3} M KCl, 12.2×10^{-3} M glucose (≥99.5%; Carl Roth, Karlsruhe, Germany), 1.25×10^{-3} M $CaCl_2$ (from $CaCl_2$*$2H_2O$; ≥99%, Merck Millipore, Darmstadt, Germany), and 1.00×10^{-3} M $MgCl_2$ solution (from $MgCl_2$ *$6H_2O$; ≥99%, Merck Millipore, Darmstadt, Germany) were used.

The pH for PBS solution was adjusted to 7 and the pH of the modified Tyrode's solution was adjusted to 7.4 with sodium hydroxide and hydrochloric acid.

Amiloride (from $C_6H_8ClN_7O \cdot HCl \cdot xH_2O$; ≥ 98%, Sigma-Aldrich, Steinheim, Germany) was used as inhibitor of the NHE. NH_3 uptake by the NHEs was performed using NH_4^+ (from NH_4Cl; ≥99.5%, Sigma-Aldrich, Steinheim, Germany). For energy depletion within the epithelial cells ATP synthesis was blocked using 2,4-dinitrophenol (from $(O_2N)_2C_6H_3OH$; Sigma-Aldrich, Steinheim, Germany).

PAH-FITC (M_w = 56 000), PAH (M_w = 15 000 g mol^{-1}), and PSS (M_w = 70 000 g mol^{-1}) were purchased from Sigma-Aldrich (Steinheim, Germany). All solutions were prepared in Milli-Q water with a resistance higher than 18.2 MΩ cm^{-1}.

Instruments: Fluorescence measurements were carried out with two incident light fluorescence microscopes (Carl Zeiss, Axiotech with electronic control gear FluoArc, AxioCam and an Eclipse 80i microscope, Nikon, s/w camera digital slight DS 2 M BWc, Nikon). A mercury vapor lamp was used as light source, and the light was focused with water immersion objective lenses with different magnifications: W Plan-Apochromat 63x/1.0 M27, W Plan-Apochromat 10x/0.5 M27 75 mm, and Nikon Plan Fluor 10x/0.30 W.

The excitation wavelength was filtered to 530–585 nm whereas the detection wavelength was 615 nm corresponding to the maximum of the InGaN NW PL emission peak.

For measurements with isolated intestinal crypts, the excitation wavelength was filtered to 465–495 nm and the detection wavelength was 515–555 nm.

The experiments were conducted in a homemade electrochemical cell with a three-electrode setup with the NW heterostructure array serving as working electrode, a platinum wire as counter electrode, and a 3 M KCl Ag/AgCl electrode as reference electrode. An external voltage source (Sourcemeter 2400, Keithley Instruments Inc., Cleveland, USA) connected to a potentiostat was used to apply a defined potential difference between the NW electrode and the electrolyte solution. The latter was continuously exchanged and a constant perfusion of the electrolyte solution was maintained throughout the measurements by a peristaltic pump with a pump velocity of $\nu = 4.84$ mL min^{-1} and 6 mL min^{-1}.

The measurements were carried out in 10×10^{-3} M PBS solution at room temperature. For the experiments with isolated intestinal crypts, modified Tyrode's solution was used.

For sample characterization, PL measurements of InGaN/GaN NW heterostructures were carried out using a laser diode with a wavelength of 405 nm for excitation. The PL signal was measured in reflection and focused on a USB-CCD-spectrometer (3648 px CCD).

All PL and fluorescence measurements were performed at room temperature.

Preparation of InGaN/GaN Electrodes: Nonintentionally doped InGaN/GaN NW heterostructures (cf. Figure 1) were grown in a self-assembled and catalyst-free growth process by plasma-assisted molecular beam epitaxy on Si (111) using nitrogen-rich conditions. The growth temperature of the GaN NW base is 720 °C and the InGaN part is deposited at a substrate temperature of 500 °C. Further details on the growth process are reported in refs. [20] and [30]. Ohmic backside contacts (80 nm Al/100 nm Ag) were deposited by thermal evaporation onto the Si substrate after removal of the native oxide layer in buffered hydrofluoric acid solution. The nanowires had a length of (307 ± 29) nm and a diameter of (56 ± 13) nm as obtained from SEM analysis. The nanowires of the arrays used for experiments with crypts were (640 ± 18) nm in length and (45 ± 11) nm in diameter. The geometry of the NW heterostructures is schematically depicted in Figure 1a. From the position of the emission maximum

 © 2018 WILEY-VCH Verlag GmbH & Co. KGaA, Weinheim

in room temperature PL spectra, the In content is calculated to be ≈33%–38% according to ref. [64]. The estimated In content from X-ray diffraction measurements yielded an In content of 10%, indicating an inhomogeneous In distribution with local In accumulations that determine the transitions energies of the PL.[30]

Modification of Silicon Substrate with Fluorescein Dye: The surface of silicon substrate was coated with polyelectrolyte solutions using a layer-by-layer method[65] and a spin coating technique. The polycationic solution of poly(allylamine) hydrochloride conjugated with fluorescein was deposited onto the Si substrate (PAH-FITC, c = 2 mg mL^{-1}, V = 20 µL, pH 6.5) for 15 min. The substrate was then spun for 1 min at 6000 rpm. After rinsing, polyanionic PSS (c = 2 mg mL^{-1}, V = 20 µL, pH 6.5) was added to the PAH-FITC layer for 15 min with following spun at 6000 rpm for 1 min. Afterward two additional PAH layers and one PSS layer were deposited onto the substrate.[39] The overall structure of FITC modified Si substrate was then Si/PAH-FITC/$(PSS/PAH)_2$ (2 corresponds to the number of polyelectrolyte bilayers).

Modification of Silicon Substrate with Quantum Dots: CdSe quantum dots were synthesized according to the previously published protocols.[66,67] Then, QDs were immobilized on the Si substrate. For this, a spin coating technique was used and a solution of CdSe QDs (V = 20 µL, c = 15.45 × 10^{-6} M in toluene) was added onto the electrode while rotating at 6000 rpm for 1 min. Then, the polyelectrolyte solutions were deposited onto the dried QDs-modified Si substrate using a layer-by-layer technique.[65] Polyanionic PSS (c = 2 mg mL^{-1}, V = 20 µL, pH 6.5) was added on the top of the QDs for 15 min. The Si substrate was spun for 1 min at 6000 rpm in order to remove the nonattached polyelectrolytes. The substrate was then rinsed with water. Afterward, polycationic PAH (c = 2 mg mL^{-1}, V = 20 µL, pH 6.5) was added to the PSS layer for 15 min and spun for 1 min at 6000 rpm. After the rinsing, another PSS/PAH bilayer was deposited following the same procedure.[39] The resulted structure of Si substrate could be expressed as follows: Si/QDs/$(PSS/PAH)_2$.

Crypt Isolation: Intestinal crypts of Wistar rats of both sexes with a body mass of about (200 ± 20) g were used. Only rats with a weight of up to 220 g exhibit intact crypts.[68] The rats were bred and housed at the Institute of Veterinary Physiology and Biochemistry of the Justus Liebig University Giessen. The ambient temperature and the relative humidity were set at 22.5 °C and 50%–55 %, respectively. Additionally, a 12 h:12 h light-dark cycle and free access to water and food were guaranteed before starting experiments.

The animals were placed in their home cage, which was covered by a CO_2 delivery lid connected to a CO_2 gas cylinder, containing ambient air (20% O_2). Anesthesia started by a CO_2 flow from the gas cylinder with a flow rate of ≈20% of the cage volume per minute. After unconsciousness (loss of righting reflex) and respiratory arrest, animals were removed from the cage and death was assured by physical methods as anesthetic effects of CO_2 were reversible. Thus, cervical dislocation was conducted, followed by exsanguination (approved by the named animal welfare officer of the Justus Liebig University Giessen, administrative number 487_M and conducted according to the German and European animal welfare law). After removing the colon, it was flushed with ice-cold Tyrode's solution and then kept in an ice-cooled bathing solution.

To obtain the enteric crypts (performed according to ref. [68]), the first step consisted in stripping away by hand the serosa and muscularis propria. Briefly, the colon was placed on a small plastic rod with a diameter of 5 mm. A circular incision was made near the anal end with a blunt scalpel and the serosa together with the lamina propria was gently removed in the proximal direction. The remaining preparation, which was the mucosa-submucosa preparation, was glued to a plastic holder using a tissue adhesive and incubated for about 5–7 min in an Ethylenediaminetetraacetic acid solution at 38 °C. The second step of isolation, following the incubation period, consisted in a short vibration (30–60 s) of the sample in a high K^+ Tyrode's buffer solution in which the isolated crypts were collected and kept until the start of experiments.

Biochemical Imaging: The intensity of the NW fluorescence was derived from fluorescence images by image analysis using ZEN 2009 (Zeiss, Germany) software. The same software settings were used for all sets of pictures taken at different U_e and pH. The whole area of the fluorescence image was analyzed, where the average value of all pixels (sum of the pixel intensities over the selected area divided by the number of pixels) in the image was calculated.

For the bioimaging experiments, the experimental procedure was as follows: the samples of the crypt suspension were collected with a Pasteur pipette and transferred onto a 35 mm petri dish. Single crypts were collected using a transmission-light microscope. Then, 20 µL of this concentrated crypt suspension was applied to the dry surface of the nanowire electrode. After an incubation period of at least 15 min allowing crypts to settle down, the peristaltic pump was started to fill the experimental chamber with modified Tyrode's solution, replacing by the same way the high K^+ buffer solution and removing unbound isolated crypts. Then, the objective lens was immersed into the solution and focused on the nanowire surface to start the measurement sequence with one image every 30 s.

For these experiments, modified Tyrode's solution with a pH of 7.4 was perfused to establish a steady state as basal activity mimicking the physiological conditions of vital tissue and cells. The medium was exchanged in an open loop system. The pump was stopped to change the buffer solution and after starting the electrolyte flow over the cell, the solution was not pumped back into the system.

To obtain the chemical contrast (cf. Figure 8), the fluorescence intensity images were converted into grey scale and the intensity differences between the images without and with additives were calculated bidirectionally to obtain the intensity changes in both ways. The intensity increase is defined as the difference of image ②/③ and the reference image ①; the intensity decrease is the difference of the reference image ① and image ②/③ (cf. Figures 8 and 9). The brightness of the difference images was adjusted by a multiplication with the same factor of 1/38. Subsequently, the grey scale images were converted into color images again attributing the applied basic color to the intensity change by a multiplication with the respective color channel. Here, red depicts the intensity increase and blue the intensity decrease. The brightness of the colored images was adjusted for better comparison and then the images were superimposed with the grey scale optical image of the crypt on the nanowire surface.

To quantitatively investigate the intensity changes due to the presence of amiloride and NH_4Cl in the buffer solutions in the transient measurement (cf. Figure 9), an individual image mask was created for each image to define the cells outline and to consider the cell movement. The mask was generated by the application of different filters. First, the image was blurred to de-focus the image. Then these images were binarized and a morphological opening was applied. The image masks for the OCE area were obtained by the inversion of the image masks of the OCE covered with crypt. The intensity images resulting from a multiplication of these image masks with the original image were spatially integrated and then divided by the area.

Supporting Information

Supporting Information is available from the Wiley Online Library or from the author.

Acknowledgements

The authors would like to acknowledge N. Sabir for modifying the Si substrate surface with fluorescent dye and QDs. S.H. acknowledges support from the "Graduiertenstipendium" of the Justus Liebig University Giessen. Parts of this work were supported by the Deutsche Forschungsgemeinschaft (Grant No. PA794/15-1 to W.J.P.).

 © 2018 WILEY-VCH Verlag GmbH & Co. KGaA, Weinheim

M.V.Z. acknowledges the Government of the Russian Federation (Grant No. 08-08) and the President's Scholarship SP-1576.2018.4.

Conflict of Interest

The authors declare no conflict of interest.

Keywords

biosensors, nanophotonics, physiology, sensors

Received: April 12, 2018
Revised: June 19, 2018
Published online:

[1] J. Yin, Y. Hu, J. Yoon, *Chem. Soc. Rev.* **2015**, *44*, 4619.
[2] K. Sokolov, M. Follen, J. Aaron, I. Pavlova, A. Malpica, R. Lotan, R. Richards-Kortum, *Cancer Res.* **2003**, *63*, 1999.
[3] R. J. Gillies, N. Raghunand, G. S. Karczmar, Z. M. Bhujwalla, *J. Magn. Reson. Imaging* **2002**, *16*, 430.
[4] A. Lambacher, M. Jenkner, M. Merz, B. Eversmann, R. A. Kaul, F. Hofmann, R. Thewes, P. Fromherz, *Appl. Phys. A* **2004**, *79*, 1607.
[5] G. Zheng, F. Patolski, Y. Cui, W. U. Wang, C. M. Lieber, *Nat. Biotechnol.* **2005**, *23*, 1294.
[6] H. Yuan, J.-X. Zhang, C. Zhang, N. Zhang, L.-X. Xu, M. Ding, P. J. Clarke, *Chin. Phys. Lett.* **2015**, *32*, 020701.
[7] M. George, W. J. Parak, H. E. Gaub, *Sens. Actuators, B* **2000**, *69*, 266.
[8] W. J. Parak, D. Gerion, T. Pellegrino, D. Zanchet, C. Micheel, S. C. Williams, R. Boudreau, M. A. Le Gros, C. A. Larabell, A. P. Alivisatos, *Nanotechnology* **2003**, *14*, R15.
[9] B. O. Dabbousi, J. Rodriguez-Viejo, F. V. Mikulec, J. R. Heine, H. Mattoussi, R. Ober, K. F. Jensen, M. G. Bawend, *J. Phys. Chem. B* **1997**, *101*, 9463.
[10] W. J. Parak, R. Boudreau, M. Le Gros, D. Gerion, D. Zanchet, C. M. Micheel, S. C. Williams, A. P. Alivisatos, C. A. Larabell, *Adv. Mater.* **2002**, *14*, 882.
[11] X. Michalet, F. F. Pinaud, L. A. Bentolila, J. M. Tsay, S. Doose, J. J. Li, G. Sundaresan, A. M. Wu, S. S. Gambhir, S. Weiss, *Science* **2005**, *307*, 538.
[12] N. Gomez, J. O. Winter, F. Shieh, A. E. Saunders, B. A. Korgel, C. E. Schmidt, *Talanta* **2005**, *67*, 462.
[13] M. Bruchez Jr., M. Moronne, P. Gin, S. Weiss, A. P. Alivisatos, *Science* **1998**, *281*, 2013.
[14] C. Y. Zhang, H. C. Yeh, M. T. Kuroki, T. H. Wang, *Nat. Mater.* **2005**, *4*, 826.
[15] J. D. Marshall, M. J. Schnitzer, *ACS Nano* **2013**, *7*, 4601.
[16] C. E. Rowland, K. Susumu, M. H. Stewart, E. Oh, A. J. Mäkinen, T. J. O'Shaughnessy, G. Kushto, M. A. Wolak, J. S. Erickson, A. L. Efros, A. L. Huston, J. B. Delehanty, *Nano Lett.* **2015**, *15*, 6848.
[17] O. K. Nag, M. H. Stewart, J. R. Deschamps, K. Susumu, E. Oh, V. Tsytsarev, Q. Tang, A. L. Efros, R. Vaxenburg, B. J. Black, Y. Chen, T. J. O'Shaughnessy, S. H. North, L. D. Field, P. E. Dawson, J. J. Pancrazio, I. L. Medintz, Y. Chen, R. S. Erzurumlu, A. L. Huston, J. B. Delehanty, *ACS Nano* **2017**, *11*, 5598.
[18] H. M. McConnell, J. W. Parce, D. H. Hafeman, *J. Electrochem. Soc.* **1987**, *134*, C523.
[19] C. Kirchner, T. Liedl, S. Kudera, T. Pellegrino, A. Munõz Javier, H. E. Gaub, S. Stölzle, N. Fertig, W. J. Parak, *Nano Lett.* **2005**, *5*, 331.
[20] J. Wallys, J. Teubert, F. Furtmayr, D. M. Hoffmann, M. Eickhoff, *Nano Lett.* **2012**, *12*, 6180.
[21] G. Steinhoff, O. Purrucker, M. Tanaka, M. Stutzmann, M. Eickhoff, *Adv. Funct. Mater.* **2003**, *13*, 841.
[22] G. Steinhoff, B. Baur, G. Wrobel, S. Ingebrandt, A. Offenhäusser, M. Stutzmann, M. Eickhoff, *Appl. Phys. Lett.* **2005**, *86*, 033901.
[23] J. Yu, S. Kumar Jha, L. Xiao, Q. Liu, P. Wang, C. Surya, M. Yang, *Biosens. Bioelectron.* **2007**, *23*, 513.
[24] B. Baur, J. Howgate, H.-G. von Ribbeck, Y. Gawlina, V. Bandalo, G. Steinhoff, M. Stutzmann, M. Eickhoff, *Appl. Phys. Lett.* **2006**, *89*, 183901.
[25] G. M. Müntze, E. Pouokam, J. Steidle, W. Schäfer, A. Sasse, K. Röth, M. Diener, M. Eickhoff, *Biosens. Bioelectron.* **2016**, *77*, 1048.
[26] M. Yoshizawa, A. Kikuchi, M. Mori, N. Fujita, K. Kishino, *Jpn. J. Appl. Phys.* **1997**, *36*, L459.
[27] F. Furtmayr, M. Vielemeyer, M. Stutzmann, M. Eickhoff, *J. Appl. Phys.* **2008**, *104*, 034309.
[28] J. Schörmann, P. Hille, M. Schäfer, J. Müßener, P. Becker, P. J. Klar, M. Kleine-Boymann, M. Rohnke, M. de la Mata, J. Arbiol, D. M. Hofmann, J. Teubert, M. Eickhoff, *J. Appl. Phys.* **2013**, *114*, 103505.
[29] S. Arafin, X. Liu, Z. Mi, *J. Nanophotonics* **2013**, *7*, 074599.
[30] T. Kehagias, G. P. Dimitrakopulos, P. Becker, J. Kioseoglou, F. Furtmayr, T. Koukoula, I. Häusler, A. Chernikov, S. Chatterjee, Th. Karakostas, H.-M. Solowan, U. T. Schwarz, M. Eickhoff, Ph. Komninou, *Nanotechnology* **2013**, *24*, 435702.
[31] K. Maier, A. Helwig, G. Müller, P. Hille, J. Teubert, M. Eickhoff, *Nano Lett.* **2017**, *17*, 615.
[32] K. Maier, A. Helwig, G. Müller, F. Furtmayr, J. Teubert, M. Eickhoff, *Sens. Actuators, B* **2014**, *197*, 87.
[33] M. Riedel, S. Hölzel, P. Hille, J. Schörmann, M. Eickhoff, F. Lisdat, *Biosens. Bioelectron.* **2017**, *94*, 298.
[34] K. D. Goodman, V. V. Protasenko, J. Verma, T. H. Kosel, H. G. Xing, D. Jena, *J. Appl. Phys.* **2011**, *109*, 084336.
[35] D. Wencel, T. Abel, C. McDonagh, *Anal. Chem.* **2014**, *86*, 15.
[36] W. Shi, X. Li, H. Ma., *Methods Appl. Fluoresc.* **2014**, *2*, 042001.
[37] M. Frasco, N. Chaniotakis, *Sensors* **2009**, *9*, 7266.
[38] A. Dowd, D. Pissuwan, M. B. Cortie, *Trends Biotechnol.* **2014**, *32*, 571.
[39] W. Khalid, G. Göbel, D. Hühn, J. M. Montenegro, P. Rivera Gil, F. Lisdat, W. J. Parak, *J. Nanobiotechnol.* **2011**, *9*, 46.
[40] D. Gerion, F. Pinaud, S. C. Williams, W. J. Parak, D. Zanchet, S. Weiss, A. P. Alivisatos, *J. Phys. Chem. B* **2001**, *105*, 8861.
[41] J. Mahmoudian, R. Hadavi, M. Jeddi-Tehrani, A. R. Mahmoudi, A. A. Bayat, E. Shaban, M. Vafakhah, M. Darzi, M. Tarahomi, R. Ghods, *Cell J. (Yakhteh)* **2011**, *13*, 169.
[42] J.-J. Zhao, J. Chen, Z.-P. Wang, J. Pan, Y.-H. Huang, *Mol. Med. Rep.* **2011**, *4*, 425.
[43] S. Bharti, G. Kaur, S. Gupta, S. K. Tripathi, *J. Lumin.* **2017**, *181*, 459.
[44] G. Kaur, S. K. Tripathi, *Mater. Chem. Phys.* **2014**, *143*, 514.
[45] V. Sharma, N. Kaur, P. Tiwari, S. M. Mobin, *J. Photochem. Photobiol., B* **2018**, *182*, 137.
[46] G. Huang, X. Chen, C. Wang, H. Zheng, Z. Huang, D. Chen, H. Xie, *RSC Adv.* **2017**, *7*, 47840.
[47] M. Diener, C. Helmle-Kolb, H. Murer, E. Scharrer, *Pflügers Arch.* **1993**, *424*, 216.
[48] M. Diener, E. Scharrer, *Comp. Biochem. Physiol.* **1997**, *118*, 375.
[49] A. Gupta, J. C. Edwards, K. A. Hruska, *Bone* **1996**, *18*, 87.
[50] M. Benchaib, R. Delorme, M. Pluvinage, P. A. Bryon, C. Souchier, *Histochem. Cell Biol.* **1996**, *106*, 253.
[51] J. Goicoechea, C. Ruiz Zamarreño, I. R. Matias, F. J. Arregui, *Sens. Actuators, B* **2007**, *126*, 41.
[52] D. Schaffhauser, M. Fine, M. Tabata, T. Goda, Y. Miyahara, *Biosensors* **2016**, *6*, 11.
[53] M. George, B. Stein, O. Müller, M. Weis-Klemm, W. J. Parak, W. K. Aicher, *Ann. Rheum. Dis.* **2004**, *63*, 67.

 © 2018 WILEY-VCH Verlag GmbH & Co. KGaA, Weinheim

[54] N. Demaurex, R. R. Romanek, J. Orlowski, S. Grinstein, *J. Gen. Physiol.* **1997**, *109*, 117.
[55] J. Orlowski, S. Grinstein, *J. Biol. Chem.* **1997**, *272*, 22373.
[56] C. S. Potten, C. Booth, D. M. Pritchard, *Int. J. Exp. Pathol.* **1997**, *78*, 219.
[57] B. Masereel, L. Pochet, D. Laeckmann, *Eur. J. Med. Chem.* **2003**, *38*, 547.
[58] J. Laurent, A. Venn, E. Tambutté, P. Ganot, D. Allemand, S. Tambutté, *FEBS J.* **2013**, *281*, 683.
[59] E. A. Arena, W. E. Longo, K. E. Roberts, P. Geibel, J. Nateqi, M. Brandstetter, J. P. Geibel, *Am. J. Physiol. Cell Physiol.* **2012**, *302*, C412.
[60] R. Ohgaki, Y. Teramura, D. Hayashi, L. Quan, S. Okuda, S. Nagamori, M. Takai, Y. Kanai, *Sci. Rep.* **2017**, *7*, https://doi.org/10.1038/s41598-017-17459-y.
[61] J. Kneipp, H. Kneipp, B. Wittig, K. Kneipp, *Nanomedicine* **2010**, *6*, 214.
[62] J. Han, K. Burgess, *Chem. Rev.* **2010**, *110*, 2709.
[63] B. Stein, M. George, H. E. Gaub, W. J. Parak, *Sens. Actuators, B* **2004**, *98*, 299.
[64] I. Vurgaftman, J. R. Meyer, L. R. Ram-Mohan, *J. Appl. Phys.* **2001**, *89*, 5815.
[65] G. Decher, *Science* **1997**, *277*, 1232.
[66] P. Reiss, J. Bleuse, A. Pron, *Nano Lett.* **2002**, *2*, 781.
[67] T. Pellegrino, L. Manna, S. Kudera, T. Liedl, D. Koktysh, A. L. Rogach, S. Keller, J. Rädler, G. Natile, W. J. Parak, *Nano Lett.* **2004**, *4*, 703.
[68] G. Schultheiss, S. L. Kocks, M. Diener, *Biol. Proced. Online* **2002**, *3*, 70.

 © 2018 WILEY-VCH Verlag GmbH & Co. KGaA, Weinheim

Manuskripte

1) Mechanisms associated to nitroxyl (HNO)-induced relaxation in the intestinal smooth muscle. (in Vorbereitung)

9. Literaturverzeichnis

Aktories, Förstermann, Hofmann, Starke (2009). Allgemeine und spezielle Pharmakologie und Toxikologie. 10te Auflage. *Elsevier Urban & Fischer*, München, pp17-20.

Aley KO, McCarter G, Levine JD (1998). Nitric oxide signaling in pain and nociceptor sensitization in the rat. *J Neurosci.*, 18:7008-7014.

Ashcroft FM, Gribble FM (2000). New windows on the mechanism of action of KATP channel openers. *Trends Pharmacol. Sci.*, 21:439-445.

Avemary J, Diener M (2010). Bradykinin-induced depolarisation and Ca^{2+} influx through voltage-gated Ca^{2+} channels in rat submucosal neurons. *Eur. J. Pharmacol*., 635:87-95.

Bell A, Althaus M and Diener M (2015). Communication between mast cells and rat submucosal neurons. *Pflügers Arch. Eur. J. Physiol.*, 467:1809-1823.

Binder HJ, Sandle GI (1994). Electrolyte transport in the mammalian colon. *In:* Physiology of the Gastrointestinal Tract, 3rd ed. LR Johnson (ed). New York, *Raven Press*, pp 2133-2172.

Blackler RW, Gemici B, Manko A, Wallace JL (2014). NSAID gastroenteropathy: new aspects of pathogenesis and prevention. *Curr. Opin. Pharmacol.*, 19:11-16.

Boeckxstaens GE, Pelckmans PA, Herman AG, Van Maercke YM (1993). Involvement of nitric oxide in the inhibitory isolation of the human isolated colon. *Gastroenterology,* 104:690-697.

Böhme M, Diener M, Rummel W (1991). Calcium- and cyclic-AMP-mediated secretory responses in isolated colonic crypts. *Pflügers Arch*., 419:144-151.

Bolz SS, Vogel L, Sollinger D, Derwand R, de Wit C, Loirand G, Pohl U (2003). Nitric oxide-induced decrease in Calcium sensitivity of resistance arteries is attributable to activation of the myosin light chain phosphatase and antagonized by the RhoA/Rho Kinase pathway. *Circulation,* 107:3081-3087.

Browning KN, Lees G.M (1996). Myenteric neurons of the rat descending colon: electrophysiological and correlated morphological properties. *Neuroscience*, 73:1029-1047.

Cairo C, Gestwicki JE, Kanai M, Kiessling LL (2002). Control of multivalent interactions by binding epitope density. *J. Am. Chem. Soc.*, 124:1615.

Canessa CM, Horisberger JD, Rossier BC (1993). Epithelial sodium channel related to proteins involved in neurodegeneration. *Nature*, 361:467-470.

Canessa CM, Schild L, Buell G, Thorens B, Gautschi I, Horisberger J-D, Rossier BC. (1994). Amiloride-sensitive epithelial Na^+channel is made of three homologous subunits. *Nature*, 367:463-467.

Chávez-Piña AE, Tapia-Alvarez GR, Navarrete A (2010). Inhibition of endogenous hydrogen sulfide synthesis by PAG protects against ethanol-induced gastric damage in the rat. *Eur. J. Pharmacol.*, 630:131-136.

Christofi FL, Wood JD (1993). Endogenously released adenosine acts at A_1 receptors to suppress slow excitatory transmission (slow EPSP) and enhance slow inhibitory transmission (slow IPSP) in the myenteric plexus of guinea-pig small intestine. *Gastroenterology*, 104:A490.

Cowart D, Venuti R, Guptill J, Noveck R, Foo S (2015). A phase 1 study of the safety and pharmacokinetics of the intravenous nitroxyl prodrug, CXL-1427. *JACC,* 65(10S).

Craven PA, DeRubertis FR (1983). Patterns of prostaglandin synthesis and degradation in isolated superficial and proliferative colonic epithelial cells compared to residual colon. *Prostaglandins*, 26:583-604.

Dernedde J, Enders S, Reissig HU, Roskamp M, Schlecht S, Yekta S (2009). Inhibition of selectin by colloidal gold with functionalized shells. *Chem. Commun.*, 8:932-934.

Dhaese I, Lefebvre AR (2009). Myosin light chain phosphatase activation is involved in the hydrogen sulfide-induced relaxation in mouse gastric fundus. *Eur. J. Pharmacol.*, 606:180-186.

Diener M, Scharrer E (1994). The effect of short-chain fatty acids on Cl^- and K^+ conductance in rat colonic crypts. *Pflügers Arch.*, 426:472-480.

Donat ME, Wong K, Staines WA, Krantis A (1999). Heme oxygenase immunoreactive neurons in the rat intestine and their relationship to nitrergic neurons. *J. Auton. Nerv. Syst.*, 77:4-12.

Dröge W (2002). Free radicals in the physiological control of cell function. *Physiol. Rev.,* 82:47-95.

Eberhardt M, Dox M, Namer B, Miljkovic J, Cordasic N, Will C, Kichko TI, De La Roche J, Fischer M, Suarez SS, Bikiel D, Dorsch K, Leffler A, Babes A, Lampert A, Kennerz JK, Jacobi J, Marti MA, Doctorovich F, Högestätt ED, Zygmunt PM, Ivanovic-Burmazovic I, Messlinger K, Reeh P, Filipovic MR (2014). H2S and NO cooperatively regulate vascular tone by activating a neuroendocrine HNO-TRPA1-CGRP signalling pathway. *Nat. Commun.*, 5:4381.

Ekundi-Valentim E, Santos KT, Camargo EA, Denadai-Souza A, Teixeira SA, Zanoni CI, Grant AD, Wallace JL, Muscará MN, Costa SK (2010). Differing effects of exogenous and endogenous hydrogen sulphide in carrageenan-induced knee joint synovitis in the rat. *Br. J. Pharmacol.*, 159:1463-1474.

Elrod JW, Calvert JW, Morrison J, Doeller JE, Kraus DW, Tao L, Jiao X, Scalia R, Kiss L, Szabo C, Kimura H, Chow CW, Lefer DJ (2007). Hydrogen sulfide attenuates myocardial ischemia-reperfusion injury by preservation of mitochondrial function. *Proc Natl Acad Sci.* 104:15560-15565.

Filipovic MR, Eberhardt M, Prokopovic V, Mikuskovic, Orescanin-Dusic Z, Reeh P, Ivanovic-Burmazovic I (2013). Beyond H_2S and NO interplay: Hydrogen sulfide and nitroprusside react directly to give nitroxyl (HNO). A new pharmacological source of HNO. *J. Med. Chem.*, 56:1499-1508.

Fiorucci S, Orlandi S, Mencarelli A, Caliendo G, Santagada Distrutti E, Santucci L, Cirino G, Wallace JL (2007). Enhancedactivity of a hydrogen sulphide-releasing derivativeof mesalamine (ATB-429) in a mouse model of colitis. *Br. J. Pharmacol.*, 150:996-1002.

Frings M, Schultheiß G, Diener M (1999). Electrogenic Ca^{2+} entry in the rat colonic epithelium. *Pfluegers Arch.*, 439:39-48.

Furness JB (2006). The Enteric Nervous System. *Blackwell Publishing*, Oxford.

Gallego D, Clavé P, Donovan J, Rahmati R, Grundy D, Jiménez M, Beyak MJ (2008). The gaseous mediator hydrogen sulphide inhibits in vitro motor patterns in the human, rat and mouse colon and jejunum. *Neurogastroenterol Motil.,* 20:1306-1316.

Gallego D, Malagelada C, Accarino A Gori A, Malagelada JR, Azpiroz F, De Giorgio R, Jimenez M (2018). Functional neuromuscular impairment in severe intestinal dysmotility. *Neurogastroenterol Motil.*, 30:e13458.

Gallego D, Malagelada C, Accarino A, De Giorgio R, Malagelada JR, Azpiroz F, Jimenez M (2014). Nitrergic and purinergic mechanisms evoke inhibitory neuromuscular transmission in the human small intestine. *Neurogastroenterol Motil.*, 26:419-429.

Gallego D, Mane N, Gil V, Martinez-cutillas M, Jimenez M (2016). Mechanisms responsible for neuromuscular relaxation in the gastrointestinal tract. *Rev. Esp Enferm Dig*., 108:721-731.

Garlid KD, Paucek P (2003). Mitochondrial potassium transport: the K^+ cycle. *Biochim. Biophys. Acta*, 1606:23-41.

Gasiorek F, Pouokam E, Diener M, Schlecht S, Wickleder M (2015). Effects of multivalent histamine supported on gold nanoparticles: Activation of histamine receptors by derivatized histamine at subnanomolar concentrations. *Organ. Biomol. Chem*., 13:9984- 9992.

Giacomini KM, Sugiyama Y (2011). Membrane Transporter and Drug Response. In: Brunton L. (ed), Chabner B. (ed), Knollman B. (ed) Goodman and Gilman's, The pharmacological basis of therapeutics. 12th Edition. *Mc Graw Hill*, New York, p 89.

Gibbons SJ, Farrugia G (2004). The role of carbon monoxide in the gastrointestinal tract. *J. Physiol.,* 556:325-336.

Gil V, Gallego D, Grasa L, Martin MT, Jimenez M (2010). Purinergic and nitrergic neuromuscular transmission mediates spontaneous neuronal activity in the rat colon. *Am. J. Physiol. Gastrointest. Liver Physiol*., 299:G158-G169.

Gil V, Gallego D, Jimenez M (2011). Effects of inhibitors of hydrogen sulphide synthesis on rat colonic motility. *Br. J. Pharmacol*., 164:485-498.

Gonzalez LM, Moeser AJ, Blikslager AT (2015). Animal models of ischemia-reperfusion-induced intestinal injury: progress and promise for translational research. *Am. J. Physiol.Gastrointest.Liver Physiol.,* 308:G63-G75.

Grasa L, Gil V, Gallego D, Jimenez M (2009). P2Y1 receptors mediate inhibitory neurotransmission in the rat colon. *Br. J. Pharmacol*., 158:1641-1652.

Greger R (2000). Role of the CFTR in the colon. *Annual Review of Physiology*, 62:467-491.

Groneberg D, König P, Wirth A, Offermans S, Koesling D, Friebe A (2010). Smooth Muscle–Specific Deletion of Nitric Oxide–Sensitive Guanylyl Cyclase Is Sufficient to Induce Hypertension in Mice. *Circulation*, 121:401-409.

Haberberger R, Schultheiss G, Diener M (2006). Epithelial muscarinic M1 receptors contribute to carbachol-induced ion secretion in mouse colon. *Eur. J. Pharmacol*., 530:229-233.

Haglund U, Bergqvist D (1999). Intestinal ischemia the basics. *Langenbeck's Arch. Sur*., 384:233-238.

Hai A, Ben-Haim D, Korbakov N, Cohen A, Shappir J, Oren R, Spira ME, Yitzchaik S (2006). Acetylcholinesterase-ISFET based system for the detection of acetylcholine and acetylcholinesterase inhibitors. *Biosens. Bioelectron.*, 22:605-612.

Hamodeh SA, Rehn M, Haschke G, Diener M (2004). Mechanismofbutyrate-induced hyperpolarization of cultured rat myenteric neurons. *Neurogastroenterol. Motil*., 16:597-604.

Haschke G, Schäfer KH, Diener M (2000). Electrophysiological characterisation of rat myenteric neurons in culture In: Neurogastroenterology - From the Basics to the Clinics. *Krammer Kluwer Academic Publishers*, Lancaster, pp. 123-128.

He XD, Goyal RK (1993). Nitric oxide involvement in the peptide VIP-associated inhibitory junction potential in the guinea pig ileum. *J. Physiol.,* 461:485-499.

Hennig B, Diener M (2009). Actions of hydrogen sulfide on ion transport across rat distal colon. *Br. J. Pharmacol*., 158:1263-1275.

Hibino H, Inanobe A, Furutani K, Murakami S, Findlay I, Kurachi Y (2010). Inwardly rectifying potassium channels: their structure, function, and physiological roles. *Physiol. Rev.*, 90:291-366.

Hölzel S, Zyuzin MV, Wallys J, Pouokam E, Müßener J, Hille P, Diener M, Parak WJ and Eickhoff M (2018). Dynamic extracellular imaging of biochemical cell activity using InGaNGaN nanowire arrays as nanophotonic probes. *Adv. Funct. Mater.,* 1802503:1-12.

Hoth M, Penner R (1992). Depletion of intracellular calcium stores activates a calcium current in mast cells. *Nature*, 355:353-356.

Hund TJ, Mohler PJ (2011). Differential roles for SUR subunits in KATP channel membrane targeting and regulation. *Am. J. Physiol. Heart Circul. Physiol.,* 300:H33-H35.

Inoue I, Nagase H, Kishi K, Higuti T (1991). ATP-sensitive K^+ channel in the mitochondrial inner membrane. *Nature*, 352:244-247.

Irvine JC, Ritchie RH, Favaloro JL, Andrews KL, Widdop RE, Kemp-Harper BK (2008). Nitroxyl (HNO): the Cinderella of the nitric oxide story. *Trends Pharmacol. Sci.*, 29:601-608.

Ishihara H, Ozaki H, Sato K, Hori M, Karaki H, Watabe S, Kato Y, Fusetani N, Hashimoto K, Uemura D (1989). Calcium-independent activation of contractile apparatus in smooth muscle by calyculin -A. *J Pharmacol Exp Ther.,* 250:388-396.

Ji Y, Pang QF, Xu G, Wang L, Wang JK, Zeng YM (2008). Exogenous hydrogen sulfide postconditioning protects isolated rat hearts against ischemia-reperfusion injury. *Eur. J. Pharmacol.,* 587:1-7.

Jimenez M, Clave P, Accarino A, Gallego D (2014). Purinergic neuromuscular transmission in the gastrointestinal tract: functional basis for future clinical and pharmacological studies. *Br. J. Pharmacol.*, 171:4360-4375.

Jöns T, Wittschieber D, Beyer A, Meier C, Brune A, Thomzig A, Ahnert-Hilger G, Veh RW (2006). K^+-ATP-channel-related protein complexes: potential transducers in the regulation of epithelial tight junction permeability. *J Cell Sci.*, 119:3087-3097.

Kanu A, Leffler CW (2007). Carbon monoxide contributes to hypotension-induced cerebrovascular vasodilatation in piglets. *Am. J. Physiol. Heart Circ. Physiol.*, 293: H3193-H3200.

Kaplan JH (1985). Ion movements throught the sodium pump. *Annu. Rev. Physiol.*, 47:535-544.

Koh SD, Campbell JD, Carl A, Sanders KM (1995). Nitric oxide activates multiple potassium channels in canine colonic smooth muscle. *J. Physiol*. 489:735-743.

Krueger D, Foerster M, Mueller K, Zeller F, Slotta-Huspenina J, Donovan J, Grundy D, Schemann M (2010). Signaling mechanisms involved in the intestinal prosecretory actions of hydrogen sulfide. *Neurogastroenterol Motil*., 22:1224-1231.

Kunzelmann K, Mall M (2002). Electrolyte transport in the mammalian colon: mechanisms and implications for disease. *Physiol. Rev.*, 82:245-289.

Lee SW, Hu YS, Hu LF, Lu Q, Dawe GS, Moore PK et al. (2006). Hydrogen sulphide regulates calcium homeostasis in microglial cells. *Glia*, 54:116-124.

Lefer DJ (2008). Potential importance of alterations in hydrogen sulphide (H_2S) bioavailability in diabetes. *Br. J. Pharmacol.*, 155:617-619.

Leung FW, Su KC, Passaro EJr, Guth PH (1992). Regional differences in gut blood flow and mucosal damage in response to ischemia and reperfusion. *Am. J. Physiol. Gastrointest. Liver Physiol.*, 263:G301-G305.

Li Y, Weisbrodt N, Lodato R, et al. (1994). Nitric oxide is involved in muscle relaxation but not in changes in short-circuit current in rat ileum. *Am. J. Physiol.*, 266:G554-559.

Lingueglia E, Voilley N, Waldmann R, et al. (1993). Expression cloning of an epithelial amiloride-sensitive Na^+channel. *FEBS Lett.*, 318:95-99.

MacNaughton W (1993). Nitric oxide donating compounds stimulate electrolyte transport in the guinea pig intestine in vitro. *Life Sci.*, 53:585-593.

Martin GR, McKnight GW, Dicay MS, Coffin CS, Ferraz JGP, Wallace JL (2010). Hydrogen sulphide synthesis in the rat and mouse gastrointestinal tract. *Dig. Liver Dis.*, 42:103-109.

Mattern A, Machka F, Wickleder MS, Ilyaskina OS, Bünemann M, Diener M, Pouokam E (2018). Potentiation of the activation of cholinergic receptors by multivalent presentation of ligands supported on gold nanoparticles. *Organ. Biomol. Chem.*, 16: 6680-6687.

Meddings JB (1997). Review article: intestinal permeability in Crohn's disease. Aliment *Pharmacol Ther.*, 11(Suppl 3):47-53.

Mescher T (2013). Basic histology. *McGraw-Hill* Education / Medical; 13th edition.

Miljkovic JL, Kenkel I, Ivanovic-Burmazovic I, Filipovic MR (2013). Generation of HNO and HSNO from nitrite by heme-iron-catalysed metabolism with H2S. *Angew. Chem. Int. Ed.,* 52:12061-12064.

Miller SM, Reed D, Sarr MG, Farrugia G, Szurszewski JH (2001). Haem oxygenase in enteric nervous system of human stomach and jejunum and co-localization with nitric oxide synthase. *Neurogastroenterol. Motil.*, 13:121-131.

Mistry DK, Garland CJ (1998). Nitric oxide (NO)-induced activation of large conductance Ca^{2+}-dependent K^{+} channels (BKca) in smooth muscle cells isolated from the rat mesenteric artery. *Br. J. Pharmacol.*, 124:1131-1140.

Motta J, Flannigan KL, Agbor TA et al (2015). Hydrogensulfide protects From colitis and restores intestinal microbiota biofilm and mucus production. *Inflammatory Bowel Diseases*, 21:1006-1017.

Müntze GM, Pouokam E, Steidle J, Schäfer W, Sasse A, Röth K, Diener M, Eickhoff M (2015). Acetylcholinesterase-modified AlGaN/GaN solution-gate field-effect transistors for in-situ monitoring of myenteric neuron activity. *Biosens. Bioelectr.*, 77:1048-1054.

Narumiya S, Ishizaki T, Ufhata M (2000). Use and properties of ROCK-specific inhibitor Y-37632. *Meth. Enzymol*., 325:273-284.

Neunlist M, Reiche D, Michel K, Pfannkuche H, Hoppe S, Schemann M (1999). The enteric nervous system and the target specific projections and neurochemical codes. *Eur J Morphol.,* 37:233-240.

Olaison G, Sjödahl R, Tagesson C (1990). Abnormal intestinal permeability in Crohn's disease. A possible pathogenic factor. *Scand. J. Gastroenterol.*, 25:321-328.

Onodera K, Pouokam E, Diener M (2013). STIM1-regulated Ca^{2+} influx across the apical and the basolateral membrane in colonic epithelium. *J. Membrane Biol.*, 246:271-285.

Paolino M, Mennuni L, Giuliani G, Anzini M, Lanza M, Caselli Gianfranco, Galimberti C, Menziani MC, Donati A, Cappelli A (2014). Dendrimeric tetravalent ligands for the serotonin-gated ion channel. *Chem. Commun.,* 50:8582-8585.

Paolocci N, Jackson MI, Lopez BE, Miranda K, Tocchetti CG, Wink DA, Hobbs AJ, Fukuto JM (2007). The pharmacology of nitroxyl (HNO) and its therapeutic potential: not just the janus face of NO. *Pharmacol Ther*., 113:442-458.

Parekh AB (2006). On the activation mechanism of store-operated calcium channels. *Pfluegers Arch*., 453:303-311.

Parekh AB, Penner R (1997). Store depletion and calcium influx. *Physiol. Rev*., 77:901-930.

Pfannkuche H, Schemann M (2015). Enterisches Nervensystem und die Innervation des Magen-Darm-Traktes. In: Physiologie der Haustiere, 5. Auflage, Hrsg: Engelhardt, Breves, Diener, Gäbel. *Enke Verlag*, Stuttgart, pp 351-414.

Pollard T, Earnshaw (2008). Cell Biology. 2. Edition. Spektrum Akademischer Verlag. In: Johnson LR (ed) Physiology of the gastrointestinal tract. *Raven Press*, New York, pp 2133-2171.

Pouokam E, Althaus M (2016). Epithelial electrolyte transport physiology and the gasotransmitter hydrogen sulfide. *Oxid. Med. Cell. Longevity*. Art. ID 4723416.

Pouokam E, Bader S, Brück B, Schmidt B, Diener M (2013). ATPsensitive K^+ channels in rat colonic epithelium. *Pflügers Arch. Eur. J. Physiol*., 465:865-877.

Pouokam E, Bell A, Diener M (2013). Actions of Angeli's salt, a nitroxyl (HNO) donor, on ion transport across mucosa-submucosa preparations from rat distal colon. *Eur. J. Pharmacol.,* 715:133-141.

Pouokam E, Diener M (2012). Modulation of ion transport across rat distal colon by cysteine. *Front Physiol.*, 3:43.

Pouokam E, Rehn M, Diener M (2009). Effects of H_2O_2 at rat myenteric neurones in culture. *Eur. J. Pharmacol.*, 615:40-49.

Pouokam E, Steidle J, Diener M (2011). Regulation of colonic ion transport by gasotransmitters. *Biol Pharm Bull.*, 34:789-793.

Purves WK, Sadava D, Orians GH, Heller HC (2006). Purves Biologie. 7te Auflage. *Spektrum Akademischer Verlag,* pp 1531-1564.

Rao R, Riviere P, Pascaud X, Junien JL, Porreca F (1994).Tonic regulation of mouse ileal ion transport by nitric oxide. *J Pharmacol Exp Ther.*, 269:626-631.

Rehn M, Diener M (2006). Effect of the stable thromboxane derivative, carbocyclic thromboxane A_2, on membrane potential of rat myenteric neurons in culture. *Neurogastroenterol Motil*., 18:1084-1092.

Rehn M, Hübschle T, Diener M (2004). TNF-α hyperpolarises membrane potential and potentiates the response to nicotinic receptor stimulation in cultured rat myenteric neurons. *Acta Physiol. Scand.*, 181:13-22.

Rolfe V, Levin RJ (1994). Enterotoxin Escherichia coli STa activates a nitric oxide dependent myenteric plexus secretory reflex in rat ileum. *J Physiol.*, 475:531-537.

Saada MC, Montero JL, Vullo D, Scozzafava A, Winum JY, Supura C. (2011). Carbonic anhydrase activators: Gold nanoparticles coated with derivatized histamine, histidine, and carnosine show enhanced activatory effects on several mammalian isoforms. *J. Med. Chem.*, 54:1170-1177.

Sakai H, Suzuki T, Murota M, Takahashi Y, Takeguchi N (2002). Nitric oxide-induced Cl^- secretion in isolated rat colon is mediated by the release of thromboxane A_2. *J Physiol.,* 543:261-271.

Sanders KM (2008). Regulation of smooth muscle excitation and contraction. *Neurogastroenterol Motil*., 20:39-53.

Sandle (1998). Salt and water absorption in the human colon: a modern appraisal. *Gut*, 43:294-299.

Sandle GI, McNicholas CM, Lomax RB (1994). The potassium channels in colonic crypts. *The lancet*, 343:22-25.

Schäfer KH, Saffrey MJ, Burnstock G, Mestres-Ventura PA (1997). New method for the isolation of myenteric plexus from the new-born rat gastrointestinal tract. *Brain Res. Prot.*, 1:109-113.

Schemann M (2005). Control of gastrointestinal motility by the "gut brain"-The enteric nervous system. *J. Pediatr. Gastroenterol. Nutr.,* 45:S4-S6.

Schemann M, Grundy D (2009). Role of hydrogen sulfide in visceral nociception. *Gut* 58:744-747.

Schicho R, Krueger D, Zeller F, von Weyhern CWH, Frieling T, Kimura H, Ishii I, De Giorgio R, Campi B, Schemann M (2006). Hydrogen sulfide is a novel prosecretory neuromodulator in the guinea-pig and human colon. *Gastroenterology*, 131:1542-1552.

Schirgi-Degen A, Beubler E (1995). Significance of nitric oxide in the stimulation of intestinal fluid absorption in the rat jejunum in vivo. *Br. J. Pharmacol.*, 114:13-18.

Schultheiss G, Hennig H, Schunack W, Prinz G, Diener M (2006). Histamine-induced ion secretion across rat distal colon: involvement of histamin H1 and H2 receptors. *Eur. J. Pharmacol.*, 546(1-3):161-170.

Schultheiss G, Ribeiro R, Schäfer KH, Diener M (2003). Activation of apical K^+-conductances by muscarinic receptor stimulation in rat distal colon: fast and slow components. *J Membr Biol.*, 195:183-196.

Schultheiss G, Seip G, Kocks SL, Diener M (2002b). Ca^{2+}-dependent and Ca^{2+}-independent Cl^- secretion stimulated by the nitric oxide donor, GEA 3162, in rat colonic epithelium. *Eur. J. Pharmacol.*, 444:21-30.

Schultheiss G, Siefjediers A, Diener M (2005). Muscarinic receptors stimulation activates a Ca^{2+}-dependent Cl^- conductance in rat colon. *J. Membr Biol.*, 204(3):117-27.

Seip G, Schultheiss G, Kocks SL, Diener M (2001). Interaction between strore-operated non-selective cation channels and the Na^+-Ca^{2+} exchanger during secretion in the rat colon. *Exp. Physiol.*, 86:461-468.

Shuttleworth CW, Sanders KM (1996). Involvement of nitric oxide in neuromuscular transmission in canine proximal colon. *Proc Soc Exp Biol Med.*, 211:16-23.

Shuttleworth CW, Xue C, Ward SM, de Vente J, Sanders KM (1993). Immunohistochemical localization of 3',5'-cyclic guanosine monophosphate in the canine proximal colon: responses to nitric oxide and electrical stimulation of enteric inhibitory neurons. *Neuroscience*, 56:513-522.

Smith TK, McCarron SL (1998). Nitric oxide modulates cholinergic reflex pathways to the longitudinal and circular muscle in the isolated guinea-pig distal colon. *J. Physiol*., 512:893-906.

Söderholm JD, Olaison G, Peterson KH, Franzén LE, Lindmark T, Wirén M, Tagesson C, Sjödahl R (2002). Augmented increase in tight junction permeability by luminal stimuli in the non-inflamed ileum of Crohn's disease. *Gut,* 50:307-313.

Stack WA, Filipowicz B, Hawkey CJ (1996). Nitric oxide donating compounds stimulate human colonic ion transport in vitro. *Gut*, 39:93-99.

Stark ME, Bauer AJ, Sarr MG, Szurszewski JH (1993). Nitric oxide mediates inhibitory nerve input in human and canine jejunum. *Gastroenterology,*104:398-409.

Steidle J, Diener M (2011). Effects of carbon monoxide on ion transport across rat distal colon. *Am. J. Physiol. Gastrointest. Liver Physiol.*, 300:G207-G216.

Stone JR, Marletta MA (1994). Soluble guanylate cyclase from bovine lung: activation with nitric oxide and carbon monoxide and spectral characterization of the ferrous and ferric states. *Biochemistry*, 33:5636-5640.

Strabel D, Diener M (1995). Evidence against direct activation of chloride secretion by carbachol in the rat distal colon. *Eur. J. Pharmacol.*, 274:181-191.

Switzer CH, Flores-Santana W, Mancardi D, Donzelli S, Basudhar D, Ridnour LA, Miranda KM, Fukuto JM, Paolocci N, Wink DA (2009). The emergence of nitroxyl (HNO) as a pharmacological agent. *Biochim. Biophys Acta*., 2009;1787:835-840. *Biochim. Biophys Acta*, 1787:835-840.

Szabo C (2007). Hydrogen sulphide and its therapeutic potential. *Nat. Rev. Drug Discovery*, 6:917-935.

Szabo Csaba (2017). Hydrogen sulphide, an enhancer of vascular nitric oxide signalling: mecahnisms and implications. *Am. J. Physiol. Cell Physiol*., 312: C3-C15.

Takeuchi K, Aihara E, Kimura M, Dogishi K, Hara T, and Hayashi S (2012). Gas mediators involved in modulating duodenal HCO_3-secretion. *Curr. Med Chem.*, 19: 43-54.

Tam FS, Hillier K (1992). The role of nitric oxide in mediating non-adrenergic non-cholinergic relaxation in longitudinal muscle of human taenia coli. *Life Sci.,* 51:1277-1284.

Tamai H, Gaginella TS (1993). Direct evidence for nitric oxide stimulation of electrolyte secretion in the rat colon. *Free Radic Res Commun.*, 19:229-39.

Tamizhselvi R, Moore PK, Bhatia M (2007). Hydrogen sulfide acts as a mediator of inflammation in acute pancreatitis: in vitro studies using isolated mouse pancreatic acinar cells. *J. Cell. Mol. Med*., 11:315-326.

Teague B, Asiedu S, Moore PK (2002). The smooth muscle relaxant effect of hydrogen sulphide in vitro:evidence for a physiological role to control intestinal contractility. *Br. J. Pharmacol*., 137:139-145.

Turkevich J, Stevenson PC, Hillier J (1951). A study of the nucleation and Growth processes in the synthesis of colloidal Gold. *Discuss Faraday Soc.*, 55–75.

Uehata M, Ishizaki T, Satoh H, Ono T, Kawahara T, Morishita T, Tamawaka H, Yamagami K, Inui J, Maekawa M, Narumiya S (1997). Calcium sensitization of smooth muscle mediated by a Rho-associated protein kinase in hypertension. *Nature,* 389:990-994.

Uthman Ed (2011). Normal small intestine mucosa. https://creativecommons.org/licenses/by/2.0

Vogalis, F, Harvey JR (2003). Altered excitability of intestinal neurons in primary culture caused by acute oxidative stress. *J. Neurophysiol.,* 89:3039-3050.

Wada-Takahashi S, Tamura K (2000). Actions of reactive oxygen species on AH/type 2 myenteric neurons in guinea pig distal colon. *Am. J. Physiol. Gastrointest. Liver Physiol.*, 279:G893-G902.

Wallace JL (2010). Physiological and pathophysiological roles of hydrogen sulfide in the gastrointestinal tract. *Antioxid Redox Signal.*, 12:1125-1133.

Wallace JL, Vong L, McKnight W, Dicay M, Gary RM (2009). Endogenous and exogenous hydrogen sulfide promotes resolution of colitis in rats. *Gastroenterology*, 137:569-578.

Wang R (2002). Two's company, three's a crowd: can H_2S be the third endogenous gaseous transmitter? *FASEB J.*, 16:1792-1798.

Wang R (2012). Physiological implications of hydrogen sulfide: a whiff exploration that blossomed. *Physiol. Rev.,* 92:791-896.

Wilson KT, Xie Y, Musch MW, Chang EB (1993). Sodium nitroprusside stimulates anion secretion and inhibits sodium chloride absorption in rat colon. *J. Pharmacol. Exp. Ther*., 266:224-230.

Wolffram S (2015). Funktionen des Dünndarms und seiner Anhangsdrüsen: In: Physiologie der Haustiere, 5. Auflage, Hrsg: Engelhardt, Breves, Diener, Gäbel. *Enke Verlag*, Stuttgart, pp 351-414.

Wood J (2004). Enteric neuroimmunophysiology and pathophysiology. *Gastroenterology*, 127:635-657.

Wood JD (2008). Enteric nervous system: reflexes, pattern generators and motility. *Curr. Opin. Gastroenterol.,* 24:149-158.

Würner L, Pouokam E, Diener M (2014). The effect of bradykinin on the electrical activity of rat myenteric neurons. *Eur. J. Pharmacol.*, 738:158-169.

Yong QC, Cheong JL, Hua F, Deng LW, Khoo YM, Lee HS, Perry A, Wood M, Whiteman M, Bian JS (2011). Regulation of heart function by endogenous gaseous mediators-crosstalk between nitric oxide and hydrogen sulfide. *Antioxid. Redox Signal.,* 14:2081-2091.

Zhang L, Qi Q, Yang J, Sun D, Li C, Xue Y, Jiang Q, Tian Y, Xu C, Wang R (2015). An anticancer role of hydrogen sulfide in human gastric cancer cells. *Oxid. Med. Cell. Longev.,* 636410.

Zhao P, Huang X, Wang ZY, Qiu ZX, Han YF, Lu HL, Kim YC, Xu WX (2009). Dual effect of exogenous hydrogen sulfide on the spontaneous contraction of the gastric smooth muscle in guinea-pig. *Eur. J. Pharmacol.*, 616:223-228.

Zhao W, Zhang J, Lu Y, Wang R (2001). The vasorelaxant effect of H_2S as a novel endogenous gaseous K_{ATP} channel opener. *EMBO J.*, 20:6008-6016.

Zheng L, Kelly CJ, Colgan SP (2015). Physiologic hypoxia and oxygen homeostasis in the healthy intestine. A review in the theme: cellular responses to hypoxia. *Am. J. Physiol. Cell Physiol.,* 309:C350-C360.

10. Anhang

10.1 Eigene Publikationen

1) **Pouokam E**, Diener M (2019). Segmental differences in ion transport in rat caecum. Pflügers Arch. Eur. J. Physiol. https://doi.org/10.1007/s00424-019-02276-1. **[2.765 Impact factor]**
2) Mattern A, Machka F, Wickleder MS, Ilyaskina OS, Bünemann M, Diener M, **Pouokam E (2018)**. Potentiation of the activation of cholinergic receptors by multivalent presentation of ligands supported on gold nanoparticles *Organ. Biomol. Chem*., 16:6680-6687; **[3.423 Impact factor]**
3) Hölzel S, Zyuzin MV, Wallys J, **Pouokam E**, Müßener J, Hille P, Diener M, Parak WJ, Eickhoff M **(2018)**. Dynamic extracellular imaging of biochemical cell activity using InGaNGaN nanowire arrays as nanophotonic probes. *Adv. Funct. Mat*er: Art. 1802503 **[13.325 Impact factor]**
4) Schindele S, **Pouokam E**, Diener M (2016). Hypoxia/reoxygenation effects on ion transport across rat colonic epithelium. *Front. Physiol*. 7:Art. 247**. [4.134 Impact factor]**
5) **Pouokam E**, Althaus M. **(2016)**. Epithelial electrolyte transport physiology and the gasotransmitter hydrogen sulfide. *Oxid. Med. Cell Longev*.,Art. ID 4723416. **[4.492 Impact factor]**
6) Müntze GM, **Pouokam E**, Steidle J, Schäfer W, Sasse A, Röth K, Diener M, Eickhoff M **(2015)**. Acetylcholinesterase-modified AlGaN/GaN solution-gate field-effect transistors for in-situ monitoring of myenteric neuron activity. *Biosens. Bioelectr.*, 77:1048-1054**. [7.476 Impact factor]**
7) Gasiorek F, **Pouokam E**, Diener M, Schlecht S, Wickleder M **(2015)**. Effects of multivalent histamine supported on gold nanoparticles: Activation of histamine receptors by derivatized histamine at subnanomolar concentrations. *Organ. Biomol. Chem.,* 13:9984-9992. **[3.56 Impact factor]**
8) Lu Z, Quack T, Hahnel S, Gelmedin V, **Pouokam E**, Diener M, Hardt M, Michel G, Baal N, Hackstein H, Grevelding CG **(2015)** Isolation, enrichment and primary characterization of vitelline cells from Schistosoma mansoni obtained by the organ-isolation method. *Int. J. Parasitol*., 45:663-672 **[3.87 Impact factor]**
9) Würner L, **Pouokam E**, Diener M **(2014)**: The effect of bradykinin on the electrical activity of rat myenteric neurons. *Eur. J. Pharmacol*., 738:158-169. **[2.53 Impact factor**
10) **Pouokam E**, Bader S, Brück B, Schmidt B, Diener M **(2013)**. ATP-sensitive K^+ channels in rat colonic epithelium. *Pflügers Arch. Eur. J. Physiol.*, 465:865-877**.[3.073 Impact factor]**
11) Onodera K, **Pouokam E**, Diener M **(2013)**: STIM1-regulated Ca^{2+} influx across the apical and the basolateral membrane in colonic epithelium. *J. Membrane Biol.*, 246:271-285. **[2.174 Impact factor]**
12) **Pouokam E**, Bell A, Diener M **(2013)**. Actions of Angeli's salt, a nitroxyl (HNO) donor, on ion transport across mucosa-submucosa preprations from rat distal colon. *Eur. J. Pharmacol*., 715:133-141. **[2.68 Impact factor]**

13) **Pouokam E**, Diener M **(2012)**. Modulation of ion transport across rat distal colon by cysteine.*Front. Physiol. Membr. Physiol. Biophys*:, 3, Art. 43. **[2.97 Impact factor]**

14) Kohr D, Singh P, Tschernatsch M, Kaps M, **Pouokam E**, Diener M, Kummer W, Birklein F, Vincent A, Goebel A, Wallukat G, Blaes F **(2011)**. Autoimmunity against the beta2 adrenergic receptor and muscarinic 2 receptor in complex regional pain syndrome. *Pain*, 152:2690-2700. **[5.777 Impact factor]**

15) **Pouokam E**, Diener M **(2011)**. Mechanims of actions of hydrogen sulfide at rat distal colonic epithelium. *Brit. J. Pharmacol.*, 162:392-404. **[4.409 Impact factor]**

16) **Pouokam E**, Steidle M, Diener M **(2011)**. Regulation of colonic ion transport by gasotransmitters. *Biol. Pharm. Bull.*, 34:789-793. **[1.657 Impact factor]**

17) **Pouokam E**, Rehn M, Diener M **(2009)**. Effects of H_2O_2 at rat myenteric neurones in culture. *Eur. J. Pharmacol.,* 615:40-49. **[2.585 Impact factor]**

18) Kamgang R, Gonsu KH, Wafo P, Mbungni JA, **Pouokam EV**, Fokam TAM, Fonkoua MC **(2007)**. Activity of aqueous ethanol extract of Euphorbia prostrata ait on Shigella dysenteriae type 1-induced diarrhea in rats. *Ind. J. Pharmacol.*, 39:240-244. **[0.69 Impact factor]**

19) Kamgang R, **Pouokam EV**, Fonkoua MC, Penlap NV, Biwole SM **(2006)**. Activities of aqueous extracts of Mallotus oppositifolium on Shigella dysenteriae1 induced diarrhoea in rats. *Clin. Exp. Pharmacol. Physiol.*, 33:89-94. **[1.780 Impact factor]**

20) Kamgang R, **Pouokam EV**, Fonkoua MC, Penlap NV, Biwole SM **(2005)**. Shigella dysenteriae type 1-induced diarrhea in rats. *Jpn. J. Infect. Dis,.* 58:335-337.**[0.776 Impact factor]**

Abstracts

1. **Pouokam E**, Muentze GM, Diener M, Eickhoff M (2015). Multifunctional screening of cell transistor hybrid systems with enzyme-modified AlGaN/GaN-type field effect transistor arrays. *Acta Physiol.* 214 Suppl. 701:3.
2. Malberg S, Al-Ibadi B, Heckmann J, Piepenbring A, Lierz M, **Pouokam E**, Diener M, Herden C (2015).Immunohistochemical markers for the enteric nervous system of the cockatiel. *J. Comp. Pathol.* 152:74.
3. **Pouokam E**, Bell A, Diener M (2013). Actions of nitroxyl (HNO) on ion transport across rat distal colon. *J. Physiol. Biochem.* 69:660.
4. **Pouokam E**, Diener M (2012). ATP-sensitive K^+ channels in rat colonic epithelium. *Genes Nutr.* 6 (Suppl. 1):S16.
5. **Pouokam E**, Diener M (2010).Changes in ion transport induced by the endogenous H2S donor, cysteine, across rat distal colon. *Genes Nutr. 5* (Suppl. 1):S49.
6. **Pouokam E**, Rehn M, Diener M (2008). Effects of H_2O_2 on Na^+ currents at rat myenteric neurones. *Leipziger Blaue Hefte 4: Proceedings 18*. Tagung der DVG-Fachgruppe Physiologie und Biochemie:50
7. **Pouokam E**, Rehn M, Diener M (2008). Effects of H_2O_2 on Na^+ currents at rat myenteric neurones. *J. Physiol. Biochem*. 64:300.
8. **Pouokam E**, Rehn M, Diener M (2007). Actions of oxidants on myenteric neurons. *J. Physiol. Biochem.* 63:69.

Dissertation:

Effects of H_2O_2 at rat myenteric neurones in culture. Ph.D.-Thesis aus dem Institut für Veterinär-Physiologie der Justus-Liebig-Universität Gießen. http://geb.uni-giessen.de/geb/volltexte/2010/7455/pdf/PouokamKamgneErvice_2010_03_01.pdf

10.2 Förderung/Drittmittelförderung

Okt-Nov. 2018	Erasmus+ Mobility Staff Stipendium nach Barcelona (Veterinär-Physiologie der Univeristat Autonoma de Barcelona)
2017-2020	DFG Förderung in Höhe von **207.500 Eur**. für Doktorandenstelle, Sachmittel und Programmpauschale zum Thema "Nitroxyl als neuer Wirkstoff in der Regulation der gastrointestinalen Motilität“
2006-2009:	Doktorandenstipendium durch den Deutschen Akademischen Austauschdienst (DAAD)
2005-2006	Deutsch Sprachkurse, Förderung des DAAD

10.3 Danksagung

Ich möchte mich hiermit herzlich bei allen, die an dieser Arbeit bzw. meinem bisherigen Werdegang im Institut für Veterinär-Physiologie und -Biochemie beteiligt waren, bedanken. Als Erster soll hier Prof. Dr. Martin Diener erwähnt werden. Ihm habe ich tatsächlich am meisten zu verdanken. Er gab mir ein Thema für meine Doktorarbeit und anschließend eine Postdoc Stelle. Dank seiner unermüdlichen Unterstützung und Hilfe bei allen Fragen zur Forschung, Lehre und privaten Angelegenheiten bin ich nun hier angekommen. Martin, danke für Alles! Als nächstes möchte ich den aktuellen und ehemaligen Mitgliedern unserer Arbeitsgruppe danken. Dr. Rehn möchte ich hier nochmals danken für die initiale und prägende Unterweisung in Zellkultur, Imaging, Elektrophysiologie Arbeiten. Weiterhin möchte ich Herrn Prof. Dr. Gerhard Schultheiß für

zahlreiche Diskussionen. Auch unseren „Laborheldinnen“ Eva Maria Haas, Barbara Schmidt, Brigitta Buß, Alice Stockinger danke ich herzlich für die tolle Assistenz sowohl im Labor als auch in der Lehre, das „Mitdenken“ und die sozialen Aspekte des Lebens. Danke nochmals für den „Kaffee“! Ein „Dankeschön“ geht auch an die Doktoranden, die ich bislang mitbetreuet habe und jetzt mitbetreue: Kaoru Onodera Ph.D, Lisa Würner Ph.D, Dr. vet, med. Sabine Schindele, Mirko Gastreich-Seelig. Die Zusammenarbeit mit euch war/ist eine Freude, sehr bereichernd. Weiterhin möchte ich Herrn Prof. Rüdiger Gerstberger, Prof. Joachim Roth, Prof. Christoph Rummel für ihre Unterstützung danken. Ich bedanke mich auch bei Doreen Marks, Jolanda Murgott, Daniella Ott für ihre Assistenz in Lehrveranstaltungen. Darüber hinaus danke ich Frau Pfeiff-Boschek für die Hilfe in allen administrativen Fragen, der Werkstatt, unseren Tierpflegern Michael Haas, Jan Fonseca. Vergessen werde ich nicht „Jungs“ des Instituts Niklas und Stephan für ihr besonderes soziales Engagement, sei es für Grill, Fußball, Streichen, Umzug. Jungs, es sind noch „Moleküle der Freude“ für euch kaltgestellt.

Doch nicht nur die Mitarbeiter unseres Instituts sollen hier Erwähnung finden. Auch institutsübergreifend habe ich viel Unterstützung erfahren: Prof. Dr. Baumgart-Vogt, Prof. Dr. Wolfgang Kummer aus der Anatomie, Prof. Dr. Franz Blaes aus der Neurologie, Prof. Dr. Christoph Gevelding aus der Parasitologie, PD Mike Althaus (aus der Biologie) , Prof. Dr. K.D. Schlüter aus der Humanphysiologie, Prof. Dr. M. Wickleder aus der Chemie (Gießen/Köln), Prof. M. Bünemann aus der Pharmakologie Marburg, Prof. Dr. Martin Eickhoff aus der Physik (Gießen/Bremen) haben mich unterstützt, mir geholfen mein Wissensspektrum zu erweitern - sei es mit konstruktiven Diskussionen, Forschungskooperationen, konstruktive Mitarbeiten. Darüber hinaus möchte ich herzlich externe Doktoranden und Mitkommilitonen für die tolle Zusammenarbeit danken: Dr. Sara Hölzel, Dr. Mareike Müntze, Dr. Friedericke Machka, Dr. Lu Z., A. Mattern, Danielle Kohr Ph.D, Pratiba Singh Ph.D, euch Dankeschön!

Herrn Prof. Dr. Marcel Jimenez Farrerons (Barcelona, Spanien) und seiner Arbeitsgruppe möchte ich für die Kooperationspartnerschaft danken.

Ohne Forderung wäre ich auch nicht hier angekommen. Somit geht ein großes „Dankeschön“ an den „DAAD“, die Deutsche Forschung Gemeinschaft und das Erasmus Programm+.

Bei dir Anca, bedanke mich für Alles!!!

Zum Schluss möchte ich meiner Familie danken. Meinen Eltern Kamgne Jacques und Metchuiam Elise, meinen Geschwistern Kamche Pelagie, Kamsu Sylvain, Feutseu Yves, Kouam Mathurine und Tameu Jacques, meinen Kindern Noah, Scarlette und Marlon möchte ich für die Unterstützung danken.

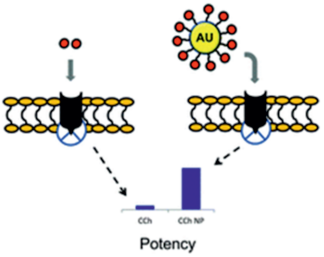

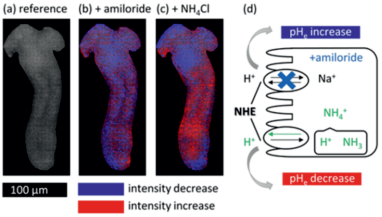

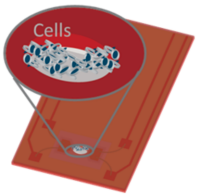

édition scientifique
VVB LAUFERSWEILER VERLAG

VVB LAUFERSWEILER VERLAG
STAUFENBERGRING 15
D-35396 GIESSEN

Tel: 0641-5599888 Fax: -5599890
redaktion@doktorverlag.de
www.doktorverlag.de

ISBN: 978-3-8359-6907-0